NASA TECHNICAL TRANSLATION

NASA TT F-823

NASA TT F-823

THEORY OF THE LIFTING AIRSCREW

V. E. Baskin, L. S. Vil'dgrube,
Ye. S. Vozhdayev, and G. I. Maykapar

Mashinostroyeniye Press
Moscow, 1973

NATIONAL AERONAUTICS AND SPACE ADMINISTRATION • WASHINGTON, D. C. • FEBRUARY 1976

General

During this translator's visit to Moscow on the occasion of the USSR-US Aeronautical Symposium in 1973, he had the pleasure of receiving, from Dr. Ye.S. Vozhdayev, a copy of the "just published" book entitled, *Theory of the Lifting Airscrew*. A cursory look at the contents seemed to confirm the claim expressed by its authors in the Preface that this is a unique publication, not only in the USSR, but in the West as well. A more thorough reading further confirmed that this, indeed, is an exceptional text in the sense that contained within its covers is probably the most thorough exposition of the application of the vortex theory to rotary-wing aerodynamics. In that respect, one might even regret that this complete reliance on the vortex theory in the presentation of the subject is not, somehow, reflected in the title.

Undoubtedly, there are some students and practitioners in the field of rotary wings, and this translator is one of them, who would believe that in a complete presentation of helicopter aerodynamics as well as that of other airscrew-type aircraft, there is room for the momentum, and combined blade-element - momentum theories[1]. However, one should also keep in mind that at the current state of technology, the vortex theory represents the basis for almost all computer programs related to aeroelastic phenomena of the rotor, as well as for many detailed performance predictions of rotary-wing aircraft. For this reason, the Russian book appeared as a potentially useful source of information for the practicing rotary-wing aerodynamicist and/or aeroelastician. It might also serve as a basic text for academic courses. Finally, its value was recognized as a useful reference book and supplementary reading material to be used with other textbooks. This latter aspect was of particular interest to this translator in conjunction with the preparation (under a USAAMRDL/NASA contract) of a textbook on fundamentals of rotary-wing aerodynamics.

In view of the above-mentioned aspects, the desirability of translating the book into English was discussed; first with Dr. I. Statler, Director of Ames Directorate; and then with Mr. P. Yaggy, Director, and Dr. R. Carlson, Deputy Director of the U.S. Army Air Mobility Research & Development Labs (USAAMRDL). They concurred that the *Theory of the Lifting Airscrew* should be made available to the English-speaking technical community. Consequently, material contained in this volume was prepared for USAAMRDL by this translator in cooperation with Mrs. Wanda L. Metz, under contract from NASA to Boeing Vertol Company.

Technical Comments

Even before starting to study the translated text, the potential reader may ask, "What is new and different in the Soviet approach from that encountered in Western literature, and in what respect does the Soviet school-of-thought appear to vary from that of ours?" In trying to answer these questions, one may run the risk of oversimplification and generalization. This is especially true when, as in this case, one is discussing or trying to describe a school-of-thought associated with an active and continuously developing field of technological and scientific endeavors. Here, one solitary researcher or small group of investigators thrusting in a new direction might completely change the already established trends. Nevertheless, accepting this risk of oversimplification, I will try to indicate what is unique in the Soviet approach to the application of the vortex theory to rotary-wing aerodynamics.

After following a survey of the field (such as that by Landgrebe and Cheney[2]), one gets the impression that in the West, two periods in the development of rotary-wing aircraft aerodynamics can be distinguished; one, up to the early '60s before the appearance of high-capacity computers, and from then to the present, where the reliance on computers plays a decisive role. However, before the appearance of high-capacity computers, the development of the vortex theory in the USSR and the West ran along two, separate, but more or less, parallel, courses.

At the dawning of the airscrew vortex theory (in the late teens and early twenties), the Soviet school had a head start with the published works of numerous Russian theoretical aero- and hydro-dynamicists; especially, those of Joukowsky and his students. In this respect, one should realize that Joukowsky, during this period, solved the problem of a stationary airscrew with an infinite number of blades through the concept of a straight cylindrical vortex wake. However, because of the lack of exchange of ideas between the USSR and the West, this translator as well as a majority of those engaged in the field of airscrew aerodynamics in the West give the credit for the originality of this approach to Knight and Hefner[3] (1937).

Although the classic works of Lamb, Glauert, Lock, Goldstein, and Betz, as well as all volumes of Durand, etc., were known to the Soviet school, contacts with the West were very limited until the sixties. Nevertheless there are indications that technical literature in the field of rotary-wing aerodynamics published in the West had penetrated to the USSR. It may be assumed,

hence, that, either directly or indirectly, the Soviet train-of-thought bears some imprint of this influence; while in contrast, the flow of thoughts in the field of rotary-wing aerodynamics from the USSR to the West was practically nonexistent until the works of Mil became available through a NASA translation in the late sixties[4], and other, rather sporadic, translations.

It appears that until the sixties, working in that atmosphere of separation, both the Western and the Soviet schools aimed at the best possible determination of the time-average velocities induced in the surrounding medium by an airscrew in general, and helicopter rotors in particular, in various regimes of flight. Making numerous simplifying assumptions regarding the shape of the wake, attempts were made to obtain solutions for the induced velocities as well as their harmonics under rather simple mathematical forms. Auxiliary graphs and tables were also made available. Works of Castles and DeLeeuw[5], ad well as Heyson and Katzoff[6], etc., can be cited as typical for that period.

With the increasing difficulties encountered in such tasks as the determination of instantaneous induced velocities taking into account the time-dependent deformation of the wake, etc., it became more and more difficult to obtain solutions, either explicitly expressed by simple mathematical formulae or with the help of special functions whose tables are generally available. In this respect, a statement by Miller[7], although referring to MIT experience, can probably be quoted as typical of the whole Western approach.

> *"The tests discussed above clearly indicated the need for an analytical tool for computing blade downwash velocities which would take into account the individual blade wake geometry and also introduce the effects of unsteady aerodynamics. Attempts to obtain a closed form solution to this problem, or one based on tabulated integrals, were not successful and it was evident that extensive computer facilities would be required to explore this problem and, hopefully, to provide a basis for obtaining simplified solutions suitable for engineering applications. In 1960, the availability of an IBM 709 computer at the MIT Computation Center and funds from a Carnegie grant permitted initiation of such a program."*

The above statement marked the beginning of the computer-oriented approach toward both aerodynamic and aeroelastic problems of rotary-wing aircraft in the West[2].

By contrast, as exemplified by this translation, it appears that in the USSR, there remained at least one strong school of thought oriented toward making use of all possible classical mathematics, including the full array of such special functions as Bessel and Legendre; elliptic integrals, theory of cylindrical functions etc.

To what extent this trend may be due to the unavailability of a large number of high capacity computers, or to what extent it reflects a mastery and love of mathematics, so typical of Russian scientists and engineers, is difficult to answer. It is also possible that their strong attachment to established tradition and patriotism may also have played some role in the development of that particular school of thought. The reader of the book will probably sense those influences by simply noticing how often the name of Joukowsky, as founder of the vortex theory, and his original solutions and approaches are mentioned with reverence throughout the text.

Review of the Text

The reader will find that material incorporated in the book is briefly reviewed in the Introduction. Using this review as a guide, additional features which should be of particular interest are pointed out.

The concept of the flat vortex wake, discussed in Ch. II, recently generated an interest in the West, as exemplified by the work of Ormiston[8], who indicated that the flat rotor wake concept is applicable down to advance ratios of $\mu \approx .15$. The Soviet authors establish the limits to the applicability of this approach in somewhat different terms of $\mu \geq 1.15\sqrt{c_T}$.

Ch. IV, dealing with various aspects of aerodynamic interactions within a two-rotor system, contains much useful information from the practical design engineering and performance estimate point of view for axial, tandem and side-by-side configurations. Here, one will also find valuable considerations of the aerodynamic influence of a lifting rotor on the tail rotor, including such problems as the significance of the vertical location of the tail rotor as far as its power requirements in various regimes of forward flight is concerned.

As to the influence of the wake structure in general, one should notice that, similar to the Western trend[2], it appears as the core of all considerations, beginning with Ch. VI. This was done with an increasing sophistication: The lifting-line approach evolved into the lifting-surface concept. Simple linear treatment of the flow problem, with its associated rigid wake, was replaced by the nonlinear, time-dependent interactions between the field of induced velocities and vortex filaments. Finally, considerations of both viscosity and compressibility were incorporated.

In the treatment of axial flow, the assumption is made that elements of free (trailing) vortices move along straight lines. This obviously means that, similar to many studies in the West during the late '50s and early '60s, contraction of the wake is not considered. However, the material presented may be quite useful for those cases where airscrews in axial translation (ascent) can be modeled by a noncontracting wake. The readily available influence coefficients should greatly reduce the time of computation.

Attention is also called to Ch. VIII, dealing with the concept of representing a rotor blade through a lifting surface. This approach considerably improves the understanding of flow in the tip region of regular blades as well as over the complete span of low-aspect ratio blades.

Ch. IX may be of particular interest, since it represents an original application of the vortex theory concept to vertical descent - the regime of flight recognized as rather elusive for pure analytical treatment. The Soviet authors attacked this problem by postulating a physico-mathematical model based on the following concept: Trailing vortices are distributed along a conical surface, while the axial pitch of the helical vortices is approximately constant. This leads to the establishment of relationships for instantaneous and time-average induced velocities, while tables of coefficients appearing in these expressions reduce the mathematical procedure to elementary operations.

In the bulk of tasks associated with the skewed flow (Chs. X-XV), ideal fluid is assumed. However, in one case, the influence of compressibility on a stationary field of induced velocities is briefly considered (end of Ch. X). Here, the application of the Biot-Savart law, modified for a compressible medium, indicates that steady-state fields of induced velocities are affected only by the Mach number $(M \equiv V/a)$ of the uniform flow directed along the axis of the skewed vortex wake, and do not depend on Mach number related to the tip speed $(M_\omega \equiv R\omega/a)$. Diffusion of vortices due to the viscosity effects is also discussed (Ch. XV.3), and the Biot-Savart law is obtained for velocities induced by the diffused vortices.

Considerations of the motion of vortex filaments within the vortex surface, which lead to ways of describing movements of the entire wake, may be of particular interest (Ch. XV.6). This approach, when adapted to simple forms of vortex surfaces, can contribute to the solution of such various problems as, (a) vortex sheet roll-up behind the blade, (b) determination of the shape of the wake (including the roll-up of the vortex surface downstream) in vertical ascent as well as hovering in- and out-of-ground effect, etc.

In the development of relationships for induced velocities (both time-average and instantaneous) and especially, their harmonic components, wide use is made of Bessel functions, Legendre polynomials and functions, etc. In addition, to facilitate actual computations, tables and graphs are provided in the text.

Most of the material presented in Chs. X-XV is based on the linear theory which leads to the movement of free vortices along the straight lines forming generatrices of skewed cylinders. However, application of the nonlinear theory to the determination of the rotor vortex system in an oblique flow is also demonstrated (Ch. XV.9). This approach, when applied to the deformation of tip vortices at various μ values (from $\mu = .07$ to $\mu = .2$) leads to results which may be compared with those of Sadler[9] (also see Ref. 2).

Discussion of vortices in a compressible medium (Ch. XVI) may be considered by some as somewhat academic as far as rotary-wings are concerned. Nevertheless, there may be a number of practical problems (especially in maneuvers) where compressibility and the resulting time delays in transmitting aerodynamic signals could play a noticeable role in the induction of velocities by vortices. For these cases as well as for those of a truly academic nature (e.g., students' theses), the material presented in this chapter may provide a valuable reference. Furthermore, the whole treatment of the subject, including the introduction of a concept of *audible zones*, should contribute to a better understanding of the physics of interaction between vortices and the surrounding medium.

For the reader interested in a review of the application of the vortex theory to lifting rotors, as well as to some problems of propellers (e.g., spinner shape for high-speed turboprops), Ch. XVII should prove of value. For instance, one of the considered problems is the determination of the optimum distribution of circulation along the blade as a function of both radius and azimuth. This would lead (as in the case of a more recent Theodorsen work for the lifting rotor[10]) to the fulfillment of the Betz condition far downstream. In the Russian text, a solution is obtained with the help of the calculus of variation.

* * * *

In order to compare current and perhaps, near-future trends of rotary-wing aerodynamics in the West with those of the USSR, let us first determine the direction in which the

Western school-of-thought is proceeding. In that respect a statement by Landgrebe and Cheney[2] may be quite illustrative: "Recent efforts have concentrated on the development of an analytic method for predicting the effect of disturbed wake geometry and unsteady aerodynamics on rotor performance." As far as predicting the effect of disturbed wake geometry is concerned, the aims of the Soviet and the Western aerodynamicist seem to coincide; in spite of the fact that the West appears to rely more on the brute capacity of the computer, in contrast to the Russian inclination toward the classical mathematical approach. However, the translated text provides little evidence of basic studies of the unsteady aerodynamic phenomena of airfoils in the rotary-wing environment which, in the West, are exemplified by the works of McCroskey[11], Philippe[12], and others.

It is, of course, possible that current Soviet efforts in that domain simply have not been incorporated in this book which, as mentioned at the beginning of these remarks, represents a fundamental text on the application of the vortex theory and to some extent, the velocity potential, to rotary-wing aerodynamics. In that respect this translator hopes that the English version will be directly useful to the aerodynamic practitioner and furthermore, provide some inspiration for both purely academic and applied research; while the mathematically-minded reader should find a true delight on these pages. Finally, translator and transcriber wish to express their indebtedness to Drs. R. Carlson and J. McCroskey, Mr. A. Morse, Drs. F. Schmitz and I. Statler for their most valuable remarks and suggestions regarding both technical and editorial matters. Our special thanks are due to Dr. R. Ormiston, who contributed his vast expertise by reading and reviewing, in detail, the manuscript of the translation.

W. Z. Stepniewski
31 January 1975

References for Annotation

1. Stepniewski, W.Z., *Basic Aerodynamics and Performance of the Helicopter*, AGARD-LS-63, April 1973.

2. Landgrebe, Anton J. and Marvin C. Cheney, Jr., *Rotor Wakes - Key to Performance Prediction*, AGARD-CPP 111, September 1972.

3. Knight, M. and R.A. Hefner, *Static Thrust Analysis of the Lifting Airscrew*, NACA TN 626, 1937.

4. Mil', M.L., et al, *Helicopters, Calculations and Design, Vol. I, Aerodynamics*, NASA TT F-494, 1967.

5. Castles, Walter, Jr. and Jacob Henri DeLeeuw, *The Normal Component of the Induced Velocity in the Vicinity of a Lifting Rotor and Some Examples of Its Application*, NACA TR No. 1184, 1954.

6. Heyson, Harry H. and S. Katzoff, *Induced Velocities near a Lifting Rotor with Nonuniform Disc Loading*, NACA TR 1319, 1956.

7. Miller, R.H., *A Discussion of Rotor Blade Harmonic Air-loading*, CAL/TRECOM Symposium, Buffalo, N.Y., June 1964.

8. Ormiston, Robert A., *An Actuator Disc Theory for Rotor Wake Induced Velocities*, AGARD-CPP-111, Sept. 1972.

9. Sadler, S.G., *Development and Application of a Method for Predicting Rotor Free Wake Positions and Resulting Rotor Blade Airloads - Model and Results*, NASA CR-1911, 1971.

10. Theodorsen, Theodore, *Theory of Static Proepllers and Helicopter Rotors*, 25th Annual Forum, American Helicopter Society No. 326, May 1969.

11. McCroskey, W.J., L.W. Carr and K.W. McAlister, *Dynamic Stall Experiments on Oscillating Airfoils*, AIAA Paper 75-125, Jan. 1975.

12. Philippe, J.J. and M. Sagner, *Calcul et Mesure des Forces Aerodynamiques sur un Profil Oscillant avec et sans Decrochage*, AGARD-CPP 111, September 1972.

TABLE OF CONTENTS

Page

Preface 1

Introduction 3

Basic Assumptions and Notions 13

Chapter I. LIFTING AIRSCREW IN FLIGHT REGIMES WITH A HORIZONTAL VELOCITY COMPONENT 22

1. Aerodynamic Forces Acting on Lifting Airscrew 22

2. Flapping Motion of the Rotor Blades 25

3. Power Required for Rotation of a Rotor 27

Chapter II. THEORY OF A ROTOR IN OBLIQUE FLOW BASED ON THE SCHEME OF A FLAT VORTEX WAKE 30

1. General Remarks 30

2. Investigation of the Flat Vortex Wake 31

3. Velocity Components Induced by the Lateral Vortex Layer . . . 38

4. Velocity Components Induced in the yOz Plane by the Free Longitudinal Vorticity Layer 45

5. Velocity Components Induced by a Longitudinal Free Vorticity Layer of Finite Length 57

6. Velocity Components Induced by a Rotor in an Arbitrary Point in Space 65

7. Mean Circulation Around Blade Section 69

Chapter III. CHARACTERISTICS OF A HINGED ROTOR IN REGIMES OF FLIGHT WITH A HORIZONTAL VELOCITY COMPONENT 78

1. Zero and First Harmonic Coefficients of Flapping Blade Motion 78

2. Thrust Coefficient 85

Page

3. Longitudinal Force Coefficient 92

4. Lateral Force Coefficient 100

5. Pitching Moment Coefficient at the Rotor Hub 107

6. Rolling Moment Coefficient at the Rotor Hub 109

7. Coefficient of Power Required to Overcome the Blade Profile Drag 111

8. Rotor Induced Power Coefficient 115

9. Optimal Distribution of the Average Circulation 118

Chapter IV. INDUCED DRAG AND POWER OF TWIN-ROTOR SYSTEMS 122

1. Induced Drag and Power of Coaxial Rotors 122

2. Average Induced Velocity in the Coaxial Configuration Generated by One Rotor in the Plane of Rotation of the Other One 126

3. Induced Resistance (Power) of Rotors in Tandem and Side-by-Side Configurations 128

4. Aerodynamic Influence of Lifting Rotor on Tail Rotor 138

Chapter V. AERODYNAMIC CHARACTERISTICS OF A RIGID LIFTING AIRSCREW 143

Chapter VI. BLADE THEORY OF LIFTING AIRSCREW IN AXIAL FLIGHT 147

1. General Integral Relationships for Instantaneous Induced Velocities 148

2. Scheme of the Discrete Vortices System of a Rotor and Basic Relationships 151

3. Computation of Circulation of Discrete Vortices (Case of Large $\overline{V}_\infty$ Values) 153

4. Aerodynamic Calculations of Airscrews (Case of High $\overline{V}_\infty$ Values) . 156

5. Numerical Example 158

6. Aerodynamic Calculations of an Airscrew in a Low Velocity Flow . 158

Page

Chapter VII. DISC THEORY OF LIFTING AIRSCREW IN AXIAL FLOW 164

1. Induced Velocity 164

2. Circulation and Aerodynamic Characteristics of Airscrews . . . 166

Chapter VIII. THEORY OF LIFTING AIRSCREW IN AXIAL FLOW BASED ON THE CONCEPT OF A THIN LIFTING SURFACE 168

1. Presentation of the Problem 168

2. Scheme of the Flow Around the Blade 169

3. Induced Velocities 171

4. Boundary Conditions and Basic Equations 173

5. Single Lifting Line 175

6. Comparison of Theory and Experiment 176

Chapter IX. AERODYNAMIC CALCULATIONS OF LIFTING AIRSCREWS IN VERTICAL DESCENT 178

1. Results of Experiments on Visualization of Tip Vortices of a Rotor 179

2. Scheme of the Rotor Vortex System 181

3. Instantaneous and Time-Average Induced Velocities 184

4. Basic Equations and Rotor Calculations 186

Chapter X. DISC THEORY OF LIFTING AIRSCREWS IN AN OBLIQUE FLOW 192

1. Some Results of Flow Visualization of Airscrew Vorticity Wake . 192

2. Scheme of the Rotor Vortex System and Basic Assumptions . . . 195

3. Instantaneous Induced Velocity 197

4. Time-Averaged Induced Velocity (General Case $\Gamma = \Gamma(\rho,\theta)$) . . . 200

5. Time-Averaged Induced Velocity (Particular Case $\Gamma = \Gamma(\rho)$) . . . 202

6. Induced Velocity at Low μ's 205

7. Harmonics of induced Velocity (Case of $\Gamma = \Gamma(\rho)$) 218

Page

8. Harmonics of Induced Velocity (General Case $\Gamma = \Gamma(\rho,\theta)$) 226

9. Stationary Field of Induced Velocities in a Compressible Flow . 238

Chapter XI. BLADE THEORY OF LIFTING AIRSCREW IN A SKEWED FLOW 243

1. Basic Assumptions and Equations 243

2. Coefficients of Basic Equations 246

Chapter XII. THEORY OF LIFTING AIRSCREW BASED ON THE THIN LIFTING SURFACE CONCEPT. 250

1. Boundary Conditions 251

2. Scheme of the Blade Vortex Wake System and Basic Equations . . 253

Chapter XIII. THEORY OF CYLINDRICAL FUNCTIONS AND TIME-AVERAGE INDUCED VELOCITIES 256

1. Vortex Wake of a Blade 256

2. Scalar Velocity Potential 257

3. Time Averaging 258

4. Potential of the Doublet-Covered Disc 260

5. Introduction of Cylindrical Functions 262

6. Application of the Theorem of Compounding 264

7. Nondimensional Form of Velocity Integrals and Modifications of $J_{n,m}$ 267

8. Interpolating Trigonometric and Legendre Polynomials 270

9. The A.V. Nekrasov Method 274

Chapter XIV. BASIC RESULTS AND COMPUTATIONAL FORMULAE FOR TIME-AVERAGE INDUCED VELOCITIES 277

1. Induced Velocities for Lift per Unit of Blade Span Independent of Azimuth Angle 277

2. Induced Velocities with Thrust per Unit of Blade Span Varying with Azimuth 283

3. Aerodynamic Forces 285

Chapter XV. FUNDAMENTALS OF THE LINEAR THEORY OF INSTANTANEOUS INDUCED VELOCITIES AND SOME OF ITS REFINEMENTS 293

1. Application of the Scheme of Lifting Line to Computations of Instantaneous Induced Velocities 293

2. Instantaneous Induced Velocities 295

3. Consideration of the Diffision of Vortices 297

4. Segregation of Induced Velocities into Proper and External Velocities. 299

5. Results of Calculations 300

6. Fundamentals of the Nonlinear Vortex Theory of Lifting Airscrews 311

7. Integral-Differential Equation of Vorticity Surface Movement 313

8. Tasks Which Can be Reduced to the Investigation of Movements of Flat Vortices and Vortex Rings 316

9. Application of Nonlinear Theory to the Determination of the Rotor Vortex System in an Oblique Flow 322

CHAPTER XVI. INDUCTION OF VORTICES IN A COMPRESSIBLE MEDIUM 330

1. Differential Equations of Gas Motion. 330

2. Scalar Potential of Gas Velocities 331

3. Discontinuous Fields of Forces (Vector Potentials of Impulses and Forces 333

4. Velocity of Gas in the Case of Smooth Fields of External Forces (Generalization of the Biot-Savart Law) 336

5. Lifting Surface in Gas 338

6. Velocity Potential of Lifting Surfaces 341

7. Velocity and Pressure of Gas Associated with Motion of a Lifting Surface 344

8. Lifting Line in Gas 348

9. Gas Velocity Associated with Motion of the Lifting Line . . . 352

10. Formulation of Principle Results for the Case of Planar Motion . 359

11. Examples 361

Chapter XVII. RESULTS OF WORK ON THE THEORY OF AIRSCREWS . 366

1. Experimental Confirmation of Basic Assumptions and Representations of the Vortex Theory 366

2. Computation of Induced Velocity 375

3. Computation of Blade Loads and Airscrew Performance, Selection of Blade Form 388

4. Propellers in a Compressible Medium 398

5. Ideal Propeller 400

6. Propeller with Finite Number of Blades in a Cylindrical Tube . . 403

7. Propellers with Wide Blades 403

8. Propellers with Noninteracting Blades and a Large Number of Blades 404

9. Flat Cascades of Airfoils in Supersonic Flow 404

10. Blade Root Sections and Spinner Shape 406

APPENDICES

I. Determination of Induced Velocity Averaged Over a Circle. . . 408

II. Determination of Coefficient $v_{s1}(\bar{r})$ for the $\sin\psi$ Development of Induced Velocity into Fourier Series 411

III. Determination of Coefficients $\bar{v}_{s(2n+1)}(\bar{r})$ and $\bar{v}_{c2n}(\bar{r})$ for the $\sin(2n+1)\psi$ and $\cos 2n\psi$ Expansion of Induced Velocity into Fourier Series 413

IV. Determination of Coefficients $\bar{v}_{s2n}(\bar{r})$ and $\bar{v}_{c(2n-1)}(\bar{r})$ for the $\sin 2n\psi$ and $\cos(2n-1)\psi$ Expansion of Induced Velocity into Fourier Series 416

V. Formulae for calculations of the $\hat{v}_y$ Coefficients 420

VI. Tables of the Influence Functions 425

VII. Calculations of $J_{m,n}$-Transforms of Exponential Functions . . 433

VIII. Calculations of $J_{n,m}$-Transforms of the Associated Legendre Polynomial. 436

IX. Tables of Function $\epsilon^{k}_{n,m}(\bar{r})$ 443

X. Some Problems Associated with Computations of Propellers 450

BIBLIOGRAPHY 453

The authors dedicate this book to the memory of the founder of the vortex theory of airscrews, a great Russian Scientist, Nikolai Egorovich Joukowsky*.

PREFACE

Airscrews found their first application as propellers of airplanes. They were designed on the basis of an elementary comparison with the well-known concept of a bolt and a nut. The difference consisted of the fact that an airscrew was moving against a non-rigid gaseous nut. (From that approach, the concept of the pitch of an airscrew was developed which is still in use at this time.) Continuous requirements of improving the performance of airplanes with reciprocating engines made it necessary to develop a theory of the airscrew which would permit not only an understanding of the mechanics of its work, but also calculations of its characteristics.

At the beginning of the second half of the 19th Century, Rankin and Froude proposed a theory of ideal propellers. It permitted a determination of upper limits of propulsive efficiencies which could be achieved by the best possible airscrew under given conditions. At the end of the 19th Century, another theory of the airscrew; namely, that by S.K. Drzewiecki, was developed and became widely known. However, that theory did not consider the existence of induced velocities generated by the airscrew in flight. A high level of development was achieved by a momentum theory which produced formulae for computations of hovering performance of helicopter rotors. That theory was developed by G.Kh. Sabinin and B.N. Yur'yev.

However, the vortex theory developed by N.E. Joukowsky * appears to be the most effective. It is based on the principle that thrust on the blades of a lifting rotor is generated by the

---

*The classical transliteration is used in this translation. However, the modern rendition of this name is *Nikolay Yegorovich Zhukovskiy*, and appears as such in the bibliography.

circulation of velocity around the contour of the blade section, while from the ends of the blades stream free vortices. This theory was later developed in the Soviet Union by the students of N.E. Joukowsky. This book is devoted to the up-to-date presentation of the vortex theory of the lifting airscrew.

Chapters I to V and Appendices I to V were written by L.S. Vil'dgrube; Chapters VI - XII and Appendix VI by Ye.S. Vozhdayev; Chapters XIII - XVI and Appendices VII - IX by V. E. Baskin; and Chapter XVII and Appendix by G.I. Maykapar. The Preface and Introduction were written by A.K. Martynov. The section of the Introduction entitled, "Basic Assumptions and Notions" were jointly written by A.K. Martynov and the authors.

The authors express their indebtedness to Professor S.M. Belotserkovskiy for his valuable advice given on the occasion of the review of this book. They also want to thank V.S. Kaplan, who undertook the effort of scientific editing.

It is requested that all critical remarks and complaints referring to the contents of this book should be directed to: Moscow, V-78, 1-St Basmannyy per., 3, "Mashinostroeniye" Press.

INTRODUCTION

Working conditions of a helicopter rotor are different from those of a wing or a propeller.* These different working conditions led to the development of a separate discipline - theory of the lifting airscrew which investigates flow around the lifting airscrew as well as forces and moments sustained by it. Strictly speaking, wing and propeller theories may be considered as special cases of the theory of the lifting airscrew. The aim of the theory of the lifting airscrew can be defined as the determination of the field of induced velocities of the airscrew and loads on the blades, as well as movements and deformation of the blades.

The main difference in the operation of lifting airscrews from that of propellers consists of the fact that the lifting airscrew (rotor) of a helicopter during horizontal flight is exposed to an airflow whose velocity is not directed along its axis as in the case of a propeller, but makes a large angle with that axis. On the side of the disc swept by the blades, tip speeds are added to the speed of flight of the helicopter while on the other side, they are subtracted. Some parts of the blade are going through *regions of reversed flow* with the result that the air velocities encountered by the blades move from the trailing toward the leading edge. We will call this type of operation of the airscrew nonaxial or *oblique flow*, in contrast to the *axial flow* existing when the velocity vector of the approaching airstream is parallel to the airscrew axis.

Oblique flow leads to special design pecularities of the lifting airscrew. In the majority of contemporary helicopters, the blades are attached to the hub through hinges or elastic joints. In recent times, some helicopters were constructed with a rigid attachment of the blades to the hub *(rigid rotors)*.

In a steady-state horizontal flight, the relative velocities of the airflow encountered by various elements of the blade as

*According to established tradition, airscrews of aircraft are called propellers.

well as aerodynamic forces experienced by those elements, change with time in a periodic way. Under the influence of those periodic loads, the blade performs complicated movements around its hinges as well as deforms as an elastic body. Consequently, the theory of the lifting airscrew must incorporate elements of unsteady aerodynamics of a lifting surface moving along a curved path. The complexity of that theory by comparison with that of a wing or propeller consists of the fact that on one hand, the blades are subjected to a curvilinear motion; while on the other, their position in space, velocity of motion and finally, their deformations, are closely related to aerodynamic loads which, in turn, depend on the velocity of flow encountered by the blade. As a result of the low rigidity of the blades, those relationships play a much more important role than in the theories of wings and propellers.

It should also be noted that in the theory of the lifting airscrew, dependence of aerodynamic loads on the field of induced velocities is much stronger than in the fixed-wing theory. Every blade of the airscrew generates not only its own field of induced velocities, but it also has to work in the field of velocities induced by other blades. The task of defining the velocity field induced by all blades represents the most complicated part of the theory of the lifting airscrew (rotor).

As is well known, the foundations of the theory of the airscrew were established through investigations of the native (Russian) authors. Those investigations were always closely related to the practice of aviation and other fields of technology. S.K. Drzewiecki first in 1892, and then in 1910, published works on the theory of the airscrew in axial translation. His theory was based on the concept of the airscrew blade consisting of elements of a wing. S.K. Drzewiecki postulated the possibility of considering *elements of the blade* as sections of a wing of infinite aspect ratio. This hypothesis became a firm part of computational methods.

In 1912-1918, N.E. Joukowsky developed the vortex theory of airscrews which became the foundation for the design of aeronautical lifting airscrews and propellers, windmills, ship propellers and other rotary-blade machines as well. According to that theory, action of the blade on the surrounding medium can be replaced by a system of vortices, some bound to the blade

and some free which spring from the blade and then move along the flow lines in a relative motion. N.E. Joukowsky investigated the field of velocities induced by those vortices and found the main part of the induced velocity values. He also determined the time-average induced velocities by replacing the helical vortices generated by the rotor with a *straight circular cylinder of vorticity*. This approach would be strictly applicable to an airscrew with an *infinite number of blades* or, in practice, it can approximate lightly loaded airscrews with a small pitch.

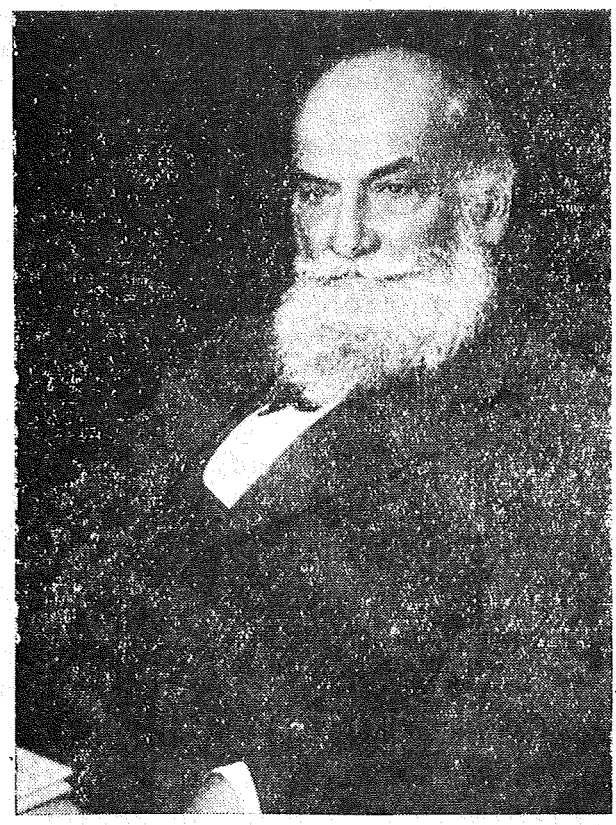

Nikolai Egorovich Joukowsky (1847-1921)

V.P. Vetchinkin, further developing the ideas of N.E. Joukowsky, solved a variational problem of optimum distribution of circulation in order to maximize propulsive efficiency

of an airscrew with an infinite number of blades. B.N. Yur'yev widely popularized the ideas of Joukowsky. He should also be credited with one of the first attempts to investigate the importance of the finite number of blades. Later, the theory of Joukowsky was further elaborated by M.V. Keldysh and F.I. Frankl' who, for an airscrew with an infinite number of blades, developed a method of defining the shape of free vortices for any level of the airscrew loading.

The theory of N.E. Joukowsky played an important role in the development of rotary-wing aircraft. The vortex theory of the lifting airscrew is based on the original works of N.E. Joukowsky and represents a development of his ideas. Problems encountered in practice required a continuous determination of the average induced velocities as well as their instantaneous values at any point in space for all regimes of the axial and oblique flow. The vortex theory of the helicopter lifting rotor helped to answer many questions encountered in practice; i.e., optimum geometry of the rotor, aerodynamic interference in two and multi-rotor configurations, detailed picture of the field of velocities and directions of flow in the whole space enveloping the rotors, precise determination of aerodynamic forces and moments acting on the rotor; characteristics of the flapping motion of the blades, etc.

In 1947, G.I. Maykapar generalized the vortex theory of Joukowsky by considering a rotor in an oblique flow with a finite and infinite number of blades. For the case of an infinite number of blades, G.I. Maykapar proposed a scheme of a skewed cylinder of vorticity. On that basis, V.Ye. Baskin and Ye.S. Vozhdayev obtained analytical solutions for the problem of finding average induced velocities. Further schemes based on the skewed cylindrical wakes and their development represent an important position in the works of native (Russian) scientists. The works of A.I. Slutskiy, N.E. Kastorskiy and A.M. Lepilkin, as well as Ye.S. Vozhdayev and other investigators, are devoted to this problem. A.A. Nikolskiy indicated an analogy between time average velocities induced by an airscrew in an oblique flow with that of a circular wing. The scheme of the cylindrical vortex wake appeared to be very useful for aerodynamic calculations. In determining loads acting on the airscrew, it became necessary to develop a theory based on a finite number of blades. At this point, the works of G.I. Maykapar, V.Ye. Baskin and Ye.S. Vozhdayev should be mentioned. A practical and sufficiently accurate method based on the vortex theory of determining on a

computer, the aerodynamic loads on the blades of a lifting rotor was developed not long ago by M.N. Tishchenko.

With the increasing speeds of the horizontal flight of helicopters, the inclination of the cylinder which represents the vortex wake increases. At sufficiently high velocities, it may be assumed that the cylindrical wake is reduced to a plane, while free vortices assume a cycloidal shape. Development of the vortex theory based on a scheme of a *flat vortex wake* and its verification with respect to engineering practice were achieved by L.S. Vil'dgrube. A.P. Proskuryakov, P.V. Zanozin, I.O. Meltz and other investigators also worked along those lines. Considerable contributions to the reduction to practice of that theory was made by G.R. Kvasha.

Wide experimental inputs obtained by M.L. Mil' and M.K. Speranskiy provided a detailed picture of the field of induced velocities and thus contributed to a further development of the theory.

The theory of the propeller also underwent an intensive development in the USSR. The investigations of N.E. Joukowsky were extended by V.P. Vetchinkin. G.I. Kuz'min was the first to make a broad comparison of the theory of Joukowsky with experimental data. During the '30s to '40s, a method of aerodynamic calculation of propellers with finite number of blades was developed and the variational problem was solved for optimum distribution of circulation along the blades. This task was accomplished by V.V. Keldysh, A.M. Lepilkin, G.I. Maykapar, B.L. Minukhin, N.N. Polyakhov, D.V. Khalezov, B.N. Yur'yev and others. The vortex theory was applied by G.I. Maykapar and other investigators to the calculation of coaxial propellers and for the establishment of aerodynamic interference between the propeller and the fuselage. He also considered the problem of oblique flow encountered by the propeller.

F.I. Frankl' developed a theory of a propeller with infinite and finite number of blades in a compressible medium. He indicated that for propellers with subsonic tip speeds, it is sufficient to limit considerations of compressibility to its influence on blade section characteristics only.

In the middle of the 1950s, large-scale wind-tunnel investigations of pressure distribution on propeller blades were undertaken. These experiments verified many theoretical assumptions

and emphasized the difference in the working conditions between the airfoil section of a wing and the airscrew blade. In the late '50s, several investigations were undertaken of the work of a propeller under conditions of supersonic velocities. This task required development of a method of calculation of the shape of the propeller spinner, shape of the root sections and establishment of the mutual influence of the blade and the spinner. In conjunction with this task, the theory of a cascade of airfoils in supersonic flow was developed. Investigations of velocity and pressure fields in a supersonic flow of compressible fluids were performed with due consideration of mutual interference of a propeller and fuselage.

It may be considered that the vortex theory of a lifting airscrew and propeller has been developed to a level satisfactory to answer basic practical questions. Now we will try to classify various segments of the vortex theory.

If every blade of an airscrew is considered separately from the remaining ones and is characterized by its individual vortex system, then such theory is called the *blade theory*. However, if the airscrew is replaced by an *active disc* where the influence of every point of the disc on the surrounding medium is considered, then such a theory is called the *disc theory*.

In the contemporary theory of the lifting airscrew, one may also distinguish linear and nonlinear approaches. Under the concept of the *linear theory*, the influence of induced velocities on the movement of free vortices is neglected. It is simply assumed that elements of free vortices move together with the undisturbed flow. Sufficiency of the linear theory was confirmed for the case of relatively high flight velocities of helicopters when average induced velocities are small in comparison with those of horizontal translation. However, if one considers that elements of free vortices are moving in the variable field of velocities which are induced by the airscrew as a whole, and the position of those elements must be determined together with the field of induced velocities, then such a theory is called the *nonlinear theory*. The nonlinear approach is of special interest for relatively low velocities of flight as well as for highly-loaded airscrews. The necessity of practical applications contributed to the development of the *quasi-linear* theory of airscrews. In this theory, the influence of the main part of the induced velocities on the movement of free

vorticities is considered and it is assumed (as in the linear theory) that those elements move in a uniform straight line flow. However, the velocity of that flow is determined as a sum of the speed of undisturbed flow and the average induced velocity. The *quasi-linear theory* permits an assumption of a skewed cylindrical vortex wake, thus making it applicable to the case of relatively low flying speeds in horizontal translation.

In this book, all segments of the above-considered classification of the theory are considered.

In Chapter I, general conditions of operation of a lifting rotor in an oblique flow are discussed. Chapter II is devoted to the theory of the lifting airscrew in horizontal translation with flight velocities much larger than the induced ones. As was mentioned before, in those regimes of flight, it is possible to assume that the vortex wake is flat. A presentation of the material is brought up to the development of computational formulae. Also, auxiliary graphs are given which should permit finding induced velocities in any desirable point of the space as well as to estimate forces and moments acting on the lifting airscrew with any given set of parameters (Chapters II-V). Rotors with articulated as well as rigidly attached blades are considered. Material included in Chapters II-V also permit the determination of characteristics of the flapping motions of the blades for articulated rotors. Mutual induced interaction of lifting airscrews of various twin-rotored configurations are also considered. Material presented in Chapters III, IV and V is characterized by a wide application of simplifying assumptions due to which it is possible to present the results under the form of simple formulae and tables. The importance of such a presentation of theoretical results for engineering practice is obvious.

In a strictly mathematical treatment, it is possible to find analytical solutions only for some special cases. For this reason, in the contemporary theory of lifting rotors, numerical methods, suitable for computer use, are widely applied. In Chapters VI to XII, numerical methods are discussed. The lifting rotor with a 3-dimensional system of vortices is considered in axial as well as in oblique flows. Both blade and disc theories are presented for those regimes of flight (Chapters VI, VII, X and XI). An approximate theory is given in Chapter IX which is based on experimental results using visualization of the vortex system of the airscrew.

The widely accepted hypothesis of using two-dimensional airfoil characteristics is not suitable for the investigation of flow existing in the tip regions. It also cannot be applied to rotors moving with high horizontal velocities and low tip speeds. In addition, a considerable increase of the airscrew loads as well as a reduction of the aspect ratio of the blades make application of that hypothesis more difficult. For this reason, in Chapters VIII and XII, theories in which rotor blades are replaced by a thin lifting surface are considered. In flight with a horizontal velocity component, elements of the blade are subjected to a varying sweep angle which changes both with the section radius and time. Furthermore, the sweep angles become larger as the speed of flight increases. For this reason, it is desirable to make an approach along the concept of a skewed (swept) lifting surface.

Basically, the same numerical method of calculation consisting of replacing a continuous vortex surface with a system of discrete closed vortices is presented for two schemes; that of lifting line and that of lifting surface. As a result, differential-integral equations for determination of the circulation are replaced by a system of algebraic equations suitable for computer solutions.

In Chapters XIII and XIV, general analytic solutions for induced velocity distribution at the rotor disc and the surrounding space is presented within the framework of the linear disc theory. The results are given in a form suitable for finding relationships between vorticities and loads. At the core of this method lies the utilization of the theory of cylindrical functions. As a result of substituting equivalent fields of dipoles for the vortex field, computation of the time-average induced velocities is reduced to the summation of velocities induced by the elementary volumes of doublets. The disc, covered by the doublets, is assumed as the elementary volume. The velocity field induced by such a disc is represented as integrals of cylindrical functions, while in the summation of velocities, the theory of addition of cylindrical functions is utilized. This permits the solution of the problem in an analytical form, both for the two and three-dimensional systems of vortices. In addition, a representation of induced velocities is obtained under the form of Fourier series with respect to the azimuth angle determining the position of a point on the disc. This approach is especially suitable for practical applications.

In Chapter XV, a theory of instantaneous induced velocities is presented and solutions of some problems of the nonlinear theory of the lifting airscrew are given.

The problem of the definition of the field of induced velocities generated by a lifting airscrew can be reduced to a general problem of finding a flow due to the action of a field of given forces. In Chapter XVI, this problem is solved under linear assumptions for the case of compressible fluid. General expressions are obtained for the speed of gas in which a loaded lifting surface or a lifting line moves in an arbitrary unsteady motion. These expressions generalize the Biot-Savart formulae for the case of compressible gas. They become identical with the classical relationships when the speed of sound becomes unlimited.

In this book, basic problems of the theory of the lifting airscrew are illuminated. However, some aspects of that theory are closely related to the propeller theory, which achieved a high level of development in conjunction with work on propellers and other rotary-blade machines. For this reason, in Chapter XVII, the results of the investigation of propellers during the last 20-25 years are given. The physical foundations of the vortex theory as well as the assumptions and basic relationships needed for finding induced velocities are reviewed. The question is also considered of loads acting on the airscrew, and the general way of solving those problems is shown for different conditions of flow encountered by the blades.

Momentum and energy theorems are used in the solution of the variational problems of optimization of the rotor. Also considered is the influence of compressibility on the characteristics of the airscrew as well as some problems brought about during practical rotary-wing development.

The majority of the material presented in this book has already been published. However, this was done with very limited circulation and for that reason, may not be known to a wide circle of specialists. Up to now, the complete vortex theory of the lifting rotor has not been published in native (Russian) literature. Furthermore, this could not have been done in the past because this theory, in a large part, was developed only recently. We also do not know of any such monograph existing abroad. Consequently, this publication should fill the gap which now exists in aerodynamic literature.

In this book, the theory of the lifting rotor is considered from different points of view. The presentation of particular problems and the approach to their solutions also varies. We believe that such arrangement of the material is achieving its objective, since it presents the current state of the art of the theory. The theory itself is advancing rapidly, new problems are continuously encountered, and new methods of solving them are generated. For this reason, any attempt to rigidly standardize the presentation of material would be premature.

In surrounding space, the lifting airscrew induces complicated unsteady fields of velocities which are combined with those of the incoming airstream. This leads to the blade loadings which considerably vary with the azimuth angle.

The aerodynamic loads dictate the position, velocity of motion, and deformation of the blade. Complicated relationships between loads, movement and deformation of the blade constitute the main aspects of the analysis of operation of the lifting airscrew (rotor). In order to facilitate the task, simplifying assumptions are made. In pure aerodynamic considerations, the real lifting airscrew is usually replaced by its idealized concept with absolutely rigid blades. This approach is also taken in this book; deformation of the blades are not considered here. It should be pointed out that such idealization is related only to the investigation of the dependency between the blade motions and loads acting on those blades. However, the methods presented below of calculation of the field of induced velocities and the determination of the general rotor characteristics can also be applied to rotors with elastic blades.

The total theory of the lifting airscrew is usually broken down into simpler, separate tasks. The first such task, which has to be performed most often, consists of the determination of aerodynamic loads and the associated field of induced velocities when the motion of the blade is given. The second task consists of the determination of aerodynamic loads when the field of induced velocities and motion of the blades are defined. The third task is represented by the requirement of finding the field of induced velocities for given loads and motions of the blades. The definition of each of these tasks and ways of accomplishing them is shown in the corresponding chapters of this book.

Presented also are considerations of approximate interrelationships between the field of velocities around the lifting airscrew and the aerodynamic loads of the blades. According to *the blade element hypothesis*, elements of the blades are considered as segments of a wing of an infinite aspect ratio, while values of their aerodynamic coefficients are determined with due consideration of angles of attack, sweep angle, and Mach and Reynolds numbers. In the first approximation, those characteristics are assumed to be the same as for the wing.

Furthermore, according to the hypothesis of a *steady flow*, values of aerodynamic coefficients of the elements of the blade in every considered moment are assumed equal to aerodynamic coefficients of a wing of infinite aspect ratio in a steady-state flow and having the same angles of attack and sweep as well as Mach and Reynolds numbers as those encountered on the blade elements at that particular instant. Comparisons of calculations with experimental data indicate the necessity of making those relationships more accurate. However, this particular aspect of the aerodynamics of the lifting airscrew is of empirical character and, as such, is not considered in this book. Many relationships, considered to be generally known, are presented here but the form of those presentations in various chapters may be somewhat different. It should also be mentioned that in some tasks related to the determination of general aerodynamic characteristics of a rotor in horizontal flight, aerodynamic loading of the blade is averaged with respect to the azimuth angles and blade radius, or the rotor disc.

Through the whole text of the book, we will make extensive use of the Biot-Savart law. For this reason, we will first review that law and later, will develop formulae for computations of velocities in compressible fluid induced by a vortex filament of an arbitrary form. Let us assume that in an unlimited volume filled with ideal fluid, there is a vortex filament S with circulation Γ (Fig. A.1). We assume a rectilinear system of coordinates $Oxyz$ and we define by $\mathbf{v}\{u, v, w\}$ the induced velocity vector in a space point $M\{x, y, z\}$. The letter N represents an arbitrary point on the curve S, $\mathbf{l}$ is the radius vector of point N with respect to point M, and l is a modulus of $\mathbf{l}$. Hence, curve S may be considered as a hodograph of the vector $\mathbf{l}$. The vorticity induced by an element $d\mathbf{l}$ of the vortex filament according to the Biot-Savart law expressed in the accepted notations would be as follows:

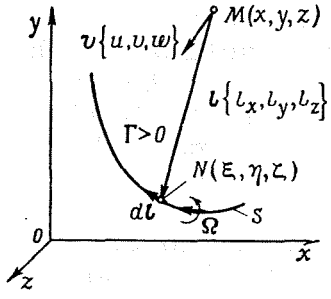

Figure A.1

$$d\mathbf{v} = \frac{\Gamma}{4\pi} \frac{\mathbf{l} \times d\mathbf{l}}{l^3}, \tag{A.1}$$

and the velocity induced by the whole line S becomes

$$\mathbf{v} = \frac{\Gamma}{4\pi} \int_S \frac{\mathbf{l} \times d\mathbf{l}}{l^3}. \tag{A.2}$$

It is necessary to apply the following rules of the signs: If the vector of rotation Ω (observer located at the end of vector Ω sees the rotation of the vortex in an anti-clockwise direction) has the same direction as vector $d\mathbf{l}$, which is tangent to the line S, then $\Gamma > 0$; if directions of vectors $d\mathbf{l}$ and Ω are opposite, then $\Gamma < 0$.

We are going to find the components of vector $\mathbf{v}$ along the axes of coordinates, assuming that the equation of the line S is given in a parametric form

$$\xi=\xi(p),\ \eta=\eta(p),\ \zeta=\zeta(p). \tag{A.3}$$

Parameter p is usually selected as either some angle (for a curved vortex line), or length of a segment on line S (for a rectilinear vortex filament). As parameter p varies from its initial value p_H to its final value p_K, point $N(\xi,\eta,\zeta)$ describes curve S. The vector $\mathbf{l}$ and its derivative $d\mathbf{l}$ can be expressed with the help of Eq. (A.3) in the following way:

$$\mathbf{l}=(\xi-x)\,\mathbf{i}+(\eta-y)\,\mathbf{j}+(\zeta-z)\,\mathbf{k};\quad d\mathbf{l}=\left(\frac{d\xi}{dp}\,dp\right)\mathbf{i}+\left(\frac{d\eta}{dp}\,dp\right)\mathbf{j}+\left(\frac{d\zeta}{dp}\,dp\right)\mathbf{k}. \tag{A.4}$$

Introducing the above expression into Eq (A.2), we obtain the sought relationships for the projections of vector $\mathbf{v}$:

$$u=\frac{\Gamma}{4\pi}\int_{p_H}^{p_K}\left[\frac{d\eta}{dp}(z-\zeta)-\frac{d\zeta}{dp}(y-\eta)\right]\frac{dp}{l^3}, \tag{A.5}$$

$$v=\frac{\Gamma}{4\pi}\int_{p_H}^{p_K}\left[\frac{d\zeta}{dp}(x-\xi)-\frac{d\xi}{dp}(z-\zeta)\right]\frac{dp}{l^3}, \tag{A.6}$$

$$w=\frac{\Gamma}{4\pi}\int_{p_H}^{p_K}\left[\frac{d\xi}{dp}(y-\eta)-\frac{d\eta}{dp}(x-\xi)\right]\frac{dp}{l^3}, \tag{A.7}$$

where

$$l=\sqrt{(x-\xi)^2+(y-\eta)^2+(z-\zeta)^2}. \tag{A.8}$$

In Eqs (A.5)-(A.7), the previously mentioned rule for the signs is applied in the following way: If, by varying p from p_H to p_K, point $N(\xi,\eta,\zeta)$ moves in the direction of vector Ω, then $\Gamma > 0$. If the point moves in the opposite direction, then $\Gamma < 0$.

Now, we are going to concentrate our attention on the problem of defining the field of velocities induced by a vortex filament in a compressible medium. Let's assume that in the space $Oxyz$ there exists a subsonic undisturbed uniform flow of ideal gas characterized by field of velocities $\mathbf{V}\{V,0,0\}$ and that there also is a nonuniform field of relatively low velocities $\mathbf{v}\{u,v,w\}$ induced by the vortex filament S. For such a case, formulae showing projections of induced velocities were developed in Ref. 79. These components may be expressed by the vector-type relationships[27]:

$$\mathbf{v}=\frac{\nu\Gamma}{4\pi}\int_S \frac{\mathbf{l}\times d\mathbf{l}}{l_\nu^3}. \tag{A.9}$$

Here,

$$l_\nu=\sqrt{\nu^2(\xi-x)^2+(\eta-y)^2+(\zeta-z)^2},\quad \nu=\frac{1}{\sqrt{1-M^2}},\quad M=\frac{V}{a},$$

a is the speed of sound in undisturbed flow. Eq (A.9) is analogous to Eq (A.2) for the case of a steady subsonic flow of compressible fluid. One should notice that the vector operations in Eqs. (A.2) and (A.9) are the same. This permits (by analogy with Eqs. (A.5)-(A.7)) to readily obtain projections of the vector $\mathbf{v}$ under the following form[27]:

$$u=\frac{\nu\Gamma}{4\pi}\int_{p_H}^{p_K}\left[\frac{d\eta}{dp}(z-\zeta)-\frac{d\zeta}{dp}(y-\eta)\right]\frac{dp}{l_\nu^3}, \tag{A.10}$$

$$v=\frac{\nu\Gamma}{4\pi}\int_{p_H}^{p_K}\left[\frac{d\zeta}{dp}(x-\xi)-\frac{d\xi}{dp}(z-\zeta)\right]\frac{dp}{l_\nu^3}, \tag{A.11}$$

$$w=\frac{\nu\Gamma}{4\pi}\int_{p_H}^{p_K}\left[\frac{d\xi}{dp}(y-\eta)-\frac{d\eta}{dp}(x-\xi)\right]\frac{dp}{l_\nu^3}. \tag{A.12}$$

The problem of the application of the Biot-Savart relationships for the computation of the field of velocities in the flows of a compressible fluid will be discussed more thoroughly in Chapter XVI.

Assuming that the reader is, in principle, familiar with the operation of the helicopter rotor, we are going to review some notations and concepts appearing in this book. A plane passing through the center of the hub and perpendicular to the axis of rotation of the rotor is called *plane of rotation*. If a rotor has horizontal hinges *(HH)*, then the plane of rotation passes through the axis of *HH*. The position of the blade (assumed as rigid) is defined by the *blade axis* coinciding with the pitch axis *(PA)*. The *plane of flapping* is defined as a plane passing through the axis of the blade and perpendicular to the plane of rotation. This plane is determined for the blade zero lag angle around the vertical hinge *(VH)*. The *blade flapping angle* β is defined as an angle between the plane of rotation and the blade axis. The angle between the blade axis and the plane of flapping is called the *lag angle* ξ. The rotation of the blade around the axis *HH* and *VH* during the operation of the rotor is called respectively, *flapping and lagging* of the blade. The blade axis of the rotating rotor generates a surface which is called the *rotor cone*. As a first approximation, the rotor cone may be considered as the *rotor disc*. Let us consider a straight line extended rearward from the rotor axis along the line of the intersection of the plane of rotation with the plane of symmetry of the helicopter (in the case of the side-by-side configurations, this would be a plane parallel to the helicopter plane of symmetry). The position of a blade on the rotor disc is defined by its *azimuth angle* ψ; i.e., an angle between the previously defined straight line and projection of the blade axis at zero lag angle (Fig. A.2). The azimuth angle is measured in the

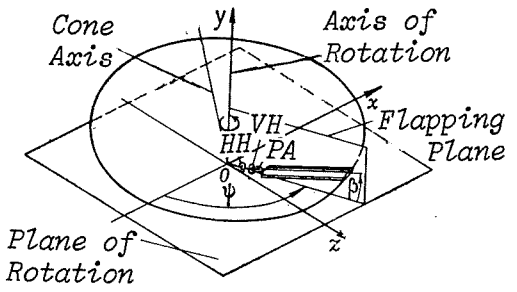

Figure A.2

direction of rotation of the rotor. For $0 < \psi < \pi$, the blades are *advancing*, while for $\pi < \psi < 2\pi$, they are *retreating*. The *angle of attack of the airscrew* (rotor) α_B is defined as an angle between the plane of rotation and vector of the distant flow toward the airscrew. The position of the blade element is defined by the *section radius* r, which is measured along the blade axis. The *blade section pitch angle* ϕ is measured as an angle between the aerodynamic chord* of the airfoil section and plane of rotation when $\beta = 0$, while the *blade pitch angle* is usually defined as that corresponding to ϕ at $r = 0,7R$. *Angle of attack of blade section* (element) α is represented by an angle between the aerodynamic chord of the airfoil section and projection of the local relative velocity of the flow on the section plane.

In this book, various coordinate systems are used and they are described in the appropriate chapters. However, as the basic coordinate system to which all other systems are related, the Cartesian system is selected with the x,y,z axes. Everywhere, except in Chapter XVII, this system is defined as in Fig. A.2. The origin, 0, is located at the point of intersection of the plane of rotation with the axis of rotor rotation (center of the hub). The x axis is located in the plane of rotation and directed forward so that its azimuth angle is equal to π. The y axis coincides with the axis of rotation and is directed upward. Axis z is located in the plane of rotation with the positive half-axis coinciding with $\psi = \pi/2$. Consequently, for an airscrew with right-hand rotation, the x,y,z coordinate system will also be of the right-hand type, and for the left rotating ones, the axis system will be of the left-hand type. Furthermore, whenever a single airscrew is considered, it is always assumed that it is of the right-hand type. As a result of this, signs of moments and angles of inclination are determined according to the right-hand-side-system sign convention.

In conclusion, a list of symbols used in this book is given.

---

*The aerodynamic chord is defined as a segment of a straight line located in the plane of airfoil section whose direction is identical with that of the distant flow toward the airfoil when the lift is zero.

R radius of lifting airscrew (rotor), in meters

r radius of section of the rotor blade, in meters

r_0 radius of the root section of the blade, in meters

b blade chord at radius r, in meters

b_7 blade chord at radius $\overline{r} = 0,7$

c blade section thickness at radius $r = 0,7$, *in meters*

l_Γ distance from axis of rotation of airscrew to horizontal hinge *(HH)*, in meters

$\eta_* = \frac{b_0}{b_1}$ blade taper (see Fig. 2.32)

$F = \pi R^2$ disc area of lifting airscrew, in meters^2

k number of blades

$\sigma = \frac{kb_7}{\pi R}$ rotor solidity ratio

ω angular velocity of lifting airscrew (rotor), in 1/sec.

V speed of flight of helicopter, in m/sec.

v induced velocity, in m/sec.

v_δ velocity due to the flapping motion, in m/sec.

W projection on the plane of rotation of the resultant velocity component, normal to the blade axis at radius r, in m/sec.

Γ velocity circulation around a contour, enclosing blade section at radius r, in meters^2/sec,

α_B angle of attack of lifting airscrew (rotor), in radians

β blade flapping angle, in radians

a_0 average coning angle

a_1 angle of the longitudinal inclination of the blade cone of lifting airscrew ($a_1 > 0$ for an aft inclination of the rotor cone)

b_1 — angle of lateral inclination of the rotor cone ($b_1 > 0$ for an inclination of the cone toward the advancing disc)

ψ — blade azimuth angle, in radians

α — angle of attack of blade section, in radians

β_1 — angle of the approaching flow at blade section, in radians

$\Delta\alpha$ — induced inflow angle at blade section, in radians

$\Delta\delta$ — inflow angle resulting from the flapping motion

*ϕ — blade section pitch angle, in radians

*ϕ_0 — blade pitch angle at $\overline{r} = 0,7$ *(representative pitch angle)* in radians

*$\Delta\phi = \phi - \phi_0$

μ — advance ratio

T — rotor thrust - projection of the rotor resultant force on axis y, in kgs.

H — longitudinal force of the rotor - projection of the resultant rotor force on axis x taken with opposite sign, in kgs

S — lateral force of the rotor - projection of the rotor resultant force on axis z, in kgs.

M_K — torque due to the aerodynamic drag encountered in rotation of the rotor, or rotating torque in kg. meters

M_x — rolling moment of lifting airscrew, in kg. meters

M_z — longitudinal (pitching) moment of lifting airscrew, in kg. meters.

c_T — thrust coefficient

c_H — longitudinal force coefficient

c_S — lateral force coefficient

m_K — torque coefficient due to aerodynamic drag, or torque coefficient

---

*In the typed text, symbols ϕ are used instead of φ appearing in formulas directly reproduced from the Russian version.

m_x rolling moment coefficient

m_z longitudinal (pitching) moment coefficient

c_y section lift coefficient

c_{y0} average (over the whole disc) blade section lift coefficient

c_x section drag coefficient

Relative (dimensionless) values are denoted by a dash over the symbols; furthermore, linear dimensions are related to R, velocities to ωR and circulation to ωR^2. Force coefficients are obtained through a division of corresponding forces by $(1/2)\rho(\omega R)^2 F$; moment coefficients by dividing corresponding moments by $(1/2)\rho(\omega R)^2 FR$, where ρ is the air density. Boldface letters are used to denote vectors.

Translator's Note: Commas are used instead of periods to designate decimals in the material reproduced from the Russian text.

Common Russian subscripts and superscripts are shown below.

ср	average	мг	instantaneous
верх	upper	пр	bound, or straight
нижн	lower	св	free (trailing)
кр	critical		
э	equivalent		
$\overline{пр}$	tandem		
сс	coaxial		
ф	fuselage		
пп	side-by-side		
рв	tail rotor		
ж	rigid		
ап	due to swashplate		
несж	incompressible		

NOTE:

Definition of c_T

$$c_T = T/\pi R^2 \tfrac{1}{2} \rho V_t^2$$

CHAPTER I

LIFTING AIRSCREW IN FLIGHT REGIMES WITH A HORIZONTAL VELOCITY COMPONENT

1. AERODYNAMIC FORCES ACTING ON LIFTING AIRSCREW

We are going to consider a blade element located at a radius r and at an azimuth angle ψ. This element encounters air velocity whose components are as follows: $W = \omega r + V \cos \alpha_B \sin \psi$ — perpendicular to the blade axis (in the plane of the disc) and $V \cos \alpha_B \cos \psi$ — along the projection of the blade axis on the plane of rotation (Fig. 1.1). We assume that the airscrew is lightly loaded, and for that reason, rotation of the slipstream due to the induced velocity will be neglected. In Fig. 1.2, the considered blade element is shown, as well as components of velocity experienced by that element plus the resulting forces. The resulting velocity of the airstream in the plane of rotation is

$$W_1 = \sqrt{W^2 + (V \sin \alpha_s + v_y + v_\delta)^2}, \tag{1.1}$$

where

$$W = \omega R \overline{W}; \quad \overline{W} = \overline{r} + \mu \sin \psi; \tag{1.2}$$

v_y is the component along the y axis of the induced velocity at the considered element; v_δ is the additional velocity resulting from the flapping motion of the blade.

The velocity v_δ, directed perpendicular to the blade axis within the plane of flapping is made up of two components. The first component is equal to $-r(d\beta/dt)$ and depends on the angular velocity of flapping (when the flapping blade moves up, the airstream flows around the element from the top down). The second

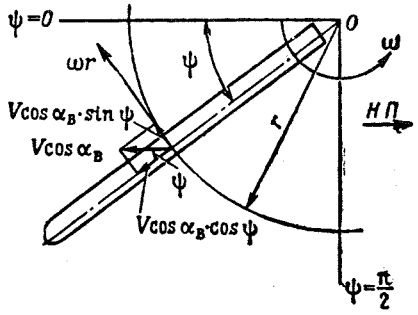

Figure 1.1

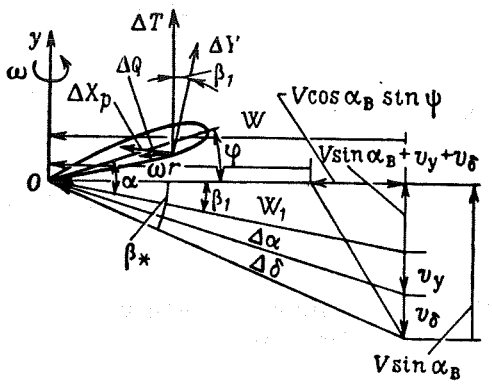

Figure 1.2

component represents a projection of the velocity component $V \cos \alpha_B \cos \psi$ parallel to the plane of rotation. Consequently,

$$v_\delta = -\left(r \frac{d\beta}{dt} + \beta V \cos \alpha_B \cos \psi\right). \tag{1.3}$$

Projecting the lifting force of the element ΔY on the rotor axis and its profile drag force ΔX_p on the plane of rotation, the thrust of the element ΔT and its resistance to rotation ΔQ are obtained.

$$\Delta T = \Delta Y \cos \beta_1 + \Delta X_p \sin \beta_1, \tag{1.4}$$

$$\Delta Q = \Delta X_p \cos \beta_1 - \Delta Y \sin \beta_1. \tag{1.5}$$

Following the hypothesis of two-dimensional blade element characteristics:

$$\Delta Y = \frac{1}{2} c_y \varrho b W_1^2 \Delta r, \tag{1.6}$$

$$\Delta X_p = \frac{1}{2} c_{xp} \varrho b W_1^2 \Delta r. \tag{1.7}$$

Force $\Delta T > 0$ when directed along the positive y axis and force $\Delta Q > 0$ if opposing rotation of the airscrew. From the triangle of velocities in Fig. 1.2, one finds:

$$\cos\beta_1 = \frac{W}{W_1}, \quad \sin\beta_1 = \frac{V\sin\alpha_в + v_y + v_i}{W_1}. \tag{1.8}$$

From Eq. (1.4):

$$\Delta Y = \frac{\Delta T - \Delta X_p \sin\beta_1}{\cos\beta_1}.$$

Substituting the above expressions into Eq. (1.5), the following is obtained:

$$\Delta Q = \frac{\Delta X_p - \Delta T\sin\beta_1}{\cos\beta_1}.$$

Expression of $sin\ \beta_1$ and $cos\ \beta_1$, according to Eq. (1.8), leads to

$$\Delta Q = \frac{1}{W}[\Delta X_p W_1 - \Delta T(V\sin\alpha_в + v_y + v_i)]. \tag{1.9}$$

The longitudinal ΔH, and side ΔS, forces generated by the blade element are determined as projections of forces ΔT and ΔQ on axes x and z, respectively. As a result of its flapping motion, the blades make a small angle β with the $x0z$ plane of coordinates which is identical with the plane of rotation. Force ΔY, perpendicular to the blade axis is also inclined by a small angle β with respect to the y axis, and consequently, it may be assumed that $\Delta Y \approx \Delta T$. Projecting forces ΔT and ΔQ on the x and z axes with a consideration of the blade flapping motion, one obtains:

$$\Delta H = \Delta Q\sin\psi - \beta\Delta T\cos\psi, \tag{1.10}$$

$$\Delta S = -\Delta Q\cos\psi - \beta\Delta T\sin\psi. \tag{1.11}$$

Knowing the forces acting on blade elements, the total forces experienced by the airscrew as a whole can be found:

$$T=\varkappa\frac{k}{2\pi}\int_0^{2\pi}d\psi\int_{r_0}^{R}dT;\quad H=\frac{k}{2\pi}\int_0^{2\pi}d\psi\int_{r_0}^{R}dH;\quad S=\frac{k}{2\pi}\int_0^{2\pi}d\psi\int_{r_0}^{R}dS. \tag{1.12}$$*

Now, we transfer formulae expressed in the rotor coordinates to those of the velocity system. In this case, one obtains the lifting force as:

$$Y_{\text{НВ}}=T\cos\alpha_{\text{В}}-H\sin\alpha_{\text{В}} \tag{1.13}$$

and the horizontal component as:

$$X_{\text{НВ}}=T\sin\alpha_{\text{В}}+H\cos\alpha_{\text{В}}. \tag{1.14}$$

Depending on the magnitude and sign of angle α_β, the horizontal component $X_{\text{НВ}}$ will be either positive or negative. This means that the rotor would either generate an aerodynamic drag or provide a propulsive force.

2. FLAPPING MOTION OF THE ROTOR BLADES

Flapping motion of articulated, rigid blade is described by the following equation[14,92].

$$\frac{d^2\beta}{d\psi^2}+\beta=\frac{1}{J_\Gamma\omega^2}\left(\varkappa\int_{l_\Gamma}^{R}rdT-M_\Gamma\right). \tag{1.15}$$

where

$$J_\Gamma=\int_{l_\Gamma}^{R}r^2dm,\quad M_\Gamma=g\int_{l_\Gamma}^{R}rdm,\quad \varkappa\int_{l_\Gamma}^{R}rdT$$

*In these formulae, and later, dT, dH...are defined according to Eqs. (1.4), (1.5)...where symbols Δ are replaced by d.

are, respectively; moment of inertia, moment of gravitational forces, and moment of the blade thrust with respect to HH, while $\varkappa$ is the tip loss coefficient[92].

The solution of that differential equation of the second order can be found, with the desired degree of accuracy, in a form of the Fourier series

$$\beta = a_0 - \sum_{n=1}^{\infty} (a_n \cos n\psi + b_n \sin n\psi). \tag{1.16}$$

Because of its wide application, the following solution (due to Glauert and Lock) and based on the first harmonic components only, is of special significance.

$$\beta \approx a_0 - a_1 \cos\psi - b_1 \sin\psi. \tag{1.17}$$

Practical experience indicates that in many cases of investigation of the aerodynamic characteristics of the rotor, the above approximation leads to sufficiently accurate results. Substituting into Eq. (1.15), the values of β expressed according to Eq. (1.17), the following is obtained:

$$\varkappa \int_{l_r}^{R} r dT = J_r \omega^2 a_0 + M_r = \text{const}. \tag{1.18}$$

This leads to an important conclusion: if flapping motion of the blades can be sufficiently accurately described by the first harmonic terms only, then the moment of the blade thrust force about the flapping hinge does not depend on the azimuth angle ψ.

It is evident from Eq. (1.17) that an absolutely rigid blade rotating around the rotor axis describes a circular cone, with the position of its axis determined by angles a_1 and b_1.

The velocity of the flow v_δ, related to ωR, and with $\psi = \omega t$ can be expressed, according to Eq. (1.3), under the following form:

$$\bar{v}_\delta = -\left(\bar{r}\frac{d\beta}{d\psi} + \beta\mu\cos\psi\right). \tag{1.19}$$

3. POWER REQUIRED FOR ROTATION OF A ROTOR

The power required for rotation of a lifting rotor (in hp) is

$$N_к = \frac{M_к \omega}{75} = \frac{k}{2\pi} \int_0^{2\pi} d\psi \int_{r_0}^{R} dN_к, \tag{1.20}$$

where $$\Delta N_к = \frac{\Delta M_к \omega}{75} = \frac{1}{75} \Delta Q \omega r. \tag{1.21}$$

According to Eq. (1.9)

$$\Delta Q \omega r = \Delta Q W - \Delta Q V \cos \alpha_в \sin \psi = \Delta X_p W_1 -$$
$$- \Delta T V \sin \alpha_в - \Delta T v_y - \Delta T v_\delta - \Delta Q V \cos \alpha_в \sin \psi.$$

With the help of Eqs. (1.3) and (1.10), the above expression can be presented under the following form

$$\Delta Q \omega r = \Delta X_p W_1 - \Delta T v_y + \Delta T r \frac{d\beta}{dt} - V (\Delta T \sin \alpha_в + \Delta H \cos \alpha_в).$$

Introducing the above expressions into Eq. (1.20) and taking into consideration Eq. (1.14), one obtains:

$$N_к = N_p + N_i + N_\delta - \frac{1}{75} V X_{нв}. \tag{1.22}$$

In the above, $N_p = \frac{1}{75} \frac{k}{2\pi} \int_0^{2\pi} d\psi \int_{r_0}^{R} W_1 dX_p$, $N_i = \frac{1}{75} \frac{k}{2\pi} \int_0^{2\pi} d\psi \int_{r_0}^{R} (-v_y) dT$

is the power required to overcome the profile drag and induced drag of the blades, respectively, while

$$N_\delta = \frac{1}{75} \frac{k}{2\pi} \int_0^{2\pi} d\psi \int_{r_0}^{R} r \frac{d\beta}{dt} dT$$

is the power lost indirectly because of the flapping motion.

Let us determine the magnitude of N_δ. The angular velocity of flapping about the horizontal hinge $d\beta/dt$ is constant along the whole length of the blade since it is considered as completely rigid in bending. Consequently,

$$N_\delta = \frac{1}{75}\,\frac{k}{2\pi}\int_0^{2\pi}\frac{d\beta}{dt}\left(\int_{l_\Gamma}^{R} r\,dT\right)d\psi. \tag{1.23}$$

Remembering that $d\beta/dt = \omega(d\beta/d\psi)$, we determine $\int_{l_\Gamma}^{R} r\,dT$ from Eq. (1.15), and then introducing that value into Eq. (1.23), we obtain:

$$N_\delta = \frac{\omega}{75}\,\frac{k}{2\pi\varkappa}\left[J_\Gamma\omega^2\int_0^{2\pi}\frac{d\beta}{d\psi}\left(\frac{d^2\beta}{d\psi^2}+\beta\right)d\psi + M_\Gamma\int_0^{2\pi}\frac{d\beta}{d\psi}\,d\psi\right].$$

Integrals appearing in the above expression can be easily determined and all of them are equal to zero. Consequently,

$$N_\delta = 0, \tag{1.24}$$

and no power is required for the flapping motion. The above was proven by Lock[108].

The helicopter rotor plays a dual role of lifting and propelling. Due to this, power required for rotating the rotor is used for generation of the lifting force (N_Y) and provision of the horizontal force (N_X). According to Eqs. (1.22), (1.24) and (1.14), we have

$$N_K = N_Y + N_X, \tag{1.25}$$

where

$$N_Y = N_p + N_i, \tag{1.26}$$

$$N_X = -\frac{1}{75}VX_{\text{нв}}. \tag{1.27}$$

Power or torque coefficients are given by the following sum

$$m_K = m_Y + m_X. \tag{1.28}$$

where

$$m_Y = m_p + m_i, \tag{1.29}$$

$$m_X = -\bar{V} c_X \tag{1.30}$$

are, respectively, the coefficients of power required to generate lifting and propulsive forces, while c_X is the coefficient of the horizontal component of the aerodynamic force, with

$$c_X = c_T \sin \alpha_B + c_H \cos \alpha_B. \tag{1.31}$$

The expression for the rotor torque is the same for rigidly attached and articulated blades. Flapping motion of the blades modifies the actual angles of attack of the blade section at various azimuth angles, thus varying numerical values of m_p, m_i, α_B and c_H, but the expression for m_K remains unchanged both for the rigidly attached and articulated blades. Eq. (1.28) is widely used for the presentation of aerodynamic rotor characteristics that are obtained either analytically or experimentally.*

---

*For instance, see Ref. 64 where this formula is used in the following form: $t_x = f(m_K/\sigma)$ where $t_x = c_X/\sigma$.

CHAPTER II

THEORY OF A ROTOR IN OBLIQUE FLOW BASED ON THE SCHEME OF A FLAT VORTEX WAKE

1. GENERAL REMARKS

Let us consider a rotor vortex system which is formed by free vortices leaving the rotor blades. In hovering, this vortex system would have a shape as that shown in Fig. 2.1. With the appearance of a horizontal velocity component, the vortex column would start deflecting to the rear and this inclination would increase with the increasing value of the horizontal component (Fig. 2.2). At sufficiently high flying

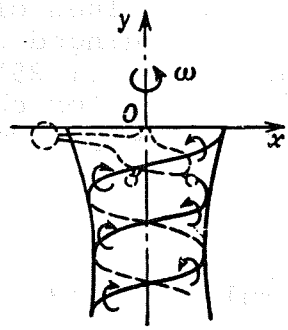

Figure 2.1

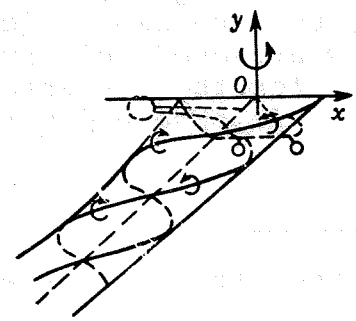

Figure 2.2

speeds, it would become flat (Fig. 2.3), while the free vortices would assume a cycloidal shape. Experience, and theoretical considerations, indicate that this system of a flat vortex wake* is completely applicable to $\bar{V} \geq 1{,}15\sqrt{c_T}$; i.e., for a considerable range of performance predictions of helicopters.

*For the first time, this scheme was investigated by L.S. Vil'dgrube in 1947. A paper was presented at the All-Union Meeting of Theoretical and Applied Mechanics in 1960[25].

2. INVESTIGATION OF THE FLAT VORTEX WAKE

A scheme of free vortices which spring from the tips of a 2-bladed rotor at $\overline{V} \approx 0{,}25$ is shown in Fig. 2.3. Since free vortices spring from all sections of the blade, they form cycloids of different dimensions and shapes (Fig. 2.4). The intensity of the free vortices leaving the same section of the blade at various azimuth angles is different. The character of the variation of the circulation around a given section of the blade (located at a radius ρ) during a complete rotor revolution depends on specific characteristics of the rotor. For instance, in a rigid rotor with non-flapping blades and not having any cyclic control of the pitch, the intensity of circulation at $\psi = (1/2)\pi$ is higher than at $\psi = (3/2)\pi$. In a rotor with articulated blades, it would be just the opposite. Let's express the value of circulation for a section at the dimensionless radius $\overline{\rho}$ in the form of

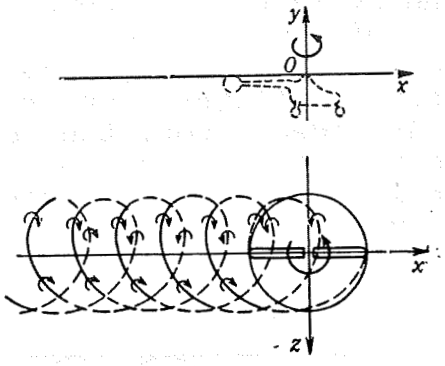

Figure 2.3

$$\Gamma(\bar{\varrho}, \psi) = \Gamma_{\varrho} + \Delta\Gamma(\bar{\varrho}, \psi), \tag{2.1}$$

where Γ_{ρ} is the average of the circulation at radius ρ for one rotor revolution, while $\Delta\Gamma(\overline{\rho}, \psi)$ is a quantity varying with the azimuth angle.

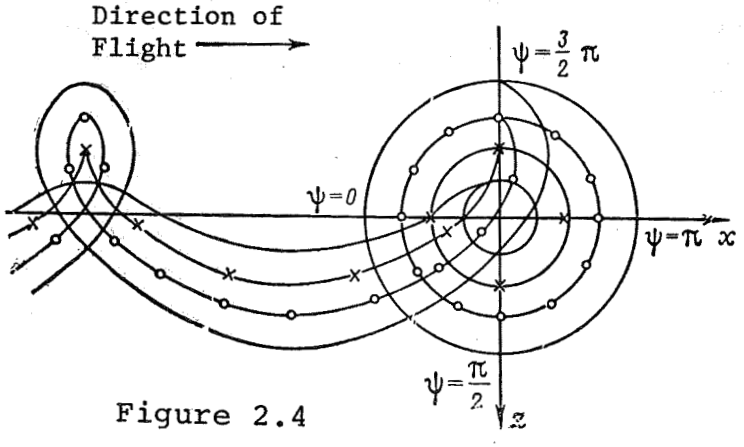

Figure 2.4

Let us consider a system of free cycloidal vortices springing from the blades at a given relative radius $\bar{\rho}$, having a circulation constant with the azimuth, and equal to the average for a complete rotor revolution. Since cruise of a helicopter is usually performed at $\bar{V} \leq 0,4$; consequently, the tip speed is about 2,5 higher than the velocity of flight. Under those circumstances, for the 3 or 4-bladed rotor, the density of free vortices would be so high that it may be assumed that the vortices form a continuous surface of vorticity (Fig. 2.5). From that continuous wake, let's separate a cycloidal free vortex

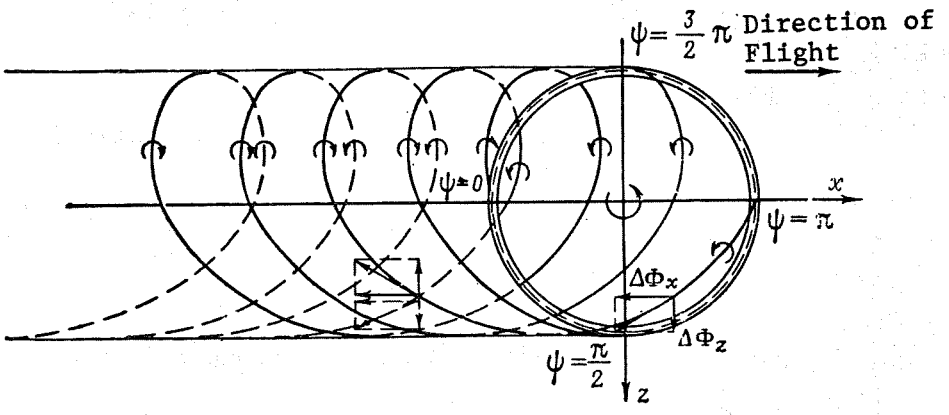

Figure 2.5

layer which springs from the blade at radius ρ and whose circulation is assumed to be constant with azimuth. Such a layer would consist of vortices which spring from all rotor blades and consequently, circulation of the layer should be equal to $k\Delta\Gamma_\rho$. Circulation of the free vortex layer of width $\Delta\rho$ which springs from one blade in that system will be (Fig. 2.6)

$$\Delta\Gamma_\varrho = -\frac{d\Gamma_\varrho}{d\varrho}\Delta\varrho. \tag{2.2}$$

The equation defining the shape of a single free vortex will be given under the following form

$$\bar{x} = \bar{V}(\psi - \psi_0) - \bar{\varrho}\cos\psi; \quad \bar{z} = \bar{\varrho}\sin\psi. \tag{2.3}$$

where ψ_0 is the azimuth angle at which the free vortex left the blade.

Let us single out an elemental vortex layer associated with two azimuth positions being different by an angle $\Delta\psi_0$. Circulation per unit length in this "vorticity" layer will be

$$\Delta\Phi = \frac{k\Delta\Gamma_\varrho}{2\pi}\,\frac{\Delta\psi_0}{\Delta s},$$

where Δs is the distance between the cycloids. From Fig. 2.7, it can be seen that

$$\Delta s = \Delta x \sin\gamma,\quad \operatorname{tg}\gamma = \frac{d\bar{z}}{d\bar{x}} = \frac{\bar{\varrho}\cos\psi}{\bar{V}+\bar{\varrho}\sin\psi}.$$

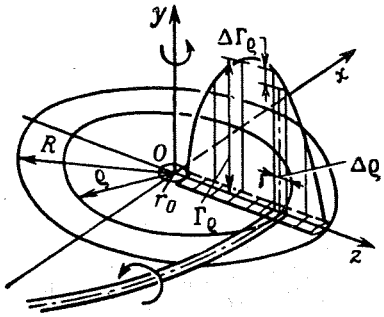

Figure 2.6

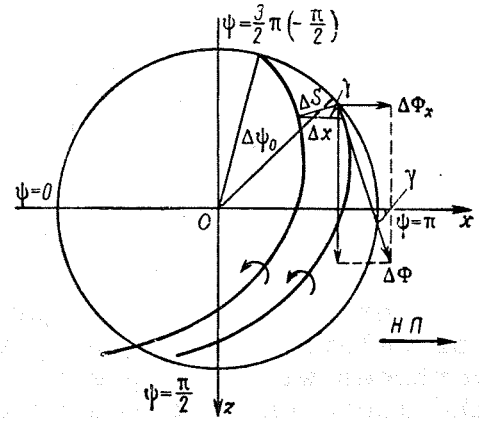

Figure 2.7

According to Eq. (2.3), the relative distance along the x axis between the cycloids encompassing the elementary vortex layer is equal to $\Delta\bar{x} = \bar{V}\Delta\psi_0$. Since $\Delta\bar{x} = \Delta x/R$,

$$\frac{\Delta\psi_0}{\Delta s} = \frac{1}{\bar{V}R\sin\gamma},\quad \Delta\Phi = \frac{k\Delta\Gamma_\varrho}{2\pi R\bar{V}}\,\frac{1}{\sin\gamma}.$$

Let us replace the free cycloidal vortex layer with two systems of vortex layers: one system of free longitudinal vortices and the second one of lateral free vortices. The components of those rectilinear layers is shown by vectors in Figs. 2.5 and 2.7. Circulation per unit length of the lateral vortex layer will be

$$\Delta\Phi_z=\begin{cases}\Delta\Phi\sin\gamma=\dfrac{k\Delta\Gamma_\varrho}{2\pi R\bar{V}} & \text{for } \dfrac{\pi}{2}<\psi<\dfrac{3}{2}\pi,\\ 0 & \text{for } \psi=\dfrac{\pi}{2} \text{ и } \psi=\dfrac{3}{2}\pi,\\ -\Delta\Phi\sin\gamma=-\dfrac{k\Delta\Gamma_\varrho}{2\pi R\bar{V}} & \text{for } -\dfrac{\pi}{2}<\psi<\dfrac{\pi}{2}.\end{cases} \qquad (2.4)^*$$

and of the longitudinal one:

$$\Delta\Phi_x=\begin{cases}\Delta\Phi\cos\gamma=\dfrac{k\Delta\Gamma_\varrho}{2\pi R\bar{V}}\,\dfrac{\bar{V}+\bar{\varrho}\sin\psi}{\bar{\varrho}\cos\psi} & \text{for } \dfrac{\pi}{2}\leqslant\psi\leqslant\dfrac{3}{2}\pi,\\ -\Delta\Phi\cos\gamma=-\dfrac{k\Delta\Gamma_\varrho}{2\pi R\bar{V}}\,\dfrac{\bar{V}+\bar{\varrho}\sin\psi}{\bar{\varrho}\cos\psi} & \text{for } -\dfrac{\pi}{2}\leqslant\psi\leqslant\dfrac{\pi}{2}.\end{cases} \qquad (2.5)$$

Free lateral rectilinear vortices will exist only within a circle of relative radius $\bar{\rho}$. Outside of this circle, the lateral vortices will disappear as a result of geometric summation of the incremental circulation (see Fig. 2.5), and only longitudinal ones will remain with doubled value of the circulation per unit length.

Fig. 2.8 shows a scheme of rectilinear vortices which replac d the cycloidal vortices that left the blade at a relative radius $\bar{\rho}$. If $\bar{z}=\bar{\rho}\sin\psi=const$, then with variation of the coordinate $\bar{x}$ due to ψ_0, values of $\Delta\Phi_x$ and $\Delta\Phi_z$ will not change. Consequently, circulation per unit length of longitudinal and lateral vortices will remain constant along the x axis. Circulation per unit length $\Delta\Phi_x$ of the longitudinal vortices for $\bar{\rho}=1$ and $\bar{V}=0{,}35$ varies in the way shown in Fig. 2.9. It can be seen that for $\bar{z}=-\bar{V}$, circulation of the longitudinal vortices $\Delta\Phi_x=0$. The direction of rotation of those vortices is opposite to the left, and to the right from the $\bar{z}=-\bar{V}$ line.

---

*Formulae 2.4 and 2.5 were obtained by A.P. Proskuryakov[76].

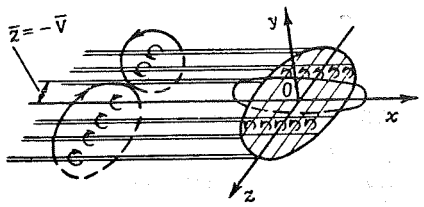

Figure 2.8

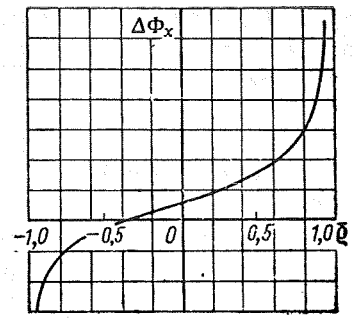

Figure 2.9

Let us approximately evaluate the variation of the circulation around the disc of a rotor with articulated blades. With the first-harmonic flapping motion of the blades, the conditions of Eq. (1.18) are fulfilled for all azimuth angles. According to the Joukowsky law of lifting force

$$dT=\varrho\Gamma(r,\psi)\ W dr, \tag{2.6}$$

where W is defined by Eq. (1.2). Upon introducing Eq. (2.6) into Eq. (1.18), we proceed to the determination of various quantities. For $l_\Gamma = 0$, after integrating and reducing the constant multipliers, we obtain

$$\int_{\bar{Q}}^{1}\Gamma(\bar{r},\psi)(\bar{r}+\mu\sin\psi)\bar{r}d\bar{r}=\frac{1}{3}\Gamma_\psi\left(1+\frac{3}{2}\mu\sin\psi\right)=\text{const}.$$

In the above, Γ_ψ represents circulation averaged over the blade length at an azimuth angle ψ while

$$\Gamma_\psi=\frac{\text{const}}{1+\frac{3}{2}\mu\sin\psi}. \tag{2.7}$$

Upon finding the average value of Γ_ψ; i.e., Γ_{cp}, we obtain

$$\Gamma_\psi=\Gamma_{cp}+\Delta\Gamma(\psi). \tag{2.8}$$

Supplementary bound vortices corresponding to the circulation variation $\Delta\Gamma(\psi)$ generate, in turn, a system of additional free vortices.

It should be noticed that the direction of rotation of these vortices would change when the sign of $\Delta\Gamma(\psi)$ changes. As a result of this, it may be assumed that for $\overline{V} < 0,4$, the time-average supplemental induced velocities resulting from the variation of circulation around the azimuth may be considered small in comparison with velocities induced by the vortex system whose average circulation remains constant with the azimuth. In other words, the time-average velocities induced by a rotor in any point of the space are primarily determined by the distribution of the circulation averaged with respect to azimuth.

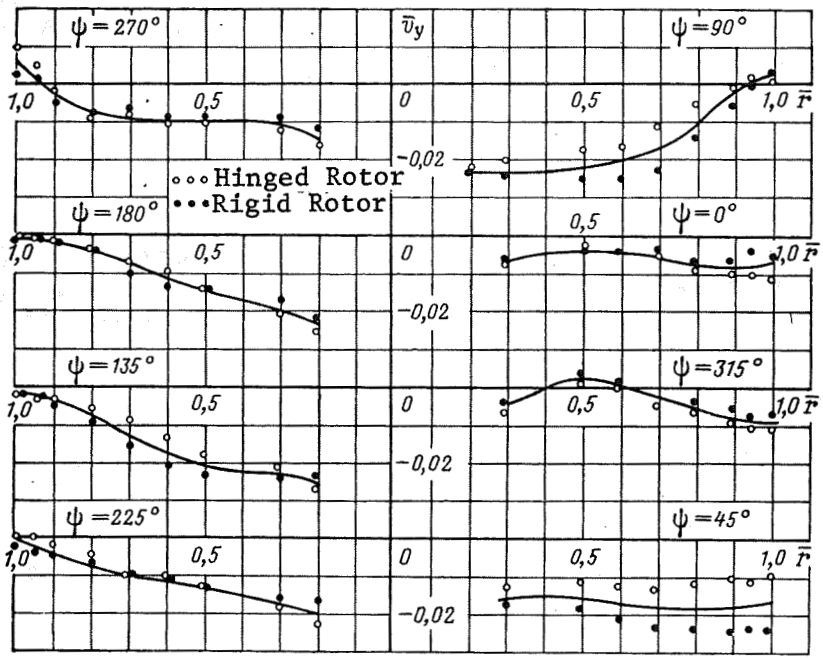

Figure 2.10

In order to verify this assumption, induced velocities were determined experimentally* for two models of a rotor of 2,5 meter diameter. Geometric shape of the blades was identical for both

*Experiments were performed by P.I. Radchenko and V.F. Antropov.

rotors; except that in one rotor, the blades were rigidly attached to the hub, while the other was of the articulated type. In Fig. 2.10, diagrams of the induced velocity distribution along the blade are shown at various azimuth angles for $\overline{V} = 0,25$, $\psi = 5°$ and $\alpha_B = -10°$. In Fig. 2.11, graphs of circulation variation at $\overline{r} = 0,7$ and $0,95$ are plotted. It can be seen from these figures that even with considerable differences in the character of variation of circulation with azimuth, as long as the average circulation remains the same, both systems would show, at the majority of azimuth angles, induced velocity distributions which, within limits acceptable for practical calculations, may be considered as identical.* The largest differences in the induced velocity distribution appear at $\psi \approx 45°$. This is also confirmed by the theoretical considerations of I.O. Meltz.

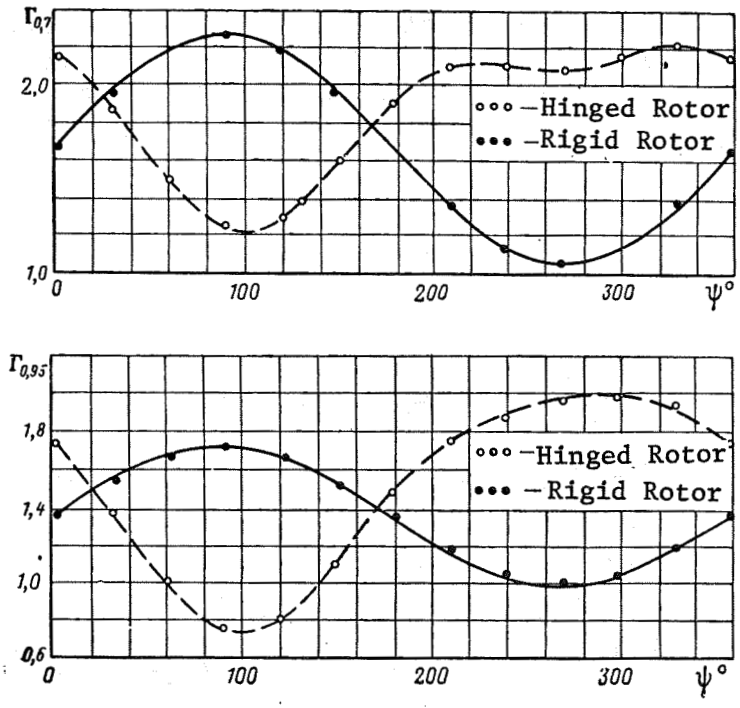

Figure 2.11

*The induced velocities shown in Fig. 2.10 do not incorporate any corrections due to the hub. These corrections would be the same for both the rigid and articulated rotors.

We will determine, at any point of the space, velocities induced by the longitudinal and lateral free vortices associated with the circulation averaged over a circle. Bound vortices having the same circulation at all azimuth angles would not generate any vertical induced velocities. However, they would produce rotational induced velocities at points located above as well as below the rotor disc. Those velocities would somewhat alter the resultant velocities experienced by various blade elements in the coaxial rotor configuration. However, since on the average, this induced rotational (in-plane) velocity represents no more than $0,5\%$ of the blade tip speed, it may be neglected.

3. VELOCITY COMPONENTS INDUCED BY THE LATERAL VORTEX LAYER

Velocity induced at a point $C(x_1, y_1, z_1)$ by the lateral vortices lies in a plane parallel to xOz. An elementary surface of the vortex layer of lateral vortices (Fig. 2.12) generates, according to the Biot-Savart law, velocity

$$d(\Delta v) = \Delta\Phi_z \frac{\sin\varphi}{4\pi a^2} dx dz.$$

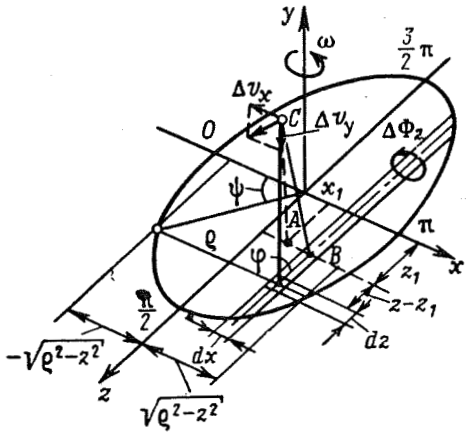

Figure 2.12

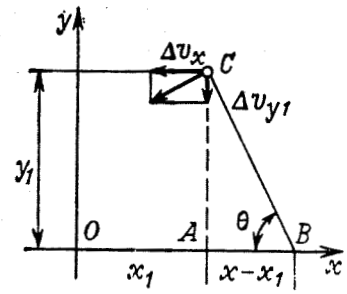

Figure 2.13

It can be seen from Figs. 2.12 and 2.13 that

$$a^2 = (x-x_1)^2 + y_1^2 + (z-z_1)^2, \quad \sin\varphi = \frac{\sqrt{(x-x_1)^2 + y_1}}{a}$$

Projections of induced velocities on axes y and x are (see Fig. 2.13):

$$d(\Delta v_{y1}) = -d(\Delta v)\cos\theta, \quad d(\Delta v_x) = -d(\Delta v)\sin\theta,$$

where

$$\sin\theta = \frac{y_1}{\sqrt{(x-x_1)^2+y_1^2}}; \quad \cos\theta = \frac{x-x_1}{\sqrt{(x-x_1)^2+y_1^2}}.$$

Subscript *"1"* at Δv_y indicates that this particular velocity is generated by the lateral vortices. Integrating the above, one obtains

$$\Delta v_{y1} = -\frac{1}{4\pi}\int_{-\varrho}^{\varrho}\Delta\Phi_z dz \int_{-\sqrt{\varrho^2-z^2}}^{\sqrt{\varrho^2-z^2}} \frac{\sin\varphi\cos\theta}{a^2}dx,$$

$$\Delta v_x = -\frac{1}{4\pi}\int_{-\varrho}^{\varrho}\Delta\Phi_z dz \int_{-\sqrt{\varrho^2-z^2}}^{\sqrt{\varrho^2-z^2}} \frac{\sin\varphi\sin\theta}{a^2}dx.$$

We substitute values for $sin\ \phi\ cos\ \theta$ and a^2, and then we find the inner integral analytically and represent it as

$$Y_y = -\frac{\bar{Y}_y}{\varrho},$$

where

$$\bar{Y}_y = \frac{1}{\sqrt{(\tilde{x}_1+\sqrt{1-\tilde{z}^2})^2+\tilde{y}_1+(\tilde{z}-\tilde{z}_1)^2}} - \frac{1}{\sqrt{(\tilde{x}_1-\sqrt{1-\tilde{z}^2})^2+\tilde{y}_1^2+(\tilde{z}+\tilde{z}_1)^2}}.$$

and

$$\tilde{x}_1 = \frac{x_1}{\varrho}, \quad \tilde{y}_1 = \frac{y_1}{\varrho}, \quad \tilde{z}_1 = \frac{z_1}{\varrho}.$$

Expressing $\Delta\Phi_z$ according to Eq. (2.4), we obtain:

$$\Delta v_{y1}=\frac{k\Delta\Gamma_0}{4\pi R\overline{V}}\Delta\hat{v}_{y1}, \tag{2.9}$$

where

$$\Delta\hat{v}_{y1}=\frac{1}{2\pi}\int_{-1}^{1}\overline{Y}_y d\tilde{z}.$$

From Eq. (2.9), the following observations can be made:

1. For $\tilde{x}_1 = 0$, i.e., for the points located in the zOy plane, velocity $\Delta\overline{v}_{y_1} = 0$. Consequently, lateral vortices do not induce vertical velocities in the zOy plane.

2. For points symmetrical with respect to the zOy plane, velocities induced by the lateral vortices are equal in magnitude, but of the opposite signs. It follows, hence that

$$\hat{v}_{y1}(-\tilde{x}) = -\Delta\hat{v}_{y1}(\tilde{x}).$$

3. $\Delta\hat{v}_{y1} \to 0$ for $\tilde{x}_1 \to \infty$.

4. $\Delta\hat{v}_{y1} \to 0$ for $\tilde{y}_1 \to \infty$.

5. In the points, symmetrical with respect to the xOz and xOy planes, the vertical components of velocities induced by the lateral vortices are equal; i.e.,

$$\Delta\hat{v}_{y1}(\tilde{y}_1)=\Delta\hat{v}_{y1}(-\tilde{y}_1);\quad \Delta\hat{v}_{y1}(\tilde{z}_1)=\Delta\hat{v}_{y1}(-\tilde{z}_1).$$

In Fig. 2.14, graphs of $\Delta\hat{v}_{y1} = f(\tilde{x}_1)$ are shown for various values of parameters $\tilde{y}_1$ and $\tilde{z}_1$.

Now, we can evaluate Δv_x. Substituting $\sin\phi$, $\sin\theta$, and a^2 into the expression for Δv_x, similarly to Eq. (2.9) we obtain,

$$\Delta v_x=\frac{k\Delta\Gamma_0}{4\pi R\overline{V}}\Delta\hat{v}_x, \tag{2.10}$$

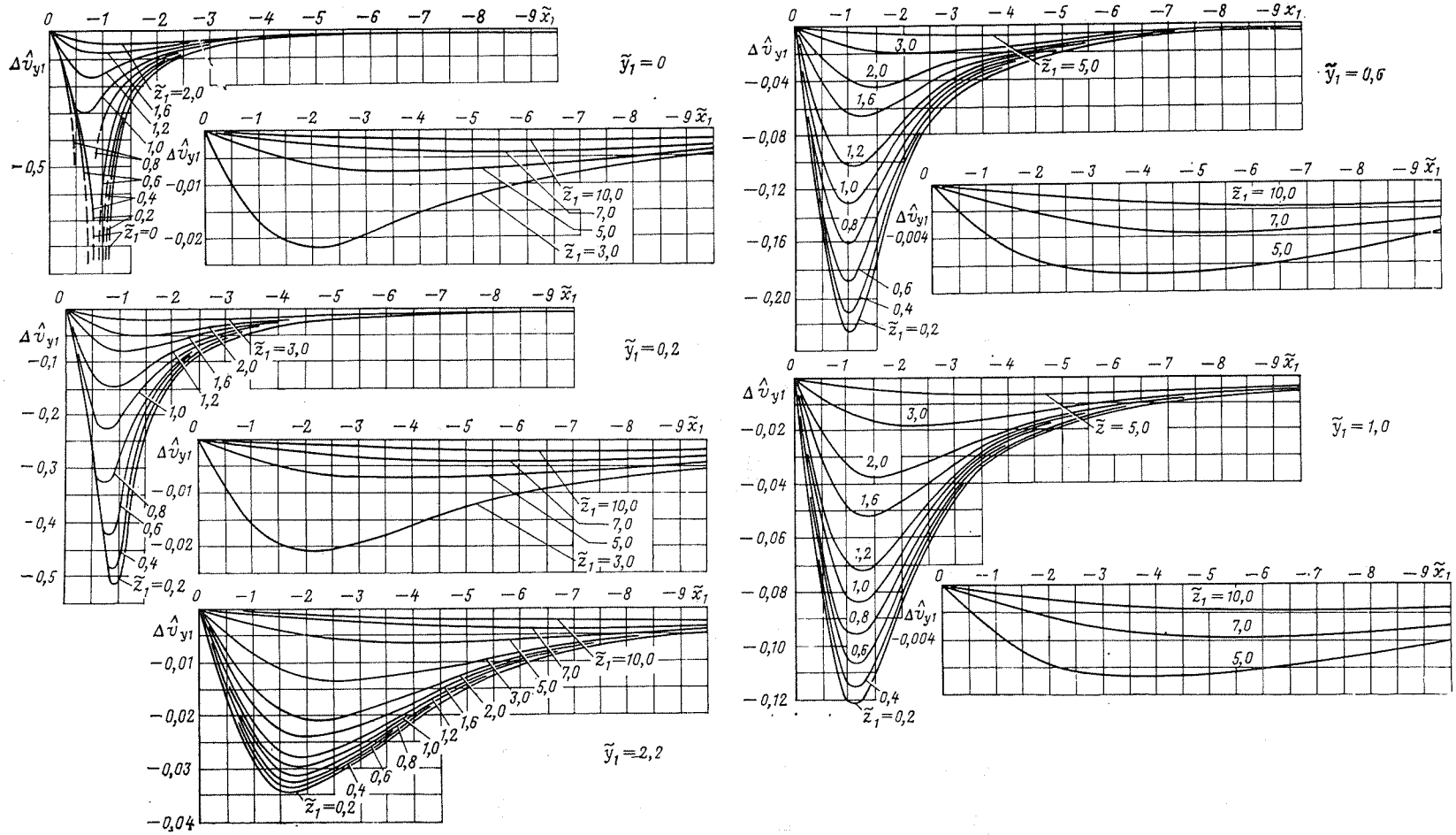
$\tilde{y}_1 = 0$
$\tilde{y}_1 = 0{,}2$
$\tilde{y}_1 = 2{,}2$
$\tilde{y}_1 = 0{,}6$
$\tilde{y}_1 = 1{,}0$
$\Delta\hat{v}_{y1}$
$\tilde{x}_1$
$\tilde{z}_1 = 0$
$\tilde{z}_1 = 0{,}2$
$\tilde{z}_1 = 0{,}4$
$\tilde{z}_1 = 0{,}6$
$\tilde{z}_1 = 0{,}8$
$\tilde{z}_1 = 1{,}0$
$\tilde{z}_1 = 1{,}2$
$\tilde{z}_1 = 1{,}6$
$\tilde{z}_1 = 2{,}0$
$\tilde{z}_1 = 3{,}0$
$\tilde{z}_1 = 5{,}0$
$\tilde{z}_1 = 7{,}0$
$\tilde{z}_1 = 10{,}0$
$\tilde{z} = 5{,}0$

Figure 2.14

where $$\Delta\hat{v}_x = -\frac{1}{2\pi}\int_{\tilde{z}=-1}^{\tilde{z}=1} \bar{Y}_x d\tilde{z},$$

$$\bar{Y}_x = \frac{\tilde{y}_1}{[\tilde{y}_1^2+(\tilde{z}-\tilde{z}_1)^2]}\left\{\frac{\tilde{x}_1+\sqrt{1-\tilde{z}^2}}{\sqrt{(\tilde{x}_1+\sqrt{1-\tilde{z}^2})^2+\tilde{y}_1^2+(\tilde{z}-\tilde{z}_1)^2}}-\right.$$

$$\left.-\frac{\tilde{x}_1-\sqrt{1-\tilde{z}^2}}{\sqrt{(\tilde{x}_1-\sqrt{1-\tilde{z}^2})^2+\tilde{y}_1^2+(\tilde{z}-\tilde{z}_1)^2}}\right\}.$$

From Eq. (2.10), the following can be deduced:

1. At the points, symmetrical with respect to the zOy plane, the values of the horizontal induced velocities are the same; i.e.,

$$\Delta\hat{v}_x(-\tilde{x}_1) = \Delta\hat{v}_x(\tilde{x}_1).$$

2. The sign of the longitudinal induced velocity is dictated by the sign of $\tilde{y}_1$. In this way, above the rotor, $\Delta\hat{v}_x < 0$, and is in the opposite direction to that of flight; while under the rotor, $\Delta\hat{v}_x > 0$, and is in the direction of flight.

3. $\Delta\hat{v}_x \to 0$ for $\tilde{x}_1 \to \infty$.

4. $\Delta\hat{v}_x \to 0$ for $\tilde{y}_1 \to \infty$.

In Fig. 2.15, graphs of $\Delta\hat{v}_x = f(\tilde{z}_1)$ are shown for various values of parameters $\tilde{x}_1$ and $\tilde{y}_1$.

The above obtained formulae define velocities induced by the lateral vortices only, which sprang from the rotor at a relative radius $\bar{\rho}$. In order to determine velocities induced by the lateral vortices which spring from all stations of the blade, it is necessary to add all the elementary velocities. In this way

$$v_{y1} = \sum_{\bar{\rho}=\bar{r}_0}^{\bar{\rho}=1,0} \Delta v_{y1}, \quad v_x = \sum_{\bar{\rho}=\bar{r}_0}^{\bar{\rho}=1,0} \Delta v_x.$$

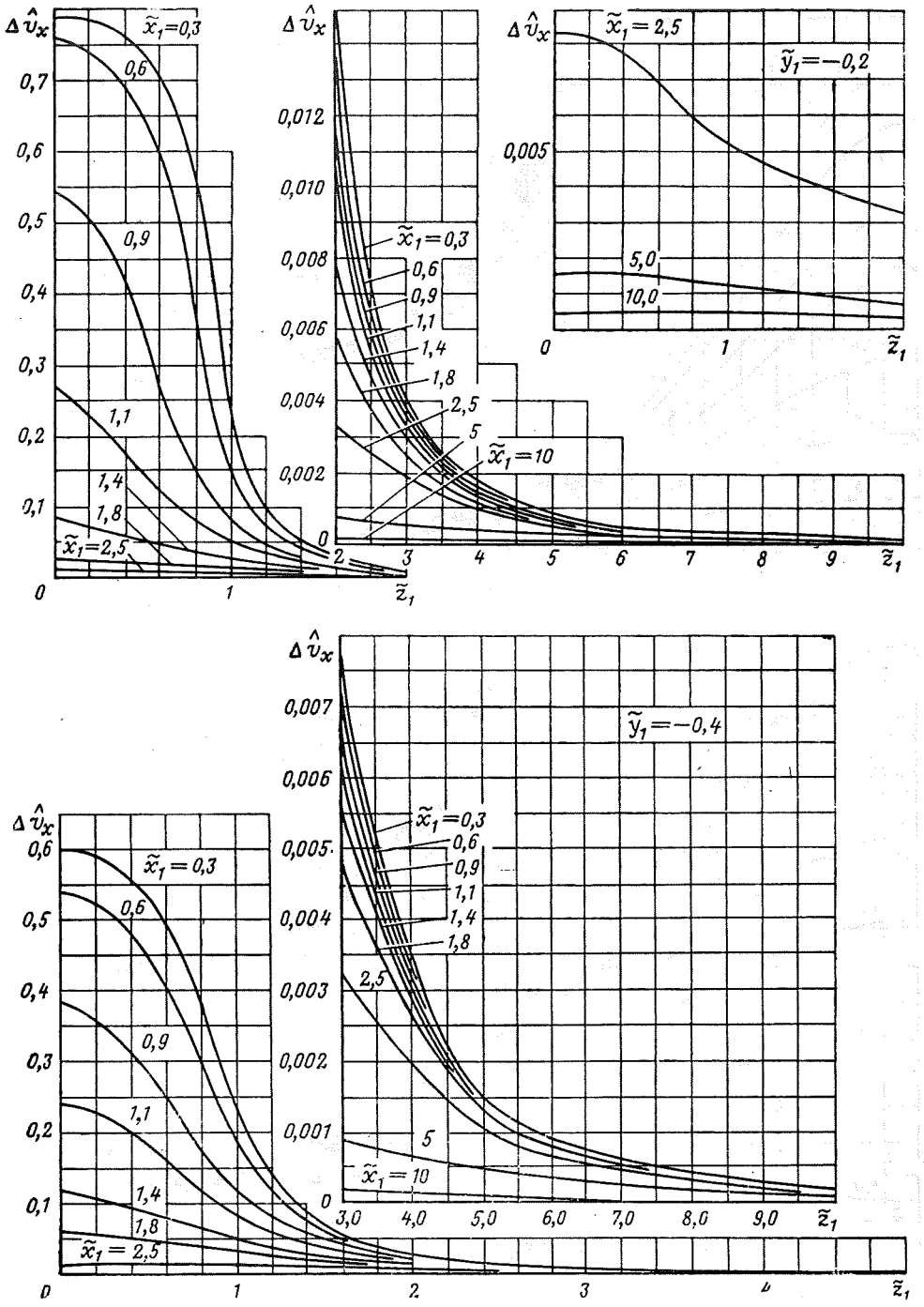
$\Delta\hat{v}_x$
$\tilde{x}_1=0,3$
0,6
0,9
1,1
1,4
1,8
$\tilde{x}_1=2,5$
$\tilde{z}_1$
$\tilde{x}_1=10$
2,5
5
$\tilde{y}_1=-0,2$
5,0
10,0
$\tilde{y}_1=-0,4$

Figure 2.15

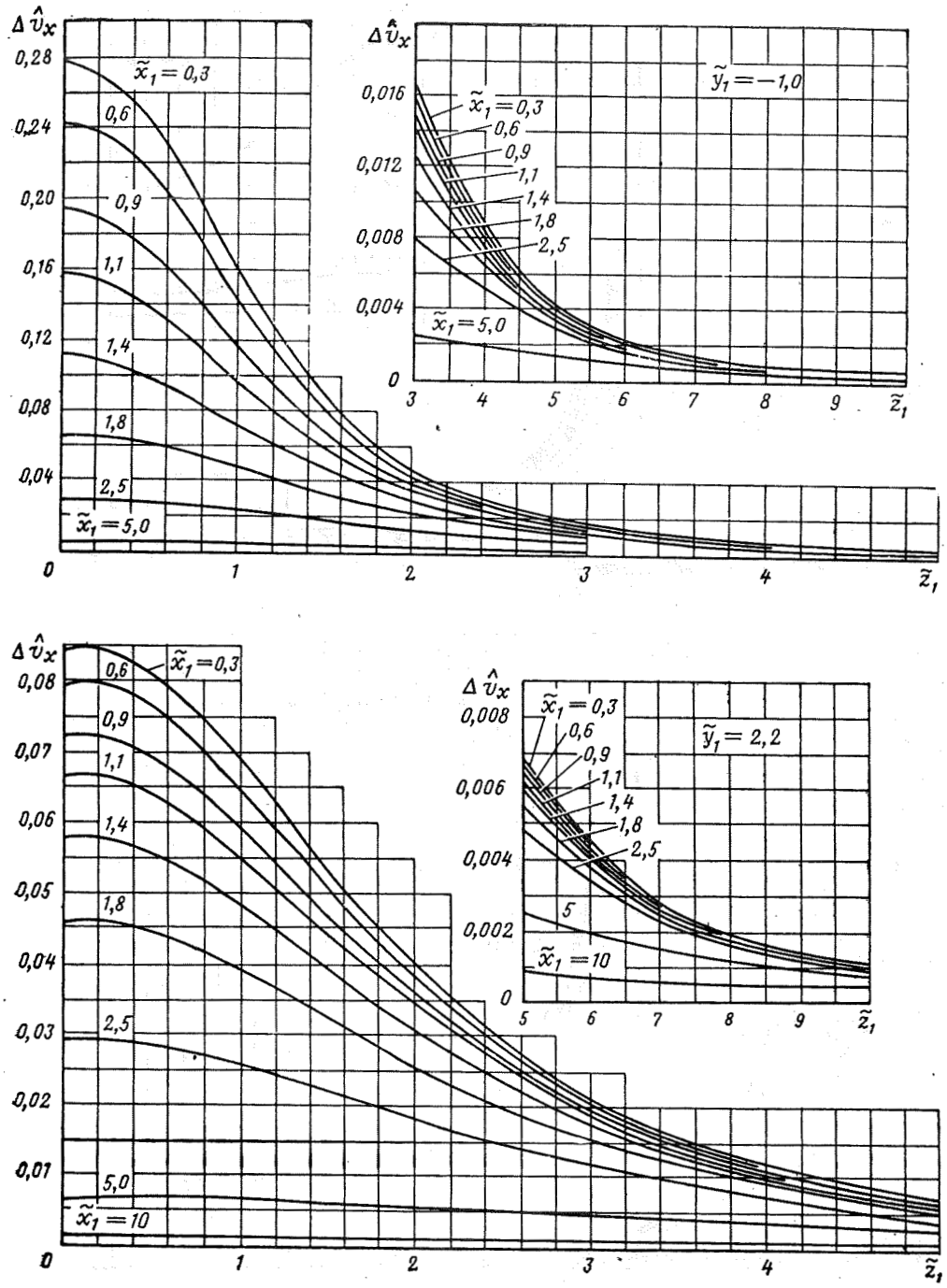

Figure 2.15 (Cont'd)

As an illustration, the distribution of v_{y_1} along the fore and aft diameter of the disc is shown in Fig. 2.16.

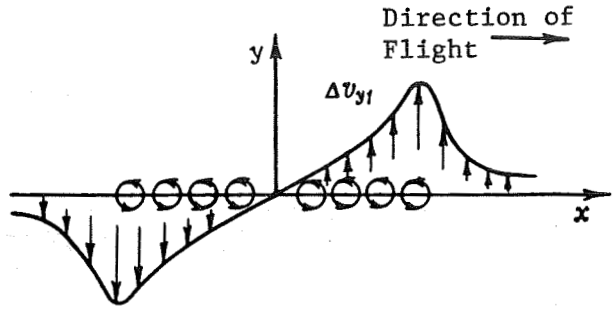

Figure 2.16

4. VELOCITY COMPONENTS INDUCED IN THE yOz PLANE BY THE FREE LONGITUDINAL VORTICITY LAYER

It has been shown that the intensity of the longitudinal vortices outside a circle of radius ρ (from whose perimeter sprang the original cycloidal free vortices) is twice as large as that inside the circle (Fig. 2.17). Velocities induced at points in the yOz plane by the longitudinal vortices located in the front half of the circle $(\pi/2 < \psi(3/2)\pi)$ as well as those in its rear half are the same. For this reason, induced velocities in the yOz plane can be determined by replacing the actual system of longitudinal vortices (see Fig. 2.8) by rectilinear longitudinal vortices extending from the Oz axis to infinity and having their circulation intensity twice as high (Fig. 2.18).

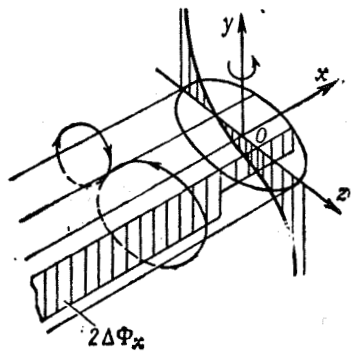

Figure 2.17

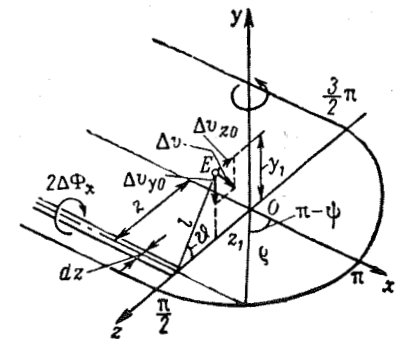

Figure 2.18

The element of the longitudinal vortex layer, dz wide and extending from the z axis to infinity along the x direction, induces the following velocity at point $E(0, \bar{y}_1, \bar{z}_1)$:

$$d(\Delta v) = -\frac{2\Delta\Phi_x}{4\pi l} dz,$$

where

$$l = \sqrt{y_1^2 + (z - z_1)^2}.$$

It can be seen from Fig. 2.18 that the vertical projection of that elementary velocity is

$$d(\Delta v_{y0}) = -d(\Delta v)\cos\vartheta, \quad \cos\vartheta = \frac{z - z_1}{l}.$$

The subscript "0" indicates that projection lies in the yOz plane. Consequently,

$$d(\Delta v_{y0}) = \frac{\Delta\Phi_x}{2\pi l^2}(z - z_1)dz.$$

Substituting $\Delta\Phi_x$ according to Eq. (2.5) into the above, and integrating (with respect to z) from $-\bar{\rho}$ to $\bar{\rho}$, we obtain:

$$\Delta v_{y0} = \frac{k\Delta\Gamma_0}{4\pi R\bar{V}} \Delta\hat{v}_{y0}, \tag{2.11}$$

where

$$\Delta\hat{v}_{y0} = \frac{1}{\pi} \int_{-\bar{\rho}}^{\bar{\rho}} \frac{(\bar{z} - \bar{z}_1)(\bar{V} + \bar{\varrho}\sin\psi)}{\left[\bar{y}_1^2 + (\bar{z} - \bar{z}_1)^2\right]\bar{\varrho}\cos\psi} d\bar{z}.$$

When the following replacements: $\bar{z} = \bar{\rho}\ sin\ \psi$, $d\bar{z} = \bar{\rho}\ cos\ \psi d\psi$ are made, then

$$\Delta\hat{v}_{y0} = -\frac{1}{\pi} \int_{\frac{\pi}{2}}^{\frac{3}{2}\pi} \frac{(\bar{\varrho}\sin\psi - \bar{z}_1)(\bar{V} + \bar{\varrho}\sin\psi)}{\bar{y}_1^2 + (\bar{\varrho}\sin\psi - \bar{z}_1)^2} d\psi.$$

After dividing the numerator and denominator of that fraction by $\overline{\rho}^2$ and rearranging the expression under the integral sign, we obtain

$$\Delta\widehat{v}_{y0}=-\frac{1}{\pi}\left\{\overline{V}_*\int\limits_{\frac{\pi}{2}}^{\frac{3}{2}\pi}\frac{(\sin\psi-\tilde{z}_1)\,d\psi}{\tilde{y}_1^2+(\sin\psi-\tilde{z}_1)^2}+\int\limits_{\frac{\pi}{2}}^{\frac{3}{2}\pi}\frac{\sin\psi(\sin\psi-\tilde{z}_1)\,d\psi}{\tilde{y}_1^2+(\sin\psi-\tilde{z}_1)^2}\right\},$$

where $\overline{V}_* = \overline{V}/\overline{\rho}$. The numerator in the second integral can be expressed under the following form:

$$\sin\psi(\sin\psi-\tilde{z}_1)=[\tilde{y}_1^2+(\sin\psi-\tilde{z}_1)^2]-\tilde{y}_1^2+\tilde{z}_1(\sin\psi-\tilde{z}_1).$$

Then,

$$\Delta\widehat{v}_{y0}=-\{1+(\overline{V}_*+\tilde{z}_1)Q-[(\overline{V}_*+\tilde{z}_1)\tilde{z}_1+\tilde{y}_1^2]P\}, \tag{2.12}$$

where

$$P=\frac{1}{\pi}\int\limits_{\frac{\pi}{2}}^{\frac{3}{2}\pi}\frac{d\psi}{\tilde{y}_1^2+(\sin\psi-\tilde{z}_1)^2};\quad Q=\frac{1}{\pi}\int\limits_{\frac{\pi}{2}}^{\frac{3}{2}\pi}\frac{\sin\psi d\psi}{\tilde{y}_1^2+(\sin\psi-\tilde{z}_1)^2}.$$

It can be seen that $P(-\tilde{z}_1) = P(\tilde{z}_1)$, $Q(-\tilde{z}_1) = -Q(\tilde{z}_1)$. If $\tilde{z}_1 = 0$, then $Q = Q_0 = 0$, and

$$P=P_0=\frac{1}{\pi}\int\limits_{\frac{\pi}{2}}^{\frac{3}{2}\pi}\frac{d\psi}{\tilde{y}_1^2+\sin^2\psi}=\frac{1}{\tilde{y}_1\sqrt{1+\tilde{y}_1^2}}. \tag{2.13}$$

Integrals P and Q were evaluated and their values are shown in Figs. 2.19 and 2.20. In the points symmetrical with respect to the xOz plane, values of the vertical induced velocities are the same:

$$\Delta v_{y0}(\tilde{y}_1)=\Delta v_{y0}(-\tilde{y}_1). \tag{2.14}$$

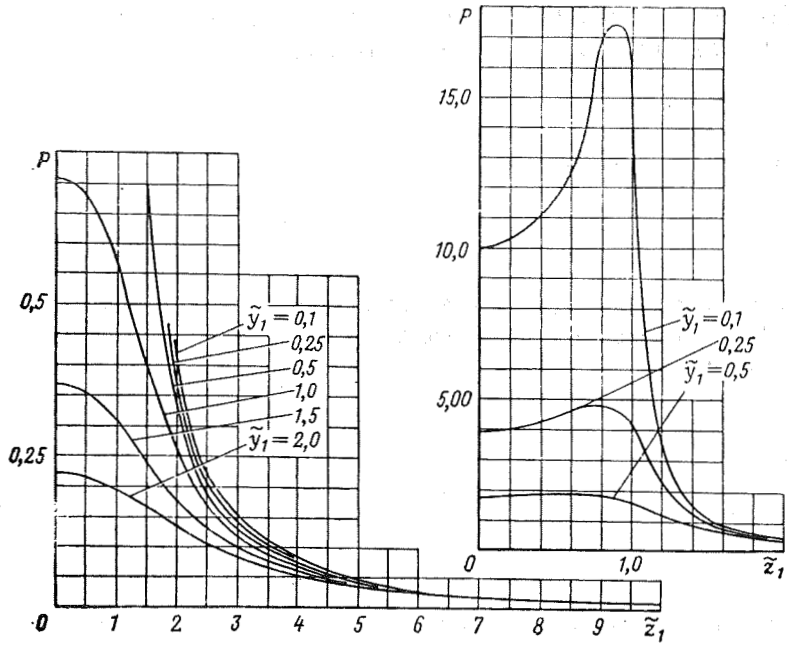

Figure 2.19

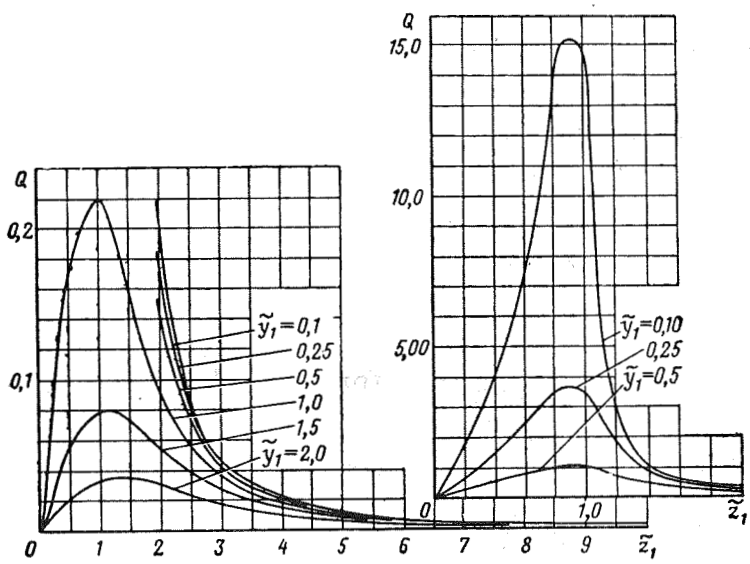

Figure 2.20

Let us consider separately, the induced velocity along the z axis. With $\tilde{y}_1 = 0$ in Eq (2.12), we obtain

$$\Delta\hat{v}_{y0} = -1-(\bar{V}_*+\tilde{z}_1)\frac{1}{\pi}\int_{\frac{\pi}{2}}^{\frac{3}{2}\pi}\frac{d\psi}{\sin\psi-\tilde{z}_1}. \tag{2.15}$$

If $-1 \leq \tilde{z}_1 \leq 1$, then the integral is improper. In order to modify it, $\psi = (\pi/2) + \alpha$ is introduced, and $\tilde{z}_1 = \cos\theta$ is substituted for $0 \leq \theta \leq \pi$. Then[33]

$$\int_{\frac{\pi}{2}}^{\frac{3}{2}\pi}\frac{d\psi}{\sin\psi-\tilde{z}_1}=\int_0^{\pi}\frac{d\alpha}{\cos\alpha-\cos\theta}=0. \tag{2.16}$$

For $\tilde{z}_1 > 1$, there is no discontinuity of the integrated function, and

$$\int_{\frac{\pi}{2}}^{\frac{3}{2}\pi}\frac{d\psi}{\sin\psi-\tilde{z}_1}=-\frac{\pi}{\sqrt{\tilde{z}_1^2-1}}.$$

For $\tilde{z}_1 < -1$ the integrated function is positive, and

$$\int_{\frac{\pi}{2}}^{\frac{3}{2}\pi}\frac{d\psi}{\sin\psi-\tilde{z}_1}=\frac{\pi}{\sqrt{\tilde{z}_1^2-1}}.$$

In this way, at $\tilde{y}_1 = 0$, we obtain

$$\Delta\hat{v}_{y0}=\begin{cases}-1-\dfrac{\bar{V}_*+\tilde{z}_1}{\sqrt{\tilde{z}_1^2-1}} & \text{for } \tilde{z}_1<-1,\\ -1 & \text{for } -1\leqslant\tilde{z}_1\leqslant 1,\\ -1+\dfrac{\bar{V}_*+\tilde{z}_1}{\sqrt{\tilde{z}_1^2-1}} & \text{for } \tilde{z}_1>1,\end{cases} \tag{2.17}$$

This means that velocity induced along the z axis by free vortices springing at a circle of radius ρ are constant inside the following intervals; $-\bar{\rho} \leq \bar{z}_1 \leq \bar{\rho}$.*

Passing through $\bar{z}_1 = 1$, the induced velocity becomes positive and varies from ∞ to 0. Fig. 2.21 graphically illustrates the variation of $\Delta\hat{v}_{y0}$ with $\bar{z}_1$. Substituting into Eq. (2.11), the expression for $\Delta\Gamma_\rho$ according to Eq. (2.2), we obtain the induced velocity on the z axis, due to all free vortices springing from the blade

$$v_{y0}(\bar{z}_1) = -\frac{k}{4\pi R\bar{V}} \int_{r_0}^{R} \Delta\hat{v}_y(\bar{z}_1) \frac{d\Gamma_\varrho}{d\varrho}\, d\varrho. \qquad (2.18)$$

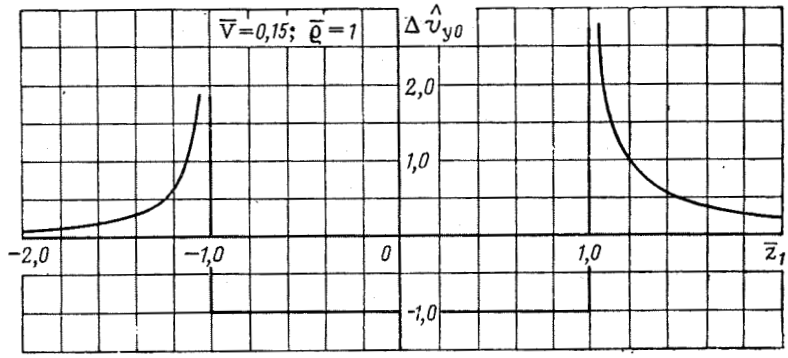

Figure 2.21

When $\bar{z}_1 < 1$; i.e., the considered point is located inside the rotor disc, then taking into consideration Eq (2.17), we obtain

$$v_{y0}(\bar{z}_1) = \frac{k}{4\pi R\bar{V}} \left[\int_{\bar{r}_0}^{\bar{z}_1} \left(1 - \frac{\bar{V}+\bar{z}_1}{\sqrt{\bar{z}_1^2 - \bar{\varrho}^2}} \right) \frac{d\Gamma_\varrho}{d\bar{\varrho}}\, d\bar{\varrho} + \int_{\bar{z}_1}^{1} \frac{d\Gamma_\varrho}{d\bar{\varrho}}\, d\bar{\varrho} \right] =$$

$$= \frac{k}{4\pi R\bar{V}} \left[\int_{\bar{r}_0}^{1} \frac{d\Gamma_\varrho}{d\bar{\varrho}}\, d\bar{\varrho} - (\bar{V}+\bar{z}_1) \int_{\bar{r}_0}^{\bar{z}_1} \frac{\frac{d\Gamma_\varrho}{d\bar{\varrho}}\, d\bar{\varrho}}{\sqrt{\bar{z}_1^2 - \bar{\varrho}^2}} \right].$$

*This solution was first obtained by A.I. Slutskiy

Since the resultant circulation of free vortices that spring from the whole blade is equal to zero; hence,

$$\int_{\bar{r}_0}^{1} \frac{d\Gamma_\varrho}{d\bar{\varrho}} d\bar{\varrho} = 0 \quad , \text{ and}$$

$$v_{y0}(\bar{r}_0 \leqslant \bar{z}_1 \leqslant 1) = -\frac{k(\bar{V}+\bar{z}_1)}{4\pi R\bar{V}} \int_{\bar{r}_0}^{\bar{z}_1} \frac{\frac{d\Gamma_\varrho}{d\bar{\varrho}} d\bar{\varrho}}{\sqrt{\bar{z}_1^2 - \bar{\varrho}^2}} . \tag{2.19}$$

If $\bar{z}_1 > 1$, then in analogy with the above, we obtain:

$$v_{y0}(\bar{z}_1 > 1) = -\frac{k(\bar{V}+\bar{z}_1)}{4\pi R\bar{V}} \int_{\bar{r}_0}^{1} \frac{\frac{d\Gamma_\varrho}{d\bar{\varrho}} d\bar{\varrho}}{\sqrt{\bar{z}_1^2 - \bar{\varrho}^2}} . \tag{2.20}$$

When $-\bar{r}_0 \geq \bar{z}_1 \geq -1$; i.e., the considered point is located on the negative side of the z axis, where the blade moves in the direction opposite to that of flight, then

$$v_{y0}(-\bar{r}_0 \geqslant \bar{z}_1 \geqslant -1) = \frac{k(\bar{V}+\bar{z}_1)}{4\pi R\bar{V}} \int_{\bar{r}_0}^{\bar{z}_1} \frac{\frac{d\Gamma_\varrho}{d\bar{\varrho}} d\bar{\varrho}}{\sqrt{\bar{z}_1^2 - \bar{\varrho}^2}} ; \tag{2.21}$$

for $\bar{z}_1 < -1$,

$$v_{y0}(\bar{z}_1 < -1) = \frac{k(\bar{V}+\bar{z}_1)}{4\pi R\bar{V}} \int_{\bar{r}_0}^{1} \frac{\frac{d\Gamma_\varrho}{d\bar{\varrho}} d\bar{\varrho}}{\sqrt{\bar{z}_1^2 - \bar{\varrho}^2}} . \tag{2.22}$$

Formulae (2.19) - (2.22) contain improper integrals, since the integrated functions in Eqs. (2.19) and (2.21) have discontinuities for $|\bar{z}_1| = \bar{\rho}$, and in Eqs. (2.20) and (2.22) for $|\bar{z}_1| = 1$. However, the existance of those integrals can be verified by Cauchy's theorems.

It is clear from Eq. (2.21) that on the negative half of the z axis, $v_{y_0} = 0$ at the point $\bar{z}_1 = -\bar{V}$. It can be deduced from Eqs. (2.17), (2.19) and (2.21) that $v_{y_0} = 0$ also, in the $-\bar{r}_0 \leq \bar{z}_1 \leq \bar{r}_0$ region of the z axis. Indeed, this region appears as the internal one for all free vortices leaving the blades between $\bar{\rho} = 1$ and $\bar{\rho} = \bar{r}_0$. Consequently, in that region,

$$\Delta\hat{v}_{y_0} = -1 = const; \text{ hence, } v_{y_0} = const \int_i^{\bar{z}_0} d\Gamma_\rho = 0. .$$

From Eqs. (2.19), (2.21), (2.20) and (2.22), it follows that,

$$\frac{v_{y0}(\bar{z}_1 > 1)}{v_{y0}(\bar{z}_1 < -1)} = -\frac{\bar{V} + |\bar{z}_1|}{\bar{V} - |\bar{z}_1|} > 1$$

and

$$\frac{v_{y0}(\bar{V} < \bar{z}_1 < \bar{z}_*)}{v_{y0}(-\bar{V} > \bar{z}_1 > \bar{z}_*)} = -\frac{\bar{V} + |\bar{z}_1|}{\bar{V} - |\bar{z}_1|} > 1,$$

where $\bar{z}_*$ is the abscissa at which

$$\int_{\bar{r}_0}^{\bar{z}_*} \frac{\frac{d\Gamma_\varrho}{d\bar{\varrho}}\, d\bar{\varrho}}{\sqrt{\bar{z}_1^2 - \bar{\varrho}^2}} = 0$$

and, consequently, $v_{y_0} = 0$. In this way, for the same values of $|z_1|$, the v_{y_0} ordinates on the positive half of the z axis are always larger than those on the negative half.

In practical computations, when Γ_ρ is given in a graphical form, finite summation should be used instead of integration. Then, for instance, for $-\bar{r}_0 \geq \bar{z}_1 \geq -1$

$$v_{y0}(\bar{z}_1) = \frac{k(\bar{V} + \bar{z}_1)}{4\pi R\bar{V}} \sum_{\bar{\varrho}=\bar{r}_0}^{\bar{\varrho}=\bar{z}} \frac{\Delta\Gamma_\varrho}{\sqrt{\bar{z}_1^2 - \bar{\varrho}^2}}, \tag{2.23}$$

where $\Delta\Gamma_\rho = \Gamma_{\rho+\Delta} + \Gamma_{\rho-\Delta}$.

In order to investigate how the distribution of circulation, averaged over the circles, influences the character of v_{y0} distribution along the $0z$ axis, let us consider a few examples.

Let us consider a triangular distribution of circulation as given by the equation* $\Gamma = a\bar{\rho}$ (Fig. 2.22). In this case, the free vorticity system would consist of a discrete vortex leaving the blade at a station $\bar{\rho} = 1,0$, and having circulation $\Gamma_1 = -a$, and a vorticity layer with intensity proportional to $d\Gamma/d\bar{\rho} = a$. Reasoning in the same way as at the development of Eq. (2.19), we obtain for the region $0 \leq \bar{z}_1 \leq 1$:

$$v_{y0}=\frac{k\Gamma_1}{4\pi R\bar{V}}+\frac{k}{4\pi R\bar{V}}\left[\int_{\bar{r}_0}^{\bar{z}_1}\frac{d\Gamma}{d\bar{\varrho}}d\bar{\varrho}-(\bar{V}+\bar{z}_1)\int_{\bar{r}_0}^{\bar{z}_1}\frac{\frac{d\Gamma}{d\bar{\varrho}}d\bar{\varrho}}{\sqrt{\bar{z}_1^2-\bar{\varrho}^2}}\right].$$

In the above expression, the first term reflects the contribution of the free tip vortex. After performing integration, assuming $\bar{r}_0 = 0$, we finally obtain

$$v_{y0}=-\frac{ka}{8R\bar{V}}(\bar{V}+\bar{z}_1). \tag{2.24}$$

For the region $\bar{z}_1 > 1$, we obtain by analogy

$$v_{y0}=\left(1-\frac{\bar{V}+\bar{z}_1}{\sqrt{\bar{z}_1^2-1}}\right)\frac{k\Gamma_1}{4\pi R\bar{V}}+$$

$$+\frac{k}{4\pi R\bar{V}}\left[\int_0^1\frac{d\Gamma}{d\bar{\varrho}}d\bar{\varrho}-(\bar{V}+\bar{z}_1)\int_0^1\frac{\frac{d\Gamma}{d\bar{\varrho}}d\bar{\varrho}}{\sqrt{\bar{z}_1^2-\bar{\varrho}^2}}\right],$$

---

*Here, the subscript "ρ" is omitted at Γ since, from now on, only circulation constant along the circle of radius ρ will be considered.

and from the above:

$$v_{y0}=\frac{ka}{4\pi R\bar{V}}(\bar{V}+\bar{z}_1)\left(\frac{1}{\sqrt{\bar{z}_1^2-1}}-\arcsin\frac{1}{\bar{z}_1}\right). \qquad (2.25)$$

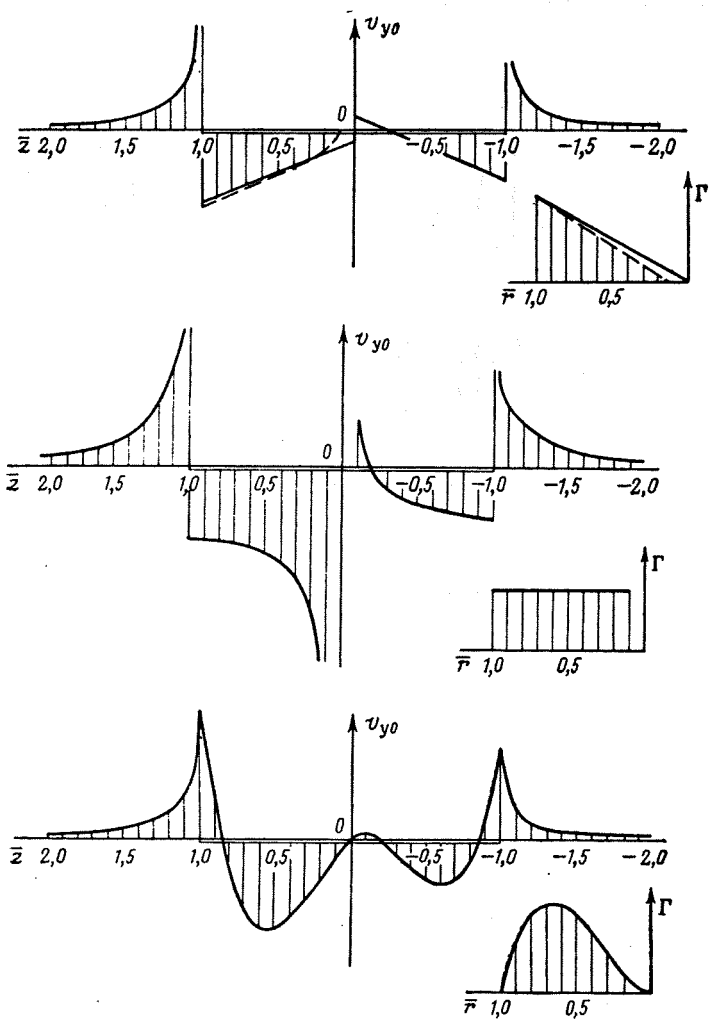

Figure 2.22

In Fig. 2.22, solid lines show the distribution of v_{y0} along the Oz axis for $\overline{V} = 0,2$. Since the circulation is extended to $\overline{\rho} = 0$, the induced velocity has a finite discontinuity at $\overline{z} = 0$, as it goes through the zero value. For $-1 \leq \overline{z} \leq 1$, the variation of v_{y0} is linear. In the same graph, the case of $\Gamma = a[(\overline{\rho} - \overline{r}_0)/(1 - \overline{r}_0)]$ is also shown for $\overline{r}_0 = 0,1$ (broken line). In this case, the expression for computation of v_{y0} takes the following form:

For $\overline{r}_0 \leq \overline{z}_1 \leq 1$,

$$v_{y0} = -\frac{ka}{8R\overline{V}} \frac{(\overline{V} + \overline{z}_1)}{(1 - \overline{r}_0)} \left(1 - \frac{2}{\pi} \arcsin \frac{\overline{r}_0}{\overline{z}_1}\right). \tag{2.26}$$

For $\overline{z}_1 > 1$,

$$v_{y0} = \frac{ka}{4\pi R\overline{V}} (\overline{V} + \overline{z}_1) \left[\frac{1}{\sqrt{\overline{z}_1^2 - 1}} - \frac{\arcsin \frac{1}{\overline{z}_1} - \arcsin \frac{\overline{r}_0}{\overline{z}_1}}{1 - \overline{r}_0} \right]. \tag{2.27}$$

The fact that Γ for the same value at the blade tip becomes zero when $\overline{\rho} = 0.1$ influenced the character of the v_{y0} graph in the $|\overline{z}_1| < 0,3$ region only (broken line on graph). There, $v_{y0} = f(\overline{z}$ becomes curvilinear and reaches zero value for $|\overline{z}_1| = 0,1$.

In Fig. 2.22, a graph of v_{y0} is also shown for the case of $\Gamma = a = const$ when free vortices leave the blade at its ends only ($\overline{\rho} = 1$ and $\overline{\rho} = \overline{r}_0 = 0,1$). Computational formulae for this case are as follows:

For $\overline{r}_0 \leq \overline{z}_1 \leq 1$,

$$v_{y0} = -\frac{\overline{V} + \overline{z}_1}{\sqrt{\overline{z}_1^2 - \overline{r}_0^2}} \frac{ka}{4\pi \overline{V} R}. \tag{2.28}$$

For $\overline{z}_1 > 1$,

$$v_{y0} = (\overline{V} + \overline{z}_1) \left(\frac{1}{\sqrt{\overline{z}_1^2 - 1}} - \frac{1}{\sqrt{\overline{z}_1^2 - \overline{r}_0^2}} \right) \frac{ka}{4\pi \overline{V} R}. \tag{2.29}$$

In Fig. 2.22, another example is given when circulation varies as follows: $\Gamma = a\bar{\rho}^2(1 - \bar{\rho})$. This relationship makes $\Gamma = 0$ at both ends of the blade, while $d\Gamma/d\bar{\rho} = a\bar{\rho}(2 - 3\bar{\rho})$. From Eq. (2.19), we will find that for $1 > \bar{z}_1 > 0$,

$$v_{y0} = -\frac{ka(\bar{V} + \bar{z}_1)}{4\pi R\bar{V}}\left[2\int_0^{\bar{z}_1}\frac{\bar{\varrho}d\bar{\varrho}}{\sqrt{\bar{z}_1^2 - \bar{\varrho}^2}} - 3\int_0^{\bar{z}_1}\frac{\bar{\varrho}^2 d\bar{\varrho}}{\sqrt{\bar{z}_1^2 - \bar{\varrho}^2}}\right],$$

and from the above, $v_{y0} = -\frac{ka(\bar{V} + \bar{z}_1)}{4\pi\bar{V}R}\left(2 - \frac{3}{4}\pi\bar{z}_1\right)\bar{z}_1$. (2.30)

By analogy with Eq. (2.20), only the upper limit of the integral is considered, thus leading, for $\bar{z}_1 > 1$, to:

$$v_{y0} = \frac{ka(\bar{V} + \bar{z}_1)}{4\pi R\bar{V}}\left[\frac{1}{2}\sqrt{\bar{z}_1^2 - 1} + \frac{3}{2}\bar{z}_1^2 \arcsin\frac{1}{\bar{z}_1} - 2\bar{z}_1\right]. \qquad (2.31)$$

It can be seen from the considered graphs (Fig. 2.22) that for $\bar{z}_1 = -\bar{V}$, $v_{y0} = 0$. If $v_{y0} > 0$ at both ends of the blade, then it becomes zero for $\bar{z}_1 = \bar{z}_{10}$, where $\bar{z}_{10}$ represents a value of $\bar{z}_1$ at which Γ becomes maximum. We should also notice that values of the positive induced velocities on the axis z are higher along its positive half (for $\psi = \pi/2$), where the blade is advancing. It is clear from the considered examples that the shape of the Γ distribution strongly influences the distribution of v_{y0}.

Let us now define the lateral component of induced velocity. It can be seen from Fig. 2.18 that

$$d(\Delta v_{z0}) = -d(\Delta v)\sin\vartheta, \quad \sin\vartheta = \frac{y_1}{l}.$$

Following the same procedure as in the development of Eq. (2.11), we obtain

$$d(\Delta v_{z0}) = \frac{2\Delta\Phi_x}{4\pi l^2} y_1 dz$$

and $\Delta v_{z0} = \frac{k\Delta\Gamma_0}{4\pi R\bar{V}}\Delta\hat{v}_{z0}$, (2.32)

where $$\Delta\bar{v}_{z0}=\frac{1}{\pi}\int_{-1}^{1}\frac{\tilde{y}_1(\bar{V}_*+\sin\psi)\,d\tilde{z}}{[\tilde{y}_1^2+(\tilde{z}-\tilde{z}_1)^2]\cos\psi}.$$

Changing the integrated variable and representing the integral as a sum of integrals similar to Eq. (2.12), we find

$$\Delta\bar{v}_{z0}=\tilde{y}_1(\bar{V}_*P+Q). \tag{2.33}$$

At points symmetrical with respect to the $x0z$ plane, induced velocities are of the same magnitude, but of the opposite sign; i.e.,

$$\Delta v_{z0}(\tilde{y}_1)=-\Delta v_{z0}(-\tilde{y}_1). \tag{2.34}$$

5. VELOCITY COMPONENTS INDUCED BY A LONGITUDINAL FREE VORTICITY LAYER OF FINITE LENGTH

We are going to determine velocities induced by longitudinal vortices in planes parallel to the $y0z$ plane. In order to evaluate those velocities, we replace the previous scheme of distribution of longitudinal vortices (see Fig. 2.17) by the three schemes shown in Fig. 2.23 and then will apply the superposition principle. Longitudinal vortices of doubled intensity and extending to infinity (Scheme 1) induce velocities in a plane parallel to the $y0z$ and passing through a coordinate x_1. These velocities, Δv_{y0} and Δv_{g0}, can be determined from Eqs. (2.11) and (2.32). Induced velocities generated by longitudinal vortices of finite length and unit intensity (shown in Schemes 2 and 3) will be called

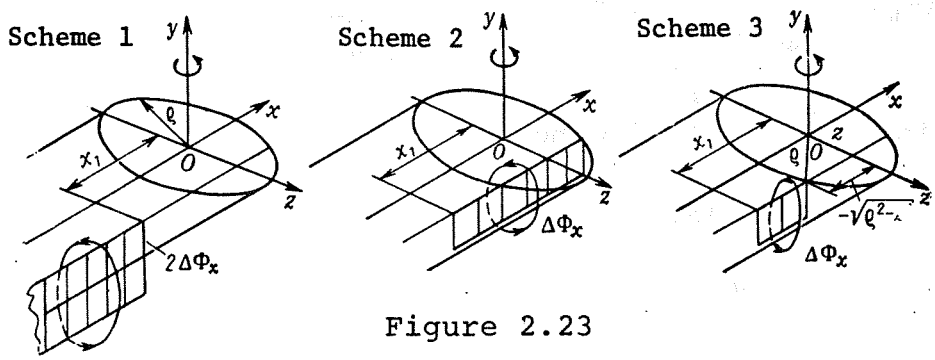

Figure 2.23

Δv_{y_2} and Δv_{z_2}. If $|x_1| < \sqrt{\rho^2 - z^2}$, then the intensity of vortices according to Scheme 3 should be negative. Elementary vortices corresponding to Schemes 2 and 3 have the same strength for the same z. An elementary vortex of Scheme 2 extends from point A to point C, and of Scheme 3 from point B to C (Fig. 2.24).

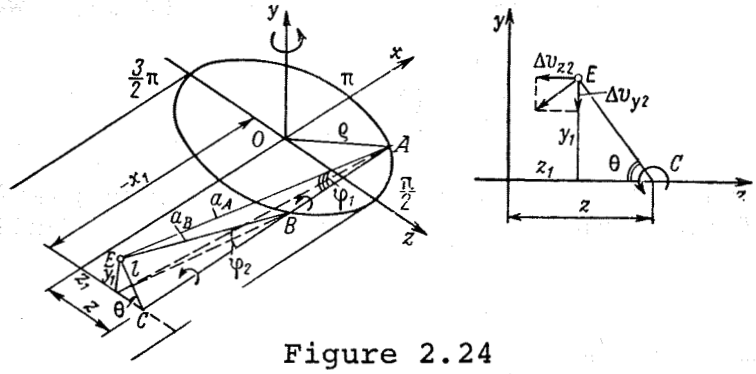

Figure 2.24

The elementary strip AC of the vorticity layer induces the following velocities at point E:

$$d(\Delta v_{AC})_y = \frac{\Delta\Phi_x}{4\pi l}\cos\varphi_1\cos\theta\,dz, \quad d(\Delta v_{AC})_z = \frac{\Delta\Phi_x}{4\pi l}\cos\varphi_1\sin\theta\,dz.$$

It can be seen from Fig. 2.24 that

$$\cos\varphi_1 = \frac{\sqrt{\rho^2 - z^2} - x_1}{a_A}, \quad a_A = \sqrt{(\sqrt{\rho^2 - z^2} - x_1)^2 + y_1^2 + (z - z_1)^2},$$

$$\sin\theta = \frac{y_1}{l}, \quad \cos\theta = \frac{z - z_1}{l}, \quad l = \sqrt{y_1^2 + (z - z_1)^2}.$$

Substituting these quantities, we obtain

$$d(\Delta v_{AC})_y = \frac{\Delta\Phi_x (z - z_1)(\sqrt{\rho^2 - z^2} - x_1)}{4\pi\left[y_1^2 + (z - z_1)^2\right]\sqrt{(\sqrt{\rho^2 - z^2} - x_1)^2 + y_1^2 + (z - z_1)^2}}\,dz,$$

$$d(\Delta v_{AC})_z = \frac{\Delta\Phi_x y_1 (\sqrt{\rho^2 - z^2} - x_1)}{4\pi\left[y_1^2 + (z - z_1)^2\right]\sqrt{(\sqrt{\rho^2 - z^2} - x_1)^2 + y_1^2 + (z - z_1)^2}}\,dz.$$

At the same point E, the elementary strip BC of the vorticity layer induces the following velocities:

$$d(\Delta v_{BC})_y = \frac{\Delta\Phi_x}{4\pi l}\cos\varphi_2\cos\theta\,dz,$$

$$d(\Delta v_{BC})_z = \frac{\Delta\Phi_x}{4\pi l}\cos\varphi_2\sin\theta\,dz.$$

It can be seen from Fig. 2.24 that

$$\cos\varphi_2=-\frac{x_1+\sqrt{\varrho^2-z^2}}{a_B},\quad a_B=\sqrt{(x_1+\sqrt{\varrho^2-z^2})^2+y_1^2+(z-z_1)^2}\ .$$

Consequently

$$d(\Delta v_{BC})_y=-\frac{\Delta\Phi_x(z-z_1)(x_1+\sqrt{\varrho^2-z^2})}{4\pi\left[y_1^2+(z-z_1)^2\right]\sqrt{(x_1+\sqrt{\varrho^2-z^2})^2+y_1^2+(z-z_1)^2}}dz,$$

$$d(\Delta v_{BC})_z=-\frac{\Delta\Phi_x y_1(x_1+\sqrt{\varrho^2-z^2})}{4\pi\left[y_1^2+(z-z_1)^2\right]\sqrt{(x_1+\sqrt{\varrho^2-z^2})^2+y_1^2+(z-z_1)^2}}dz.$$

In the above, we substitute Eq. (2.5) for $\Delta\Phi_x$ and introduce the necessary quantities. Upon replacing $\tilde{z}$ by $\sin\psi$, we integrate with respect to ψ instead of z. In this way, we obtain:

$$\Delta v_{y2}=(\Delta v_{AC})_y+(\Delta v_{BC})_y=\frac{k\Delta\Gamma_Q}{4\pi R\overline{V}}\Delta\widehat{v}_{y2}, \tag{2.35}$$

where $$\Delta\widehat{v}_{y2}=-\frac{1}{2}(\overline{V}_*\widetilde{M}+\widetilde{N}), \tag{2.36}$$

$$\widetilde{M}=\frac{\widetilde{L}-\widetilde{z}_1\widetilde{K}}{\widetilde{y}_1}, \tag{2.37}$$

$$\widetilde{L}=\frac{\widetilde{y}_1}{\pi}\int_{\frac{\pi}{2}}^{\frac{3}{2}\pi}\frac{\sin\psi}{\widetilde{y}_1^2+(\sin\psi-\widetilde{z}_1)^2}\widetilde{W}d\psi, \tag{2.38}$$

$$\widetilde{W}=\frac{\cos\psi-\widetilde{x}_1}{\sqrt{(\cos\psi-\widetilde{x}_1)^2+\widetilde{y}_1^2+(\sin\psi-\widetilde{z}_1)^2}}-$$

$$-\frac{\cos\psi+\widetilde{x}_1}{\sqrt{(\cos\psi+\widetilde{x}_1)^2+\widetilde{y}_1^2+(\sin\psi-\widetilde{z}_1)^2}},$$

$$\widetilde{K}=\frac{\widetilde{y}_1}{\pi}\int_{\frac{\pi}{2}}^{\frac{3}{2}\pi}\frac{\widetilde{W}d\psi}{\widetilde{y}_1^2+(\sin\psi-\widetilde{z}_1)^2}, \tag{2.39}$$

$$\widetilde{N}=\widetilde{U}-\frac{\widetilde{z}_1}{\widetilde{y}_1}\widetilde{L}, \tag{2.40}$$

$$\tilde{U}=\frac{1}{\pi}\int_{\frac{\pi}{2}}^{\frac{3}{2}\pi}\frac{\tilde{W}\sin^2\psi d\psi}{\tilde{y}_1^2+(\sin\psi-\tilde{z}_1)^2}. \tag{2.41}$$

It follows, from Eqs. (2.38) and (2.39), that

$$\tilde{L}(\tilde{x}_1,\tilde{y}_1,-\tilde{z}_1)=-\tilde{L}(\tilde{x}_1,\tilde{y}_1,\tilde{z}_1), \tag{2.42}$$

$$\tilde{K}(\tilde{x}_1,\tilde{y}_1,-\tilde{z}_1)=\tilde{K}(\tilde{x}_1,\tilde{y}_1,\tilde{z}_1) \tag{2.43}$$

and with respect to Eq. (2.37),

$$\tilde{M}(\tilde{x}_1,\tilde{y}_1,-\tilde{z}_1)=-\tilde{M}(\tilde{x}_1,\tilde{y}_1,\tilde{z}_1). \tag{2.44}$$

According to Eqs (2.40) and (2.41), we obtain

$$\tilde{U}(\tilde{x}_1,\tilde{y}_1,-\tilde{z}_1)=\tilde{U}(\tilde{x}_1,\tilde{y}_1,\tilde{z}_1) \tag{2.45}$$

and

$$\tilde{N}(\tilde{x}_1,\tilde{y}_1,-\tilde{z}_1)=\tilde{N}(\tilde{x}_1,\tilde{y}_1,\tilde{z}_1). \tag{2.46}$$

It can be seen from Eq. (2.36) that

$$\Delta\hat{v}_{y2}(-\tilde{x}_1,\tilde{y}_1,\tilde{z}_1)=-\Delta\hat{v}_{y2}(\tilde{x}_1,\tilde{y}_1,\tilde{z}_1) \tag{2.47}$$

and

$$\Delta\hat{v}_{y2}(\tilde{x}_1,-\tilde{y}_1,\tilde{z}_1)=\Delta\hat{v}_{y2}(\tilde{x}_1,\tilde{y}_1,\tilde{z}_1). \tag{2.48}$$

By analogy with Eq. (2.35), we have:

$$\Delta v_{z2}=\frac{k\Delta\Gamma_0}{4\pi R\bar{V}}\Delta\hat{v}_{z2}, \tag{2.49}$$

where

$$\Delta\hat{v}_{z2}=-\frac{1}{2}(\bar{V}\cdot\tilde{K}+\tilde{L}). \tag{2.50}$$

The sign of $\Delta\hat{v}_{z2}$ is defined by the sign of $\tilde{y}_1$. At points symmetrical with respect to the plane of rotation of the rotor (the xOz plane), velocities $\Delta\hat{v}_{z2}$ are of the same magnitude, but of the opposite signs; i.e.,

$$\Delta\hat{v}_{z2}(\tilde{x}_1,-\tilde{y}_1,\tilde{z}_1)=-\Delta\hat{v}_{z2}(\tilde{x}_1,\tilde{y}_1,\tilde{z}_1). \tag{2.51}$$

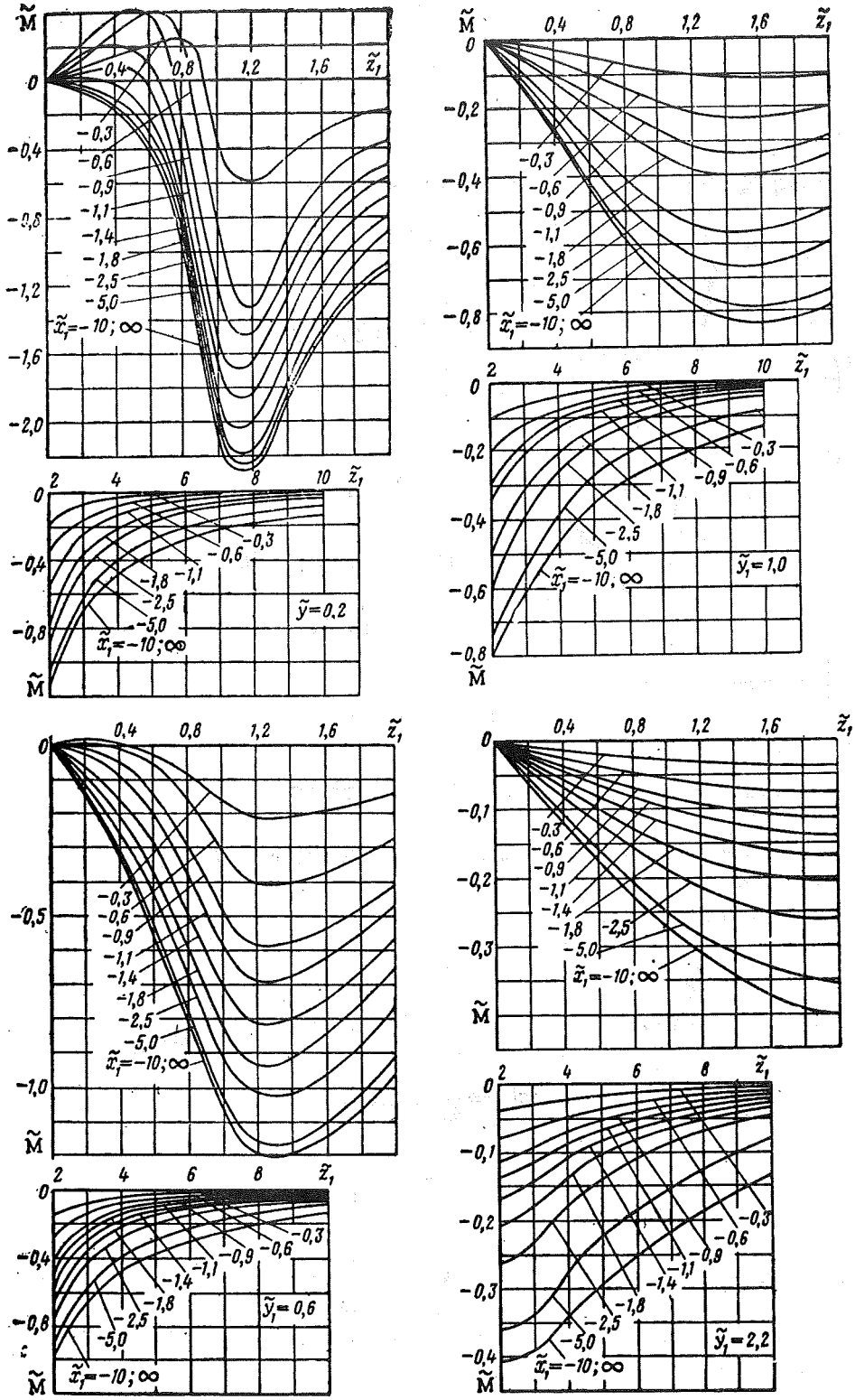

Figure 2.25

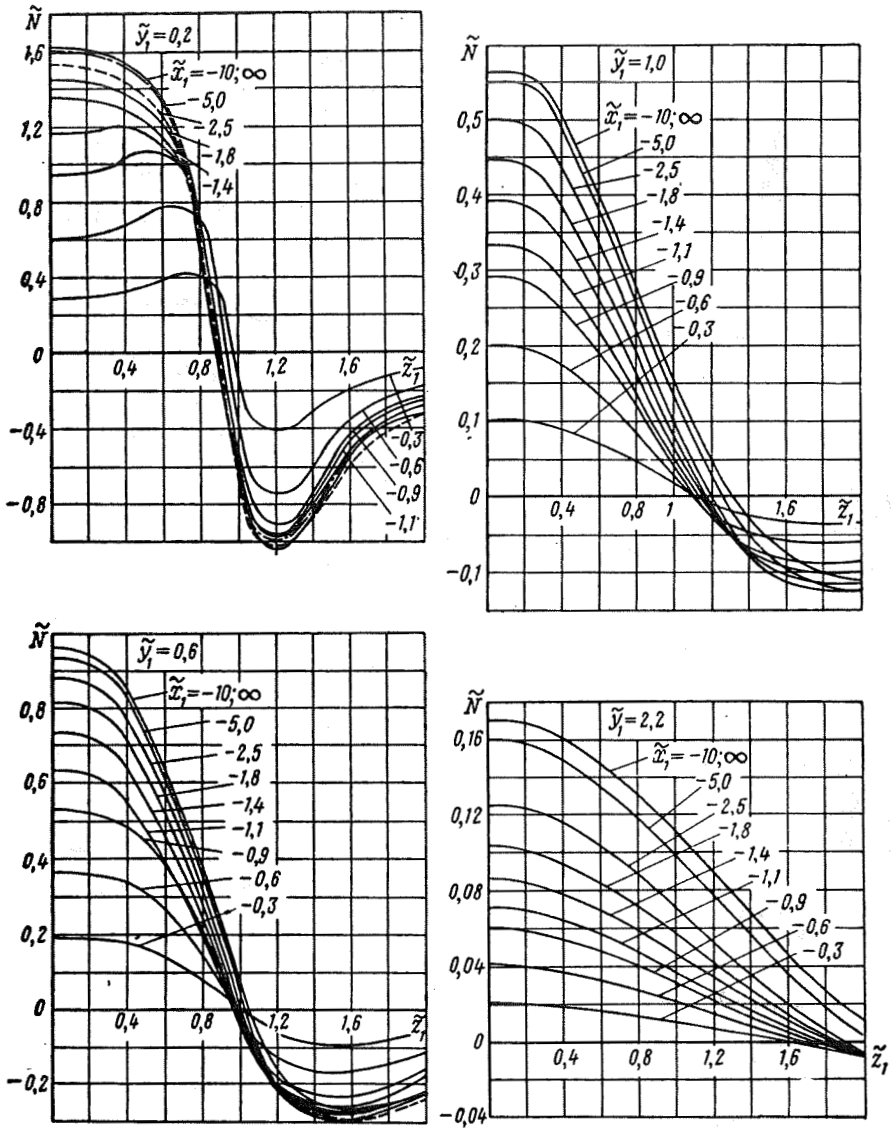
$\tilde{N}$
$\tilde{y}_1 = 0,2$
$\tilde{x}_1 = -10; \infty$
-5,0
-2,5
-1,8
-1,4
1,6
1,2
0,8
0,4
0
-0,4
-0,8
0,4
0,8
1,2
1,6
$\tilde{z}_1$
-0,3
-0,6
-0,9
-1,1
$\tilde{N}$
$\tilde{y}_1 = 1,0$
$\tilde{x}_1 = -10; \infty$
-5,0
-2,5
-1,8
-1,4
-1,1
-0,9
-0,6
-0,3
0,5
0,4
0,3
0,2
0,1
0
-0,1
0,4
0,8
1
1,6
$\tilde{z}_1$
$\tilde{N}$
$\tilde{y}_1 = 0,6$
$\tilde{x}_1 = -10; \infty$
-5,0
-2,5
-1,8
-1,4
-1,1
-0,9
-0,6
-0,3
0,8
0,6
0,4
0,2
0
-0,2
0,4
0,8
1,2
1,6
$\tilde{z}_1$
$\tilde{N}$
$\tilde{y}_1 = 2,2$
$\tilde{x}_1 = -10; \infty$
-5,0
-2,5
-1,8
-1,4
-1,1
-0,9
-0,6
-0,3
0,16
0,12
0,08
0,04
0
-0,04
0,4
0,8
1,2
1,6
$\tilde{z}_1$

Figure 2.26

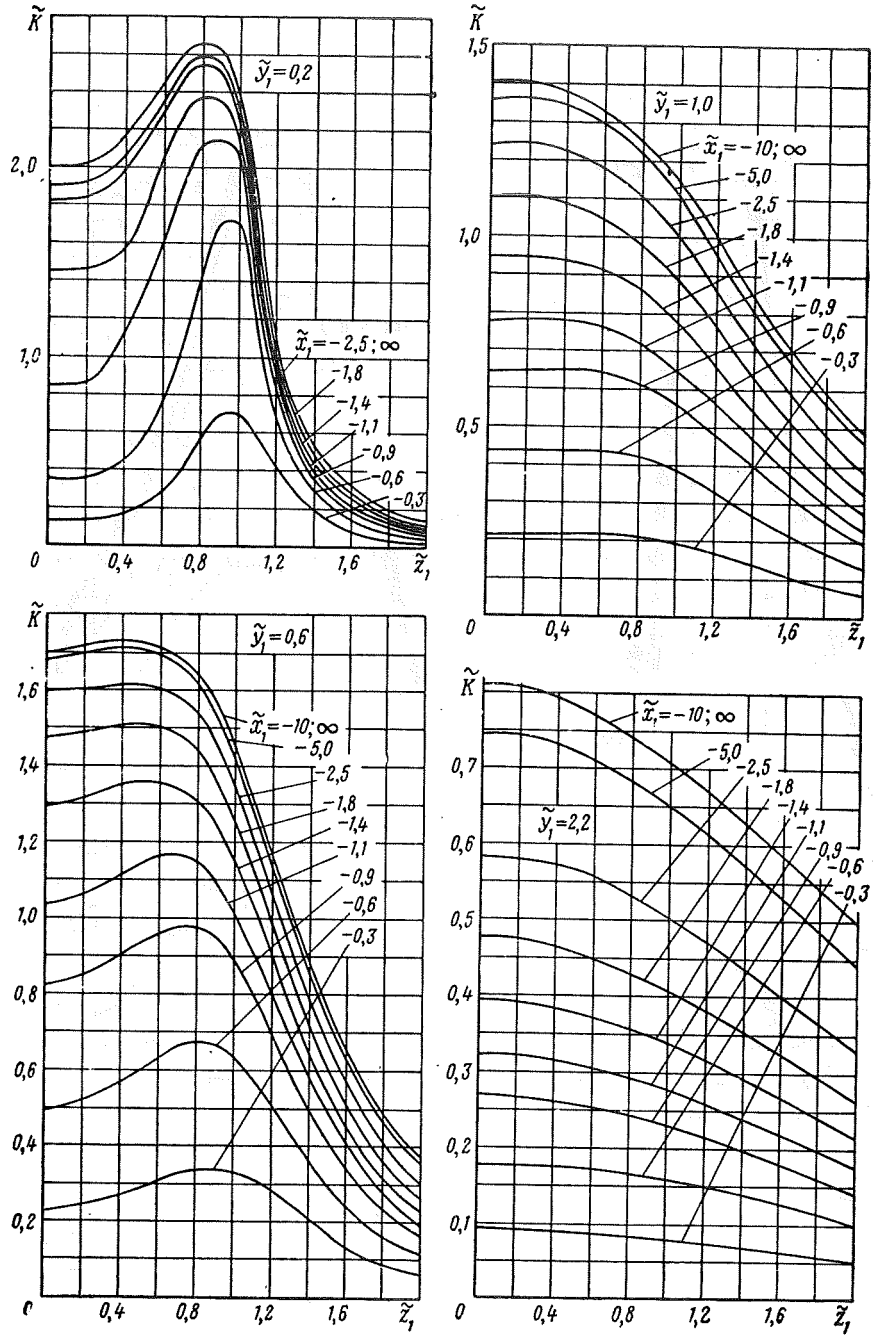
$\tilde{K}$
$\tilde{y}_1=0,2$
$\tilde{x}_1=-2,5;\infty$
-1,8
-1,4
-1,1
-0,9
-0,6
-0,3
2,0
1,0
0
0,4
0,8
1,2
1,6
$\tilde{z}_1$
$\tilde{y}_1=1,0$
$\tilde{x}_1=-10;\infty$
-5,0
-2,5
-1,8
-1,4
-1,1
-0,9
-0,6
-0,3
1,5
1,0
0,5
$\tilde{y}_1=0,6$
$\tilde{x}_1=-10;\infty$
-5,0
-2,5
-1,8
-1,4
-1,1
-0,9
-0,6
-0,3
1,6
1,4
1,2
1,0
0,8
0,6
0,4
0,2
$\tilde{y}_1=2,2$
$\tilde{x}_1=-10;\infty$
-5,0
-2,5
-1,8
-1,4
-1,1
-0,9
-0,6
-0,3
0,7
0,6
0,5
0,4
0,3
0,2
0,1

Figure 2.27

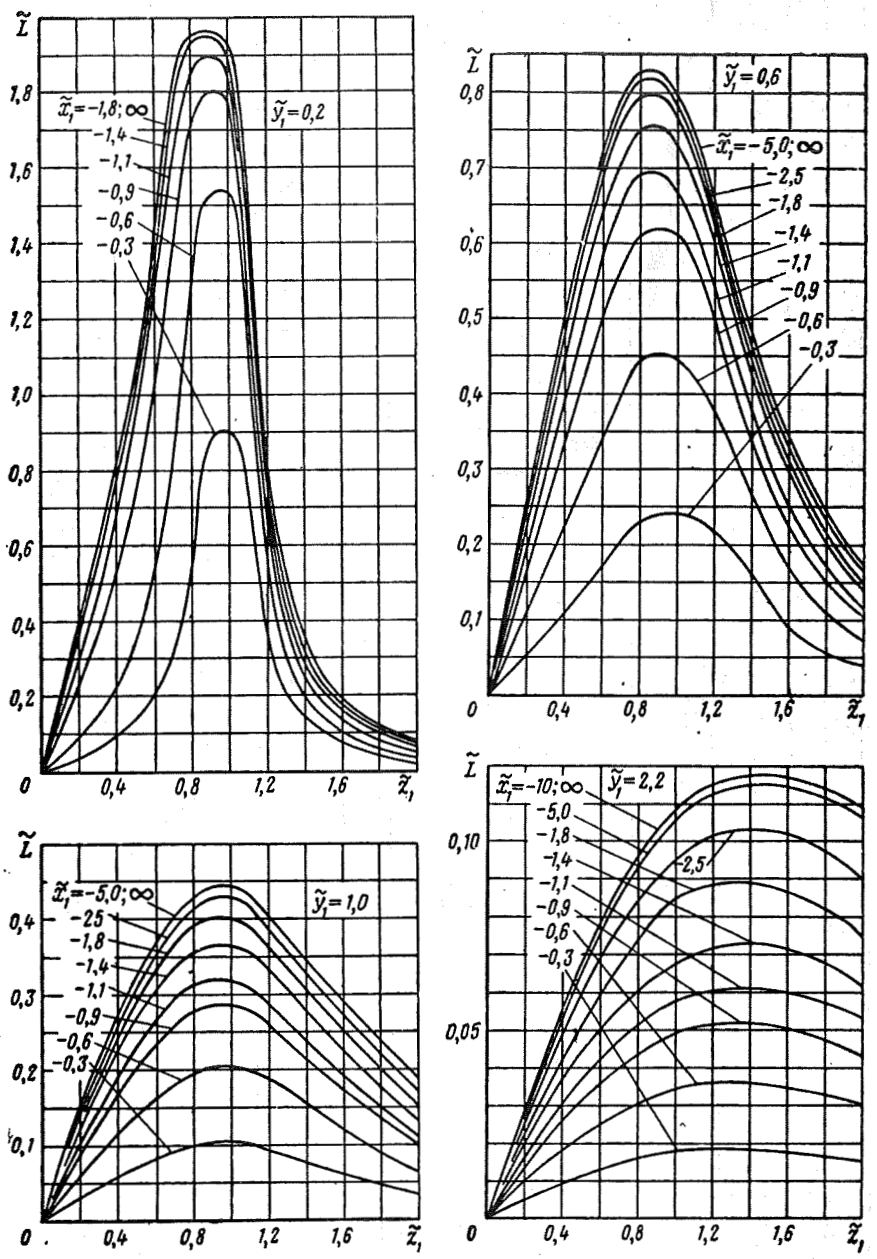
$\tilde{L}$
$\tilde{x}_1$=−1,8; ∞
−1,4
−1,1
−0,9
−0,6
−0,3
$\tilde{y}_1$=0,2
$\tilde{z}_1$
$\tilde{y}_1$=0,6
$\tilde{x}_1$=−5,0; ∞
−2,5
−1,8
−1,4
−1,1
−0,9
−0,6
−0,3
$\tilde{y}_1$=1,0
$\tilde{y}_1$=2,2
$\tilde{x}_1$=−10; ∞
−5,0
−2,5

Figure 2.28

From the expression for $\Delta\hat{v}_{z2}$, it also results that

$$\Delta\hat{v}_{z2}(-\tilde{x}_1, \tilde{y}_1, \tilde{z}_1) = -\Delta\hat{v}_{z2}(\tilde{x}_1, \tilde{y}_1, \tilde{z}_1). \tag{2.52}$$

From the relationships expressed by Eqs. (2.36) - (2.50), we conclude that

$$\Delta\hat{v}_{y2}(\tilde{x}_1, \tilde{y}_1, -\tilde{z}_1) = \frac{1}{2}\left[\overline{V}_* \tilde{M}(\tilde{x}_1, \tilde{y}_1, \tilde{z}_1) - \tilde{N}(\tilde{x}_1, \tilde{y}_1, \tilde{z}_1)\right] \tag{2.53}$$

and

$$\Delta\hat{v}_{z2}(\tilde{x}_1, \tilde{y}_1, -\tilde{z}_1) = -\frac{1}{2}\left[\overline{V}_* \tilde{K}(\tilde{x}_1, \tilde{y}_1, \tilde{z}_1) - L(\tilde{x}_1, \tilde{y}_1, \tilde{z}_1)\right]. \tag{2.54}$$

In this way, $\Delta\hat{v}_{y2}$ and $\Delta\hat{v}_{z2}$ can be found for the negative values of $\tilde{z}_1$ by knowing the functions $\tilde{K}$, $\tilde{L}$, $\tilde{M}$ and $\tilde{N}$ for the positive $\tilde{z}$ only. In Figs. 2.25 - 2.28, there are graphs of $\tilde{M}$, $\tilde{N}$, $\tilde{K}$ and $\tilde{L}$ as functions of $\tilde{z}$ for various values of parameters $\hat{x}_1$ and $\hat{y}_1$. It can be seen from Eqs. (2.35) and (2.11) that for $x_1 \to \infty$, $\Delta\hat{v}_{y2} \to \Delta\hat{v}_{y0}$. By comparing Eqs. (2.32) and (2.49), we also conclude that $\Delta\hat{v}_{z2} \to \Delta\hat{v}_{z0}$. From the accompanying graphs, one can find that for $\tilde{x}_1 < -10$, the functions $\tilde{M}$, $\tilde{N}$, $\tilde{K}$ and $\tilde{L}$ remain practically unchanged. Due to this, it is possible to assume, with sufficient accuracy, that

$$\Delta\hat{v}_{y2}(\tilde{x}_1 \leqslant -10, \tilde{y}_1, \tilde{z}_1) = \Delta\hat{v}_{y0}(\tilde{y}_1, \tilde{z}_1), \tag{2.55}$$

$$\Delta\hat{v}_{z2}(\tilde{x}_1 \leqslant -10, \tilde{y}_1, \tilde{z}_1) = \Delta\hat{v}_{z0}(\tilde{y}_1, \tilde{z}_1). \tag{2.56}$$

6. VELOCITY COMPONENTS INDUCED BY A ROTOR IN AN ARBITRARY POINT OF SPACE

In the preceding sections, we obtained formulae for the velocity components induced by various systems of vorticity layers equivalent to the free vorticity layer that left the periphery of a circle of radius ρ. Now, we can sum all those components and present the results in a final form:

$$\Delta v_x = \frac{k\Delta\Gamma}{4\pi R\overline{V}}\Delta\hat{v}_x, \tag{2.57}$$

$$\Delta v_y = \frac{k\Delta\Gamma}{4\pi R\bar{V}}\Delta\hat{v}_y, \tag{2.58}$$

$$\Delta v_z = \frac{k\Delta\Gamma}{4\pi R\bar{V}}\Delta\hat{v}_z. \tag{2.59}$$

where

$$\Delta\hat{v}_y = \Delta\hat{v}_{y1} + \Delta\hat{v}_{y02}, \tag{2.60}$$

$$\Delta\hat{v}_{y02} = \Delta\hat{v}_{y0} + \Delta\hat{v}_{y2}, \tag{2.61}$$

$$\Delta\hat{v}_z = \Delta\hat{v}_{z0} + \Delta\hat{v}_{z2}. \tag{2.62}$$

According to Eqs. (2.36) and (2.55); (2.50) and (2.56):

$$\Delta\hat{v}_{y02} = -\frac{1}{2}[\bar{V}_*(\tilde{M}_\infty + \tilde{M}) + (\tilde{N}_\infty + \tilde{N})], \tag{2.63}$$

$$\Delta\hat{v}_z = -\frac{1}{2}[\bar{V}_*(\tilde{K}_\infty + \tilde{K}) + (\tilde{L}_\infty + \tilde{L})]. \tag{2.64}$$

Formulae and graphs for determination of $\Delta\hat{v}_x$ and $\Delta\hat{v}_{y1}$ are given in Section 3, and for $\Delta\hat{v}_{y2}$ and $\Delta\hat{v}_z$, in Section 5. It is apparent from the considered formulae that for $x \to \infty$

$$\Delta\hat{v}_{y1} \to 0, \quad \Delta\hat{v}_y \to 2\Delta\hat{v}_{y0}.$$

In this way, it is possible to postulate the following theorem: At sufficiently large distances downstream from the lifting airscrew, the vertical component of induced velocity is equal to twice its value in the xOz plane, as long as the y coordinates remain the same. Similarly, for $x \to \infty$, $\Delta\hat{v}_z \to 2\Delta\hat{v}_{z0}$.

In order to define velocity induced at a given point in space $(\bar{x}_1, \bar{y}_1, \bar{z}_1)$ by the free vortices springing from all sections of the blade, it is necessary to sum the values of Δv_x, Δv_y, Δv_z. For instance, for the projection of induced velocity on the x axis, we have

$$v_x(\bar{x}_1, \bar{y}_1, \bar{z}_1) = \sum_{\bar{\varrho}=\bar{r}}^{\bar{\varrho}=1,0} \Delta v_x^{(\varrho)}(\bar{x}_1, \bar{y}_1, \bar{z}_1) =$$

$$= \frac{k}{4\pi R\bar{V}} \sum_{\bar{\varrho}=\bar{r}_0}^{\bar{\varrho}=} \Delta\hat{v}_x^{(\varrho)}(\ldots)\Delta\Gamma_\varrho, \tag{2.65}$$

where $$\Delta\Gamma_\varrho = \Gamma_{\varrho-\Delta} - \Gamma_{\varrho+\Delta}. \qquad (2.66)$$

According to Eq. (2.2), the signs of $\Delta\Gamma_\rho$ will be determined from Eq. (2.66) (see Fig. 2.29).

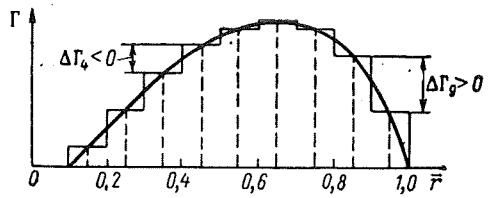

Figure 2.29

If the distribution of circulation along the blade is averaged for one revolution and given as a curve, then by replacing it with elements of straight lines (as in Fig. 2.29), we can obtain an approximate graph. Such graph is suitable for calculations, as it gives incremental variations of circulation at stations $\bar{\rho} = 1,0;\ 0,9;\ \ldots;\ 0,1$, while values between points $1,0 - 0,9;\ 0,9 - 0,8$, etc., remain constant. In Fig. 2.29, segments of constant circulation are assumed to be $\Delta\bar{\rho} = 0,1$. Making intervals of $\Delta\bar{\rho}$ smaller and increasing the number of intervals in Eqs. (2.70) - (2.72), it is possible to approach the original curve of the circulation distribution with any desired degree of accuracy. However, actual experience indicates that for practical calculations, it is sufficient to select $\Delta\bar{\rho} = 0,1$. Going now to the relative values

$$\bar{v}_x = \frac{v_x}{\omega R}, \quad \bar{\Gamma} = \frac{\Gamma}{\omega R^2}, \quad \Delta\tilde{\Gamma}_\varrho = \frac{\Delta\bar{\Gamma}_\varrho}{\bar{\Gamma}_{cp}}, \text{ we obtain}$$

$$\bar{v}_x(\bar{x}_1, \bar{y}_1, \bar{z}_1) = \frac{k\bar{\Gamma}_{cp}}{4\pi\bar{V}}\hat{v}_x(\bar{x}_1, \bar{y}_1, \bar{z}_1), \qquad (2.67)$$

$$\bar{v}_y(\bar{x}_1, \bar{y}_1, \bar{z}_1) = \frac{k\bar{\Gamma}_{cp}}{4\pi\bar{V}}\hat{v}_y(\bar{x}_1, \bar{y}_1, \bar{z}_1), \qquad (2.68)$$

$$\bar{v}_z(\bar{x}_1, \bar{y}_1, \bar{z}_1) = \frac{k\bar{\Gamma}_{cp}}{4\pi\bar{V}}\hat{v}_z(\bar{x}_1, \bar{y}_1, \bar{z}_1), \qquad (2.69)$$

where

$$\hat{v}_x(\bar{x}_1, \bar{y}_1, \bar{z}_1) = \sum_{\bar{\varrho}=\bar{r}_0}^{\bar{\varrho}=1,0} \Delta\hat{v}_x^{(\varrho)}(\ldots)\Delta\tilde{\Gamma}_\varrho, \qquad (2.70)$$

$$\hat{v}_y(\bar{x}_1, \bar{y}_1, \bar{z}_1) = \sum_{\bar{\varrho}=\bar{r}_0}^{\bar{\varrho}=1,0} \Delta\hat{v}_y^{(\varrho)}(\bar{x}_1, \bar{y}_1, \bar{z}_1)\Delta\tilde{\Gamma}_\varrho, \qquad (2.71)$$

$$\hat{v}_z(\bar{x}_1, \bar{y}_1, \bar{z}_1) = \sum_{\bar{\varrho}=\bar{r}_0}^{\bar{\varrho}=1,0} \Delta\hat{v}_z^{(\varrho)}(\ldots)\Delta\tilde{\Gamma}_\varrho. \qquad (2.72)$$

Here, Γ_{cp} represents relative circulation averaged over the disc, and determination of its value is given in Section 1 of Chapter III.

In order to illustrate the application of the graphical approach to the determination of $\Delta\hat{v}^{\rho}_{x}$, $\Delta\hat{v}^{\rho}_{y}$ and $\Delta\hat{v}^{\rho}_{z}$ appearing in Eqs. (2.70) - (2.72) we will consider an example of establishing a working formula for $\hat{v}_z(\overline{x}_1, \overline{y}_1, \overline{z}_1)$ when $\overline{V} = 0,2$; $\overline{x}_1 = -1,2$; $\overline{y}_1 = 0,2$; $\overline{z}_1 = 0,2$. In the expanded form, Eq. (2.72) can be written as follows:

$$\hat{v}_z(\ldots)=\Delta\hat{v}_z^{(1)}(\ldots)\Delta\tilde{\Gamma}_1+\Delta\hat{v}_z^{(2)}\Delta\tilde{\Gamma}_2+\ldots+\Delta\hat{v}_z^{(9)}\Delta\tilde{\Gamma}_9+\Delta\hat{v}_z^{(10)}\Delta\tilde{\Gamma}_{10}.$$

Here, $\Delta\tilde{\Gamma}_1 \ldots \Delta\tilde{\Gamma}_{10}$ represents the difference in the ordinate values corresponding to the relative radii $\overline{\rho} = .1 \ldots \overline{\rho} = 1$.

1. For $\overline{\rho} = .1$, we find $\tilde{x}_1 = \overline{x}_1/\overline{\rho} = -12$;

$$\tilde{y}_1=\frac{\overline{y}_1}{\overline{\rho}}=2; \quad \tilde{z}_1=\frac{\overline{z}_1}{\overline{\rho}}=2; \quad \overline{V}_*=\frac{\overline{V}}{\overline{\rho}}=2.$$

From Fig. 2.27, we find that for the given $\tilde{x}_1$ and $\tilde{z}_1$, $\tilde{K}_{12} = \tilde{K}_{\infty} = 0,520$ when $\tilde{y}_1 = 1,6$ and $\tilde{K}_{12} = \tilde{K}_{\infty} = 0,490$ when $\tilde{y}_1 = 2,2$. Using linear interpolation, we find that for $\tilde{y}_1 = 2,0$, $\tilde{K}_{12} = \tilde{K}_{\infty} = 0,500$. Similarly, from Fig. 2.28, we find that when $\tilde{y}_1 = 1,6$ then $\tilde{L}_{12} = \tilde{L}_{\infty} = 0,155$; at $\tilde{y}_1 = 2,2$, $\tilde{L}_{12} = \tilde{L}_{\infty} = 0,109$. Again interpolating linearly, we find that for $\tilde{y}_1 = 2,0$, $\tilde{L}_{12} = \tilde{L}_{\infty} = 0,124$. From Eq. (2.64), we obtain

$$\Delta\hat{v}_z^{(1)}(-1,2;\ 0,2;\ 0,2)=-\frac{1}{2}[2(0,5+0,5)+(0,124+0,124)]=-1,124.$$

2. For $\overline{\rho} = 0,2$, we have $\tilde{x} = -6,0$, $\tilde{y} = 1,0$, $\tilde{z} = 1,0$, $\overline{V}_* = 1,0$. From Fig. 2.27, we find that for $\tilde{y}_1 = 1,0$, $\tilde{L}_6 = \tilde{L}_{\infty} = 0,45$. Eq. (2.64) gives

$$\Delta\hat{v}_z^{(2)}(-1,2;\ 0,2;\ 0,2)=-\frac{1}{2}[1(1,11+1,13)+(0,45+0,45)]=-1,57.$$

In a similar way, we find all the remaining values of $\Delta v_z^{(\rho)}$. Finally, we obtain

$$\hat{v}_z(-1,2;\ 0,2;\ 0,2)=-0,726\Delta\tilde{\Gamma}_{10}-0,831\Delta\tilde{\Gamma}_9-0,929\Delta\tilde{\Gamma}_8-1,063\Delta\tilde{\Gamma}_7-$$
$$-1,213\Delta\tilde{\Gamma}_6-1,403\Delta\tilde{\Gamma}_5-1,612\Delta\tilde{\Gamma}_4-1,760\Delta\tilde{\Gamma}_3-1,570\Delta\tilde{\Gamma}_2-1,124\Delta\tilde{\Gamma}_1.$$

In Appendix V, one can find tables of coefficients for the formulae needed to determine $\hat{v}_y(\overline{r})$ at $\overline{V} = 0,15$; $0,25$; $0,35$ and various values of ψ. From those formulae, we can obtain the induced velocity distribution in the rotor plane.

7. MEAN CIRCULATION AROUND BLADE SECTION

It was shown in the preceding considerations that in order to determine components of the induced velocity, it is necessary to know the distribution of the mean circulation along the blade (averaged over one revolution).

According to Eq. (2.1):

$$\Gamma_0=\frac{1}{2\pi}\int_0^{2\pi}\Gamma(\bar{\varrho},\psi)\,d\psi.$$

However, in a theory that would take into account only mean circulation; i.e., assuming its constant value for any blade station around a complete rotor revolution, it is possible to relay the magnitude of that circulation to the average thrust developed during one rotor revolution. According to Eq. (1.12)

$$T=\varkappa\frac{k}{2\pi}\int_0^{2\pi}d\psi\int_{r_0}^{R}\frac{dT}{dr}\,dr.$$

Changing the order of integration, the above expression can be rewritten as

$$T=\varkappa k\int_{r_0}^{R}\left(\frac{1}{2\pi}\int_0^{2\pi}\frac{dT}{dr}\,d\psi\right)dr, \tag{2-73}$$

where, according to Eq. (2.6):

$$\frac{dT}{dr}=\varrho\Gamma(r,\psi)W.$$

Expressing the above relationship in relative quantities, we obtain

$$\frac{d\overline{T}}{d\bar{r}}=\overline{\Gamma}(\bar{r},\psi)\overline{W}. \tag{2.74}$$

At a given blade station, value of $d\overline{\Gamma}/d\overline{r}$ corresponding to one rotor revolution will be

$$\frac{1}{2\pi}\int_0^{2\pi}\frac{d\overline{T}}{d\bar{r}}\,d\psi=\frac{1}{2\pi}\int_0^{2\pi}\overline{\Gamma}(\bar{r},\psi)\overline{W}\,d\psi. \tag{2.75}$$

We take the circulation out of the integral sign, define its average value as $\bar{\Gamma}_r$, and consider that it represents an average over the circle of radius r.

Then, in the light of Eq. (1.2), we obtain

$$\bar{\Gamma}_r = \frac{1}{2\pi\bar{r}} \int_0^{2\pi} \bar{\Gamma}(\bar{r}, \psi) \overline{W} d\psi. \tag{2.76}$$

Consideration of Eqs. (2.74), (1.4), (1.6) and (1.7) leads to:

$$\bar{\Gamma}(\bar{r}, \psi) \overline{W} = \frac{1}{2} \bar{b} \overline{W}_1^2 (c_y \cos\beta_1 + c_{xp} \sin\beta_1).$$

From this, taking into account Eq. (1.8), we find

$$\bar{\Gamma}(\bar{r}, \psi) = \frac{1}{2} c_y \bar{b} \overline{W} \frac{1 + \frac{c_{xp}}{c_y} \operatorname{tg}\beta_1}{\cos\beta_1} \approx \frac{1}{2} c_y \bar{b} \overline{W}. \tag{2.77}$$

In accordance with the hypothesis of the validity of the application of static values of blade section lift coefficients, we have $c_y = a_\infty \alpha$, where $a_\infty = dc_y/d\alpha$ is the slope of the $c_y = f(\alpha)$ curve for infinite aspect ratio ($\lambda = \infty$). The above approach is acceptable for $\alpha < \alpha_{KP}$. In the *reversed flow region**, blade sections exceed stall angles of attack for $\bar{r} < -\mu \sin\psi$ and $\pi < \psi < 2\pi$. It should be noted that blade sections of a rotor may also experience local stall due to the interaction with blade tip vortices[3]. However, those local increases of the angle of attack have no practical influence on the magnitude of forces and moments averaged over the whole disc, and thus may be neglected.

It can be seen from Fig. 1.2 that the actual angle of attack of a blade section is

$$\alpha = \varphi + \beta_* + \Delta\alpha + \Delta\delta = \varphi + \beta_1. \tag{2.78}$$

If one takes into consideration the flight control inputs and influence of the flapping control devices, then the pitch angle of a blade section would be**:

$$\varphi = \varphi_0 + \Delta\varphi - \bar{k}\beta + \theta_1 \cos\psi + \theta_2 \sin\psi. \tag{2.79}$$

---

*For instance, see Refs. 14 and 92
**For details, see Refs. 66, 75 and 92

Here, θ_1 and θ_2 are, respectively, the blade pitch angles due to control inputs at $\psi = 0$ and $\psi = \pi/2$. From Fig. 1.2, we find:

$$\beta_1 \approx \operatorname{tg}\beta_1 = \frac{\overline{V}\sin\alpha_в + \bar{v}_y + \bar{v}_\delta}{\overline{W}}, \tag{2.80}$$

$$\Delta\alpha = \frac{\bar{v}_y}{\overline{W}}, \quad \Delta\delta = \frac{\bar{v}_\delta}{\overline{W}},$$

$$\beta_* = \frac{V\sin\alpha_в}{W} = \frac{\mu\operatorname{tg}\alpha_в}{\overline{W}} \approx \frac{\mu\alpha_в}{\overline{W}}. \tag{2.81}$$

We introduce the above expressions into Eq. (2.78), express β according to Eq. (1.17), and substitute the obtained results into Eq. (2.77); then

$$\bar{\Gamma}(\bar{r}, \psi) = \frac{1}{2} a_\infty \bar{b}\left[(\varphi_э + \theta_{1э}\cos\psi + \theta_{2э}\sin\psi)\overline{W} + \bar{v}_y(\bar{r}, \psi) + \bar{v}_\delta + \mu\alpha_в\right]. \tag{2.82}$$

Here, the following notations are introduced:

$$\varphi_э = \varphi_{0э} + \Delta\varphi, \quad \varphi_{0э} = \varphi_0 - \bar{k}a_0, \quad \theta_{1э} = \theta_1 + \bar{k}a_1, \quad \theta_{2э} = \theta_2 + \bar{k}b_1.$$

After performing integration indicated by Eq. (2.76), we obtain an expression for the average circulation at station r.

$$\bar{\Gamma}_r = \frac{1}{2} a_\infty \bar{b}\left[\varphi_э \bar{r}\left(1 + \frac{1}{2}\frac{\mu^2}{\bar{r}^2}\right) + \mu(\alpha_в + \theta_{2э}) + \right.$$

$$\left. + \bar{v}_W(\bar{r}) + \frac{1}{2\pi\bar{r}}\int_0^{2\pi} \bar{v}_\delta \overline{W} d\psi\right]. \tag{2.83}$$

If the flapping motion is of the first-harmonic type, then

$$\int_0^{2\pi} \bar{v}_\delta \overline{W} d\psi = 0, \tag{2.84}$$

This means that although the flapping motion varies the circulation at different azimuth angles, it does not influence its average (mean) value which remains proportional to the average thrust*.

---

*Glauert[14] showed that flapping motion described by the first harmonic of the Fourier series has no influence on the rotor thrust.

Let us determine

$$\bar{v}_W(\bar{r}) = \frac{1}{2\pi\bar{r}} \int_0^{2\pi} \bar{v}_y(\bar{r}, \psi)\, \overline{W} d\psi = \frac{1}{2\pi} \int_0^{2\pi} \bar{v}_y(\bar{r}, \psi)\, d\psi +$$

$$+ \frac{\mu}{2\pi\bar{r}} \int_0^{2\pi} \bar{v}_y(\bar{r}, \psi) \sin\psi d\psi. \qquad (2.85)$$

The first term represents induced velocity corresponding to a given blade station; averaged over one revolution:

$$\bar{v}_r = \frac{1}{2\pi} \int_0^{2\pi} \bar{v}_y(\bar{r}, \psi)\, d\psi. \qquad (2.86)$$

Instead of integrating along the whole circle, from 0 to 2π, it is possible to do it along a half-circle within the intervals of $\pi/2 \leq \psi \leq (3/2)\pi$ and represent the result as a sum of velocities at points symmetrical with respect to the Oz axis (Points A and B in Fig. 2.30). In this way, we obtain:

$$\bar{v}_r = \frac{1}{2\pi} \int_{\frac{\pi}{2}}^{\frac{3}{2}\pi} [\bar{v}_y(\bar{r}, \psi) + \bar{v}_y(\bar{r}, \pi - \psi)]\, d\psi. \qquad (2.87)$$

As shown in Sections 4 - 6,

$$\bar{v}_y(\bar{r}, \psi) = \bar{v}_{y0}(\bar{z}) + \bar{v}_{y1}(\bar{r}, \psi) + \bar{v}_{y2}(\bar{r}, \psi), \quad (\bar{z} = \bar{r}\sin\psi). \qquad (2.88)$$

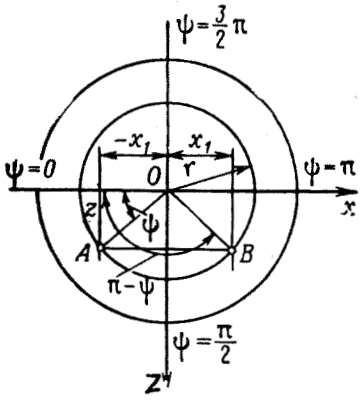

Figure 2.30

It was indicated in Sections 3 and 5 that at points symmetrical with respect to the plane of coordinates v_{y1} and v_{y2} are of equal magnitude, but of the opposite signs. Consequently,

$$\bar{v}_y(\bar{r}, \psi) + \bar{v}_y(\bar{r}, \pi - \psi) = 2\bar{v}_{y0}(\bar{z}). \qquad (2.89)$$

Introducing the above expression into Eq. (2.87), we obtain

$$\bar{v}_r = \frac{1}{\pi} \int_{\frac{\pi}{2}}^{\frac{3}{2}\pi} \bar{v}_{y0}(\bar{z})\, d\psi, \qquad (2.90)$$

This means that the induced velocity at a blade station, when averaged over one revolution depends only on $v_{y0}(\bar{z})$; in other words, velocity induced on the Oz axis by longitudinal

straight-line vortices extending from the z axis to infinity (see Fig. 2.18). The integral of Eq. (2.90) is computed in Appendix I, where it is shown that

$$\bar{v}_r = -\frac{k\bar{\Gamma}_\rho(\bar{r})}{4\pi\bar{V}}.$$

If, according to the previously formulated assumption, we substitute $\bar{\Gamma}_r$ for $\bar{\Gamma}_\rho(\bar{r})$, then we will have

$$\bar{v}_r = -\frac{k\bar{\Gamma}_r}{4\pi\bar{V}}. \tag{2.91}$$

From this, the following theorem can be deduced: Induced velocity, averaged over a circle lying inside of the rotor disc, depends only on the circulation value, also averaged over this circle.

In other words, average induced velocity at a given blade station is not influenced by the free vortices springing from other stations. This presentation is in complete accord with the vortex theory of N.E. Joukowsky for propellers. For the propeller, induced velocity at an elementary ring is defined only by circulation along this ring. If the velocity of axial displacement of the airscrew is large in comparison with the axial induced velocity, then it may be assumed that $V_1 = V + v \approx V$, where V is the velocity of axial displacement. In this case, the expression for the axial induced velocity at radius r, as given in the Joukowsky vortex theory of propellers, becomes identical* with Eq. (2.91). Consequently, the relationships expressed by Eq. (2.91) represent an extension of the Joukowsky propeller theory to the oblique flow regions of an airscrew. It should be noted that Eq. (2.91) indicates the possibilities of determining induced velocities, averaged over the circle, also through the momentum theory of Yur'yev-Sabinin[92].

We determine the second integral in Eq. (2.85) by designating it

$$\bar{v}_\mu(\bar{r}) = \frac{\mu}{2\bar{r}}\bar{v}_{s1}, \tag{2.92}$$

where

$$\bar{v}_{s1}(\bar{r}) = \frac{1}{\pi}\int_0^{2\pi}\bar{v}_y(\bar{r}, \psi)\sin\psi\, d\psi. \tag{2.93}$$

*See formula on p. 99 of Ref. 21.

The quantity $\bar{v}_{s1}(\bar{r})$ represents a coefficient at $\sin\psi$ in the development of $\bar{v}_y(\bar{r},\psi)$ into the Fourier series. Here, we are going to pursue the same approach as in the development of the formula for $\bar{v}_r$; i.e., we take a sum of induced velocities at points symmetrical with respect to the Oz axis (see Fig. 2.30). As a result, we obtain

$$\bar{v}_\mu(\bar{r})=\frac{\mu}{2\pi\bar{r}}\int_{\frac{\pi}{2}}^{\frac{3}{2}\pi}\left[\bar{v}_y(\psi,\bar{r})\sin\psi+\bar{v}_y(\pi-\psi,\bar{r})\sin(\pi-\psi)\right]d\psi.$$

Here (as in the determination of $\bar{v}_r$), induced velocities $\bar{v}_{y1}$ and $\bar{v}_{y2}$ are cancelled, and in analogy with Eq. (2.90), we have

$$\bar{v}_\mu(\bar{r})=\frac{\mu}{\pi\bar{r}}\int_{\frac{\pi}{2}}^{\frac{3}{2}\pi}\bar{v}_{y0}(\bar{z})\sin\psi\,d\psi. \tag{2.94}$$

The quantity $\bar{v}_\mu(\bar{r})$ appears as a result of action on a circle of radius r of free (trailing) vortices springing from all sections of the blade. Similarly to Eq. (2.18), we can define

$$\bar{v}_\mu(\bar{r})=-\frac{k}{4\pi\bar{V}}\int_{\bar{r}_0}^{1}\Delta\hat{v}_\mu^{(\varrho)}(\bar{r})\frac{d\bar{\Gamma}_\varrho}{d\bar{\varrho}}\,d\bar{\varrho}. \tag{2.95}$$

This integral is evaluated in Appendix II, where it is shown that

$$\bar{v}_\mu(\bar{r})=-\frac{\mu}{\bar{r}^2}\frac{k\bar{\Gamma}_\varrho(\bar{r})}{4\pi}.$$

Substituting $\bar{\Gamma}_r$ for $\bar{\Gamma}_\rho(\bar{r})$, we have

$$\bar{v}_\mu(\bar{r})=-\frac{\mu}{\bar{r}^2}\frac{k\bar{\Gamma}_r}{4\pi}. \tag{2.96}$$

Taking into consideration Eqs. (2.85), (2.86), (2.91), (2.92), (2.93) and (2.96), we finally obtain

$$\bar{v}_w(\bar{r})=-\left(1+\frac{\mu\bar{V}}{\bar{r}^2}\right)\frac{k\bar{\Gamma}_r}{4\pi\bar{V}}. \tag{2.97}$$

Now, substituting Eq. (2.97) into Eq. (2.83) and solving the equation with respect to $\bar{\Gamma}_r$, we find

$$\bar{\Gamma}_r = B\left[\varphi_э \bar{r}\left(1+\frac{1}{2}\,\frac{\mu^2}{\bar{r}^2}\right)+\mu\alpha_э\right], \qquad (2.98)$$

where $$B=\frac{4\pi a_\infty \mu \bar{b}}{8\pi\mu + a_\infty k\bar{b}\left(1+\frac{\mu^2}{\bar{r}^2}\right)},\quad \alpha_э=\alpha_в+\theta_{2э}.$$

The above performed substitution of μ for $\bar{V}$ does not introduce any noticeable error. It should be noted that for $\bar{r} < \mu$, $\bar{\Gamma}_r$ begins to decrease smoothly from its value at $\bar{r} = \mu$, becoming zero at the blade root station ($r = r_0$). For $\bar{V} \leq 0,45$, no noticeable influence of that approximation ($\mu \approx \bar{V}$) on the final results can be detected.

To illustrate the agreement between analytical predictions and experimental data, Fig. 2.31 is shown.

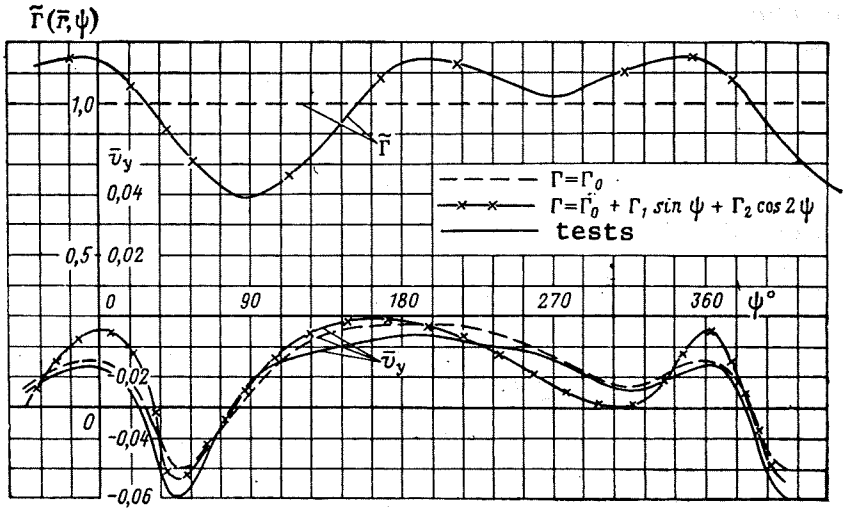

Figure 2.31

Here, both calculated and experimentally obtained curves of $\bar{v}_y = f(\psi)$ are plotted for $\bar{r} = 0,7$, $\bar{y}_1 = -0,1$ (below the rotor disc) and $\mu = 0,15$.

A comparison was made for the following parameter values: $\eta_* = 1$;* $\Delta\phi_\Sigma = 0$; $\alpha_э = 0$; $c_т = 0,012$; $\sigma = 0,07$. Calculations were performed; first assuming that induced velocity depends

*For determination of η_*, see Fig. 2.32

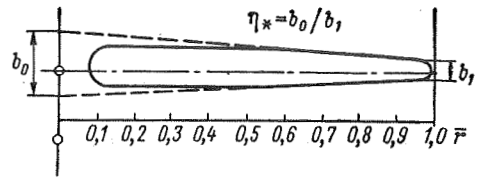

Figure 2.32

only on the circulation value averaged with respect to the azimuth (i.e., at $\partial\tilde{\Gamma}/\partial\psi = 0$); and second, that circulation varies according to the following law: $\tilde{\Gamma} = \tilde{\Gamma}_0 + \tilde{\Gamma}_1 \sin\psi + \tilde{\Gamma}_2 \cos 2\psi$, which was established by P.V. Zanozin in 1961 in his extension of the theory of the airscrew with a flat vortex wake. This law* of the $\tilde{\Gamma}$ variation is shown in Fig. 2.31. These graphs show to what extent $\bar{v}$ is influenced by the variation of $\tilde{\Gamma}$ with respect to ψ. Graphs of $\bar{v}_x$, $\bar{v}_y$ and $\bar{v}_z$, which were obtained according to the above presented theory, as well as as the experimental values measured by G.R. Kvasha and P.M. Novoselov are shown in Figs. 2.33-2.35. Agreement between theory and tests is satisfactory.

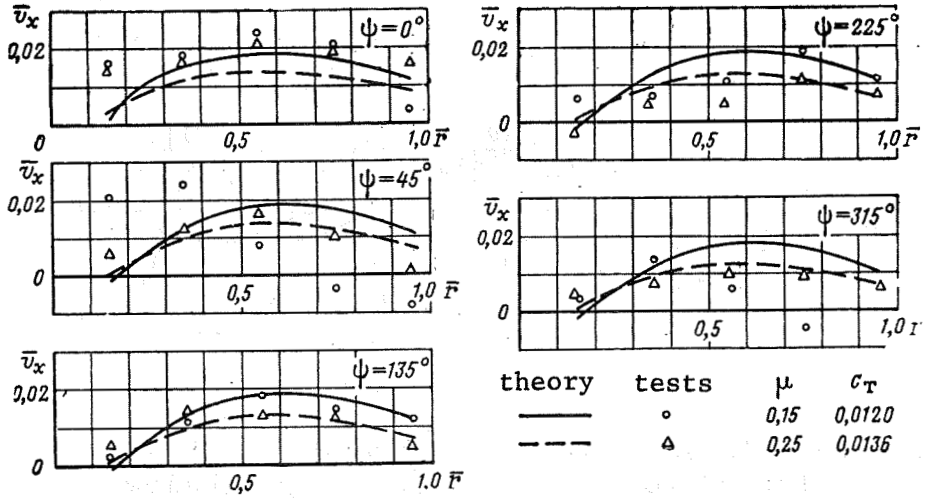

Figure 2.33

*It is shown in Section 3 of Chapter III that the assumed number of harmonics in the Fourier series is sufficient.

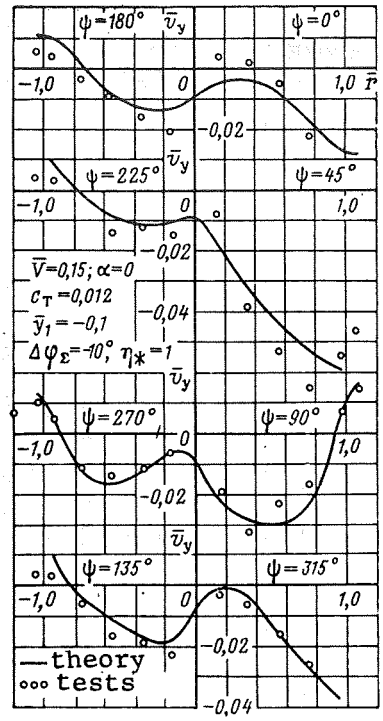

Figure 2.34

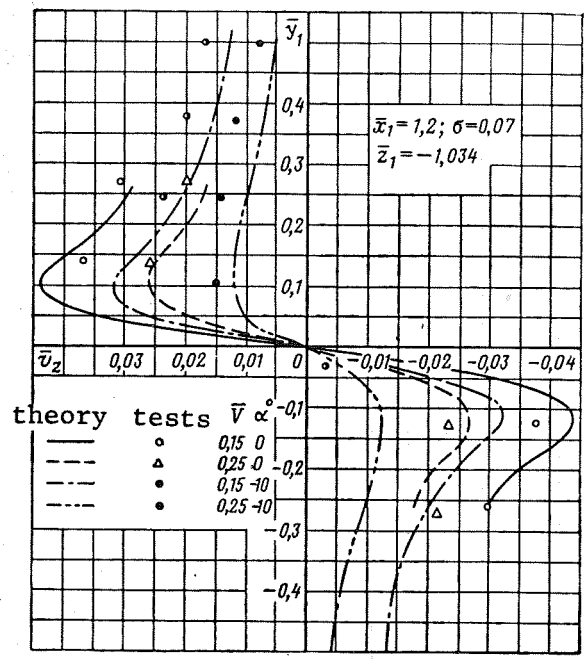

Figure 2.35

CHAPTER III

CHARACTERISTICS OF A HINGED ROTOR IN REGIMES OF FLIGHT WITH A HORIZONTAL VELOCITY COMPONENT

1. ZERO AND FIRST HARMONIC COEFFICIENTS OF FLAPPING BLADE MOTION

It is well-known that aerodynamic characteristics of a rotor with hinged blades depend on their flapping motion. For this reason, in order to perform aerodynamic calculations, one must know expressions for coefficients of the flapping motion, taking into account the nonuniformity of the induced velocity distribution.

Upon substituting Eq. (2.6) into Eq. (1.15) and using dimensionless values, we obtain

$$\frac{d^2\beta}{d\psi^2}+\beta=c_1\varkappa\int_{\bar{l}_r}^{1}\bar{r}\bar{\Gamma}(\bar{r},\ \psi)\,\overline{W}d\bar{r}-\Delta a_0, \tag{3.1}$$

where

$$c_1=\frac{\varrho R^5}{J_r},\qquad \Delta a_0=\frac{M_r}{J_r\omega^2}.$$

Let us integrate the left and right sides of this equation within the limits of 0 to 2π. After expressing β according to Eq. (1.16), we find

$$a_0=c_1\varkappa\frac{1}{2\pi}\int_0^{2\pi}d\psi\int_{\bar{l}_r}^{1}\bar{r}\bar{\Gamma}(\bar{r},\ \psi)\,\overline{W}d\bar{r}-\Delta a_0. \tag{3.2}$$

Changing the order of integration, and taking into account Eq. (2.76), we have:

$$\frac{1}{2\pi}\int_0^{2\pi}d\psi\int_{\bar{l}_r}^{1}\bar{r}\bar{\Gamma}(\bar{r},\ \psi)\,\overline{W}d\bar{r}=\int_{\bar{l}_r}^{1}\bar{r}\left[\frac{1}{2\pi}\int_0^{2\pi}\bar{\Gamma}(\bar{r},\ \psi)\,\overline{W}d\psi\right]=\int_{\bar{l}_r}^{1}\bar{r}^2\bar{\Gamma}_r d\bar{r}. \tag{3.3}$$

Consequently,

$$a_0=c_1\varkappa\int_{\bar{l}_r}^{1}\bar{r}^2\bar{\Gamma}_r d\bar{r}-\Delta a_0. \tag{3.4}$$

Let us rearrange the expression for the coefficient c_1:

$$c_1=\frac{\varrho a_\infty b_7 R^4}{2J_\Gamma}\,\frac{2}{a_\infty}\,\frac{\pi R}{kb_7}\,\frac{k}{\pi}=\frac{2k\gamma}{\pi\sigma a_\infty}. \tag{3.5}$$

The quantity Δa_0 represents an increment of the average coning angle a_0 resulting from the weight $G_л$ of the blade. For a uniform mass distribution along the blade, and assuming $l_\Gamma = 0$, we obtain:

$$M_\Gamma=\frac{1}{2}\,RG_л,\quad J_\Gamma=\frac{1}{3}\,R^2\frac{G_л}{g},\qquad \Delta a_0=\frac{3}{2}\,\frac{R_g}{(\omega R)^2}. \tag{3.6}$$

For $\omega R \approx 206\ m/sec$, we will have

$$\Delta a_0{}^\circ\approx 0{,}01\,D. \tag{3.7}$$

For large rotor diameters, this quantity becomes noticeable. For $D = 35\,m$, $\Delta a_0 = 0{,}35^\circ$. Introducing Eq. (3.5) into Eq. (3.4), we rind

$$a_0=2\,\frac{\gamma}{\sigma a_\infty}\,\frac{k}{\pi}\,\varkappa\int_{\bar r_\Gamma}^{1}\bar r^2\bar\Gamma_r d\bar r-\Delta a_0. \tag{3.8}$$

Taking into consideration Eqs. (2.73), (2.75), (2.76), and using the coefficient form, we obtain

$$c_\Gamma=\varkappa\,\frac{k}{\pi}\,\bar\Gamma_{cp}, \tag{3.9}$$

where

$$\bar\Gamma_{cp}=2\int_{\bar r_0}^{1}\bar r\bar\Gamma_r d\bar r. \tag{3.10}$$

Taking advantage of the relative quantity* defined in Sect. 6 of Ch. II

$$\tilde\Gamma=\frac{\bar\Gamma_r}{\bar\Gamma_{cp}}, \tag{3.11}$$

---

*For the sake of simplicity, instead of $\tilde\Gamma_r$ we will use $\tilde\Gamma$.

we obtain from Eq. (3.10) the following important relationship:

$$\int_{\bar{r}_0}^{1} \bar{r}\tilde{\Gamma}d\bar{r}=\frac{1}{2}. \tag{3.12}$$

We will express now

$$\int_{\bar{l}_\Gamma}^{1} \bar{r}^2\bar{\Gamma}_r d\bar{r}=\bar{r}_*\int_{\bar{l}_\Gamma}^{1} \bar{r}\bar{\Gamma}_r d\bar{r}, \tag{3.13}$$

where for $\bar{r}_0 = \bar{l}_\Gamma$,

$$\bar{r}_*=\frac{\int_{\bar{l}_\Gamma}^{1} \bar{r}^2\bar{\Gamma}_r d\bar{r}}{\int_{\bar{l}_\Gamma}^{1} \bar{r}\bar{\Gamma}_r d\bar{r}}=2\int_{\bar{l}_\Gamma}^{1} \bar{r}^2\tilde{\Gamma}d\bar{r}. \tag{3.14}$$

After substituting Eqs. (3.13), (3.10) and (3.9) into Eq. (3.4), and also taking into consideration Eqs. (3.5) and (3.6), we will have

$$a_0=\frac{\gamma}{a_\infty}\bar{r}_*\frac{c_\Gamma}{\sigma}-\Delta a_0. \tag{3.15}$$

For a rectangular blade (see Fig. 3.3) with a twist $\Delta\phi_\Sigma = 3^\circ$ at $\alpha_э \approx -10^\circ$, relative circulation will be $\tilde{\Gamma} \approx (3/2)\bar{r}$. Consequently, according to Eq. (3.14), $r_* = 3/4$. If $\tilde{\Gamma} = 1$ (approximately corresponding to $\alpha_э = 0$ at $\eta_* = 1$ and $\Delta\phi_\Sigma = 10^\circ$; or $\eta_* = 3$, and $\Delta\phi_\Sigma = 5^\circ$), then $\bar{r}_* = 2/3$. Usually, distributions of $\tilde{\Gamma}$ as obtained from Eq. (2.98) lie between the above considered values. Taking $r_*/a_\infty \approx 0,125$ as an average value, and neglecting Δa_0, we obtain:

$$a_0\approx 0,125\,\gamma\frac{c_\Gamma}{\sigma}. \tag{3.16}$$

In determining the blade flapping angle according to the Glauert-Lock theory, we will consider only first harmonics of the Fourier series. This means that we assume

$$\beta=a_0-a_{10}\cos\psi-b_{10}\sin\psi. \tag{3.17}$$

Here, a_{10} and b_{10} are blade flapping coefficients in the absence of any flapping governor ($\bar{k} = 0$) and when the controls are in neutral position ($\theta_1 = \theta_2 = 0$).

According to Eqs. (2.6), (2.77) and the scheme in Fig. 1.2

$$\Delta T = a_\infty \frac{\rho}{2} bW^2 (\varphi + \beta_1) \Delta r, \tag{3.18}$$

where

$$\beta_1 \approx \frac{\mu a_\vartheta + \bar{v}_y + \bar{v}_\delta}{W}, \tag{3.19}$$

and $\bar{v}_\delta$ is expressed by Eq. (1.19). In this case, we represent the induced velocity under the following form:

$$\bar{v}_y = \bar{v}_r + \bar{v}_{c1}(\bar{r}) \cos\psi + \bar{v}_{s1}(\bar{r}) \sin\psi, \tag{3.20}$$

where $\bar{v}_r$, $\bar{v}_{c_1}(\bar{r})$ and $\bar{v}_{s_1}(\bar{r})$ are determined according to Eqs. (I.7), (II.11) and (IV.4) developed in the Appendices.

Introducing Eq. (3.18) into Eq. (1.18), and equating to zero coefficients at $sin\ \psi$ and $cos\ \psi$, we obtain:

$$a_{10} = \frac{1}{\left(E_3 - \frac{1}{4}\mu^2 E_1\right)} \left[2\mu(\varphi_0 E_2 + E_2^\varphi) + \mu^2 a_\vartheta E_1 + \hat{V}_a\right], \tag{3.21}$$

$$b_{10} = \frac{a_0 \mu E_2 - \hat{V}_b}{E_3 + \frac{1}{4}\mu^2 E_1}, \tag{3.22}$$

where

$$E_2^\varphi = \int_{\bar{r}_0}^{1} \Delta\varphi \bar{r}^2 \tilde{b} d\bar{r}, \tag{3.23}$$

$$\hat{V}_a = \int_{\bar{r}_0}^{1} \bar{r}\tilde{b}(\mu\bar{v}_r + \bar{r}\bar{v}_{s1}) d\bar{r}, \tag{3.24}$$

$$\hat{V}_b = \int_{\bar{r}_0}^{1} \bar{r}^2 \tilde{b} \bar{v}_{c1} d\bar{r}. \tag{3.25}$$

Quantities E_1, E_2 and E_3 are defined by the following expression:

$$E_n = \int_{\bar{r}_0}^{1} \bar{r}^n \tilde{b} d\bar{r}. \tag{3.26}$$

We introduce Eqs. (I.7) and (II.11) into Eq. (3.24); then taking into consideration Eqs. (3.9) and (3.11) as well as assuming $\bar{V} \approx \mu$, we obtain

$$\hat{V}_a = -\frac{3}{4}\frac{c_T}{\varkappa}\int_{\bar{r}_0}^{1}\bar{r}\tilde{b}\tilde{\Gamma}d\bar{r}. \tag{3.27}$$

For $\tilde{b} = 1$, Eq. (3.12) gives:

$$\hat{V}_a = -\frac{3}{8}\frac{c_T}{\varkappa}. \tag{3.28}$$

Calculations indicate that for $\tilde{\Gamma} = 1$ and $\eta_* = 3$,

$$\int_{\bar{r}_0}^{1}\bar{r}\tilde{b}\tilde{\Gamma}d\bar{r} = 0{,}525,$$

and for $\tilde{\Gamma} = (2/3)\bar{r}$ and $\eta_* = 3$, the value of the above integral is equal to $0{,}47$. In this way, it may be assumed that Eq. (3.28) is applicable to the tapered blades as well.

Assuming uniform velocity distribution, we would have, according to Glauert's theory, $\bar{V}_a = -c_T/8\varkappa$. Consideration of the nonuniformity of induced velocities makes their influence 3 times as important.

For a linear twist of the blade, when

$$\Delta\varphi = \Delta\varphi_\Sigma(0{,}7 - \bar{r}), \tag{3.29}$$

where $\Delta\phi_\Sigma = \Delta\phi_{\bar{r}=0} - \Delta\phi_{\bar{r}=1}$, we obtain

$$a_{10} = \frac{1}{\left(E_3 - \frac{1}{4}\mu^2 E_1\right)}\left\{2\mu\left[E_2\varphi_0 + (0{,}7E_2 - E_3)\Delta\varphi_\Sigma\right] + \mu^2 E_1\alpha_э - \frac{3}{8}\frac{c_T}{\varkappa}\right\}. \tag{3.30}$$

For a flat, constant-chord blade ($\tilde{b} = 1$, $\Delta\phi_\Sigma = 0$)

$$a_{10} = \frac{4}{\left(1 - \frac{1}{2}\mu^2\right)}\left(\frac{2}{3}\mu\varphi_0 + \frac{1}{2}\mu^2\alpha_э - \frac{3}{8}\frac{c_T}{\varkappa}\right). \tag{3.31}$$

Eq. (3.31) has the same form as in Glauert's theory, and differs only by the coefficient at c_T.

When $\bar{k} = 0$, the collective pitch of the blade is $\phi_0 = \phi_{0э}$. Now, we substitute, into Eq. (3.30), the ϕ_0 value given by Eq. (3.51), and neglecting small-value terms, we obtain for $\tilde{b} = 1$ and $\varkappa \approx 0{,}94$

$$a_{10} \approx (1{,}5\mu - 0{,}6\sigma)\frac{c_T}{\sigma} - 1{,}64\mu^2\alpha_э. \tag{3.32}$$

In the case considered by Glauert ($\bar{v}_y = const$), the first term in Eq. (3.32) would be $(1{,}5\mu + 0{,}49\sigma)c_T/\sigma$. It can be seen, hence, that consideration of the nonuniformity in the induced velocity distribution varies the influence of σ on a_{10}.

For a constant chord blade, Eq. (3.22) gives:

$$b_{10} = \frac{\frac{4}{3}\mu a_0 - 4\hat{V}_b}{1 + \frac{1}{2}\mu^2}. \tag{3.33}$$

According to Eqs. (IV.4) and (3.9), for $\tilde{b} = 1$

$$\hat{V}_b = \frac{c_T}{4\pi\bar{V}} \int_{\bar{r}_0}^{1} \bar{r}^2 \tilde{v}_{c1} d\bar{r} = \frac{c_T}{4\pi\bar{V}} A_2^{(1)}. \tag{3.34}$$

In Fig. 3.1, graphs are shown of the quantity $A_2^{(1)}$ for three types of distribution of the average circulations: $\tilde{\Gamma}_I = (3/2)\bar{r}$, $\tilde{\Gamma}_{II} = 10\bar{r}^2(1 - \bar{r})$ and $\tilde{\Gamma}_{III} = 1$. These graphs are computed from the $\hat{v}_{c1}(\bar{r})$ formula in Appendix IV. For the given types of circulation, $\hat{v}_{c1}(\bar{r})$ is shown in Fig. 3.2.

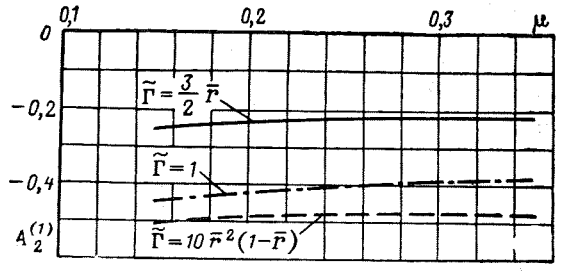

Figure 3.1

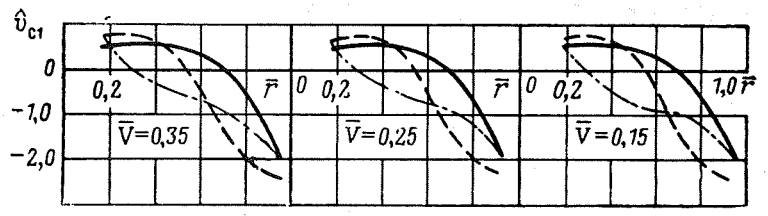

Figure 3.2

The quantity $A_2^{(1)}$ can be determined for any blade configuration and any regimes of flight. In order to do this, it is necessary (as recommended in Sect. 6 of Ch. II) to find $\Delta\tilde{\Gamma}_\rho = \Delta\bar{\Gamma}_\rho/\bar{\Gamma}_{cp}$ and substitute the thus obtained values into

expressions for $\hat{v}_{c1}(\bar{r})$. In order to facilitate computation of the relationship of $\tilde{\Gamma} = \bar{\Gamma}_r/\bar{\Gamma}_{cp}$, it is possible to take a direct advantage of the following formula, obtained from Eqs. (2.98) and (3.9) for $\bar{V} \approx \mu$:

$$\tilde{\Gamma} = 4\mu \frac{\varkappa}{c_T} \tilde{c} \left(\varphi_э \bar{r} \frac{\bar{r}^2 + \frac{1}{2}\mu^2}{\bar{r}^2 + \tilde{c}\mu^2} + \mu \alpha_э \frac{\bar{r}^2}{\bar{r}^2 + \tilde{c}\mu^2} \right), \tag{3.35}$$

where the coefficient

$$\tilde{c} = \frac{a_\infty \sigma \tilde{b}}{8\mu + a_\infty \sigma \tilde{b}}. \tag{3.36}$$

In Fig. 3.3 graphs of $\tilde{\Gamma}$ are shown at various values of μ and α, for a rotor with constant-chord, linearly twisted blades and $\sigma = 0,07$ when $c_T/\sigma = 0,17$.

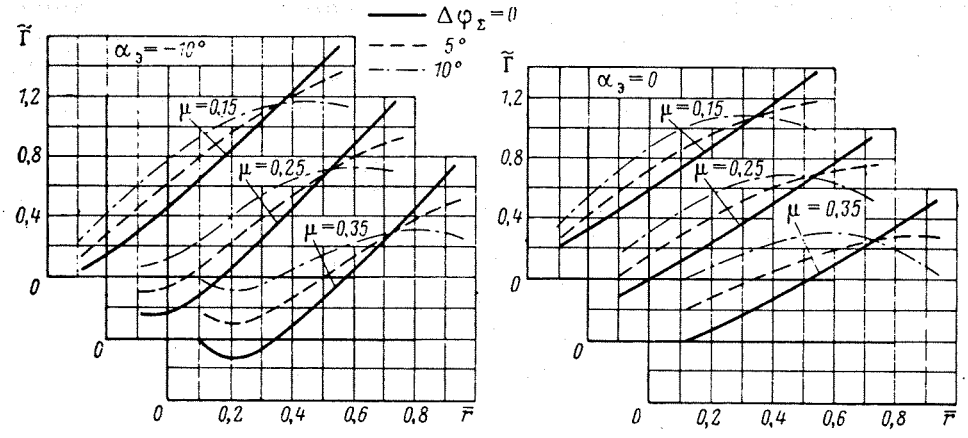

Figure 3.3

After introducing Eqs. (3.16) and (3.34) into Eq. (3.33), we obtain

$$b_{10} \approx \frac{4}{3} \mu a_0 \left(1 + \tilde{G} \frac{\sigma}{\gamma \mu^2}\right). \tag{3.37}$$

If the circulation corresponds to the type $\tilde{\Gamma}_I$, then the quantity $\tilde{G} \approx 1,4$; if it is of the $\tilde{\Gamma}_{III}$ type, then $\tilde{G} = 2,5$. For a uniform distribution of induced velocity, $\tilde{G} = 0$. Consequently, taking into consideration the nonuniformity of velocity distribution would change the b_{10} coefficient by a factor of 1,25-1,5.

In the presence of a flapping governor (say δ_3) or displacement of the swashplate, flapping coefficients with respect to the x, y, z axes can be determined from the well-known formulae of A.N. Mihailov[66] which may be expressed in the following way:

$$a_1 = a_{10} + \theta_{2э}, \tag{3.38}$$

$$b_1 = b_{10} - \theta_{1э}. \tag{3.39}$$

where the quantities $\theta_{1э}$ and $\theta_{2э}$ are determined according to Eq. (2.82).

2. THRUST COEFFICIENT

General expressions for the thrust coefficient c_T were given in Eqs. (3.9), (3.10) and (2.98). It should be noted that if, in Eq. (2.91), $\bar{\Gamma}_{cp}$ is substituted instead of $\bar{\Gamma}_r$, then $\bar{v}_{cp}$ (the average induced velocity over the rotor disc) will be obtained. Next, expressing $\bar{\Gamma}_{cp}$ in terms of c_T according to Eq. (3.9), we find that:

$$\bar{v}_{cp} = -\frac{c_T}{4\varkappa \bar{V}}. \tag{3.40}$$

We multiply the right and left sides of the above equation by ωR, and then we multiply and divide the right side of the equation by $(\rho/2)F$. Assuming next that $\varkappa \approx 1$, we obtain

$$v_{cp} = -\frac{T}{2\rho F V}. \tag{3.41}$$

The above formula for the case of $V_1 \approx V$ becomes identical with the relationship proposed as a hypothesis by Glauert and thus, proves that hypothesis.

In order to develop relationships for c_T, we substitute $\phi_э = \phi_{0э} + \Delta\phi$ into Eq. (2.98), and taking into account Eqs. (3.10) and (3.9), after performing some transformations, we finally have

$$c_T = \sigma(\bar{c}_0 + \bar{c}_1\varphi_{0э} + \bar{c}_2\alpha_э). \tag{3.42}$$

Here,

$$\bar{c}_0 = 2\varkappa a_\infty \int_{\bar{r}_0}^{1} \Delta\varphi \bar{r}^2 \tilde{B} \left(1 + \frac{\mu^2}{2\bar{r}^2}\right) d\bar{r}, \tag{3.43}$$

$$\bar{c}_1 = 2\varkappa a_\infty \int_{\bar{r}_0}^{1} \bar{r}^2 \tilde{\tilde{B}} \left(1 + \frac{\mu^2}{2\bar{r}^2}\right) d\bar{r}, \tag{3.44}$$

$$\bar{c}_2 = 2\varkappa a_\infty \mu \int_{\bar{r}_0}^{1} \bar{r}\tilde{\tilde{B}}d\bar{r}, \tag{3.45}$$

where

$$\tilde{B} = \frac{4\mu\tilde{b}}{8\mu + a_\infty \sigma\tilde{b}\left(1 + \frac{\mu^2}{\bar{r}^2}\right)}, \tag{3.46}$$

It is evident from the above formulae that the blade twist influences only the first term in Eq. (3.42); namely, $\bar{c}_0$. Influence of the "reversed flow region" may be accounted for by a proper increase of the relative cut-out radius, $\bar{r}_0$. In the particular case of constant-chord, untwisted, blade ($\Delta\phi = 0$, $\tilde{b} = 1$ and $\bar{r}_0 = 0$) expressions for $\bar{c}_1$ and $\bar{c}_2$ take a simple form:

$$\bar{c}_1 = 4\frac{\varkappa\hat{c}}{\mu\sigma}\left[\frac{2}{3} + (\mu^2 - 2\hat{c})\left(1 - \sqrt{\hat{c}}\operatorname{arctg}\frac{1}{\sqrt{\hat{c}}}\right)\right], \tag{3.47}$$

$$\bar{c}_2 = 4\varkappa\frac{\hat{c}}{\sigma}\left(1 - \hat{c}\ln\frac{1+\hat{c}}{\hat{c}}\right), \tag{3.48}$$

$$\hat{c} = \frac{a_\infty \sigma\mu^2}{8\mu + a_\infty \sigma}. \tag{3.49}$$

If the blade is twisted according to Eq. (3.29) and $\tilde{b} = 1$, then

$$\bar{c}_0 = \Delta\varphi_\Sigma\left[0{,}7\bar{c}_1 - 0{,}5\mu\bar{c}_2\left(1 - 2\frac{\hat{c}}{\mu^2}\right) - 2\frac{\varkappa\hat{c}}{\sigma\mu}\right]. \tag{3.50}$$

Let us solve Eq. (3.42) with respect to $\phi_{0,3/4}$. After transformations and neglecting small quantities of the second order, we obtain

$$\varphi^\circ_{0,3/4} \approx 21{,}8\,\frac{c_T}{\sigma}\left(1{,}43 + \frac{\sigma}{\mu}\right) - 1{,}35\mu\alpha^\circ_{3/4} + 0{,}05\,\Delta\varphi^\circ_\Sigma. \tag{3.51}$$

Example: For $c_T = 0{,}01$; $\sigma = 0{,}08$, $\mu = 0{,}25$ and $\Delta\phi_\Sigma = 8^\circ$; effective collective pitch angle would be $\phi_{0,3/4} = 7{,}9^\circ$ for $\alpha_{3/4} = -8^\circ$, and $\phi_{0,3/4} = 2{,}5^\circ$ when $\alpha_{3/4} = 8^\circ$. For the preliminary evaluations, it is possible to use Eq. (3.51) for tapered blades as well.

Let us establish dependence of c_T on the geometric representative blade pitch angle ϕ_0 when the flapping is zero. In

order to do this, we substitute $\phi_{0_3} = \phi_0 - \bar{k}a_0$ into Eq. (3.42). Next we substitute a_0, assuming for the sake of generality that the twist is nonlinear. According to Eq. (3.8), a_0 for $\Delta a_0 \approx 0$ can be expressed under a form similar to Eqs. (3.42)-(3.45). This would result in the following:

$$c_T = c_{T0} + c_T^{\varphi}\varphi_0 + c_T^{\alpha}\alpha_3, \tag{3.52}$$

where

$$\frac{c_{T0}}{\sigma} = \bar{c}_0 - \frac{\bar{k}_3\bar{c}_1\bar{A}_0}{1+\bar{k}_3\bar{A}_1}, \tag{3.53}$$

$$\frac{c_T^{\varphi}}{\sigma} = \bar{c}_1\left(1 - \frac{\bar{k}_3\bar{A}_1}{1+\bar{k}_3\bar{A}_1}\right), \tag{3.54}$$

$$\frac{c_T^{\alpha}}{\sigma} = \bar{c}_2 - \frac{\bar{k}_3\bar{c}_1\bar{A}_2}{1+\bar{k}_3\bar{A}_1}, \tag{3.55}$$

$$\bar{A}_0 = A_0 a_\infty, \quad \bar{A}_1 = A_1 a_\infty, \quad \bar{A}_2 = A_2 a_\infty, \quad \bar{k}_3 = \bar{k}\frac{\gamma}{a_\infty}, \tag{3.56}$$

$$A_0 = 2\varkappa\int_{\bar{r}_0}^{1} \Delta\varphi\bar{r}^3\tilde{B}\left(1+\frac{\mu^2}{2\bar{r}^2}\right)d\bar{r}, \tag{3.57}$$

$$A_1 = 2\varkappa\int_{\bar{r}_0}^{1} \bar{r}^3\tilde{B}\left(1+\frac{\mu^2}{2\bar{r}^2}\right)d\bar{r}, \tag{3.58}$$

$$A_2 = 2\varkappa\mu\int_{\bar{r}_0}^{1} \bar{r}^2\tilde{B}d\bar{r}. \tag{3.59}$$

And, in the case of a linear twist,

$$\frac{c_{T0}}{\sigma} = \Delta\varphi_\Sigma\frac{c_{T0}^{(0)}}{\sigma}.$$

Graphs of $c_{T0}^{(0)}/\sigma$; c_T^{ϕ}/σ; c_T^{α}/σ are shown in Fig. 3.4 as a function of μ for various values of parameters σ and $\bar{k}_3$, when $\eta_* = 1$. In the graphs of Fig. 3.4 it was assumed that $x = 0,94$ and $a_\infty = 5,6$. It can be seen from those graphs that variation in the blade taper ratio, η_*, has little influence on the c_T^{ϕ}/σ and c_T^{α}/σ levels. This means that those particular quantities are practically independent from the blade planform. Also, variations in the solidity ratio, σ, do not appreciably alter those quantities. However, the shape of the blade, as described by η_* and $\Delta\phi_\Sigma$, strongly influences the $c_{T0}^{(0)}/\sigma$ values. Quantities c_T^{α}/σ and c_T^{ϕ}/σ considerably vary with the variation of $\bar{k}_3$ (characterizing the influence of flapping controlling devices). With a variation of $\bar{k}_3$ from 0 to 0,8, they decrease to almost one-half of their original values. A comparison of the computed c_T^{α}/σ values with those obtained by P.M. Novoselov and P.I.

Radchenko on a model of the Mi-1 rotor with rigid blades ($D = 2,5\,m$, $\sigma = 0,05$) indicated a satisfactory agreement.

It was shown in Sect. 2 of Ch. I that due to the blade flapping motion, section angles of attack α, as well as their lift coefficients, c_y, are higher in those areas where the velocities of the flow, W, encountered by the blade are lower. Consequently, the highest values of the average blade lift coefficient $c_{y\psi}$ corresponds to the azimuth angle $\psi = (3/2)\pi$. The highest allowable value of $c_{y\psi}$ in the excess of which a local stall begins, is c_{ymax}. This value depends on the Mach and Reynolds numbers, $M = W/a$ and $Re = Wb/\nu$, but it is also influenced by the unsteady aerodynamic phenomena and action of inertial forces on the blade boundary layer. At $c_{y\psi} > c_{ymax}$, the rotor power required and blade vibrations increase, and controlability deteriorates, while control loads become higher. All those phenomena determine the critical value of the average lift coefficient, c_{y0}, averaged over the whole disc area.

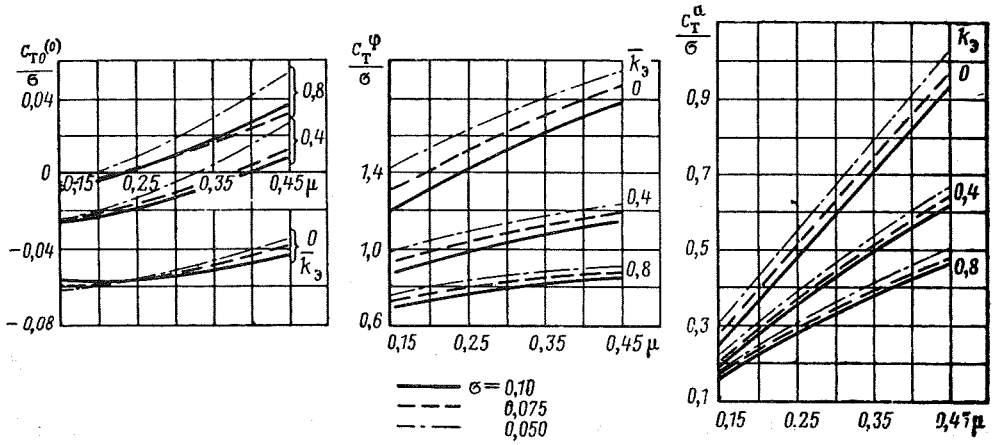

Figure 3.4

It was shown before that in aerodynamic calculations at moderate advance ratios ($\mu \leq 0,45$), it is sufficient to consider only first harmonics of the flapping motion. Eq. (1.18) indicates that under the above approximations, the blade lifting force moment related to the flapping hinge is the same at all azimuth angles. Let us take into consideration the relationships expressed by Eqs. (2.74) and (2.77). Then, using relative (dimensionless) quantities and neglecting constant coefficients, we obtain

$$\int_{\bar{r}_0}^{1} \bar{r} c_y \bar{b} \bar{W}^2 d\bar{r} = \text{const.} \qquad (3.60)$$

Assuming, for simplicity, $\bar{b} = const$ and $\bar{r}_0 = 0$, we have

$$\int_0^1 \bar{r} c_y \overline{W}^2 d\bar{r} = c_{y\psi} \int_0^1 \bar{r} \overline{W}^2 d\bar{r} =$$

$$= \frac{1}{4} c_{y\psi} \left(1 + \frac{8}{3} \mu \sin\psi + 2\mu^2 \sin^2\psi\right). \qquad (3.61)$$

Integrating, with respect to ψ, the right side of Eq. (3.61) from 0 to 2π, we find

$$\frac{1}{2\pi} \int_0^{2\pi} d\psi \int_0^1 \bar{r} c_y \overline{W}^2 d\bar{r} = \frac{1}{4} c_{y_0} (1+\mu^2). \qquad (3.62)$$

Equating Eqs. (3.61) and (3.62), we have

$$c_{y\psi} = c_{y_0} f(\psi),$$

where

$$f(\psi) = \frac{1+\mu^2}{1 + 2{,}67\,\mu \sin\psi + 2\mu^2 \sin^2\psi}. \qquad (3.63)$$

The critical value of the average rotor lift coefficient (averaged over the whole disc) becomes:

$$c_{y_0\,кр} = \frac{c_{y\,max}}{f\left(\frac{3}{2}\pi\right)}. \qquad (3.64)$$

Since the magnitude of the average blade lift coefficient $c_{y\psi}$ can be approximated by the c_y at $\bar{r} = 0{,}7$, its maximum value $c_{y_{max}}$ can be found for

$$W = \omega R (0{,}7 - \mu) \qquad (3.65)$$

from basic airfoil characteristics, and its value increased due to the unsteady flow phenomena and then $c_{y_0 kp}$ can be computed according to Eq. (3.64). For preliminary calculations, one can assume $c_{y_{max}} = 1{,}25$. The first graph of $c_{y_0 kp} = f(\mu)$, computed according to Eq. (3.64), was published in 1947[24]. In 1951, that curve appeared in many foreign technical journals.* The relationship $c_{y_0 kp} = f(\mu)$ is called the *safe stall limits*. This problem of establishing the safe stall limit was considered by I. P. Bratukhin, K. N. Baburin-Bel'chikov,

---

*For instance, see *Helicopter Rotor Performance Possibilities* by J. Stuart III, American Helicopter Society, Proceedings of the Seventh Annual Forum, April 26-29, 1951, Washington.

Ts.V. Solov'yev and experimentally investigated by A.S. D'yachenko and R.M. Shikhina-Zanozina. It was also considered in Ref 64. K.N. Baburin-Bel'chikov computed the stall limit more exactly, taking into account the 2nd and 3rd harmonics of the flapping motion. This gave considerably higher values for c_{y0kp} at $\mu > 0,2$. Ts.V. Solov'yev determined the safe stall limit for high μ's. In Fig. 3.5, one can find a graph of

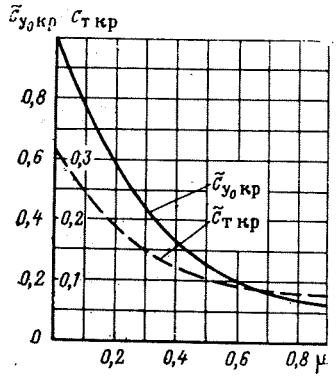

Figure 3.5

$$\tilde{c}_{y0kp} = c_{y0kp}/c_{ymax}.$$

The presented results were obtained for rectangular blades, but they may be considered approximately correct for any blade form.

Let us now relay the rotor thrust coefficients c_T to the average lift coefficient c_{y0}. After substituting Eqs. (2.74) and (2.77) into Eq. (1.12), we switch to relative (dimensionless) quantities. Then for $\bar{r}_0 = 0$,

$$c_т = \varkappa \frac{k}{2\pi^2}\int_0^{2\pi} d\psi \int_0^1 c_y \bar{b}\bar{W}^2 d\bar{r} = \varkappa\sigma \frac{1}{2\pi}\int_0^{2\pi} c_{y\psi}^{т} \int_0^1 \tilde{b}\bar{W}^2 d\bar{r}. \qquad (3.66)$$

Assuming that approximately,

$$c_{y\psi}^{т} = \frac{\int_0^1 c_y \tilde{b}\bar{W}^2 d\bar{r}}{\int_0^1 \tilde{b}\bar{W}^2 d\bar{r}} \approx \frac{\int_0^1 \bar{r} c_y \bar{W}^2 d\bar{r}}{\int_0^1 \bar{r}\bar{W}^2 d\bar{r}} = c_{y\psi}.$$

We next substitute Eq. (3.63) into Eq. (3.66), and obtain

$$c_т = \varkappa\sigma c_{y_0} \frac{1}{2\pi}\int_0^{2\pi} f(\psi)\, d\psi \int_0^1 \tilde{b}\bar{W}^2 d\bar{r} = \varkappa\sigma c_{y_0} \tilde{b}_{ср} \frac{1}{2\pi}\int_0^{2\pi} f(\psi)\, d\psi \int_0^1 \bar{W}^2 d\bar{r}, \qquad (3.67)$$

$$\tilde{b}_{ср} = \frac{\int_0^{2\pi} f(\psi)\, d\psi \int_0^1 \tilde{b}\bar{W}^2 d\bar{r}}{\int_0^{2\pi} f(\psi)\, d\psi \int_0^1 \bar{W}^2 d\bar{r}}. \qquad (3.68)$$

Let us define

$$k_т = \tilde{b}_{ср} = \frac{\bar{b}_{ср}}{\bar{b}_7}. \qquad (3.69)$$

Coefficient k_T reflects the influence of the blade planform on the thrust coefficient. We substitute $f(\psi)$ according to Eq. (3.63) and compute the integral

$$\frac{1}{2\pi}\int_0^{2\pi} f(\psi)\,d\psi \int_0^1 \overline{W}^2 d\bar{r} = \frac{1}{3}(1+\mu^2)\frac{1}{2\pi}\int_0^{2\pi}\frac{1+3\mu\sin\psi+3\mu^2\sin^2\psi}{1+2{,}67\,\mu\sin\psi+2\mu^2\sin^2\psi}\,d\psi \approx$$

$$\approx \frac{1}{3}(1+1{,}2\mu^2). \tag{3.70}$$

Then, according to Eqs. (3.67), (3.69) and (3.70)

$$c_T = \frac{1}{3}\varkappa(1+1{,}2\mu^2)\sigma k_T c_{y_0}. \tag{3.71}$$

For $\varkappa \approx 0.94$

$$c_T = 0{,}313(1+1{,}2\,\mu^2)\sigma k_T c_{y_0}. \tag{3.72}$$

In the case of a tapered blade (see Fig. 2.32),

$$\bar{b} = \bar{b}_1[1+(\eta_*-1)(1-\bar{r})] \tag{3.73}$$

and

$$\tilde{b} = \frac{1+(\eta_*-1)(1-\bar{r})}{1+0{,}3(\eta_*-1)}. \tag{3.74}$$

Upon substituting Eq. (3.74) into Eq. (3.68), and after integrating, we obtain, according to Eq. (3.69):

$$k_T = \frac{\eta_* - 0{,}75(\eta_*-1)\dfrac{1+\mu^2}{1+1{,}2\mu^2}}{0{,}7+0{,}3\eta_*}. \tag{3.75}$$

A graph giving the k_T values is shown in Fig 3.6. From Eq. (3.72), we find

$$\tilde{c}_{T.кр} = \frac{c_{T.кр}}{\sigma c_{y\,max}\,k_T} = 0{,}313(1+1{,}2\mu^2)\,\tilde{c}_{y_0\,кр}. \tag{3.76}$$

The dependence of $\tilde{c}_{T.kp}$ on μ is presented in Fig. 3.5.

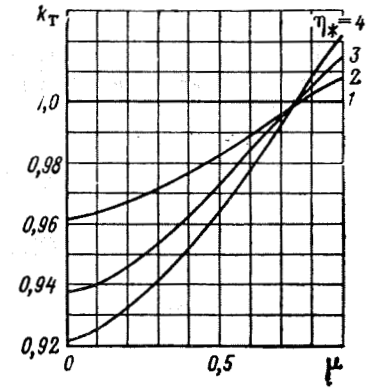

Figure 3.6

Let us express new relationships between c_{y_0} and c_{y_r} - the average blade section lift coefficient at radius r (i.e., averaged over a complete circumference of a circle of radius r). According to Eq. (3.66), for $\overline{r}_0 \neq 0$

$$c_T = \varkappa \frac{k}{\pi} \int_{\bar{r}_0}^{1} \bar{b} \left(\frac{1}{2\pi} \int_0^{2\pi} c_y \overline{W}^2 d\psi \right) d\bar{r} = \varkappa \frac{k}{\pi} \int_{\bar{r}_0}^{1} \bar{b} c_{y_r} \left(\frac{1}{2\pi} \int_0^{2\pi} \overline{W}^2 d\psi \right) d\bar{r} =$$

$$= \varkappa\sigma \int_{\bar{r}_0}^{1} \tilde{b} c_{y_r} \left(\frac{1}{2\pi} \int_0^{2\pi} \overline{W}^2 d\psi \right) d\bar{r} = \varkappa\sigma \int_{\bar{r}_0}^{1} \tilde{b} c_{y_r} \left(\bar{r}^2 + \frac{1}{2} \mu^2 \right) d\bar{r} =$$

$$= \varkappa\sigma c_{y_0} \int_{\bar{r}_0}^{1} \tilde{b} \left(\bar{r}^2 + \frac{1}{2} \mu^2 \right) d\bar{r}. \tag{3.77}$$

where

$$c_{y_r} = \frac{\frac{1}{2\pi} \int_0^{2\pi} c_y \overline{W}^2 d\psi}{\bar{r}^2 + \frac{1}{2} \mu^2} \tag{3.78}$$

and

$$c_{y_0} = \frac{\int_{\bar{r}_0}^{1} \tilde{b} c_{y_r} \left(\bar{r}^2 + \frac{1}{2} \mu^2 \right) d\bar{r}}{\int_{\bar{r}_0}^{1} \tilde{b} \left(\bar{r}^2 + \frac{1}{2} \mu^2 \right) d\bar{r}}. \tag{3.79}$$

Comparing Eqs. (3.9) and (3.10) with Eq. (3.78), we obtain one more expression for c_{y_r}

$$c_{y_r} = \frac{2\bar{r}\overline{\Gamma}_r}{\bar{b} \left(\bar{r}^2 + \frac{1}{2} \mu^2 \right)} = \frac{c_T}{\varkappa\sigma} \frac{2\bar{r}\tilde{\Gamma}}{\tilde{b} \left(\bar{r}^2 + \frac{1}{2} \mu^2 \right)}. \tag{3.80}$$

It may be shown that the formulae for $\overline{\Gamma}_r$, c_T, a_0, a_{10} and b_{10} may be considered sufficiently accurate up to $\alpha_1 \approx -30°$.

3. LONGITUDINAL FORCE COEFFICIENT

In Sect. 1 of Ch. I, expressions were developed for ΔH - longitudinal force component of a blade element. According to Eqs. (1.9) and (1.10)

$$\Delta H = \Delta H_p + \Delta H_\alpha + \Delta H_v + \Delta H_\beta, \tag{3.81}$$

where

$$\Delta H_p = \Delta X_p \frac{W_1}{W} \sin\psi, \tag{3.82}$$

$$\Delta H_{\alpha} = -\Delta T \frac{V \sin \alpha_э}{W} \sin \psi, \tag{3.83}$$

$$\Delta H_{v} = -\Delta T \frac{v_y}{W} \sin \psi, \tag{3.84}$$

$$\Delta H_{\beta} = -\Delta T \left(\frac{v_\delta}{W} \sin \psi + \beta \cos \psi \right). \tag{3.85}$$

Substituting, first, Eq. (1.7) into Eq. (3.28); and then, Eq. (3.82) into Eq. (1.12) and switching to relative (dimensionless) quantities, we obtain an expression for that part of the elementary longitudinal force which depends on the blade profile drag.

$$\Delta c_{Hp} = \frac{k}{2\pi^2} \int_0^{2\pi} \sin \psi d\psi \int_{\bar{r}_0}^{1} c_{xp} \bar{b} \overline{W}_1^2 d\bar{r} = \sigma \int_{\bar{r}_0}^{1} \tilde{b} \left(\frac{1}{2\pi} \int_0^{2\pi} c_{xp} \overline{W}_1^2 \sin \psi d\psi \right) d\bar{r}. \tag{3.86}$$

We introduce the average value of the profile drag coefficient

$$c_{xpr}^{H} = \frac{\frac{1}{2\pi} \int_0^{2\pi} c_{xp} \overline{W}_1^2 \sin \psi d\psi}{\frac{1}{2\pi} \int_0^{2\pi} \overline{W}_1^2 \sin \psi d\psi}. \tag{3.87}$$

According to Eq. (1.1) for small $\alpha_э$, $\overline{W}_1 \approx \overline{W}$. At large inclinations of the rotor axis; neglecting $\overline{v}_y$ in comparison with $\mu tg\, \alpha_э + \overline{v}_\delta$, we obtain

$$\overline{W}_1^2 \approx \overline{W}^2 + (\mu \operatorname{tg} \alpha_э + \overline{v}_\delta)^2. \tag{3.88}$$

Introducing Eqs (1.19) and (1.17) into the above relationships, we have

$$\frac{1}{2\pi} \int_0^{2\pi} \overline{W}_1^2 \sin \psi d\psi = \bar{r} \mu \varkappa_H, \tag{3.89}$$

where

$$\varkappa_H = 1 - a_{10} \operatorname{tg} \alpha_э - \frac{1}{4} a_{10}^2 + \frac{1}{4} b_{10}^2 - \frac{1}{4} \mu \frac{a_0 b_{10}}{\bar{r}}. \tag{3.90}$$

Computations at $\overline{V} = 0,5$, $\alpha_э = -30°$ and $c_T/\sigma = 0,141$ indicate that it may be assumed with sufficient accuracy that

$$\varkappa_H \simeq 1 - a_{10}\left(\operatorname{tg}\alpha_э + \frac{1}{4}a_{10}\right). \tag{3.91}$$

In this case, $\varkappa_H \approx 1,13$. From Eqs. (3.87) and (3.89), we find

$$c^H_{xpr} = \frac{\frac{1}{2\pi}\int_0^{2\pi} c_{xp}\overline{W}_1^2 \sin\psi d\psi}{\bar{r}\mu\varkappa_H}. \tag{3.92}$$

Substituting Eqs. (3.87) and (3.89) into Eq. (3.86), we obtain

$$\frac{\Delta c_{Hp}}{c_т} = \frac{1}{2}\mu\varkappa_H\frac{\sigma}{c_т}c_{xpH}, \tag{3.93}$$

where

$$c_{xpH} = c^H_{xpn} + \Delta c^H_{xp},\quad c^H_{xpn} = 2\int_{\bar{r}_0}^{1}\bar{r}\tilde{b}c^H_{xpr}d\bar{r}. \tag{3.94}$$

In Fig. 3.7, one can find a graph of $c^H_{xpn} = f(\bar{V})$ with c_{y0} and $\alpha_э$ considered as parameters. This graph was obtained by V.N. Kvokov at $\omega R = 220$ m/sec for blades whose characteristics are shown in Fig. 3.8. In that approximate computation, α was determined from Eq. (2.78), while flapping motion of the first harmonic type was defined according to Eqs. (3.16), (3.32) and (3.37) with $\tilde{G} = 1,4$ and $\sigma = 0,1$; and coefficients of induced velocity $\hat{v}_y(\bar{r},\psi)$ were calculated from relationships given in Appendix V for $\bar{V} = 0,35$ and $\tilde{\Gamma} = (2/3)\bar{r}$.

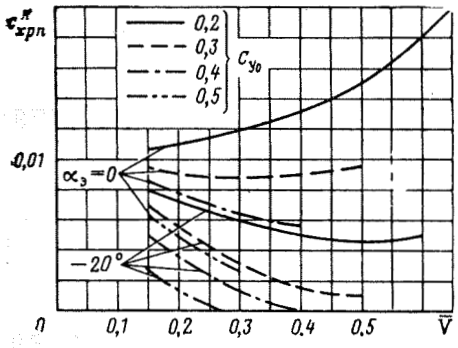

Figure 3.7

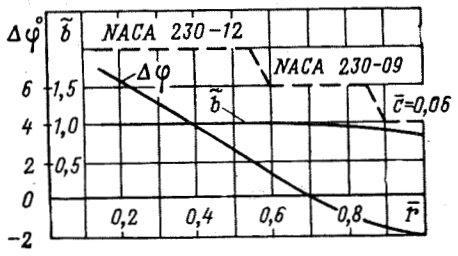

Figure 3.8

Coefficient Δc^H_{xp} takes into consideration the influence of the radial component of the flow, $V_R = V\cos\alpha_э\cos\psi$, which increases the aerodynamic drag of the blade because of the skin friction. It may be assumed that approximately,

$$\Delta c^H_{xp} \approx 0,01.$$

Now, we will determine the $\Delta c_{H\alpha}$ coefficient. Assuming that

$$\frac{V \sin \alpha_э}{W} \approx \frac{\mu \alpha_э}{\overline{W}} \tag{3.95}$$

and taking into consideration, Eqs. (2.74), (3.9)-(3.11) and (3.83), from Eq. (1.12) we will get

$$\Delta c_{H\alpha} = -\mu \alpha_э \frac{k}{\pi^2} \int_0^{2\pi} \sin \psi d\psi \int_{\bar{r}_0}^{1} \bar{\Gamma}(\bar{r}, \psi) d\bar{r} =$$

$$= -2\mu \alpha_э \frac{c_т}{\varkappa} \int_{\bar{r}_0}^{1} \left[\frac{1}{2\pi} \int_0^{2\pi} \tilde{\Gamma}(\bar{r}, \psi) \sin \psi d\psi \right] d\bar{r}. \tag{3.96}$$

It was shown in Sect. 2 of Ch. II that if the blade flapping motion can be sufficiently accurately described by the first harmonics, then the relationship given by Eq. (2.7) is valid.

The main role in the generation of aerodynamic forces and moments is played by the effective part of the blade, whose representative section may be assumed to be located close to $\bar{r} = 0,7$. Also, it may be assumed that the average relative circulation $\tilde{\Gamma}_\psi$ is approximately equal to the relative local circulation at that station $\bar{r} = 0,7$. Calculations indicate that Eq. (2.7), valid for the average circulation, can be generalized, with sufficient accuracy, by assuming

$$\frac{\bar{\Gamma}(\bar{r}, \psi)}{\bar{\Gamma}_{ср}} = \tilde{\Gamma}(\bar{r}, \psi) \approx \frac{\tilde{\Gamma}}{1 + \frac{3}{2} \mu \sin \psi}. \tag{3.97}$$

For $\mu < 2/3$, it is possible to develop the above expression into the following series:

$$\tilde{\Gamma}(\bar{r}, \psi) \approx \tilde{\Gamma} [1 + 1,12\mu^2 (1 + 1,7\mu^2) - 1,5\mu (1 + 1,7\mu^2) \sin \psi -$$
$$- 1,12\mu^2 (1 + 2,25\mu^2) \cos 2\psi + 0,844\mu^3 \sin 3\psi + 0,633\mu^4 \cos 4\psi + \ldots].$$

Here, $\tilde{\Gamma} = \tilde{\Gamma}(\bar{r})$ is the relative circulation averaged over a circumference of a circle of a given radius. Substituting Eq. (3.97) into the internal integral of Eq. (3.96), we obtain

$$\frac{1}{2\pi} \int_0^{2\pi} \tilde{\Gamma}(\bar{r}, \psi) \sin \psi d\psi \approx \tilde{\Gamma} \frac{1}{2\pi} \int_0^{2\pi} \frac{\sin \psi \, d\psi}{1 + \frac{3}{2} \mu \sin \psi} \approx -\frac{3}{4} \mu (1 + 1,7\,\mu^2) \tilde{\Gamma}. \tag{3.98}$$

Consequently,

$$\Delta c_{Ha} = \frac{3}{2}\mu^2(1+1{,}7\mu^2)\alpha_s \frac{c_T}{\varkappa}\int_{\bar{r}_0}^{1}\tilde{\Gamma}d\bar{r}. \qquad (3.99)$$

For $\tilde{\Gamma} = (3/2)\bar{r}$ and $\bar{r}_0 \approx 0{,}1$, the integral in that expression is equal to $0{,}74$. If one assumes $\varkappa = 0{,}94$, then

$$\frac{\Delta c_{Ha}}{c_T} = 1{,}12\mu^2(1+1{,}7\mu^2)\alpha_s. \qquad (3.100)$$

In the case of $\tilde{\Gamma} = 1$

$$\frac{\Delta c_{Ha}}{c_T} = 1{,}35\mu^2(1+1{,}7\mu^2)\alpha_s. \qquad (3.101)$$

Similarly, substituting Eq. (3.84) into Eq. (1.12), we will obtain that component of the longitudinal force coefficient which depends on the induced velocity.

$$\Delta c_{Hv} = -2\frac{c_T}{\varkappa}\int_{\bar{r}_0}^{1}\left[\frac{1}{2\pi}\int_0^{2\pi}\bar{v}_y\tilde{\Gamma}(\bar{r},\psi)\sin\psi d\psi\right]d\bar{r}. \qquad (3.102)$$

According to relationships of Eqs. (2.68), (3.9) and (3.97) for $\bar{V} \approx \mu$

$$\Delta c_{Hv} = -\frac{c_T^2}{2\varkappa 2\mu}\int_{\bar{r}_0}^{1}\tilde{\Gamma}\left[\frac{1}{2\pi}\int_0^{2\pi}\frac{\hat{v}_y\sin\psi d\psi}{1+\frac{3}{2}\mu\sin\psi}\right]d\bar{r}. \qquad (3.103)$$

Let us develop the nondimensional induced velocity $\bar{v}_y$ into a Fourier series

$$\bar{v}_y(\bar{r},\psi) = \bar{v}_r + \bar{v}_{c1}(\bar{r})\cos\psi + \bar{v}_{s1}(\bar{r})\sin\psi + \bar{v}_{c2}(\bar{r})\cos 2\psi + \\ + \bar{v}_{s2}(\bar{r})\sin 2\psi + \bar{v}_{c3}(\bar{r})\cos 3\psi + \bar{v}_{s3}(\bar{r})\sin 3\psi + \ldots \qquad (3.104)$$

Then,

$$\frac{1}{2\pi}\int_0^{2\pi}\frac{\hat{v}_y(\bar{r},\psi)\sin\psi d\psi}{1+\frac{3}{2}\mu\sin\psi} = -0{,}76\mu(1+1{,}7\mu^2)\hat{v}_r + \\ + 0{,}5(1+1{,}69\mu^2+3{,}17\mu^4)\hat{v}_{s1}(\bar{r}) + 0{,}376\mu(1+2{,}24\mu^2)\hat{v}_{c2}(\bar{r}) - \\ - 0{,}282\mu^2(1+2{,}81\mu^2)\hat{v}_{s3}(\bar{r}) - 0{,}211\mu^3\hat{v}_{c4} + 0{,}158\mu^4\hat{v}_{s5}(\bar{r}) + \ldots \qquad (3.105)$$

In the determination of $\hat{v}_{c_2}$, $\hat{v}_{s_3}$, $\hat{v}_{c_4}$, $\hat{v}_{s_5}$, we take advantage of Eqs. (III.52) and (III.29) which means that we accept the approximation of $\tilde{\Gamma} = (3/2)\bar{r}$. Then

$$\hat{v}_{c2}(\bar{r})=-\frac{2}{3}\hat{v}_r, \qquad \hat{v}_{s3}(\bar{r})=\frac{1}{3}\hat{v}_{s1}(\bar{r}),$$
$$\hat{v}_{c4}(\bar{r})=-\frac{2}{15}\hat{v}_r, \qquad \hat{v}_{s5}(\bar{r})=\frac{1}{5}\hat{v}_{s1}(\bar{r}). \tag{3.106}$$

Introducing Eq. (3.106) into Eq. (3.105), we obtain

$$\frac{1}{2\pi}\int_0^{2\pi}\frac{\tilde{v}_y(\bar{r},\psi)\sin\psi}{1+\frac{3}{2}\mu\sin\psi}d\psi\approx-\mu(1+1{,}8\mu^2)\hat{v}_r+$$
$$+\frac{1}{2}[1+1{,}5\mu^2(1+1{,}8\mu^2)]\hat{v}_{s1}(\bar{r}). \tag{3.107}$$

According to Eqs. (I.7) and (II.11),

$$\hat{v}_r=-\tilde{\Gamma}, \quad \hat{v}_{s1}(\bar{r})=-2\bar{V}\frac{\tilde{\Gamma}}{\bar{r}}. \tag{3.108}$$

Let us quantitatively evaluate the influence of a nonuniform induced velocity distribution. If $\hat{v} = const = \hat{v}(\bar{r} = 0{,}7)$, then from Eq. (3.105)

$$\frac{1}{2\pi}\int_0^{2\pi}\frac{\hat{v}_y\sin\psi}{1+\frac{3}{2}\mu\sin\psi}d\psi=-0{,}76\mu(1+1{,}7\mu^2)\hat{v}_r(0{,}7).$$

According to Eq. (3.108), Eq. (3.107) for $\hat{v} \neq const$ will take the following form:

$$\frac{1}{2\pi}\int_0^{2\pi}\frac{\hat{v}_y(\bar{r},\psi)\sin\psi}{1+\frac{3}{2}\mu\sin\psi}d\psi\approx0{,}43\mu[1+0{,}79\mu^2(1+11{,}3\mu^2)]\hat{v}_r(\bar{r}=0{,}7).$$

In this way, in the presence of a nonuniform induced velocity distribution, the considered integral will even change its sign. Now, taking into consideration, Eq. (3.108), we substitute Eq. (3.107) into Eq. (3.103). Then for $\bar{V} \approx \mu$

$$\Delta c_{Hv}=\frac{1}{2\varkappa^2}\left\{[1+1{,}5\mu^2(1+1{,}8\mu^2)]\int_{\bar{r}_0}^{1}\frac{\tilde{\Gamma}^2}{\bar{r}}d\bar{r}-(1+1{,}8\mu^2)\int_{\bar{r}_0}^{1}\tilde{\Gamma}^2d\bar{r}\right\}c_\tau^2. \tag{3.109}$$

At $\tilde{\Gamma} = (3/2)\bar{r}$, $\bar{r}_0 = 0,1$ and $\varkappa = 0,94$, we obtain

$$\frac{\Delta c_{Hv}}{c_\tau} \approx 0,2\,[1 + 0,9\mu^2(1 + 9,5\mu^2)]\, c_\tau. \tag{3.110}$$

If $\tilde{\Gamma} = 1$, $\varkappa = 0,94$ and $\bar{r} = 0,1$, then

$$\frac{\Delta c_{Hv}}{c_\tau} \approx 0,8\,[1 + 1,32\mu^2(1 + 3,36\mu^2)]\, c_\tau. \tag{3.111}$$

For $\tilde{\Gamma} = (5/4)(\bar{r})^{1/2}$ (intermediate scheme of circulation) and the previous values of $\bar{r}_0$ and $\varkappa$

$$\frac{\Delta c_{Hv}}{c_\tau} \simeq 0,42\,[1 + \mu^2(1 + 5,2\mu^2)]\, c_\tau. \tag{3.112}$$

Now, we will define that part of the longitudinal force coefficient which depends on the flapping motion. Using relative quantities, after substituting Eq. (1.19), we obtain

$$\frac{\bar{v}_\delta}{\bar{W}} + \beta\cos\psi = -\bar{r}\,\frac{\frac{d\beta}{d\psi}\sin\psi - \beta\cos\psi}{\bar{W}}. \tag{3.113}$$

We will consider only first harmonics of the flapping motion. In accordance with the theory of the so-called *equivalent* rotor[66,75], it is possible to do the following: Instead of a rotor equipped with flapping control devices (e.g., δ_3), having the swashplate displaced from its neutral position, and its plane of rotation making an angle α_B with respect to the velocity vector and plane of rotation, while collective pitch angle is ϕ_0; it is possible to consider a rotor without any flapping control devices, with all controls in neutral, and whose angle of attack is equal to $\alpha_э = \alpha_B + \theta_{2э}$, $(\theta_{2э} = \theta_2 + \bar{k}b_1)$ and whose collective pitch angle* is $\phi_{0э} = \phi_0 - \bar{k}a_0$. Both of those rotors will have the same aerodynamic characteristics. We will consider such *equivalent* rotor whose longitudinal axis of coordinates, x, lies in the effective plane of rotation which, makes, with the hub plane, an angle $\theta_{2э}$. Flapping motion with respect to the effective plane of rotation is given by Eq. (3.17). We substitute Eq. (3.17) into Eqs. (3.113) and (3.85). Then, we find the longitudinal force component which is associated with the flapping motion

$$\Delta H_\beta = \Delta T\bar{r}\,\frac{a_{10} - a_0\cos\psi}{\bar{W}}. \tag{3.114}$$

*See Eqs. (2.82) and (2.98)

Next, we substitute Eq. (3.114) into Eq. (1.12) and switch from forces to coefficients. Then, taking into consideration Eq. (2.74), and changing the order of integration, we obtain

$$\Delta c_{H\beta}=2\,\frac{k}{\pi}\int\limits_{\bar r_0}^{1}\bar r\left[\frac{1}{2\pi}\int\limits_{0}^{2\pi}\Gamma(\bar r,\ \psi)(a_{10}-a_0\cos\psi)\,d\psi\right]d\bar r. \tag{3.115}$$

According to Eqs. (3.9), (3.11) and (3.97)

$$\Delta c_{H\beta}=2\,\frac{c_\tau}{\varkappa}\int\limits_{\bar r_0}^{1}\bar r\tilde\Gamma\left[\frac{1}{2\pi}\int\limits_{0}^{2\pi}\frac{a_{10}-a_0\cos\psi}{1+\frac{3}{2}\,\mu\sin\psi}\,d\psi\right]d\bar r, \tag{3.116}$$

where

$$\frac{1}{2\pi}\int\limits_{0}^{2\pi}\frac{a_{10}-a_0\cos\psi}{1+\frac{3}{2}\,\mu\sin\psi}\,d\psi\approx[1+1{,}12\mu^2(1+1{,}7\mu^2)]\,a_{10}. \tag{3.117}$$

Taking into consideration Eq. (3.12), we finally obtain

$$\frac{\Delta c_{H\beta}}{c_\tau}\approx 1{,}06\,[1+1{,}12\mu^2(1+1{,}7\mu^2)]\,a_{10}. \tag{3.118}$$

Calculations indicate that coefficient $\Delta c_{H\beta}$ is not appreciably affected by the character of $\tilde\Gamma$ distribution.

Unifying the obtained results, we will have

$$\frac{c_H}{c_\tau}=\frac{1}{2}\,\varkappa_H\mu\ \frac{\sigma}{c_\tau}\,c_{xpH}+\tilde H_1\mu^2(1+1{,}7\mu^2)\,a_9+\tilde H_2\,[1+\tilde H_3\mu^2(1+\tilde H_4\mu^2)]\,c_\tau+$$
$$+1{,}06\,[1+1{,}12\mu^2(1+1{,}7\mu^2)]\,a_{10}. \tag{3.119}$$

Values of the $\tilde H_\eta$ coefficients are given in Table 3.1.

$\tilde\Gamma$	$\tilde H_1$	$\tilde H_2$	$\tilde H_3$	$\tilde H_4$
$\frac{3}{2}\,\bar r$	1,20	0,2	0,9	9,5
1,0	1,44	0,8	1,32	3,36

Table 3.1

The most important role in Eq. (3.119) is played by the last term containing a_{10} and the second one, dependent on $\alpha_э$. A comparison with experimental data was favorable when computations were performed according to the above formula with the following coefficients:

$$\frac{c_H}{c_т}=\frac{1}{2}\varkappa_H\mu\,\frac{\sigma}{c_т}c_{xpH}+1{,}3\mu^2(1+1{,}7\mu^2)\alpha_э+0{,}5\,[1+1{,}1\mu^2(1+6{,}4\mu^2)]\,c_т+$$
$$+1{,}06\,[1+1{,}12\mu^2(1+1{,}7\mu^2)]\,a_{10}. \qquad (3.120)$$

The results were compared with experimental data obtained by M.K. Speranskiy from rotor tests *(D = 12,5m; σ = 0,086; ωR = 131 m/sec)*. In addition, comparisons were made between computed and measured values for a rotor model with *D = 2,01m* and *σ = 0,105*. In order to give some idea regarding the order of magnitude of various quantities appearing in Eq. (3.120), their numerical values are shown (for *μ = 0,30* and *D = 12,5*) retaining the same sequence of terms as in the original equation:

$$\frac{c_н}{c_т}=0{,}0047-0{,}0474+0{,}0087+0{,}155=0{,}121.$$

Comparisons of computed and tested values are shown in Table 3.2.

$D_м$	μ	$\alpha_э^\circ$	$\frac{c_т}{\sigma}$	$\left(\frac{c_н}{c_т}\right)_{test}$	$\left(\frac{c_н}{c_т}\right)_{calc}$	$\frac{c_{н\,calc}}{c_{н\,test}}$
12,5	0,30	—17	0,172	0,122	0,121	0,99
12,5	0,20	—12	0,157	0,0640	0,0620	0,97
2,01	0,39	0	0,129	0,107	0,101	0,94

Table 3.2

4. LATERAL FORCE COEFFICIENT

In Sect. 1 of Ch. I, an expression was developed for ΔS - the lateral component of the blade element force. After substituting Eq. (1.9) into Eq. (1.11), we obtain for the latter

$$\Delta S=\Delta S_p+\Delta S_\alpha+\Delta S_v+\Delta S_\beta, \qquad (3.121)$$

where

$$\Delta S_p=-\Delta X_p\frac{W_1}{W}\cos\psi, \qquad (3.122)$$

$$\Delta S_\alpha = \Delta T \frac{V \sin \alpha_э}{W} \cos \psi, \tag{3.123}$$

$$\Delta S_v = \Delta T \frac{v_y}{W} \cos \psi, \tag{3.124}$$

$$\Delta S_\beta = \Delta T \left(\frac{v_\delta}{W} \cos \psi - \beta \sin \psi \right). \tag{3.125}$$

Let us examine Eq. (3.122). After taking into consideration Eqs. (1.7) and (1.12), switching to relative quantities, and assuming $W_1 \approx W$, we will have one component of the lateral force coefficient

$$\Delta c_{Sp} = -\frac{k}{2\pi^2} \int_0^{2\pi} \cos \psi d\psi \int_{\bar{r}_0}^1 c_{xp} \bar{b} \bar{W}^2 d\bar{r} = -\frac{\sigma}{2\pi} \int_0^{2\pi} \cos \psi d\psi c_{xp\psi} \int_{\bar{r}_0}^1 \bar{b} \bar{W}^2 d\bar{r}. \tag{3.126}$$

The quantity $c_{xp\psi}$ varies with the azimuth ψ as well as W and $c_{y\psi}$. However, at points symmetrical with respect to the Oz axis; i.e., for azimuth angles ψ and $\pi - \psi$, values of $c_{xp\psi}$ are approximately the same. For this reason, Eq. (3.126) can be presented under the following form:

$$\Delta c_{Sp} \approx -\frac{\sigma}{2\pi} \int_{\frac{\pi}{2}}^{\frac{3}{2}\pi} \left\{ c_{xp\psi} \int_{\bar{r}_0}^1 \bar{b} \bar{W}^2 d\bar{r} \left[\cos \psi + \cos (\pi - \psi) \right] \right\} d\psi. \tag{3.127}$$

The expression within the square brackets is equal to zero. Consequently,

$$\Delta c_{Sp} \approx 0. \tag{3.128}$$

Now, we are going to consider the coefficient $\Delta c_{S\alpha}$. By analogy with the development of Eq. (3.96), we obtain

$$\Delta c_{S\alpha} = 2\mu\alpha_э \frac{c_\tau}{\varkappa} \int_{\bar{r}_0}^1 \left[\frac{1}{2\pi} \int_0^{2\pi} \tilde{\Gamma}(\bar{r}, \psi) \cos \psi d\psi \right] d\bar{r}. \tag{3.129}$$

Introducing Eq. (3.97) into the above, we will have

$$\frac{1}{2\pi} \int_0^{2\pi} \tilde{\Gamma}(\bar{r}, \psi) \cos \psi d\psi = \tilde{\Gamma} \frac{1}{2\pi} \int_0^{2\pi} \frac{\cos \psi d\psi}{1 + \frac{3}{2} \mu \sin \psi} = 0. \tag{3.130}$$

And again,

$$\Delta c_{S\alpha}=0. \tag{3.131}$$

Substituting Eq. (3.124) into Eq. (1.12), and passing from forces to their coefficients, we obtain

$$\Delta c_{SV}=2\frac{c_\tau}{\varkappa}\int_{\bar r_0}^{1}\left[\frac{1}{2\pi}\int_0^{2\pi}\bar v_y\tilde\Gamma(\bar r,\psi)\cos\psi d\psi\right]d\bar r. \tag{3.132}$$

According to Eqs. (2.68), (3.9) and (3.07),

$$\Delta c_{SV}=\frac{c_\tau^2}{2\varkappa^2\mu}\int_{\bar r_0}^{1}\tilde\Gamma\left[\frac{1}{2\pi}\int_0^{2\pi}\frac{\hat v_y\cos\psi}{1+\frac{3}{2}\mu\sin\psi}d\psi\right]d\bar r. \tag{3.133}$$

Similar to the development of the expression for Δc_{Hv}, we expand $\bar v_y$ into a series (Eq. (3.104)). Then, after determination of the integrals, we find

$$\begin{aligned}\Delta c_{SV}=\frac{c_\tau^2}{4\varkappa^2}\Bigg\{&\left[\frac{1}{\mu}+0{,}56\mu(1+1{,}12\mu^2)\right]\int_{\bar r_0}^{1}\hat v_{c1}\tilde\Gamma d\bar r-\\&-0{,}75(1+1{,}12\mu^2)\int_{\bar r_0}^{1}\hat v_{s2}\tilde\Gamma d\bar r-0{,}56\mu(1+1{,}7\mu^2)\int_{\bar r_0}^{1}\hat v_{c3}\tilde\Gamma d\bar r+\\&+0{,}42\mu^2\int_{\bar r_0}^{1}\hat v_{s4}\tilde\Gamma d\bar r+0{,}32\mu^3\int_{\bar r_0}^{1}\hat v_{c5}\tilde\Gamma d\bar r\Bigg\}.\end{aligned} \tag{3.134}$$

In Appendix IV, explicit expressions are given for the determination of $\hat v_{c1}, \ldots, \hat v_{c5}$ for any law of the $\tilde\Gamma$ distribution. In Sect. 6 of Ch. II and Sect. 1 of Ch. III, recommended ways of performing those computations are shown (see Eq. (3.35)). Graphs of $\hat v_{c1}$ for the three considered schemes of the $\tilde\Gamma$ distribution are given in Fig. 3.2. Graphs of $\hat v_{s2}$, $\hat v_{c3}$, $\hat v_{c5}$ and $\hat v_{c4}$ are shown in Figs. 3.9-3.11. We will limit ourselves to the development of working formulae for Δc_{Sv} for $\tilde\Gamma = (3/2)\bar r$ and $\tilde\Gamma = 1$. Assuming $\tilde\Gamma = (3/2)\bar r$, in Eq. (3.134), we will obtain integrals of the following types:

$$A_1^{(1)}=\int_{\bar r_0}^{1}\bar r\hat v_{c1}(\bar r)\,d\bar r,\qquad B_1^{(2)}=\int_{\bar r_0}^{1}\bar r\hat v_{s2}(\bar r)\,d\bar r,$$
$$A_1^{(3)}=\int_{\bar r_0}^{1}\bar r\hat v_{c3}(\bar r)\,d\bar r,\qquad B_1^{(4)}=\int_{\bar r_0}^{1}\bar r\hat v_{s4}(\bar r)\,d\bar r,\qquad (3.135)$$
$$A_1^{(5)}=\int_{\bar r_0}^{1}\bar r\hat v_{c5}(\bar r)\,d\bar r.$$

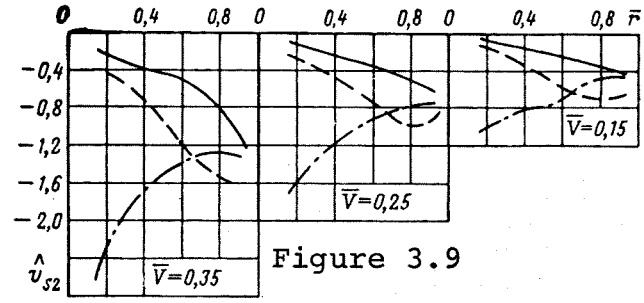

Figure 3.9

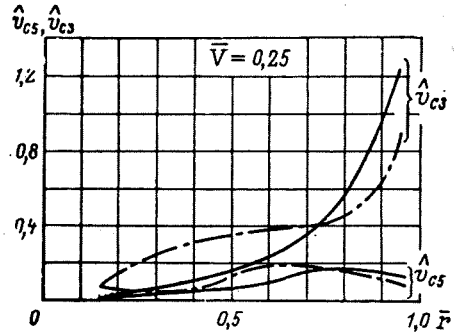

Figure 3.10

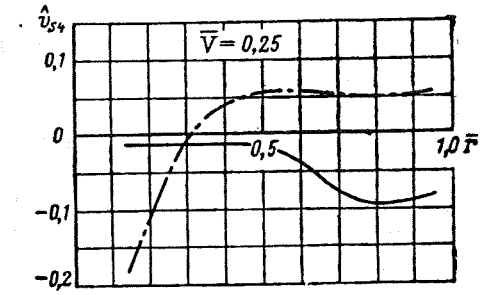

Figure 3.11

In Figs. 3.12 and 3.13, graphs of $A_1^{(1)}$ and $B_1^{(2)}$ are shown. From those graphs, we find that for $\bar V = 0,25$ and $\tilde\Gamma = (3/4)\bar r$, $A_1^{(1)} = -0,2$ and $B_1^{(2)} = -0,22$; while from Figs. 3.10 and 3.11, for $\bar r_0 = 0,1$, $A_1^{(3)} = 0,246$; $A_1^{(5)} = 0,06$; $B_1^{(4)} = -0,029$. Those figures represent approximate values of A_1^n and B_1^m; also for $\bar V \neq 0,25$. Substituting the thus obtained values into Eq. (3.134), assuming $\varkappa \approx 0,94$ and neglecting small terms, we obtain

$$\frac{\Delta c_{SV}}{c_T}=-0,085\left(\frac{1}{\mu}-0,83+1,25\mu\right)c_T. \qquad (3.136)$$

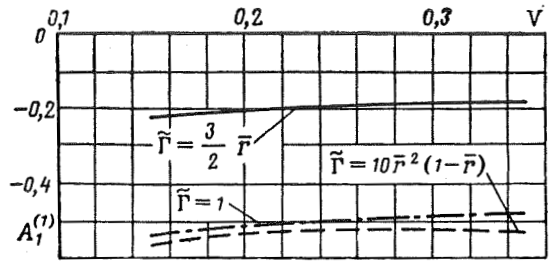

Figure 3.12

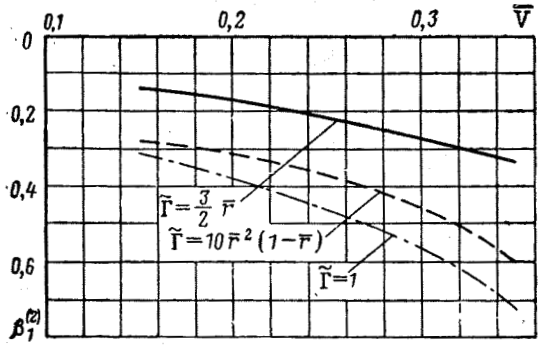

Figure 3.13

Substituting $\tilde{\Gamma} = 1$ into Eq. (3.134), we obtain the following integrals:

$$A_0^{(1)}=\int_{\bar{r}_0}^{1}\hat{v}_{c1}(\bar{r})\,d\bar{r},\qquad B_0^{(2)}=\int_{\bar{r}_0}^{1}\hat{v}_{s2}(\bar{r})\,d\bar{r},\qquad A_0^{(3)}=\int_{\bar{r}_0}^{1}\hat{v}_{c3}(\bar{r})\,d\bar{r},$$

$$B_0^{(4)}=\int_{\bar{r}_0}^{1}\hat{v}_{s4}(\bar{r})\,d\bar{r},\qquad A_0^{(5)}=\int_{\bar{r}_0}^{1}\hat{v}_{c5}(\bar{r})\,d\bar{r}. \tag{3.137}$$

In Figs. 3.14 and 3.15, graphs of $A_0^{(1)}$ and $B_0^{(2)}$ are given and we find that for $\overline{V} = 0,25$ and $\tilde{\Gamma} = 1$, $A_0^{(1)} = -0,6$; $B_0^{(2)} = -1$. From Figs. 3.10 and 3.11, for $\tilde{\Gamma} = 1$ and $\overline{r}_0 = 0,1$, we obtain computed values of $A_0^{(3)} = 0,343$; $B_0^{(4)} = 0,01$; $A_0^{(5)} = 0,091$. The above magnitudes of A_0^n and B_0^m are also approximately correct for $\overline{V} \neq 0,25$. Substituting those quantities into Eq. (3.134), assuming $\varkappa = 0,94$, and neglecting small terms, we obtain

$$\frac{\Delta c_{SV}}{c_T}=0{,}256\left[\frac{1}{\mu}-1{,}25+0{,}88\mu\,(1-1{,}43\mu)\right]c_T. \tag{3.138}$$

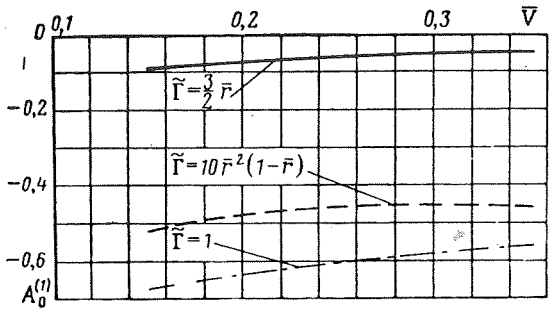

Figure 3.14

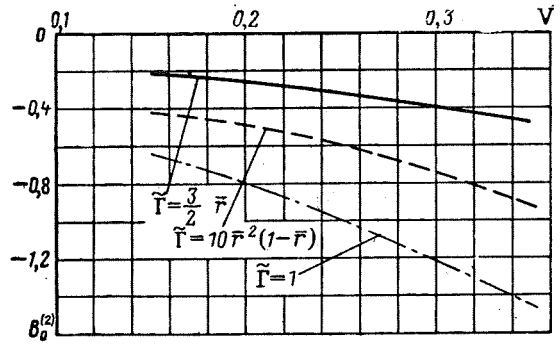

Figure 3.15

A comparison of Eq. (3.138) with Eq. (3.136) would indicate that changes to the average circulation can triple the Δc_{sv} value.

Now, we are going to evaluate the $\Delta c_{s\beta}$ coefficient. By substituting Eq. (1.19) into Eq. (3.125) and making a change toward relative quantities, we obtain

$$\frac{\bar{v}_\delta}{\bar{W}}\cos\psi-\beta\sin\psi=-\frac{1}{\bar{W}}\left(\bar{r}\frac{d\beta}{d\psi}\cos\psi+\mu\beta+\bar{r}\beta\sin\psi\right). \tag{3.139}$$

Switching from forces to their coefficients and taking into consideration, Eqs. (3.97) and (3.12), we find, similar to the preceding case, that

$$\frac{\Delta c_{s\beta}}{c_\tau}=\frac{1}{\varkappa}\left(\left[1+1{,}12\mu^2(1+1{,}7\mu^2\right)\left(1-1{,}34\int_{\bar{r}_0}^{1}\tilde{\Gamma}d\bar{r}\right]\right)b_{10}+$$

$$+0{,}75\mu\left\{1+1{,}7\mu^2-2{,}67\left[1+1{,}12\mu^2(1+1{,}7\mu^2)\right]\int_{\bar{r}_0}^{1}\tilde{\Gamma}d\bar{r}\right\}a_0\cdot\Big). \tag{3.140}$$

For $\tilde{\Gamma} = (3/2)\bar{r}$; $\bar{r}_0 = 0{,}1$ and $\varkappa = 0{,}94$,

$$\frac{\Delta c_{S\beta}}{c_T} = 1{,}06 b_{10} - 0{,}8\mu(1 - 0{,}87\mu^2) a_0. \qquad (3.141)$$

In the case of $\tilde{\Gamma} = 1$; $\bar{r} = 0{,}1$ and $\varkappa = 0{,}94$

$$\frac{\Delta c_{S\beta}}{c_T} \approx 1{,}02 b_{10} - 1{,}12\mu(1 + \mu^2) a_0. \qquad (3.142)$$

By unifying the obtained results, we find that

$$\frac{c_S}{c_T} = \tilde{S}_1 b_{10} - \tilde{S}_2 \mu(1 - \tilde{S}_3 \mu^2) a_0 - \tilde{S}_4 \left(\frac{1}{\mu} - \tilde{S}_5 + \tilde{S}_6 \mu - \tilde{S}_7 \mu^2\right) c_T. \qquad (3.143)$$

Values of the $\tilde{S}_n$ coefficients are given in Table 3.3.

$\tilde{\Gamma}$	$\tilde{S}_1$	$\tilde{S}_2$	$\tilde{S}_3$	$\tilde{S}_4$	$\tilde{S}_5$	$\tilde{S}_6$	$\tilde{S}_7$
$\frac{3}{2}\bar{r}$	1,06	0,80	1,36	0,085	0,83	1,25	0
1,0	1,02	1,12	1,00	0,256	1,25	0,88	1,26

Table 3.3

To illustrate the application of the developed formulae, we will consider the following example. Let $\mu = 0{,}25$; $c_T/\sigma = 0{,}18$; $\sigma = 0{,}09$; $\gamma = 5{,}6$. Then from Eq. (3.16) $a_0 = 0{,}126$. From Eq. (3.37) we find that when $\tilde{\Gamma} = (3/2)\bar{r}$, then $b_{10} = 0{,}0573$ and for $\tilde{\Gamma} = 1$, b_{10} becomes $b_{10} = 0{,}069$. Retaining the original order of terms in Eq. (3.143), we find from the latter that for $\tilde{\Gamma} = (3/2)\bar{r}$, we have

$$\frac{c_S}{c_T} = 0{,}0607 - 0{,}0266 - 0{,}008 = 0{,}0261,$$

and for $\tilde{\Gamma} = 1$

$$\frac{c_S}{c_T} = 0{,}0705 - 0{,}0375 - 0{,}020 = 0{,}0130.$$

The above results emphasize the importance of $\tilde{\Gamma}$ as far as the c_S/c_T values are concerned. It should also be noted that under the assumption of $\hat{v} = const$, the term containing c_T would be zero and $c_S/c_T = 0{,}0391$ for both $\tilde{\Gamma} = (3/2)\bar{r}$ and $\tilde{\Gamma} = 1$. It can be seen from the above example that consideration of the nonuniformity of induced velocity at $\tilde{\Gamma} = 1$ reduces to $1/3$, the c_S/c_T value.

5. PITCHING MOMENT COEFFICIENT AT THE ROTOR HUB

Axes of the flapping hinges are located at a distance l_Γ from the rotor axis. Due to this, the rotor hub experiences a longitudinal moment generated by aerodynamic and inertial forces[14]. The magnitude of that moment, at $l_\Gamma = r_0$ will be

$$M_z = -\frac{kl_\Gamma}{2\pi}\int_0^{2\pi}\sum_\psi \cos\psi d\psi, \tag{3.144}$$

where

$$\sum_\psi = \varkappa\int_{r_0}^{R} dT - \frac{M_\Gamma}{g}\frac{d^2\beta}{dt^2} - G_\pi \tag{3.145}$$

is an equivalent force acting at the flapping hinge at a given azimuth position, and resulting from all axially-directed rotor forces. It can be seen that moment M_z is composed of a moment due to the aerodynamic forces, M_{za}, and another one, M_{zm}, generated by the inertial forces.

$$M_z = M_{za} + M_{zm}, \tag{3.146}$$

where

$$M_{za} = -l_\Gamma\varkappa\frac{k}{2\pi}\int_0^{2\pi}\cos\psi d\psi\int_{r_0}^{R}\frac{dT}{dr}\,dr, \tag{3.147}$$

and

$$M_{zm} = l_\Gamma\frac{k}{2\pi}\int_0^{2\pi}\cos\psi\left(\frac{M_\Gamma}{g}\frac{d^2\beta}{dt^2} + G_\pi\right)d\psi = l_\Gamma\frac{M_\Gamma}{g}\frac{k}{2\pi}\int_0^{2\pi}\frac{d^2\beta}{dt^2}\cos\psi d\psi. \tag{3.148}$$

We substitute Eq. (2.74) into Eq. (3.147), switch to relative quantities, and after changing the order of integration, we obtain

$$m_{za} = -2\bar{l}_\Gamma\varkappa\frac{k}{\pi}\int_{\bar{r}_0}^{1}\left[\frac{1}{2\pi}\int_0^{2\pi}\bar{\Gamma}(\bar{r},\,\psi)\,\overline{W}\cos\psi d\psi\right]d\bar{r}. \tag{3.149}$$

Taking into consideration, Eqs. (3.9), (3.11) and (3.97) we have

$$m_{za} = -2\bar{l}_\Gamma c_T\int_{\bar{r}_0}^{1}\tilde{\Gamma}\left[\frac{1}{2\pi}\int_0^{2\pi}\frac{\bar{r}\cos\psi + \mu\sin\psi\cos\psi}{1+\frac{3}{2}\mu\sin\psi}d\psi\right]d\bar{r}. \tag{3.150}$$

The internal integral is equal to zero; consequently,

$$m_{za}=0. \tag{3.151}$$

In other words, longitudinal hub moment of aerodynamic forces equals zero as long as the flapping motion of the blades is of the first-harmonic type.

Now, we will define m_{zm}; i.e., coefficient of the pitching moment resulting from the inertial (mass) forces. Remembering that $t = \psi/\omega$, and in considering Eq. (3.17), we obtain

$$\frac{1}{2\pi}\int_0^{2\pi}\frac{d^2\beta}{dt^2}\cos\psi d\psi=\frac{1}{2}\omega^2 a_{10}. \tag{3.152}$$

We introduce the following quantity

$$r_r=\frac{J_r}{M_r}g. \tag{3.153}$$

For a uniform mass distribution along the blade, $r_\Gamma = (2/3)R$.

Expressing those relationships in relative quantities and taking into consideration, Eq. (3.5), we will have

$$m_{zm}=\frac{1}{2}\bar{l}_r\frac{\sigma}{\bar{r}_r}\frac{a_\infty}{\gamma}a_{10}. \tag{3.154}$$

Let us rewrite the above expression. Expressing $(\sigma/\gamma)a_\infty$ with a_0 from Eq. (3.15), and neglecting Δa_0, we obtain

$$m_{zm}=\frac{\bar{l}_r}{2a_0}\frac{\bar{r}_*}{\bar{r}_r}c_T a_{10}. \tag{3.155}$$

Calculations show that $\bar{r}_*:\bar{r}_\Gamma \approx 1$. Consequently,

$$m_{zm}\approx\frac{\bar{l}_r}{2a_0}c_T a_{10}. \tag{3.156}$$

This formula gives the coefficient of longitudinal moment due to the inertial forces acting at the horizontal hinge axis and directed along the effective rotor axis, perpendicular to the effective plane of rotation. However, in the presence of a flapping control device (say, δ_3) and the swashplate inclination, the effective (virtual) axis of rotation is displaced from the rotor mechanical axis through an angle δ_z. As a result, there will appear components of the centrifugal force δ_z Ц $\cos\psi$, normal to the rotor hub plane. Those normal components will generate, with respect to the z_1 axis, a supplementary longitudinal moment:

$$M_{z\text{Ц}}=\delta_z l_r \frac{k\text{Ц}}{2\pi}\int_0^{2\pi}\cos^2\psi d\psi, \quad \text{where} \quad \text{Ц}=\omega^2\frac{M_r}{g}. \tag{3.157}$$

Performing the indicated integration, we obtain

$$M_{z\text{Ц}}=\frac{1}{2}\frac{kM_r}{g}l_r\delta_z\omega^2, \tag{3.158}$$

from which, by analogy with Eq. (3.156), we obtain

$$m_{z\text{Ц}}\approx\frac{\bar{l}_r}{2a_0}c_r\delta_z. \tag{3.159}$$

Combining quantities m_{zm} and $m_{z\mu}$, and keeping in mind, Eq. (3.38) with $\theta_{29} = \delta_z$, we will obtain the resultant longitudinal-moment coefficient due to all mass forces, under the following form:

$$m_{zm}\approx\frac{\bar{l}_r}{2a_0}c_r a_1. \tag{3.160}$$

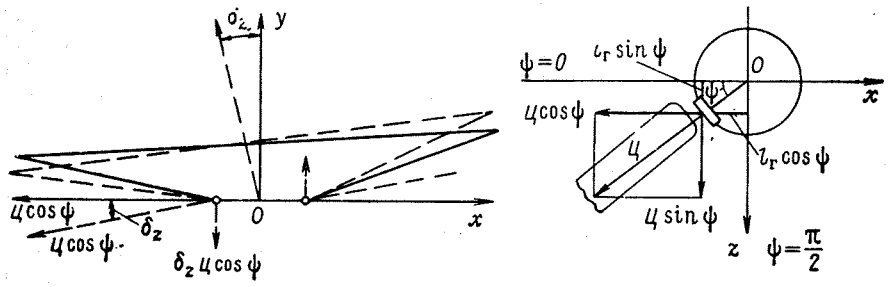

Figure 3.16

6. ROLLING MOMENT COEFFICIENT AT THE ROTOR HUB

Rolling moment at the rotor hub, generated by aerodynamic as well as inertial forces will be

$$M_x=-\frac{kl_r}{2\pi}\int_0^{2\pi}\sum_\psi \sin\psi d\psi. \tag{3.161}$$

The magnitude of the resultant Σ_ψ is given by Eq. (3.145).

It can be seen from this equation that M_x is composed of the aerodynamic moments, M_{xa}; and inertial (mass) forces, M_{xm}:

$$M_x = M_{xa} + M_{xm}. \tag{3.162}$$

Here,

$$M_{xa} = -l_r \varkappa \frac{k}{2\pi} \int_0^{2\pi} \sin\psi d\psi \int_{r_0}^{R} dT, \tag{3.163}$$

and

$$M_{xm} = l_r \frac{M_r}{g} \frac{k}{2\pi} \int_0^{2\pi} \frac{d^2\beta}{dt^2} \sin\psi d\psi. \tag{3.164}$$

In analogy with Eq. (3.150), we may write

$$m_{xa} = -2\bar{l}_r c_T \int_{\bar{r}_0}^{1} \tilde{\Gamma} \left[\frac{1}{2\pi} \int_0^{2\pi} \frac{\bar{r}\sin\psi + \mu\sin^2\psi}{1 + \frac{3}{2}\mu\sin\psi} d\psi \right] d\bar{r}, \tag{3.165}$$

$$\frac{1}{2\pi} \int_0^{2\pi} \frac{\bar{r}\sin\psi + \mu\sin^2\psi}{1 + \frac{3}{2}\mu\sin\psi} d\psi \approx \frac{1}{2}\mu(1 + 1{,}7\mu^2)\left(1 - \frac{3}{2}\bar{r}\right). \tag{3.166}$$

Substituting that expression into Eq. (3.165) and taking into consideration Eq. (3.12), we obtain

$$\frac{m_{xa}}{c_T} = -\mu(1 + 1{,}7\mu^2)\bar{l}_r \left(\int_{\bar{r}_0}^{1} \tilde{\Gamma} d\bar{r} - \frac{3}{4} \right). \tag{3.167}$$

If $\tilde{\Gamma}_I = (3/2)\bar{r}$ and $\bar{r}_0 \leq 0{,}1$, then $m_{xa} \approx 0$. For $\tilde{\Gamma}_{III} = 1$ and $\bar{r}_0 = 0{,}1$

$$\frac{m_{xa}}{c_T} = -0{,}15\mu(1 + 1{,}7\mu^2)\bar{l}_r. \tag{3.168}$$

The quantity $m_{xa}/c_T < 0$ and is usually very small. For instance, at $\mu = 0{,}3$ and $\bar{l}_r \approx 0{,}01$, $m_{xa}/c_T = -0{,}00045$. In the physical sense, the ratio m_{xa}/c_T represents a relative arm on which the rotor thrust would act in order to produce moment m_{xa}. In the above considered example, that arm amounts to $0{,}045\%$ of the blade radius, while the moment is directed toward the retreating blade side. The rolling moment coefficient associated with the inertial forces, in analogy with Eq. (3.160) will be

$$\frac{m_{xm}}{c_T} \approx \frac{\bar{l}_r}{2a_0} b_1, \tag{3.169}$$

where b_1 is determined from Eq. (3.39), assuming $\theta_{1\vartheta} = -\delta_x$.

7. COEFFICIENT OF POWER REQUIRED TO OVERCOME THE BLADE PROFILE DRAG

It was shown in Sect. 3 of Ch. I, that

$$75N_p = \frac{k}{2\pi}\int_0^{2\pi} d\psi \int_{r_0}^{R} W_1 dX_p. \tag{3.170}$$

Introducing Eq. (1.7) into the above, we will obtain the following relationship for the power coefficient.

$$m_{pn} = \frac{k}{2\pi^2}\int_0^{2\pi} d\psi \int_{\bar{r}_0}^{1} c_{xp}\bar{b}\overline{W}_1^3 d\bar{r} = \sigma\frac{1}{2\pi}\int_{\bar{r}_0}^{1}\bar{b}\,d\bar{r}\int_0^{2\pi} c_{xp}\overline{W}_1^3 d\psi. \tag{2.171}$$

We present the above expression under the following form:

$$m_{pn} = \sigma\int_{\bar{r}_0}^{1}\bar{b}\,c_{xpr}\left(\frac{1}{2\pi}\int_0^{2\pi}\overline{W}_1^3 d\psi\right)d\bar{r}, \tag{3.172}$$

where

$$c_{xpr} = \frac{\frac{1}{2\pi}\int_0^{2\pi} c_{xp}\overline{W}_1^3 d\psi}{\frac{1}{2\pi}\int_0^{2\pi}\overline{W}_1^3 d\psi} \tag{3.171}$$

is the mean value (averaged over a circle of radius r) of the blade section profile drag coefficient. The quantity $c_{xp}(\bar{r},\psi)$ appearing under the integral sign, is determined from the two-dimensional blade airfoil characteristics with due consideration of $c_y(\bar{r},\psi)$ as well as Mach $(M = W_1(\bar{r},\psi)/a)$ and Reynolds $(R_e)\bar{r},\psi))$ numbers. Let us take to the front of the integral sign, the quantity c_{xp_0} - blade profile drag coefficient, averaged over the whole rotor disc. Then

$$m_{pn} = \sigma k_p c_{xp_0}\int_{\bar{r}_0}^{1}\left(\frac{1}{2\pi}\int_0^{2\pi}\overline{W}_1^3 d\psi\right)d\bar{r}, \tag{3.174}$$

where

$$k_p = \frac{\int_{\bar{r}_0}^{1}\bar{b}\left(\frac{1}{2\pi}\int_0^{2\pi}\overline{W}_1^3 d\psi\right)\bar{d}r}{\int_{\bar{r}_0}^{1}\left(\frac{1}{2\pi}\int_0^{2\pi}\overline{W}_1^3 d\psi\right)d\bar{r}} \tag{3.175}$$

and

$$c_{xp_0}=\frac{\int\limits_{\bar{r}_0}^{1}\tilde{b}c_{xp_r}\left(\frac{1}{2\pi}\int\limits_{0}^{2\pi}\overline{W}_1^3 d\psi\right)d\bar{r}}{k_p\int\limits_{\bar{r}_0}^{1}\left(\frac{1}{2\pi}\int\limits_{0}^{2\pi}\overline{W}_1^3 d\psi\right)d\bar{r}}. \tag{3.176}$$

Similar to Eq. (3.88), we have

$$\overline{W}_1^3\simeq\overline{W}^3+\frac{3}{2}\overline{W}(\mu\operatorname{tg}\alpha_э+\bar{v}_\delta)^2. \tag{3.177}$$

We substitute Eq. (1.2) for $\overline{W}$ and Eq. (1.19) for $\overline{v}_\delta$. Then

$$\int\limits_0^1\left(\frac{1}{2\pi}\int\limits_0^{2\pi}\overline{W}_1^3 d\psi\right)d\bar{r}=\frac{1}{4}(1+3\mu^2+3\mu^2\operatorname{tg}^2\alpha_э+\Delta_\delta). \tag{3.178}$$

Here

$$\Delta_\delta=\frac{3}{4}\left[\left(1+\frac{1}{2}\mu^2\right)a_{10}^2+2\mu^2a_0^2+\left(1+\frac{3}{2}\mu^2\right)b_{10}^2-2{,}67\left(1+\frac{3}{4}\mu^2\right)a_0b_{10}\right].$$

For $\overline{V}=0{,}5$; $\alpha_э=-30°$; $c_T/\sigma=0{,}141$; $\sigma=0{,}11$, we would have, with an error of less than 1%

$$\Delta_\delta\approx\frac{3}{4}\left(1+\frac{1}{2}\mu^2\right)a_{10}^2. \tag{3.179}$$

In addition,

$$1+3\mu^2+3\mu^2\operatorname{tg}^2\alpha_э=1+3\overline{V}^2.$$

After substituting those expressions into Eq. (3.174), we obtain

$$m_{pn}=\frac{1}{4}(1+\Delta_\delta+3\overline{V}^2)\sigma k_pc_{xp_0}. \tag{3.180}$$

Let us consider the k_p coefficient. If we assume that approximately, $\overline{v}_\delta=0$, then

$$\frac{1}{2\pi}\int\limits_0^{2\pi}\overline{W}_1^3 d\psi\approx\bar{r}\left(\bar{r}^2+\frac{3}{2}\overline{V}^2\right). \tag{3.181}$$

According to Eq. (3.175), the coefficient k_p, partially

accounting for the influence of the blade planform* on the m_p value, will be

$$k_p = \frac{4}{1+3\bar{V}^2}\int_{\bar{r}_0}^{1}\bar{r}\tilde{b}\left(\bar{r}^2+\frac{3}{2}\bar{V}^2\right)d\bar{r}. \qquad (3.182)$$

For the trapezoidal blades, $\tilde{b}$ is expressed by Eq. (3.74). We introduce that relationship into Eq. (3.182), and for $r_0 = 0$, we obtain

$$k_p = \frac{\eta_* - 0{,}8(\eta_* - 1)\dfrac{1+2{,}5\bar{V}^2}{1+3\bar{V}^2}}{0{,}7+0{,}3\eta_*}. \qquad (3.183)$$

Graphs of $k_p = f(\bar{V})$ are shown in Fig. 3.17.

Graphs of $c_{y_0} = f(k_p c_{xp_0})$ for various values of parameters $\bar{V}$ and $\alpha_э$ are shown in Fig. 3.18. They were obtained analytically by V.N. Kvokov at $\omega R = 220$ m/sec for blades whose geometric characteristics are given in Fig. 3.8. Coefficients c_{y_0} were computed according to Eq. (3.79). The computations were performed, as in the case of the determination of coefficient c_{xpH}, according to Eq. (3.94). For $\bar{V} < 0{,}2$, it is recommended to use the relationships shown in Fig. 3.18 for $\bar{V} = 0{,}2$. With the increasing forward inclination of the rotor axis, its profile and wave drag also increases. This can be explained by an increase of the speed of flow encountered by the blade sections as well as by higher values of $c_y(\bar{r}, \psi)$ in the tip regions ($\bar{r} > 0{,}7$) at azimuth angles $220° < \psi° < 320°$. For $\omega R \neq 220$ m/sec, corrections to the c_{xp_0} values can be made from the graphs in Fig. 3.19. The total blade profile power coefficient will be

$$m_p = m_{pn} + \Delta m_p. \qquad (3.184)$$

Coefficient Δm_p takes into account the influence of the radial component of the velocity of flow $V_R = V \cos \alpha_э \cos \psi$ (see Fig. 1.1). This increase of the aerodynamic drag resulting from the friction forces can be approximated by the following expression:

$$\Delta m_p \simeq 5 \cdot 10^{-3}\bar{V}^2\sigma. \qquad (3.185)$$

---

*According to Eq. (3.176), c_{xp_0} also depends on the blade form. The coefficient k_p fully reflects the significance of the blade planform on the profile drag only when c_{xp_r} along the blade span does not change.

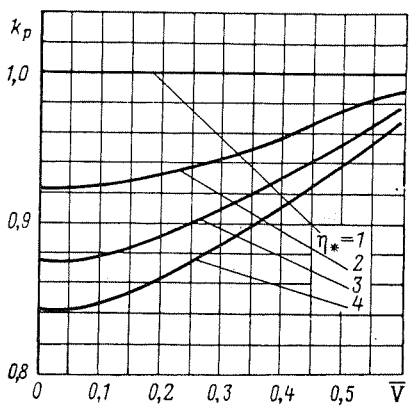

Figure 3.17

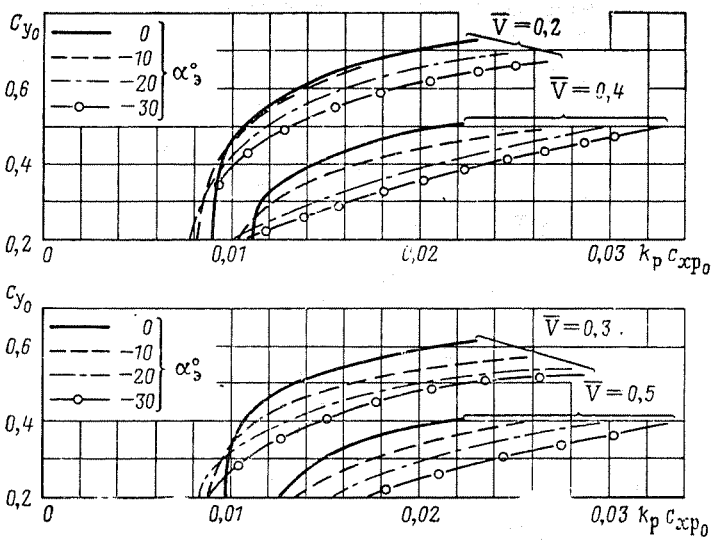

Figure 3.18

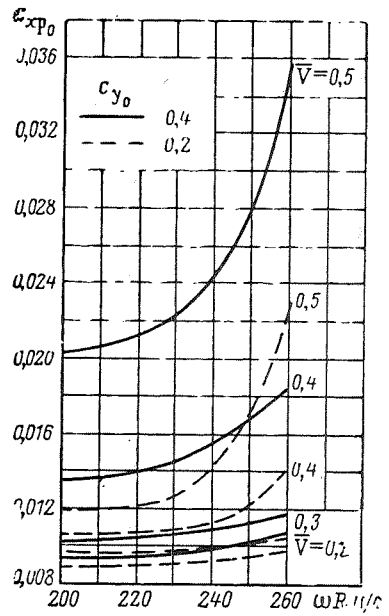

Figure 3.19

8. ROTOR INDUCED POWER COEFFICIENT

It is known from Sect. 3 of Ch. I that

$$75N_i=\frac{k}{2\pi}\int_0^{2\pi}d\psi\int_{r_0}^{R}(-v_y)\,dT. \tag{3.186}$$

Dividing the left and right sides of the above equation by $(\rho/2)(\omega R)^3F$ and taking into consideration Eq. (2.74), we will have

$$m_i=\frac{k}{\pi^2}\int_0^{2\pi}d\psi\int_{\bar r_0}^{1}(-\bar v_y)\,\overline{W}\bar\Gamma(\bar r,\psi)\,d\bar r. \tag{3.187}$$

Now, we introduce Eqs. (2.68), (3.9) and (3.11) into the above. Then,

$$m_i=\frac{c_\tau^2}{4\varkappa^2\overline{V}}\,I, \tag{3.188}$$

where

$$I=\frac{1}{\pi}\int_0^{2\pi}d\psi\int_{\bar r_0}^{1}(-\hat v_y)\,\overline{W}\tilde\Gamma(\bar r,\psi)\,d\bar r. \tag{3.189}$$

Quantity I represents the induction coefficient of the lifting airscrew, and it depends on the character of distribution over the disc of $\hat v_y(\bar r,\psi)$ coefficient of the vertical component of induced velocity and relative circulation $\tilde\Gamma(\bar r,\psi)$. They, in turn, depend on the blade form and regime of flight of the airscrew. According to Glauert's theory when $v_y = const$ and $\hat v_y = -1$, the induction coefficient $I = 1$. Let us substitute Eq. (3.189) into Eq. (3.97). Changing the order of the integration, we obtain

$$I=2\int_{\bar r_0}^{1}\tilde\Gamma\left[\frac{1}{2\pi}\int_0^{2\pi}\frac{(-\hat v_y)(\bar r+\mu\sin\psi)}{1+\frac{3}{2}\mu\sin\psi}d\psi\right]d\bar r. \tag{3.190}$$

This integral can be found in the same way as used in the determination of Δc_{Hv}. We expand induced velocity into a series (Eq. (3.104)) with coefficients $\hat v_r$ and $\hat v_{s1}$ defined by Eq. (3.108). In the determination of other coefficients, we assume that $\tilde\Gamma \approx (3/2)\bar r$ and take advantage of the relationships by Eq. (3.106). Then, assuming that $\overline{V} \approx \mu$, we find that

$$I=2\int_{\bar{r}_0}^{1}\bar{r}\tilde{\Gamma}^2\left\{1+1{,}5\mu^2\left[1+1{,}8\mu^2-\frac{1{,}7}{\bar{r}}(1+1{,}6\mu^2)+\frac{0{,}7}{\bar{r}^2}(1+1{,}5\mu^2)\right]\right\}d\bar{r}. \qquad (3.191)$$

Eq. (3.191) should be sufficiently accurate for any type of $\tilde{\Gamma}$ distribution. The above relationship can be conveniently presented under the following form:

$$I=2\int_{\bar{r}_0}^{1}\bar{r}\tilde{\Gamma}^2\left(g_2+\frac{g_1}{\bar{r}}+\frac{g_0}{\bar{r}^2}\right)d\bar{r}, \qquad (3.192)$$

where $g_2=1+1{,}5\mu^2(1+1{,}8\mu^2)$; $g_1=-2{,}5\mu^2(1+1{,}6\mu^2)$; $g_0=\mu^2(1+1{,}5\mu^2)$.

In actual computations, it is important to watch for the fulfillment of the condition expressed by Eq. (3.12). For this reason, it is desirable to present Eq. (3.35) for a blade of an arbitrary shape under the following form:

$$\tilde{\Gamma}=\varphi_{0\vartheta}\tilde{\Gamma}_\varphi+\tilde{\Gamma}_\Delta+\alpha_\vartheta\tilde{\Gamma}_\alpha, \qquad (3.193)$$

where $$\tilde{\Gamma}_\varphi=4\mu\frac{\varkappa}{c_T}\tilde{c}\bar{r}\frac{\bar{r}^2+\frac{1}{2}\mu^2}{\bar{r}^2+\tilde{c}\mu^2}; \qquad (3.194)$$

$$\tilde{\Gamma}_\Delta=\Delta\varphi\tilde{\Gamma}_\varphi; \qquad (3.195)$$

$$\tilde{\Gamma}_\alpha=4\mu^2\frac{\varkappa}{c_T}\frac{\tilde{c}\bar{r}^2}{\bar{r}^2+\tilde{c}\mu^2}. \qquad (3.196)$$

In order to fulfill the condition of Eq. (3.12), the effective collective blade pitch angle* $\phi_{0\vartheta}$ should be found from the following ratio:

$$\varphi_{0\vartheta}=\frac{\frac{1}{2}-\int_{\bar{r}_0}^{1}\bar{r}\tilde{\Gamma}_\Delta d\bar{r}-\alpha_\vartheta\int_{\bar{r}_0}^{1}\bar{r}\tilde{\Gamma}_\alpha d\bar{r}}{\int_{\bar{r}_0}^{1}\bar{r}\tilde{\Gamma}_\varphi d\bar{r}}. \qquad (3.197)$$

*See Sect. 2 of Ch. III

Using the above-developed formula, values of the induction coefficient I were computed for a rotor having $\sigma = 0,07$; $c_T/\sigma = 0,17$. The results are shown in Fig. 3.20. Various twist distributions, as well as magnitudes of $\alpha_э$ and μ were considered for $\eta_* = 1$.

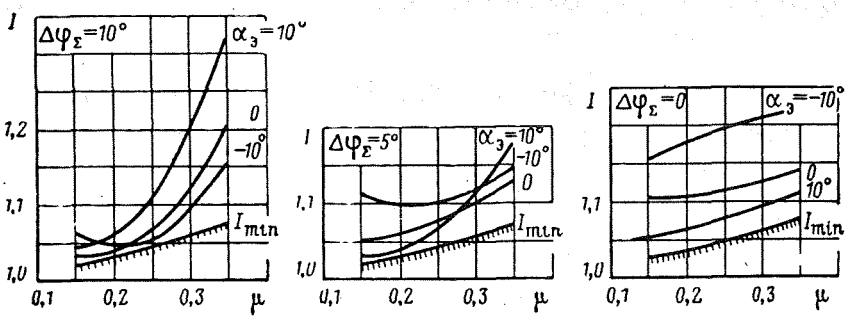

Figure 3.20

At the conclusion of this section, we are going to compare the analytical predictions with test results. Let us assume a rotor of diameter $D = 12,5m$ with $\sigma = 0,086$ and geometric characteristics of the blades as shown in Fig. 3.21. Fig. 3.22 gives a comparison for $c_T = f(m_k)$ for several values of $\alpha_э$. There, the stall limit, established according to Fig. 3.5 is also shown. Torque coefficients were computed according to Eq. (1.28), m_p was obtained from Eq. (3.180), and values of c_H were found from Eq. (3.120). Tests were performed at $\omega R = 131m/sec$. A satisfactory agreement between analytical and test data should be noted.

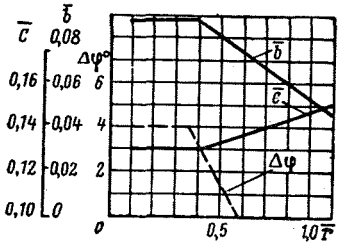

Figure 3.21

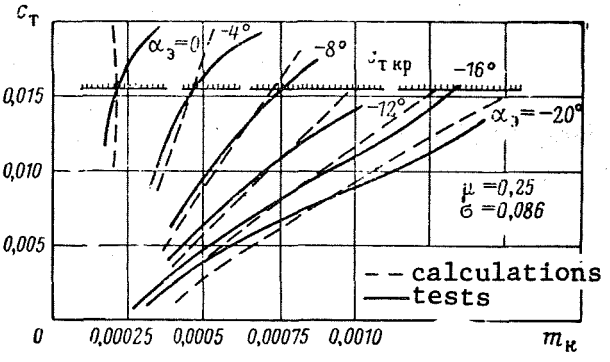

Figure 3.22

9. OPTIMAL DISTRIBUTION OF THE AVERAGE CIRCULATION

The induced drag will be considered first. The task of finding such distribution of the circulation that would result in the lowest value of the m_i coefficient at a given magnitude of the thrust coefficient c_T, is reduced to the problem of solving the isoperimetric problem of the calculus of variation of finding such $\tilde{\Gamma}_{opt_1} = f(\bar{r})$ which would make the integral given by Eq. (3-192) a minimum, while the condition expressed by Eq. (3.12) is fulfilled. The subintegral functions in Eqs. (3.192) and (3.12) do not depend on the derivative $d\tilde{\Gamma}/d\bar{r}$, and depend only on the sought function, $\tilde{\Gamma}$. For this reason, we can find the optimal distribution of $\tilde{\Gamma}_{opt}$ from the following necessary condition

$$\frac{dL}{d\tilde{\Gamma}}=0, \tag{3.198}$$

where $$L=L_1-aL_2 \ (a=\text{const}); \quad L_1=\bar{r}\tilde{\Gamma}^2\left(g_2+\frac{g_1}{\bar{r}}+\frac{g_0}{\bar{r}^2}\right); \quad L_2=\bar{r}\tilde{\Gamma}. \tag{3.199}$$

We find from Eq. (3.198) that

$$\tilde{\Gamma}_{\text{opt 1}}=\frac{0{,}5a}{g_2+\frac{g_1}{\bar{r}}+\frac{g_0}{\bar{r}^2}}. \tag{3.200}$$

Substituting Eq. (3.200) into Eq. (3.12), we obtain

$$a=\frac{2g_2}{F_1(\mu)}, \tag{3.201}$$

where $$F_1(\mu)=1-2\bar{g}_1+(\bar{g}_1^2-\bar{g}_0)\ln\frac{(1+\bar{g}_1+\bar{g}_0)}{\bar{g}_0}-$$

$$-\frac{\bar{g}_1(\bar{g}_1^2-3\bar{g}_0)}{\sqrt{\bar{g}_0-\frac{\bar{g}_1^2}{4}}}\left(\operatorname{arc\,tg}\frac{1+\frac{\bar{g}_1}{2}}{\sqrt{\bar{g}_0-\frac{\bar{g}_1^2}{4}}}-\operatorname{arc\,tg}\frac{\frac{\bar{g}_1}{2}}{\sqrt{\bar{g}_0-\frac{\bar{g}_1^2}{4}}}\right),$$

$$\bar{g}_1=\frac{g_1}{g_2}, \quad \bar{g}_0=\frac{g_0}{g_2}.$$

We introduce Eq. (3.201) into Eq. (3.200), and obtain

$$\tilde{\Gamma}_{\text{opt 1}}=\frac{\bar{r}^2}{F_1(\mu)(\bar{r}^2+\bar{g}_1\bar{r}+\bar{g}_0)}. \tag{3.202}$$

Next, substituting Eq. (3.202) into Eq. (3.192), we find that

$$I_{\min}=\frac{g_2}{F_1(\mu)}. \tag{3.203}$$

In Fig. 3.23, one can find $\tilde{\Gamma}_{opt_1}$ distributions; while in Fig. 3.20, graphs of I_{min} (lowest values of the induction coefficients) are shown. With decreasing μ, optimum character of $\tilde{\Gamma}_{opt_1}$ approaches a uniform distribution. As the limit with $\mu \to 0$ and $c_T \to 0$, the relative circulation $\tilde{\Gamma}_{opt_1} \to 1$. Having ordinates of $\tilde{\Gamma}_{opt}$, it is possible to find optimum twist distribution $\Delta\phi_{opt_1}$ of a blade when its planform is given. From Eq. (3.35) we can find the effective pitch angle of the blade sections.

$$\varphi_э=\frac{c_T}{\varkappa\sigma}F_3(\bar{r},\mu,\sigma,\tilde{b})-\alpha_э F_2(\bar{r},\mu) \tag{3.204}$$

and $$\Delta\varphi_э=\varphi_э-\varphi_{0э}. \tag{3.205}$$

Here,

$$F_2(\bar{r},\mu)=\frac{\mu\bar{r}}{\bar{r}^2+0{,}5\mu^2}, \tag{3.206}$$

$$F_3(\bar{r},\mu,\sigma,\tilde{b})=\frac{1}{4}\cdot\frac{\tilde{\Gamma}}{\mu\bar{r}}\cdot\frac{\sigma}{\tilde{c}}\cdot\frac{\bar{r}^2+\tilde{c}\mu^2}{\bar{r}^2+0{,}5\mu^2}. \tag{3.207}$$

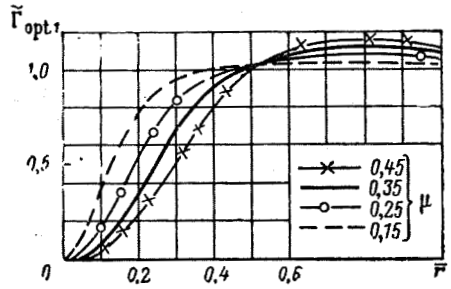

Figure 3.23

Fig. 3.24 illustrates blade twist distribution which would result in I_{min} for $c_T/\sigma = 0{,}156$. It should be noted that with increasing μ values, optimum twist angles decrease for sections located at $\bar{r} < 0{,}7$ while for $\bar{r} > 0{,}7$, they remain practically unchanged.

Now, we are going to find optimum circulation that would minimize m_Y. We multiply and divide by c_{y_r} the function appearing under the integral in Eq. (3.172). Then, according to

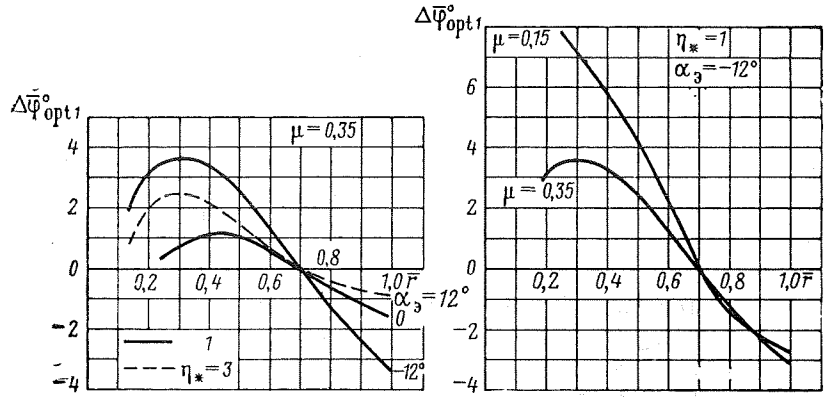

Figure 3.24

Eqs. (3.80), (3.172), (3.181), (3.188) and (3.192), we obtain

$$m_Y=2\frac{c_T}{\varkappa}\int_{\bar{r}_0}^{1}\left[\left(\frac{c_{xp_r}}{c_{y_r}}\right)F_5(\bar{r},\mu)+\frac{c_T}{4\varkappa\mu}\bar{r}\tilde{\Gamma}F_4(\bar{r},\mu)\right]\tilde{\Gamma}d\bar{r}. \tag{3.208}$$

Here, $$F_4(\bar{r},\mu)=g_2+\frac{g_1}{\bar{r}}+\frac{g_0}{\bar{r}^2}, \tag{3.209}$$

$$F_5(\bar{r},\mu)=\frac{\bar{r}^2(\bar{r}^2+1{,}5\mu^2)}{\bar{r}^2+0{,}5\mu^2}. \tag{3.210}$$

The $c_{y_r}=f(c_{xp_r})$ relationships are computed from Eqs. (3.173) and (3.78). $c_{y_{r_{opt}}}$ can be found from the condition of making c_{xp_r}/c_{y_r} a minimum. Let us find the optimal relative circulation $\tilde{\Gamma}_{opt2}=f(\bar{r})$ which would minimize m_Y, while fulfilling conditions of Eq. (3.12). Taking the same approach as in the development of Eq. (3.200) and after making some regrouping, we find

$$\tilde{\Gamma}_{opt\,2}=\tilde{\Gamma}_{opt\,1}+\Delta\tilde{\Gamma}_{opt}, \tag{3.211}$$

where $$\Delta\tilde{\Gamma}_{opt}=2\frac{\varkappa}{c_T}\bar{V}F_7(\bar{r},\mu), \tag{3.212}$$

$$F_7(\bar{r},\mu)=2\tilde{\Gamma}_{opt1}F_6(\mu)-\frac{c_{xp_r}}{c_{y_r}}\frac{F_5(\bar{r},\mu)}{\bar{r}F_4(\bar{r},\mu)}, \tag{3.213}$$

$$F_6(\mu)=\int_{\bar{r}_0}^{1}\left(\frac{c_{xp_r}}{c_{y_r}}\right)\frac{F_5(\bar{r},\mu)}{F_4(\bar{r},\mu)}d\bar{r}. \qquad (3.214)$$

$\tilde{\Gamma}_{opt1}$ and $\tilde{\Gamma}_{opt2}$ are shown in Fig. 3.25 for $\mu = 0,25$. Values of $c_{y r_{opt}}$ and $(c_{xp_r}/c_{y_r})_{min}$ are given in Table 3.4.

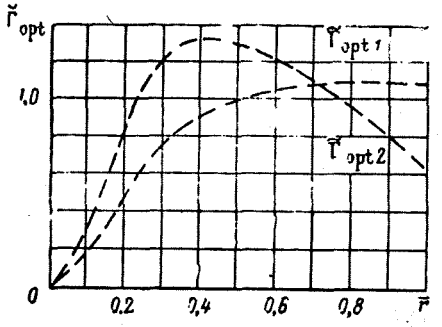

Figure 3.25

$\bar{r}$	0,2	0,4	0,6	0,8	0,95
$c_{y_r\,opt}$	0,45	0,62	0,53	0,43	0,35
$\left(\frac{c_{x\,p_r}}{c_{y_r}}\right)_{min}$	0,014	0,022	0,032	0,038	0,04

Table 3.4

Knowing $\tilde{\Gamma}_{opt_2}$ and $c_{y r_{opt}}$, we can find $\tilde{b}_{opt}$ from Eq. (3.80). It appeared, in the considered case, that the optimum blade would have a planform close to the trapezoidal one with a taper ratio of $\eta_* = 3$. For $\eta_* = 3$, we can determine $\Delta\phi_{э opt}$ from Eqs. (3.204)-(3.207). Computations performed according to Eq. (3.208) indicate that the m_Y value corresponding to $\eta_* = 3$ is approximately 13% lower than that resulting from $\eta_* = 1$. The $\Delta\phi_{э\,opt}$ distribution is close to that corresponding to $\eta_* = 1$ and $\mu = 0,35$ shown in Fig. 3.24.

Eqs. (3.204) and (3.207) permit one to select $\Delta\phi_э$ and b that would, on one hand, satisfy manufacturing and technological requirements, while on the other, would assure a circulation close to the optimum.

CHAPTER IV

INDUCED DRAG AND POWER OF TWIN-ROTOR SYSTEMS

1. INDUCED DRAG AND POWER OF COAXIAL ROTORS

Let us assign an index *"1"* to the lower rotor in the coaxial system, and *"2"* to the upper one. According to Eq. (3.187), the coefficient of power required to overcome the induced drag of the lower rotor will be

$$m_{i1}=\frac{k}{\pi^2}\int_0^{2\pi}d\psi\int_{\bar r_0}^{1}(-v_\Sigma^{(1)})\bar\Gamma_1(\bar r,\psi)\overline{W}d\bar r. \qquad (4.1)$$

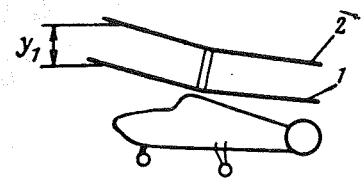

Figure 4.1

where $\bar v_\Sigma^{(1)}=\bar v_y^{(1)}+\bar v_g^{(2)}$ (4.2)

represents the resultant induced velocity at any point of the disc of the lower rotor. It consists of a sum of the proper induced velocity $\bar v_y^{(1)}$ of the lower rotor and an additional velocity $\bar v_g^{(2)}$ generated by the upper rotor at that particular point of the lower disc. The magnitude of $\bar v_g^{(2)}$ depends on the distance, y_1, between the two rotors (Fig. 4.1).

Let us consider a particular case of the coaxial system; namely, that which was used in the high-speed concept of Sikorsky (ABC): Two rotors with rigid blade attachment to the hub are closely located to each other and have opposite directions of rotation. It will be assumed, for simplicity, that $y_1 = 0$. Then, $\bar v_g^{(2)} = \bar v_y^{(2)}$. Since, in the coaxial configurations, the upper and lower rotors rotate in opposite directions; hence, the z axes of the upper and lower rotors will be pointing in opposite directions.

The vertical component of the induced velocity of the lower rotor can be presented as a Fourier series

$$\bar v_y^{(1)}(\bar r,\psi)=\bar v_r^{(1)}+\sum_{n=1}^{n=\infty}\left[\bar v_{cn}^{(1)}(\bar r)\cos n\psi+\bar v_{sn}^{(1)}(\bar r)\sin n\psi\right]. \qquad (4.3)$$

Induced velocity of the upper rotor, expressed in the coordinate system of the lower one, will be:

$$\bar v_y^{(2)}(\bar r,\psi)=\bar v_r^{(2)}+\sum_{n=1}^{n=\infty}\left[\bar v_{cn}^{(2)}(\bar r)\cos n\psi-\bar v_{sn}^{(2)}(\bar r)\sin n\psi\right], \qquad (4.4)$$

where, due to the change in the direction of the z axis, the coefficients at $\sin n\psi$ have opposite signs to those in Eq. (4.3).

Let us present the circulation at blade sections of the rotor under the following form:

$$\bar{\Gamma}(\bar{r},\psi)\approx\bar{\Gamma}_r(c_0+c_1\sin\psi+c_2\cos 2\psi). \tag{4.5}$$

The above expression is valid for all types of blade attachments.

In the case of articulated blades, executing the flapping motion described by the first harmonic relationships, we have, from Eq. (3.97)

$$c_0=1+1{,}12\,\mu^2(1+1{,}7\,\mu^2);\ c_1=-1{,}5\,\mu(1+1{,}7\,\mu^2);$$
$$c_2=-1{,}12\,\mu^2(1+2{,}25\,\mu^2). \tag{4.6}$$

For absolutely rigid attachment of rigid blades and $\alpha_B \approx -5^\circ$, calculations show (see Fig. 2.11) that

$$c_0=1,\ c_1=1{,}5\,\mu,\ c_2=0. \tag{4.7}$$

If the blades execute elastic oscillations leading to uniformity of circulation with respect to angles ψ, then

$$c_0=1,\ c_1=c_2=0. \tag{4.8}$$

In this way, knowing composition of the blade and its elastic oscillations, it should be possible to compute the law of variation of circulation with the azimuth angle at the $\bar{r}\approx 0{,}7$ section. Now it should be possible to select coefficients c_0, c_1 and c_2 which would make Eq. (4.5) to approximate, with sufficient accuracy, the actual variation of circulation.

Substituting Eqs. (4.2) and (4.5) into Eq. (4.1), we obtain

$$m_{i1}=2\,\frac{k}{\pi}\int_{\bar{r}_0}^{1}\bar{\Gamma}_{r_1}\left\{\frac{1}{2\pi}\int_0^{2\pi}(-\bar{v}_y^{(1)}-\bar{v}_y^{(2)})\left[c_0\bar{r}+\frac{1}{2}c_1\mu+\right.\right.$$
$$+\left(c_1\bar{r}+c_0\mu-\frac{1}{2}c_2\mu\right)\sin\psi+\left(c_2\bar{r}-\frac{1}{2}c_1\mu\right)\cos 2\psi+$$
$$\left.\left.+\frac{1}{2}c_2\mu\sin 3\psi\right]d\psi\right\}d\bar{r}. \tag{4.9}$$

We evaluate the internal integral, taking into consideration Eqs. (2.68), (3.9), (4.3), (4.4), and (III.2)-(III.4)

$$\frac{1}{2\pi}\int_0^{2\pi}\ldots d\psi=\frac{c_{T1}}{4k\bar{V}}\left[\left(c_0\bar{r}+\frac{1}{2}c_1\mu\right)\left(-\hat{v}_r^{(1)}-\hat{v}_r^{(2)}\frac{c_{T2}}{c_{T1}}\right)+\right.$$
$$+\frac{1}{2}\left[c_1\bar{r}+\mu\left(c_0-\frac{1}{2}c_2\right)\right]\left(-\hat{v}_{s1}^{(1)}+\hat{v}_{s1}^{(2)}\frac{c_{T2}}{c_{T1}}\right)+$$
$$\left.+\frac{1}{2}\left(c_2\bar{r}-\frac{1}{2}c_1\mu\right)\left(-\hat{v}_{c2}^{(1)}-\hat{v}_{c2}^{(2)}\frac{c_{T2}}{c_{T1}}\right)+\frac{1}{4}c_2\mu\left(-\hat{v}_{s3}^{(1)}+\hat{v}_{s2}^{(2)}\frac{c_{T2}}{c_{T1}}\right)\right]. \qquad (4.10)$$

Here, c_{T1} and c_{T2} are the thrust coefficients of the lower and upper rotors, respectively. In general $c_{T1} \neq c_{T2}$.

From the equilibrium condition about the vertical axis: $M_{K1} = M_{K2}$.

Kinematic conditions of operation of the upper and lower rotors when $y \neq 0$ are somewhat different. In Sect. 3 of Ch. II the v_x components of the induced velocity are determined. Those components in the action of the upper rotor on the lower one would reduce the μ values of the latter. By contrast, the action of the lower rotor on the upper rotor would result in an increase of μ's.

$$\mu^{(1)}=\frac{V\cos\alpha_э-|v_{xcp}^{(2)}|}{\omega R},\quad \mu^{(2)}=\frac{V\cos\alpha_э+|v_{xcp}^{(1)}|}{\omega R}.$$

According to calculations of G.R. Kvasha for an average $\mu_{cp} = 0,15$, $\mu^1 \approx 0,147$ and $\mu^2 \approx 0,153$. In this way, $\mu^1 < \mu^2$ and equilibrium is realized at $c_{T1} \neq c_{T2}$. We assume as before that dependence of $\hat{v}_{c2}$ from $\hat{v}_r$, and $\hat{v}_{s3}$ from $\hat{v}_{s1}$ is expressed by Eq. (3.106). Then

$$\frac{1}{2\pi}\int_0^{2\pi}\ldots d\psi=\frac{c_{T1}}{4k\bar{V}}\left\{\left[\bar{r}\left(c_0-\frac{1}{3}c_2\right)+\frac{2}{3}c_1\mu\right]\left(-\hat{v}_r^{(1)}-\hat{v}_r^{(2)}\frac{c_{T2}}{c_{T1}}\right)+\right.$$
$$\left.+\frac{1}{2}\left[c_1\bar{r}+\mu\left(c_0-\frac{1}{3}c_2\right)\right]\left(-\hat{v}_{s1}^{(1)}+\hat{v}_{s1}^{(2)}\frac{c_{T2}}{c_{T1}}\right)\right\}. \qquad (4.11)$$

In aerodynamic computations, we are interested in the average values of m_i for the upper and lower rotors. Experience shows that it is permissible to assume $c_{T1} = c_{T2} = c_T$ and $\tilde{\Gamma}_1 = \tilde{\Gamma}_2 = \tilde{\Gamma}$. Substituting Eqs. (4.11) and (3.108) into Eq. (4.9); for m_i, we obtain Eq. (3.188) in which the induction coefficient for rigid attachment of the blade and $\bar{V} \approx \mu$ would be

$$I^{*}_{cc}=4\int_{\bar{r}_0}^{1}\bar{r}\tilde{\Gamma}^2\left(c_0-\frac{1}{3}c_2+\frac{2}{3}c_1\frac{\mu}{\bar{r}}\right)d\bar{r}. \qquad (4.12)$$

Let us compare the induction coefficient I^{*}_{cc} of the coaxial system with that of a rigid rotor (I^{*}) whose solidity is twice that of either rotor in the coaxial configuration. Then the coaxial system may be considered as a single rotor with a doubled solidity. Thus, in Eq. (4.12), the coefficient *4* will be replaced by *2*. After substitution of coefficients c_0, c_1 and c_2 according to Eq. (4.7), the expression for I^{*}_{cc} will have the following form:

$$I^{*}_{cc\text{э}}=2\int_{\bar{r}_0}^{1}\bar{r}\tilde{\Gamma}^2\left(1+\frac{\mu^2}{\bar{r}}\right)d\bar{r}. \qquad (4.13)$$

After a substitution of $c_{T_2}=0$ into Eq. (4.11), we will obtain, in a similar way, a general expression for the induction coefficient of a single rotor. This will be in the same form as Eq. (3.192), in which

$$g_2\approx c_0-\frac{1}{3}c_2,\ g_1=\frac{5}{3}c_1\mu,\ g_0=\mu^2 g_2. \qquad (4.14)$$

From the above, taking into consideration Eq. (4.7), we obtain

$$I^{*}=2\int_{\bar{r}_0}^{1}\bar{r}\tilde{\Gamma}^2\left[1+\frac{\mu^2}{\bar{r}}\left(2{,}5+\frac{1}{\bar{r}}\right)\right]d\bar{r}. \qquad (4.15)$$

Results of computation of I^{*} and $I^{*}_{cc\text{э}}$ for $\tilde{\Gamma}=(3/2)\bar{r}$ are shown in Table 4.1.

It can be seen from Table 4.1 that a coaxial system with rigidly attached blades rotating in opposite directions, and consequently, characterized by aerodynamic loadings and induced velocities symmetrically distributed with respect to the longitudinal axis, shows a lower induced power than a single rotor of the same diameter and developing the same thrust.

μ	0,15	0,25	0,35
I^{*}	1,24	1,50	1,86
$I^{*}_{cc\text{э}}$	1,16	1,22	1,31
$I^{*}/I^{*}_{cc\text{э}}$	1,07	1,23	1,42

Table 4.1

For an articulated or elastic attachment of the blades, the coaxial rotors must be separated by some distance, y_1. Actual experience shows that for coaxial rotors with articulated blades $-\bar{y}_1 \approx 0,2$. Then, it is necessary to compute $v_g^{(2)}$ in Eq. (4.2) in the way shown in Sect. 6 of Ch. II. The induction coefficient of coaxial rotors with flapping hinges and thus, having $\bar{y}_1 > 0$ can be approximated as follows:

$$I_{c.c} \approx I(1+\varkappa_{c.c}), \tag{4.16}$$

where $$\varkappa_{cc} = \frac{\bar{v}_{cp}(\bar{y}=\bar{y}_1)}{\bar{v}_{cp}(\bar{y}=0)} \tag{4.17}$$

is the ratio of velocity averaged over the disc induced at the lower rotor by the upper one; to the self-induced average velocity at the disc of the upper rotor.

2. AVERAGE INDUCED VELOCITY IN THE COAXIAL CONFIGURATION GENERATED BY ONE ROTOR IN THE PLANE OF ROTATION OF THE OTHER ONE

It is possible to show that the magnitude of the mean rotor induced velocity, averaged over the disc, is close to its value at $\bar{r} = 0,7$. This means that

$$\bar{v}_{cp}(\bar{y}=\bar{y}_1) \approx \bar{v}_r(r=0,7;\ \bar{y}=\bar{y}_1). \tag{4.18}$$

In order to determine that mean induced velocity, it is necessary to have its coefficients* $\Delta\hat{v}_r^{(\rho)}(\tilde{r}, \tilde{y}_1)$, where $\tilde{r} = \bar{r}/\rho$, $\tilde{y}_1 = \bar{y}/\rho$. In analogy with Eq. (I.3) from Appendix I we will write

$$\Delta\hat{v}_r^{(\rho)}(\tilde{r}, \tilde{y}_1) = \frac{1}{\pi}\int_{\frac{\pi}{2}}^{\frac{3}{2}\pi} \Delta\hat{v}_{y0}^{(\rho)}(\tilde{z}_1, \tilde{y}_1)\, d\psi, \tag{4.19}$$

where $\Delta\hat{v}_{y0}^{(\rho)}(\tilde{z}_1, \tilde{y}_1)$ is determined by Eq. (2.12). Substituting $\tilde{z} = \tilde{r}\sin\psi$, we obtain

$$\Delta\hat{v}_r^{(\rho)}(\tilde{r}, \tilde{y}_1) = -1 - \frac{1}{\pi}\left[\bar{V}_* \int_{\frac{\pi}{2}}^{\frac{3}{2}\pi} Q\, d\psi + \tilde{r}\int_{\frac{\pi}{2}}^{\frac{3}{2}\pi} Q\sin\psi\, d\psi - \right.$$

$$\left. - \bar{V}_*\tilde{r}\int_{\frac{\pi}{2}}^{\frac{3}{2}\pi} P\sin\psi\, d\psi - \tilde{r}^2\int_{\frac{\pi}{2}}^{\frac{3}{2}\pi} P\sin^2\psi\, d\psi - \tilde{y}_1^2\int_{\frac{\pi}{2}}^{\frac{3}{2}\pi} P\, d\psi\right]. \tag{4.20}$$

*See Appendix I

As a result of Eq. (2.12)

$$\int_{\frac{\pi}{2}}^{\frac{3}{2}\pi} Qd\psi=\int_{\frac{\pi}{2}}^{\pi} Qd\psi+\int_{\pi}^{\frac{3}{2}\pi} Qd\psi=0,$$

since

$$\int_{\frac{\pi}{2}}^{\pi} Qd\psi=-\int_{\pi}^{\frac{3}{2}\pi} Qd\psi.$$

By analogy

$$\int_{\frac{\pi}{2}}^{\frac{3}{2}\pi} P\sin\psi d\psi=0,\quad \int_{\frac{\pi}{2}}^{\frac{3}{2}\pi} Pd\psi=2\int_{\frac{\pi}{2}}^{\pi} Pd\psi,$$

$$\int_{\frac{\pi}{2}}^{\frac{3}{2}\pi} P\sin^2\psi d\psi=2\int_{\frac{\pi}{2}}^{\pi} P\sin^2\psi d\psi,\quad \int_{\frac{\pi}{2}}^{\frac{3}{2}\pi} Q\sin\psi d\psi=2\int_{\frac{\pi}{2}}^{\pi} Q\sin\psi d\psi.$$

Then

$$\Delta\hat{\bar{v}}_r^0(\hat{\bar{y}}_1)=-1+\tilde{R}, \tag{4.21}$$

where

$$\tilde{R}=\frac{2}{\pi}\left(\tilde{\bar{r}}^2\int_{\frac{\pi}{2}}^{\pi} P\sin^2\psi d\psi+\tilde{\bar{y}}_1^2\int_{\frac{\pi}{2}}^{\pi} Pd\psi-\tilde{\bar{r}}\int_{\frac{\pi}{2}}^{\pi} Q\sin\psi d\psi\right). \tag{4.22}$$

We should emphasize that $\Delta\hat{v}_r^{\rho}(\tilde{\bar{y}}_1)$ is independent of μ. According to Eq. (4.19) and Eq. (I.2) from Appendix I,

$$\bar{v}_r(\bar{y}_1)\approx-\frac{k}{4\pi\bar{V}}\int_{\bar{Q}=\bar{r}_0}^{\bar{Q}=1}\Delta\hat{\bar{v}}_r^0(\bar{r}=0{,}7;\ \bar{y}_1)\,d\bar{\Gamma}=$$

$$=-\frac{k\bar{\Gamma}_{cp}}{4\pi\bar{V}}\int_{\bar{Q}=\bar{r}_0}^{\bar{Q}=1}\Delta\hat{\bar{v}}_r^{(0)}(\bar{r}=0{,}7;\ \bar{y}_1)\,d\tilde{\Gamma}. \tag{4.23}$$

Substituting $\bar{\Gamma}_{cp}$ instead of $\bar{\Gamma}_r$ in Eq. (2.91), we will obtain $\bar{v}_{cp}$ - the mean induced velocity averaged over the disc. Then, according to Eq. (4.17),

$$\varkappa_{cc}\approx\int_{\bar{Q}=\bar{r}_0}^{\bar{Q}=1}\Delta\hat{\bar{v}}_r^0(0{,}7;\ \bar{y}_1)\,d\tilde{\Gamma}\approx-\sum_{\bar{Q}=1,0}^{\bar{Q}=\bar{r}_0}\Delta\hat{\bar{v}}_r^0(0{,}7;\ y_1)\,\Delta\tilde{\Gamma}_c. \tag{4.24}$$

The quantity $\Delta\tilde{\Gamma}_\rho$ is determined from a formula analogous to Eq. (2.66). Computation of $\varkappa_{cc}$ was performed at various values of $\bar{y}_1$ for two types of average circulation distribution along the blade: $\tilde{\Gamma} = (3/2)\bar{r}$ and $\tilde{\Gamma} = 1$. As mentioned before, those two cases may be considered as limits containing all the distributions encountered in practice. Calculations indicated that for the case of $y_1 \neq 0$, the coefficient $\varkappa_{cc}$ depends little on the shape of the blade and angle of attack of the rotor. Average values of $\varkappa_{cc}$ are shown in Fig. 4.2. It can be seen from this figure that in the coaxial configuration, the elevation of one rotor above the other strongly influences the value of the additional induced velocity. According to calculations at $\bar{y}_1 = 0,2$, the coaxial system has induced resistance (power) 22% lower than a single rotor of the same diameter and doubled solidity.

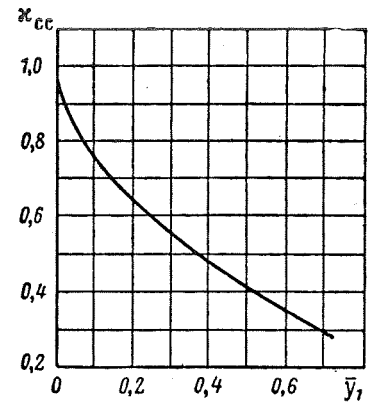

Figure 4.2

3. INDUCED RESISTANCE (POWER) OF ROTORS IN TANDEM AND SIDE-BY-SIDE CONFIGURATIONS

Velocities induced ahead of the rotor disc are very small. For this reason, it is possible to assume that in a tandem configuration with $-\bar{x}_* \geq 1,5$, the rear rotor has no practical influence on the front one. Consequently, the front rotor can be considered as isolated and all its aerodynamic characteristics can be found as for a single rotor.

The rear rotor remains under a strong influence of the front one, since with the increasing distance from the front rotor axis, its induced velocities increase.

It is shown in Sect. 6 of Ch. II that at a point infinitely far behind a lifting airscrew, the induced velocity is twice as high as that at a point having the same coordinates of $\bar{y}_1$ and $\bar{z}_1$, but located in a plane passing through the lateral diameter of the rotor disc ($\bar{x}_1 = 0$). Induced velocity distribution along a fore-and-aft section of an isolated rotor is shown in Fig. 4.3.

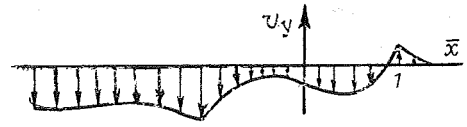

Figure 4.3

It can be seen from this figure that not too far behind the trailing edge of the rotor disc, the induced velocity becomes practically constant. Calculations indicate that in practice, doubling of induced velocity occurs at $\bar{x}_1 = -1,3$. It may be assumed, hence, that the velocity induced by the front rotor remains constant in the region of the disc of the rear rotor (Fig. 4.4). In every section, it is equal to twice the velocity induced by the front rotor in a point of the $y0z$ plane; with an ordinate y_1 equal to the effective elevation of the rear rotor with respect to the front one. If one represents that additional induced velocity under a form of the Fourier series in analogy with Eq. (4.3), then terms containing cosines of odd, and sines of even, harmonics would disappear; i.e.,

$$\bar{v}^g_{c(2n-1)}(\bar{r}) = \bar{v}^g_{s(2n)}(\bar{r}) = 0.$$

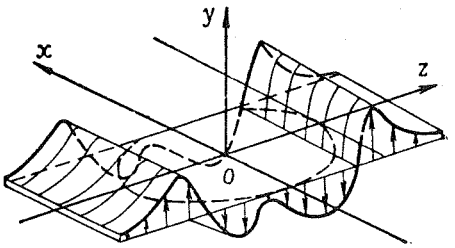

Figure 4.4

In the tandem configuration, the average additional velocity induced at the rear rotor by the front one will be two times higher than in the case of the coaxial system. Consequently,

$$\varkappa_{\text{пр}} = 2\varkappa_{\text{сс}}. \qquad (4.25)$$

where the subscript пр denotes tandem, and сс, coaxial, configurations.

Elevation of the rear rotor over the front one is defined by the distance between the vortex wakes of these two rotors. That elevation may be defined (see Fig. 4.5) as follows:

$$y_1 \approx \bar{y}_{10} - \bar{x}_* \alpha_\Phi, \qquad (4.26)$$

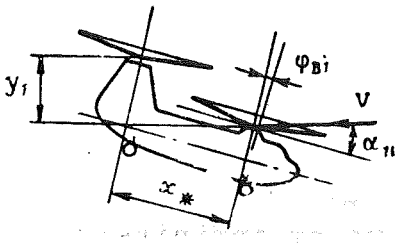

Figure 4.5

where $\bar{y}_{10}$ is the relative structural elevation of the rear rotor as determined for zero angle of attack of the fuselage (α_Φ); $\bar{x}_*$ is the relative distance between the axes of the two rotors. In order to make calculations more conservative, angle α_Φ may be determined without consideration of the inflow angle due to the front rotor. In other words, it is possible to assume that

$$\alpha_\Phi \approx \alpha_{э1} - \delta_{z1} - \varphi_{B1}. \qquad (4.27)$$

Here, $\alpha_{э1}$ is the effective angle of attack of the front rotor; δ_{z1} - angle of inclination of the thrust vector with respect to the rotor axis, and ϕ_{B1} - angle between the shaft axis of the

front rotor and perpendicular to the fuselage axis*. Experimental results of G.R. Kvasha and P.V. Zanozin confirmed the validity of Eq. (4.26).

Let us assign the subscript "1" to all quantities referring to the front rotor and "2" to those associated with the rear one. On the basis of the previous considerations, the induced power coefficient of the front rotor can be defined, according to Eq. (3.188), as:

$$m_{i1}=\frac{c_{T1}^2}{4\varkappa^2\bar{V}}I_{\text{пр1}}, \tag{4.28}$$

where the induction coefficient ($I_{\text{пр}1}$) can be found from Eq. (3.192). The induced power coefficient of the rear rotor can also be obtained from Eq. (3.188)

$$m_{i2}=\frac{c_{T2}^2}{4\varkappa^2\bar{V}}I_{\text{пр2}}, \tag{4.29}$$

The approximate value of $I_{\text{пр}2}$ can be found from Eq. (4.16) by substituting coefficient $\varkappa_{\text{пр}}$ for $\varkappa_{cc}$. Even with identical geometry of the front and rear rotor blades, distributions of $\tilde{\Gamma}_1$ and $\tilde{\Gamma}_2$ will be somewhat different due to the aerodynamic influence of the front rotor on the rear one. However, calculations show that actual differences in the $\tilde{\Gamma}$ distributions are not appreciable, and thus may be neglected. For this reason, upon averaging the induction coefficients of the front and rear rotors at c_{T1} and c_{T2} and taking into consideration, Eq. (4.25), we obtain

$$I_{\text{пр}}=\frac{1}{2}(I_{\text{пр1}}+I_{\text{пр2}})=I_{cc}. \tag{4.30}$$

In this way, the average induction coefficient $I_{\text{пр}}$ of the the tandem configuration with a longitudinal rotor separation of $\bar{x}_* > 1{,}5$ will be the same as that of the coaxial system with the same vertical separation of the rotors, $\bar{y}_1$.

If the directions of rotation of both rotors in the tandem configuration were the same, then in the absence of the elevation of the rear rotor over the front one, the ratio $I_{\text{пр}}/I = 2$. This means that induced resistance (power) of two lifting airscrews

---

*It should be remembered that $\delta_{z1} > 0$ and $\phi_{B1} > 0$ if they are inclined backward from the rotor shaft axis.

arranged in tandem is four times higher than that of the separated rotor. For opposite directions of rotation of the two rotors in the tandem configuration, $I_{пр}/I < 2$ and decreases with increasing μ (i.e., with the increasing nonuniformity of the induced velocity distribution).

Let us now determine $\tilde{\Gamma}_{2_{opt}}$ - optimum distribution of circulation for the rear rotor of the tandem configuration when $\bar{y}_1 = 0$. By analogy with Eqs. (4.9) and (4.11), we will obtain an expression for m_{i2} (in this case, a coefficient "2" will appear in front of $\bar{v}_y$, $\hat{v}_r$, $\hat{v}_{s1}$, $\hat{v}_{c2}$ and $\hat{v}_{s3}$). Accepting the relationships expressed in Eq. (3.106), we have

$$m_{i2}=\frac{c_{т2}^2}{4\varkappa 2\bar{V}} I_{пр2}, \tag{4.31}$$

where

$$I_{пр2}=2\int_{\bar{r}_0}^{1}\tilde{\Gamma}_2\left[B_1\left(\tilde{\Gamma}_2+2\tilde{\Gamma}_1\frac{c_{т1}}{c_{т2}}\right)+B_2\frac{\mu}{\bar{r}}\left(\tilde{\Gamma}_2-2\tilde{\Gamma}_1\frac{c_{т1}}{c_{т2}}\right)\right]d\bar{r}. \tag{4.32}$$

Here,

$$B_1=\bar{r}\left(c_0-\frac{1}{3}c_2\right)+\frac{2}{3}c_1\mu, \quad B_2=c_1\bar{r}+\mu\left(c_0-\frac{1}{3}c_2\right). \tag{4.33}$$

We will find $\tilde{\Gamma}_{2opt_1}$, for which $I_{пр2}$ would have the lowest value, while conditions expressed by Eq. (3.12) are still fulfilled. As in Sect. 9 of Ch. III, we find

$$\tilde{\Gamma}_{2opt1}=\frac{a_2\bar{r}}{2\left(B_1+\frac{\mu}{\bar{r}}B_2\right)}-\frac{c_{т1}}{c_{т2}}\tilde{\Gamma}_1F_*, \tag{4.34}$$

$$F_*=\frac{B_1-\frac{\mu}{\bar{r}}B_2}{B_1+\frac{\mu}{\bar{r}}B_2}. \tag{4.35}$$

Substituting Eq. (4.33) into Eqs. (4.34) and (4.35), and taking into consideration, Eq. (4.14), we obtain

$$\tilde{\Gamma}_{2opt1}=\frac{0{,}5a_2}{g_2+\frac{g_1}{\bar{r}}+\frac{g_0}{\bar{r}^2}}-\tilde{\Gamma}_1 F_{*1}\frac{c_{T1}}{c_{T2}}, \tag{4.36}$$

$$F_*=\frac{g_2-\frac{1}{5}\frac{g_1}{\bar{r}}-\frac{g_0}{\bar{r}^2}}{g_2+\frac{g_1}{\bar{r}}+\frac{g_0}{\bar{r}^2}}. \tag{4.37}$$

Comparing the first term in Eq. (4.36) with Eq. (3.200), we conclude that

$$\frac{0{,}5a_2}{g_2+\frac{g_1}{\bar{r}}+\frac{g_0}{\bar{r}^2}}=c_3\tilde{\Gamma}_{opt1}, \tag{4.38}$$

This means that the first term in Eq. (4.36) is proportional to the circulation of the front rotor working as an isolated rotor. Then, assuming $\tilde{\Gamma}_1 = \tilde{\Gamma}_{opt_1}$, we obtain

$$\tilde{\Gamma}_{2opt1}=c_3\tilde{\Gamma}_{opt1}-F_{10}\frac{c_{T1}}{c_{T2}}, \tag{4.39}$$

$$F_{10}=\tilde{\Gamma}_{opt1}F_{*1}=f(\bar{r},\mu). \tag{4.40}$$

According to Eq. (3.12),

$$c_3=1+2F_{11}\frac{c_{T1}}{c_{T2}}, \tag{4.41}$$

$$F_{11}=\int_{\bar{r}_0}^{1}\bar{r}F_{10}d\bar{r}. \tag{4.42}$$

Distributions of $\tilde{\Gamma}_{2opt_1}$ and $\tilde{\Gamma}_{1opt_1} = \tilde{\Gamma}_{opt_1}$ are shown in Fig. 4.6.

It can be seen that modification of the common induced field strongly influenced the shape of $\tilde{\Gamma}_{2opt_1}$; making the inboard part of the blade more highly loaded.

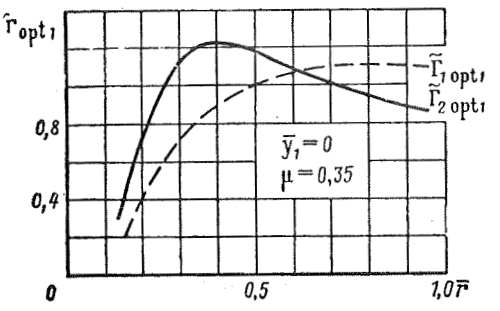

Figure 4.6

From Eqs. (3.204)-(3.207), the difference $\Delta\phi_2 = \phi_{2opt} - \phi_{1opt}$ is defined. A graph of $\Delta\phi_2 = f(\bar{r})$ is shown in Fig. 4.7. It can be seen from that figure that for the rear rotor, the blade section pitch angles should be higher by $3,5^\circ$ at $\bar{r} \approx 0,3$ than for the front rotor. At $\mu = 0,35$, the optimization process can save 14% of induced power by comparison with a conventional design.

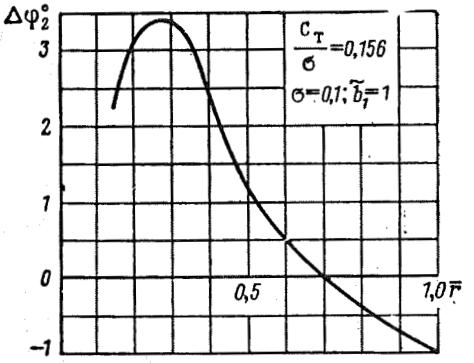

Figure 4.7

The inflow angle generated by the front rotor lowers the thrust coefficient of the rear rotor. Calculations show that at $\mu = 0,25$, $\bar{y}_1 = 0,2$ and $\phi_{02} = \phi_{01}$, the rear rotor thrust coefficient c_{T2} is approximately 14% lower than the c_{T1} of the front one. In order to increase c_{T2} to the required value, it is necessary to increase the collective pitch of the rear rotor. It can be seen from Eq. (2.83) that in order to compensate the effect of the increased inflow due to the front rotor so that $\bar{\Gamma}_{r2}$ and also c_{T2} would remain the same, it is necessary to increase the collective pitch of the rear rotor by an increment of $\Delta\phi_{02}$, defined as follows:

$$\Delta\varphi_{02}\bar{r}_{cp}\left(1+\frac{1}{2}\,\frac{\mu^2}{\bar{r}_{cp}^2}\right)+\varkappa_{np}\bar{v}_W^{(1)}(\bar{r}_{cp})=0. \qquad (4.43)$$

Upon expressing $\overline{v}_W^{(1)}(\overline{r}_{cp})$ according to Eq. (2.97), and after performing the usual transformations, and assuming $\overline{V} \approx \mu$, we obtain

$$\Delta\varphi_{02} \approx 22 \frac{1+2\mu^2}{\mu(1+\mu^2)} c_{T1} \varkappa_{np}. \qquad (4.44)$$

From the above formula, we find that in the considered example, it is necessary to increase the collective pitch of the rear rotor by $\Delta\phi_{02} \approx 1,5^\circ$. For the coaxial configuration, the $\Delta\phi$ value would amount to only 1/2 of the above. Inductive interference of the front rotor on the rear one can be considerably diminished by flying the helicopter in a yawed position (Fig. 4.8). In this case, the vorticity wake of the front rotor will take such position with respect to the rear rotor disc that negative induced velocities will be generated over one part of the disc, while positive ones will be present in the other. As a result of this, the average of the additional induced velocity becomes lower and coefficient $\varkappa_{cc}$ decreases. In Fig. 4.9, a graph of $\varkappa_{cc} = f(\overline{z}_*)$ is shown as obtained by P.V. Zanozin for the tandem shown in Fig. 4.8, with $\overline{x}_* = 1,65$.

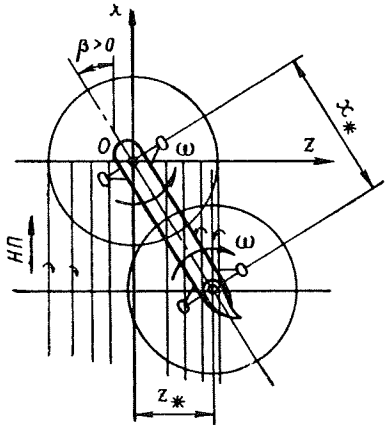

Figure 4.8

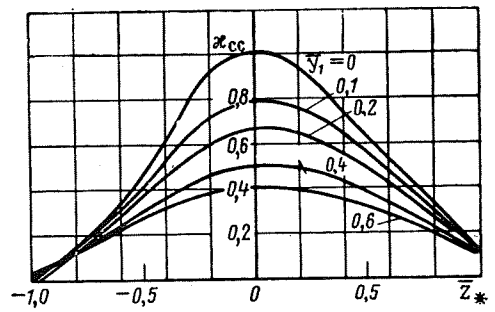

Figure 4.9

The relative distance between the rotor axes is

$$\overline{z}_* = \overline{x}_* \sin\beta. \qquad (4.45)$$

One rotor in the side-by-side configuration is located in the field of additional induced velocities directed upward. Those additional velocities are induced by the other rotor. In Fig. 4.10, an example is given of induced velocities generated along the lateral disc diameter by the vortex system with an average circulation of $\overline{\Gamma} = (3/2)\overline{r}$. This average circulation corresponds to the aerodynamic loading distributions shown in Fig. 4.10 for a rotor with articulated blades. Distribution

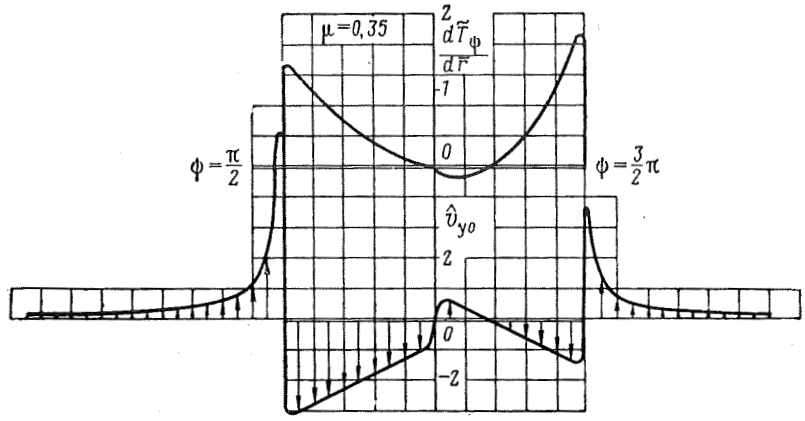

Figure 4.10

over the disc of the self-generated vertical induced velocities as well as the additional ones due to the other rotor, depend on the direction of rotation of the rotors, as well as the amount of intermesh as characterized by the $\bar{z}_*$ value.

The induction coefficient of a lifting airscrew in the side-by-side configuration can be expressed as

$$I_{\text{пп}}=I+\Delta I_{\text{пп}}. \tag{4.46}$$

Here, I is the self-induction coefficient as defined by Eq. (3.189), and $\Delta I_{\pi\pi}$ is the complementary-induction coefficient, reflecting the mutual interaction of the rotors. According to Eqs. (4.1), (4.2) and (3.189)

$$\Delta I_{\text{пп}}=\frac{1}{\pi}\int_0^{2\pi} d\psi \int_{\bar{r}_0}^{1} (-\hat{v}_g)\,\tilde{\Gamma}(\bar{r},\psi)\,\overline{W}\,d\bar{r}.$$

From Eq. (3.97), $\tilde{\Gamma}(\overline{r},\psi) = \tilde{\Gamma}(\overline{r},\pi-\psi)$. Taking into consideration Eqs. (2.88) and (2.89), we obtain

$$\Delta I_{\text{пп}}=2\int_{\bar{r}_0}^{1}\tilde{\Gamma}\left[\frac{1}{\pi}\int_{\frac{\pi}{2}}^{\frac{3}{2}\pi}\frac{(-\hat{v}_{y0})\,\overline{W}\,d\psi}{1+1{,}5\mu\sin\psi}\right]d\bar{r}. \tag{4.47}$$

From Eqs. (2.24), (2.25) and (2.68), for $\tilde{\Gamma} = (3/2)\bar{r}$ we find

$$\hat{v}_{y0} = -\frac{3}{4}\pi(\bar{V}+\bar{z}) \quad \text{for} \quad 0 \leqslant \bar{z} \leqslant 1,$$

$$\hat{v}_{y0} = \frac{3}{4}\pi(\bar{V}+\bar{z}) \quad \text{for} \quad -1 \leqslant \bar{z} \leqslant 0,$$

$$\hat{v}_{y0} = \frac{3}{2}(\bar{V}+\bar{z})\left(\arcsin\frac{1}{\bar{z}} - \frac{1}{\sqrt{\bar{z}^2-1}}\right) \quad \text{for} \quad z \geqslant 1,$$

$$\hat{v}_{y0} = -\frac{3}{2}(\bar{V}+\bar{z})\left(\arcsin\frac{1}{\bar{z}} + \frac{1}{\sqrt{\bar{z}^2-1}}\right) \quad \text{for} \quad \bar{z} < -1. \qquad (4.48)$$

Depending on the direction of rotation of the rotors, the blades over the fuselage are either advancing *(internally leading)*, or retreating *(externally leading)*. Graphs of the load and induced velocity distributions for the internally leading and externally leading rotor configurations are shown in Figs. 4.11-4.13. Those graphs are for $\mu = 0,35$, representative of cruise conditions, and refer to intermeshing and non-intermeshing schemes. A comparison of the $\hat{v}_{y0}$ ordinates at $\psi = \pi/2$ of the isolated rotor (see Fig. 4.10) with the ordinates of this curve for the inside region of the side-by-side scheme shows that for $\psi = \pi/2$ of the latter configuration, the $\hat{v}_{y0}$ are lower (see Fig. 4.11) at the same values of the blade unit loading; proportional to $d\tilde{T}_\psi/d\bar{r}$. Results of calculations are shown in Fig. 4.14.

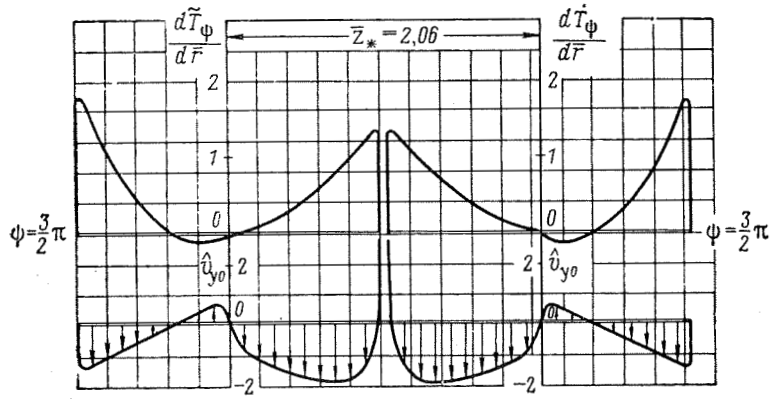

Figure 4.11

Attention was called first by L.S. Vil'dgrube to the benefits (from the point of view of reduced induced power) of the internally leading configurations. A quantitative determination of the dependence of $\Delta I_{\pi\pi}$ on the direction of rotation

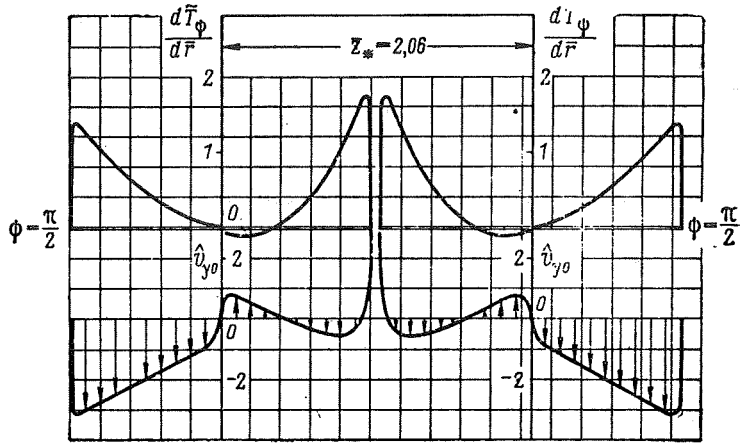

Figure 4.12

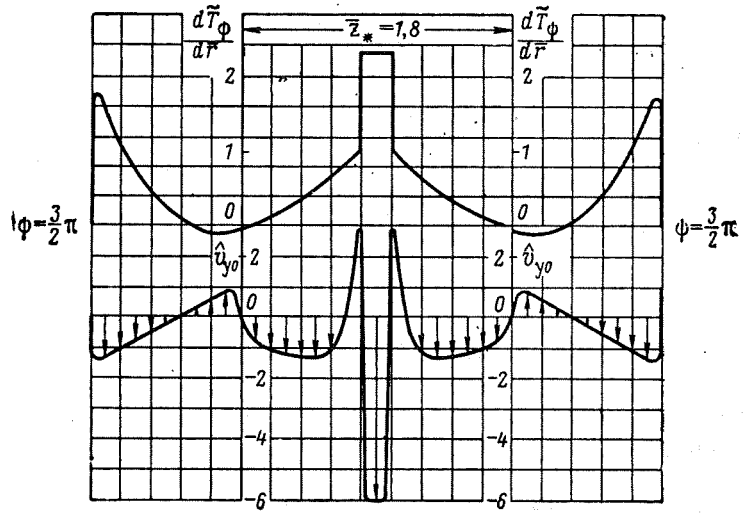

Figure 4.13

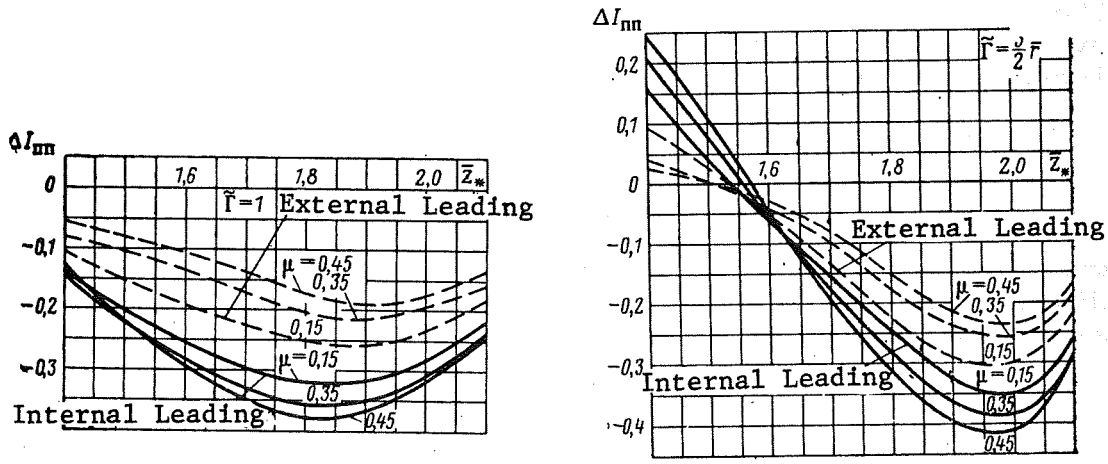

Figure 4.14

was accomplished by G.R. Kvasha. The ratio of the $\Delta I_{\pi\pi}$ coefficients for the externally leading configuration to those of the internally leading one is, in the average, equal to *0,6-0,7* which is in agreement with the data presented in Fig. 4.14.

Let us consider next, the influence of the form of distribution of average circulation on the magnitude of $\Delta I_{\pi\pi}$. Assuming $\tilde{\Gamma} = 1$, we will find from Eqs (2.28), (2.29) and (2.68) that

$$\hat{v}_{y0} = -\frac{\bar{V}+\bar{z}}{\bar{z}} \text{ at } |\bar{z}| \leqslant 1,$$

$$\hat{v}_{y0} = -\frac{\bar{V}+\bar{z}}{\bar{z}}\left(1-\frac{\bar{z}}{\sqrt{\bar{z}^2-1}}\right) \text{ at } \bar{z} > 1, \qquad (4.49)$$

$$\hat{v}_{y0} = -\frac{\bar{V}+\bar{z}}{\bar{z}}\left(1+\frac{\bar{z}}{\sqrt{\bar{z}^2-1}}\right) \text{ at } \bar{z} < -1.$$

In Fig. 4.14, one can find graphs of $\Delta I_{\pi\pi}$ for this case. It can be seen that $\Delta I_{\pi\pi max}$ for $\tilde{\Gamma} = (3/2)\bar{r}$ is higher than for $\tilde{\Gamma} = 1$. This can be explained by the fact that at $\tilde{\Gamma} = (3/2)\bar{r}$ tip vortices with higher circulations stream out from the rotor disc.

4. AERODYNAMIC INFLUENCE OF LIFTING ROTOR ON TAIL ROTOR

The main influence is exerted by the lateral component, v_z, of the induced velocity. This component is parallel to the tail rotor axis and thus, considerably influences the values of angles of attack of its blade sections (Fig. 4.15). As a result of this, the collective pitch angle of the tail rotor required to produce the necessary thrust $Tp.в$ as well as the blade flapping motion of its blades, varies. In order to overcome that additional induced resistance to rotation, an increment in power is needed

$$\Delta N_{\text{р.в}} = \frac{1}{75}(-v_{z\,\text{ср}})T_{\text{р.в}}, \qquad (4.50)$$

where $v_{z\,ср}$ is the side velocity averaged over the tail rotor disc. From the condition of equilibrium about the vertical axis, the thrust of the tail rotor is

$$T_{\text{р.в}} = \frac{M_{\text{к}}}{x_{\text{р.в}}} = \frac{75N_{\text{к}}}{\omega R\bar{x}_{\text{р.в}}}. \qquad (4.51)$$

Substituting Eq. (4.51) into Eq. (4.50), we obtain

$$\frac{\Delta N_{\text{р.в}}}{N_{\text{к}}} = -\frac{\bar{v}_{z\,\text{ср}}}{\bar{x}_{\text{р.в}}}. \tag{4.52}$$

According to Eqs. (2.69) and (3.9),

$$\bar{v}_z = \frac{c_{\text{т}}}{4\varkappa}\,\frac{\hat{v}_z}{\bar{V}}. \tag{4.53}$$

Let us consider flight without side-slip. In this case, it can be assumed that the plane of the tail rotor disc practically coincides with the xOy plane. Depending on the helicopter regimes of flight, the axis of the tail rotor can be either above, or below the Ox axis (Fig. 4.16). Usually, $\bar{x}_{p.\text{в}} = 1{,}2\text{-}1{,}3$. Calculations performed according to formulae from Sect. 6 of Ch. II, as well as experimental data, indicate that for $\bar{x}_1 = 1{,}3$,

$$\bar{v}_z \approx 2\hat{v}_{z0}. \tag{4.54}$$

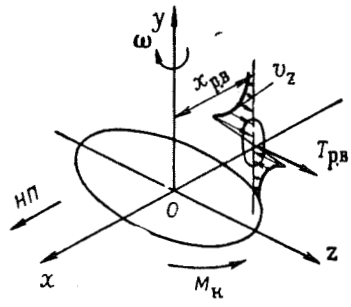

Figure 4.15

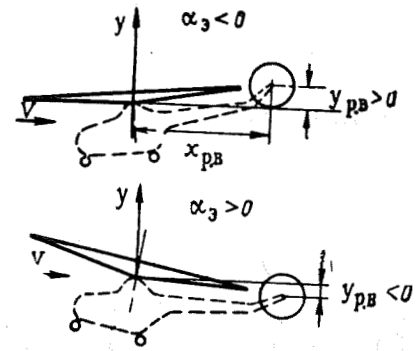

Figure 4.16

In analogy to Eq. (2.18) and taking into consideration Eq. (2.2), we will present the coefficient of the lateral component of induced velocity in the yOz plane in the following form:

$$\hat{v}_{z0} = -\int_{\bar{r}_0}^{1} \Delta\hat{v}_{z0}\, d\bar{\Gamma}. \tag{4.55}$$

The quantity $\Delta\hat{v}_{z0}$ is determined according to Eq. (2.33). For $\bar{z}_1 = 0$ and $\bar{x}_1 > 1{,}2$, Eqs. (2.13) and (4.54) show that

$$\Delta\hat{\bar{v}}_z = -\frac{2\bar{V}}{\sqrt{\bar{\varrho}^2+\bar{y}_1^2}}, \tag{4.56}$$

$$\frac{\hat{\bar{v}}_z}{\bar{V}} = 2\int_{\bar{r}_0}^{1}\frac{\frac{d\tilde{\Gamma}}{d\bar{\varrho}}}{\sqrt{\bar{\varrho}^2+\bar{y}_1^2}}d\bar{\varrho}. \tag{4.57}$$

By comparing Eqs. (4.53) and (4.57), we can see that $\bar{v}_z$ values in the $x0y$ plane depend only on the magnitude of the thrust coefficient of the lifting rotor, c_T, and character of the $\tilde{\Gamma}$ distribution. Variation of $\bar{V}$ has no direct influence on $\bar{v}_z$.

Let us determine $\hat{v}_z/\bar{V}$ for the three common cases of circulation distribution.

For the uniform distribution, $\tilde{\Gamma} = 1$, two distinct vortices spring from both ends of the blades, with the following circulations: $\Delta\tilde{\Gamma}_1 = 1$ and $\Delta\tilde{\Gamma}_{\bar{r}_0} = -1$. According to Eqs. (2.72) and (2.66),

$$\hat{\bar{v}}_z = \Delta\hat{\bar{v}}_z^{\bar{\varrho}=\bar{r}_0}\Delta\tilde{\Gamma}_{\bar{r}_0} + \Delta\hat{\bar{v}}_z^{\bar{\varrho}=1}\Delta\tilde{\Gamma}_1. \tag{4.58}$$

Substituting Eq. (4.56) into the above, we obtain

$$\frac{\hat{\bar{v}}_z}{\bar{V}} = 2\left(\frac{1}{\sqrt{\bar{r}_0^2+\bar{y}_1^2}} - \frac{1}{\sqrt{1+\bar{y}_1^2}}\right). \tag{4.59}$$

In the case of a linear (triangular) distribution of circulation, $\tilde{\Gamma} = a(\bar{\varrho} - \bar{r}_0)$. A continuous sheet of vorticity with circulation per unit length of $d\tilde{\Gamma}/d\bar{\varrho} = a$ comes off the blade plus a tip vortex whose circulation is $\Delta\tilde{\Gamma}_1 = -a(1 - \bar{r}_0)$. According to Eqs. (4.58) and (4.57),

$$\frac{\hat{\bar{v}}_z}{\bar{V}} = 2a\left(\ln\frac{1+\sqrt{1+\bar{y}_1^2}}{\bar{r}_0+\sqrt{\bar{r}_0^2+\bar{y}_1^2}} - \frac{1-\bar{r}_0}{\sqrt{1+\bar{y}_1^2}}\right). \tag{4.60}$$

From the condition expressed by Eq. (3.12), we find that

$$a = \frac{3}{2-3\bar{r}_0+\bar{r}_0^3}. \tag{4.61}$$

If $\tilde{\Gamma} = 10\bar{\rho}^2(1 - \bar{\rho})$, then the vorticity surface has a circulation per unit length of $d\tilde{\Gamma}/d\bar{\rho} = 10\bar{\rho}(2 - 3\bar{\rho})$. From Eq. (4.57), after integration and transformations, we obtain

$$\frac{\hat{v}_z}{\bar{V}} = 10\left(\sqrt{1+\bar{y}_1^2} - 4\bar{y}_1 + 3\bar{y}_1^2 \ln\frac{1+\sqrt{1+\bar{y}_1^2}}{\bar{y}_1}\right). \qquad (4.62)$$

According to Eq. (2.34), for negative values of $\bar{y}_1$, the coefficient $\hat{v}_z$ also becomes negative.

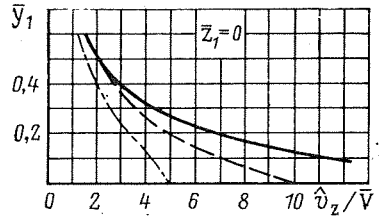

Figure 4.17

In Fig. 4.17, graphs of $\hat{v}_z/\bar{V}$ are shown. In this figure, the continuous line corresponds to $\tilde{\Gamma} = 1$; the dash line to $\tilde{\Gamma} = 10\bar{\rho}^2(1 - \bar{\rho})$, and the dash-dot line to $\tilde{\Gamma} = 1{,}76(\bar{\rho} - 0{,}1)$. From this graph, it can be seen that the type of distribution of the average circulation strongly influences $\hat{v}_z$ values. With an increase of the inboard blade chords and a decrease of $\bar{r}_0$, the coefficient $\hat{v}_z$ increases. Let us make a quantative evaluation of the influence of the main rotor on the operation of the tail rotor. From Eqs. (4.52) and (4.53), one finds,

$$\frac{\Delta N_{\text{p.в}}}{N_{\text{к}}} = -\frac{c_{\text{т}}}{4\varkappa\bar{x}_{\text{p.в}}}\frac{\hat{v}_{z\,\text{ср}}}{\bar{V}}. \qquad (4.63)$$

In the helicopter regime of flight ($\alpha_э < 0$), the tail rotor is above the main rotor vorticity wake and $\hat{v}_{z_{ср}} > 0$. Consequently, at $\alpha_э < 0$, the influence of the main rotor causes a decrease of power required by the tail rotor. For simplicity, let us assume that the ordinate of the tail rotor axis $y_{p.B} > R_{p.B}$ (where $R_{p.B}$ is the tail rotor radius). This means that the tail rotor is completely above the Oz axis. Then, it may be assumed with sufficient accuracy that $\hat{v}_{z_{ср}}$ (average) would be equal to $\hat{v}_z$ at the tail rotor axis. From Fig. 4.17, one can find that in the average, $\hat{v}_{z_{ср}}/\bar{V} = 4{,}5$. For $x_{p.B} \approx 1{,}21$, $\varkappa = 0{,}94$ and $c_{\text{т}} = 0{,}012$, we obtain $\Delta N_{p.B}/Nk \approx -0{,}0118$.

Calculations indicate that without considerations of the influence of the main rotor, the tail rotor absorbs 5-7% of the main rotor power. The influence of the vortex system of the main rotor can reduce the power required by the tail rotor by as much as 17-24%. This would occur in those regimes of flight where the flying speed is sufficiently high so that the tail rotor is above the vortex wake of the main rotor.

In power-off conditions, the main rotor goes into autorotation, $\alpha_э > 0$, and the tail rotor finds itself below the main rotor vortex wake (see Fig. 4.16). Under those conditions, $\hat{v}_{z\,ср} < 0$, and the thrust of the tail rotor automatically decreases. It should be noted that at $\alpha_э > 0$, ordinates of $\tilde{\Gamma}$ at small $\bar{r}$ values increase, and thus the coefficient $\hat{v}_z$ will change its sign, while its absolute value will be higher than in the helicopter regime of flight.

On the basis of the above presented considerations, it may be estimated that reduction of the power required by the tail rotor, resulting from the aerodynamic influence of the main rotor, can be approximated by the following formula:

$$\frac{\Delta N_{р.в}}{N_к} = -c_т. \tag{4.64}$$

Let us now determine the coefficient $\hat{v}_y$ of the vertical component of velocity induced in the xOy plane by the main rotor when $\bar{x}_1 \approx 1{,}3$. In analogy with Eq. (4.54), we obtain

$$\hat{v}_y \approx 2\hat{v}_{y0}. \tag{4.65}$$

For $\bar{z}_1 = 0$, Eqs. (2.12) and (2.13) indicate that

$$\Delta\hat{v}_y = -2\left(1 - \frac{\bar{y}_1}{\sqrt{\bar{\varrho}^2 - \bar{y}_1^2}}\right). \tag{4.66}$$

From a relationship similar to Eq. (4.55), we find

$$\hat{v}_y = 2\left(\int_{\bar{r}_0}^{1} d\tilde{\Gamma} - \bar{y}_1 \int_{\bar{r}_0}^{1} \frac{\frac{d\tilde{\Gamma}}{d\bar{\varrho}}}{\sqrt{\bar{\varrho}^2 + \bar{y}_1^2}} d\bar{\varrho}\right) \tag{4.67}$$

In the development of Eq. (2.19), it was stated that the first integral is equal to zero, and the second one can be expressed (Eq. (4.57)) in terms of $\hat{v}_z$. Then,

$$\hat{v}_y = -\bar{y}_1 \frac{\bar{v}_z}{\bar{V}} \tag{4.68}$$

and the vertical component of relative induced velocity, v_y, can be found from Eqs. (2.68) and (3.9).

CHAPTER V

AERODYNAMIC CHARACTERISTICS OF A RIGID LIFTING AIRSCREW

The absence of flapping motion in rigidly attached blades considerably influences the distribution of the actual angles of attack along their sections, and consequently, affects the distribution of aerodynamic loads. However, according to Eq. (2.84), flapping oscillations of the first harmonic type do not influence the thrust magnitude of an articulated rotor. In this way, the circulation $\tilde{\Gamma}_r$ averaged over one rotor revolution and the thrust coefficient c_T of such a rotor are determined for $\bar{k}_\vartheta = 0$ by Eqs. (2.98) and (3.12), which were established for rotors with articulated blades.

For the development of all other formulae, it will be assumed that the flapping angle β and v_δ are zero. Then, from Eqs. (1.9), (1.10) and (1.12), after some transformations and substitution of $a_\infty\alpha$ for c_y, where α is given by Eq. (2.78), we obtain

$$\frac{c_H^{\text{ж}}}{c_T} \approx \frac{1}{2}\mu\frac{\sigma}{c_T}\left\{c_{xpH} + 3{,}7\,\frac{c_T}{\mu}\left[\varphi_0(1-0{,}7\mu^2) + 2{,}4\mu(1-\mu)\alpha_в\right] - \right.$$
$$\left. - 5\mu\alpha\varphi_0 - 2{,}2\frac{c_T^2}{\mu^2}\left(1-\mu^2+\frac{0{,}05}{\mu}\right)\right\}. \qquad (5.1)$$

The quantity c_{xpH}, determined from Eq. (3.94), is higher than for articulated blades since $c_{y\psi}^{\text{ж}}$ in the $40° \leq \psi \leq 140°$ region will be higher than $c_{y\psi}$ from Eq. (3.63). For preliminary calculations, the following formulae can be used:

$$c_{y\psi}^{\text{ж}} \approx 2{,}13\,\frac{c_T}{\sigma}\left[1{,}43 + \frac{\sigma}{\mu}\left(1 + \frac{\varkappa_\psi}{1+1{,}43\mu\sin\psi}\right)\right] +$$
$$+ 0{,}136\mu^2\alpha_в^0\left[\mu - 1{,}43(1+1{,}5\mu^2)\sin\psi - \mu\cos 2\psi + 0{,}72\mu^2\sin 3\psi\right] + \Delta c_{y\psi}(\theta), \qquad (5.2)$$

where
$$\Delta c_{y\psi}(\theta) = 0{,}1\,(\theta_1^\circ\cos\psi + \theta_2^\circ\sin\psi) - 0{,}132\mu\theta_2^\circ. \qquad (5.3)$$

Values of $\varkappa_\psi$ are shown in Table 5.1.

Eq. (5.1) was obtained for $\tilde{\Gamma} = (3/2)\bar{r}$. To illustrate the order of magnitude of $c_H^{\text{ж}}/c_T$, its values are shown in Table 5.2 for $\mu = 0{,}25$; $c_T/\sigma = 0{,}134$; $\sigma = 0{,}10$. Variations of σ and $\tilde{\Gamma}$ have little influence on the $c_H^{\text{ж}}/c_T$ level. A comparison of results obtained under the assumption of nonuniform induced velocity distribution with those computed assuming that $v_y = const$[33] indicates that the nonuniformity of induced velocities increases

$c_H^{ж}$ by 16% at $\mu = 0,25$ and $\alpha_B < 0$, and makes it 2-4 times higher for $\alpha_B > 0$.

$\psi°$	0	45	90	135	180	225	270	315
$\varkappa_\psi$	0,1	—3,4	—1,75	—0,5	—0,1	—0,3	—0,1	—1,3

Table 5.1

$\alpha_в°$	—10	+10
$c_H^{ж}/c_т$	0,045	0,016

Table 5.2

From Eqs. (1.9), (1.11) and (1.12) and similar to Eq. (5.1), we obtain

$$\frac{c_S^{ж}}{c_т} \approx -\tilde{S}_8 \frac{\sigma}{\mu}\left[\varphi_0(1+\mu)+\tilde{S}_9\mu\alpha_в-\tilde{S}_{10}\frac{c_т}{\mu}(1+\tilde{S}_{11}\mu)\right]. \qquad (5.4)$$

Values of the $\tilde{S}_n$ coefficients are given in Table 5.3.

We should notice that at $\mu = 0,25$, the $c_S{}^{ж}$ value is not high and represents no more than 1% of thrust. If one assumes $v_y = const$, then $c_S{}^{ж} = 0$, as obtained by Glauert[33].

The longitudinal moment generated by a blade element will be $\Delta M_z = -r\Delta T \cos\psi$. After routine substitutions and transformations, we obtain

$$\frac{m_z^{ж}}{c_т} \approx \tilde{z}\frac{\sigma}{\mu}\left(1+\frac{1}{2}\mu\right). \qquad (5.5)$$

Values of $\tilde{z}$ are given in Table 5.4.

$\tilde{\Gamma}$	$\tilde{S}_8$	$\tilde{S}_9$	$\tilde{S}_{10}$	$\tilde{S}_{11}$
$\frac{3}{2}\bar{r}$	0,15	0,7	1,0	2
1,0	0,37	2,7	0,72	5

Table 5.3

$\tilde{\Gamma}$	$\tilde{z}$
$\frac{3}{2}\bar{r}$	0,154
1,0	0,33

Table 5.4

Coefficient $m_z^{ж}$ depends very strongly on the type of $\tilde{\Gamma}$ distribution. For $\mu = 0,25$; $\sigma = 0,075$ and $\tilde{\Gamma} = (3/2)\bar{r}$, the ratio of $m_z^{ж}/c_T \approx 0,052$. This quantity represents the relative distance of the point of application of the rotor thrust

from its axis. Pitching moment increases with increasing σ. Experiments* performed with a model of high solidity ratio ($\sigma = 0,255$) at $\mu = 0,21$ and $c_T = 0,033$ confirmed the correctness of Eq. (5.5). It should be emphasized that non-zero values of $m_z^{ж}$ result from nonuniform distribution of induced velocity. Should $\overline{v}_y = const$, then $m_z^{ж} = 0$.

With a displacement of the swashplate from its neutral position (see Eq. (2.79)), an additional moment will be generated whose coefficient will be

$$\Delta m_{z\,an}^{ж} \simeq -0,66\sigma(1+0,5\mu^2)\theta_1. \tag{5.6}$$

Comparing Eqs. (5.5) and (5.6), we can find the angle of the blade rotation in pitch, θ_1, at $\psi = 0$, at which the longitudinal moment will be cancelled.

Rolling moment produced by a blade element will be $\Delta M_x = -r\Delta T \sin\psi$. From this, in analogy with the development of Eq. (5.5), we find

$$m_x^{ж} \approx -1,08\mu\sigma\left[\frac{c_T}{\sigma}\left(1-0,52\frac{\sigma}{\mu}\right)-1,1\mu\alpha_в\right]. \tag{5.7}$$

Displacement of the swashplate from neutral would produce an additional moment, whose coefficient would be:

$$\Delta m_{x\,an}^{ж} \approx -0,66\sigma\left(1+\frac{2}{3}\mu^2\right)\theta_2. \tag{5.8}$$

From this we can find an angle $\theta_2 < 0$, required to cancel the rolling moment.

The profile power coefficients can be determined from Eqs. (3.184) and (3.180), assuming $v_\delta = 0$. The average profile drag coefficient $c_{xp_0}^{ж}$ may be computed from Eqs. (3.176) and (3.181). To give a better feeling, results of some comparative calculations are presented. At $\overline{V} = 0,35$; $c_T/\sigma = 0,157$, $\alpha_в = -5°$ and $\theta_2 = 0$, a rigid rotor requires 1,73 more power to overcome the profile drag than a rotor with identical blades but attached through flapping hinges. At $\theta_2 = -2,5°$, values of the $c_{y\psi}$ coefficients around $\psi = \pi/2$ become lower and consequently, $c_{xp_0}^{ж}$ is lowered by 14%. With the decreasing $\overline{V}$ levels, differences in profile drag (power) values of the rigid and flapping configurations become less significant. Coefficients of power

---

*Performed by V.D. Voronitzev and I.A. Serov

required to overcome induced drag are given by Eq. (3.188). The induction coefficient of the rigid rotor I^{κ} can be determined from Eq. (4.15). If $\Gamma_{\psi} \approx const$, then it is necessary to use Eq. (4.8) instead of Eq. (4.7), and induced power becomes lower. It should be emphasized that from an aerodynamic point of view, it is beneficial for the rigid rotor to maintain $\theta_2 < 0$.

CHAPTER VI

BLADE THEORY OF LIFTING AIRSCREW IN AXIAL FLIGHT

The blade theory of propellers was developed in great detail (see Refs. 21, 63, and others) and applied to the two, three and four-bladed propellers at sufficiently high speeds of flight when the influence of induced velocities on the shape of free vortices may be neglected (linear theory). For lifting airscrews which usually operate at low speeds of vertical translation, that influence of induced velocities is quite considerable and thus, cannot be neglected. Rigorous treatment of the problem of flight of a rotor at low vertical velocities is quite complicated, since determination of the shape of free vorticity wake, distribution of circulation within it, and definition of the field of induced velocities should be accomplished simultaneously (nonlinear theory).

This problem is solved below in an approximate way through numerical methods. Furthermore, general assumptions of the propeller theory are applied, as well as well-known hypotheses applicable to the case of low flying speeds: (1) the blade is represented by a radial segment of the lifting line with circulation varying along its span, (2) blade airfoil sections work under the two-dimensional flow conditions (hypothesis of narrow elements), (3) variation of the blade lift coefficient with angle of attack is assumed linear, and (4) elements of free (trailing) vortices which spring from any point of the rotating lifting line move in the space in a rectilinear motion with a speed equal to the sum of the undisturbed flow approaching the rotor, and induced velocity averaged over the disc.

Hypothesis No. (4) takes into consideration the principal part of the influence of the induced velocity field on the vortices movements. Indeed, it will be shown later that the airscrew theory based on this hypothesis assures results sufficiently accurate for practice.

Principles of the considered numerical methods are based on the substitution of a system of discrete horseshoe vortices for a continuous vorticity layer. This approach found a broad application to the theory of vorticity layer[12] since it is quite descriptive, leads to a simple alogrithm, and consequently, is suitable for computer computations. Transition to a system of discrete blade vortices leads to a replacement of the basic integral-differential equation determining the law of circulation distribution along a lifting line by a system of linear algebraic equations. Coefficients appearing at the sought circulation of discrete vortices contained in this system are

determined by nonelementary functions (influence functions). Their determination represents the most difficult part of the computation. In order to reduce the presented theory to practice, the influence functions are presented in a tabular form for a number of blades from 3 to 5. As a result, the task is reduced to the solution of systems of linear algebraic equations with known coefficients. Programs for such solutions are available in the libraries of practically all computers.

1. GENERAL INTEGRAL RELATIONSHIPS FOR INSTANTANEOUS INDUCED VELOCITIES

Let us assume that a k-bladed airscrew of $2R$ diameter is located in a uniform flow with velocity V_∞ and that a stationary Cartesian system of coordinates $Oxyz$ (Fig. 6.1) originates in the center of its hub. The airscrew rotates around the y axis with an angular velocity ω. The airscrew blades are indexed by a number $n(n=1,2,\ldots,k)$. Azimuth angle θ_n of the nth blade is measured from the negative half-axis of x and is counted in the direction of rotation. If we define by θ the azimuth angle of the blade with the number $n=1$, then

$$\theta_n=\theta+\delta_n,\quad \delta_n=\frac{2\pi}{k}(n-1). \tag{6.1}$$

Let it be assumed that circulation distribution along the lifting line is given by a continuous function, $\Gamma = \Gamma(\rho)$. Then, according to the Helmholtz theory, elementary vortices will continuously spring from any point of the lifting line which, moving together with the flow, would form an elementary free vortex. An assembly of such vortices springing from the lifting line would form a vorticity wake.

Now we develop parametric equations of the vortex surface. In order to do this, we will investigate the movement of an arbitrary element E of the free vortex (Fig. 6.2). Element E was formed in that instant when the segment $OB = \rho$ of the lifting line occupied position OA. After its separation from the lifting line in point A, the element E started to move parallel to the axis with a speed $V = V_\infty - v$ (hypothesis (4)), where v is the induced velocity generated by the airscrew at point A of the lifting line. Let us introduce a supplementary parameter: angle ϑ between segments OA and OB measured from segment OB. During time ϑ/ω, segment OA moves to the position of OB with an azimuth angle θ_n, while the vortex element travels distance

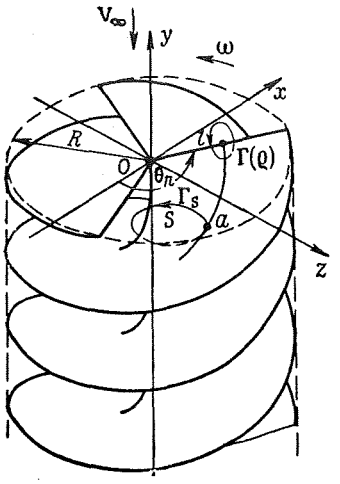

Figure 6.1

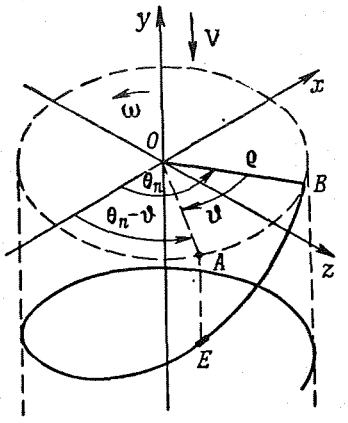

Figure 6.2

$AE = V\vartheta/\omega(\overline{AE} = \overline{V}\vartheta)$. It can be seen, hence, from Fig. 6.2 that Cartesian coefficients of element E expressed in non-dimensional form will be:

$$\bar{\xi} = -\bar{\varrho}\cos(\theta_n - \vartheta),\quad \bar{\eta} = -\overline{V}\vartheta,\quad \bar{\zeta} = \bar{\varrho}\sin(\theta_n - \vartheta),$$
$$0 \leqslant \theta_n \leqslant 2n,\quad 0 \leqslant \vartheta < \infty,\quad \bar{\varrho}_0 \leqslant \bar{\varrho} \leqslant 1, \tag{6.2}$$

where $\bar{\rho}_0$ is the relative* radius of the non-working part of the blade. Eq. (6.2) gives the sought parametric equation of the vortex wake. For given values of $\bar{\rho}$, those relationships represent equations of a helix (with parameter ϑ) along which extends an elementary free vortex. As angle ϑ varies from zero to infinity, the running point moves along the vortex (Fig. 6.2) further and further away from the lifting line, up to infinity. In the case of $\vartheta = 0$, Eq. (6.2) represents equations of the lifting line (with a parameter $\bar{\rho}$):

$$\xi = -\bar{\varrho}\cos\theta_n,\quad \bar{\eta} = 0,\quad \bar{\zeta} = \bar{\varrho}\sin\theta_n. \tag{6.3}$$

Before analyzing the induced velocities, let us establish a relationship between circulation of the free elementary

---

*For the sake of brevity, this adjective will be omitted in in following considerations.

vortex with circulation of the lifting line. First of all, let us establish rules regarding a closed contour along which velocity circulation is computed. Let an arbitrary closed line be drawn around a vortex with a prescribed direction of movement of the running point (ξ, η, ζ). We will assume that an observer moving along this vortex together with the running point and looking in the direction opposite to his movement sees the movement around the enclosing contour in an anti-clockwise direction. Guided by the above-established rules, let us imagine an arbitrary closed-contour curve S, with circulation $\overline{\Gamma}_S$, which pierces the vorticity surface at some point "a" of the trailing vortex springing from the lifting line at radius $\overline{\rho}$ (see Fig. 6.1). We also draw another closed-contour line "l" with circulation $\overline{\Gamma}$, which constricts the lifting line at that point. We tighten contour S around the lifting line by having point "a" move along the indicated free vortex towards the lifting line. This operation should be performed in such a way that the continuously deforming contour S would cut the vortex wake only at the moving point a. Then, according to the first theorem of Helmholtz, it is possible to conclude that circulation $\overline{\Gamma}_S$ would remain constant throughout the whole process of the transformation of contour S. If we realize that the transformed contour S differs from contour "l" only by direction of movement, then $\overline{\Gamma}_S = -\overline{\Gamma}$, from which one can obtain a formula for an elementary free (trailing) vortex.

$$d\overline{\Gamma}_S = -\frac{d\overline{\Gamma}}{d\overline{\varrho}}\, d\overline{\varrho}. \tag{6.4}$$

Let us define by $d\overline{v}$, the axial velocity induced by an elementary free vortex in a point with the following coordinates:

$$\overline{x} = -\overline{r}\cos\psi, \quad y = 0, \quad \overline{z} = \overline{r}\sin\psi, \tag{6.5}$$

where $\overline{r}$ and ψ, respectively, are the polar radius and azimuth angle of that point. Angle ψ is counted from the negative half-axis x in the direction of rotor rotation. We substitute Eqs. (6.2), (6.4) and (6.5) into Eq. (A.6) and, in the latter, assume $p = \mathfrak{d}$. After a few transformations, we find

$$d\overline{v} = \frac{1}{4\pi}\left(\frac{d\overline{\Gamma}}{d\overline{\varrho}}\, d\overline{\varrho}\right)\int_0^{\infty} \frac{\overline{\varrho}^2 - \overline{\varrho}\,\overline{r}\cos(\theta - \psi + \delta_n - \vartheta)}{[\overline{V}^2\vartheta^2 + \overline{\varrho}^2 + \overline{r}^2 - 2\overline{\varrho}\,\overline{r}\cos(\theta - \psi + \delta_n - \vartheta)]^{3/2}}\, d\vartheta.$$

Then instantaneous velocity induced by the whole system of free vortices will be

$$\bar{v}=\frac{1}{4\pi}\sum_{n=1}^{k}\int_{\bar{\varrho}_0}^{1}\int_{0}^{\infty}\frac{d\bar{\Gamma}}{d\bar{\varrho}}\,\frac{\bar{\varrho}^2-\bar{\varrho}\bar{r}\cos(\theta-\psi+\delta_n-\vartheta)}{[\bar{V}^2\vartheta^2+\bar{\varrho}^2+\bar{r}^2-2\bar{\varrho}\bar{r}\cos(\theta-\psi+\delta_n-\vartheta)]^{3/2}}\,d\vartheta d\bar{\varrho}. \tag{6.6}$$

In the particular case when velocity $\bar{v}=\bar{v}(\bar{r},\psi)$ is computed at the lifting line ($\theta=\psi$), Eq. (6.6) is transformed into the following:

$$\bar{v}=\frac{1}{4\pi}\sum_{n=1}^{k}\int_{\bar{\varrho}_0}^{1}\int_{0}^{\infty}\frac{d\bar{\Gamma}}{d\bar{\varrho}}\,\frac{\bar{\varrho}^2-\bar{\varrho}\bar{r}\cos(\delta_n-\vartheta)}{[\bar{V}^2\vartheta^2+\bar{\varrho}^2+\bar{r}^2-2\bar{\varrho}\bar{r}\cos(\delta_n-\vartheta)]^{3/2}}\,d\vartheta d\bar{\varrho}. \tag{6.7}$$

Let us develop new formulae for instantaneous velocity induced in point (6.5) by lifting lines of the rotor. We substitute Eqs. (6.3) and (6.5) into Eq. (A.6), assuming in the latter that $p=\bar{\rho}$. After some simple transformations, we will find the sought expression for velocity induced by the lifting lines:

$$\bar{v}_{\text{H}}=-\frac{1}{4\pi}\sum_{n=1}^{k}\int_{\bar{\varrho}_0}^{1}\frac{\bar{\Gamma}\bar{r}\sin(\theta-\psi+\delta_n)}{[\bar{\varrho}^2+\bar{r}^2-2\bar{\varrho}\bar{r}\sin(\theta-\psi+\delta_n)]^{3/2}}\,d\bar{\varrho}. \tag{6.8}$$

In the case of $\theta=\psi$, we have $\bar{v}_{\text{H}}=0$. This means that induced velocities at the lifting lines are only induced by the free vortices.

2. SCHEME OF THE DISCRETE VORTICES SYSTEM OF A ROTOR AND BASIC RELATIONSHIPS

Let us substitute a system of discrete vortices for the continuous layer of vorticity coming from the blade (Fig. 6.3). In order to do this, the lifting line is divided into m segments. To the points of division, we assign an index i ($i=1,2,3,\ldots,m+1$). The location of those points on the y axis are designated by $\bar{\rho}_i$. A vortex with the index i consists of a segment of the lifting line between points i and $i+1$, and two free vortices trailing from those points. Circulation of the i-th vortex is designated as $\bar{\Gamma}_i$. Between the two cylindrical surfaces with radii $\bar{\rho}_i$ and $\bar{\rho}_{i+1}$ there are k horseshoe vortices with the same index number, i. Induced velocities are computed at the so-called control points j ($j=1,2,3,\ldots,m$) located between points i. Velocity induced by the airscrew at point j is designated as $\bar{v}_j$. In this case, for a given discrete scheme, the following relationship, analogous to Eq. (6.7), can be obtained

$$\bar{v}=\sum_{i=1}^{m}\bar{v}_{ij}\bar{\Gamma}_i\quad(j=1,2,3,\ldots,m), \tag{6.9}$$

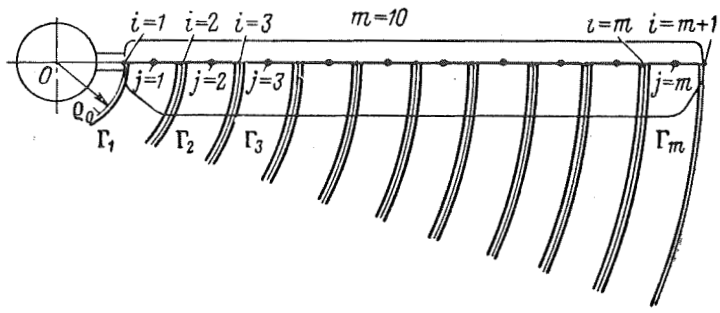

Figure 6.3

where

$$\bar{v}_{ij}=\frac{1}{4\pi}\sum_{n=1}^{k}\int_0^{\infty}[P_{ij}(n,\vartheta)-P_{i+1,j}(n,\vartheta)]\,d\vartheta, \qquad (6.10)$$

$$P_{ij}(n,\vartheta)=\frac{\bar{\varrho}_i^2-\bar{\varrho}_i\bar{r}_j\cos(\delta_n-\vartheta)}{[\bar{V}^2\vartheta^2+\bar{\varrho}_i^2+\bar{r}_j^2-2\bar{\varrho}_i\bar{r}_j\cos(\delta_n-\vartheta)]^{3/2}}.$$

It is easy to see that with unlimited replacement of the lifting line by points i (with $\max(\bar{\rho}_{i+1}-\bar{\rho}_i)\to 0$), Eq. (6.9) changes into Eq. (6.7).

Coefficients v_{ij} in Eq. (6.10) are called *influence functions*. An influence function represents the velocity induced at point j by vortices with the same index i and circulation equal to unity. Coefficients $\bar{v}_{ij}$ from Eq. (6.9) are not expressed through elementary functions; for this reason, in order to facilitate aerodynamic computations of rotors, they are presented in a tabular form (see Appendix VI). It was assumed in the calculations that: $m = 10$; $\bar{\rho}_i = 0{,}2,\ 0{,}28,\ 0{,}36,\ \ldots,\ 1{,}0$; $\bar{\rho}_j = 0{,}24,\ 0{,}32,\ 0{,}4,\ \ldots,\ 0{,}96$; $k = 3,\ 4,\ 5$. In order to widen the range of velocities, tables are arranged with respect to parameter

$$\sin\beta_R=\frac{\bar{V}}{\sqrt{1+\bar{V}^2}}.$$

Integration of Eq. (6.10) was performed on a computer using Simpson's rule with an automatic selection of the step of integration and the upper limit, so that the absolute error of the obtained results would not exceed 10^{-4}. Selection of $m = 10$ is

based on actual computational experience, showing that this particular number is close to optimum because of the accuracy of computations as well as difficulties of calculations.

The quantities given in the tables permit one to directly evaluate the importance of the number of blades on induced velocities. In every table, it can be seen that a decisive role is played by elements located along the principal diagonal. Every one of those elements characterize the magnitude of induced velocity generated in point j by vortices $i = j$. It is clear from the tables that with an increase in the number of blades, the influence of vortices $i \neq j$ decreases. In this case, helixes of vortex filaments are distributed more tightly in the space and with $k \to \infty$, they would form a cylindrical vorticity surface. As is known for $k \to \infty$, the influence of $i \neq j$ vortices disappears ($\overline{v}_{ij} = 0$ for $i \neq j$). With increasing velocity $\overline{V}$ and a constant number of blades, distances between helixes of the vortex filaments increase and thus, the influence of a finite number of blades becomes more significant. Consequently, vortices $i \neq j$, being closer to point j, begin to play a more important role.

In the case of a sufficiently high velocity of the flow when $\overline{V} \approx \overline{V}_\infty$, then Eq. (6.9) and tabulated data permit one to find, in an elementary way, induced velocities $\overline{v}_j$, once circulations $\overline{\Gamma}_i$ are known. Let us concentrate our attention on the determination of circulations $\overline{\Gamma}_i$.

3. COMPUTATION OF CIRCULATION OF DISCRETE VORTICES (CASE OF LARGE $\overline{V}_\infty$ VALUES)

Let us consider the flow around an airfoil section located at radius $\overline{r}_j$ (Fig. 6.4). The aerodynamic chord forms, with plane of rotation, a pitch angle $\phi_j = \phi_0 + \Delta\phi_j$; where ϕ_0 is the pitch angle of the representative blade section, and $\Delta\phi_j$ is the geometric twist angle. An angle of attack α_j is formed between the aerodynamic chord and the flow approaching the airfoil at velocity W_{pj}. Velocity W_{pj} is a vectorial sum of the following components: $\overline{V}_\infty$ - speed of translation; $\overline{u}_j = \overline{r}_j$ - peripheral velocity due to rotation of the blade; and $\overline{v}_{pj}$ - complete induced velocity which, in turn, has two components, $\overline{v}_j$ and $\overline{v}_{\tau j}$. Here, $\overline{v}_{\tau j}$ is the rotational induced velocity. Velocity

$$\overline{W}_j = \sqrt{\overline{V}_\infty^2 + \overline{r}_j^{\,2}}$$

makes, with the plane of rotation, an angle $\beta_j = tg^{-1}(\overline{V}_\infty/\overline{r}_j)$ which will be called the *inflow angle*. Velocities $\overline{W}_{pj}$ and $\overline{W}_j$ make an angle $\Delta\beta_j$ which will be called the *induced flow angle*. Since angle $\Delta\beta_j$ is small, it may be assumed hence, that it is equal to $\overline{v}_{pj}/\overline{W}_j$. If it is assumed that velocity $\overline{v}_{pj}$ is perpendicular to the helical line[63], then $\overline{v}_{pj} = \overline{v}_j/\cos\beta_j$ and

consequently, $\Delta\beta_j = -\bar{v}_j/\bar{r}_j$. In this case, the profile angle of attack and the corresponding lift coefficient can be expressed as follows:

$$\alpha_j = \varphi_0 + \Delta\varphi_j - \beta_j + \frac{v_j}{\bar{r}_j}, \tag{6.11}$$

$$c_{yj} = a_{\infty j}\left(\varphi_0 + \Delta\varphi_j - \beta_j + \frac{\bar{v}_j}{\bar{r}_j}\right), \tag{6.12}$$

where $a_{\infty j}$ is the lift slope (associated with the lift coefficient c_{yj}).

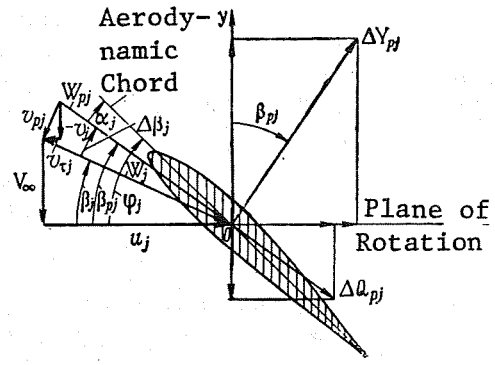

Figure 6.4

Now, we find a relationship between lift coefficient c_{yj} and circulation $\bar{\Gamma}_i = \bar{\Gamma}_j$. According to the Joukowsky theory,

$$Y_{pj} = \varrho W_{pj}\Gamma_j.$$

Here, Y_{pj} is the lift per unit of span of infinite aspect ratio wing; ρ is the air density. On the other hand, it is known from experiemntal aerodynamics that

$$Y_{pj} = \frac{1}{2} c_{yj}\varrho W_{pj}^2 b_j,$$

where b_j is the airfoil section chord. Equating the right sides of the above equations and assuming that $W_{pj} = W_j$ (because of small $\Delta\beta_j$), we obtain the well-known equation

$$\bar{\Gamma}_j = \frac{1}{2} c_{yj}\bar{b}_j\bar{W}_j. \tag{6.13}$$

We substitute Eq. (6.9) into Eq. (6.12), and Eq. (6.12) into Eq. (6.13). As a result of simple calculations, we obtain a system of linear algebraic equations defining the sought circulations

$$\sum_{i=1}^{m} \bar{\gamma}_{ij}\bar{\Gamma}_j = \bar{q}_j, \tag{6.14}$$

where

$$\gamma_{ij}=\begin{cases}\dfrac{\bar{v}_{ij}}{k} & \text{for } i\neq j,\\ \dfrac{\bar{v}_{ij}}{k}-\dfrac{2\cos\beta_j}{a_{\infty j}k\bar{b}_j} & \text{for } i=j,\end{cases} \tag{6.15}$$

$$\bar{g}_j=-\frac{\bar{\varrho}_j}{k}\varphi_0\pm\frac{\bar{\varrho}_j}{k}(\beta_j-\Delta\varphi_j). \tag{6.16}$$

In the developed form, system given by Eq. (6.14) can be written in the following way:

$$\left.\begin{aligned}&\bar{\gamma}_{11}\bar{\Gamma}_1+\bar{\gamma}_{21}\bar{\Gamma}_2+\bar{\gamma}_{31}\bar{\Gamma}_3+\ldots+\bar{\gamma}_{m1}\bar{\Gamma}_m=\bar{g}_1,\\ &\gamma_{12}\bar{\Gamma}_1+\gamma_{22}\bar{\Gamma}_2+\bar{\gamma}_{32}\bar{\Gamma}_3+\ldots+\bar{\gamma}_{m2}\bar{\Gamma}_m=\bar{g}_2,\\ &\ldots\ldots\ldots\ldots\ldots\ldots\\ &\bar{\gamma}_{1m}\bar{\Gamma}_1+\bar{\gamma}_{2m}\bar{\Gamma}_2+\bar{\gamma}_{3m}\bar{\Gamma}_3+\ldots+\bar{\gamma}_{mm}\bar{\Gamma}_m=\bar{g}_m.\end{aligned}\right\} \tag{6.17}$$

Quantities $\bar{v}_{ij}/k$, appearing in coefficients $\bar{\gamma}_{ij}$ are taken from tables in Appendix VI with respect to parameter

$$\sin\beta_R=\frac{\bar{V}_\infty}{\sqrt{1+\bar{V}_\infty^2}}.$$

With the given characteristics of an airscrew: ϕ_ϱ, $\Delta\phi_j$, $a_{\infty j}$ and velocity $\bar{V}_\infty$, all coefficients γ_{ij} and $\bar{g}_j$ become known; hence, the system of Eqs. (6.14) can be solved on a computer, using standard methods. It is also possible to obtain a solution through a simple iteration without using a computer. We will demonstrate the application of the latter method on an example of the system given by Eq. (6.17). Every equation of that system should be solved with respect to the sought value of circulation appearing on the principal diagonal:

$$\left.\begin{aligned}&\bar{\Gamma}_1=\frac{1}{\bar{\gamma}_{11}}(\bar{g}_1-\bar{\gamma}_{21}\bar{\Gamma}_2-\bar{\gamma}_{31}\bar{\Gamma}_3-\ldots-\bar{\gamma}_{m1}\bar{\Gamma}_m),\\ &\bar{\Gamma}_2=\frac{1}{\bar{\gamma}_{22}}(\bar{g}_2-\bar{\gamma}_{12}\bar{\Gamma}_2-\bar{\gamma}_{32}\bar{\Gamma}_3-\ldots-\bar{\gamma}_{m2}\bar{\Gamma}_m),\\ &\ldots\ldots\ldots\ldots\ldots\ldots\ldots\\ &\bar{\Gamma}_m=\frac{1}{\bar{\gamma}_{mm}}(\bar{g}_m-\bar{\gamma}_{1m}\bar{\Gamma}_1-\bar{\gamma}_{2m}\bar{\Gamma}_2-\ldots-\bar{\gamma}_{m-1,m}\bar{\Gamma}_{m-1}).\end{aligned}\right\} \tag{6.18}$$

Since the most important role of all terms appearing in the parentheses is played by coefficients $\bar{g}_j$ (this results from the smallness of quantity $\bar{\gamma}_{ij}$ for $i \neq j$), it may be assumed, hence, as a first approximation that values of the sought circulations are

$$\bar{\Gamma}_1^{(1)} = \frac{\bar{g}_1}{\bar{\gamma}_{11}}, \quad \bar{\Gamma}_2^{(1)} = \frac{\bar{g}_2}{\bar{\gamma}_{22}}, \quad \ldots, \quad \bar{\Gamma}_m^{(1)} = \frac{\bar{g}_m}{\bar{\gamma}_{mm}}. \tag{6.19}$$

Substituting results from Eq. (6.19) into Eqs. (6.18), we will obtain circulations $\bar{\Gamma}_i^{(2)}$, representing second approximation. This process of consecutive approximations is quickly converging and thus, two or three approximations suffice.

Usually, airscrew calculations for given $\bar{V}_\infty$ are performed with ϕ_0 values connected with $\bar{g}_j$ through Eq. (6.16). In order to avoid the necessity of solving a system of Eqs. (6.14) for every ϕ_0 value, we make the following exact transformation: we represent circulation $\bar{\Gamma}_i$ and coefficient $\bar{g}_j$ as the following sums[63]:

$$\bar{\Gamma}_i = \bar{\Gamma}_i' + \varphi_0 \bar{\Gamma}_i'', \tag{6.20}$$

$$\bar{g}_j = \bar{g}_j' + \varphi_0 \bar{g}_j'', \tag{6.21}$$

where, according to Eq. 6.16)

$$\bar{g}_j' = \frac{\bar{\varrho}_j}{k}(\beta_j - \Delta\varphi_j), \quad \bar{g}_j'' = -\frac{\bar{\varrho}_j}{k}. \tag{6.22}$$

If one substitutes Eqs. (6.20) and (6.21) into the system of Eqs. (6.14), then the latter breaks down into two independent systems:

$$\sum_{i=1}^{m} \bar{\gamma}_{ij} \bar{\Gamma}_i' = \bar{g}_j', \quad \sum_{i=1}^{m} \bar{\gamma}_{ij} \bar{\Gamma}_i'' = \bar{g}_j'', \tag{6.23}$$

not containing ϕ_0. Solution of the system of Eqs. (6.23) gives quantities $\bar{\Gamma}_i'$ and $\bar{\Gamma}_j''$ permitting one to calculate, from Eq. (6.20), circulation $\bar{\Gamma}_i$ for any number of the ϕ_0 values. As the next step, through elementary calculations, induced velocities $\bar{v}_j$ can be found from Eq. (6.9).

4. AERODYNAMIC CALCULATIONS OF AIRSCREWS (CASE OF HIGH $\bar{V}_\infty$ VALUES)

We will develop expressions for thrust and torque. Let us consider a blade segment $\Delta r_j = \rho_{i+1} - \rho_i$. Here, every value of index "i" corresponds to the same index value of "j". For

sufficiently small values of Δr_j, it is possible to consider that all parameters characterizing flow at the considered segment are constant for its entire length and equal to their respective values at point j in the middle of the segment. The following forces act on the segment: lift ΔY_{pj} and drag ΔQ_{pj}. Lifting force is perpendicular to velocity W_{pj} making, with the plane of rotation, an angle $\beta_{pj} = \beta_j + \Delta\beta_j$. Force ΔQ_{pj} is directed along velocity W_{pj}. Projecting forces ΔY_{pj} and ΔQ_{pj} on axis y and the plane of rotation, we obtain thrust ΔT_j developed by the segment (parallel to the y axis) and its corresponding drag ΔQ_j, perpendicular to the lifting line and directed opposite to the airscrew rotation:

$$\Delta T_j = \Delta Y_{pj}\cos\beta_{pj} - \Delta Q_{pj}\sin\beta_{pj}, \quad \Delta Q_j = \Delta Y_{pj}\sin\beta_{pj} + \Delta Q_{pj}\cos\beta_{pj}.$$

We introduce $\mu_{pj} = c_{xpj}/c_{yj}$ which represents a reverse of the lift to drag ratio of section j. Then, taking into consideration Eq. (6.13), as well as the following expressions,

$$\Delta Y_{pj} = c_{yj}\frac{\varrho}{2}W_{pj}^2 b_j \Delta r_j, \quad \Delta Q_{pj} = c_{xpj}\frac{\varrho}{2}W_{pj}^2 b_j \Delta r_j,$$

$$W_{pj}\cos\beta_{pj} = \omega r_j - v_{\tau j}, \quad W_{pj}\sin\beta_j = V_\infty - v_j,$$

we obtain the following relationships:

$$\Delta T_j = \varrho\left[\omega r_j - v_{\tau j} - \mu_{pj}(V_\infty - v_j)\right]\Gamma_j \Delta r_j,$$
$$\Delta Q_j = \varrho\left[V_\infty - v_j + \mu_{pj}(\omega r_j - v_{\tau j})\right]\Gamma_j \Delta r_j.$$

Torque generated by the segment is $\Delta M_{Kj} = \Delta Q_j \Delta r_j$. Total values of thrust and torque of the airscrew will be expressed as follows:

$$T = k\sum_{j=1}^{m}\Delta T_j, \quad M_K = k\sum_{j=1}^{m}\Delta M_{Kj}.$$

For practical calculations, the above formulae are presented in a nondimensional form:

$$c_T = \frac{2k}{\pi}\sum_{j=1}^{m}\left[\bar r_j - \bar v_{\tau j} - \mu_{pj}(\bar V_\infty - \bar v_j)\right]\bar\Gamma_j \Delta\bar r_j, \tag{6.24}$$

$$m_K = \frac{2k}{\pi}\sum_{j=1}^{m}\left[\bar V_\infty - \bar v_j + \mu_{pj}(\bar r_j - \bar v_{\tau j})\right]\bar\Gamma_j \bar r_j \Delta\bar r_j. \tag{6.25}$$

If one assumes that velocity $\bar v_{pj}$ is perpendicular to the helical line, then $\bar v_{\tau j} = -\bar v_j \bar V_\infty / \bar r_j$.

In order to determine μ_{pj}, it is first necessary to compute angles of attack α_j given by Eq. (6.12). Values of μ_{pj} are taken from experimental airfoil data at corresponding Reynolds and Mach numbers

$$\mathrm{Re}_j = \frac{\overline{W}_j b_j}{\nu}\omega R^2 \quad \text{and} \quad M_j = \frac{\overline{W}_j}{a}\omega R,$$

where ν and a are, respectively, kinematic coefficients of viscosity and speed of sound in the undisturbed flow.

Airscrew efficiency will obviously be defined by the following:

$$\eta_B = c_T \overline{V}_\infty / m_K.$$

5. NUMERICAL EXAMPLE

As an illustration of the above presented method, let us consider an example of aerodynamic calculations for an airscrew of $18\ m$ diameter, having four blades of constant chord, $b = 1{,}131m$ and a linear twist $\Delta\phi_j = \Delta\phi_\Sigma(0{,}7 - \overline{r}_j)$; $\Delta\phi_\Sigma = \pi/6$. Let $\omega R = 260\ m/sec$, $V_\infty = 195\ m/sec$, $\phi_0 = 50°$. We also assume that flight is performed at an altitude of $2\ km$ in standard atmosphere. Then, $a = 332{,}5\ m/sec$, $\nu = 0{,}1715 \times 10^{-4}$. It is required to determine the following: circulations $\overline{\Gamma}_i$, induced velocities $\overline{v}_j$ and $\overline{v}_{\tau j}$, actual angles of attack α_j; and then, thrust coefficient c_T, torque coefficient m_k and airscrew efficiency η_B. In order to be able to use Table VI-2, we have to calculate parameter

$$\sin\beta_R = \overline{V}_\infty / \sqrt{1 + \tilde{V}_\infty^2} = 0{,}6.$$

Initial data required for calculation of circulations $\overline{\Gamma}_i$ are shown in Table 6.1

Now we construct an enlarged matrix of coefficients from Eq. (6.23). That matrix is given in Table 6.2 Diagonal terms are taken from the 13th row of Table 6.1 and nondiagonal terms $\overline{\gamma}_{ij} = \overline{v}_{ij}/k$, for $i \neq j$, from Table VI.2. The quantities $\overline{g}_j'$ and $\overline{g}_j''$ are taken from the 10th and 11th rows of Table 6.1. Taking that matrix to the computer, and using standard programs of solving systems of the type given by Eq. (6.23), we find values of $\overline{\Gamma}_i'$ and $\overline{\Gamma}_i''$. Results of the further calculations are shown in Table 6.3.

A comparison of the blade and disc theories indicates that the blade theory gives results better approximating experimental data. According to the disc theory, $\eta_B = 0{,}795$.

6. AERODYNAMIC CALCULATIONS OF AN AIRSCREW IN A LOW VELOCITY FLOW

At high $\overline{V}_\infty$ values, calculations of an airscrew are performed on the basis of an assumption that the shape of the vortex wake is determined only by the magnitude of $\overline{V}_\infty$. However, at low

Row No.	Characteristics \ j	1	2	3	4	5	6	7	8	9	10
1	$\bar{r}_j$	0,240	0,320	0,400	0,480	0,560	0,640	0,720	0,800	0,880	0,960
2	$\bar{b}_j$	0,1257	0,1257	0,1257	0,1257	0,1257	0,1257	0,1257	0,1257	0,1257	0,1257
3	$\overline{W}_j = \sqrt{\bar{r}_j^2 + \overline{V}_\infty^2}$	0,7875	0,8154	0,8500	0,8904	0,9360	0,9860	1,0390	1,0960	1,1560	1,2190
4	$\mathrm{Re}_j = \frac{1}{\nu}\overline{W}_j b_j \omega R^2$	$13,5\cdot10^6$	$14,0\cdot10^6$	$14,6\cdot10^6$	$15,3\cdot10^6$	$16,0\cdot10^6$	$16,9\cdot10^6$	$17,8\cdot10^6$	$18,8\cdot10^6$	$19,8\cdot10^6$	$20,9\cdot10^6$
5	$M_j = \frac{1}{a}\overline{W}_j \omega R$	0,6175	0,6375	0,6646	0,6962	0,7320	0,7711	0,8123	0,8571	0,9040	0,9533
6	$a_{\infty j} = dc_{yj}/d\alpha_j$	6,65	6,70	6,75	6,85	7,20	7,70	8,10	14,9	14,7	13,0
7	$\Delta\varphi_j$, rad.	0,2408	0,1919	0,1511	0,1152	0,0733	0,0314	—0,0105	—0,0523	—0,0942	—0,1361
8	$\cos\beta_j = \bar{\varrho}_j/\overline{W}_j$	0,3047	0,3924	0,4705	0,5390	0,5982	0,6490	0,6929	0,7280	0,7612	0,7875
9	β_j, rad.	1,2611	1,1675	1,0808	1,0010	0,9294	0,8644	0,8058	0,7531	0,7058	0,6632
10	$\bar{g}'_j = (\beta_j - \Delta\varphi_j)\frac{\bar{\varrho}_j}{K}$	0,0612	0,0775	0,0924	0,1063	0,1198	0,1333	0,1469	0,1611	0,1760	0,1918
11	$\bar{g}''_j = -\bar{\varrho}_j/k$	—0,060	—0,080	—0,100	—0,120	—0,140	—0,160	—0,180	—0,200	—0,220	—0,240
12	$\bar{v}_{jj}/k$ (see Table VI.2)	—0,3152	—0,400	—0,4763	—0,5435	—0,6017	—0,6518	—0,6946	—0,7311	—0,7622	—0,7888
13	$\bar{\nu}_{jj} = \frac{\bar{v}_{jj}}{k} - \frac{2\cos\beta_j}{a_\infty \bar{b}_j k}$	—0,4976	—0,6330	—0,7536	—0,8565	—0,9322	—0,9871	—1,0347	—0,9259	—0,9681	—1,0299

Table 6.1

VALUES OF COEFFICIENTS $\bar{\gamma}_{ij}$

j \ i	1	2	3	4	5	6	7	8	9	10	$\bar{g}'_j$	$\bar{g}''_j$
1	—0,4976	0,0938	0,0148	0,0048	0,0019	0,0009	0,0004	0,0002	0,0001	0,0001	0,0612	—0,060
2	0,1176	—0,6330	0,1248	0,0213	0,0074	0,0032	0,0015	0,0008	0,0004	0,0002	0,0775	—0,080
3	0,0214	0,1447	—0,7536	0,1522	0,0271	0,0098	0,0044	0,0022	0,0012	0,0007	0,0924	—0,100
4	0,0075	0,0269	0,1679	—0,8565	0,1762	0,0322	0,0120	0,0056	0,0029	0,0016	0,1063	—0,120
5	0,0032	0,0096	0,0315	0,1878	—0,9322	0,1969	0,0366	0,0139	0,0066	0,0035	0,1198	—0,140
6	0,0015	0,0044	0,0117	0,0352	0,2047	—0,9871	0,2145	0,0404	0,0155	0,0075	0,1333	—0,160
7	0,0008	0,0022	0,0054	0,0133	0,3840	0,2191	—1,0347	0,2295	0,0435	0,0169	0,1469	—0,180
8	0,0004	0,0011	0,0028	0,0062	0,0145	0,0410	0,2314	—0,9259	0,2422	0,0462	0,1611	—0,200
9	0,0002	0,0006	0,0014	0,0031	0,0068	0,0156	0,0432	0,2420	—0,9681	0,2530	0,1760	—0,220
10	0,0001	0,0003	0,0008	0,0017	0,0035	0,0074	0,0165	0,0452	0,2510	—1,0299	0,1918	—0,240

Table 6.2

$\varphi_0 = 0,8727$

Row No.	Characteristics \ j	1	2	3	4	5	6	7	8	9	10
1	$\bar{\Gamma}'_i$	—0,1764	—0,2188	—0,2422	—0,2631	—0,2901	—0,3307	—0,4414	—0,4262	—0,3986	—0,3133
2	$\bar{\Gamma}''_i$	0,1776	0,2301	0,2604	0,2989	0,3396	0,3956	0,5330	0,5239	0,4941	0,3898
3	$\bar{\Gamma}_i = \bar{\Gamma}'_i + \varphi_0 \bar{\Gamma}''_i$	—0,0214	—0,0180	—0,0106	—0,0023	0,0062	0,0145	0,0237	0,0309	0,0325	0,0268
4	$\bar{v}_j$ [Eq. (6.9)]	0,0197	0,0139	0,0087	0,0039	—0,0011	—0,0058	—0,0083	—0,0306	—0,0371	—0,0446
5	$\bar{v}_{\tau j} = -\bar{v}_j \bar{V}_\infty \bar{r}_j$	—0,0616	—0,023	—0,0163	—0,0061	0,0014	0,0069	0,0087	0,0287	0,0316	0,0349
6	$\alpha^\circ_j = 57,3\alpha_j$	—3,760	—5,280	—1,680	—0,286	0,830	1,750	2,560	1,655	1,740	1,535
7	$\mu_{pj} = c_{xpj}/c_{yj}$	—0,0204	—0,0205	—0,0450	—0,260	0,0667	0,0354	0,0391	0,0448	0,0542	0,0488
8	c_τ [Eq. (6.24)]	0,0165									
9	$m_к$ [Eq. (6.25)]	0,016									
10	$\eta_b = c_\tau V_\infty / m_к$	0,774									

Table 6.3

values of $\bar{V}_\infty$, the shape of the vortex wake depends to a large degree, also on induced velocities whose values are not known in advance and represent one of the objects of calculations. In this way, the task leads to a necessity of establishing a unique relationship between induced velocities, shape of the vorticity wake and circulation of discrete vortices.

According to Hypothesis No. 4, the velocity of movement of the elements of free vortices is equal to the sum of velocity of the undisturbed flow and induced velocity averaged over the disc. This velocity can be easily computed from the momentum theory:

$$\bar{V}=\frac{1}{2}\left(\bar{V}_\infty+\sqrt{\bar{V}_\infty^2+c_T}\right). \tag{6.26}$$

In view of the low values of $\bar{V}_\infty$, it is possible to simplify Eqs. (6.24) for the thrust and (6.25) for the torque coefficients. In this case, angle of inclination of the helical line with respect to the plane of rotation given by the relationship $\beta_{*j} = tg^{-1}(\bar{V}/\bar{r}_j)$ is very small. For this reason, peripheral induced velocity $\bar{v}_{\tau j} = \bar{v}_j \operatorname{tg} \beta_{*j}$ is very low in comparison with $\bar{r}_j$. The product of $\mu_{pj}(\bar{V}_\infty - \bar{v}_j)$ is also small in comparison with $\bar{r}_j$. Consequently, Eqs. (6.24) and (6.25) can be rewritten as follows:

$$c_T=\frac{2k}{\pi}\sum_{j=1}^{m}\bar{\Gamma}_j\bar{r}_j\Delta\bar{r}_j, \tag{6.27}$$

$$m_K=\frac{2k}{\pi}\sum_{j=1}^{m}(\bar{V}_\infty-\bar{v}_j+\mu_{pj}\bar{r}_j)\bar{\Gamma}_j\bar{r}_j\Delta\bar{r}_j. \tag{6.28}$$

We now turn toward the task of determining circulation $\bar{\Gamma}_j$. At low $\bar{V}_\infty$ values, the angle of the induced inflow can obviously be computed as $\Delta\beta_j = -\bar{v}_j/\bar{r}_j$. For this reason, for airscrew calculations, one may use Eqs. (6.29). For given values of $\bar{V}_\infty$ and c_T, we calculate $\bar{V}$ (Eq. (6.26)) and parameter

$$\sin \beta_R = \bar{V}/\sqrt{1 + \bar{V}^2}$$

and next, we find coefficients $\bar{v}_{ij}/k$ from Tables VI.1-VI.3. Then, we solve the system of Eqs. (6.23) and determine the values of $\bar{\Gamma}_i'$ and $\bar{\Gamma}_i''$. However, computation of circulation $\bar{\Gamma}_i$ from Eq. (6.20) is difficult due to the fact that the magnitude of ϕ_0 corresponding to the given coefficient c_T is not known. This difficulty can be surmounted through the method of consecutive approximations. But a more convenient, direct method of determining ϕ_0 is given below.

We substitute Eq. (6.20) into Eq. (6.27). Then,

where

$$c_T = c_T' + c_T'' \varphi_0,$$

$$c_T' = \frac{2k}{\pi} \sum_{j=1}^{m} \bar{\Gamma}_j' \bar{r}_j \Delta \bar{r}_j, \quad c_T'' = \frac{2k}{\pi} \sum_{j=1}^{m} \bar{\Gamma}_j'' \bar{r}_j \Delta r_j. \tag{6.29}$$

Since all quantities appearing in Eq. (6.29) are known, hence, it is not difficult to find the sought value of ϕ_0 for given c_T

$$\varphi_0 = \frac{c_T - c_T'}{c_T''}. \tag{6.30}$$

Now, we can calculate circulation $\bar{\Gamma}_i$ from Eq. (6.20) and induced velocities $\bar{v}_j$ from Eq. (6.9). Reverse values of the lift-to-drag ratios of airfoil sections are obtained in the same way as in the previously considered case of high $\bar{V}_\infty$ values. Next, we calculate m_k from Eq. (6.28). For the assumed c_T values at a given velocity $\bar{V}_\infty$, we obtain the corresponding values of m_k and, in this way, we obtain the $c_T = c_T(m_k)$ curve for an airscrew.

In Figs. 6.5-6.7, results of calculations are shown in comparison with experimental results obtained by A.V. Sharov.

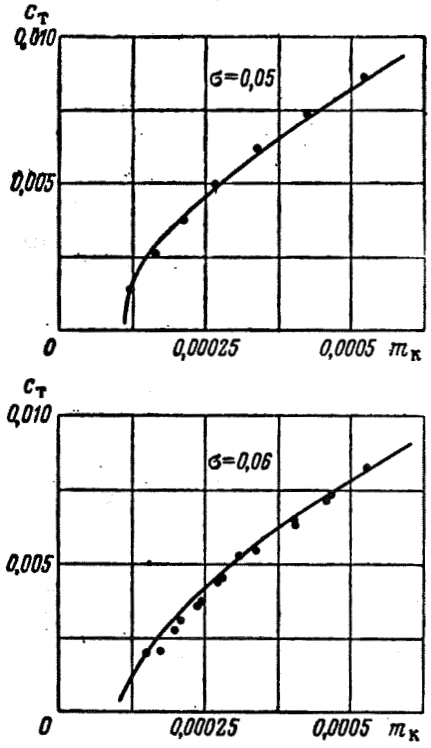

Figure 6.5

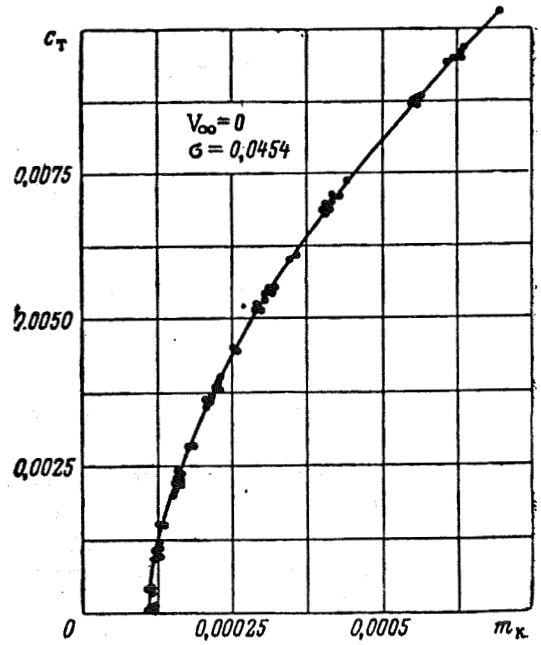

Figure 6.6

In Fig. 6.8, typical results of calculations of the $c_T/\sigma = c_T(m_k/\sigma)$ relationships for airscrews with different number of blades, but identical solidity, are given. It can be seen that for the number of blades $k > 3$, the curves become practically identical. The previously mentioned calculations were performed for the case of hovering of airscrews with rectangular blades having a linear twist $\Delta\phi_\Sigma = -7,7°$ and radius of the inboard cutout $\bar{\rho}_0 = 0,2$. The airscrew solidity ratio was $\sigma = 0,11$, while the tip speed was $\omega R = 220$ m/sec.

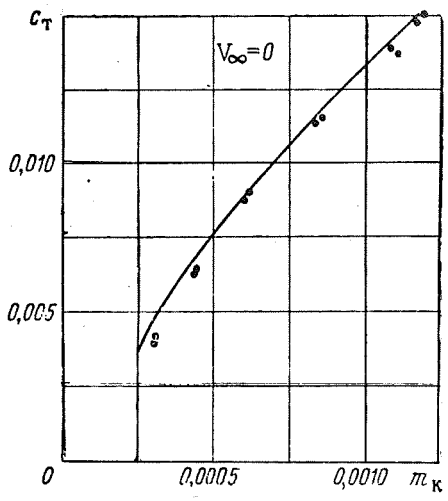

Figure 6.7

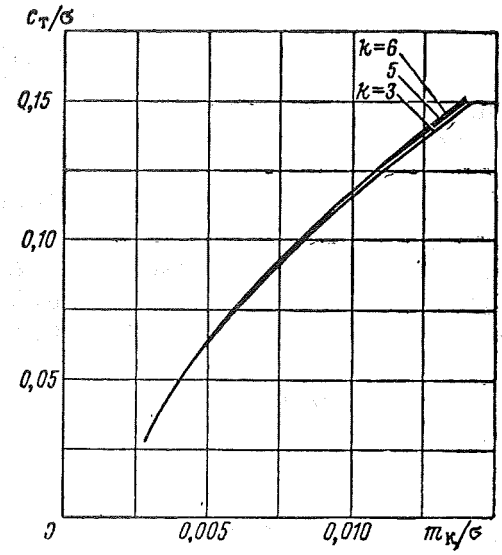

Figure 6.8

It may be concluded, hence, that the task of determining airscrew characteristics in practical operations is accomplished.

CHAPTER VII

DISC THEORY OF LIFTING AIRSCREW IN AXIAL FLOW

Disc theory offers a very reliable operational technique for prediction of general characteristics of airscrews with number of blades $k > 3$ and operating at low $\bar{V}_\infty$ levels when instantaneous and average induced velocities are not much different. An extension of Joukowsky's thoeory to the case of a low velocity $\bar{V}_\infty$ is presented below. This is done by taking into account the influence of induced velocities on the pitch of the free helical vortices.

1. INDUCED VELOCITY

The lifting airscrew, having a finite number of blades, induces, at a point (Eq. (6.5)), an instantaneous velocity $\bar{v}^{M\Gamma}$ equal to the sum of velocities given by Eqs. (6.6) and (6.7):

$$\bar{v}^{M\Gamma}=\frac{1}{4\pi}\sum_{n=1}^{k}\int_0^{\infty}\int_{\bar{\varrho}_0}^{1}\frac{d\bar{\Gamma}}{d\bar{\varrho}}\,\frac{\bar{\varrho}^2-\bar{\varrho}\bar{r}\cos(\theta-\psi+\delta_n-\vartheta)}{[\bar{V}^2\vartheta^2+\bar{\varrho}^2+\bar{r}^2-2\bar{\varrho}\bar{r}\cos(\theta-\psi+\delta_n-\vartheta)]^{3/2}}\,d\bar{\varrho}d\vartheta+$$

$$+\frac{1}{4\pi}\sum_{n=1}^{k}\int_{\bar{\varrho}_0}^{1}\bar{\Gamma}(\bar{\varrho})\,\frac{-\bar{r}\sin(\theta-\psi+\delta_n)}{[\bar{\varrho}^2+\bar{r}^2-2\bar{\varrho}\bar{r}\cos(\theta-\psi+\delta_n)]^{3/2}}\,d\bar{\varrho}. \tag{7.1}$$

Induced velocity $\bar{v}^{M\Gamma}$ at a fixed point (Eq. (6.5)) will be a periodic function of angle θ.

Going to the disc theory, we will average, with respect to time, the instantaneous induced velocity at a point defined by Eq. (6.5). This will be identical with finding an average with respect to angle θ. If we define the averaged velocity by the symbol $\bar{v}$, then

$$\bar{v}=\frac{1}{2\pi}\int_0^{2\pi}\bar{v}^{M\Gamma}d\theta. \tag{7.2}$$

Substituting Eq. (7.1) into Eq. (7.2), we obtain

$$\bar{v}=\frac{1}{8\pi^2}\sum_{n=1}^{k}\int_0^{2\pi}\int_0^{\infty}\int_{\bar{\varrho}_0}^{1}\frac{d\bar{\Gamma}}{d\bar{\varrho}}\,\frac{\bar{\varrho}^2-\bar{\varrho}\bar{r}\cos(\theta-\psi+\delta_n-\vartheta)}{[\bar{V}^2\vartheta^2+\bar{\varrho}^2+\bar{r}^2-2\bar{\varrho}\bar{r}\cos(\theta-\psi+\delta_n-\vartheta)]^{3/2}}\,d\bar{\varrho}d\vartheta d\theta+$$

$$+\frac{1}{8\pi^2}\sum_{n=1}^{k}\int_0^{2\pi}\int_{\bar{\varrho}_0}^{1}\bar{\Gamma}(\bar{\varrho})\,\frac{-\bar{r}\sin(\theta-\psi+\delta_n)}{[\bar{\varrho}^2+\bar{r}^2-2\bar{\varrho}\bar{r}\cos(\theta-\psi+\delta_n)]^{3/2}}\,d\bar{\varrho}d\theta. \tag{7.3}$$

Eq. (7.3) can be considerably simplified if one takes advantage of the known properties of the 2π integral of periodic functions

$$\int_0^{2\pi} f(\theta+a)\,d\theta=\int_0^{2\pi} f(\theta)\,d\theta, \tag{7.4}$$

where a is independent from θ. On the basis of that property, we omit all components with the exception of θ in the arguments of the trigonometric functions in Eq. (7.3). Then, integrated functions appear independent from n and k. For this reason, the sum symbol in Eq. (7.3) can be replaced by the factor k. In addition, the integrated function of the second component of Eq. (7.3) appears to be odd with respect to parameter θ. As a result of this, that component becomes zero. Finally, we have

$$\bar{v}=\frac{k}{8\pi^2}\int_0^{2\pi}\int_0^{\infty}\int_{\bar{\varrho}_0}^{1}\frac{d\bar{\Gamma}}{d\bar{\varrho}}\,\frac{\bar{\varrho}^2-\bar{\varrho}\bar{r}\cos\theta}{\left[\bar{V}^2\vartheta^2+\bar{\varrho}^2+\bar{r}^2-2\bar{\varrho}\bar{r}\cos\theta\right]^{3/2}}\,d\bar{\varrho}\,d\vartheta\,d\theta.$$

The above relationship can be still further simplified. Let us rewrite it as follows:

$$\bar{v}=\int_{\bar{\varrho}_0}^{1}\frac{d\bar{\Gamma}}{d\bar{\varrho}}\,\Phi\,d\bar{\varrho}, \tag{7.5}$$

$$\Phi=\frac{k}{8\pi^2}\int_0^{2\pi}\left(\bar{\varrho}^2-\bar{\varrho}\bar{r}\cos\theta\right)F\,d\theta, \tag{7.6}$$

$$F=\int_0^{\infty}\frac{d\vartheta}{\left[\bar{V}^2\vartheta^2+\bar{\varrho}^2+\bar{r}^2-2\bar{\varrho}\bar{r}\cos\theta\right]^{3/2}}. \tag{7.7}$$

Integration of Eq. (7.7) results in

$$F=\frac{1}{\bar{V}}\,\frac{1}{\bar{\varrho}^2+\bar{r}^2-2\bar{\varrho}\bar{r}\cos\theta}.$$

Substituting the above expression into Eq. (7.6) and integrating it, we obtain

$$\Phi=\begin{cases}\dfrac{k}{4\pi\bar{V}} & \text{for } \bar{\varrho}>\bar{r},\\[2ex] \dfrac{k}{8\pi\bar{V}} & \text{for } \bar{\varrho}=\bar{r},\\[2ex] 0 & \text{for } \bar{\varrho}<\bar{r}.\end{cases} \tag{7.8}$$

Now, it results from Eqs. (7.5) and (7.8) that

$$\bar{v}=\frac{k}{4\pi}\int_{\bar{r}}^{1}\frac{d\bar{\Gamma}}{d\bar{\varrho}}\frac{d\bar{\varrho}}{\bar{V}}. \tag{7.9}$$

where $\bar{V}$ is the velocity of movement of the elements of free vortices. If this velocity is identical for all the elements, then Eq. (7.9) transfers itself into the classical formula of Joukowsky.

$$\bar{v}(\bar{r})=-\frac{k\Gamma(\bar{r})}{4\pi\bar{V}}. \tag{7.10}$$

Eq. (7.10) shows that induced velocity at any station of the blade depends only on circulation at that station and does not depend on circulation at other stations. N.E. Joukowsky developed that relationship using a scheme of an airscrew with an infinite number of blades. In the above analysis, no such assumption is directly made, while the average value of the fluctuating induced velocity, generated by an airscrew with a finite number of blades at a fixed point of the plane of rotation is determined. It can be seen that the time-averaged induced velocity of an airscrew with a finite number of blades and induced velocity of an airscrew with infinite number of blades are conceptually the same.

2. *CIRCULATION AND AERODYNAMIC CHARACTERISTICS OF AIRSCREWS*

We will consider a method of airscrew calculations, based on Hypothesis No. 4 as expressed by Eq. (6.26). Let us rewrite Eq. (7.1) in the following form:

$$\bar{v}_j=-\frac{k\bar{\Gamma}_j}{4\pi\bar{V}}(j=1,2,3,\ldots,m) \tag{7.11}$$

and substitute Eq. (7.11) into Eq. (6.12), and Eq. (6.12) into Eq. (6.13). As a result of this, we obtain

$$\bar{\Gamma}_j=\bar{\Gamma}'_j+\varphi_0\bar{\Gamma}''_j, \tag{7.12}$$

where

$$\bar{\Gamma}'_j=\frac{A_j}{1+B_j}(\Delta\varphi_j-\beta_j),\quad \bar{\Gamma}''_j=\frac{B_j}{1+B_j}, \tag{7.13}$$
$$A_j=\frac{1}{2}a_{\infty j}\bar{b}_j\bar{W}_j,\quad \bar{B}_j=\frac{kA_j}{4\pi\bar{V}\bar{r}_j}.$$

With given values of $a_{\infty j}$, $\bar{b}_j$, $\Delta\phi_j$, $\bar{V}_\infty$ and c_T, magnitudes of $\bar{\Gamma}'_j$ and $\bar{\Gamma}''_j$ are determined on the basis of Eqs. (6.26) and (7.13). Next, from Eq. (6.29), coefficients c_T' and c_T'' are obtained, while the angle of the collective airscrew pitch is computed from Eq. (6.30). Then, circulations and induced velocities are determined from Eqs. (7.12) and (7.11). Finally, from Eq. (6.28), torque coefficients m_k are computed. Repeating the above outlined calculations for several assumed c_T values, we will find the corresponding m_k's, so that a curve of $c_T = f(m_k)$ or $c_T/\sigma = f(m_k/\sigma)$ can be drawn. Application of the presented method results in a good agreement between predicted and measured general characteristics of airscrews without the necessity of using empirical correction factors. In Fig. 7.1, a comparison is shown between calculations based on the disc theory (Curve 1) and those resulting from the blade theory (Curve 2). It can be seen that the results are quite close.

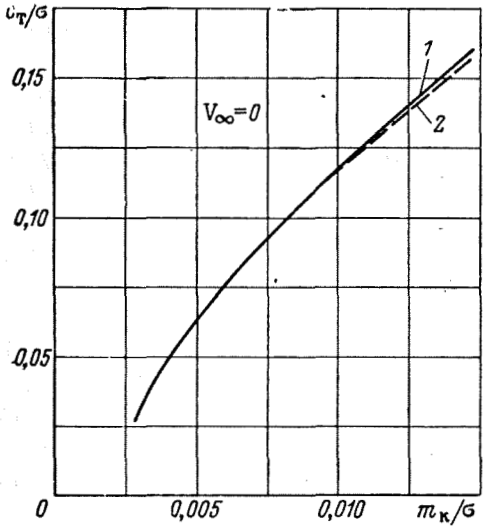

Figure 7.1

CHAPTER VIII

THEORY OF LIFTING AIRSCREW IN AXIAL FLOW BASED ON THE CONCEPT OF A THIN LIFTING SURFACE

The application of the scheme of a lifting surface to calculation of the airscrew results from the necessity of learning about the flow around the blade tip where the classical approach of the lifting line is not applicable. Going to the concept of lifting surface is also useful in the study of blades of low aspect ratio. For this reason, this approach has found application in the theory of marine propellers[73].

1. PRESENTATION OF THE PROBLEM

The rotor or propeller blade is modeled by a thin lifting surface whose form and description of motion is assumed to be known. It is necessary to define the velocity field and distribution of aerodynamic loading over this lifting surface.

In the general case, the problem is reduced to the integration of the equation of continuity (div $\boldsymbol{V} = 0$).

The boundary condition of the problem would be a condition of the smooth and unstalled flow according to which, the normal velocity component on the lifting surface is equal to 0. The condition of Chaplygin-Joukowsky of the finite velocity at the trailing edge guarantees the uniqueness of the solution of the problem.

The lifting surface may be replaced by a layer of interconnected vortices whose intensity depends on their position on the surface. According to the theories of nondestructiveness of circulation of the bound vortices, elements of free vortices must also be considered. Those free elementary vortices first move along the lifting surface and then leave that surface and move along the slipstream, forming a free vortex sheet. Within the framework of quasi-stationary theory, we will assume that elements move with the velocity of the flow $\overline{V}$ (Eq. 6.26)) corresponding to the outside flow. The relationship between the vector of induced velocity and the intensity of the vortex sheet is expressed through an integral relationship based on the Biot-Savart law. This relationship corresponds to the solution of the continuity equation. For this reason, the problem is reduced to the calculation of the intensity of the vortex layer on the basis of the above-mentioned principle conditions. From a mathematical point of view, this problem is

reduced to a solution of the basic integral equation of the first order of the Friedholm type. From the calculated distribution of the intensity of the bound vortex, aerodynamic loads are calculated according to the Joukowsky theory[12].

For practical calculation, the vortex sheet is represented by an assembly of discrete horseshoe vortices similar to those used in the theory of the wing[12].

As a result of this approach, the basic integral equation is replaced by a system of linear algebraic equations, defining the circulation of discrete vortices.

2. SCHEME OF THE FLOW AROUND THE BLADE

We define, by n $(n=1, 2, \ldots, k)$, the blade number of a k-bladed airscrew and we introduce a Cartesian system of coordinates $Oxyz$ (Fig. 8.1) attached to blade number 1. Axis y coincides with the axis of rotation of the airscrew, while axis z goes along the axis of blade number 1. The lifting surface which we substitute for blade number n is defined by the following parametric equations:

$$\bar{x}=\bar{\varrho}\sin(\delta_n-\vartheta),\quad \bar{y}=f(\bar{\varrho},\vartheta),\quad \bar{z}=\bar{\varrho}\cos(\delta_n-\vartheta). \tag{8.1}$$

Here, $\delta_n = 2\pi(n-1)/k$; $\bar{\rho}$ and ϑ represent polar coordinates of point $(\bar{x},0,\bar{z})$ for $n = 1$. Angle ϑ is considered positive when moving away from axis z in the direction opposite to the rotation of the airscrew.

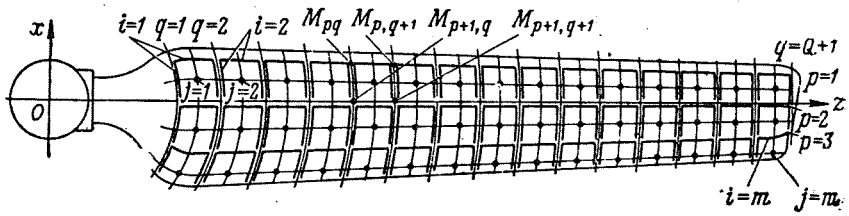

Figure 8.1

Cylindrical surfaces,

$$\bar{x}^2+\bar{z}^2=\bar{\varrho}_q^2\ (q=1,2,3,\ldots,\vartheta+1) \tag{8.2}$$

divide surface 8.1 into Q segments. Lines of intersection of surfaces (8.1) and (8.2) are defined by an index "q". Each of the q lines is divided into P segments of equal length. Points corresponding to 1/4 lengths of each segment of line q are counted from the leading edge of the blade and are given index numbers "p" ($p = 1, 2, 3, \ldots, P$). Through the points with identical index numbers along the span of the blades are extended lines also defined by p. In this way, on the surface (8.1), a net of lines p and q with nodes M_{pq} is obtained.

The vortex system of blade number 1 is replaced by a system of discrete horseshoe-shaped vortices $i = 1, 2, 3, \ldots, m$, where $m = PQ$. The vortex i consists of a segment of attached (bound) vortex extending along the line p between the neighboring nodes M_{pq} and $M_{p,q+1}$ and a pair of free vortices extending from those nodes. Free vortex consists of a part extending along the line q between points p and P, and half infinite helical vortex extending from point P. Induced velocities are computed at control points j ($j = 1, 2, 3, \ldots, m$), located between bound and free vortices on the surface (8.1) for $n = 1$.

Let's now consider a helical surface generated by the axis of blade n cutting through the filaments of the uniform rectilinear flow coming toward the airscrew. The parametric equation of this surface becomes

$$\bar{x} = -\bar{\varrho}\sin(\delta_n - \vartheta),\quad \bar{y} = -\bar{V}\vartheta,\quad \bar{z} = \bar{\varrho}\cos(\delta_n - \vartheta). \tag{8.3}$$

The angles between surfaces (8.1) and (8.3) are small; hence, for the simplification of analysis, the whole network of lines p and q can be transferred to the surface (8.3) along the lines parallel to axis y. In this case, horseshoe vortices of blade n will be located on the surface (8.3) and coordinates of the nodes of the network will be

$$\bar{x}_{pq} = \bar{\varrho}_q \sin(\delta_n - \vartheta_{pq}),\quad \bar{y}_{pq} = -\bar{V}\vartheta_{pq},\quad \bar{z}_{pq} = \bar{\varrho}_q\cos(\delta_n - \vartheta_{pq}), \tag{8.4}$$

where ϑ_{pq} is the polar angle of points $(\bar{x}_{pq}, 0, \bar{y}_{pq})$ for $n = 1$. Double subscripts in Eq. (8.4) give the number of lines p and q whose intersection forms a node of the net. Transferring points j $(\bar{x}_j, \bar{y}_j, \bar{z}_j)$ to surface (8.3) for $n = 1$, we obtain

$$\bar{x}_j = -\bar{r}_j \sin\vartheta_j,\quad \bar{y}_j = -\bar{V}\vartheta_j,\quad \bar{z}_j = \bar{r}_j\cos\vartheta_j. \tag{8.5}$$

In order to simplify the calculations, we replace line p by segments of straight lines extending between the nodes of the net. Then parametric equations of the straight-line segment of the bound vortex can be expressed in the following way:

$$\bar{\xi}_s=\bar{x}_{pq}+s\Delta\bar{x}_p,\ \bar{\eta}_s=\bar{y}_{pq}+s\Delta\bar{y}_p,\ \bar{\zeta}_s=\bar{z}_{pq}+s\Delta\bar{z}_p, \tag{8.6}$$

where

$$\Delta\bar{x}_p=\bar{x}_{p,q+1}-\bar{x}_{pq},\ \Delta\bar{y}_p=\bar{y}_{p,q+1}-\bar{y}_{pq},\ \Delta\bar{z}_p=\bar{z}_{p,q+1}-\bar{z}_{pq}$$

are the increments of the coordinates of the end of the segment with respect to its beginning, while $s(0 \leq s \leq 1)$ is a parameter. Functions appearing in (8.6) are defined by Eqs. (8.4). Parametric equations of free vortex leaving the node M_{pq} can be in consideration of (8.3) and (8.4), expressed in the following form:

$$\bar{\xi}_\vartheta=\bar{\varrho}_q\sin(\delta_n-\vartheta_{pq}-\vartheta),\ \bar{\eta}_\vartheta=-\bar{V}(\vartheta_{pq}-\vartheta),\ \bar{\zeta}_\vartheta=\bar{\varrho}_q\cos(\delta_n-\vartheta_{pq}-\vartheta)\ldots, \tag{8.7}$$

where $\vartheta(0 \leq \vartheta < \infty)$ is a parameter.

We define, by $\bar{\Gamma}_i$, the circulation of the vorticity along the closed contour enclosing the bound segment of vortex i. Direction of the path of the contours is defined by the rules given in Section 1 of Chapter VI. On the basis of this rule, circulation of free vortices leaving from nodes M_{pq} and $M_{p,q+1}$ of this segment will be equal to $-\bar{\Gamma}_i$ and $\bar{\Gamma}_i$, respectively.

3. INDUCED VELOCITIES

We define, by $\bar{u}_{pj}$, $\bar{v}_{pj}$, $\bar{w}_{pj}$, components of induced velocity at point j generated by the segment of bound vortex of unit circulation. Introducing Eq. (8.6) into corresponding Eqs. (B.5)-(B.7), we find:

$$\begin{aligned}\bar{u}_{pj}&=\frac{1}{4\pi}(\Delta\bar{y}_p\Delta\bar{z}_j-\Delta\bar{z}_p\Delta\bar{y}_j)\,I_s,\\ \bar{v}_{pj}&=\frac{1}{4\pi}(\Delta\bar{z}_p\Delta\bar{x}_j-\Delta\bar{x}_p\Delta\bar{z}_j)\,I_s,\\ \bar{w}_{pj}&=\frac{1}{4\pi}(\Delta\bar{x}_p\Delta\bar{y}_j-\Delta\bar{y}_p\Delta\bar{x}_j)\,I_s,\end{aligned} \tag{8.8}$$

where

$$\Delta\bar{x}_j=\bar{x}_j-\bar{x}_{pq},\ \Delta\bar{y}_j=\bar{y}_j-\bar{y}_{pq},\ \Delta\bar{z}_j=\bar{z}_j-\bar{z}_{pq},$$

$$I_s=\int_0^1\frac{ds}{(\sqrt{as^2-2bs+c})^{3/2}}. \tag{8.9}$$

Here,

$$a=\Delta\bar{x}_p^2+\Delta\bar{y}_p^2+\Delta\bar{z}_p^2,\quad b=\Delta\bar{x}_p\Delta\bar{x}_j+\Delta\bar{y}_p\Delta\bar{y}_j+\Delta\bar{z}_p\Delta\bar{z}_j,$$
$$c=\Delta\bar{x}_j^2+\Delta\bar{y}_j^2+\Delta\bar{z}_j^2.$$

Upon integration indicated in Eq. (8.9), we obtain

$$I_s=\frac{1}{ac-b^2}\left(\frac{a-b}{\sqrt{a-2b+c}}+\frac{b}{\sqrt{c}}\right). \tag{8.10}$$

Now, we will develop formulae for the velocity components induced by a free helical vortex with circulation equal to *-1*. Upon substituting Eqs. (8.5) and (8.7) into the relationships of Eqs. (B-5) - (B-7), we will find the desired components

$$\bar{u}_{qj}=\frac{\bar{V}}{4\pi}\int_0^\infty F_u(\vartheta)\frac{d\vartheta}{\bar{l}^3},\quad \bar{v}_{qj}=\frac{1}{4\pi}\int_0^\infty F_\vartheta(\vartheta)\frac{d\vartheta}{\bar{l}^3},\quad \bar{w}_{qj}=\frac{\bar{V}}{4\pi}\int_0^\infty F_w(\vartheta)\frac{d\vartheta}{\bar{l}^3}, \tag{8.11}$$

where
$$F_u(\vartheta)=\bar{r}_j\cos\vartheta_j-\bar{\varrho}_q\cos(\delta_n-\vartheta_{pq}-\vartheta)-(\vartheta_j-\vartheta_{pq}-\vartheta)\,\bar{\varrho}_q\sin(\delta_n-\vartheta_{pq}-\vartheta),$$
$$F_v(\vartheta)=\bar{\varrho}_q^2-\bar{\varrho}_q\bar{r}_j\cos(\delta_n-\vartheta_j-\vartheta_{pq}-\vartheta),$$
$$F_w(\vartheta)=\bar{r}_j\sin\vartheta_j+\bar{\varrho}_q\sin(\delta_n-\vartheta_{pq}-\vartheta)-(\vartheta_j-\vartheta_{pq}-\vartheta)\,\bar{\varrho}_q\cos(\delta_n-\vartheta_{pq}-\vartheta),$$
$$\bar{l}^2=\bar{V}^2(\vartheta_j-\vartheta_{pq}-\vartheta)^2+\bar{\varrho}_q^2+\bar{r}_j^2-2\bar{\varrho}_q\bar{r}_j\cos(\delta_n-\vartheta_j-\vartheta_{pq}-\vartheta).$$

With the help of Eqs. (8.8) and (8.11), we can find the relationships for velocity components induced by the horseshoe vortex i equal to unity and located on blade n:

$$\bar{u}_{ij}^n=\bar{u}_{pj}+\bar{u}_{qj}-\bar{u}_{q+1\,j},$$
$$\bar{v}_{ij}^n=\bar{v}_{pj}+\bar{v}_{qj}-\bar{v}_{q+1,j},\quad \bar{w}_{ij}^n=\bar{w}_{pj}+\bar{w}_{qj}-\bar{w}_{q+1,j}. \tag{8.12}$$

Velocities $\bar{u}_{q+1}$, $\bar{v}_{q+1,j}$, $\bar{w}_{q+1,j}$ can also be defined from Eq. (8.11) by changing index "q" to "$q+1$!".

Programming of Eqs. (8.11) and (8.12) should be done in such a way that first, velocities of components are computed from Eq. (8.11) for $p = P$. For computation of velocities induced by the helical vortices extending from nodes of the line $p = P - 1$, there is no need to again perform the integration according to Eq. (8.11) along the semi-infinite region. It is sufficient to add to previously obtained velocities, the velocities generated by segments of helical vortices included between lines $p = P - 1$, and $p = P$. The velocities induced by those segments are defined by Eq. (8.11) with upper limit of integration equal to ϑ_{pq} with $p = P$. We follow a similar procedure also in determining induced velocities from helical vortices springing from the line $p = P - 2, P - 3, \ldots, 1$. Corresponding values of the upper integration limits in Eq. (8.11) must be taken as ϑ_{pq} with $p = P - 1, P - 2, \ldots, 2$. It is possible to have a simplified procedure consisting of

a substitution for the line q of broken lines with apexes at the nodes of the network. In that case, induced velocity from the straight segments of free vortices can be computed from Eqs. (8.8) with opposite signs, in which increments $\Delta\bar{x}_p$, $\Delta\bar{y}_p$, $\Delta\bar{z}_p$ will be as follows:

$$\Delta\bar{x}_p=\bar{x}_{p+1,q}-\bar{x}_{pq}, \quad \Delta\bar{y}_p=\bar{y}_{p+1,q}-\bar{y}_{pq}, \quad \Delta\bar{z}_p=\bar{z}_{p+1,q}-\bar{z}_{pq}.$$

Now, we can concentrate on the considerations of induced velocities $\bar{v}_j\{\bar{u}_j, \bar{v}_j, \bar{w}_j\}$ generated by the airscrew at the control point j of blade 1. We calculate components of velocity vector $\bar{v}_{ij}\{\bar{u}_{ij}, \bar{v}_{ij}, \bar{w}_{ij}\}$ induced by the vortices with the identical indices "i" and having circulation equal to unity. Summing velocities (8.12) corresponding to number n, we obtain

$$\bar{u}_{ij}=\sum_{n=1}^{k}\bar{u}_{ij}^{n}, \quad \bar{v}_{ij}=\sum_{n=1}^{k}\bar{v}_{ij}^{n}, \quad \bar{w}_{ij}=\sum_{n=1}^{k}\bar{w}_{ij}^{n}. \tag{8.13}$$

Since vortices with identical indices "i" have the same circulation $\bar{\Gamma}_i$; hence, the desired components of vector $\bar{v}_j$ will be

$$\bar{u}_j=\sum_{i=1}^{m}\bar{u}_{ij}\bar{\Gamma}_i, \quad \bar{v}_j=\sum_{i=1}^{m}\bar{v}_{ij}\bar{\Gamma}_i, \quad \bar{w}_j=\sum_{i=1}^{m}\bar{w}_{ij}\bar{\Gamma}_i. \tag{8.14}$$

In this way, computation of velocities (8.14) corresponding to given values of $\bar{\Gamma}_i$ is reduced to the determination of coefficients (8.13) on a computer. The problem now consists of the necessity of determining circulation $\bar{\Gamma}_i$ on the basis of boundary conditions.

4. BOUNDARY CONDITIONS AND BASIC EQUATIONS

Let's present Eq. (8.1) for $n = 1$ under the following form:

$$\bar{y} = f(\bar{x}, \bar{z}) \tag{8.15}$$

with function $F = \bar{y} - f(\bar{x}, \bar{z}) = 0$. The unit vector normal with respect to surface (8.15) is

$$\mathbf{n}^0=\frac{\operatorname{grad}F}{|\operatorname{grad}F|}, \tag{8.16}$$

where projections of the vector of grad F on the x, y, z axes are

$$\frac{\partial F}{\partial\bar{x}}=-f_x, \quad \frac{\partial F}{\partial\bar{y}}=1, \quad \frac{\partial F}{\partial\bar{z}}=-f_z, \tag{8.17}$$

where $f_x=\frac{\partial f}{\partial \bar{x}}$, $f_z=\frac{\partial f}{\partial \bar{z}}$.

Let $\bar{\boldsymbol{V}}_j\{\bar{V}_{xj}, \bar{V}_{yj}, \bar{V}_{zj}\}$ be the corresponding resultant velocity of flow at point j on surface (8.15), while $\boldsymbol{n}^\circ$ is vector (8.16) at the same point. Then, the boundary condition of non-penetration of surface (8.15) can be expressed by the following scalar product:

$$\bar{\mathbf{V}}_j \cdot \mathbf{n}^\circ = 0. \tag{8.18}$$

If we consider that components of circumferential velocity of rotation at point j in this motion are $\{-\bar{z}_j, 0, \bar{x}_j\}$, then projections of vector $\bar{V}_j$ can be expressed in the following way:

$$\bar{V}_{xj}=\bar{u}_j-\bar{z}_j, \quad \bar{V}_{yj}=\bar{v}_j-\bar{V}_\infty, \quad \bar{V}_{zj}=\bar{w}_j+\bar{x}_j. \tag{8.19}$$

Now, expanding the scalar product of Eq. (8.18) with the help of the projection of cofactors of Eqs. (8.17) and (8.19), we obtain the principal condition of Eq. (8.18) under the following form:

$$\bar{v}_j-\bar{u}_j f_{xj}-\bar{w}_j f_{zj}=\bar{x}_j f_{zj}-\bar{z}_j f_{xj}+\bar{V}_\infty. \tag{8.20}$$

Derivatives f_{xj} and f_{zj} are determined at points j from geometry of the blade and given collective pitch angle.

Now, Eq. (8.14) is substituted into Eq. (8.20). After rearranging, we obtain a system of linear algebraic equations defining the sought circulation:

$$\sum_{i=1}^{m} \bar{\gamma}_{ij}\bar{\Gamma}_i=g_j, \tag{8.21}$$

where

$$\bar{\gamma}_{ij}=\bar{v}_{ij}-\bar{u}_{ij}f_{xj}-\bar{w}_{ij}f_{zj}, \quad \bar{g}_j=\bar{x}_j f_{zj}-\bar{z}_j f_{xj}+\bar{V}_\infty. \tag{8.22}$$

Numerical calculations for conventional airscrews indicate that as the first order approximation, $\bar{w}_{ij}f_{zj}$ and $\bar{x}_j f_{zj}$ can be neglected, thus obtaining

$$\bar{\gamma}_{ij}=\bar{v}_{ij}-\bar{u}_{ij}f_{xj}, \quad \bar{g}_j=\bar{V}_\infty-\bar{z}_j f_{xj}.$$

If $\bar{V}_\infty$ is low, then $|\bar{u}_{ij}| << |\bar{x}_{ij}|$ and correspondingly, $\bar{V}_{ij} \approx \bar{v}_{ij}$.

One should note that for the considered distribution of discrete vortices and control points, the condition of Chaplygin-Joukowsky is automatically fulfilled.

5. SINGLE LIFTING LINE

Let's now consider the simplest scheme of lifting surface under the form of a single lifting line coinciding with the blade axis (Fig. 8.2). The theory based on this scheme is usually called the 3/4 theory due to the fact that control points are located at the 3/4 distance of the chord from the leading edge of the blade. The lifting line is located at 1/4 chord from the leading edge.

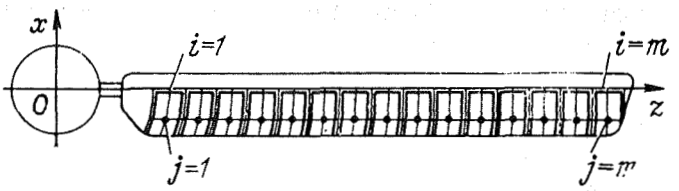

Figure 8.2

To calculate circulation $\bar{\Gamma}_i$, Eq. (8.21) is used, and to calculate coefficients $\bar{u}_{ij}$, $\bar{v}_{ij}$, $\bar{w}_{ij}$, corresponding equations, (8.12) and (8.13), are utilized. We first define the velocities $\bar{u}_{pj}$, $\bar{v}_{pj}$, $\bar{w}_{pj}$ appearing in Eq. (8.12). Since, in the considered case, $\vartheta_{pq} = 0$, then on the basis of Eqs. (8.4)-(8.6), increments of coordinates from Eq. (8.8) will be equal to:

$$\Delta\bar{x}_p=(\bar{\varrho}_{q+1}-\bar{\varrho}_q)\sin\delta_n,\quad \Delta\bar{y}_p=0,\quad \Delta\bar{z}_p=(\bar{\varrho}_{q+1}-\bar{\varrho}_q)\cos\delta_n,$$
$$\Delta\bar{x}_j=-\bar{r}_j\sin\vartheta_j-\bar{\varrho}_q\sin\delta_n,\quad \Delta\bar{y}_j=-\bar{V}\vartheta_j,\quad \Delta\bar{z}_j=\bar{r}_j\cos\vartheta_j-\bar{\varrho}_q\cos\delta_n.$$

Substituting the above expressions into Eq. (8.8), we obtain:

$$\bar{u}_{pj}=\frac{1}{4\pi}H\bar{V}\vartheta_j\cos\delta_n,\quad \bar{v}_{pj}=-\frac{1}{4\pi}H\bar{r}_j\sin(\delta_n+\vartheta_j),$$
$$\bar{w}_{pj}=-\frac{1}{4\pi}H\bar{V}\vartheta_j\sin\delta_n,$$

where

$$H=\frac{I_{q+1}-I_q}{\bar{V}^2\vartheta_j^2+\bar{r}_j^2\sin^2(\delta_n-\vartheta_j)},\qquad I_q=\frac{\bar{\varrho}_q-\bar{r}_j\cos(\delta_n-\vartheta_j)}{\bar{V}^2\vartheta_j^2+\bar{\varrho}_q^2+\bar{r}_j^2-2\bar{\varrho}_q\bar{r}_j\cos(\delta_n-\vartheta_j)}$$

Velocities $\bar{u}_{qj}$, $\bar{v}_{qj}$, $\bar{w}_{qj}$ appearing in Eq. (8.12) are defined from Eq. (8.11) for $\vartheta_{pq} = 0$. Derivatives from Eq. (8.22) can be found from the expression

where $$f_{xj}=\operatorname{tg}(\varphi_j+\delta\varphi_j),\quad f_{zj}=\operatorname{tg}a_0,$$

ϕ_j — pitch angle of the airfoil at section $\bar{z}_j$;

$\delta\phi_j$ — angle between airfoil chord and tangent to the midline of the airfoil at point j;

a_0 — coning angle of the blade.

A scheme of the single lifting line can be used for calculation of blades of large elongation.

6. COMPARISON OF THEORY AND EXPERIMENT

In Figs. 8.3 and 8.4, results are shown of calculation of distribution of circulation along the span of the blade based on the scheme of lifting surface (Curve 2) and that of the lift-line according to Prandtl (Curve 1). There, also, are the experimental results based on the measured aerodynamic loads

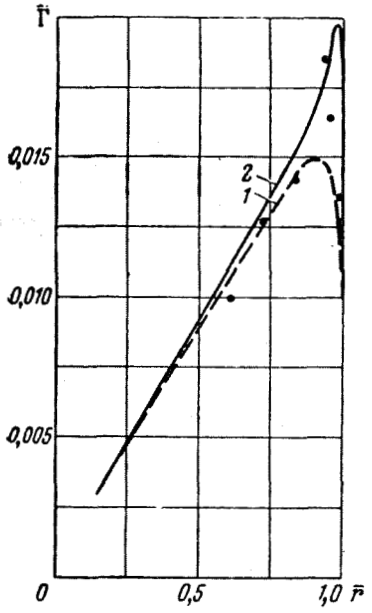

Figure 8.3

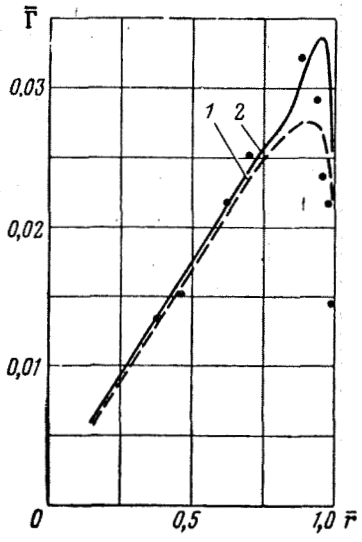

Figure 8.4

which, in turn, were recalculated into values of circulation by using N.E. Joukowsky's expressions. The considered models of lifting airscrews were about 2 meters in diameter. The blades of those airscrews were of rectangular planform, untwisted, with airfoil sections of NACA 230-12 along the whole span. In Fig. 8.3, calculated and experimental dependencies $\Gamma = \Gamma(\bar{r})$ obtained for a model airscrew with a blade chord $b = 0,08m$ and collective pitch angle $\phi_0 = 8,9^\circ$ are shown, and in Fig. 8.4, the results of calculations and experiment are shown for a model of an airscrew with blade chord $b = 0,11m$ and collective pitch angle $\phi_0 = 11,2^\circ$ (definition of the curves are the same as in Fig. 8.3).

It can be seen that the theory of the lifting surface shows a better agreement with tests in distribution of circulation at the blade tips than that predicted by the lifting-line

theory. Nevertheless, some discrepancies between calculated and experimental values can still be found as a result of imperfection of the scheme of the lifting surface and assumptions of quasi-linear theories. For this reason, it is necessary to have a detailed experimental study of the flow in the blade tip region in order to introduce the necessary corrections into that theory.

CHAPTER IX

AERODYNAMIC CALCULATIONS OF LIFTING AIRSCREWS IN VERTICAL DESCENT

There is a large amount of literature (see Refs. 32, 45, 78, 88, 95, 116, etc.) dealing with problems of vertical descent of lifting airscrews. Nevertheless, that regime of flight is not completely understood. In particular, up to now, no one attacked the basic problem of the determination of circulation and induced velocities along the blades at an arbitrary rate of descent. This can be explained by the fact that the phenomena occurring in the flow during descent of a rotor are very difficult to analyze theoretically. In contrast to the case of vertical ascent, the undisturbed flow slows down (brakes) the speed of air particles accelerated by the rotor. As a result of this, at low speeds of descent, those particles move slowly, and consequently, processes of diffusion and mutual interaction of vortices begin to play an important role. This leads to considerable complexities in the vortex system of the rotor and its field of induced velocities. Development of a rotor theory rigorously taking into account those phenomena would represent a very complicated task, as it would be connected with some difficult problems of the mechanics of viscous fluids (in particular, those of turbulence). For this reason, it is of interest to solve the above-mentioned task in a simplified form.

As is well known, the classic propeller theory accepts the hypothesis of the continuity of velocity of the vortices' movements. According to this hypothesis, vortex elements which separate themselves from the lifting line move along straight lines at a speed equal to that of the undisturbed flow approaching the propeller; thus forming a wake of regular helical form. This hypothesis is correct for large values of $\bar{V}_\infty$ when the influence of induced velocities is relatively small, and thus, can be neglected.

The classical propeller theory can be extended to the case of low values of $\bar{V}_\infty$ if concepts of the approaching flow is now interpreted in the light of a sum of velocities; that of flow approaching the propeller and that of the induced velocity, averaged over the disc. In spite of the fact that elements of free vortices actually move at different speeds, a theory based on the previously discussed assumptions gives satisfactory results as far as general airscrew characteristics are concerned. This is due to the fact that accounting for the variation of the pitch of the helixes formed by trailing vortices, the main part of the influence of induced velocities on movement of the vortices is evaluated. The above outlined approach is acceptable for any

values of V_∞, with the exception of the regime corresponding to the *"vortex ring state."*

Visualization of the tip blade vortices in the vortex ring state indicated that a special peculiarity of this regime of flight consists of widening of the vortex system accompanied by fluctuations and diffusion of vortices. Experiments show that in the proximity of the rotor, tip vortices are distributed over an approximately conical surface, while the axial pitch of the vortices does not change very much. These results* showed the possibilities for the following simple generalization of the above-discussed hypothesis to the case of the vortex ring state: At a given velocity of the undisturbed flow, elements of free vortices move with a constant axial velocity, V_y, and a constant radial velocity, V_r.

On the basis of the above-formulated general hypothesis, we will construct a conical scheme of the vortex system of an airscrew and develop parametric equations of the vorticity wake. Next, on the basis of simplifying assumptions, we establish a relationship between parameters of this scheme and the airscrew rate of descent. In essence, the task is reduced to the determination of circulation and induced velocities for a given scheme of the vortex system.

1. RESULTS OF EXPERIMENTS ON VISUALIZATION OF TIP VORTICES OF A ROTOR

Visualization was performed with smoke produced by a smoke generator and fed to the blade tips through the rotor hub and then through a tubular spar of the blade. The hub was equipped with a strain-guage balance in order to measure general rotor characteristics. Pressure distributions on the blade surface were also measured. High-speed movie camera provided a graphical coverage.

The vortex system of a rotor in vertical ascent can be seen in Fig. 9.1. In this case, the vortex system of N. E. Joukowsky is correct. In descent, phenomena occurring in the flow are quite different. Elements of free vortices move much more slowly and hence, they begin to deteriorate when still in the proximity of the rotor. At some low speed of the undisturbed flow, a process of widening of the vortex system occurs.

---

*First experiments of visualization of tip vortices in the air, including some regimes of vertical descent, were performed in TsAGI in 1957 by A.S. D'yachenko. Later, those experiments were continued and expanded by V. G. Kolkov. In this book, some results of Kolkov's tests are presented.

Velocities induced by free vortices are of the same order of magnitude as the speed of the movement of the vortex elements. Restricted system (because of diffusion) of free vortices induces radial velocities which, obviously, contribute to the widening of the system.

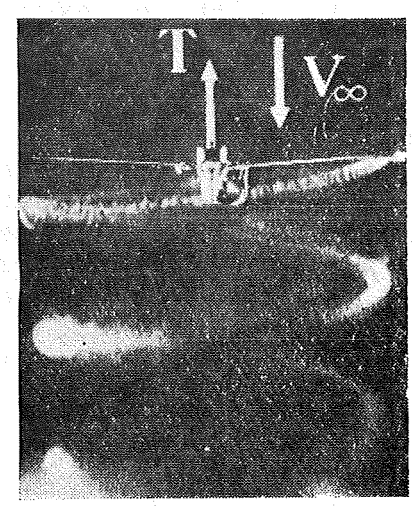

Figure 9.1

With the increasing rate of descent, free vortices come closer to the plane of rotation of the rotor. As a result of this, induced velocities in this plane increase. Tip vortices have a complicated spiral form (Fig. 9.2). This is the vortex ring state, whose peculiarity manifests itself through ring-type-movement of the air masses around spiral vortices (Fig. 9.3). In that regime, induced velocities at the disc plane reach their maximum values. The field of induced velocities becomes, to a large extent, unsteady. During translation, free vortices execute complicated fluctuating movements. Physical concept of the vortex ring becomes clearer. In the flow stream, diffusion of free vortices generates large-scale turbulence. All those processes cause an increase in the helicopter roughness.

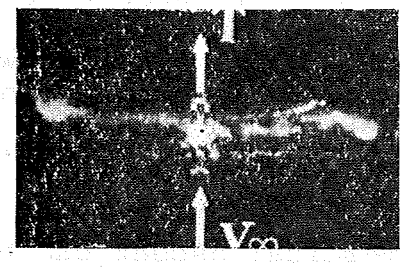

Figure 9.2

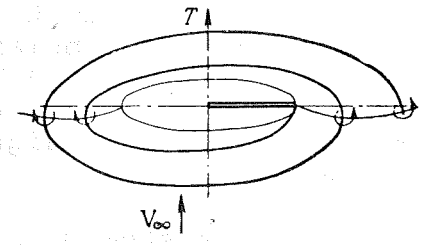

Figure 9.3

With the increasing rate of descent, free vortices float up with the flow (Figs. 9.4 and 9.5), and that leads to a decrease in induced velocities. One can see in Fig. 9.4, the dark core of a vortex of a blade without smoke. As can be seen, smoke from the outside does not penetrate into the vortex core. This means that the vortex filament in the proximity of the rotor consists of the same air particles (vortex filament moves together with the air flow) as stated by the Helmholtz theory regarding vortices in an ideal fluid. It appears, hence, that in this case, diffusion of vortices close to the rotor is insignificant and thus, can be neglected. At

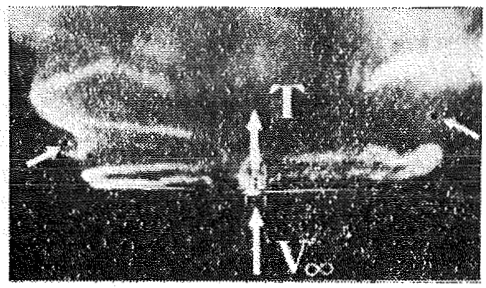

Figure 9.4

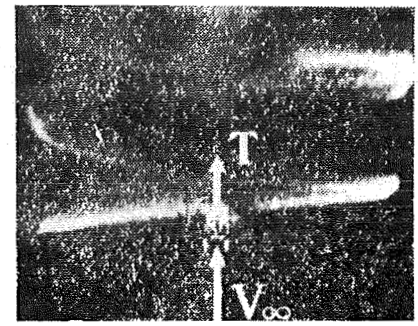

Figure 9.5

sufficiently high rates of descent, the Joukowsky-type vortex system appears again. In this case, mutual interaction of vortices becomes weak due to the low magnitude of induced velocities in comparison with the speed of the undisturbed flow.

Experimental results indicate that the surface of revolution along which tip vortices are distributed can be considered as approximately generated by a straight line. In that region, at fixed values of c_T and $\overline{V}_\infty$, the axial pitch of tip vortices does not change very much and thus, may be assumed as constant. Those peculiarities will be reflected in the development of a scheme of the rotor vortex system.

Let v_B be the average (over the whole disc) induced velocity in hovering, $(\overline{v}_B = -0,5\sqrt{c_T})$. Results of the above described experiments conducted at various combinations of $\overline{V}_\infty$ and c_T values showed that a significant widening of the vortex system occurs at $\tilde{V}_\infty = \overline{V}/|\overline{v}_B|$ values being within the following limits:

$$-2,5 < \tilde{V}_\infty < -0,5, \tag{9.1}$$

It should also be noted that a definite shape of the rotor vortex system corresponds to every value of parameter $\tilde{V}_\infty$ in Eq. (9.1). Outside of the range given by Eq. (9.1), i.e., at

$$\tilde{V}_\infty \geqslant -0,5, \quad \tilde{V}_\infty \leqslant -2,5 \tag{9.2}$$

the cylindrical vortex scheme of Joukowsky is applicable. Inequalities of Eqs. (9.1) and (9.2) will be used later in the computational analysis.

2. SCHEME OF THE ROTOR VORTEX SYSTEM

For practical applications, it is sufficient to estimate the position of vortices in the proximity of the rotor. The position of the far vortices may be roughly estimated as they little influence the flow patterns at the blades. As a result of the above, only principle characteristics of the shape of the near vortices are taken into consideration.

Let us assume that it is possible to substitute a straight line for an actual curve generating a surface of revolution on which tip vortices are located, and to further assume that vortices themselves assume a helical shape with a constant pitch (Fig. 9.6). Let us also assume that there is no fluctuation of the vortices. Those assumptions correspond to the generalized hypothesis of the constancy of velocity of vortices movement. On the basis of this hypothesis, it is possible to formulate the following parametric equations of the free vorticity layer of the *nth* blade *(n = 1, 2, ... k)*:

$$\left.\begin{aligned} \bar{\xi} &= -\bar{\varrho}\left(1+\frac{\bar{V}_r}{\bar{\varrho}}\,\vartheta\right)\cos(\theta_n-\vartheta),\\ \bar{\eta} &= -\bar{V}_y\vartheta,\\ \bar{\zeta} &= \bar{\varrho}\left(1+\frac{\bar{V}_r}{\bar{\varrho}}\,\vartheta\right)\sin(\theta_n-\vartheta). \end{aligned}\right\} \qquad (9.3)$$

The quantities appearing in Eq. (9.3) have the same meaning as those in Eq. (6.2).

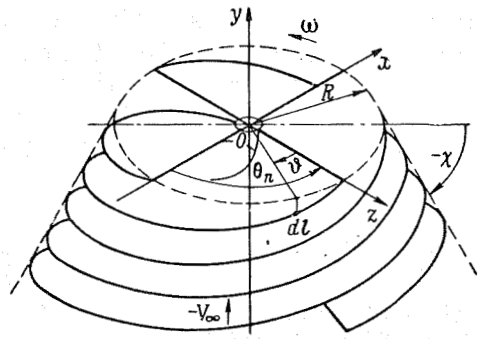

Figure 9.6

In Eq. (9.3), $\bar{V}_r$ and $\bar{V}_y$ are unknown. We are going to determine them. Hypothesis of the constant velocity of vortices movement in the flight regimes defined by Eq. (9.2) can be expressed, according to the momentum theory, as follows:

$$\left.\begin{aligned} \tilde{V}_y &= \frac{\tilde{V}_\infty}{2}+\sqrt{\left(\frac{\tilde{V}_\infty}{2}\right)^2+1} \quad (\tilde{V}_\infty \geqslant -0{,}5),\\ \tilde{V}_y &= \frac{\tilde{V}_\infty}{2}-\sqrt{\left(\frac{\tilde{V}_\infty}{2}\right)^2-1} \quad (\tilde{V}_\infty \leqslant -2{,}5), \end{aligned}\right\} \qquad (9.4)$$

where $\tilde{V}_y = \bar{V}_y/|\bar{v}_B|$. The task would consist now of determining the function $\tilde{V}_y(\tilde{V}_\infty)$ within the limits given by Eq. (9.1).

Let us assume that the above function is smooth everywhere. Then on the basis of Eq. (9.4), one can determine the value of

the sought function and its first derivative at the limits of the range given by Eq. (9.1). In addition, experimental results show that for $\tilde{V}_\infty \approx -1,5$, tip vortices concentrate close to the xz plane, and generate the largest induced velocities on that plane. In the accepted scheme of the vortex wake, the $\tilde{V}_y = 0$ case would correspond to this particular regime (flat vortex wake). In this way, in the region given by Eq. (9.1), we could know 3 values of the function and two of its derivatives. Let us assume that a polynomial of the lowest degree satisfying the above five conditions also approximates, with sufficient accuracy, the function $\tilde{V}_y(\tilde{V}_\infty)$. A graph of such a polynomial, of the fourth degree, is shown in Fig. 9.7.

Let us direct our attention now toward determination of function $\tilde{V}_r(\tilde{V}_\infty)$. We introduce, into our considerations, an auxiliary parameter : angle χ (see Fig. 9.6). It is obvious that

$$\tilde{V}_r = \tilde{V}_y \operatorname{ctg} \chi. \tag{9.5}$$

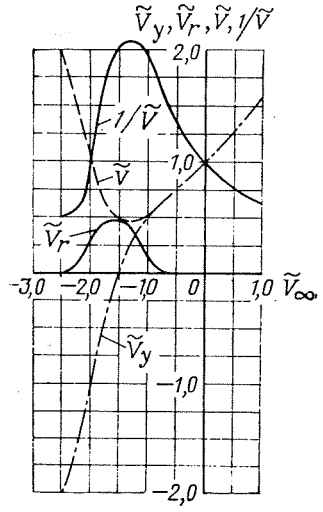

Figure 9.7

Now, let us determine function $\chi(\tilde{V}_\infty)$. At $\tilde{V}_\infty \geq -0,5$, the cylindrical wake of Joukowsky is acceptable and, hence, $\chi = -\pi/2$. At $\tilde{V}_\infty \leq -2,5$, again that form is correct, and consequently, $\chi = \pi/2$. From the assumption of differentiability of function $\chi(\tilde{V}_\infty)$, it follows that at the limits of the region given by Eq. (9.1), derivatives of that function are also known, $\chi' = 0$. In addition, it was mentioned that for $\tilde{V}_\infty = -1,5$, $\tilde{V}_y = 0 (\chi = 0)$. From those five conditions, an interpolating function describing $\chi(\tilde{V}_\infty)$ is developed. With the help of that function and Eq. (9.5), it is easy to find an approximate expression for $\tilde{V}_r(\tilde{V}_\infty)$. Graphical presentation of that expression is also shown in Fig. 9.7. In addition, in Fig. 9.7, a graph of function

$$\tilde{V} = \sqrt{\tilde{V}_y^2 + \tilde{V}_r^2}$$

is given, determining the resultant velocity of translation of a vortex element on the generated conical surface.

So, functions $\tilde{V}_y(\tilde{V}_\infty)$ and $\tilde{V}_r(\tilde{V}_\infty)$ are defined for any value of $\tilde{V}_\infty$. For given values of $\overline{V}_\infty$ and c_T (or $\overline{v}_B$), it is now possible to compute $\tilde{V}_\infty = \tilde{V}_\infty / |\overline{v}_B|$; then, from the graphs of Fig. 9.7 to find $\tilde{V}_y$ and $\tilde{V}_r$ and finally, to get values of $\overline{V}_y = \tilde{V}_y |\overline{v}_B|$ and $\overline{V}_r = \tilde{V}_r |\overline{v}_B|$ appearing in Eq. (9.3). In this way, a scheme of the rotor vortex system is defined. The next task would consist of finding, for blades of known geometric characteristics, the distribution of circulation and induced velocities along the blade which correspond to the given values of $\overline{V}_\infty$ and c_T, as well as determining the representative collective pitch angle of the blades and rotor torque coefficient.

3. INSTANTANEOUS AND TIME-AVERAGE INDUCED VELOCITIES

Let us develop the formulae for the axial component of instantaneous velocity generated by a rotor at a fixed point:

$$\bar{x}=-\bar{r}\sin\psi,\quad \bar{y}=0,\quad \bar{z}=\bar{r}\sin\psi. \tag{9.6}$$

We assume that circulation is continuously distributed along the blade span ($\bar{\Gamma}=\bar{\Gamma}(\bar{\rho})$). The relative circulation of a vortex strip of the wake defined by Eq. (9.3), included between radii $\bar{\rho}$ and $\bar{\rho}+d\bar{\rho}$ will be $(d\bar{\Gamma}/d\bar{\rho})d\bar{\rho}$. We will use Eq. (B.6) assuming that, in it, $p=\vartheta$. In considering that parameter ϑ varies within the limits of $0\leq\vartheta\leq\infty$, we obtain the following expression for instantaneous velocity, induced by an elementary strip of vorticity:

$$d\bar{v}^{\text{инд}}=-\frac{1}{4\pi}\left(\frac{d\bar{\Gamma}}{d\bar{\varrho}}d\bar{\varrho}\right)\int_0^\infty\left[\frac{d\bar{\zeta}}{d\vartheta}(\bar{x}-\bar{\xi})-\frac{d\bar{\xi}}{d\vartheta}(\bar{z}-\bar{\zeta})\right]\frac{d\vartheta}{\bar{l}^3}. \tag{9.7}$$

We substitute Eqs. (9.3) and (9.6) into Eq. (9.7). Summing up induced velocities generated by all vorticity strips of the rotor, we obtain instantaneous velocity

$$\bar{v}^{\text{инд}}=\frac{1}{4\pi}\sum_{n=1}^{k}\int_{\bar{c}_0}^{1}\frac{d\bar{\Gamma}}{d\bar{\varrho}}\left(\int_0^\infty\frac{F(\vartheta)}{F^{3/2}(\vartheta)}d\vartheta\right)d\bar{\varrho}, \tag{9.8}$$

where

$$E(\vartheta)=\bar{\varrho}^2-\bar{\varrho}\bar{r}\cos(\theta_n-\psi-\vartheta)+\bar{V}_r\bar{r}\sin(\theta_n-\psi-\vartheta)+$$
$$+\bar{V}_r\{\bar{\varrho}+[\bar{\varrho}-\bar{r}\cos(\theta_n-\psi-\vartheta)]\}\vartheta+\bar{V}_r^2\vartheta^2,$$
$$F(\vartheta)=(\bar{V}_y^2+\bar{V}_r^2)\vartheta^2+2\bar{V}_r[\bar{\varrho}-\bar{r}\cos(\theta_n-\psi-\vartheta)]\vartheta+$$
$$+\bar{\varrho}^2+\bar{r}^2-2\bar{\varrho}\bar{r}\cos(\theta_n-\psi-\vartheta).$$

It is easy to see that for $\bar{V}_r=0$, Eq. (9.8) becomes identical to the known Eq. (6.6), giving instantaneous induced velocity according to the blade theory. It is interesting to notice that although the internal integral in Eq. (9.8) becomes divergent, Eq. (9.8) has a meaning with the exclusion of points located on the lifting lines ($\theta_n=\psi$). On the lifting line, induced velocity becomes infinite because free (trailing) vortices are no longer perpendicular to the lifting line. However, if one realizes that values of $\bar{V}_y$ and $\bar{V}_r$ are very low for the region defined by Eq. (9.1) and consequently, density of the vortex filaments is very high, then it may be assumed with sufficient accuracy that instantaneous velocity at a point (Eq. (9.6)) is no different than its time-average value. Then the above discussed difficulty disappears automatically.

For practical computations, let us represent the vorticity wake as an assembly of horseshoe vortices i ($i=1,2,3,\ldots,m$) with

corresponding circulations $\bar{\Gamma}_i$ (Fig. 9.8). Vortex i consists of two free (trailing) helical vortices springing from the neighboring points on the lifting line, i and $i+1$, and a straight segment of bound vortex extending between those two points. Let us define, by $j (j=1, 2, 3, \ldots, m)$, the points located between points i. The distances of points i and j from axis y will be defined, respectively, as $\bar{\rho}_i$ and $\bar{r}_j$. Induced velocities are determined at point

$$\bar{x}_j = -\bar{r}_j \cos\psi, \quad \bar{y}_j = 0, \quad \bar{z}_j = \bar{r}_j \sin\psi. \tag{9.9}$$

We define, by $\bar{v}_{ij}^{M\Gamma}$, the instantaneous velocity at the point defined by Eq. (9.9) induced by vortices with identical indices "i" and unit circulation. Then, on the basis of Eq. (9.8)

$$\bar{v}_{ij}^{M\Gamma} = \frac{1}{4\pi} \sum_{n=1}^{k} \int_0^{\infty} \left(\frac{E_i(\vartheta)}{F_i(\vartheta)} - \frac{E_{i+1}(\vartheta)}{F_{i+1}(\vartheta)} \right) d\vartheta, \tag{9.10}$$

where

$$\begin{aligned} E_i(\vartheta) &= \bar{\varrho}_i^2 - \bar{\varrho}_i \bar{r}_j \cos(\theta_n - \psi - \vartheta) + \bar{V}_r \bar{r}_j \sin(\theta_n - \psi - \vartheta) + \\ &+ \bar{V}_r \{\bar{\varrho}_i + [\bar{\varrho}_i - \bar{r}_j \cos(\theta_n - \psi - \vartheta)]\} \vartheta + \bar{V}_r^2 \vartheta^2, \\ F_i(\vartheta) &= (\bar{V}_y^2 + \bar{V}_r^2) \vartheta^2 + 2\bar{V}_r [\bar{\varrho}_i - \bar{r}_j \cos(\theta_n - \psi - \vartheta)] \vartheta + \\ &+ \bar{\varrho}_i^2 + \bar{r}_j^2 - 2\bar{\varrho}_i \bar{r}_j \cos(\theta_n - \psi - \vartheta). \end{aligned} \tag{9.11}$$

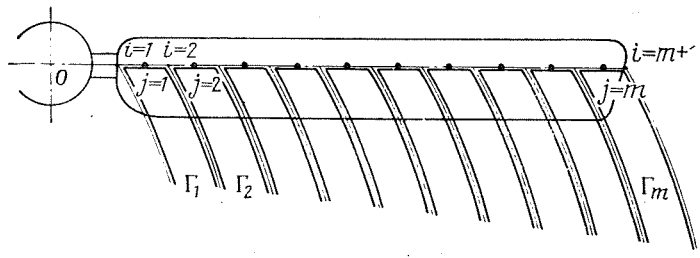

Figure 9.8

The quantities $E_{i+1}(\vartheta)$ and $F_{i+1}(\vartheta)$ are obtained from Eq. (9.11) by changing index "i" to index "$i+1$".

Switching to the disc theory, we average the velocity given by Eq. (9.10) at a fixed point (Eq. (9.9)) with respect to time:

$$\bar{v}_{ij} = \frac{1}{2\pi} \int_0^{2\pi} \bar{v}_{ij}^{M\Gamma} d\theta. \tag{9.12}$$

Integration in Eq. (9.12) is performed with respect to the azimuth angle θ of blade *1*. We substitute Eq. (9.10) into Eq. (9.12), and skipping the intermediate steps, we write the final result as

$$\bar{v}_{ij}=\frac{k}{4\pi\bar{V}}I_{ij}, \tag{9.13}$$

where $$I_{ij}=\frac{1}{2\pi}\int_0^{2\pi}(\Phi_i-\Phi_{i+1})\,d\theta, \tag{9.14}$$

$$\Phi_i=\frac{1}{\bar{l}^2-\frac{\bar{V}_r^2}{\bar{V}^2}\bar{P}_i}\left[(\bar{\varrho}_i\bar{P}_i+\bar{V}_r\bar{r}_j\sin\theta)\left(1-\frac{\bar{V}_r}{\bar{V}}\right)\left(1-\frac{\bar{V}_r}{\bar{V}}\frac{\bar{P}_i}{\bar{l}_i}\right)+\right.$$

$$+\frac{\bar{V}_r}{\bar{V}}(\bar{P}_i+\bar{\varrho}_i)\left(\bar{l}_i-\frac{\bar{V}_r}{\bar{V}}\bar{P}_i\right)+\frac{\bar{V}_r^2}{\bar{V}^2}\left(2\frac{\bar{V}_r^2}{\bar{V}^2}\bar{P}_i^2-\frac{\bar{V}_r}{\bar{V}}\bar{P}_i\bar{l}_i-\bar{l}_i^2\right)-$$

$$\left.-\frac{\bar{V}_r^2}{\bar{V}^2}\ln\left|\bar{l}_i+\frac{\bar{V}_r}{\bar{V}}\bar{P}_i\right|\right],$$

$$\bar{l}_i^2=\bar{\varrho}_i^2+\bar{r}_j^2-2\bar{\varrho}_i\bar{r}_j\cos\theta,\quad \bar{P}_i=\bar{\varrho}_i-\bar{r}_j\cos\theta.$$

Since the function given by Eq. (9.14) is very complicated, hence, to facilitate calculations, values of that function are given in Table 9.1. Let us designate, by $\bar{v}_j$, the velocity induced by the rotor at point j. Since vortices with identical indices "i" have identical circulation $\bar{\Gamma}_i$, hence, taking into account Eq. (9.13), we obtain the sought velocity in the following form:

$$\bar{v}_j=\frac{k}{4\pi\bar{V}}\sum_{i=1}^{m}\bar{\Gamma}_iI_{ij}\,(j=1,2,3,\ldots,m). \tag{9.15}$$

It can be seen that with the help of the tables, giving values of I_{ij}, computation of $\bar{v}_j$, corresponding to given circulation $\bar{\Gamma}_i$ can be reduced to elementary operations.

4. BASIC EQUATIONS AND ROTOR CALCULATIONS

In order to obtain basic equations, let us substitute Eq. (9.15) into Eq. (6.12), and Eq. (6.12) into Eq. (6.13). After transformations, we end up with a system of linear algebraic equations

$\bar{r}_j$	$\tilde{V}_\infty$	I_{ij}									
		$i=1$	$i=2$	$i=3$	$i=4$	$i=5$	$i=6$	$i=7$	$i=8$	$i=9$	$i=10$
0,24 ($j=1$)	0	—1,0000	0	0	0	0	0	0	0	0	0
	—0,4	—1,0000	0	0	0	0	0	0	0	0	0
	—0,8	—1,0197	0,0243	0,0088	0,0049	0,0034	0,0025	0,0020	0,0016	0,0014	0,0012
	—1,2	—0,8213	0,2369	0,1208	0,0816	0,0670	0,0553	0,0475	0,0417	0,0373	0,0337
	—1,8	—0,8218	0,2366	0,1206	0,0815	0,0699	0,0552	0,0474	0,0416	0,0372	0,0337
	—2,2	—1,0196	0,0242	0,0087	0,0049	0,0033	0,0025	0,0020	0,0016	0,0014	0,0012
	—2,5	—1,0000	0	0	0	0	0	0	0	0	0
0,32 ($j=2$)	0	0	—1,0000	0	0	0	0	0	0	0	0
	—0,4	0	—1,0000	0	0	0	0	0	0	0	0
	—0,8	—0,0537	—1,0145	0,0262	0,0097	0,0055	0,0037	0,0027	0,0021	0,0018	0,0015
	—1,2	—0,2717	—0,8142	0,2313	0,1162	0,0812	0,0635	0,0526	0,0452	0,0388	0,0356
	—1,8	—0,2716	—0,8147	0,2310	0,1160	0,0810	0,0634	0,0526	0,0451	0,0387	0,0356
	—2,2	—0,0534	—1,0144	0,0260	0,0096	0,0055	0,0037	0,0027	0,0021	0,0017	0,0015
	—2,5	0	—1,0000	0	0	0	0	0	0	0	0
0,40 ($j=3$)	0	0	0	—1,0000	0	0	0	0	0	0	0
	—0,4	0	0	—1,0000	0	0	0	0	0	0	0
	—0,8	—0,0299	—0,0508	—1,0112	0,0275	0,0104	0,0059	0,0040	0,0029	0,0023	0,0019
	—1,2	—0,1454	—0,2607	—0,8099	0,2279	0,1132	0,0786	0,0613	0,0507	0,0435	0,0383
	—1,8	—0,1453	—0,2605	—0,8104	0,2276	0,1130	0,0785	0,0612	0,0507	0,0435	0,0382
	—2,2	—0,0298	—0,0504	—1,0112	0,0273	0,0103	0,0059	0,0040	0,0029	0,0023	0,0019
	—2,5	0	0	—1,0000	0	0	0	0	0	0	0

TABLE 9.1

0,48 (j=4)	0	0	0	0	—1,0000	0	0	0	0	0	0
	—0,4	0	0	0	—1,0000	0	0	0	0	0	0
	—0,8	—0,0219	—0,0279	—0,0488	—1,0089	0,0285	0,0110	0,0063	0,0043	0,0031	0,0025
	—1,2	—0,1044	—0,1376	—0,2534	—0,8068	0,2255	0,1110	0,0767	0,0596	0,0483	0,0422
	—1,8	—0,1043	—0,1375	—0,2533	—0,8073	0,2253	0,1109	0,0766	0,0595	0,0482	0,0422
	—2,2	—0,0217	—0,0278	—0,0484	—1,0089	0,0283	0,0109	0,0063	0,0043	0,0031	0,0024
	—2,5	0	0	0	—1,0000	0	0	0	0	0	0
0,56 (j=5)	0	0	0	0	0	—1,0000	0	0	0	0	0
	—0,4	0	0	0	0	—1,0000	0	0	0	0	0
	—0,8	—0,0175	—0,0204	—0,0266	—0,0473	—1,0071	0,0292	0,0115	0,0066	0,0045	0,0034
	—1,2	—0,0828	—0,0984	—0,1322	—0,2483	—0,8046	0,2239	0,1094	0,0752	0,0583	0,0481
	—1,8	—0,0828	—0,0983	—0,1321	—0,2481	—0,8051	0,2236	0,1093	0,0751	0,0582	0,0480
	—2,2	—0,0174	—0,0203	—0,0264	—0,0470	—1,0071	0,0290	0,0114	0,0066	0,0045	0,0034
	—2,5	0	0	0	0	—1,0000	0	0	0	0	0
0,64 (j=6)	0	0	0	0	0	0	—1,0000	0	0	0	0
	—0,4	0	0	0	0	0	—1,0000	0	0	0	0
	—0,8	—0,0147	—0,0164	—0,0193	—0,0255	—0,0462	—1,0059	0,0299	0,0119	0,0069	0,0047
	—1,2	—0,0692	—0,0781	—0,0941	—0,1282	—0,2444	—0,8029	0,2226	0,1082	0,0741	0,0573
	—1,8	—0,0692	—0,0780	—0,0941	—0,1281	—0,2442	—0,8034	0,2223	0,1081	0,0740	0,0572
	—2,2	—0,0146	—0,0162	—0,0192	—0,0254	—0,0459	—1,0059	0,0297	0,0119	0,0068	0,0047
	—2,5	0	0	0	0	0	—1,0000	0	0	0	0
0,72 (j=7)	0	0	0	0	0	0	0	—1,0000	0	0	0
	—0,4	0	0	0	0	0	0	—1,0000	0	0	0
	—0,8	—0,0127	—0,0138	—0,0155	—0,0185	—0,0247	—0,0453	—1,0048	0,0304	0,0122	0,0072
	—1,2	—0,0597	—0,0653	—0,0746	—0,0909	—0,1251	—0,2414	—0,8015	0,2216	0,1072	0,0732
	—1,8	—0,0597	—0,0653	—0,0745	—0,0908	—0,1251	—0,2412	—0,8020	0,2214	0,1071	0,0731

TABLE 9.1 (Cont'd)

$\bar{r}_j$	$\tilde{V}_\infty$	I_{ij}									
		$i=1$	$i=2$	$i=3$	$i=4$	$i=5$	$i=6$	$i=7$	$i=8$	$i=9$	$i=10$
	—2,2	—0,0126	—0,0137	—0,0154	—0,0184	—0,0245	—0,0450	—1,0048	0,0302	0,0121	0,0072
	—2,5	0	0	0	0	0	0	—1,0000	0	0	0
0,80 ($j=8$)	0	0	0	0	0	0	0	0	—1,0000	0	0
	—0,4	0	0	0	0	0	0	0	—1,0000	0	0
	—0,8	—0,0112	—0,0119	—0,0131	—0,0148	—0,0178	—0,0240	—0,0446	—1,0039	0,0309	0,0125
	—1,2	—0,0527	—0,0565	—0,0624	—0,0719	—0,0884	—0,1227	—0,2389	—0,8204	0,2208	0,1065
	—1,8	—0,0526	—0,0564	—0,0624	—0,0718	—0,0883	—0,1226	—0,2388	—0,8009	0,2206	0,1063
	—2,2	—0,0112	—0,0119	—0,0130	—0,0147	—0,0177	—0,0239	—0,0443	—1,0040	0,0307	0,0124
	—2,5	0	0	0	0	0	0	0	—1,0000	0	0
0,88 ($j=9$)	0	0	0	0	0	0	0	0	0	—1,0000	0
	—0,4	0	0	0	0	0	0	0	0	—1,0000	0
	—0,8	—0,0101	—0,0106	—0,0114	—0,0125	—0,0143	—0,0173	—0,0235	—0,0440	—1,0032	0,0313
	—1,2	—0,0472	—0,0469	—0,0539	—0,0601	—0,0687	—0,0863	—0,1207	—0,2369	—0,7995	0,2202
	—1,8	—0,0471	—0,0469	—0,0539	—0,0600	—0,0687	—0,0863	—0,1207	—0,2368	—0,7999	0,2199
	—2,2	—0,0100	—0,0105	—0,0113	—0,0124	—0,0142	—0,0172	—0,0233	—0,0437	—1,0032	0,0310
	—2,5	0	0	0	0	0	0	0	0	—1,0000	0
0,96 ($j=10$)	0	0	0	0	0	0	0	0	0	0	—1,0000
	—0,4	0	0	0	0	0	0	0	0	0	—1,0000
	—0,8	—0,0092	—0,0095	—0,0101	—0,0109	—0,0120	—0,0138	—0,0169	—0,0230	—0,0435	—1,0026
	—1,2	—0,0428	—0,0447	—0,0477	—0,0519	—0,0582	—0,0680	—0,0846	—0,1191	—0,2353	—0,7987
	—1,8	—0,0428	—0,0447	—0,0477	—0,0519	—0,0582	—0,0679	—0,0846	—0,1190	—0,2351	—0,7991
	—2,2	—0,0092	—0,0095	—0,0100	—0,0108	—0,0120	—0,0137	—0,0168	—0,0229	—0,0432	—1,0026
	—2,5	0	0	0	0	0	0	0	0	0	—1,0000

TABLE 9.1 (Cont'd)

$$\sum_{i=1}^{m} \gamma_{ij}\bar{\Gamma}_i = \bar{g}_j, \tag{9.16}$$

in which

$$\bar{\gamma}_{ij} = \begin{cases} I_{ij} & (i \neq j), \\ I_{ij} - \dfrac{8\pi \bar{V} \cos \beta_j}{k a_{\infty j} \bar{b}_j} & (i = j), \end{cases}$$

$$\bar{g}_j = \frac{4\pi}{k} \bar{V} \bar{r}_j (\beta_j - \varphi_0 - \Delta\varphi_j).$$

In order to facilitate computations, with the help of Eqs. (6.20) and (6.21) we divide the system of Eq. (9.16) into two systems

$$\sum_{i=1}^{m} \bar{\gamma}_{ij} \bar{\Gamma}'_i = \bar{g}'_j, \quad \sum_{i=1}^{m} \bar{\gamma}_{ij} \bar{\Gamma}''_j = \bar{g}''_j, \tag{9.17}$$

where

$$\bar{g}'_j = \frac{4\pi}{k} \bar{r}_j (\beta_j - \Delta\varphi_j), \quad \bar{g}''_j = -\frac{4\pi}{k} \bar{r}_j.$$

Since all coefficients in the systems of Eq. (9.17) for given values of $\bar{V}_\infty$ and c_T are known, hence, the magnitudes of $\bar{\Gamma}_i'$ and $\bar{\Gamma}_i''$ can be easily calculated on a computer. Then, from Eqs. (6.30) and (6.29), the blade pitch angle ϕ_0 is found, while Eqs. (6.20) and (9.15) would give values of $\bar{\Gamma}_i$ and $\bar{v}_j$. The sequence of further calculations of the rotor are analogous to that presented in Sect. 6 of Ch. VI.

Let us examine results of calculations for a model of a two-bladed rotor with rectangular flat blades, having a chord $\bar{b} = 0{,}085$ and NACA 230-12 airfoil section along the whole span. We consider descent of the rotor at $\bar{V}_\infty = -0{,}037$ and $c_T = 0{,}0076$. Distribution of circulation along the lifting line is given in Fig. 9.9. In that figure, experimental results* obtained from aerodynamic loading and recalculated to circulation using the Joukowsky formula are also shown. It can be seen that with the exception of the blade tip, analytical and experimental results show an acceptable agreement. It is interesting to note that similar discrepancies were observed in the case of $\bar{V}_\infty = 0$ (see Figs. 8.3 and 8.4) when the classical lifting line scheme was used for analytical predictions. It appears that one of the

*Tests performed by A.S. D'yachenko

main causes of the discrepancy between the calculated and test data lies in that the flow at the blade tip is of three-dimensional character and does not correspond to the hypothesis of two-dimensional flow. It may be expected, hence, that application of the lifting surface scheme should lead to a better agreement between predicted and measured data. Induced velocity distribution along the blade, corresponding to the circulation distribution of Fig. 9.9, is shown in Fig. 9.10.

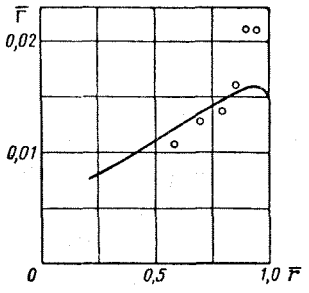

Figure 9.9

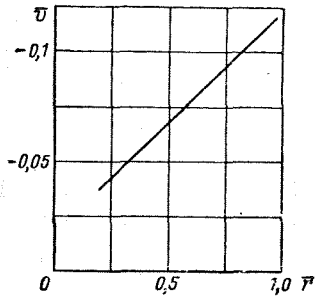

Figure 9.10

In conclusion, let us consider the problem of an average, over the disc, induced velocity $\bar{v}_{cp}$ corresponding to a constant circulation along the blade, $\bar{\Gamma}_{cp}$. Using Eq. (9.15), we find an approximate expression

$$\bar{v}_{cp} = -\frac{k\bar{\Gamma}_{cp}}{4\pi V} \quad \text{or} \quad \bar{v}_{cp} = -\frac{1}{\tilde{V}}, \tag{9.18}$$

where $\tilde{v}_{cp} = \bar{v}_{cp}/|\bar{v}_B|$. A graph of function $1/\tilde{V}$ is shown in Fig. 9.7. That function agrees favorably with experimental data.

As is known from the Joukowsky formula, induced velocity, averaged over the disc is

$$\bar{v}_{cp} = -\frac{k\bar{\Gamma}_{cp}}{4\pi|\bar{V}_y|} \quad \text{or} \quad \bar{v}_{cp} = \frac{1}{|\tilde{V}_y|}. \tag{9.19}$$

The difference between Eqs. (9.18) and (9.19) consists of that in Eq. (9.18), it was assumed that elements of the free vortices move along the conical surface with a speed of

$$\bar{V} = \sqrt{\bar{V}_y^2 + \bar{V}_r^2},$$

while Eq. (9.19) reflects the movement of vortices along a cylindrical surface with a speed of $\bar{V} = \bar{V}_y$. When $\bar{V}_r = 0$, both formulae become identical. Eq. (9.19) cannot be applied to the vortex-ring case, as with a decrease of the absolute value of $\bar{V}_y$, induced velocity grows to infinity.

CHAPTER X

DISC THEORY OF LIFTING AIRSCREWS IN AN OBLIQUE FLOW

1. SOME RESULTS OF FLOW VISUALIZATION OF AIRSCREW VORTICITY WAKE

We will examine some results of experiments where vorticity wakes of airscrews at arbitrary angles of attack were investigated.* In Figs. 10.1 and 10.2, photographs are shown of tip vortices of a rotor in climb at a low velocity and moderate loading ($\mu = 0{,}05$; $c_T = 0{,}0129$). It can be seen that

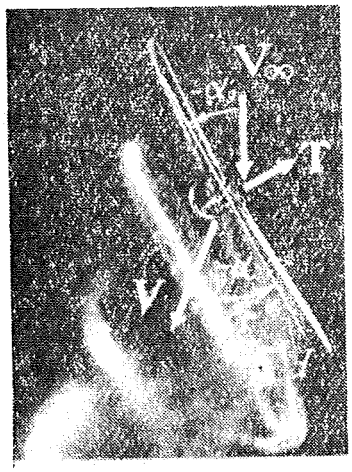

Here, *I* is the rotor Plane of Rotation

Figure 10.1

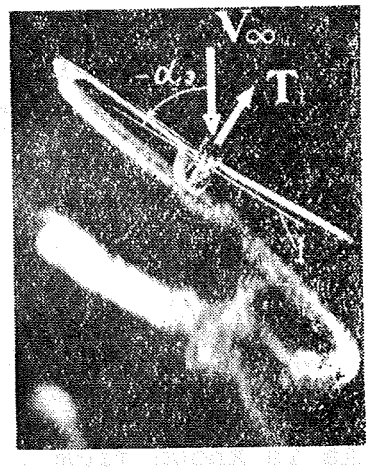

Figure 10.2

vortices are distributed over a surface that may be practically considered as a cylinder with an elliptical cross-section, while vortices themselves form a helix with constant pitch. From these observations, an important conclusion can be drawn: Vortex elements move in space together with particles of a uniform rectilinear flow with velocity V. It can also be seen that the axis of the elliptical cylinder does not coincide with the direction of the undisturbed flow V_∞. This is due to the influence of induced velocities on the movement of the vortices.

*Experiments performed by V.G. Kolkov

Results of the experiments can be sufficiently accurately described through a hypothesis of the constancy of velocity of the vortices movement which may be expressed by the following vectorial relationship:

$$V = V_\infty + v_{cp}, \tag{10.1}$$

where v_{cp} is a vector of induced velocity averaged over the disc. With the increasing V_∞, the hypothesis expressed by Eq. (10.1) remains satisfactory, while at sufficiently high speeds V_∞, $V = V_\infty$.

At flight regimes corresponding to low values of V_∞ and low angles of attack of the rotor, movement of vortices becomes more complicated. Due to a decrease of the component perpendicular to the plane of rotation due to the velocity of undisturbed flow, a greater influence on movement of the vortices is acquired by nonuniformity of the induced velocity distributions. This is especially true at high c_T values. At sufficiently high velocities of the undisturbed flow ($\mu > \sqrt{c_T}$), vortex systems becomes practically flat while free (trailing) vortices acquire a cycloidal shape (Fig. 10.3).

Let us consider power-off descents which have been, until now, the least investigated of all regimes of flight. In Fig. 10.4, a shows a case of descent at a very low speed and a very low loading ($\mu = 0,05$; $c_T = 0,005$). It can be seen that the vortices movement corresponds to the hypothesis of Eq. (10.1).

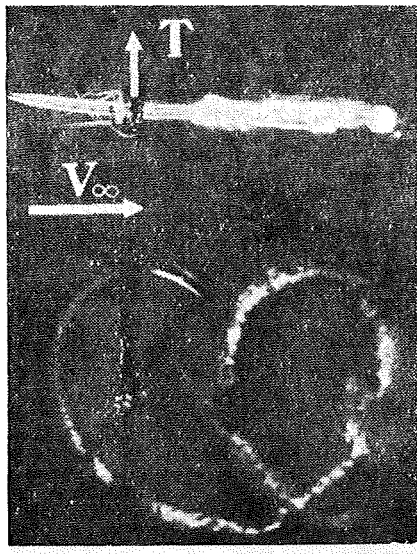

Figure 10.3

Figure 10.4

In descent of a highly loaded rotor at low velocity, a strong interaction between the vortices takes place. This results in

complicated unsteady movements and deformations of the vortices (see Fig. 10.7, *а*, σ, β). At very low velocities of vortices movements, diffusion starts to play a role in vortices being near the rotor (see Fig. 10.4, σ and 10.7, β). It is interesting to note that at $\alpha = +30^\circ$ and $\mu = 0{,}05$, an increase of c_T causes a visible variation in the appearance of the vortex system (see Fig. 10.4, *а*, σ).

It is important to call one's attention to a significant difference between ascent and descent. In the case of ascent, induced velocities accelerate the movement of the vortex elements, while in descent, they provide a decelerating influence. This slowing down of the vortices movement is especially visible in the disc trailing edge region, where induced velocities are high. In that region, vortices appear to be "packed" very tightly (Figs. 10.5 and 10.6).

Results of the experiments, only some of which are quoted here, permitted the establishment of approximate limits for the application of existing theoretical methods. They also allowed an approximate evaluation of the influence of basic parameters (μ, $\alpha_э$, c_T) on the form of the rotor wake structure. It was established, for instance, that for regimes of flight with low angles of attack $\alpha_э$ and at $\mu < \sqrt{c_T}$, it is expedient to use a three-dimensional vortex system. Furthermore, it is also expedient to apply the same approach to cases of high μ values in combination with large, either positive or negative, angles of attack. At $\mu > \sqrt{c_T}$ and low angles of attack, it is recommended to use the theory based on the flat rotor vortex wake concept. Experimental results also give a basis for further expansion of the theory to the cases of more complicated motions and diffusion of the vortices. The theory presented below is based on the hypothesis of Eq. (10.1) which permits the use of the well-known three-dimensional scheme of G. I. Maykapar[61].

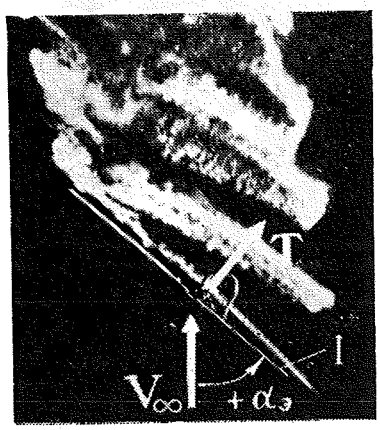

Figure 10.5

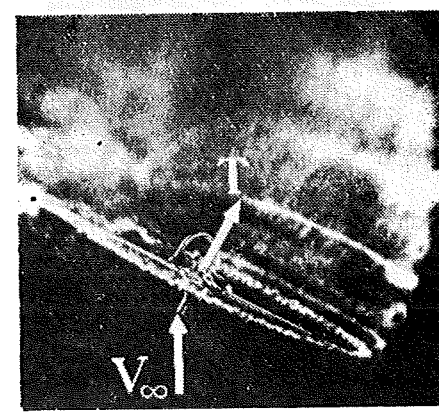

Figure 10.6

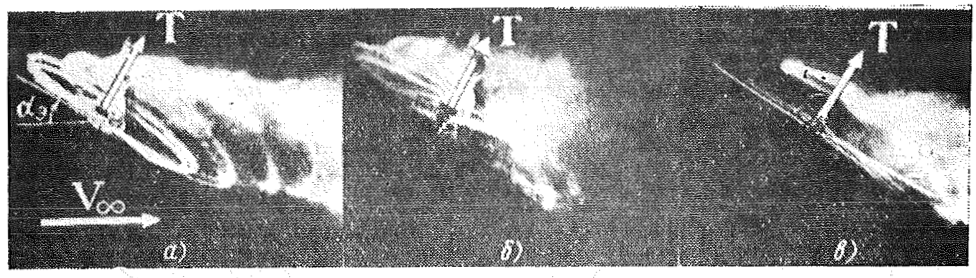

Figure 10.7

2. SCHEME OF THE ROTOR VORTEX SYSTEM AND BASIC ASSUMPTIONS

Let a k-bladed rotor be submerged in a uniform rectilinear air stream flowing with velocity V. Let the center of the hub coincide with the origin of a Cartesian system of coordinates $Oxyz$ (Fig. 10.8). The rotor rotates about the y axis with an angular velocity ω. The rotor blade is modeled by a segment of the lifting line with circulation varying with the radius, $\bar{\rho}$ and blade azimuth angle, θ: $\Gamma = \Gamma(\rho, \theta)$. The plane of rotation makes an arbitrary angle α_B with vector V. Without any loss of generality of this approach, it is possible to assume that vector $V(V_x, V_y, V_z)$ is parallel to the xy plane, so that

$$V_x = -V\cos\alpha_B, \quad V_y = V\sin\alpha_B, \quad V_z = 0. \tag{10.2}$$

If one's attention is concentrated on elements of vortices continuously separating themselves from an arbitrary point on the rotating lifting line, then one would notice that those elements moving in the space $Oxyz$ with a velocity V would form a free vortex shaped as a skewed helix. Vortex elements that spring from the whole lifting line form a vortex wake shaped as a skewed helical surface.

Let us write parametric equations of that surface. In order to do this, we will investigate the movement of an arbitrary vortex element which has separated from the lifting line (Fig. 10.9). Element E was generated at the instant when segment $OB = \rho$ of the lifting line was in the position OA. After its separation at point A, the element began to move with speed V and reached point E at the moment when segment OA moved to position OB. Coordinates at point A are

$$\xi_A = -\varrho\cos(\theta - \vartheta), \quad \eta_A = 0, \quad \zeta_A = \varrho\sin(\theta - \vartheta). \tag{10.3}$$

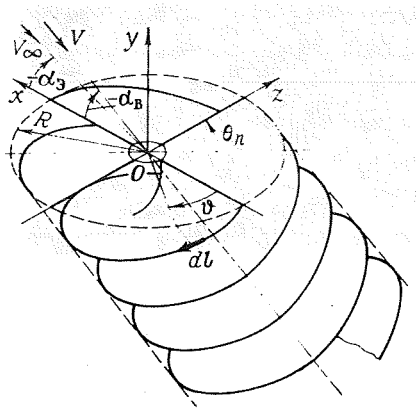

Figure 10.8

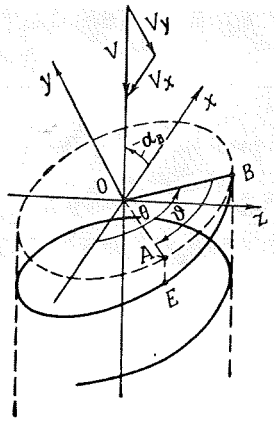

Figure 10.9

Time of rotation of the lifting line from its position *OA* to position *OB*, obviously, is ϑ/ω, where ϑ is the angle between segments *OB* and *OA*, measured from segment *OB*. During that time, the considered vortex element is displaced, according to Eq. (10.2), with respect to point *A* by the following:

$$\Delta\xi_A = -V\frac{\vartheta}{\omega}\cos\alpha_B,\quad \Delta\eta_A = V\frac{\vartheta}{\omega}\sin\alpha_B,\quad \Delta\zeta_A = 0. \tag{10.4}$$

In this way, taking into consideration Eqs. (10.3) and (10.4), coordinates at point *E* can be presented in the following, nondimensional form:

$$\bar{\xi} = -\bar{V}\vartheta\cos\alpha_B - \bar{\varrho}\cos(\theta-\vartheta),\quad \bar{\eta} = \bar{V}\vartheta\sin\alpha_B,\quad \zeta = \bar{\varrho}\sin(\theta-\vartheta), \tag{10.5}$$

where $\bar{\varrho}_0 \leqslant \bar{\varrho} \leqslant 1,\quad 0 \leqslant \theta \leqslant 2\pi,\quad 0 \leqslant \vartheta < \infty.$

The relationships in Eq. (10.5) become the desired parametric equations of the vortex wake. If, in Eq. (10.5), we assume $\bar{\rho} = const$, $\theta = const$, then for given values of $\bar{V}$ and α_B, we will get equations (with respect to parameter ϑ) of a skewed helical curve. If radius $\bar{\rho}$ varies in a continuous manner within the limits of $\bar{\rho}_0 \leq \bar{\rho} \leq 1$, then we would obtain a family of such lines, completely covering the vortex wake surface. Along those lines extend the so-called elementary longitudinal (trailing) vortices with circulation

$$-\frac{\partial}{\partial\bar{\varrho}}\bar{\Gamma}(\bar{\varrho}, \theta-\vartheta)\,d\bar{\varrho}. \tag{10.6}$$

The appearance of longitudinal vortices is related to variation of circulation along the lifting-line span - just as in the wing theory. The reason for the "-" sign before the derivative in Eq. (10.6) is explained in Sect. 1 of Ch. VI.

If, in Eq. (10.5), one assumes $\theta = const$, $\vartheta = const$, then for given values of $\overline{V}$ and α_B, one would get equations of a segment of straight line - a trace of the lifting line with respect to parameter $\overline{\rho}$. Should angle ϑ vary in a continuous manner within the limits $0 \leq \vartheta < \infty$, then a family of those segments would completely cover the vorticity wake. On those segments would be located the so-called elementary lateral (shed) vortices with circulations

$$-\frac{\partial \overline{\Gamma}}{\partial \vartheta}\overline{\Gamma}(\overline{\varrho}, \theta - \vartheta)\, d\vartheta. \tag{10.7}$$

Generation of the lateral vortices is associated with the unsteadiness of flow encountered by the blade. In their nature, lateral vortices are analogous to the starting and stopping vortices observed in an unsteady flow encountered by a wing. Eq. (10.7) results from the following considerations. To a rotation of the blade about the rotor axis through an angle $d(\theta - \vartheta)$, corresponds variation of circulation of the lifting line by the following value

$$\frac{\partial}{\partial(\theta-\vartheta)}\overline{\Gamma}(\overline{\varrho}, \theta-\vartheta)\, d(\theta-\vartheta) = \frac{\partial}{\partial \vartheta}\overline{\Gamma}(\overline{\varrho}, \theta-\vartheta)\, d\vartheta.$$

According to the Thompson theory (of constancy of circulation within a closed contour), from the lifting line should spring a lateral vortex with circulation of the opposite sign; i.e., with the circulation given in Eq. (10.7).

The material presented so far in this section should be sufficient to permit solution of one of the basic tasks of the theory; namely, of determining the induced velocity distribution according to a known law for $\overline{\Gamma}(\overline{\rho}, \theta)$. This task will be solved through time-averaging of instantaneous induced velocities.

3. INSTANTANEOUS INDUCED VELOCITY

INSTANTANEOUS VELOCITY, INDUCED BY LONGITUDINAL VORTICES

A formula for velocity induced by a rectilinear vortex with circulation given by Eq. (10.6) follows from the relationship of Eq. (I.6) with $p = \vartheta$; i.e.,

$$d\bar{v}_{\text{пр}}^{\text{мг}} = \frac{1}{4\pi} \int_0^{\infty} \left[\frac{\partial}{\partial \bar{\varrho}} \bar{\Gamma}(\bar{\varrho}, \theta - \vartheta)\, d\bar{\varrho} \right] \frac{F}{\bar{l}^3}\, d\vartheta, \tag{10.8}$$

where

$$\left.\begin{aligned} F &= \frac{\partial \bar{\xi}}{\partial \vartheta}(\bar{z} - \bar{\zeta}) - \frac{\partial \zeta}{\partial \vartheta}(\bar{x} - \bar{\xi}), \\ \bar{l}^2 &= (\bar{x} - \bar{\xi})^2 + (\bar{y} - \bar{\eta})^2 + (z - \bar{\zeta})^2. \end{aligned}\right\} \tag{10.9}$$

Induced velocity is calculated at point

$$\bar{x} = -\bar{r}\cos\psi, \quad \bar{y} = 0, \quad \bar{z} = \bar{r}\sin\psi. \tag{10.10}$$

Substituting Eqs. (10.5) and (10.10) into Eq. (10.9), and after some transformations, we obtain

$$F = G\vartheta + H, \quad \bar{l} = \sqrt{\bar{V}^2\vartheta^2 + g\vartheta + h}, \tag{10.11}$$

where

$$\begin{aligned} G &= [\bar{\varrho}\cos(\theta - \vartheta)]\, \bar{V}\cos\alpha_{\text{в}}, \\ H &= \bar{\varrho}^2 - \bar{\varrho}\bar{r}\cos(\theta - \vartheta - \psi) + [\bar{\varrho}\sin(\theta - \vartheta) - \bar{r}\sin\psi]\, \bar{V}\cos\alpha_{\text{в}}, \\ g &= 2[\bar{\varrho}\cos(\theta - \vartheta) - \bar{r}\cos\psi]\, \bar{V}\cos\alpha_{\text{в}}, \\ h &= \bar{\varrho}^2 + \bar{r}^2 - 2\bar{\varrho}\bar{r}\cos(\theta - \vartheta - \psi). \end{aligned} \tag{10.12}$$

We substitute Eq. (10.11) into Eq. (10.8) and sum the induced velocities generated by all elementary free vortices which spring from the lifting line. Then

$$\bar{v}^{\text{мг}} = \frac{1}{4\pi} \int_{\bar{\varrho}_0}^{1} \int_0^{\infty} \frac{\partial \bar{\Gamma}(\bar{\varrho}, \theta - \vartheta)}{\partial \bar{\varrho}} \frac{G\vartheta + H}{(\bar{V}^2\vartheta^2 + g\vartheta + h)^{3/2}}\, d\vartheta d\bar{\varrho}. \tag{10.13}$$

With the given function $\bar{\Gamma}(\bar{\rho}, \theta - \vartheta)$, the double integral of Eq. (10.13) can be computed, for points not located on the lifting line, through numerical integration. On the lifting line ($\theta = \psi$), induced velocity becomes infinite. This is due to the fact that free vortices are not perpendicular to the lifting line. Components of the vorticity surface parallel to the lifting line (boundary of the surface) induce at that boundary, according to the well-known law of hydrodynamics, infinite velocities (if the intensity of the layer at that boundary does not become either zero, or infinite). It is possible to avoid those unrealistic results if we would replace the blade by a lifting surface. Then induced velocities would be calculated, not at the boundary of the vorticity layer, but inside it where they are finite. Distribution of intensity

over the vorticity surface is determined according to the known boundary conditions (non-penetration of the airfoil contour and finite magnitudes of velocities at the trailing edge).

This task can be simplified if the hypothesis of two-dimensional airfoil characteristics is accepted. Then, flow around any blade section is considered as two-dimensional flow around airfoil sections whose trailing edges lie on the lifting line. In this way, strictly speaking, such usual concepts of the blade theory as the induced inflow at the airfoil and true (local) angle of attack are not applicable any more. However, through time averaging of the instantaneous induced velocities, those difficulties are removed. Induced velocity becomes finite and the lifting-line scheme with its accepted notions becomes applicable.

INSTANTANEOUS VELOCITY INDUCED BY FREE LATERAL VORTICES

Formulae for velocities induced by free lateral vortices can be obtained from Eq. (A.6) for $p = \bar{\rho}$. Assuming that circulation of that vortex is as given by Eq. (10.7), we obtain the sought formula

$$d\bar{v}^{\text{мг}}_{\text{пп}} = \frac{1}{4\pi} \int_{\bar{\varrho}_0}^{1} \left[\frac{\partial \bar{\Gamma}(\bar{\varrho}, \theta - \vartheta)}{\partial (\theta - \vartheta)} d(\theta - \vartheta) \right] \frac{\Phi}{\bar{l}^3} d\bar{\varrho}, \tag{10.14}$$

where

$$\Phi = \frac{\partial \bar{\xi}}{\partial \bar{\varrho}} (\bar{z} - \bar{\zeta}) - \frac{\partial \bar{\zeta}}{\partial \bar{\varrho}} (\bar{x} - \bar{\xi}). \tag{10.15}$$

Substituting Eqs. (10.5) and (10.10) into Eq. (10.15), we obtain

$$\Phi = P\vartheta + Q, \tag{10.16}$$

where

$$P = -\bar{V} \cos \alpha_{\text{в}} \sin(\theta - \vartheta), \quad Q = \bar{r} \sin(\theta - \vartheta - \psi). \tag{10.17}$$

Substituting Eq. (10.16) into Eq. (10.14), and after summing up induced velocities due to the lateral vortices located on the surface defined by Eq (10.5), we find the sought formula

$$\bar{v}^{\text{мг}}_{\text{пп}} = \frac{1}{4\pi} \int_{\bar{\varrho}_0}^{1} \int_{0}^{\infty} \frac{\partial \bar{\Gamma}(\bar{\varrho}, \theta - \vartheta)}{\partial (\theta - \vartheta)} \frac{P\vartheta + Q}{(\bar{V}^2 \vartheta^2 + g\vartheta + h)^{3/2}} d(\theta - \vartheta) d\bar{\varrho}. \tag{10.18}$$

INSTANTANEOUS VELOCITY INDUCED BY THE LIFTING LINE

Parametric equations of the lifting line follow from Eq. (10.5) with $\vartheta = 0$; i.e.,

$$\bar{\xi} = -\bar{\varrho}\cos\theta, \quad \bar{\eta} = 0, \quad \bar{\zeta} = \bar{\varrho}\sin\theta. \tag{10.19}$$

Formulae for velocities, induced by the lifting line, can be found from the relationship given by Eq. (A.6) when $p = \bar{\rho}$:

$$\bar{v}_{\text{н}}^{\text{мг}} = \frac{1}{4\pi}\int_{\bar{\varrho}_0}^{1} \bar{\Gamma}(\bar{\varrho}, \theta)\left[\frac{\partial\bar{\zeta}}{\partial\bar{\varrho}}(\bar{x}-\bar{\xi}) - \frac{\partial\bar{\xi}}{\partial\bar{\varrho}}(\bar{z}-\bar{\zeta})\right]\frac{\partial\bar{\varrho}}{\bar{l}^3}. \tag{10.20}$$

Substituting Eqs. (10.19) and (10.10) into Eq. (10.20), we finally get

$$\bar{v}_{\text{н}}^{\text{мг}} = -\frac{1}{4\pi}\int_{\bar{\varrho}_0}^{1} \bar{\Gamma}(\bar{\varrho}, \theta)\frac{\bar{r}\sin(\theta-\psi)}{[\bar{\varrho}^2 + \bar{r}^2 - 2\bar{\varrho}\bar{r}\cos(\theta-\psi)]^{3/2}}d\bar{\varrho}. \tag{10.21}$$

4. TIME-AVERAGED INDUCED VELOCITY (GENERAL CASE $\Gamma = \Gamma(\rho, \theta)$)

VELOCITY INDUCED BY LONGITUDINAL FREE VORTICES

Computation of the time-averaged velocity, induced by the longitudinal vortices of a k-bladed rotor, leads to the determination of the following integral:

$$v_{\text{пр}} = \frac{k}{2\pi}\int_0^{2\pi} \bar{v}_{\text{пр}}^{\text{мг}} d\theta. \tag{10.22}$$

Upon substitution of Eq. (10.13) into Eq. (10.22), we obtain the following triple integral

$$\bar{v}_{\text{пр}} = \frac{k}{8\pi^2}\int_{\bar{\varrho}_0}^{1}\int_0^{\infty}\int_0^{2\pi}\frac{\partial\bar{\Gamma}(\bar{\varrho}, \theta-\vartheta)}{\partial\bar{\varrho}}\frac{G\vartheta + H}{(\bar{V}^2\vartheta^2 + g\vartheta + h)^{3/2}}d\theta d\vartheta d\bar{\varrho}. \tag{10.23}$$

Let us consider the internal integral in Eq. (10.23). On the basis of Eq. (7.4), we neglect parameter ϑ in the arguments of periodic functions in Eq. (10.23). Then, taking into consideration Eq. (10.12), we obtain

$$\bar{v}_{\text{пр}} = \frac{1}{8\pi^2}\int_{\bar{\varrho}_0}^{1}\int_0^{2\pi}\int_0^{\infty}\frac{\partial\bar{\Gamma}(\bar{\varrho}, \theta)}{\partial\bar{\varrho}}\frac{G_1\vartheta + H_1}{[\bar{V}^2\vartheta^2 + 2L_x\bar{V}\vartheta\cos\alpha_{\text{в}} + L^2]^{3/2}}d\vartheta d\theta d\bar{\varrho}, \tag{10.24}$$

where

$$G_1=\bar{V}\bar{\varrho}\cos\theta\cos\alpha_в,\quad H_1=\bar{\varrho}^2-\bar{\varrho}\bar{r}\cos(\theta-\psi)+\bar{V}L_z\cos\alpha_в,$$
$$L_x=\bar{\varrho}\cos\theta-\bar{r}\cos\psi,\quad L_z=\bar{\varrho}\sin\theta-\bar{r}\sin\psi, \tag{10.25}$$
$$L=\sqrt{\bar{\varrho}^2+\bar{r}^2-2\bar{\varrho}\bar{r}\cos(\theta-\psi)}.$$

After some simplifications, the internal integral of Eq. (10.24) is reduced to the following two integrals

$$\left.\begin{aligned}\int_0^\infty\frac{\vartheta d\vartheta}{[\bar{V}^2\vartheta^2+2L_x\bar{V}\vartheta\cos\alpha_в+L^2]^{3/2}}&=\frac{\bar{V}^{-2}}{L+L_x\cos\alpha_в},\\ \int_0^\infty\frac{d\vartheta}{[\bar{V}^2\vartheta^2+2L_x\bar{V}\vartheta\cos\alpha_в+L^2]^{3/2}}&=\frac{(\bar{V}L)^{-1}}{L+L_x\cos\alpha_в}.\end{aligned}\right\} \tag{10.26}$$

Now, we substitute Eq. (10.26) into Eq. (10.24). After some simple transformations, we arrive at the sought formula

$$\bar{v}_{пр}=\frac{k}{8\pi^2\bar{V}}\int_{\bar{\varrho}_0}^{1}\int_0^{2\pi}\frac{\partial\bar{\Gamma}(\bar{\varrho},\theta)}{\partial\bar{\varrho}}\left\{\frac{\bar{r}L_z\bar{\varrho}\sin(\theta-\psi)\cos\alpha_в}{L^2(L+L\cos\alpha_в)}+\right.$$
$$\left.+\frac{L_z\bar{V}\cos\alpha_в}{L(L+L_x\cos\alpha_в)}+\frac{\bar{\varrho}^2-\bar{\varrho}\bar{r}\cos(\theta-\psi)}{L^2}\right\}d\theta d\bar{\varrho}. \tag{10.27}$$

VELOCITIES INDUCED BY LATERAL VORTICES AND LIFTING LINES

Time-averaged velocity, induced by the lateral vortices of a k-bladed rotor, is given by the following relationship

$$\bar{v}_{пп}=\frac{k}{2\pi}\int_0^{2\pi}\bar{v}_{пп}^{мг}d\theta. \tag{10.28}$$

Substituting Eq. (10.18) into Eq. (10.27), and taking advantage of the property expressed by Eq. (7.4), we obtain

$$\bar{v}_{пп}=\frac{k}{8\pi^2}\int_{\bar{\varrho}_0}^{1}\int_0^{2\pi}\int_0^{\infty}\frac{\partial\bar{\Gamma}(\bar{\varrho},\theta)}{\partial\theta}\,\frac{\bar{r}\sin(\theta-\psi)-\bar{V}\vartheta\sin\theta\cos\alpha_в}{[\bar{V}^2\vartheta^2+2L_x\bar{V}\vartheta\cos\alpha_в+L^2]^{3/2}}\,d\vartheta d\theta d\bar{\varrho}.$$

As in the preceding case, the integral with respect to the variable ϑ is determined analytically. Taking into consideration Eq. (10.26), we finally obtain

$$\bar{v}_{пп}=\frac{k}{8\pi^2\bar{V}}\int_{\bar{\varrho}_0}^{1}\int_0^{2\pi}\frac{\partial\bar{\Gamma}(\bar{\varrho},\theta)}{\partial\theta}\left\{\frac{\bar{r}}{L}\sin(\theta-\psi)-\sin\theta\cos\alpha_в\right\}\frac{d\theta d\bar{\varrho}}{L+L_x\cos\alpha_в}. \tag{10.29}$$

On the basis of Eq. (10.21), the time average of velocity induced by the lifting lines will be

$$\bar{v}_{\text{н}} = -\frac{k}{8\pi^2}\int_{\bar{\varrho}_0}^{1}\int_{0}^{2\pi}\bar{\Gamma}(\bar{\varrho},\,\theta)\,\frac{\bar{r}\sin(\theta-\psi)}{[\bar{\varrho}^2+\bar{r}^2-2\bar{\varrho}\bar{r}\cos(\theta-\psi)]^{3/2}}\,d\theta d\bar{\varrho}. \tag{10.30}$$

Finally, induced velocity generated by the vortex system of a rotor can be expressed as

$$\bar{v} = \bar{v}_{\text{пр}} + \bar{v}_{\text{пп}} + \bar{v}_{\text{н}}, \tag{10.31}$$

where the components are defined by Eqs. (10.27), (10.29) and (10.30).

5. TIME-AVERAGED INDUCED VELOCITY (PARTICULAR CASE $\Gamma = \Gamma(\rho)$)

In practical computations performed on the basis of the disc theory, it is often assumed that circulation of the lifting line remains constant with the blade azimuth angle. It is well known that the above assumption does not introduce any appreciable errors to calculations of induced velocities at low μ's, while considerably simplifying the analysis. We want to emphasize that this assumption is applied only to the determination of induced velocities which, in turn, are used for calculations of the actual angles of attack of blade airfoil sections and variable circulation $\bar{\Gamma}(\bar{\rho},\theta)$ which are necessary for computations of rotor characteristics.

Under the condition of $\bar{\Gamma} = \bar{\Gamma}(\bar{\rho})$, induced velocities due to the lateral vortices and lifting lines become zero, and consequently, Eq. (10.31) assumes the following form:

$$\bar{v} = \frac{k}{4\pi\bar{V}}\int_{\bar{\varrho}_0}^{1}\frac{\partial\bar{\Gamma}}{\partial\bar{\varrho}}\,\Phi_p d\bar{\varrho} + \frac{k}{4\pi\bar{r}}\int_{\bar{\varrho}_0}^{1}\frac{\partial\bar{\Gamma}}{\partial\bar{\varrho}}\,\Phi_q d\bar{\varrho} + \frac{k}{4\pi\bar{V}}\int_{\bar{\varrho}_0}^{1}\frac{\partial\bar{\Gamma}}{\partial\bar{\varrho}}\,\Phi_r d\bar{\varrho}\ldots, \tag{10.32}$$

where

$$\Phi_p = \frac{1}{2\pi}\int_{0}^{2\pi}\frac{\bar{r}L_z\bar{\varrho}\sin(\theta-\psi)\cos\alpha_{\text{в}}}{L^2(L+L_x\cos\alpha_{\text{в}})}\,d\theta, \tag{10.33}$$

$$\Phi_q = \frac{1}{2\pi}\int_{0}^{2\pi}\frac{\bar{r}\,L_z\cos\alpha_{\text{в}}}{L\,(L+L_x\cos\alpha_{\text{в}})}\,d\theta, \tag{10.34}$$

$$\Phi_r = \frac{1}{2\pi}\int_{0}^{2\pi}\frac{\bar{\varrho}^2-\bar{\varrho}\bar{r}\cos(\theta-\psi)}{\bar{\varrho}^2+\bar{r}^2-2\bar{\varrho}\bar{r}\cos(\theta-\psi)}\,d\theta. \tag{10.35}$$

The integral (Eq. 10.35)) is determined analytically. It should be noted that $\Phi_r = 0,5(1 + J_r)$, where

$$J_r = \frac{1}{2\pi} \int_0^{2\pi} \frac{\bar{\varrho}^2 - \bar{r}^2}{\bar{\varrho}^2 + \bar{r}^2 - 2\bar{\varrho}\bar{r}\cos(\theta - \psi)} d\theta$$

is the Poisson integral expressed by equalities

$$J_r = \begin{cases} 1 & \text{for } \bar{\varrho} > \bar{r}, \\ 0 & \text{for } \bar{\varrho} = \bar{r}, \\ -1 & \text{for } \bar{\varrho} < \bar{r}. \end{cases}$$

Therefore,

$$\Phi_r = \begin{cases} 1 & \text{for } \bar{\varrho} > \bar{r}, \\ \frac{1}{2} & \text{for } \bar{\varrho} = \bar{r}, \\ 0 & \text{for } \bar{\varrho} < \bar{r}. \end{cases} \tag{10.36}$$

Consequently, if we now define the third component in Eq. (10.32) as $\bar{v}_r$, then

$$\bar{v}_r = \frac{k}{4\pi\bar{V}} \int_{\bar{r}}^{0} \frac{\partial\bar{\Gamma}}{\partial\bar{\varrho}} d\bar{\varrho} = -\frac{k\bar{\Gamma}(\bar{r})}{4\pi\bar{V}}. \tag{10.37}$$

Let us explain the physical meaning of Eq. (10.37). In order to do this, we calculate induced velocity averaged over a circle of radius $\bar{r}$. Taking advantage of Eq. (10.32), we obtain

$$\frac{1}{2\pi} \int_{-\pi}^{\pi} \bar{v} d\psi = \frac{k}{4\pi\bar{V}} \int_{\bar{\varrho}_0}^{1} \frac{\partial\bar{\Gamma}}{\partial\bar{\varrho}} \Psi_p d\bar{\varrho} + \frac{k}{4\pi\bar{r}} \int_{\bar{\varrho}_0}^{1} \frac{\partial\bar{\Gamma}}{\partial\bar{\varrho}} \Psi_q d\bar{\varrho} + \bar{v}_r, \tag{10.38}$$

where

$$\Psi_p = \frac{1}{4\pi^2} \int_{-\pi}^{\pi} \int_{-\pi}^{\pi} \frac{\bar{r} L_z \bar{\varrho} \sin(\theta - \psi)\cos\alpha_в}{L^2 (L + L_x \cos\alpha_в)} d\theta d\psi, \tag{10.39}$$

$$\Psi_q = \frac{1}{4\pi^2} \int_{-\pi}^{\pi} \int_{-\pi}^{\pi} \frac{\bar{r} L_z \cos\alpha_в}{L (L + L_x \cos\alpha_в)} d\theta d\psi. \tag{10.40}$$

Taking into consideration the relationships of Eq. (10.25), we see that by changing the variables θ and ψ respectively, to $-\theta$, $-\psi$, the subintegral function in Eq. (10.40) only changes

its sign. It is obvious from this that $\Psi_q = 0$. We will show that $\Psi_p = 0$ also. We start from the easily proved identities obtained from Eq. (10.25):

$$L_x = L\cos(\psi+\varphi),\ L_z = L\sin(\psi+\varphi), \tag{10.41}$$

where parameter ϕ is determined from the following formulae

$$\sin\varphi = \frac{1}{L}\bar{\varrho}\sin(\theta-\psi),\quad \cos\varphi = \frac{1}{L}\left[\bar{\varrho}\cos(\theta-\psi)-\bar{r}\right].$$

We substitute Eq. (10.41) into Eq. (10.39) and on the basis of the property expressed by Eq. (7.4), we neglect angle ψ in arguments $(\theta-\psi)$. Hence, on the same basis, we also neglect parameter ϕ. Then the integral in Eq. (10.39) will have the following form:

$$\Psi_p = \frac{1}{4\pi^2}\int_{-\pi}^{\pi}\int_{-\pi}^{\pi}\frac{\bar{\varrho}\bar{r}\sin\theta\sin\psi\cos\alpha_в}{(\bar{\varrho}^2+\bar{r}^2-2\bar{\varrho}\bar{r}\cos\theta)(1+\cos\psi\cos\alpha_в)}\,d\theta d\psi. \tag{10.42}$$

Since the subintegral function in Eq. (10.42) appears odd with respect to θ (or ψ); hence, $\Psi_p = 0$, which had to be proven. Now, Eq. (10.38) will have the form of

$$\bar{v}_r = \frac{1}{2\pi}\int_{-\pi}^{\pi}\bar{v}\,d\psi = -\frac{k\Gamma(\bar{r})}{4\pi\bar{V}}.$$

Consequently, Eq. (10.37) determines induced velocity, averaged over a circle of radius $\bar{r}$ for an arbitrary angle α. It can be seen that this velocity is expressed by the classical Joukowsky formula from his propeller theory (also see Ch. XIV of this book).

Taking into account Eq. (10.37), we rewrite Eq. (10.32) as follows:

$$\bar{v} = -\frac{k\bar{\Gamma}(\bar{r})}{4\pi\bar{V}} + \frac{4}{4\pi\bar{V}}\int_{\bar{\varrho}_0}^{1}\frac{\partial\bar{\Gamma}}{\partial\bar{\varrho}}\Phi_p\,d\bar{\varrho} + \frac{k}{4\pi\bar{r}}\int_{\bar{\varrho}_0}^{1}\frac{\partial\bar{\Gamma}}{\partial\bar{\varrho}}\Phi_q\,d\bar{\varrho}. \tag{10.43}$$

Practical application of Eq. (10.43) is somewhat difficult, since integrals Φ_p and Φ_q cannot be expressed through elementary functions. These integrals can be expressed as combinations of elliptical integrals (or other special functions). However, such relationships would not be convenient for practical applications. For this reason, in calculations we make use of either tables or graphs of auxiliary functions (Eqs. (10.33) and (10.34)) which facilitate the determination of induced velocities. The volume of the graphs or tables can be reduced by rewriting Eqs. (10.33) and (10.34) under the following form:

$$\Phi_p = \frac{1}{2\pi}\int_0^{2\pi} \frac{\tilde{L}_z \tilde{\varrho}\sin(\theta-\psi)\cos\alpha_в}{\tilde{L}^2(\tilde{L}+\tilde{L}_x\cos\alpha_в)}\,d\theta,$$

$$\Phi_q = \frac{1}{2\pi}\int_0^{2\pi} \frac{\tilde{L}_z\cos\alpha_в}{\tilde{L}(\tilde{L}+\tilde{L}_x\cos\alpha_в)}\,d\theta. \qquad (10.44)$$

Here,

$$\tilde{\varrho} = \frac{\bar{\varrho}}{\bar{r}}, \qquad \tilde{L} = \sqrt{1+\tilde{\varrho}^2-2\tilde{\varrho}\cos(\theta-\psi)},$$

$$\tilde{L}_x = \tilde{\varrho}\cos\theta - \cos\psi, \quad \tilde{L}_z = \tilde{\varrho}\sin\theta - \sin\psi.$$

The quantities $\tilde{\rho}$, α and ψ serve as parameters of functions Φ_p and Φ_q where, in addition, the following equalities exist

$$\Phi_p(\psi) = \Phi_p(-\psi), \quad \Phi_q(\psi) = -\Phi_q(-\psi),$$

which also facilitate computations. In particular, it follows from the above that the second term in Eq. (10.43) represents the symmetrical, with respect to the x axis, component of the velocity field, and the third one - antisymmetrical.

Graphs of functions Φ_p and Φ_q are given in Figs. 10.10 - 10.15. These functions at $\bar{\rho} = \bar{r}$ have an integral singularity of the form $\ell n|\bar{\rho} - \bar{r}|$; consequently, in general, improper integrals exist in Eq. (10.43). The sequence of computation of integrals in Eqs. (10.33) and (10.34) with the given function $\bar{\Gamma}(\bar{\rho})$ is as follows. We select $\bar{\rho}$ values and for given value of $\bar{r}$ we determine the corresponding value of $\tilde{\rho}$. Next, from Eq. (10.44) or Figs. 10.10-10.15, we determine values of Φ_p and Φ_q. Now, the integrals in Eq. (10.43) can be computed by any method of numerical integration, with the exclusion of a small region ε around point $\bar{\rho} = \bar{r}$. With sufficient accuracy for practical application, it is possible to assume $\varepsilon = 0{,}04$.

As an illustration of the application of Eq. (10.43), Fig. 10.16 is shown where the field of induced velocities in the plane of rotation is presented for the Mi-6 helicopter in cruising flight ($\mu = 0{,}33$; $\alpha_э = -15°$; $c_T = 0{,}015$).

6. INDUCED VELOCITY AT LOW μ's

We are going to consider the problem of determining induced velocities for the case of very low μ values. Here, it is possible to establish a simple analytical relationship between the induced velocity and angle ψ, and to present a convenient method of calculation.

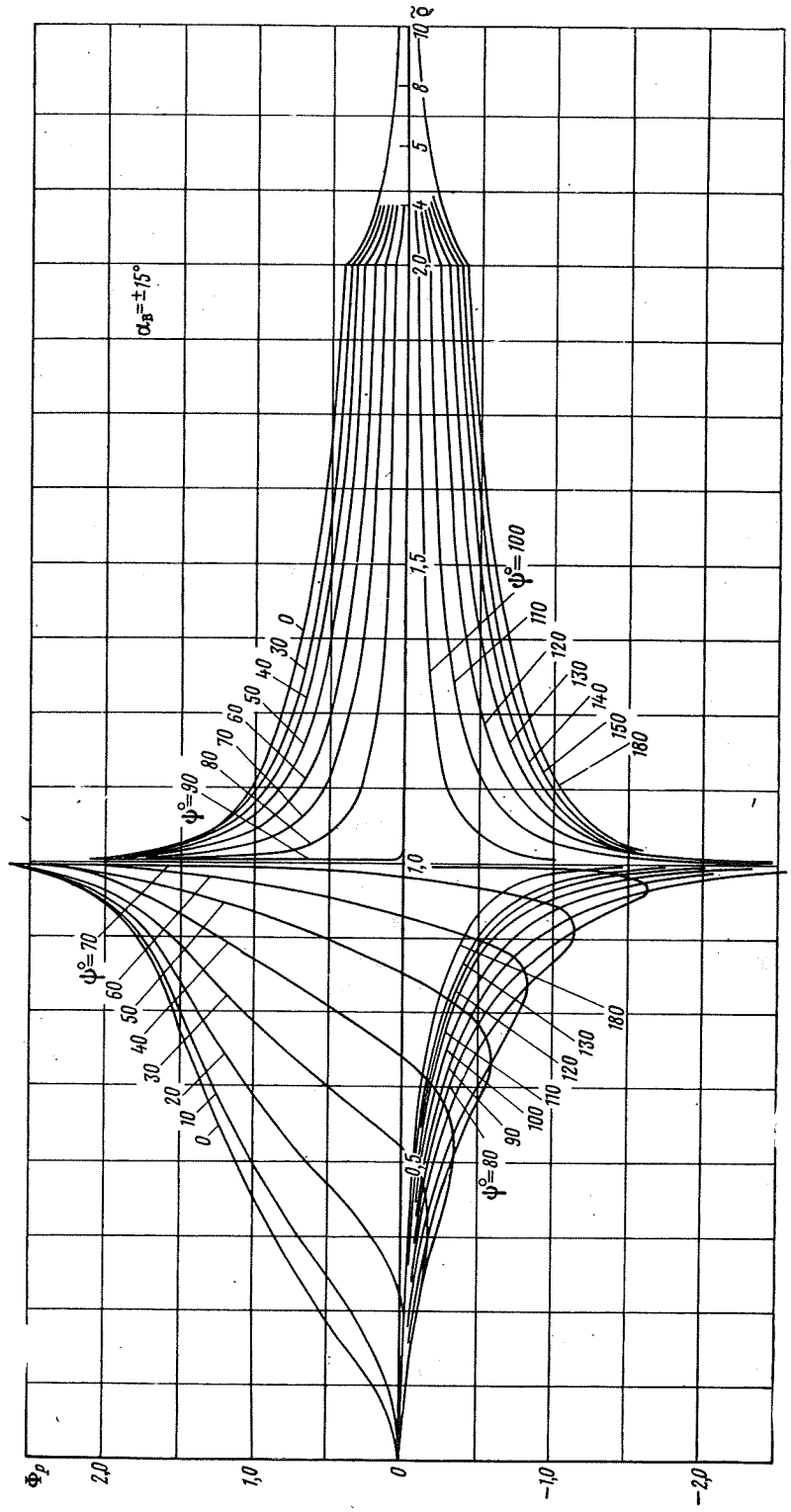
$\bar{c}$
10
8
5
4
2,0
1,5
1,0
0,5
$\alpha_в = \pm 15°$
$\psi° = 0$
30
40
50
60
70
80
90
100
110
120
130
140
150
160
180
Φ_p
2,0
1,0
0
-1,0
-2,0

Figure 10.10

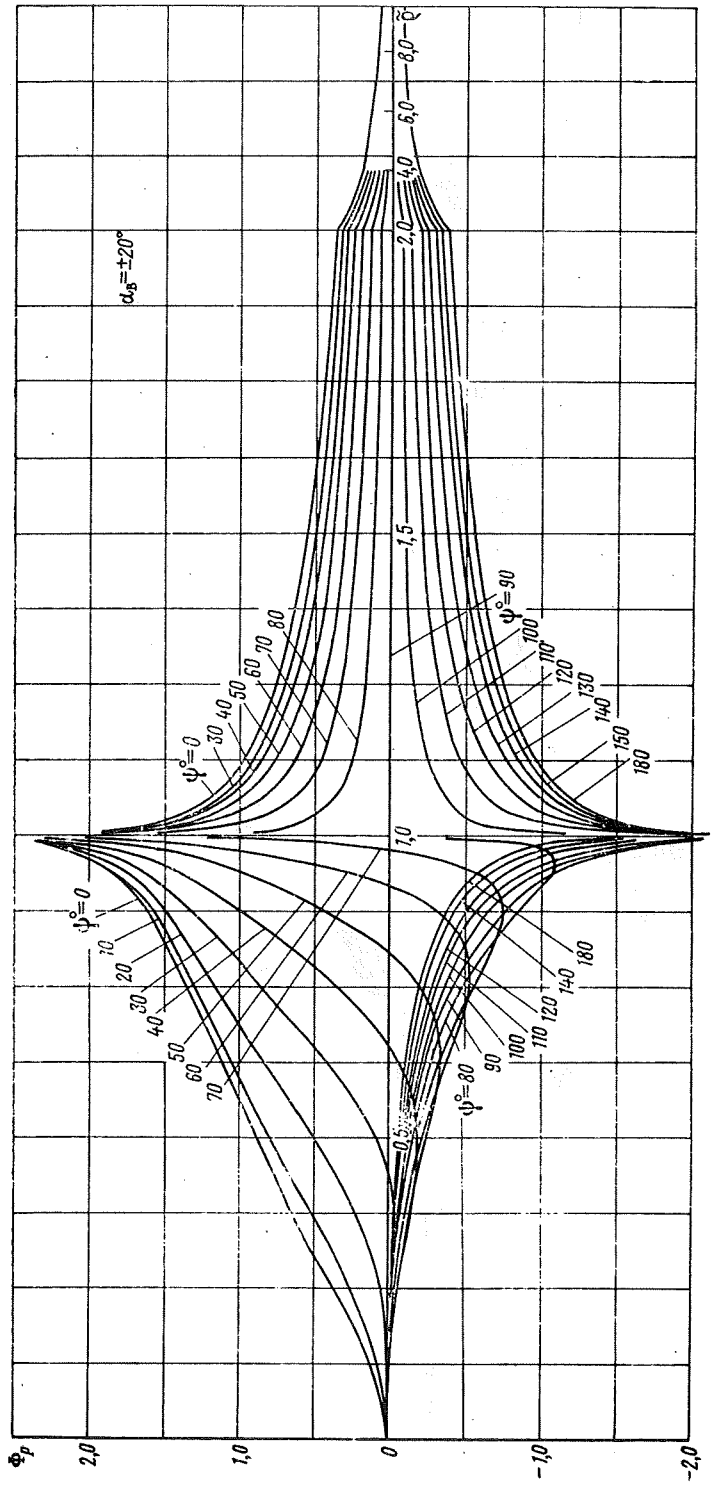
$\alpha_B = \pm 20°$
8,0
6,0
4,0
2,0
1,5
1,0
0,5
0
$\psi° = 0$
10
20
30
40
50
60
70
80
$\psi° = 90$
100
110
120
130
140
150
180
$\psi° = 0$
10
20
30
40
50
60
70
$\psi° = 80$
90
100
110
120
140
180
Φ_p
2,0
1,0
0
-1,0
-2,0

Figure 10.11

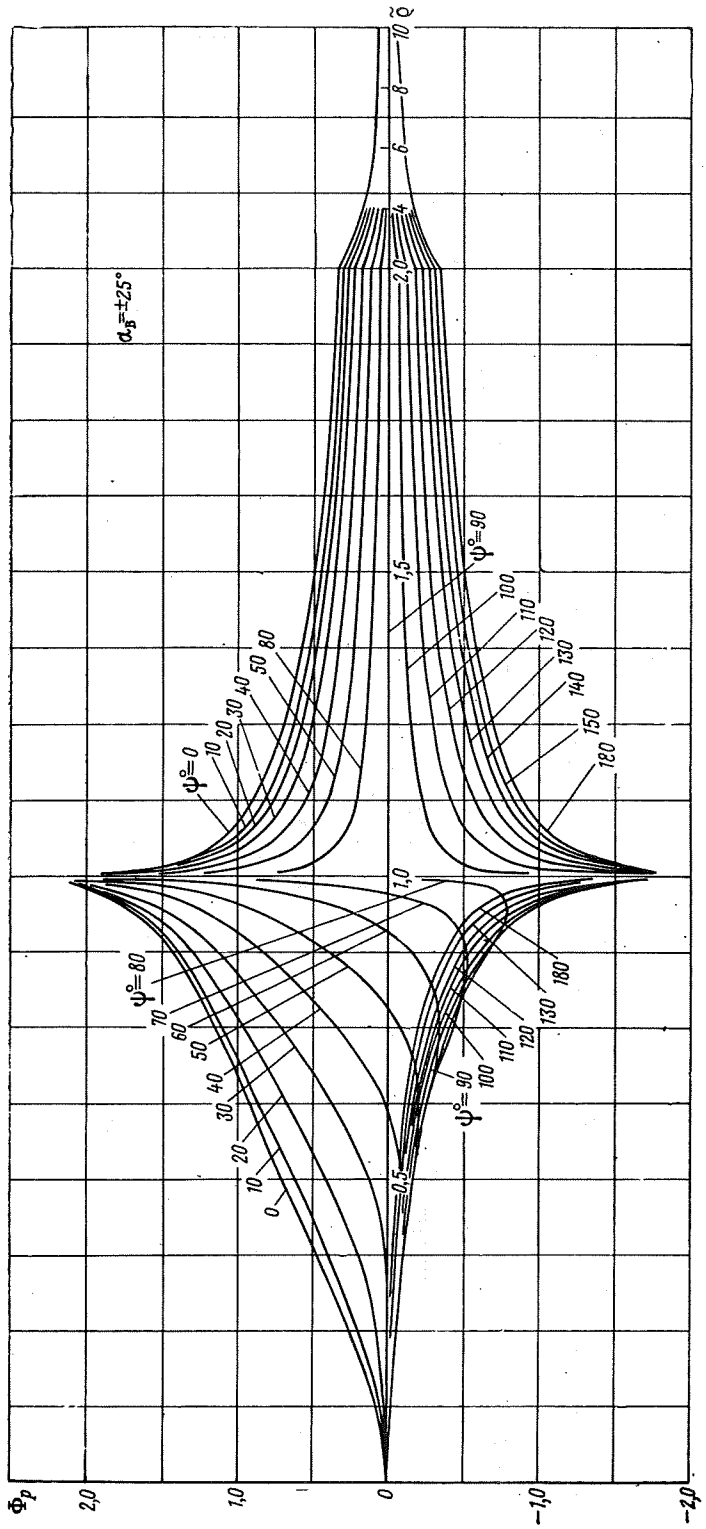
$\tilde{Q}$
10
8
6
4
2,0
1,5
1,0
0,5
$\alpha_B = \pm 25°$
$\psi° = 0$
10
20
30
40
50
80
$\psi° = 90$
100
110
120
130
140
150
180
$\psi° = 80$
70
60
50
40
30
20
10
0
Φ_p
2,0
1,0
0
-1,0
-2,0

Figure 10.12

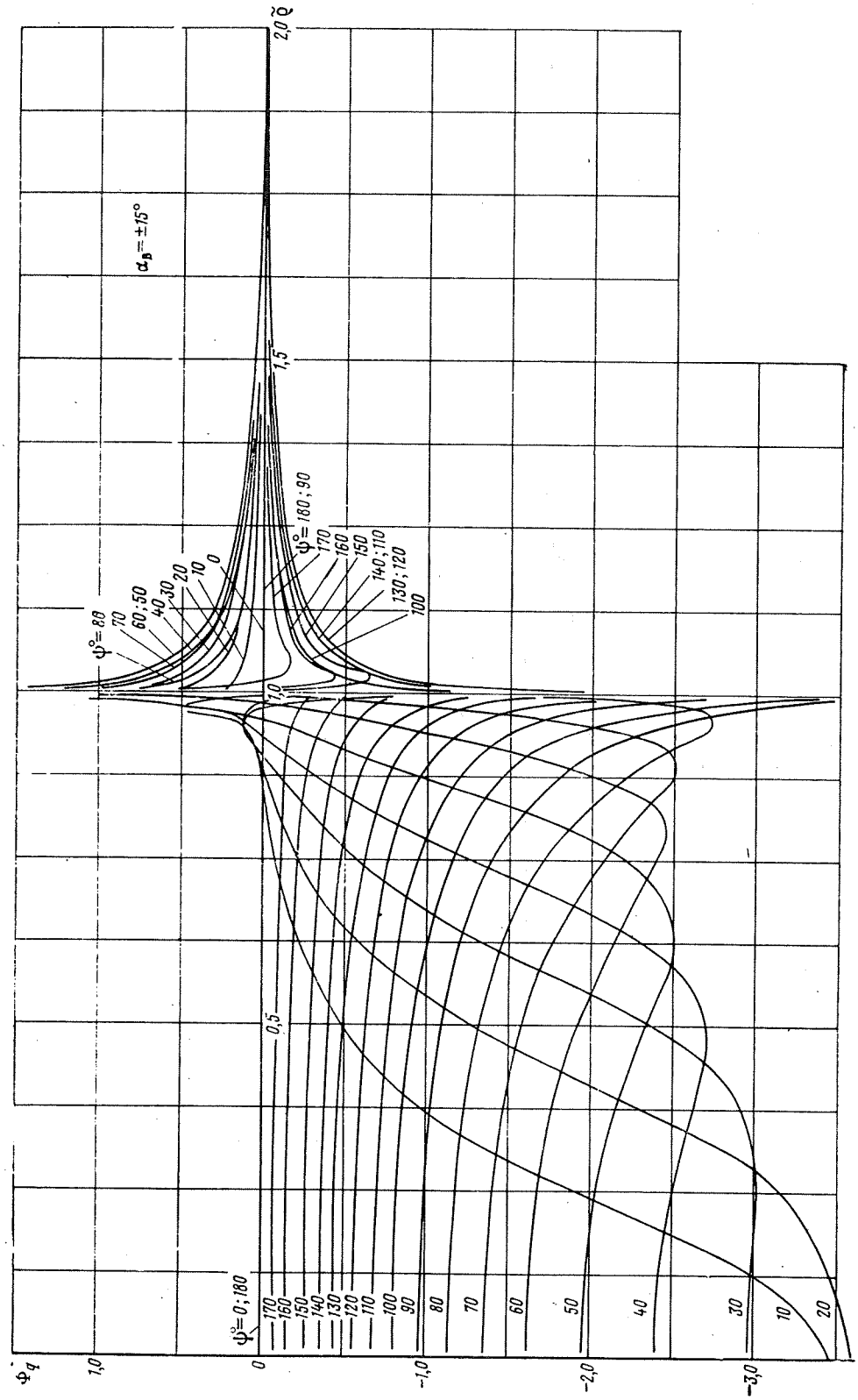
$\bar{\rho}$
2,0
1,5
1,0
0,5
0
-1,0
-2,0
-3,0
Φ_q
1,0
$\alpha_B = \pm 15°$
$\psi° = 180;90$
170
160
150
140;110
130;120
100
$\psi° = 80$
70
60;50
40
30
20
10
0
$\psi° = 0;180$
170
160
150
140
130
120
110
100
90
80
70
60
50
40
30
10
20

Figure 10.13

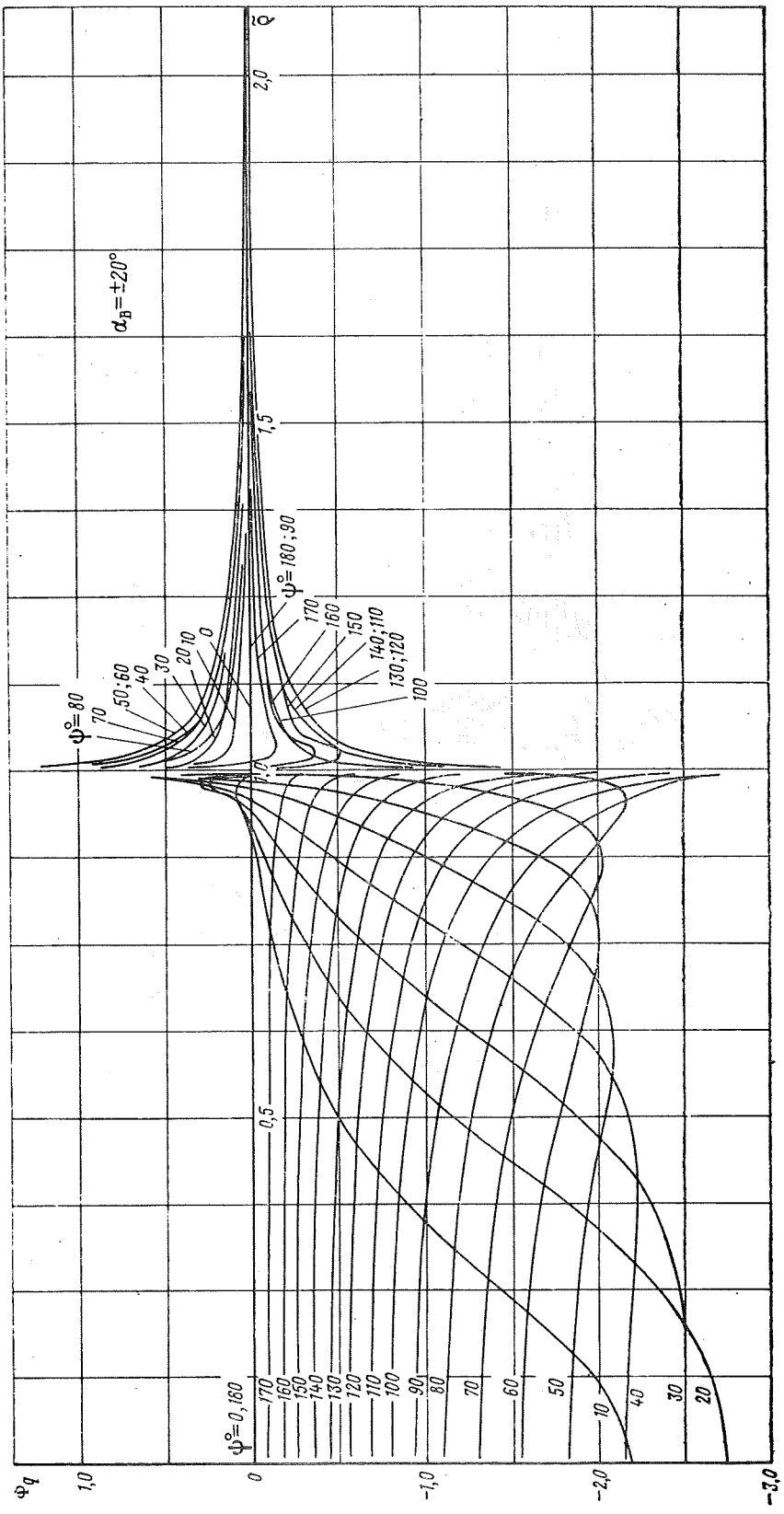
Q
2,0
1,5
1,0
0,5
0
$\alpha_B = \pm 20°$
$\psi° = 180;90$
170
160
150
140;110
130;120
100
$\psi° = 80$
70
50;60
40
30
20
10
0
$\psi° = 0,180$
170
160
150
140
130
120
110
100
90
80
70
60
50
40
30
20
10
Φ_q
1,0
0
-1,0
-2,0
-3,0

Figure 10.14

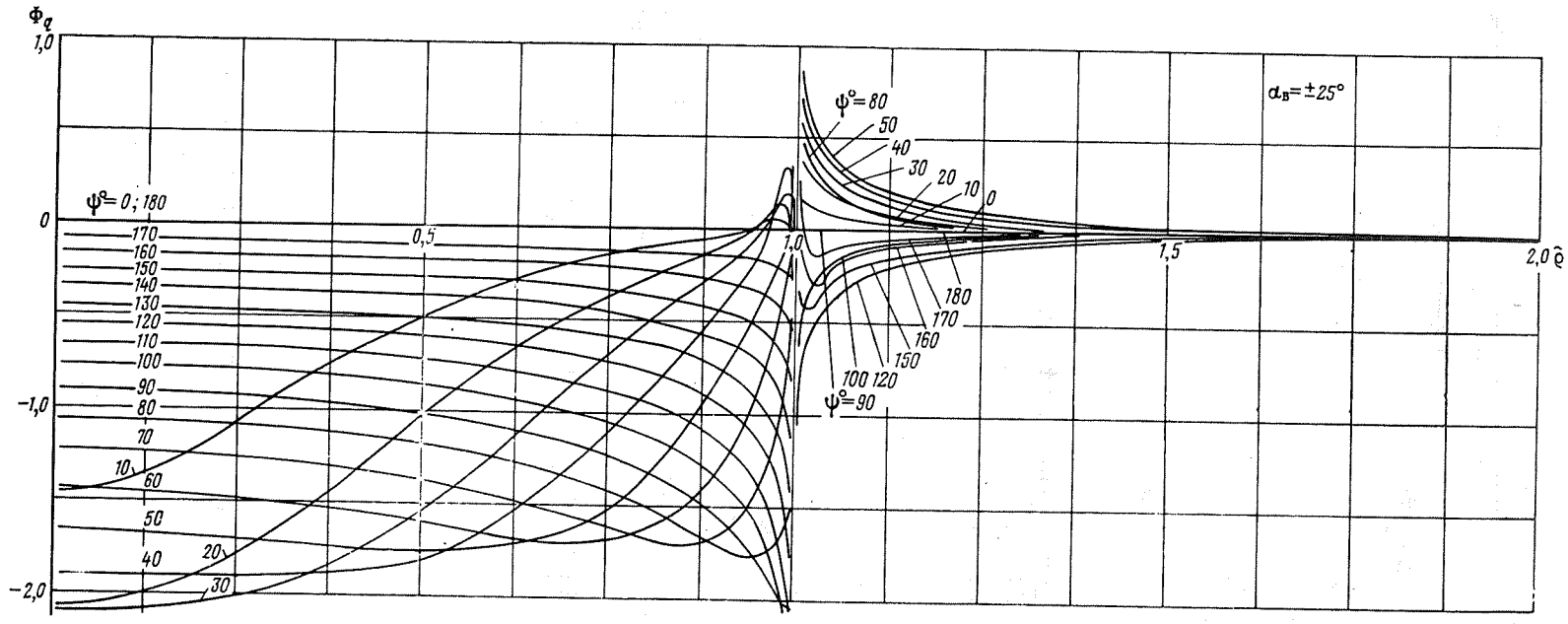
Φ_q
1,0
0
−1,0
−2,0
$\psi^\circ = 0; 180$
170
160
150
140
130
120
110
100
90
80
70
10
60
50
40
20
30
0,5
1,0
1,5
2,0 $\bar{q}$
$\psi^\circ = 80$
50
40
30
20
10
0
$\alpha_B = \pm 25°$
180
170
160
150
100
120
$\psi^\circ = 90$

Figure 10.15

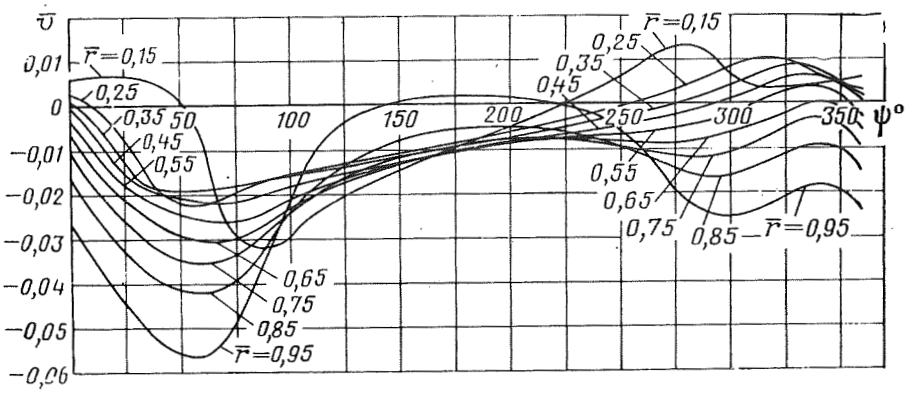

Figure 10.16

Let us concentrate our attention on the determination of integrals in Eqs. (10.33) and (10.34). To facilitate the process of integration, we replace the function

$$R_* = \frac{1}{1 + \frac{L_x}{L}\cos\alpha_в}$$

with an infinite series

$$R_* = \sum_{n=0}^{\infty} (-1)^n \frac{L_x^n}{L^n} \cos^n \alpha_в, \quad n = 0, 1, 2, \ldots \tag{10.45}$$

This expansion makes sense, since $|L_x| \leq L$, $|\cos \alpha_B| < 1$. Assuming that values of $\cos^2\alpha_B$ are small in comparison with unity, we limit the series of Eq. (10.45) to its section containing the first two terms (for $n = 0$ and $n = 1$). Then, integrals of Eqs. (10.33) and (10.34) have the following form:

$$\Phi_p = \frac{1}{2\pi} \int_0^{2\pi} \frac{\bar{r} L_z}{L^3} \left(1 - \frac{L_x}{L}\cos\alpha_в\right) \bar{\varrho} \sin(\theta - \psi) \cos\alpha_в d\theta, \tag{10.46}$$

$$\Phi_q = \frac{1}{2\pi} \int_0^{2\pi} \frac{\bar{r} L_z}{L^2} \left(1 - \frac{L_x}{L}\cos\alpha\right) \cos\alpha_в d\theta. \tag{10.47}$$

We break the integral in Eq. (10.46) down into two components

$$\Phi_p = \frac{1}{\pi}(f_p \cos\psi - \varphi_p \cos 2\psi \cos\alpha_в)\cos\alpha_в, \tag{10.48}$$

where

$$f_p = \frac{1}{2} \int_0^{2\pi} \frac{\bar{\varrho}^2 \bar{r} \sin^2\theta d\theta}{(\bar{\varrho}^2 + \bar{r}^2 - 2\bar{\varrho}\bar{r}\cos\theta)^{3/2}}, \tag{10.49}$$

$$\varphi_p = \frac{1}{2}\int_0^{2\pi} \frac{(\bar{\varrho}\cos\theta - \bar{r})\,\bar{\varrho}^2\bar{r}\sin^2\theta d\theta}{(\bar{\varrho}^2 + \bar{r}^2 - 2\bar{\varrho}\bar{r}\cos\theta)^2}. \tag{10.50}$$

The integral of Eq. (10.49) can be transformed, with the help of substituting $\theta = \pi + 2\lambda$, into the elliptic integral C:

$$f_p = \frac{8\tilde{\varrho}^2}{(1+\tilde{\varrho})^3}\,\mathrm{C}, \tag{10.51}$$

where

$$\mathrm{C} = \frac{1}{k_1^2}\left\{\left(\frac{2}{k_1^2} - 1\right)\mathrm{K} - \frac{2}{k_1^2}\,\mathrm{E}\right\}.$$

Here, K and E are the complete elliptic integrals of the first and second kind with respect to parameters

$$k_1 = \frac{2\sqrt{\tilde{\varrho}}}{1+\tilde{\varrho}}. \tag{10.52}$$

Graphs of the function given by Eq. (10.51) are shown in Fig. 10.17.

The integral in Eq. (10.50) is determined analytically:

$$\varphi_p = \begin{cases} -\dfrac{\pi}{2}\,\tilde{\varrho}^2 & \text{for } \tilde{\varrho} < 1, \\ -\dfrac{\pi}{4} & \text{for } \tilde{\varrho} = 1, \\ 0 & \text{for } \tilde{\varrho} > 1. \end{cases} \tag{10.53}$$

We now turn our attention to the integral of Eq. (10.47). Let us represent it as

$$\Phi_q = \frac{1}{2\pi}(f_q \sin\psi - \varphi_q \sin 2\psi \cos\alpha_в)\cos\alpha_в, \tag{10.54}$$

where

$$f_q = \int_0^{2\pi} \frac{\bar{\varrho}\bar{r}\cos\theta - \bar{r}^2}{\bar{\varrho}^2 + \bar{r}^2 - 2\bar{\varrho}\bar{r}\cos\theta}\,d\theta, \tag{10.55}$$

$$\varphi_q = \frac{1}{2}\int_0^{2\pi} \frac{\bar{r}d\theta}{\sqrt{\bar{\varrho}^2 + \bar{r}^2 - 2\bar{\varrho}\bar{r}\cos\theta}} - 2f_p. \tag{10.56}$$

As a result of integrating Eq. (10.55), we find

$$f_q=\begin{cases}0 & \text{for} \quad \tilde{\varrho}>1,\\ -\pi & \text{for} \quad \tilde{\varrho}=1,\\ -2\pi & \text{for} \quad \tilde{\varrho}<1.\end{cases} \tag{10.57}$$

The integral in Eq. (10.56) leads to the complete elliptic integral of the first kind; hence,

$$\varphi_q=\frac{2}{1+\tilde{\varrho}}K-2f_p. \tag{10.58}$$

Graphs of function ϕ_q are given in Fig. 10.18.

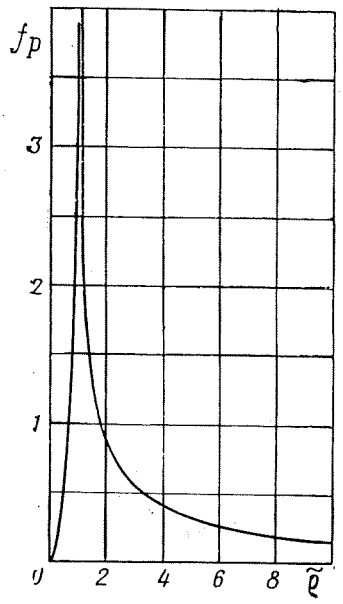

Figure 10.17

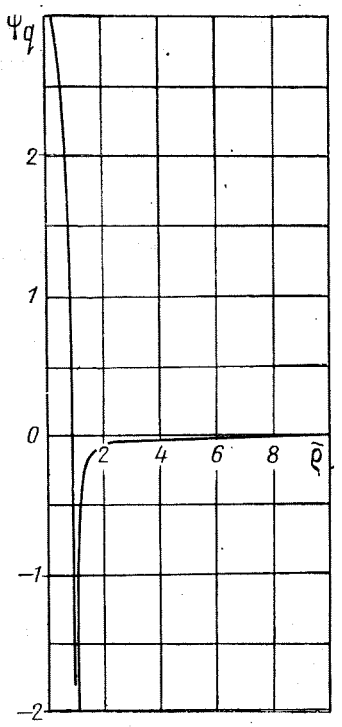

Figure 10.18

Substituting Eqs. (10.48), (10.53), (10.54) and (10.57) into Eq. (10.43), we find the desired formulae for induced velocities at low μ values

$$\bar{v}=\frac{k}{4\pi\bar{V}}\left\{(F\cos\psi+G\cos 2\psi\cos\alpha_в)\cos\alpha_в-\right.$$
$$\left.-\frac{1}{\bar{r}}\left[(\bar{r}+\mu\sin\psi)\,\Gamma(\bar{r})+\mu H\sin 2\psi\cos\alpha_в\right]\right\}, \tag{10.59}$$

where $F = F(\bar{r})$, $G = G(\bar{r})$ and $H = H(\bar{r})$ are functions of the same parameter $\bar{r}$ and are determined by the following integrals

$$F=\frac{1}{\pi}\int_{\bar{\varrho}_0}^{1}\frac{\partial\bar{\Gamma}}{\partial\bar{\varrho}}f_p d\bar{\varrho}, \tag{10.60}$$

$$G=\frac{1}{2}\int_{\bar{\varrho}_0}^{\bar{r}}\frac{\partial\bar{\Gamma}}{\partial\bar{\varrho}}\tilde{\varrho}^2 d\bar{\varrho}, \tag{10.61}$$

$$H=\frac{1}{2\pi}\int_{\bar{\varrho}_0}^{1}\frac{\partial\bar{\Gamma}}{\partial\bar{\varrho}}\varphi_q d\bar{\varrho}. \tag{10.62}$$

In practical calculations, a continuous representation of $\bar{\Gamma}(\bar{\rho})$ is often approximated by the finite steps approach, assuming that between closely located points i and $i+1$, circulation of the lifting line may be considered as constant. Functions given by Eqs. (10.60)-(10.62) are determined at points $j\,(j=1,2,3,\ldots,m)$, located between points i. Then, integrals of Eqs. (10.60) and (10.62) have the following form:

$$F_j=\frac{1}{\pi}\sum_{i=1}^{m}f_{ij}\bar{\Gamma}_i,\quad H_j=\frac{1}{2\pi}\sum_{i=1}^{m}\varphi_{ij}\bar{\Gamma}_i, \tag{10.63}$$

where

$$f_{ij}=f_p(\tilde{\varrho}_j)-f_p(\tilde{\varrho}_{i+1}),\quad \varphi_{ij}=\varphi_q(\tilde{\varrho}_i)-\varphi_q(\tilde{\varrho}_{i+1}),\quad \tilde{\varrho}_i=\bar{\varrho}_i/\bar{r}_j.$$

Numerical coefficients f_{ij} and ϕ_{ij} are determined with the help of Eqs. (10.51) and (10.58).

After making necessary calculations for $\bar{\rho}_0 = 0{,}2$; $m = 10$ and equally-spaced distribution at points i and j along the blade radius, we developed tables of values for coefficients f_{ij} and ϕ_{ij} (Tables 10.1 and 10.3).

The function of Eq. (10.61) can be presented under the following form

$$G_j=\sum_{i=1}^{j}g_{ij}\bar{\Gamma}_i \tag{10.64}$$

or in the expanded form,

$$G_1 = g_{11}\bar{\Gamma}_1,$$

$$G_2 = g_{12}\bar{\Gamma}_1 + g_{22}\bar{\Gamma}_2,$$

$$G_3 = g_{13}\bar{\Gamma}_1 + g_{23}\bar{\Gamma}_2 + g_{33}\bar{\Gamma}_3,$$

$$\cdots\cdots\cdots\cdots$$

$$G_m = g_{1m}\bar{\Gamma}_1 + g_{2m}\bar{\Gamma}_2 + g_{3m}\bar{\Gamma}_3 + \ldots + g_{mm}\bar{\Gamma}_m.$$

Numerical coefficients g_{ij} are determined according to Eq. (10.61) as follows:

$$g_{ij} = \begin{cases} (\bar{\varrho}_i^2 - \bar{\varrho}_{i+1}^2)/2\bar{r}_j & \text{for } i < j, \\ \bar{\varrho}_i^2/2\bar{r}_j & \text{for } i = j, \\ 0 & \text{for } i > j. \end{cases} \tag{10.65}$$

After performing computations of the coefficients given by Eq. (10.65) for the above-defined conditions, we obtain a triangular matrix of numerical values of g_{ij} (see Table 10.2). For given values of $\bar{\Gamma}_i$, the functions given by Eqs. (10.63 and (10.64) can be easily determined with the help of Tables 10.1 and 10.2. Then, the sought induced velocity $\bar{v}_j = \bar{v}_j(\bar{r}_j, \psi)$ is determined, according to Eq. (10.59), as follows:

$$\bar{v}_j = \frac{k}{4\pi\bar{V}} \left\{ (F_j \cos\psi + G_j \cos 2\psi \cos\alpha_в) - \right.$$

$$\left. - \frac{1}{\bar{r}_j} \left[(\bar{r}_j + \mu \sin\psi)\, \Gamma(\bar{r}_j) + \mu H_j \sin 2\psi \cos\alpha_в \right] \right\}.$$

The obtained solutions for induced velocity consider only the first two terms of the series in Eq. (10.45) and contain sines and cosines of ψ and 2ψ. If one limits oneself to the first term only of that series, then the well-known solution of G.I. Maykapar which contains only $\sin\psi$ and $\cos\psi$ will be obtained. This solution can be directly obtained from Eq. (10.59) by neglecting in it the terms with $\sin 2\psi$ and $\cos 2\psi$. When the third term in the series of Eq. (10.45) is considered, then the solution would contain terms with $\sin 3\psi$ and $\cos 3\psi$. In general, consideration of the nth term in the series (Eq. (10.45)) would lead to the appearance of $\sin n\psi$ and $\cos n\psi$. An increase of the number of considered terms in Eq. (10.45) means an expansion of the range of μ values included in the

Values of Coefficients f_{ij}

$\bar{r}_j$ \ i	1	2	3	4	5	6	7	8	9	10
0,24 (j=1)	—0,510	0,865	0,315	0,175	0,128	0,094	0,068	0,051	0,044	0,035
0,32 (j=2)	—1,208	—0,440	0,915	0,335	0,200	0,137	0,098	0,077	0,063	0,053
0,40 (j=3)	—0,557	—1,185	—0,400	1,022	0,288	0,224	0,131	0,110	0,083	0,065
0,48 (j=4)	—0,350	—0,590	—1,180	—0,430	1,100	0,330	0,230	0,150	0,110	0,095
0,56 (j=5)	—0,251	—0,352	—0,590	—1,170	—0,530	1,200	0,390	0,220	0,160	0,120
0,64 (j=6)	—0,177	—0,255	—0,385	—0,520	—1,170	—0,550	1,180	0,450	0,190	0,160
0,72 (j=7)	—0,125	—0,208	—0,267	—0,375	—0,550	—1,170	—0,510	1,130	0,560	0,220
0,80 (j=8)	—0,100	—0,153	—0,207	—0,273	—0,392	—0,541	—1,180	—0,354	1,118	0,442
0,88 (j=9)	—0,083	—0,122	—0,173	—0,197	—0,290	—0,395	—0,520	—1,190	—0,365	1,115
0,96 (j=10)	—0,072	—0,093	—0,140	—0,170	—0,210	—0,295	—0,380	—0,535	—1,190	—0,265

TABLE 10.1

Values of Coefficients g_{ij}

$\bar{r}_j$ \ i	1	2	3	4	5	6	7	8	9	10
0,24	0,347									
0,32	—0,187	0,382								
0,4	—0,120	—0,160	0,405							
0,48	—0,083	—0,111	—0,139	0,420						
0,56	—0,061	—0,082	—0,102	—0,122	0,431					
0,64	—0,047	—0,062	—0,078	—0,094	—0,109	0,438				
0,72	—0,037	—0,049	—0,062	—0,074	—0,087	—0,098	0,444			
0,8	—0,030	—0,040	—0,050	—0,060	—0,071	—0,080	—0,090	0,453		
0,88	—0,025	—0,033	—0,041	—0,050	—0,058	—0,066	—0,074	—0,083	0,456	
0,96	—0,021	—0,028	—0,035	—0,042	—0,049	—0,055	—0,062	—0,069	—0,076	0,458

TABLE 10.2

Values of Coefficients ϕ_{ij}

$\bar{r}_j$ \ i	1	2	3	4	5	6	7	8	9	10
0,24 (j=1)	1,400	—0,337	—0,073	—0,033	—0,014	—0,006	—0,004	—0,002	—0,001	—0
0,32 (j=2)	1,700	1,300	—0,690	—0,080	—0,047	—0,025	—0,011	—0,007	—0,003	—0,002
0,40 (j=3)	0,813	1,617	1,250	—0,895	—0,093	—0,050	—0,032	—0,020	—0,011	—0,007
0,48 (j=4)	0,580	0,712	1,570	1,238	—1,060	—0,105	—0,058	—0,033	—0,029	—0,015
0,56 (j=5)	0,320	0,480	0,910	1,530	1,060	—1,100	—0,140	—0,060	—0,035	—0,028
0,64 (j=6)	0,220	0,320	0,530	0,800	1,490	1,060	—1,100	—0,145	—0,075	—0,035
0,72 (j=7)	0,170	0,260	0,340	0,520	0,780	1,480	0,950	—1,050	—0,220	—0,080
0,80 (j=8)	0,140	0,190	0,270	0,380	0,560	0,790	1,460	0,800	—1,000	—0,300
0,88 (j=9)	0,120	0,150	0,220	0,280	0,370	0,560	0,900	1,400	0,600	—0,820
0,96 (j=10)	0,100	0,120	0,170	0,220	0,320	0,380	0,520	0,840	1,380	0,600

TABLE 10.3

obtained result. With increasing μ values (decrease of $|\alpha_B|$), the complexity of the structure of the induced velocity field increases, which leads to more complicated computational formulae. This problem is discussed in greater detail in the following section.

7. HARMONICS OF INDUCED VELOCITY (CASE OF $\Gamma = \Gamma(\rho)$)

We are going to consider an analytical method of induced velocity calculations along the lines of the disc theory of G.I. Maykapar. Velocity is presented in the form of Fourier Series. Coefficients of that series will be determined directly from the integral relationship for the induced velocity which later will be represented under a form of special functions.

The difficulty of that transformation is due to the fact that these expressions have no visible connections with the known integral representation of special functions. In conjunction with this, in order to achieve a transformation of the integral expressions into special functions, the hypergeometric equation of Gauss was used, the particular solutions of which form a large class of special functions.

If an assumption that the obtained integrals belong to that class is correct, then they must represent solutions of the Gauss equation. It turned out that under the defined conditions imposed on the parameters of the Gauss equation, and with a special selection of the independent variable, the expressions for coefficients appear to be the solutions of this equation and consequently, they are hypergeometric functions. It became evident that those functions are the Legendre functions which, depending on the number of velocity harmonics, change either into the Legendre polynomial or into the Legendre functions of the first and second kind which, in turn, can be represented through the complete elliptic integrals of the first and second kind. In this way, new integral representations of the Legendre polynomials and functions are developed. Transition to the Legendre functions considerably simplifies methods of calculations, since it permits one to take advantage of their useful properties and, in particular, of the recurring relationships.

INTEGRAL REPRESENTATION OF THE INDUCED VELOCITY HARMONICS

Let us represent induced velocity through the Fourier series

$$\bar{v}=\bar{v}_r+\sum_{n=1}^{\infty}\{\bar{v}_{cn}\cos n\psi+\bar{v}_{sn}\sin n\psi\} \tag{10.66}$$

and define the coefficients

$$\bar{v}_{cn}=\frac{1}{\pi}\int_0^{2\pi}\bar{v}\cos n\psi d\psi;\quad \bar{v}_{sn}=\frac{1}{\pi}\int_0^{2\pi}\bar{v}\sin n\psi d\psi, \tag{10.67}$$

taking advantage of Eq. (10.43) in which we change functions Φ_p and Φ_q to the following form

where
$$\Phi_p=\frac{1}{2\pi}\int_0^{2\pi}\frac{L_z\bar{\varrho}\sin\theta\cos\alpha_в}{L^2(L+L_x\cos\alpha_в)}d\theta;\quad \Phi_q=\frac{1}{2\pi}\int_0^{2\pi}\frac{L_z\cos\alpha_в}{L(L+L_x\cos\alpha_в)}d\theta,$$

$$\left.\begin{aligned} L_x&=(\tilde{\varrho}\cos\theta-1)\cos\psi-\tilde{\varrho}\sin\theta\sin\psi,\\ L_z&=(\tilde{\varrho}\cos\theta-1)\sin\psi+\tilde{\varrho}\sin\theta\cos\psi,\quad L=\sqrt{1+\tilde{\varrho}^2-2\tilde{\varrho}\cos\theta}. \end{aligned}\right\} \tag{10.68}$$

First, we integrate Eq. (10.67) with respect to ψ. In order to do this, we introduce

$$t=\psi+\varphi, \tag{10.69}$$

where the auxiliary parameter ϕ is found from the following formulae

$$\cos\varphi=\frac{1}{L}(\tilde{\varrho}\cos\theta-1), \quad \sin\varphi=\frac{1}{L}\tilde{\varrho}\sin\theta. \tag{10.70}$$

If we introduce Eq. (10.43) into the relationships of Eq. (10.67) and consider the equalities in Eqs. (10.68)-(10.70), then we obtain

$$\bar{v}_{cn}=-\frac{kK_{\alpha}^{n}}{4\pi\bar{V}}\int_{\bar{\varrho}_0}^{1}\frac{\partial\bar{\Gamma}}{\partial\bar{\varrho}}C_n d\bar{\varrho}, \tag{10.71}$$

$$\bar{v}_{sn}=-\frac{kK_{\alpha}^{n}}{4\pi\bar{r}}\int_{\bar{\varrho}_0}^{1}\frac{\partial\bar{\Gamma}}{\partial\bar{\varrho}}S_n d\bar{\varrho}, \tag{10.72}$$

where

$$K_{\alpha}^{n}=-\frac{1}{2\pi}\int_{0}^{2\pi}\frac{\sin t\sin nt\cos\alpha_{\text{в}}}{1+\cos t\cos\alpha_{\text{в}}}dt, \tag{10.73}$$

$$C_n=\frac{1}{\pi}\int_{0}^{2\pi}\frac{1}{L}\sin\varphi\sin n\varphi d\theta, \quad S_n=\frac{1}{\pi}\int_{0}^{2\pi}\frac{1}{L}\cos n\varphi d\theta. \tag{10.74}$$

The integral in Eq. (10.73) is found in an elementary way

$$K_{\alpha}^{n}=\left(\frac{-\cos\alpha_{\text{в}}}{1+|\sin\alpha_{\text{в}}|}\right)^{n}, \tag{10.75}$$

while it is convenient to present the integrals from Eq. (10.74) as

$$C_n=\frac{1}{\pi}\int_{0}^{\pi}\frac{1}{L}[T_{n-1}(\cos\varphi)-T_{n+1}(\cos\varphi)]\,d\theta, \tag{10.76}$$

$$S_n=\frac{2}{\pi}\int_{0}^{\pi}\frac{1}{L}T_h(\cos\varphi)\,d\theta, \tag{10.77}$$

where $T_n(\cos\phi) = \cos n\phi$ is the Tchebycheff polynomial of the first kind. Transition to the Tchebycheff polynomials is convenient due to the fact that it excludes from the considerations, the second equality in Eq. (10.70). From Eqs. (10.76) and (10.77), the following important conclusion can be drawn:

$$C_n = \frac{1}{2}(S_{n-1} - S_{n+1}), \qquad (10.78)$$

which permits one to establish a simple relationship between the coefficients of Eqs. (10.71) and (10.72):

$$\bar{v}_{cn} = \frac{\bar{r}}{2\bar{V}}\left(K_\alpha \bar{v}_{s,n-1} - \frac{1}{K_\alpha}\bar{v}_{s,n+1}\right). \qquad (10.79)$$

Here, K_α is determined according to Eq. (10.75) for $n=1$.

It follows from Eqs. (10.76) and (10.77) that the kernels C_n and S_n of the integrals in Eqs. (10.71) and (10.72) do not depend on the parameters characterizing the regime of flight.

ANALYTICAL REPRESENTATIONS OF KERNELS S_n FOR UNEVEN NUMBERS $n = 2m + 1$ $(m=0, 1, 2, \ldots)$

The integral in Eq. (10.77) can be transformed into hypergeometric functions. In order to achieve that transformation, we will take advantage of the above-outlined procedure. It is possible to show that the integral in Eq. (10.77) represents a solution of the Gauss equation for the initial conditions of $\eta(0) = -2$, $\eta'(0) = 2m(m+1)$, if $\xi = \tilde{\rho}^2$, $\alpha = -m$, $\beta = m+1$, $\gamma = 1$. In the light of this, the integral of Eq. (10.77) appears as a hypergeometric function of the type

$$S_{2m+1} = \begin{cases} -2F(-m, m+1, 1; \tilde{\varrho}^2) & \text{for } \tilde{\varrho} < 1; \\ 0 & \text{for } \tilde{\varrho} > 1. \end{cases} \qquad (10.80)$$

The function F in Eq. (10.80) is the Legendre polynomial $P_m(x)$ for $x = 1-2\tilde{\rho}^2$. Expression of kernels in Eq. (10.77) through Lengendre polynomials takes the form of

$$S_{2m+1} = \begin{cases} -2P_m(1-2\tilde{\varrho}^2) & \text{for } \tilde{\varrho} < 1, \\ 0 & \text{for } \tilde{\varrho} > 1. \end{cases} \qquad (10.81)$$

For lower values of index m, Eq. (10.81) leads to elementary formulae for the sought kernels

$$\left.\begin{aligned} S_1 &= -2, \\ S_3 &= -2+4\tilde{\varrho}^2, \\ S_5 &= -2+12\tilde{\varrho}^2-12\tilde{\varrho}^4. \end{aligned}\right\} \qquad (10.82)$$

For computation of the kernels at higher values of index m, it is convenient to take advantage of the recurring formula

$$S_{2m+3}=\frac{2m+1}{m+1}(1-2\tilde{\varrho}^2)S_{2m+1}-\frac{m}{m+1}S_{2m-1}, \qquad (10.83)$$

resulting from the theory of Legendre functions. Graphs of functions S_{2m+1} are given in Fig. 10.19

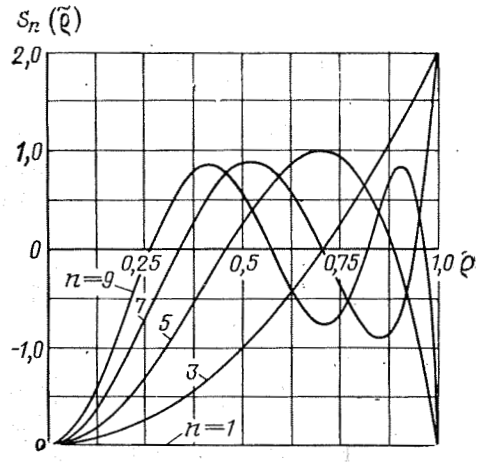

Figure 10.19

INTEGRAL PRESENTATIONS OF LEGENDRE'S POLYNOMIAL

Transformation of kernels S_{2m+1} to the form of Eq. (10.81) leads not only to convenient practical results as in Eqs. (10.82) and (10.83), but also gives the following integral presentation of Legendre's polynomials, containing Tchebycheff's polynomials:

$$P_m(\cos\theta)=-\frac{1}{\pi}\int_0^{\pi} T_{2m+1}(p)\,\frac{d\vartheta}{l},$$

where

$$p=\frac{1}{l}\left(\sin\frac{\theta}{2}\cos\vartheta-1\right), \quad l=\sqrt{1+\sin^2\frac{\theta}{2}-2\sin\frac{\theta}{2}\cos\vartheta},$$

$$0\leqslant\theta\leqslant\pi, \quad m=0,\ 1,\ 2,\ldots$$

$\bar{v}_{sn}$ COEFFICIENTS FOR ODD INDICES n

Since, according to Eq. (10.81), kernels S_{2m+1} for $\tilde{\rho} > 1$ are equal to zero, Eq. (10.72) is transformed to the following form:

$$\bar{v}_{s,2m+1}=\frac{k}{4\pi\bar{r}}\left(\frac{\cos\alpha_{\text{в}}}{1+|\sin\alpha_{\text{в}}|}\right)^{2m+1}\int\limits_{\bar{Q}_0}^{\bar{r}}\frac{\partial\bar{\Gamma}}{\partial\bar{Q}}S_{2m+1}d\bar{Q}. \tag{10.84}$$

In the particular case of $m = 0$, it follows from Eq. (10.84) that for $S_1 = -2$

$$\bar{v}_{s1}=-\frac{k}{2\pi\bar{r}}\frac{\cos\alpha_{\text{в}}}{1+|\sin\alpha_{\text{в}}|}\bar{\Gamma}(\bar{r}). \tag{10.85}$$

This relationship was obtained by Wan Shi-Tzoun by a different method. The results shown in Eq. (10.85) were also obtained earlier, in a different form, by V.Ye. Baskin.

At $m > 0$, the coefficients given by Eq. (10.84) can be simply determined through numerical methods. In order to obtain an analytical solution, we rewrite Eq. (10.84) as follows:

$$\bar{v}_{s\,2m+1}=\frac{k}{2\pi\bar{r}}\left(\frac{\cos\alpha_{\text{в}}}{1+|\sin\alpha_{\text{в}}|}\right)^{2m+1}\int\limits_{-1}^{+1}\frac{\partial\bar{\Gamma}}{\partial x}P_m(x)\,dx, \tag{10.86}$$

where $x = 1 - 2\tilde{\rho}^2$, while the derivative of circulation is expanded into Legendre's polynomials

$$\frac{\partial\bar{\Gamma}}{\partial x}=\sum_{\mu=0}^{\infty}h_\mu P_\mu(x). \tag{10.87}$$

Then, taking into consideration the orthogonality of Legendre's polynomials, on the basis of Eq. (10.86), the following analytical expression is obtained,

$$\bar{v}_{s.2m+1}=\frac{k}{\pi\bar{r}}\frac{h_m}{2m+1}\left(\frac{\cos\alpha_{\text{в}}}{1+|\sin\alpha_{\text{в}}|}\right)^{2m+1},$$

which shows that the coefficient $\bar{v}_{s.\,2m+1}$ is influenced by only one coefficient from the series of Eq. (10.87); namely, that with the index $\mu = m$.

ANALYTICAL REPRESENTATION OF KERNELS S_n FOR EVEN INDICES $n = 2m$

Taking advantage of Gauss equation, as in the transformation of Eq. (10.81), it is possible to show that the integral of Eq. (10.77) can be expressed through the following hypergeometric functions

$$S_{2m}=\begin{cases}2F\left(-m+\frac{1}{2}\,m+\frac{1}{2},\ 1;\ \tilde{\varrho}^2\right) & \text{for } \tilde{\varrho}<1,\\ \frac{(-1)^m(2m-1)!!}{2^{3m-1}m!}\,\tilde{\varrho}^{-2m-1}\,F\left(m+\frac{1}{2},\ m+\frac{1}{2},\ 2m+1;\ \frac{1}{\tilde{\varrho}^2}\right) & \\ & \text{for } \tilde{\varrho}>1,\end{cases} \tag{10.88}$$

which can be written in terms of Legendre's functions of the first and second kind:

$$S_{2m}=\begin{cases}2P_{m-\frac{1}{2}}\left(1-2\tilde{\varrho}^2\right) & \text{for } \tilde{\varrho}<1,\\ (-1)^m\frac{4}{\pi}\,Q_{m-\frac{1}{2}}\left(2\tilde{\varrho}^2-1\right) & \text{for } \tilde{\varrho}>1.\end{cases} \tag{10.89}$$

Presentation of Eq. (10.89) is convenient because the following recurring formula results from it

$$S_{2m+2}=\frac{4m}{2m+1}\left(1-2\tilde{\varrho}^2\right)S_{2m}-\frac{2m-1}{2m+1}\,S_{2m-2}. \tag{10.90}$$

For the convenience of practical calculations, we change the hypergeometric functions of Eq. (10.88) into the complete elliptic integrals of the first and second kinds, postulating that these integrals have the following form:

$$\mathbf{K}(x)=\frac{\pi}{2}\,F\left(\frac{1}{2},\ \frac{1}{2},\ 1;\ x^2\right),\quad \mathbf{E}(x)=\frac{\pi}{2}\,F\left(-\frac{1}{2},\ \frac{1}{2},\ 1;\ x^2\right).$$

Assuming, in Eq. (10.88), that $m = 0$ and $m = 1$, we get the following relationships:

$$S_0=\begin{cases}\frac{4}{\pi}\,\mathbf{K}(\tilde{\varrho}) & \text{for } \tilde{\varrho}<1,\\ \frac{4}{\pi\tilde{\varrho}}\,\mathbf{K}\left(\frac{1}{\tilde{\varrho}}\right) & \text{for } \tilde{\varrho}>1,\end{cases}$$

$$S_2=\begin{cases}\frac{4}{\pi}\left[2\mathbf{E}(\tilde{\varrho})-\mathbf{K}(\tilde{\varrho})\right] & \text{for } \tilde{\varrho}<1,\\ \frac{4}{\pi\tilde{\varrho}}\left[2\tilde{\varrho}^2\mathbf{E}\left(\frac{1}{\tilde{\varrho}}\right)-\left(2\tilde{\varrho}^2-1\right)\mathbf{K}\left(\frac{1}{\tilde{\varrho}}\right)\right] & \text{for } \tilde{\varrho}>1.\end{cases}$$

With the help of the above relationships, the recurring function of Eq. (10.90) permits one to easily determine kernels S_{2m} for any arbitrary natural number m. Graphs of those kernels are shown in Fig. 10.20.

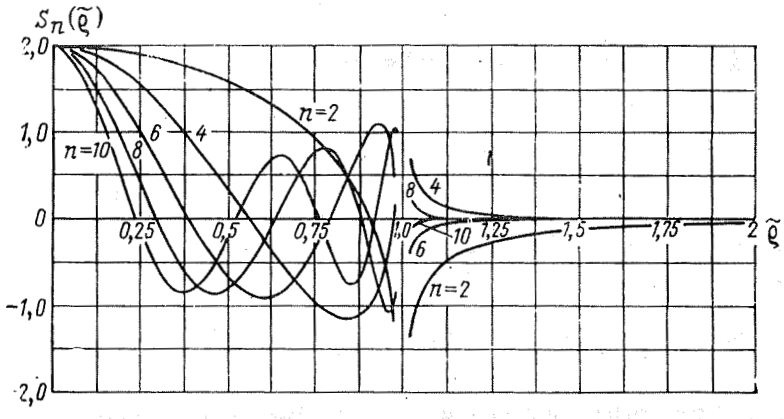

Figure 10.20

INTEGRAL REPRESENTATION OF LEGENDRE'S EQUATIONS WITH HALF-INTEGER INDICES

Transformation of the integral in Eq. (10.77) into a form of Eq. (10.99) permits one to obtain the following representation of Legendre's functions of the first and second kinds:

$$P_{m-\frac{1}{2}}(1-2x^2)=I_{2m}(x) \qquad \text{for } 0 \leqslant x < 1,$$

$$Q_{m-\frac{1}{2}}(2x^2-1)=(-1)^m \frac{\pi}{2} I_{2m}(x) \quad \text{for } x>1,$$

where

$$I_{2m}=\frac{1}{\pi}\int_0^{2\pi} T_{2m}(p)\,\frac{d\vartheta}{l} \quad (m=0,\ 1,\ 2,\ldots).$$

Here, $T_{2m}(p)$ is Tchebycheff's polynomial of the first kind with respect to parameter

$$p=\frac{1}{l}(x\cos\vartheta-1), \quad \text{for } l=\sqrt{1+x-2x\cos\vartheta}.$$

EXPRESSIONS FOR KERNELS C_n

If kernels S_n and coefficients $\overline{v}_{sn}$ have already been computed, then there is no necessity of expressing kernels C_n through special functions and then determining coefficients $\overline{v}_{cn}$ using Eq. (10.71). In order to obtain numerical values of $\overline{v}_{cn}$, it is necessary to use the elementary relationships of Eq. (10.79). Expressing kernels C_n through special functions makes sense, mostly for getting a better insight into the structure of the coefficients $\overline{v}_{cn}$.

For evenly numbered indices $n = 2m$, kernels C_n can be expressed according to Eqs. (10.78) and (10.81) through Legendre's polynomials

$$C_{2m}=\begin{cases}P_m(1-2\tilde{\varrho}^2)-P_{m-1}(1-2\tilde{\varrho}^2) & \text{for } \tilde{\varrho}<1,\\ 0 & \text{for } \tilde{\varrho}>1,\end{cases}$$

which can be unified into Jacoby's polynomial

$$C_{2m}=-2\tilde{\varrho}^2P_{m-1}^{(1,0)}(1-2\tilde{\varrho}^2). \tag{10.91}$$

For low values of index m, Eq. (10.91) yields the following elementary formulae

$$C_2=-2\tilde{\varrho}^2;\quad C_4=-2\tilde{\varrho}^2(2-3\tilde{\varrho}^2);\quad C_6=-2\tilde{\varrho}^2(3-12\tilde{\varrho}^2+10\tilde{\varrho}^4).$$

Kernels C_n for odd indices n can be expressed with the help of Eqs. (10.89) and (10.78) as Jacoby's functions of the first and second kinds which, in turn, are expressed through the complete elliptic integrals. For the lower indexes n, we have

$$C_1=\begin{cases}\frac{4}{\pi}\left[\mathbf{K}(\tilde{\varrho})-\mathbf{E}(\tilde{\varrho})\right] & \text{for } \tilde{\varrho}<1,\\ \frac{4}{\pi}\tilde{\varrho}\left[\mathbf{K}\left(\frac{1}{\tilde{\varrho}}\right)-\mathbf{E}\left(\frac{1}{\tilde{\varrho}}\right)\right] & \text{for } \tilde{\varrho}>1,\end{cases}$$

$$C_3=\begin{cases}\frac{4}{3\pi}\left[(1-4\tilde{\varrho}^2)\mathbf{K}(\tilde{\varrho})-(1-8\tilde{\varrho}^2)\mathbf{E}(\tilde{\varrho})\right] & \text{for } \tilde{\varrho}<1,\\ \frac{4}{3\pi}\tilde{\varrho}\left[(5-8\tilde{\varrho}^2)\mathbf{K}\left(\frac{1}{\tilde{\varrho}}\right)-(1-8\tilde{\varrho}^2)\mathbf{E}\left(\frac{1}{\tilde{\varrho}}\right)\right] & \text{for } \tilde{\varrho}>1.\end{cases}$$

Graphs of kernels C_n are given in Figs. 10.21 and 10.22.

Obtaining simple formulae for the induced velocity harmonics proves the effectiveness of the application of the theory of hypergeometric functions to the airscrew theory. With the help of this approach, it is possible to consider various variations of integral transformations and select from them the most suitable solutions.

8. HARMONICS OF INDUCED VELOCITY (GENERAL CASE $\Gamma = \Gamma(\rho, \theta)$)

Let us represent circulation of a lifting line under the form of Fourier series

$$\bar{\Gamma}=\bar{\Gamma}(\bar{\varrho})+\sum_{\nu=1}^{\infty}\{\bar{\Gamma}_{c\nu}(\bar{\varrho})\cos\nu\theta+\bar{\Gamma}_{s\nu}(\bar{\varrho})\sin\nu\theta\} \tag{10.92}$$

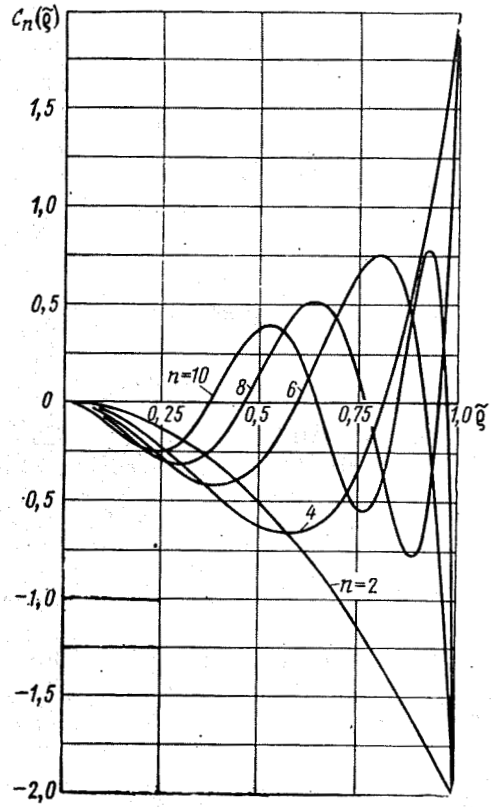

Figure 10.21

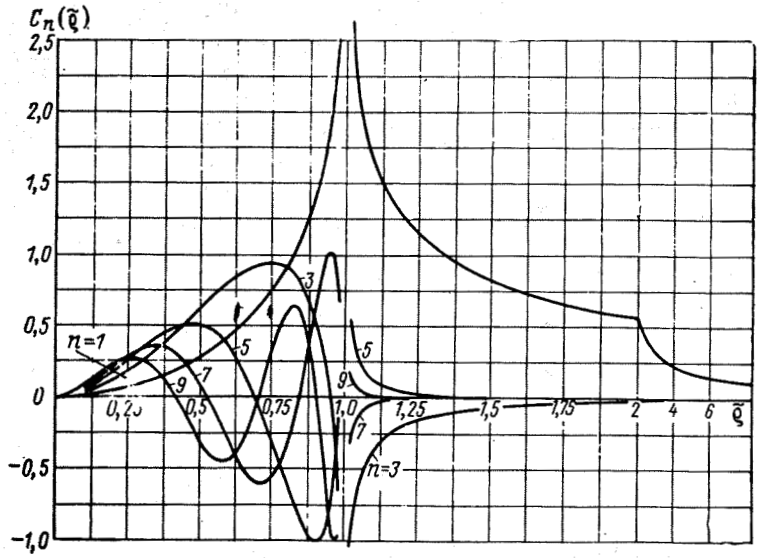

Figure 10.22

and define the coefficients

$$\bar{v}_r = \frac{1}{2\pi}\int_0^{2\pi} \bar{v}\, d\psi, \tag{10.93}$$

$$\bar{v}_{cn} = \frac{1}{\pi}\int_0^{2\pi} \bar{v}\cos n\psi\, d\psi, \tag{10.94}$$

$$\bar{v}_{sn} = \frac{1}{\pi}\int_0^{2\pi} \bar{v}\sin n\psi\, d\psi \tag{10.95}$$

of the Fourier series for induced velocities separately for each group of vortices which together make the vortex system of an airscrew.

VELOCITY HARMONICS INDUCED BY LIFTING LINES

The symbols of coefficients given by Eqs. (10.93)-(10.95) will be supplemented in this case with a superscript "*H*". We substitute Eq. (10.30) into Eq. (10.93), thus obtaining

$$\bar{v}_r^H = \frac{k}{8\pi^2\bar{r}^2}\int_{\bar{\varrho}_0}^{1}\int_0^{2\pi}\bar{\Gamma}\left\{\frac{1}{2\pi}\int_0^{2\pi}\frac{\sin(\psi-\theta)\,d\psi}{[1+\tilde{\varrho}^2-2\tilde{\varrho}\cos(\psi-\theta)]^{3/2}}\right\}d\theta\, d\bar{\varrho} = 0,$$

since the integral in the "{}" brackets is zero.

Let us turn our attention now to coefficients $\bar{v}_{cn}^H$ and $\bar{v}_{sn}^H$. If one takes into consideration, Eqs. (10.30), (10.94) and (10.95), then these coefficients would have the following form

$$\left.\begin{aligned}\bar{v}_{cn}^H &= -\frac{k}{4\pi\bar{r}^2}\sum_{\nu=1}^{8}\int_{\bar{\varrho}_0}^{1}\bar{\Gamma}_{s\nu}(\bar{\varrho})\, J_{n\nu}\, d\bar{\varrho},\\ \bar{v}_{sn}^H &= \frac{k}{4\pi\bar{r}^2}\sum_{\nu=1}^{\infty}\int_{\bar{\varrho}_0}^{1}\bar{\Gamma}_{c\nu}(\bar{\varrho})\, K_{n\nu}\, d\bar{\varrho},\end{aligned}\right\} \tag{10.96}$$

where

$$J_{n\nu} = \frac{1}{2\pi^2}\int_0^{2\pi}\int_0^{2\pi}\frac{\sin\psi\sin n\psi\sin\nu\theta\sin n\theta}{(1+\tilde{\varrho}^2-2\tilde{\varrho}\cos\psi)^{3/2}}\, d\theta\, d\psi,$$

$$K_{n\nu} = \frac{1}{2\pi^2}\int_0^{2\pi}\int_0^{2\pi}\frac{\sin\psi\sin n\psi\cos\nu\theta\cos n\theta}{(1+\tilde{\varrho}^2-2\tilde{\varrho}\cos\psi)^{3/2}}\, d\theta\, d\psi.$$

It is possible to show that

$$J_{n\nu}=K_{n\nu}=\begin{cases}0 & \text{for } n\neq\nu,\\ J_n & \text{for } n=\nu,\end{cases}$$

where

$$J_n=\frac{1}{2\pi}\int_0^{2\pi}\frac{\sin\psi\sin n\psi d\psi}{(1+\tilde{\varrho}^2-2\tilde{\varrho}\cos\psi)^{3/2}}. \tag{10.97}$$

Now, Eq. (10.96) becomes much simpler, as the summation disappears

$$\left.\begin{aligned}\bar{v}_{cn}^{\text{н}}&=-\frac{k}{4\pi\bar{r}^2}\int_{\bar{\varrho}_0}^{1}\bar{\Gamma}_{sn}(\bar{\varrho})J_n d\bar{\varrho},\\ \bar{v}_{sn}^{\text{н}}&=\frac{k}{4\pi\bar{r}^2}\int_{\bar{\varrho}_0}^{1}\bar{\Gamma}_{cn}(\bar{\varrho})J_n d\bar{\varrho}.\end{aligned}\right\} \tag{10.98}$$

An important conclusion follows from Eq. (10.98): The coefficient of the *nth* harmonic of velocity is influenced only by the *nth* harmonic coefficient of the circulation.

The present task consists of computing the integral in Eq. (10.97) for an arbitrary number n. This integral cannot be expressed by elementary functions; however, it is possible to transform it into hypergeometric functions

$$J_n=\frac{(2n-1)!!}{2^n(n-1)!}\frac{\tilde{\varrho}^{n-1}}{(1+\tilde{\varrho})^{2n+1}}F\left[n+\frac{1}{2},\ n+\frac{1}{2},\ 2n+1,\ \frac{4\tilde{\varrho}}{(1+\tilde{\varrho})^2}\right],$$

which, in turn, may be expressed through Legendre's function of the second kind $Q_{n-\frac{1}{2}}(x)$ при $x=(1+\tilde{\varrho}^2)/2\tilde{\varrho}$:

$$J_n=\frac{n}{\pi}\tilde{\varrho}^{-\frac{3}{2}}Q_{n-\frac{1}{2}}\left(\frac{1+\tilde{\varrho}^2}{2\tilde{\varrho}}\right). \tag{10.99}$$

Practical significance of the transformation to Eq. (10.99) is due to the presence of the recurring formula

$$J_n=\frac{2n}{2n-1}\frac{1+\tilde{\varrho}^2}{\tilde{\varrho}}J_{n-1}-\frac{n}{n-2}\frac{2n-3}{2n-1}J_{n-2}, \tag{10.100}$$

resulting from the relationship of Eq. (10.99) and a recurring formula for Legendre's functions. In this way, for computation of function J_n for any arbitrary rational number $n > 2$, it is sufficient to determine functions J_1 and J_2. These functions

can easily by expressed through the complete elliptic integrals of the first and second kinds.

$$J_1=\begin{cases}\frac{2}{\pi}\frac{1}{\tilde{\varrho}^2}\left[\mathbf{K}(\tilde{\varrho})-\mathbf{E}(\tilde{\varrho})\right] & \text{for } \tilde{\varrho}<1,\\ \frac{2}{\pi}\frac{1}{\tilde{\varrho}}\left[\mathbf{K}\left(\frac{1}{\tilde{\varrho}}\right)-\mathbf{E}\left(\frac{1}{\tilde{\varrho}}\right)\right] & \text{for } \tilde{\varrho}>1,\end{cases}$$

$$J_2=\begin{cases}\frac{4}{3\pi}\frac{1}{\tilde{\varrho}^3}\left[(2+\tilde{\varrho}^2)\mathbf{K}(\tilde{\varrho})-2(1+\tilde{\varrho}^2)\mathbf{E}(\tilde{\varrho})\right] & \text{for } \tilde{\varrho}<1,\\ \frac{4}{3\pi}\frac{1}{\tilde{\varrho}^2}\left[(1+2\tilde{\varrho}^2)\mathbf{K}\left(\frac{1}{\tilde{\varrho}}\right)-2(1+\tilde{\varrho}^2)\mathbf{E}\left(\frac{1}{\tilde{\varrho}}\right)\right] & \text{for } \tilde{\varrho}>1.\end{cases} \qquad (10.101)$$

Eqs. (10.98) and (10.101) complete the task of finding harmonics of velocity induced by the lifting lines of airscrews.

HARMONICS OF VELOCITY INDUCED BY FREE LONGITUDINAL VORTICES

In the general case of $\bar{\Gamma} = \bar{\Gamma}(\bar{\rho},\theta)$, coefficients of components (Eqs. (10.93)-(10.95)) generated by free (trailing) longitudinal vortices will be designated by the superscript "πp" and presented in the following form:

$$\bar{v}_r^{\pi p}=\bar{v}_r+\bar{v}_r^c+\bar{v}_r^s, \qquad (10.102)$$

$$\bar{v}_{cn}^{\pi p}=\bar{v}_{cn}+\bar{v}_{cn}^c+\bar{v}_{cn}^s, \qquad (10.103)$$

$$\bar{v}_{sn}^{\pi p}=\bar{v}_{sn}+\bar{v}_{sn}^c+\bar{v}_{sn}^s. \qquad (10.104)$$

The first terms in Eqs. (10.102)-(10.104) represent coefficients of components due to the first term in the expansion of circulation (Eq. 10.92)). Those components were already determined in the preceding considerations. We will designate the components by superscripts "c" and "s" respectively, corresponding to the coefficients appearing at the sine and cosine terms in the series of Eq. (10.92).

Let us first consider the coefficients $\bar{v}_r^c$ and $\bar{v}_r^s$. It is possible to show that after a substitution of Eqs. (10.27) and (10.92) into Eq. (10.93) and an integration with respect to parameter ψ, the following formulae will result

$$\bar{v}_r^c=\frac{k}{4\pi\bar{V}}\sum_{\nu=1}^{\infty}\left\{K_\alpha^\nu\int_{\bar{\varrho}_0}^{1}\frac{\partial\bar{\Gamma}_{c\nu}}{\partial\bar{\varrho}}P_\nu d\bar{\varrho}\right\}, \qquad (10.105)$$

$$\bar{v}_r^s = -\frac{k}{4\pi\bar{r}} \sum_{\nu=1}^{\infty} \left\{ K_\alpha^\nu \int_{\bar{\varrho}_0}^{1} \frac{\partial \bar{\Gamma}_{s\nu}}{\partial \bar{\varrho}} Q_\nu d\bar{\varrho} \right\}. \tag{10.106}$$

Here, $K_\alpha^\nu = \left(\frac{-\cos \alpha_B}{1 + |\sin \alpha_B|} \right)^\nu$,

$$P_\nu = \frac{1}{2}(Q_\nu - Q_{\nu-1}), \tag{10.107}$$

$$Q_\nu = \frac{1}{\pi} \int_0^{\pi} \frac{1}{L} T_n(\cos \Psi) d\theta, \tag{10.108}$$

where $T_n(\cos \Psi)$ is Tchebycheff's polynomial of the first kind of parameters

$$\cos \Psi = \frac{\tilde{\varrho} - \cos \theta}{L}, \quad L = \sqrt{1 + \tilde{\varrho}^2 - 2\tilde{\varrho} \cos \theta}. \tag{10.109}$$

In order to compute coefficients $\bar{v}_r^c$ and $\bar{v}_r^s$, it is necessary to determine kernel Q_ν. This kernel can be transformed into Legendre's functions. For odd values of index $\nu = 2m + 1$, the integral of Eq. (10.108) is transformed into Legendre's polynomial $P_m(x)$ at $x = 1 - (2/\tilde{\rho}^2)$:

$$Q_{2m+1} = \begin{cases} 0 & \text{for } \tilde{\varrho} < 1, \\ \frac{1}{\tilde{\varrho}} P_m \left(1 - \frac{2}{\tilde{\varrho}^2} \right) & \text{for } \tilde{\varrho} > 1. \end{cases} \tag{10.110}$$

For the low values of index m, the following elementary formulae are obtained from Eq. (10.110):

$$Q_1 = \frac{1}{\tilde{\varrho}},$$

$$Q_3 = \frac{1}{\tilde{\varrho}} \left(1 - \frac{2}{\tilde{\varrho}^2} \right),$$

$$Q_5 = \frac{1}{\tilde{\varrho}} \left(1 - \frac{6}{\tilde{\varrho}^2} + \frac{6}{\tilde{\varrho}^4} \right).$$

Computation of functions Q_{2m+1} for large values of index m can be conveniently performed through the use of recurring formula

$$Q_{2m+3} = \frac{2m+1}{m+1} \left(1 - \frac{2}{\tilde{\varrho}^2} \right) Q_{2m+1} - \frac{m}{m+1} Q_{2m-1}.$$

From Eqs. (10.107) and (10.11), it is possible to obtain kernels P_ν for even values of index $\nu = 2m$ under the form of Jacoby's polynomials:

$$P_{2m}=\begin{cases} 0 & \text{for } \tilde{\varrho}<1, \\ \frac{1}{\tilde{\varrho}^3} P_{m-1}^{(1,0)}\left(1-\frac{2}{\tilde{\varrho}^2}\right) & \text{for } \tilde{\varrho}>1, \end{cases} \tag{10.111}$$

from which simple formulae are obtained for the lower index m values

$$P_2=\frac{1}{\tilde{\varrho}^3}; \quad P_4=\frac{1}{\tilde{\varrho}^3}\left(2-\frac{3}{\tilde{\varrho}^3}\right); \quad P_6=\frac{1}{\tilde{\varrho}^3}\left(3-\frac{12}{\tilde{\varrho}^2}+\frac{10}{\tilde{\varrho}^4}\right).$$

Let us turn our attention to kernels from Eq. (10.108) for even values of index $\nu = 2m$. These kernels can be transformed into Legendre's functions of the first and second kinds

$$Q_{2m}=\begin{cases} (-1)^m \frac{2}{\pi\tilde{\varrho}} Q_{m-\frac{1}{2}}\left(\frac{2}{\tilde{\varrho}^2}-1\right) & \text{for } \tilde{\varrho}<1, \\ \frac{1}{\tilde{\varrho}} P_m\left(1-\frac{2}{\tilde{\varrho}^2}\right) & \text{for } \tilde{\varrho}>1. \end{cases} \tag{10.112}$$

For $m = 0$ and $m = 1$, Eq. (10.112) can be expressed through elliptic integrals:

$$Q_0=\begin{cases} \frac{2}{\pi}\mathrm{K}(\tilde{\varrho}) & \text{for } \tilde{\varrho}<1, \\ \frac{2}{\pi\tilde{\varrho}}\mathrm{K}\left(\frac{1}{\tilde{\varrho}}\right) & \text{for } \tilde{\varrho}>1, \end{cases}$$

$$Q_2=\begin{cases} \frac{2}{\pi}\left[\frac{2}{\tilde{\varrho}^2}\mathrm{E}(\tilde{\varrho})-\left(\frac{2}{\tilde{\varrho}^2}-1\right)\mathrm{K}(\tilde{\varrho})\right] & \text{for } \tilde{\varrho}<1, \\ \frac{2}{\pi\tilde{\varrho}}\left[2\mathrm{E}\left(\frac{1}{\tilde{\varrho}}\right)-\mathrm{K}\left(\frac{1}{\tilde{\varrho}}\right)\right] & \text{for } \tilde{\varrho}>1. \end{cases}$$

In order to compute function Q_{2m} for any natural number m, we will take advantage of the following recurring formula, known in the Legendre function theory:

$$Q_{2m+2}=\frac{4m}{2m+1}\left(1-\frac{2}{\tilde{\varrho}^2}\right)Q_{2m}-\frac{2m-1}{2m+1}Q_{2m-2}.$$

Function P_ν for odd numbers of ν is determined with respect to Q_{2m} with the help of Eq. (10.107). In this way, kernels of integrals in Eqs. (10.105)-(10.106) are determined. Now, coefficients $\bar{v}_r^c$ and $\bar{v}_r^s$ can be determined either directly through numerical calculations, or through the expansion of the derivatives of circulation into Legendre's functions.

We will now investigate coefficients $\bar{v}_{cn}^c$ and $\bar{v}_{cn}^s$ from Eq. (10.103). After a substitution of Eqs. (10.27) and (10.92) into Eq. (10.94), the following relationships are obtained

$$\bar{v}_{cn}^c = \frac{k}{2\pi\bar{V}} \sum_{\nu=1}^{\infty} \int_{\bar{Q}_0}^{1} \frac{\partial \bar{\Gamma}_{c\nu}}{\partial \bar{Q}} (C_{n\nu}^c + C_n^c)\, d\bar{Q}, \tag{10.113}$$

$$\bar{v}_{cn}^s = \frac{k}{2\pi\bar{r}} \sum_{\nu=1}^{\infty} \int_{\bar{Q}_0}^{1} \frac{\partial \bar{\Gamma}_{s\nu}}{\partial \bar{Q}} C_{n\nu}^s d\bar{Q}, \tag{10.114}$$

where

$$C_{n\nu}^c = \frac{1}{4\pi^2} \int_0^{2\pi} \int_0^{2\pi} \frac{\tilde{L}_z \tilde{Q} \sin(\theta - \psi) \cos \nu\theta \cos n\psi \cos \alpha_B}{\tilde{L}^2 (\tilde{L} + \tilde{L}_x \cos \alpha_B)} d\theta d\psi, \tag{10.115}$$

$$C_n^c = \frac{1}{4\pi^2} \int_0^{2\pi} \int_0^{2\pi} \frac{\tilde{Q}^2 - \tilde{Q} \cos(\theta - \psi)}{\tilde{L}^2} \cos \nu\theta \cos n\psi d\theta d\psi, \tag{10.116}$$

$$C_{n\nu}^s = \frac{1}{4\pi} \int_0^{2\pi} \int_0^{2\pi} \frac{L_z \sin \nu\theta \cos n\psi \cos \alpha_B}{\tilde{L}(\tilde{L} + L_x \cos \alpha_B)} d\theta d\psi. \tag{10.117}$$

Here, functions $\tilde{L}_x$, $\tilde{L}_z$ and $\tilde{L}$ are determined according to Eq. (10.44).

Upon completion of integration with respect to ψ in Eq. (10.115), we obtain

$$C_{n\nu}^c = \frac{1}{8} \left[K_\alpha^{n+\nu} (S_{n+1}^{-\nu} - S_{n-1}^{-\nu}) - \delta_{n\nu} K_\alpha^{|n-\nu|} (S_{n+1}^{\nu} - S_{n-1}^{\nu}) \right], \tag{10.118}$$

$$C^s_{n\nu}=\frac{1}{4}\left(\delta_{n\nu}K^{|n-\nu|}_{\alpha}S^{\nu}_{n}-K^{n+\nu}_{\alpha}S^{-\nu}_{n}\right), \tag{10.119}$$

where

$$S^{\nu}_{n}=\frac{2}{\pi}\int_0^{\pi}\frac{1}{L}\cos\left[n\varphi+\nu(\theta-\varphi)\right]d\theta. \tag{10.120}$$

Here, angle ϕ is found from Eq. (10.70), and symbol $\delta_{n\nu}$ means

$$\delta_{n\nu}=\begin{cases}1 & \text{for } \nu\leqslant n,\\ -1 & \text{for } \nu=n.\end{cases}$$

Functions with negative superscripts in Eqs. (10.118) and (10.119) are determined from Eq. (10.120) with a change of ν to $-\nu$. Similar to the integral in Eq. (10.77), the integral in Eq. (10.120) can be expressed through special functions. However, the resulting relationships would be complicated. For this reason, it is more convenient to use tables of that integral.

The integration with respect to ψ performed in Eq. (10.116) leads to the following results:

$$C^c_n=\begin{cases}0\\ \dfrac{1}{4\pi}\displaystyle\int_0^{2\pi}\frac{\tilde{\varrho}^2-\tilde{\varrho}\cos\theta}{1+\tilde{\varrho}^2-2\tilde{\varrho}\cos\theta}\cos\nu\theta d\theta & \text{for } \nu=n,\end{cases}$$

or, finally,

$$C^c_n=\begin{cases}-\dfrac{1}{8}\left(1+\tilde{\varrho}^2\right)\tilde{\varrho}^{n-1} & \text{for } \tilde{\varrho}<1,\\ 0 & \text{for } \tilde{\varrho}=1,\\ \dfrac{1}{8}\left(1+\tilde{\varrho}^2\right)\dfrac{1}{\tilde{\varrho}^{n+1}} & \text{for } \tilde{\varrho}>1.\end{cases} \tag{10.121}$$

Since, for $\nu\neq n$, function C^c_n is equal to zero, hence Eq. (10.113) somewhat simplifies

$$\bar{v}^c_{cn}=\frac{k}{2\pi\bar{V}}\left\{\sum_{\nu=1}^{\infty}\int_{\bar{\varrho}_0}^{1}\frac{\partial\bar{\Gamma}_{c\nu}}{\partial\bar{\varrho}}C^c_{n\nu}d\bar{\varrho}+\int_{\bar{\varrho}_0}^{1}\frac{\partial\bar{\Gamma}_{cn}}{\partial\bar{\varrho}}C^c_n d\bar{\varrho}\right\}. \tag{10.122}$$

Eqs. (10.114) and (10.122), together with Eqs. (10.118), (10.119) and (10.121) represent the final solution of the task of determining coefficient $\bar{v}^{\pi p}_{cn}$.

Let us now switch our attention to coefficient $\bar{v}^{\pi p}_{sn}$ defined by Eq. (10.104), and examine the coefficients $\bar{v}^c_{sn}$ and $\bar{v}^s_{sn}$

which appear in $\bar{v}_{sn}^{\pi p}$. After substituting Eqs. (10.27) and (10.92) into Eq. (10.95), and after accomplishing the necessary transformations, we obtain

$$\bar{v}_{sn}^{c}=\frac{k}{4\pi\bar{r}}\sum_{\nu=1}^{\infty}\int_{\bar{\varrho}_0}^{1}\frac{\partial\bar{\Gamma}_{c\nu}}{\partial\bar{\varrho}}\,S_{n\nu}^{c}\,d\bar{\varrho}, \tag{10.123}$$

$$\bar{v}_{sn}^{s}=\frac{k}{2\pi\bar{V}}\sum_{\nu=1}^{\infty}\int_{\bar{\varrho}_0}^{1}\frac{\partial\bar{\Gamma}_{s\nu}}{\partial\bar{\varrho}}\,(S_{n\nu}^{s}+S_{n}^{s})\,d\bar{\varrho}, \tag{10.124}$$

where

$$\left.\begin{aligned}
S_{n\nu}^{c}&=\frac{1}{4\pi^2}\int_0^{2\pi}\int_0^{2\pi}\frac{\tilde{L}_z\cos\nu\theta\sin n\psi\cos\alpha_{\text{в}}}{\tilde{L}\,(\tilde{L}+\tilde{L}_x\cos\alpha_{\text{в}})}\,d\theta d\psi,\\
S_{n\nu}^{s}&=\frac{1}{4\pi^2}\int_0^{2\pi}\int_0^{2\pi}\frac{\tilde{L}_z\tilde{\varrho}\sin(\theta-\psi)\sin\nu\theta\sin n\psi\cos\alpha_{\text{в}}}{\tilde{L}^2(\tilde{L}+\tilde{L}_x\cos\alpha_{\text{в}})}\,d\theta d\psi,\\
S_{n}^{s}&=\frac{1}{4\pi^2}\int_0^{2\pi}\int_0^{2\pi}\frac{1}{\tilde{L}^2}\left[\tilde{\varrho}^2-\tilde{\varrho}\cos(\theta-\psi)\right]\sin\nu\theta\sin n\psi d\theta d\psi.
\end{aligned}\right\} \tag{10.125}$$

After an integration with respect to the variable ψ, Eq. (10.125) will have the following form:

$$S_{n\nu}^{c}=\frac{1}{4}\left(\delta_{n\nu}K_{\alpha}^{|n-\nu|}S_{n}^{\nu}-K_{\alpha}^{n+\nu}S_{n}^{-\nu}\right), \tag{10.126}$$

$$S_{n\nu}^{s}=\frac{1}{8}\left[\delta_{n\nu}K_{\alpha}^{|n-\nu|}\left(S_{n+1}^{\nu}-S_{n-1}^{\nu}\right)-K_{\alpha}^{n+\nu}\left(S_{n+1}^{-\nu}-S_{n-1}^{-\nu}\right)\right], \tag{10.127}$$

$$S_{n}^{s}=\begin{cases}0 & \text{for}\quad \nu\neq n,\\ \dfrac{1}{4\pi}\displaystyle\int_0^{2\pi}\frac{\tilde{\varrho}^2-\tilde{\varrho}\cos\theta}{1+\tilde{\varrho}^2-2\tilde{\varrho}\cos\theta}\cos\nu\theta\,d\theta & \text{for}\quad \nu=n.\end{cases}$$

This latter integral can be determined in an elementary way:

$$S_{n}^{s}=\begin{cases}-\dfrac{1}{8}(1+\tilde{\varrho}^2)\,\tilde{\varrho}^{n-1} & \text{for}\ \tilde{\varrho}<1,\\ 0 & \text{for}\ \tilde{\varrho}=1,\\ \dfrac{1}{8}(1+\tilde{\varrho}^2)\dfrac{1}{\tilde{\varrho}^{n+1}} & \text{for}\ \tilde{\varrho}>1.\end{cases} \tag{10.128}$$

By comparing Eqs. (10.126), (10.127) and (10.128) with Eqs. (10.118), (10.119) and (10.121), we would note the following useful properties:

$$S_{n\nu}^{c}=C_{n\nu}^{s},\quad S_{n\nu}^{s}=-C_{n\nu}^{c},\quad S_{n}^{s}=C_{n}^{c}.$$

Now, final expressions for the coefficients in Eqs. (10.123) and (10.124) can be rewritten

$$\bar{v}^c_{sn} = \frac{k}{4\pi\bar{r}} \sum_{\nu=1}^{\infty} \int_{\bar{\varrho}_0}^{1} \frac{\partial \bar{\Gamma}_{c\nu}}{\partial \bar{\varrho}} C^s_{n\nu} d\bar{\varrho},$$

$$\bar{v}^s_{sn} = \frac{k}{2\pi\bar{V}} \left(\int_{\bar{\varrho}_0}^{1} \frac{\partial \bar{\Gamma}_{sn}}{\partial \bar{\varrho}} C^c_n d\bar{\varrho} - \sum_{\nu=1}^{\infty} \int_{\bar{\varrho}_0}^{1} \frac{\partial \bar{\Gamma}_{s\nu}}{\partial \bar{\varrho}} C_{n\nu} d\bar{\varrho} \right).$$

So, harmonics of velocity induced by the longitudinal free vortices are defined.

HARMONICS OF VELOCITY INDUCED BY FREE LATERAL (SHED) VORTICES

In this case, the coefficients given by Eqs. (10.93)-(10.95) will be defined by the superscript "$\pi\pi$". Let us consider the coefficient $\bar{v}^{\pi\pi}_r$. It is possible to show that if Eq. (10.29) is substituted into Eq. (10.93), then the resulting relationship would have the following form:

$$\bar{v}^{\pi\pi}_r = -\frac{k}{4\pi\bar{V}\bar{r}} \sum_{\nu=1}^{\infty} \nu \int_{\bar{\varrho}_0}^{1} \bar{\Gamma}_{c\nu}(\bar{\varrho}) \bar{Q}^{\pi\pi}_\nu d\bar{\varrho}, \qquad (10.129)$$

where

$$Q^{\pi\pi}_\nu = \frac{1}{4\pi^2} \int_0^{2\pi} \int_0^{2\pi} \left[\frac{\sin(\theta-\psi)}{\tilde{L}} - \sin\theta \cos\alpha_в \right] \frac{\sin\nu\theta}{\tilde{L} + \tilde{L}_x \cos\alpha_в} d\theta\, d\psi.$$

After an integration with respect to ψ, the above integral can be rewritten as follows:

$$Q^{\pi\pi}_\nu = \frac{K^\nu_\alpha}{2\pi} \int_0^{2\pi} \frac{1}{L} \cos\Psi \cos\nu\Psi d\theta, \qquad (10.130)$$

where the angle Ψ is given by Eq. (10.109). It can be noticed that the integral in Eq. (10.130) can be expressed through function Q_ν, defined by Eq. (10.108) and expressed through Legendre's functions, Eqs. (10.110) and (10.111):

$$Q^{\pi\pi}_\nu = \frac{1}{2} K^\nu_\alpha (Q_{\nu-1} - Q_{\nu+1}).$$

This gives a solution to the task of determining the kernel of the integral in Eq. (10.129). The final form of Eq. (10.129) will be

$$\bar{v}_r^{\pi\pi} = -\frac{k}{8\pi\bar{V}\bar{r}} \sum_{\nu=1}^{\infty} \left[\nu K_\alpha^\nu \int_{\bar{\varrho}_0}^{1} \bar{\Gamma}_{c\nu} (Q_{\nu-1} + Q_{\nu+1}) d\bar{\varrho} \right]. \tag{10.131}$$

Let us investigate coefficient $\bar{v}_{cn}^{\pi\pi}$. If we substitute Eqs. (10.29) and (10.92) into Eq. (10.94), then the following relationship is obtained

$$\bar{v}_{cn}^{\pi\pi} = -\frac{k}{4\pi\bar{V}\bar{r}} \sum_{\nu=1}^{\infty} \nu \int_{\bar{\varrho}_0}^{1} \bar{\Gamma}_{c\nu}(\bar{\varrho}) P_{n\nu}^{\pi\pi} d\bar{\varrho}, \tag{10.132}$$

where

$$P_{n\nu}^{\pi\pi} = \frac{1}{2\pi^2} \int_0^{2\pi} \int_0^{2\pi} \left[\frac{\sin(\theta - \psi)}{\tilde{L}} - \sin\theta \cos\alpha_B \right] \frac{\sin \nu\theta \cos n\psi}{\tilde{L} + \tilde{L}_x \cos\alpha_B} d\theta d\psi.$$

As the result of an integration with respect to ψ, we find

$$P_{n\nu}^{\pi\pi} = \frac{1}{4} \{ K_\alpha^{n+\nu} [S_n^{-(\nu+1)} + S_n^{-(\nu-1)}] - \delta_{n\nu} k_\alpha^{|n-\nu|} [S_n^{\nu+1} + S_n^{\nu-1}] \}, \tag{10.133}$$

where functions S_n^ν are defined by Eq. (10.120).

Finally, we turn our attention to coefficient $\bar{v}_{sn}^{\pi\pi}$. After a substitution of Eqs. (10.29) and (10.92) into Eq. (10.95), we find that this coefficient has the following form

$$\bar{v}_{sn}^{\pi\pi} = \frac{k}{4\pi\bar{V}\bar{r}} \sum_{\nu=1}^{\infty} \nu \int_{\bar{\varrho}_0}^{1} \bar{\Gamma}_{s\nu}(\tilde{\varrho}) Q_{n\nu}^{\pi\pi} d\bar{\varrho}, \tag{10.134}$$

where

$$Q_{n\nu}^{\pi\pi} = \frac{1}{2\pi^2} \int_0^{2\pi} \int_0^{2\pi} \left[\frac{\sin(\theta - \psi)}{\tilde{L}} - \sin\theta \cos\alpha_B \right] \frac{\sin n\psi \cos \nu\theta}{\tilde{L} + \tilde{L}_x \cos\alpha_B} d\theta d\psi. \tag{10.135}$$

After an integration with respect to ψ, that equation is transformed into the following relationship

$$Q_{n\nu}^{\pi\pi} = \frac{1}{4} \{ K_\alpha^{n+\nu} [S_n^{-(\nu+1)} + S^{-(\nu-1)}] + \delta_{n\nu} K_\alpha^{|n-\nu|} [S_n^{\nu+1} + S_n^{\nu-1}] \}. \tag{10.136}$$

It can be seen that there are identical terms in Eqs. (10.133) and (10.134) which should facilitate calculations.

So, Eqs. (10.131), (10.132) and (10.134), together with

Eqs. (10.133) and (10.136) complete the task of determining the harmonics of velocity induced by the free lateral (shed) vortices of the rotor. Harmonics of velocity induced by the whole vortex system of a rotor are determined as a sum of velocity harmonics related to each of these groups of vortices.

9. STATIONARY FIELD OF INDUCED VELOCITIES IN A COMPRESSIBLE FLOW

The works of F.I. Frankl', L.A. Simonov, S.A. Khristianovich, G.I. Maykapar, V.V. Keldysh, G.I. Taganov, D.V. Khalezov, etc., are devoted to the theory of aircraft propellers in a compressible flow (see bibliography at the end of this book). In this section, theoretical problems of a lifting airscrew in a compressible flow are considered.

Let a lifting airscrew, whose hub center coincides with the origin of coordinates, be located within an undisturbed flow with velocity V, directed along the abscissa axis of a stationary Cartesian coordinate system OXYZ (Fig. 10.23). The airscrew blade is modeled by a segment of the bound vortex whose circulation varies along the radius, but remains constant with respect to the azimuth. The velocity vector of the undisturbed flow makes an arbitrary angle of attack, α_B, with the rotor plane of rotation. In the OXYZ coordinate system, vortices are distributed on the surface given by the following:

$$\bar{\xi}=\bar{\varrho}\cos(\theta-\vartheta)\cos\alpha_в+\bar{V}\vartheta,\quad \bar{\eta}=-\bar{\varrho}\cos(\theta-\vartheta)\sin\alpha_в,$$
$$\bar{\zeta}=-\bar{\varrho}\sin(\theta-\vartheta). \qquad (10.137)$$

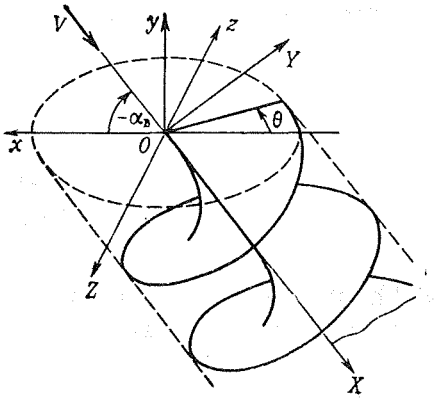

Figure 10.23

Let us also introduce the usual Cartesian coordinate system Oxyz connected with the rotor.

Induced velocity $\mathbf{v}$, generated by the rotor, is the sum of velocity $v_п$ induced by the bound vortices, and velocity v_c, induced by the free vortices:

$$\bar{\mathbf{v}}\{\bar{u}, \bar{v}, \bar{w}\} = \bar{\mathbf{v}}_п\{\bar{u}_п, \bar{v}_п, \bar{w}_п\} + \bar{\mathbf{v}}_c\{u_c, v_c, w_c\}.$$

We first define the time-averaged velocity $\bar{\mathbf{v}}_п\{\bar{u}_п, \bar{v}_п, \bar{w}_п\}$ induced at an arbitrary point in space $(\bar{x}, \bar{y}, \bar{z})$ by the bound vortices of a k-bladed rotor. Let us assume that $\bar{x} = -\bar{r}\cos\psi$, $\bar{z} = \bar{r}\sin\psi$. We substitute Eq. (10.137) with $\vartheta = 0$ into Eqs. (I.10)-(I.12) and average the thus obtained results with respect to time. Then we make a transfer to the Oxyz coordinates and obtain

$$\bar{u}_п = \frac{-\nu k}{8\pi^2}\int_0^{2\pi}\int_{\bar{Q}_0}^{1}\bar{\Gamma}\frac{\bar{y}\sin\theta}{\bar{l}_\nu^3}d\bar{Q}d\theta,$$

$$\bar{v}_п = \frac{-\nu k}{8\pi^2}\int_0^{2\pi}\int_{\bar{Q}_0}^{1}\bar{\Gamma}\frac{\bar{r}\sin(\theta-\psi)}{\bar{l}_\nu^3}d\bar{Q}d\theta, \qquad (10.138)$$

$$\bar{w}_п = \frac{-\nu k}{8\pi^2}\int_0^{2\pi}\int_{\bar{Q}_0}^{1}\bar{\Gamma}\frac{\bar{y}\cos\theta}{\bar{l}_\nu^3}d\bar{Q}d\theta,$$

where

$$\bar{l}_\nu^2 = L^2 + \bar{y}^2 + (\nu^2+1)\bar{l}_\xi^2; \quad \bar{l}_\xi = \bar{y}\sin\alpha_в - L_x\cos\alpha_в.$$

Here, the functions L and L_x are defined by Eq. (10.25).

It follows from Eq. (10.138) that in a compressible medium, the $\bar{v}_п$ velocity field is different from zero. At the same time, for $\nu = 1$ (incompressible fluid), the $\bar{v}_п$ velocity field disappears.

Let us now average the velocity given by Eq. (10.138) over the circle of radius $\bar{r}$:

$$\bar{v}_{r\,п} = \frac{-\nu k}{16\pi^3}\int_0^{2\pi}\int_0^{2\pi}\int_{\bar{Q}_0}^{1}\bar{\Gamma}\frac{\bar{r}\sin(\theta-\psi)}{\bar{l}_\nu^3}d\bar{Q}d\theta d\psi.$$

It can be seen from the above that by changing the independent variables θ and ψ to $-\theta$ and $-\psi$, the integrated function changes its sign. In this way, the following theorem can be formulated: Component of the velocity field $\bar{v}_п$ is asymmetric with respect to axis x.

We now switch our attention to the field of velocities $\bar{v}_c(\bar{u}_c, \bar{v}_c, \bar{w}_c)$ induced in space (x, y, z) by the free vortices. We substitute Eq. (10.137) into Eqs. (I.10)-(I.12) and average the obtained results with respect to time. Then, we transfer

the results to the $Oxyz$ coordinate system, and obtain

$$\bar{u}_c=\frac{k}{8\pi^2\bar{V}}\int_0^{2\pi}\int_{\bar{\varrho}_0}^{1}\frac{\partial\bar{\Gamma}}{\partial\bar{\varrho}}\left[P_x-\bar{\varrho}l_x\cos\theta\sin\alpha_в\cos\alpha_в-\right.$$
$$\left.-\frac{\cos\alpha}{\bar{l}\nu}(\nu^2P_xl_x-\bar{\varrho}\bar{l}^2\cos\theta\,\mathrm{tg}\,\alpha_в)\right]\frac{d\bar{\varrho}d\theta}{l^2-\nu^2l_x\cos^2\alpha_в},$$
$$\bar{v}_c=\frac{k}{8\pi^2\bar{V}}\int_0^{2\pi}\int_{\bar{\varrho}_0}^{1}\frac{\partial\bar{\Gamma}}{\partial\bar{\varrho}}\left[P_y-\bar{\varrho}l_x\cos\theta\cos^2\alpha_в-\right.$$
$$\left.-\frac{\cos\alpha_в}{l\nu}(\nu^2P_yl_x-\bar{\varrho}l^2\cos\theta)\right]\frac{d\bar{\varrho}d\theta}{l^2-\nu^2l_x^2\cos^2\alpha_в}, \qquad (10.139)$$
$$\bar{w}_c=\frac{k}{8\pi^2\bar{V}}\int_0^{2\pi}\int_{\bar{\varrho}_0}^{1}\frac{\partial\bar{\Gamma}}{\partial\bar{\varrho}}\left[P_z+\bar{\varrho}l_x\sin\theta\sin\alpha_в\cos\alpha_в-\right.$$
$$\left.-\frac{\cos\alpha_в}{l\nu}(\nu^2P_zl_x+\bar{\varrho}l^2\sin\theta\,\mathrm{tg}\,\alpha_в)\right]\frac{d\bar{\varrho}d\theta}{l^2-\nu^2l_x^2\cos^2\alpha_в},$$

where

$$P_x=\mu(\bar{z}-\bar{\varrho}\sin\theta)\,\mathrm{tg}\,\alpha_в-\bar{\varrho}\bar{y}\cos\theta,$$
$$P_y=\bar{\varrho}^2-\bar{\varrho}(\bar{z}-\mu)\sin\theta+\bar{\varrho}\bar{x}\cos\theta-\mu\bar{z},$$
$$P_z=\bar{y}(\mu+\bar{\varrho}\sin\theta)-(\bar{x}+\bar{\varrho}\cos\theta)\mu\,\mathrm{tg}\,\alpha_в,$$
$$l=\sqrt{\bar{x}^2+\bar{y}^2+\bar{z}^2+\bar{\varrho}^2+2\bar{\varrho}(\bar{x}\cos\theta-\bar{z}\sin\theta)},$$
$$l_x=\bar{x}-\bar{y}\,\mathrm{tg}\,\alpha_в+\bar{\varrho}\cos\theta,\quad \mu=\bar{V}\cos\alpha_в.$$

For points in the plane of rotation, where $\bar{x} = -\bar{r}\cos\psi$ and $\bar{z} = \bar{r}\sin\psi$, Eq. (10.139) yields

$$\bar{v}_c=\frac{k}{8\pi^2\bar{V}}\int_0^{2\pi}\int_{\bar{\varrho}_0}^{1}\frac{\partial\bar{\Gamma}}{\partial\bar{\varrho}}\left[\bar{\varrho}^2-\bar{\varrho}\bar{r}\cos(\theta-\psi)+\mu L_z+\right.$$
$$\left.+\frac{1}{\nu}L\bar{\varrho}\cos\theta\cos\alpha_в\right]\frac{d\bar{\varrho}d\theta}{L(L+\nu L_x\cos\alpha_в)}, \qquad (10.140)$$

while function L_z is determined from Eq. (10.25).

If, in Eq. (10.140), $\alpha_B = \pm 90°$ is assumed, then that formula changes into the following:

$$\bar{v}_c=\frac{k}{8\pi^2\bar{V}}\int_0^{2\pi}\int_{\bar{\varrho}_0}^{1}\frac{\partial\bar{\Gamma}}{\partial\bar{\varrho}}\left[\bar{\varrho}^2-\bar{\varrho}\bar{r}\cos(\theta-\psi)\right]\frac{d\bar{\varrho}d\theta}{L^2}. \qquad (10.141)$$

Taking into consideration Eq. (10.35), from Eq. (10.141) we obtain

$$\bar{v}_c = \frac{k}{8\pi^2 \bar{V}} \int_{\bar{r}}^{1} \frac{\partial \bar{\Gamma}}{\partial \bar{\varrho}} d\bar{\varrho} = -\frac{k\bar{\Gamma}(\bar{r})}{4\pi \bar{V}},$$

which is the Joukowsky formula. This shows that compressibility of air has no influence on induced velocities of an airscrew in axial flow. This result is well known.

In order to facilitate calculations, we will represent Eq. (10.140) in the following form:

$$\bar{v}_c = \bar{v}_p + \bar{v}_q + \bar{v}_r, \tag{10.142}$$

where

$$\bar{v}_p = \frac{k}{4\pi \bar{V}} \int_{\bar{\varrho}_0}^{1} \frac{\partial \bar{\Gamma}}{\partial \bar{\varrho}} \Phi_p d\bar{\varrho}, \quad \bar{v}_q = \frac{k}{4\pi \bar{r}} \int_{\bar{\varrho}_0}^{1} \frac{\partial \bar{\Gamma}}{\partial \bar{\varrho}} \Phi_q d\bar{\varrho}, \quad \bar{v}_r = \frac{-k\bar{\Gamma}(\bar{r})}{4\pi \bar{V}}.$$

Here

$$\Phi_p = \frac{1}{2\pi} \int_0^{2\pi} \frac{\nu \bar{r} L_z \bar{\varrho} \sin(\theta - \psi) + \left(\frac{1}{\nu} - \nu\right) \cos\theta}{L^2 (L + L_x \nu \cos \alpha_в)} \cos \alpha_в d\theta,$$

$$\Phi_q = \frac{1}{2\pi} \int_0^{2\pi} \frac{\bar{r} L_z \cos \alpha_в}{L (L + L_x \nu \cos \alpha_в)} d\theta.$$

It can be seen that for $a = \infty$ (incompressible fluid), $\nu = 1$, and Eq. (10.142) transforms into Eq. (10.32). Function Φ_p represents the symmetrical, with respect to the x axis, and Φ_q, antisymmetrical, components of the varying field of induced velocities.

It is important to call one's attention to the following important circumstances: The stationary field of induced velocities does not depend on the Mach number M_ω related to the rotation of the airscrew ($M_\omega = \omega r/a$), but depends only on Mach number $M = V/a$ of the uniform flow directed along the axis of the skewed cylindrical vorticity wake. An explanation of this can be found in the fact that generation of velocity at an arbitrary point in space by a rotating airscrew with an infinite number of blades is equivalent to the generation of velocity by a stationary vortex system of an airscrew (an observer located at that point sees an immobile field of vortices).

In order to illustrate the quantitative influence of compressibility, we perform calculations according to Eqs. (10.138) and (10.142). Some results of the induced velocity calculations are shown in Fig. 10.24. In those calculations, the following

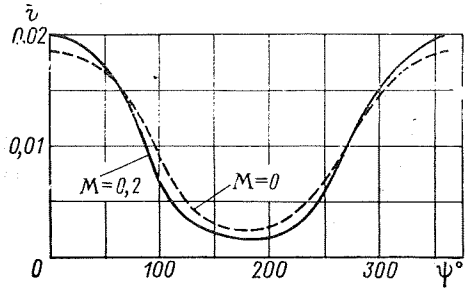

Figure 10.24

assumptions were made: $\Gamma = c_T(\pi/k)\omega R^2$; $c_T = 0,014$; $\omega R = 221$ m/sec; $\mu = 0,3$; $\alpha_B = -18°$ for both $M = 0 (a = \infty)$ and $M = 0,2$. It can be seen that the influence of compressibility is insignificant. However, since the formulae determining the velocity fields in compressible flows are not much more complicated from those for the incompressible case; hence, it may be justified to consider the influence of compressibility.

CHAPTER XI

BLADE THEORY OF LIFTING AIRSCREW IN A SKEWED FLOW

1. BASIC ASSUMPTIONS AND EQUATIONS

Let us make the following assumptions: (1) lifting rotor is lightly loaded; (2) blades are modeled by lifting lines with circulation varying both with the radius and azimuth; (3) flow encountered by the blade sections can be considered as two-dimensional *(two-dimensional hypothesis)*; (4) variation of the airfoil section lift coefficient with angle of attack is linear; (5) forces acting on the airfoil sections are determined on the basis of steady-state data *(stationary data hypothesis)*; (6) elements of free vortices move in space at a speed of uniform and rectilinear flow.

Some of the above-presented assumptions have already been considered. We want to emphasize only that the hypothesis of a two-dimensional flow does not represent the actual flow at the blade, especially in the regimes of forward flight. It follows from the two-dimensional hypothesis that the aerodynamic loads at the blade tip and root are zero, while actually, they periodically strongly increase when both ends of the blade encounter flow similar to that experienced by the blade leading edge. This drawback is partially eliminated when the lifting surface concept is applied. Also assumption No. (4) is not fully acceptable for regimes of flight involving high angles of attack; in some cases, blade airfoil sections work at angles of attack being outside of the linear part of the $c_y = c_y(\alpha_B)$ relationship. However, comparisons of analytical data with test results indicate that calculations based on nonlinaer relationships, as obtained experimentally under steady-state conditions still do not agree too well with tests. This is due to the fact that steady aerodynamics data is only applicable to the low airfoil angles of attack (for oscillation frequencies, characteristic of helicopter rotors). Interesting experimental results of unsteady aerodynamics also point out the unsuitability of using steady aerodynamics data for cases involving high airfoil angles of attack. It was shown that in unsteady aerodynamics, the range of the linear dependence of $c_y(\alpha_B)$ extends considerably and $c_{y_{max}}$ values substantially increase, while the nose-down airfoil pitching moments become much larger (airfoil center of pressure moves aft). It was also shown that the sweep angle of the blade and radial flow within the boundary layer also exert considerable influence on the character of flow experienced by the airfoil sections. For these reasons, the presented theory satisfactorily agrees with test data only for low speeds of

flight, when the blade sweep angles are small and airfoil angles of attack are low over a large portion of the rotor disc.

We will concentrate our attention on the development of the rotor vortex system. Equations of the vortex wake will be as given by Eq. (10.5). For practical calculations, we conceive a scheme based on a system of discrete vortices (Fig. 11.1). Development of this scheme is performed as follows: The lifting line is divided into m segments with the points of division $q = 1,2,3,\ldots,m+1$. The center of each segment is designated by an index "j" ($j=1,2,3,\ldots,m$) and is called the control point. Distances of points q and j from the rotor axis are called, respectively, $\bar{\rho}_q$ and $\bar{r}_j$. On the surface given by Eq. (10.5), one puts a network of "longitudinal" and "lateral" lines with nodes

$$\begin{aligned} \bar{\xi}_{pq} &= -\bar{V}\vartheta_p \cos\alpha_в - \bar{\varrho}_q \cos(\theta_n - \vartheta_p), \\ \bar{\eta}_{pq} &= \bar{V}\vartheta_p \sin\alpha_в, \\ \bar{\zeta}_{pq} &= \bar{\varrho}_q \sin(\theta_n - \vartheta_p), \end{aligned} \tag{11.1}$$

where ϑ_p is the azimuth angle of the dividing points of the longitudinal lines $\bar{\rho}_q = const$ ($p=0,1,2,\ldots,\infty$). Nodes of the p and q network are designated by M_{pq}. Intersection of a pair of lines q and $q+1$ with a pair of lines p and $p+1$ forms a cell with the two "upper", M_{pq} and $M_{p,q+1}$, and two "lower", $M_{p+1,q}$ and $M_{p+1,q+1}$, nodes.

A closed discrete vortex with circulation $\bar{\Gamma}_i$ extends along the boundaries of a cell. It is easy to realize that circulation $\bar{\Gamma}_i$ is equal to the lifting line circulation on the segment $q,q+1$ in that instant when the blade was in the position $\theta_n - \vartheta_p$.

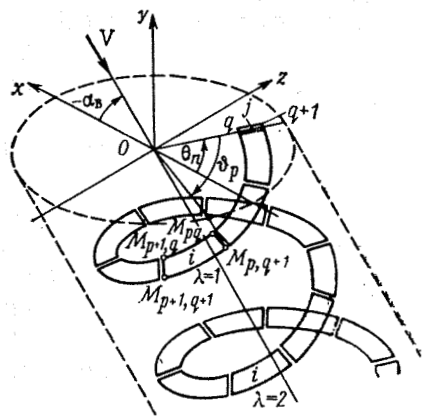

Figure 11.1

If, within the range $0 \leq \vartheta_p \leq 2\pi$, index "$p$" runs through the values $p=0,1,2,\ldots,P$, then the quantity of the sought values of Γ_i in that range will be mP. To facilitate the computation without limiting its generality, we will assume that the number P is a multiple of the number of blades. If we now consider that circulations of the closed vortices distributed along a line parallel to the axis of the elliptical cylinder have the same value $\bar{\Gamma}_i$, then the total number of unknown values for any number of blades will obviously be $m_* = mP$.

In order to determine the unknown values of $\bar{\Gamma}_i$, it is necessary to establish m_* equations for m control points on the considered blade, sequentially taking P azimuth positions $\theta - \vartheta$ within the interval $\theta - 2\pi \leq \theta - \vartheta_p \leq \theta$.

Let $\lambda=1,2,3,\ldots$ be the number of closed vortices of the same configuration distributed along the generatrix of the elliptical cylinder. Numbering starts from the rotor plane of rotation. The number of vortices is selected in such a way that the length of the vortex system is approximately equal to the rotor diameter. Also, let $\bar{v}_{ij}^{\lambda}$ be the axial induced velocity at point j of blade 1, generated by one of those vortices with a circulation equal to unity. Then λ vortices induce the following velocity at point j

$$\bar{v}_{ij}=\sum_{\lambda}\bar{v}_{ij}^{\lambda},$$

while the induced velocity of the rotor vortex system will be

$$\bar{v}_j=\sum_{i=1}^{m_*} v_{ij}\bar{\Gamma}_i. \tag{11.2}$$

Here, "i" should be understood as the consecutive number of the row of closed vortices with the same circulation $\bar{\Gamma}_i$. The initial equation for the determination of velocity circulation has a form of

$$\bar{\Gamma}_j=\frac{1}{2}c_{yj}\bar{b}_j\bar{W}_j, \tag{11.3}$$

where

$$c_{yj}=a_j\left(\bar{\varphi}_j+\operatorname{arc\,tg}\frac{\bar{W}_{yj}}{\bar{W}_j}+\frac{\bar{v}_j}{\bar{W}_j}\right),$$

$$\bar{W}_j=\bar{r}_j+\mu\sin\theta,\quad \bar{W}_{yj}=\bar{V}_\infty\sin\alpha_s-\mu\beta\cos\theta-\bar{r}_j\frac{d\beta}{d\theta}.$$

Substituting Eq. (11.2) into Eq. (11.3), we obtain a system of algebraic equations

$$\sum_{i=1}^{m_*}\bar{\gamma}_{ij}\bar{\Gamma}_i=\bar{g}_j, \tag{11.4}$$

where

$$\bar{\gamma}_{ij}=\begin{cases} -\bar{v}_{ij} & \text{for } i\neq j, \\ -\bar{v}_{ij}+\dfrac{2}{a_j\bar{b}_j} & \text{for } i=j, \end{cases} \tag{11.5}$$

$$\bar{g}_j=\overline{W}_j\left(\bar{\varphi}_j+\operatorname{arc\,tg}\frac{\overline{W}_{yj}}{\overline{W}_j}\right). \tag{11.6}$$

In coefficients $\bar{\gamma}_{ij}$, values of $\bar{v}_{ij}$ appear as unknowns. We are going to determine them.

2. COEFFICIENTS OF BASIC EQUATIONS

Let $\bar{v}^{\lambda}_{qj}$ be the induced velocity due to the curvilinear segment of the longitudinal vortex with a unitary circulation, joining side nodes M_{pq} and $M_{p+1,q}$ of a cell. Let this segment belong to the vortex wake of a blade with an azimuth angle $\theta_n = \theta + \delta_n$, $\delta_n = (2\pi/k)(n-1)$, (θ is the azimuth angle of blade No. 1). Induced velocity is determined at point

$$\bar{x}_j=-\bar{r}_j\cos\theta,\quad \bar{y}_j=0,\quad \bar{z}_j=\bar{r}_j\sin\theta.$$

We take advantage of Eq. (10.13), substituting in it angle θ_n for θ and angle θ for ψ. From that formula comes

$$\bar{v}^{\lambda}_{qj}=\frac{1}{4\pi}\int_{\vartheta_p}^{\vartheta_{p+1}}\frac{G\vartheta+H}{(\bar{V}^2\vartheta^2+g\vartheta+h)^{3/2}}\,d\vartheta, \tag{11.7}$$

where

$$G=\left[\bar{\varrho}_q\cos(\theta_n-\vartheta)\right]\bar{V}\cos\alpha_{\text{в}},\quad H=\bar{\varrho}_q^2-\bar{\varrho}_q\bar{r}_j\cos(\delta_n-\vartheta)+$$
$$+\left[\bar{\varrho}_q\sin(\theta_n-\vartheta)-\bar{r}_j\sin\theta\right]\bar{V}\cos\alpha_{\text{в}},$$
$$g=2\left[\bar{\varrho}_q\cos(\theta_n-\vartheta)-\bar{r}_j\cos\theta\right]\bar{V}\cos\alpha_{\text{в}},$$
$$h=\bar{\varrho}_q^2+\bar{r}_j^2-2\bar{\varrho}_q\bar{r}_j\cos(\delta_n-\vartheta).$$

We determine velocity $\bar{v}^{\lambda}_{pj}$ due to the nonlinear vortex segment with a unitary circulation which joins the upper nodes M_{pq} and M_{pq+1} of that cell. To do this, we will use Eq. (10.18) in which we change the variables in a way similar to the previous case. In addition, we modify the denominator in Eq. (10.18) in order to facilitate integration with respect to $\bar{\rho}$. After suitable transformations, we obtain

$$\bar{v}^{\lambda}_{pj}=\frac{1}{4\pi}\int_{\bar{\varrho}_q}^{\bar{\varrho}_{q+1}}\frac{\bar{V}\sin(\theta_n-\vartheta_p)\cos\alpha_{\text{в}}-\bar{r}_j\sin(\delta_n-\vartheta_p)}{[\bar{\varrho}^2+g_*\bar{\varrho}+h_*]^{3/2}}\,d\bar{\varrho},$$

where

$$g_*=2\left[\bar{V}\cos(\theta_n-\vartheta_p)\cos\alpha_{\text{в}}-\bar{r}_j\cos(\delta_n-\vartheta_p)\right],$$
$$h_*=\bar{V}^2\vartheta_p^2+\bar{r}_j^2-2\bar{V}\bar{r}_j\cos\theta\cos\alpha_{\text{в}}.$$

After determining this integral, we find

$$\bar{v}_{pj}^{\lambda}=\frac{2P_*}{\Delta}(I_q-I_{q+1}), \tag{11.8}$$

where

$$P_*=\bar{V}\sin(\vartheta_n-\vartheta_p)\cos\alpha_в-\bar{r}_j\sin(\delta_n-\vartheta_p),$$

$$\Delta=4h_*-g_*^2, \qquad I_q=\frac{2\bar{\varrho}_q+g_*}{\sqrt{\bar{\varrho}_q^2+g_*\bar{\varrho}_q+h_*}}.$$

Eqs. (11.7) and (11.8) permit one to determine velocity induced by a vortex cell

$$\bar{v}_{ij}^{\lambda}=\bar{v}_{qj}^{\lambda}-\bar{v}_{q+1,j}^{\lambda}-\bar{v}_{pj}^{\lambda}-\bar{v}_{p+1,j}^{\lambda}. \tag{11.9}$$

The above formula is correct for all closed vortices with the exception of those with an index $i=j$ at $\lambda=1$; i.e., the vortices which border the lifting line of the considered blade No. 1. The core of this matter is that with an unlimited reduction in size of the elements in the p,q net, induced velocity becomes infinite.

In order to overcome this difficulty, we replace the blade lifting line by a thin vortex strip whose width is equal to the blade chord. We will represent the surface of the vortex strip as a part of the surface defined in Eq. (10.5), within the range of the angle ϑ variation corresponding to the interval $(-\Delta\vartheta_j, \Delta\vartheta_j)$. It is assumed that unitary density of vorticity is constant along the strip width. This assumption does not limit the generality of the considered problem since the above approach was undertaken only in order to avoid a singularity in the process of integration. This singularity will disappear, since parts of the vortex system located on both sides of the lifting line induce infinite velocities on the line. However, they are of opposite signs which result in a finite value of the sought velocity.

It is also convenient to replace the vortex strip with a set of discrete vortices. In the simplest case, this vortex strip can be replaced by two segments of bound vortices of equal strength and located on the straight lines of Eq. (11.1) with $\delta_n = 0$, $\vartheta = -\Delta\vartheta_j$ and $\vartheta = \Delta\vartheta_j$. If circulation of the lifting line was $\bar{\Gamma}_i$, then circulation of each of those segments would be $\bar{\Gamma}_i/2$ (Fig. 11.2). In this way, a scheme of a closed vortex $i=j$ for $\lambda=1$ is developed. Bound segments of this vortex induce velocities of opposite signs at points j. It can be shown by evaluation that their sum is negligibly small. For this reason, velocity induced by vortex $i=j$ can be approximately given by the following sum of velocities

$$\bar{v}_{ij}^{\lambda}=\bar{v}_{qj}^{\lambda}-\bar{v}_{q+1,j}^{\lambda}-\bar{v}_{p+1,j}^{\lambda} \quad (p=0,\ \lambda=1),$$

where

$$\bar{v}_{qj}=\frac{1}{4\pi}\left\{\frac{1}{2}\int_{-\Delta\vartheta_j}^{\Delta\vartheta_j}\frac{G\vartheta+H}{(\bar{V}^2\vartheta^2+g\vartheta+h)^{3/2}}\,d\vartheta+\right.$$

$$\left.+\int_{\Delta\vartheta_j}^{\vartheta_p}\frac{G\vartheta+H}{(\bar{V}^2\vartheta^2+g\vartheta+h)^{3/2}}\,d\vartheta\right\}\ (p=1).$$

The formula for $\bar{v}_{p+1}$ remains unchanged.

After determination of the $\bar{v}_{ij}^{\lambda}$ values, we calculate coefficients $\bar{v}_{ij}$ belonging to the system of Eq. (11.5). In order to solve this system, it is necessary to previously determine the function $\beta = \beta(\psi)$ which appears in coefficients g_j. This will be done using the equation of flapping motion. It is advisable to first determine the approximate values of circulation appearing in that equation using the theory of a rotor with an infinite number of blades or from Glauert's theory.

Next, the system of Eq. (11.5) is solved and values of $\bar{v}_j$ and $\bar{\Gamma}_i$ determined. If necessary, it is possible to repeat the solution of the flapping motion equation with the above-obtained values to improve the accuracy of calculations of circulation and induced velocities in the system of Eq. (11.5).

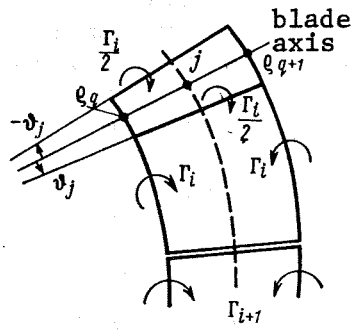

Figure 11.2

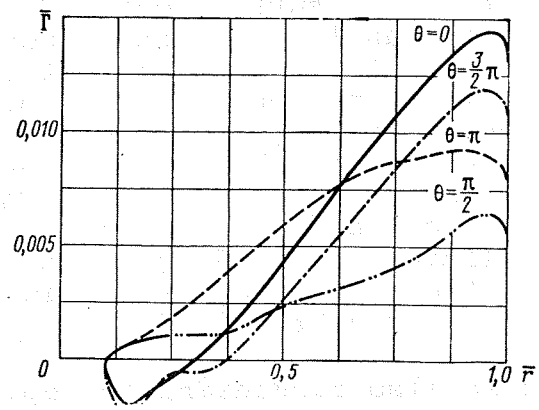

Figure 11.3

The presented method is flexible and permits considerable simplification in concrete cases of calculations. For instance, by assuming that distant lateral vortices have little influence on velocities induced in the plane of rotation, it is possible to limit considerations to the near lateral vortices only. It may be assumed that the rest of the vortex system is free from lateral vortices while the intensity of longitudinal vortices

is constant along their length. This approach reduces computer time. In order to illustrate the presented method, typical graphs of function $\bar{\Gamma} = \bar{\Gamma}(\bar{r}, \theta)$, as applied to a three-bladed rotor at $\mu = 0{,}3$, are shown in Fig. 11.3.

CHAPTER XII

THEORY OF LIFTING AIRSCREW BASED ON THE THIN LIFTING SURFACE CONCEPT

It was mentioned before that one of the pecularities of the operation of lifting airscrews in horizontal flight is the varying sweep angle in the flow encountered by the blade elements. Application of the lifting line scheme in the blade theory is, strictly speaking, justified only in the cases of negligible sweep angles; i.e., at low μ values. Figs. 12.1 and 12.2 show flow patterns obtained with a rotor model*. It can be seen that at $\mu = 0,46$, the sweep angles are quite considerable, especially in the blade root area. Root sections of the blade periodically work as either leading or trailing edges. With increasing μ, regions of large sweep angles become greatly enlarged (Fig. 12.3 for $\mu = 1,0$ and Fig. 12.4 for $\mu = 3,0$). Under those conditions, the lifting line and two-dimensional flow hypotheses become inapplicable. For this reason, it is necessary to switch to the lifting surface concept.

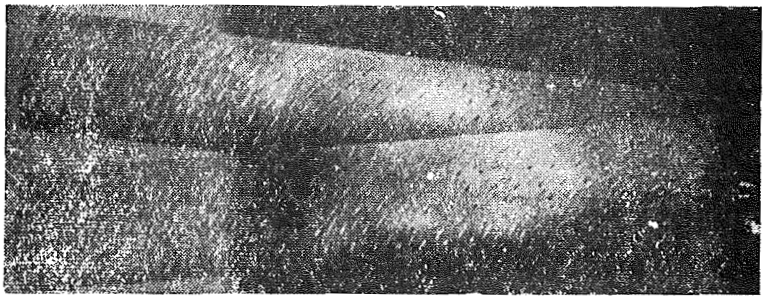

Figure 12.1

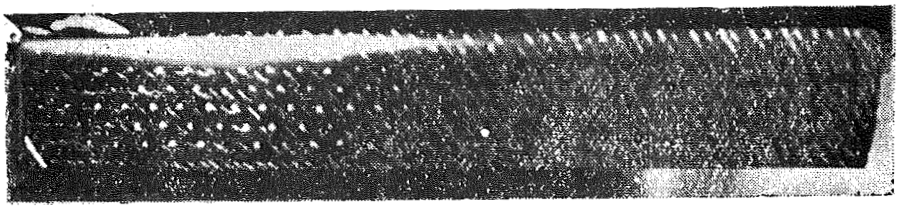

Figure 12.2

Formulation of this problem is, in general, similar to that discussed in Sect. 1 of Ch. VIII. In this problem, a

*Tests performed by L.S. Pavlov

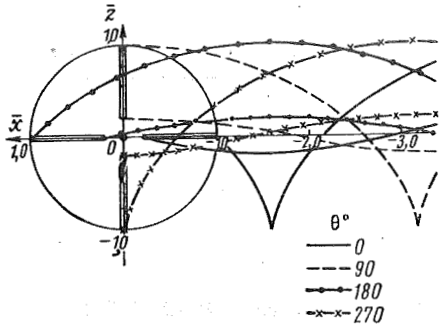

Figure 12.3

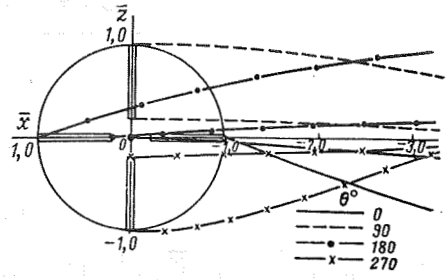

Figure 12.4

smooth flow around a blade modeled by a thin lifting surface is considered; geometry of the blade and the law of its motion are assumed to be known. In the beginning, boundary conditions on the surface were examined and on this basis, a system of linear algebraic equations for the determination of circulation was established.

1. BOUNDARY CONDITIONS

Let us introduce two systems of Cartesian coordinates; one, $Oxyz$, being stationary and another, $O\xi\eta\zeta$, rotating with the blade around the Oy axis with rotational speed ω. Origins of both coordinate systems as well as their Oy and $O\eta$ axes coincide. Position of the $O\zeta$ axis is defined by the azimuth angle θ, measured from the negative half-axis x. (Fig. 12.5). The equation of the blade surface in the $O\xi\eta\zeta$ system is given under the following form

$$\bar{\eta} = f(\bar{\xi}, \bar{\zeta}). \tag{12.1}$$

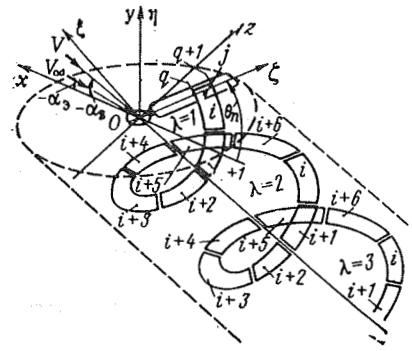

Figure 12.5

Boundary conditions are fulfilled at the control points $j(\bar{\xi}_j, \bar{\eta}_j, \bar{\zeta}_j)$. In general, coordinates of those points depend on θ due to the periodic flapping motion, accompanied by bending and torsional deformations of the blade. Boundary conditions stating the non-penetrability of the surface (Eq. (12.1)) can be expressed under the following form

$$\bar{\mathbf{V}}_j \cdot \mathbf{n}_j^0 = 0. \tag{12.2}$$

Here, $\bar{\boldsymbol{V}}_j\{\bar{V}_{xj}, \bar{V}_{yj}, \bar{V}_{zj}\}$ is the vector of the resultant relative velocity at point j, and $\mathbf{n}_j^0$ is the unit vector perpendicular to the surface (Eq. (12.1)) at that point. Components at that point of the undisturbed velocity vector are $\bar{V}_\infty \cos \alpha_э \sin \theta_n$, $\bar{V}_\infty \sin \alpha_э$, $\bar{V}_\infty \cos \alpha_э \cos \theta_n$, while components of vector $\bar{\mathbf{u}}_j$ of flow rotational velocity in the relative motion will be $\bar{\zeta}_j, 0, \bar{\xi}$.

Let $\bar{\mathbf{v}}_j\{\bar{u}_j, \bar{v}_j, \bar{w}_j\}$ be the vector of induced velocity, and $\bar{v}_j^\delta\{\bar{u}_j, \bar{v}_j^\delta, \bar{w}_j^\delta\}$, the vector of the flapping motion of point j. Then, the vector $\bar{\boldsymbol{V}}_j$ can be expressed as the following sum

$$\bar{\mathbf{V}}_j = \bar{\mathbf{V}}_\infty + \bar{\mathbf{u}}_j + \bar{\mathbf{v}}_j - \bar{\mathbf{v}}_j^\delta. \tag{12.3}$$

In order to find vector $\mathbf{n}_j^0$, we will present Eq. (12.1) in the form of $F(\bar{\xi}, \bar{\eta}, \bar{\zeta}) = 0$, where $F = \bar{\eta} - f(\bar{\xi}, \bar{\zeta})$. Then, the unit vector normal to the surface is expressed as

$$\mathbf{n}_j^0 = \frac{\operatorname{grad} F}{|\operatorname{grad} F|}, \tag{12.4}$$

where in addition, projections of vector *grad F* are determined according to Eq. (12.1). As a result of Eqs. (12.2)-(12.4), boundary condition of the non-penetrability of the lifting surface takes the following form:

$$\begin{aligned}&(\bar{V}_\infty \cos \alpha_э \cos \theta_n + \bar{\zeta}_j + \bar{u}_j^\delta - \bar{u}_j) f_{\xi j} - \\ &- (V_\infty \cos \alpha_э \cos \theta_n + \bar{\xi}_j - \bar{w}_j^\delta + \bar{w}_j) f_{\zeta j} + \bar{V}_\infty \sin \alpha_э - \bar{v}_j^\delta + \bar{v}_j = 0.\end{aligned} \tag{12.5}$$

Since it is assumed that geometric characteristics of the blades and the law of its motion are known; hence, in Eq. (12.5), only velocities $\bar{u}_j$, $\bar{v}_j$, $\bar{w}_j$ remain unknown. Velocities $\bar{u}_j$ and $\bar{w}_j$ are small in comparison with $\bar{v}_j$. In addition, derivatives $f_{\xi j}$ and $f_{\zeta j}$ are small in comparison to one. For this reason, Eq. (12.5) can be linearized in the following way

$$(\bar{\zeta}_j + \bar{V}_\infty \cos \alpha_э \sin \theta_n) f_{\xi j} - (\bar{V}_\infty \cos \alpha_э \cos \theta_n) f_{\zeta j} + \bar{v}_j - \bar{v}_j^\delta + \bar{V}_\infty \sin \alpha_э = 0. \tag{12.6}$$

2. SCHEME OF THE BLADE VORTEX WAKE SYSTEM AND BASIC EQUATIONS

Cylindrical surfaces with cycloidal directrix given by

$$\bar{x} = -\bar{\varrho}_q \cos(\theta_n - \vartheta) - \bar{V}\vartheta \cos\alpha, \quad \bar{z} = \bar{\varrho}_q \sin(\theta_n - \vartheta) \tag{12.7}$$

divide the blade into Q sections (Fig. 12.6). Lines of intersection of the surface given by Eq. (12.1) with that described by Eq. (12.7) are designated by an index "q" ($q=1, 2, \ldots, Q+1$). Each of the q lines is divided into P segments of equal length.

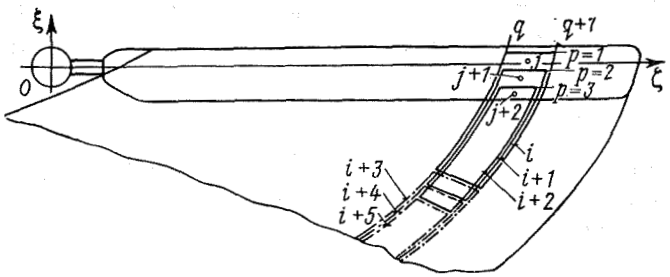

Figure 12.6

Points corresponding to the 1/4 length (measured from the airfoil leading edge) of each segment of line q are designated by index "p" ($p=1, 2, 3, \ldots, P$). Broken lines along the blade span, also designated by q, are drawn through points p having the same indices. Lines q can be replaced by broken lines with apexes at points p. Eventually, on the surface given by Eq. (12.1), a network of lines p and q is formed. Through the points corresponding to the 3/4 length of each segment of the q lines, lines are drawn on which control points j are located between the q lines.

Segments of bound vortices extend along lines p, and along lines q on the blade extend segments of free vortices. Continuous variation of circulation along the longitudinal vortices, resulting from the unsteadiness of the flow encountered by the blade, is replaced by the step-type variation. For this, longitudinal vortices behind the blade are divided by straight lines (Eq. (12.7)) with $\vartheta = \vartheta_r (r=0, 1, 2\ldots)$ into segments within which the circulation may be considered as constant. It is convenient to select values of the azimuth pitch $\vartheta_{r+1} - \vartheta_r$ as a multiple of the index angle between the neighboring blades. On the boundaries of segments where circulation is varying in a step fashion, lateral vortices which compensate for the variation of circulation of the longitudinal vortices are present.

The thus obtained vorticity system is transformed into an equivalent assembly of discrete closed vortices (Fig. 12.6). It can be seen that circulations of the closed vortices, distributed along the generatrix of the elliptical cylinder, are the same. We designate the row number of those vortices by $i\,(i=1,2,3,\ldots,m)$, and the consecutive number of a closed vortex in that row, by $\lambda\,(\lambda=1,2,\ldots)$. Let $\bar{v}_{ij}^{\lambda}$ also be the axial velocity generated at point j by a closed vortex with unit circulation. All closed vortices of row i induce axial velocity

$$\bar{v}_{ij}=\sum_{\lambda}\bar{v}_{ij}^{\lambda}.$$

To facilitate calculations and reduce computer time, we will assume that the closed vortices consist of rectilinear segments of vortices connecting the nodes of a vortex cell. Induced velocities generated by those segments are calculated from Eq. (8.8).

If the circulation of a closed vortex is equal to $\bar{\Gamma}_i$, then the induced velocity generated by the rotor vortex system is obtained as the following sum

$$\bar{v}_j=\sum_{i=1}^{m}\bar{v}_{ij}\bar{\Gamma}_i. \tag{12.8}$$

Substituting Eq. (12.8) into Eq. (12.6), we obtain a system of linear algebraic equations,

$$\sum_{i=1}^{m}\bar{\gamma}_{ij}\bar{\Gamma}_i=\bar{g}_j, \tag{12.9}$$

in which

$$\left.\begin{aligned}&\bar{\gamma}_{ij}=\bar{v}_{ij},\ \bar{g}_j=(\bar{V}_\infty\cos\alpha_э\cos\theta_n)f_{\zeta j}-\\&-(\bar{\zeta}_i+\bar{V}_\infty\cos\alpha_э\sin\theta_n)f_{\xi j}+\bar{v}_j^{\delta}-\bar{V}_\infty\sin\alpha_э=0.\end{aligned}\right\} \tag{12.10}$$

In the case of axial flow, the relationships given by Eqs. (12.9) and (12.10) become identical with those developed in Sect. 4 of Ch. VIII.

A comparison of the results of computations obtained on the basis of the lifting line approach (Curve I) and those obtained from the application of the lifting surface scheme (Curve II) is shown in Fig. 12.7. From this figure, it can be seen that substantial differences in the computed results appear in the blade tip regions.

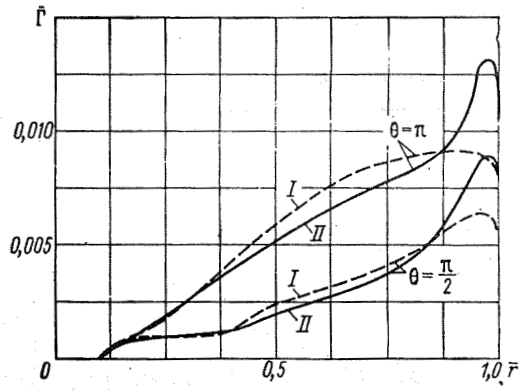

Figure 12.7

CHAPTER XIII

THEORY OF CYLINDRICAL FUNCTIONS AND TIME-AVERAGE INDUCED VELOCITIES

The theory of cylindrical functions can be effectively applied to the task of determining a field of time-averaged induced velocities. Special attempts to apply those methods can be found in Refs. 107 and 109. A general solution of the task of finding a field of the time-average induced velocities for the case of a three-dimensional vortex system and circulation varying over the disc was obtained on the basis of methods reported in those references. This solution can be used for airscrews as well as circular wings.

1. VORTEX WAKE OF A BLADE

Let us replace helicopter rotor blades by R-long segments of bound vortices which rotate around the Oy rotor axis with a constant angular velocity ω and remain in the Oxz plane. Circulation Γ of the blade bound vortex is assumed to be a function of the distance ρ from a point on the vortex to the axis of rotation, and a periodic function of the blade azimuth angle ψ: $\Gamma = \Gamma(\rho, \psi)$. As a result of the Γ variation with both ρ and ψ, a vortex wake, whose elements move at the speed of the fluid particles, springs from the blade. We will examine the movement of those particles in the $Oxyz$ coordinate system connected with the helicopter.

After a vortex element leaves the blade from radius ρ at instant τ and blade azimuth ϑ_τ, it will move within some field of velocities $V(r, t)$ so that at time t, its position will be defined by the following radius vector

$$\mathbf{r}(t) = \mathbf{r}^*(\tau) + \int_{t'=\tau}^{t'=t} \mathbf{V}'(\mathbf{r}(t'), t')\, dt'. \qquad (13.1)$$

Here, $\boldsymbol{r}^*$ is the radius vector of the blade point at the instance of the vortex separation, and is expressed as follows:

$$\mathbf{r}^*(\tau) = -\mathbf{i}\rho\cos\vartheta + \mathbf{k}\rho\sin\vartheta.$$

Accepting the assumptions of the linear vortex theory, we assume that the velocity $\boldsymbol{V}'$ appearing in Eq. (13.1) of the transport of vortices is constant. Let V_x and V_y be, respectively, projections of the helicopter translational velocity on axes Ox and Oy. Let us determine by V'_y, a sum of velocity V_y and induced velocity averaged over the disc; then the transport velocity of the vortices will be

$$\mathbf{V}' = -\mathbf{i}V_x - \mathbf{j}V'_y.$$

If one integrates Eq. (13.1) assuming $V' = const$, and expresses times t and τ in Eq. (13.1) through azimuth angles ψ and ϑ corresponding to those instances, then the coordinates x, y, z of point $\boldsymbol{r}$ on the vorticity surface will be

$$\begin{aligned} x &= -\varrho\cos\vartheta + V_x\frac{\vartheta-\psi}{\omega}, \\ y &= \frac{V'_y}{\omega}(\vartheta-\psi), \\ z &= \varrho\sin\vartheta, \end{aligned} \tag{13.2}$$

where $0 \leq \rho \leq R$, $-\infty < \vartheta \leq \psi$.

Eq. (13.2) represents parametric equations defining the shape of surface S_ψ (vorticity wake). The vorticity wake represents a skewed helical surface which is generated by segment MN of length R (which was in the initial moment at the position of the blade), if we imagine that it rotates with an angular velocity opposite to ω (of the rotor) while at the same time, its point M moves with velocity V', making some angle with the plane of rotation of segment MN (Fig. 13.1). Parameters ρ, ψ, ϑ may be considered as curvilinear "skewed helix" coordinates of points in space, while the coordinate surface corresponding to $\psi = const$, coincides with the skewed helical surface, S_ψ. Assuming $\vartheta = const$ in Eq. (13.2) we will obtain segments of straight lines, and making $\rho = const$, we will obtain skewed helical lines. For $\rho = 0$, Eq. (13.2) defines a straight line, which may be called the axis of the S_ψ surface. In the particular case of $V'_y \to 0$ $(V_x \neq 0)$ the surface S changes into a flat figure with overlapping regions (this case was considered in Ch. II).

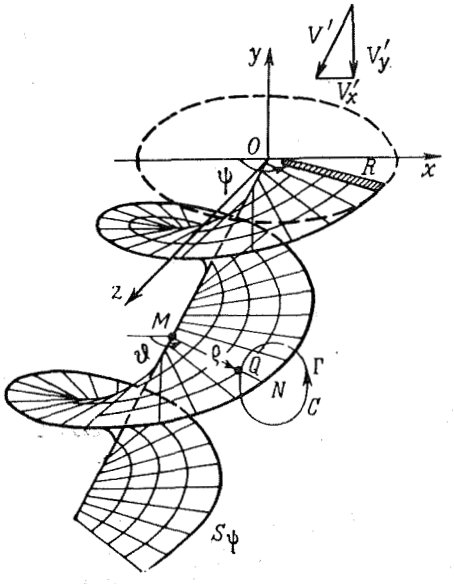

Figure 13.1

2. SCALAR VELOCITY POTENTIAL

Vorticity wake S_ψ consists of free vortices which, together with the bound vortices, make the complete vortex system generated by the blades. These vortices induce, in the surrounding

air, a field of velocities $\mathbf{v}$, depending on the shape of surface S_ψ. The velocity circulation Γ_C along a closed contour C piercing the vorticity wake in an arbitrary point $Q(\rho, \vartheta)$ is equal, as can easily be seen, to the circulation of the bound vortex at the instant of its cutting the C contour; i.e., $\Gamma_C = \Gamma(\rho, \vartheta)$.

Velocity potential Φ of velocities generated by the vortices covering surface S_ψ can be obtained by locating on that surface, doublets of intensity $\Gamma(\rho, \vartheta)$ oriented along the normals to the surface. Then, for the potential of the wake which left the blade at an azimuth angle ψ, we obtain the following expression:

$$\Phi(\psi, \mathbf{r}_0) = -\int_{S_\psi} \frac{\Gamma(\varrho, \vartheta)}{4\pi} \frac{\partial}{\partial n}\left(\frac{1}{l}\right) dS. \qquad (13.3)$$

Here, $l = |\mathbf{r} - \mathbf{r}_0|$ is the distance from point $(\mathbf{r}_0)$ in which the potential is calculated to the point of integration $(\mathbf{r})$; the symbol $\partial/\partial n$ means differentiation with respect to the coordinates of point (r) in the direction of $\mathbf{n}$, a normal to surface S_ψ. Taking advantage of the following relationships,

$$\frac{\partial}{\partial n}\left(\frac{1}{l}\right) = \mathbf{n}\,\mathrm{grad}\left(\frac{1}{l}\right), \quad \mathbf{n}\,dS = \left[\frac{\partial \mathbf{r}}{\partial \vartheta} \times \frac{\partial \mathbf{r}}{\partial \varrho}\right] d\varrho d\vartheta,$$

it is possible to give the following form, in expressing potential Φ, to Eq. (13.3):

$$\Phi(\psi, \mathbf{r}_0) = -\int_{S_\psi} \frac{\Gamma(\varrho, \vartheta)}{4\pi} \left[\frac{\partial \mathbf{r}}{\partial \vartheta} \times \frac{\partial \mathbf{r}}{\partial \varrho}\right] \mathrm{grad}\left(\frac{1}{l}\right) dS$$

or, by expanding the mixed vectorial product, we obtain

$$\Phi(\psi, \mathbf{r}_0) = \int_0^R \int_{-\infty}^{\psi} \frac{\Gamma(\varrho, \vartheta)}{4\pi\omega} \left\{(\omega\varrho + V_x \sin\vartheta)\frac{\partial}{\partial y}\left(\frac{1}{l}\right) - \right.$$
$$\left. - V_y' \left[\frac{\partial}{\partial x}\left(\frac{1}{l}\right)\sin\vartheta + \frac{\partial}{\partial z}\left(\frac{1}{l}\right)\cos\vartheta\right]\right\} d\varrho d\vartheta. \qquad (13.4)$$

When integrating Eq. (13.4) along the surface, it is necessary to first compute the derivatives of $1/l$ and to represent coordinates x, y, z appearing in the obtained expressions as functions of parameters ρ and ϑ. In this approach the potential will depend on blade azimuth ψ which appears in the limits of integration as well as in the subintegral function.

3. TIME AVERAGING

The time average potential, $\Phi_{cp}(\mathbf{r}_0)$ of velocities induced by free vortices generated by the rotor is obtained in the

following way: Potential $\Phi(\psi, r)$ of the vortex wake springing from each of the k blades is averaged with respect to ψ, and the thus obtained expressions are summed up. In this way,

$$\Phi_{cp}(r_0)=\frac{k}{2\pi}\int_0^{2\pi}\Phi(\psi, r_0)\,d\psi \tag{13.5}$$

or, in an expanded form,

$$\Phi_{cp}=\int_0^{2\pi}d\psi\int_0^{R}d\varrho\int_{-\infty}^{\psi}\frac{k\Gamma(\varrho,\vartheta)}{8\pi^2\omega}\times$$
$$\times\left\{W'_x\frac{\partial\left(\frac{1}{l}\right)}{\partial y}-V'_y\left[\frac{\partial\left(\frac{1}{l}\right)}{\partial x}\sin\vartheta+\frac{\partial\left(\frac{1}{l}\right)}{\partial z}\cos\vartheta\right]\right\}d\vartheta, \tag{13.6}$$

where $W'_x = \omega\rho + V_x \sin\vartheta$, and x, y, z are defined by Eq. (13.2).

The integrand of Eq. (13.4) has singularities; hence, during integration of potential $\Phi(\psi, r_0)$ with respect to ψ, it is necessary that point (r_0) is not located on surface S_ψ. Consequently, Eq. (13.5) defines the velocity potential at points located outside of the skewed half-cylinder K (Fig. 13.2). The base of this cylinder coincides with the rotor disc, while its generatrices are parallel to the translatory velocity of vortices (vector V'). The flow is potential (irrotational) only on the outside of this cylinder while inside, the flow is rotational.

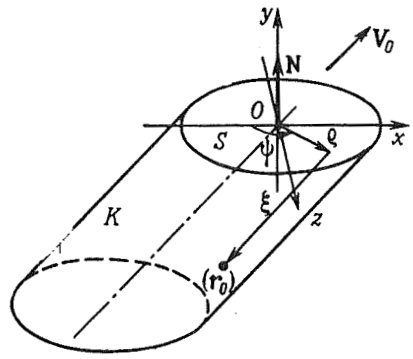

Figure 13.2

Instead of "skewed helical" coordinates ρ, ψ, ϑ, let us introduce "skewed cylindrical" coordinates ρ, ψ, ξ (see Fig. 13.2) which are related to the Cartesian coordinates in the following way:

$$x = -\varrho\cos\psi - \frac{V_x}{V'}\xi,$$
$$y = -\frac{V'_y}{V'}\xi, \qquad (13.7)$$
$$z = \varrho\sin\psi.$$

Parameter ξ represents a distance along the axis of the skewed cylinder from a point on the rotor disc with polar coordinates ρ,ψ to a point (x,y,z). Switching, in the integral of Eq. (13.6), to the new coordinates, we obtain

$$\Phi_{cp} = \frac{k}{8\pi^2 V'}\int_0^\infty d\xi \int_0^R\int_0^{2\pi} \Gamma(\varrho,\psi)\times$$
$$\times\left\{W_x\frac{\partial\left(\frac{1}{l}\right)}{\partial y} - V'_y\left[\frac{\partial\left(\frac{1}{l}\right)}{\partial x}\sin\psi + \frac{\partial\left(\frac{1}{l}\right)}{\partial z}\cos\psi\right]\right\} d\varrho d\psi, \qquad (13.8)$$

where $W_x = \omega\rho + V_x \sin\psi$, while x,y,z depend on ρ,ψ,ξ according to Eq. (13.7).

Eq. (13.8) represents the potential of doublets distributed inside cylinder K with volumetric density

$$\mathbf{D} = -\frac{k}{2\pi V'_y \varrho}\Gamma(\varrho,\psi)\{W_x\mathbf{j} - V'_y(\sin\psi\mathbf{i} + \cos\psi\mathbf{k})\}. \qquad (13.9)$$

4. POTENTIAL OF THE DOUBLET-COVERED DISC

Let us consider transformation of the integral in Eq. (13.8) into a form more suitable for computations. First of all, let us assume that

$$\Phi_{cp}(\mathbf{r}_0) = \frac{1}{V'}\int_0^\infty \varphi(\mathbf{r}_0,\xi)\,d\xi, \qquad (13.10)$$

where

$$\varphi(\mathbf{r}_0,\xi) = \frac{k}{8\pi^2}\int_0^R\int_0^{2\pi}\Gamma(\varrho,\psi)\times$$
$$\times\left\{W_x\frac{\partial\left(\frac{1}{l}\right)}{\partial y} - V'_y\left[\frac{\partial\left(\frac{1}{l}\right)}{\partial x}\sin\psi + -\frac{\partial\left(\frac{1}{l}\right)}{\partial z}\cos\psi\right]\right\} d\varrho d\psi. \qquad (13.11)$$

The quantity $\phi(r_0, \xi)$ can be interpreted as a potential of velocities induced by the doublet-covered disc S_ξ. The latter represents an element of the skewed cylinder, cut out from it by two infinitismally close surfaces, parallel to the $x0z$ plane and intersecting the cylinder axis at a point ξ distant from the rotor disc center. Eq. (13.10) reduced the computation of Φ_{cp} at a fixed point (x_0, y_0, z_0) to a summation of potential $\phi(r_0, \xi)$ with respect to the displacement of disc S_ξ.

The subintegral expression in Eq. (13.11) indicates that a part of the doublets located on disc S_ξ is oriented along the normal $-N$. The surface intensity of such doublets is

$$\sigma_1(\varrho, \psi) = \frac{k}{2\pi\varrho} \Gamma(\varrho, \psi) W_{x'}. \tag{13.12}$$

The remaining doublets on disc S_ξ are oriented in the direction of increasing ψ along tangents to the circles $\rho = const$, and their surface intensity is

$$\sigma_2(\varrho, \psi) = \frac{k}{2\pi\varrho} \Gamma(\varrho, \psi) V'_y. \tag{13.13}$$

According to the Joukowsky formula, in the expressions for $\rho_0\sigma_1$ and $\rho_0\sigma_2$, the multipliers of $k/2\pi\rho$ are lift and drag per unit length of the blade bound vortex. (Here, and afterwards, ρ_0 is the air density.)

Let us transform Eq. (13.11) into a form more convenient for calculations. In order to do this, we introduce a new coordinate system $O'x'y'z'$, obtained from the $Oxyz$ system through a parallel displacement of the coordinates origin O into the center of the disc S_ξ. As can be seen from Fig. 13.3

$$x' = x + \frac{V_x}{V'}\xi, \quad y' = y + \frac{V'_y}{V'}\xi, \quad z' = z. \tag{13.14}$$

Cylindrical coordinates corresponding to the $O'x'y'z'$ system will be defined as r', y', ϑ'. In that coordinate system, integral of Eq. (13.11) in light of Eqs. (13.14) and (13.13), can be rewritten as

$$\varphi(r_0, \xi) = \frac{1}{4\pi} \int_0^R \int_0^{2\pi} \left[\sigma_1(r', \vartheta') \frac{\partial\left(\frac{1}{l}\right)}{\partial y'} - \sigma_2(r', \vartheta') \frac{\partial\left(\frac{1}{l}\right)}{r'\partial\vartheta'} \right] r' dr' d\vartheta', \tag{13.15}$$

where

$$l = \sqrt{(x' - x'_0)^2 + (y' - y'_0)^2 + (z' - z'_0)^2},$$

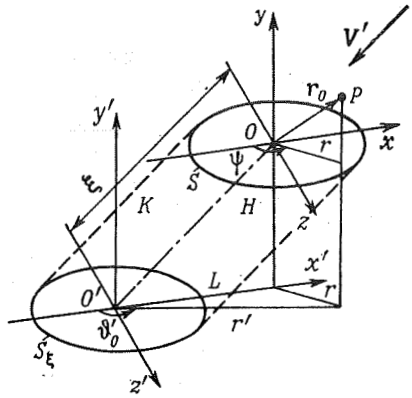

Figure 13.3

and variables of integration x', y', z' depend on r' and ϑ' in the following way

$$x' = -r' \cos \vartheta', \; y' = 0, \; z' = r' \sin \vartheta'.$$

Taking advantage of directly proven relationships,

$$\frac{\partial}{\partial y_0'}\left(\frac{1}{l}\right) = -\frac{\partial}{\partial y'}\left(\frac{1}{l}\right), \; \frac{\partial}{\partial \vartheta_0'}\left(\frac{1}{l}\right) = -\frac{\partial}{\partial \vartheta'}\left(\frac{1}{l}\right)$$

and taking differentiation outside of the integral signs, Eq. (13.15) can be presented in the following form:

$$\varphi(\mathbf{r}_0, \xi) = \frac{\partial \varphi_1}{\partial y_0'} - \frac{\partial \varphi_2}{\partial \vartheta_0'}, \tag{13.16}$$

where

$$\varphi_i(\mathbf{r}_0, \xi) = -\frac{1}{4\pi} \int_0^{2\pi} \int_0^R \frac{F_i(r', \vartheta')}{l} r' dr' d\vartheta' \quad (i = 1, 2).$$
$$F_1 = \sigma_1, \; F_2 = \sigma_2 / r'. \tag{13.17}$$

As can be seen from Eq. (13.17), function ϕ_i represents the velocity potential generated by sources distributed over disc S_ξ with density F_i.

5. INTRODUCTION OF CYLINDRICAL FUNCTIONS

By expanding potential with the help of cylindrical functions, Eq. (13.17) can be replaced by an expression suitable for calculations. Potential ϕ_i of disc S_ξ covered with sources has the following characteristics which would permit one to explicitly define ϕ_i, still omitting Eq. (13.17):

(1) With the exception of disc S_ξ, function $\phi_i(\mathbf{r}_0, \xi)$ satisfies the Laplace equation.

(2) At infinite distances from disc S_ξ, function ϕ_i approaches zero.

(3) If a point moves toward the $y'=0$ plane (in which lies disc S_ξ) from the side of the positive y', then the following boundary condition are fulfilled:

$$\lim_{y'\to+0}\frac{\partial\varphi_i}{\partial y'}=\begin{cases}F_i/2 & \text{for } r'<R,\\ 0 & \text{for } r'>R.\end{cases} \tag{13.18}$$

For $y'\geq 0$, the above given conditions are satisfied by the following solution of the Laplace equation in cylindrical coordinates r', ϑ', y':

$$\varphi_i(\mathbf{r},\xi)=-\frac{1}{2}\sum_{m=-\infty}^{\infty}\int_0^\infty d\varkappa\int_0^R e^{-\varkappa y'}J_m(\varkappa r')J_m(\varkappa\varrho)\times$$
$$\times\left[F_m^{ci}(\varrho)\cos m\vartheta'+F_m^{si}(\varrho)\sin m\vartheta'\right]\varrho\,d\varrho, \tag{13.19}$$

where $J_m(z)$ is the Bessel function of the first kind of order m and of argument z[77], while

$$F_m^{ci} \quad \text{and} \quad F_m^{si}$$

are the coefficients of an expansion of F_i into Fourier series,

$$F_i(\varrho,\vartheta)=\sum_{m=-\infty}^{\infty}\left[F_m^{ci}(\varrho)\cos m\vartheta+F_m^{si}(\varrho)\sin m\vartheta\right], \tag{13.20}$$

where, in addition, it is assumed that $F_m^{ci}=F_{-m}^{ci}$, $F_m^{si}=-F_{-m}^{si}$. Eq. (13.19) represents superposition of an infinite number of particular solutions of the Laplace equation in cylindrical coordinates of the following form,

$$\chi_1=e^{-\varkappa y'}J_m(\varkappa z')\sin m\vartheta', \quad \chi_2=e^{-\varkappa y'}J_m(\varkappa z')\cos m\vartheta'$$

and for this reason, it also satisfies the Laplace equation. In order to verify that the boundary conditions of Eq. (13.18) are also fulfilled, it is sufficient to differentiate Eq. (13.19) and, going to the limit with $y'\to 0$, take advantage of the Hankel integral

$$f(\varrho)=\int_0^\infty tJ_m(\varrho t)\,dt\int_0^\infty sf(s)J_m(st)\,ds,$$

which is analogous to the Fourier integral of Bessel functions ($f(p)$ is an arbitrary function).

For the condition of $y' \geq 0$, the integrals in Eq. (13.19) converge. As a result of the uniqueness of the solution of the corresponding boundary condition of the Laplace equation, they give the same values of ϕ_i as Eq. (13.17).

Substituting Eq. (13.19) into Eq. (13.16) and differentiating under the integral sign, we will obtain, for $\phi(r_0, \xi) = \phi(r_0', \vartheta_0', y_0')$ at $y_0' > 0$, the following expression containing integrals of Bessel functions

$$\varphi(r_0', \vartheta_0', y_0') = \frac{1}{2} \sum_{m=-\infty}^{\infty} \int_0^{\infty} \varkappa d\varkappa \int_0^R e^{-\varkappa y_0'} J_m(\varkappa r_0') J_m(\varkappa \varrho) \times$$

$$\times \left\{ \left[F_m^{c1}(\varrho) + \frac{m}{\varkappa} F_m^{s2}(\varrho) \right] \cos m\vartheta_0' + \left[F_m^{s1}(\varrho) - \frac{m}{\varkappa} F_m^{c2}(\varrho) \right] \sin m\vartheta_0' \right\} \varrho d\varrho. \quad (13.21)$$

In order to find potential $\Phi_{cp}(r_0)$ of induced velocities, it is necessary, according to Eq. (13.10), to integrate Eq. (13.21) with respect to variable ξ, while the position in space of the computed point (r_0) remains fixed in the $Oxyz$ system. But, during the determination of the integral in Eq. (13.21), coordinates y_0', r_0', ϑ_0' of that point would vary, depending on ξ. Taking into consideration Eqs. (13.14) and going from Cartesian to cylindrical coordinates, we obtain the following relationships defining variations of r_0', ϑ_0' y_0' with respect to ξ:

$$r_0' = \sqrt{r^2 + L^2 - 2rL \sin \psi},$$

$$e^{2i\vartheta_0'} = \frac{L - re^{i\psi}}{L - re^{-i\psi}}, \quad (13.22)$$

$$y_0' = y + \frac{V_y'}{V'} \xi, \; L = \frac{V_x}{V} \xi.$$

Coordinates r, y and ψ of point r_0 do not change when integrating with respect to ξ.

It can be seen that dependence of the subintegral function in Eq. (13.21) on ξ is quite complicated. Nevertheless, taking advantage of the known theorem of compounding[77], it is generally possible to integrate Eq. (13.4) with respect to ξ, from 0 to ∞ which, strictly speaking, justifies such a form of representing ϕ_i.

6. APPLICATION OF THE THEOREM OF COMPOUNDING

We take advantage of Graeffe's theorem of summation, known in the theory of cylindrical functions (see Ref. 77, Eq. 6.541,1*)

*According to the numbering system of equations in Ref. 77)

according to which the following equalities are correct

$$\cos m\vartheta_0' J_m(\varkappa r_0') = (-1)^m \sum_{n=-\infty}^{\infty} J_n(\varkappa r) J_{n+m}(\varkappa L) \cos n\psi,$$
$$\sin m\vartheta_0' J_m(\varkappa r_0') = -(-1)^m \sum_{n=-\infty}^{\infty} J_n(\varkappa r) J_{n+m}(\varkappa L) \sin n\psi, \tag{13.23}$$

where parameters r, ψ, r_0', ϑ_0' and L are associated with each other through the relationship in Eq. (13.22). From the geometric point of view, L, r and r_0' represent lengths of the sides of a triangle; ψ is the angle between sides L and r; ϑ_0' is the external angle between sides L and r (see Fig. 13.3). Replacing products $J_m(\varkappa r_0') \sin m\vartheta_0'$ and $J_m(\varkappa r_0') \cos m\vartheta_0'$ appearing in Eq. (13.21) with their expressions from Eq. (13.23), and returning to coordinates y, r, ψ of point r_0, it is possible to write

$$\varphi(\mathbf{r}, \xi) = \frac{1}{2} \sum_{m=-\infty}^{\infty} (-1)^m \int_0^{\infty} \varkappa d\varkappa \int_0^R e^{-\varkappa\left(y+\xi\frac{V_y'}{V'}\right)} J_m(\varkappa\varrho) \sum_{n=-\infty}^{\infty} J_{n+m}\left(\varkappa\frac{V_x'}{V'}\xi\right) \times$$
$$\times J_n(\varkappa r)\left\{\left[F_m^{c1}(\varrho) + \frac{m}{\varkappa} F_m^{s2}(\varrho)\right]\cos n\psi - \left[F_m^{s1}(\varrho) - \frac{m}{\varkappa} F_m^{c2}(\varrho)\right]\sin n\psi\right\} \varrho d\varrho. \tag{13.24}$$

Although the above expressions contain a product of not two, but already, three, cylindrical functions, it is much more convenient than Eq. (13.21). This is due to the fact that the relationship of the subintegral function to variable ξ (with respect to which, integration should be performed) is much simpler; since the quantities ψ and r, in contrast to r_0' and ϑ_0', remain constant when ξ varies. We substitute Eq. (13.24) into Eq. (13.10) and change the order of integration and summation. Then, we obtain

$$\Phi_{cp}(r, \psi, y) = \frac{1}{2V'} \sum_{n=-\infty}^{\infty} \sum_{m=-\infty}^{\infty} (-1)^m \int_0^{\infty} d\xi \int_0^{\infty} \varkappa d\varkappa \int_0^R e^{-\varkappa\left(y+\xi\frac{V_y'}{V'}\right)} J_n(\varkappa r) \times$$
$$\times J_m(\varkappa\varrho) J_{m+n}\left(\varkappa\frac{V_x}{V'}\xi\right)\left\{\left[F_m^{c1}(\varrho) + \frac{m}{\varkappa} F_m^{s2}(\varrho)\right]\cos n\psi - \right.$$
$$\left. - \left[F_m^{s1}(\varrho) - \frac{m}{\varkappa} F_m^{c2}(\varrho)\right]\sin n\psi\right\} \varrho d\varrho. \tag{13.25}$$

It should be noted that in the above expression, in contrast to Eq. (13.21), parameter ψ (azimuth angle of a point on the rotor disc) is under the sign of the trigonometric functions; so that Eq. (13.25) gives an expansion of potential Φ_{cp} into the Fourier series with respect to ψ.

The integral of variable ξ which appears in Eq. (13.25) corresponds to the summation of induced velocities along the vorticity cylinder and can be computed, according to Eq. (4.421.1) of Ref. 77, as

$$\int_0^\infty e^{-\alpha x} J_p(\beta x)\, dx = \frac{(\sqrt{\alpha^2+\beta^2}-\alpha)^p}{\beta^p \sqrt{\alpha^2+\beta^2}} \quad (p \geqslant 0), \tag{13.26}$$

Furthermore, in the case of Bessel functions with a negative index, it is necessary to take advantage of the relationship $J_{-p}(x) = (-1)^p J_p(x)$. After suitable transformations, we obtain from Eq. (13.25)

$$\Phi_{\text{ср}}(r, \psi, y) = \frac{1}{2} \sum_{n=-\infty}^{\infty} \sum_{m=-\infty}^{\infty} (-1)^m A_{n+m} \int_0^\infty e^{-\varkappa y} d\varkappa \int_0^R J_n(\varkappa r) J_m(\varkappa \varrho) \times$$
$$\times \left\{ \left[F_m^{c1}(\varrho) + \frac{m}{\varkappa} F_m^{s2}(\varrho) \right] \cos n\psi - \left[F_m^{s1}(\varrho) - \frac{m}{\varkappa} F_m^{c2}(\varrho) \right] \sin n\psi \right\} \varrho d\varrho, \tag{13.27}$$

where

$$A_p = \frac{1}{V'} \left(\frac{V' - V_y'}{V_x} \right)^p, \quad A_{-p} = (-1)^p A_p \quad (p = 0, 1, 2, 3, \ldots).$$

Once Eq. (13.27) giving expressions for the potential is obtained, one can find the induced velocity components

$$v_y = \frac{\partial \Phi_{\text{ср}}}{\partial y}, \quad v_r = \frac{\partial \Phi_{\text{ср}}}{\partial r}, \quad v_\psi = \frac{1}{r} \frac{\partial \Phi_{\text{ср}}}{\partial \psi}$$

After a differentiation under the integral sign and utilization of the formula for the derivative of Bessel function $2J_p'(z) = J_{p-1}(z) - J_{p+1}(z)$, we obtain

$$v_y(r, \psi, y) = -\frac{1}{2} \sum_{n=-\infty}^{\infty} \sum_{m=-\infty}^{\infty} (-1)^m A_{n+m} \int_0^\infty e^{-\varkappa y} \varkappa\, d\varkappa \int_0^R J_n(\varkappa r) J_m(\varkappa \varrho) \times$$
$$\times \left\{ \left[F_m^{c1}(\varrho) + \frac{m}{\varkappa} F_m^{s2}(\varrho) \right] \cos n\psi - \left[F_m^{s1}(\varrho) - \frac{m}{\varkappa} F_m^{c2}(\varrho) \right] \sin n\psi \right\} \varrho d\varrho, \tag{13.28}$$

$$v_\psi(r, \psi, y) = -\frac{1}{2r} \sum_{n=-\infty}^{\infty} \sum_{m=-\infty}^{\infty} (-1)^m A_{n+m} \int_0^\infty e^{-\varkappa y} d\varkappa \int_0^R J_n(\varkappa r) J_m(\varkappa \varrho) \times$$
$$\times \left\{ \left[F_m^{s1}(\varrho) - \frac{m}{\varkappa \varrho} F_m^{c2}(\varrho) \right] n \cos n\psi + \left[F_m^{c1}(\varrho) + \frac{m}{\varkappa \varrho} F_m^{s2}(\varrho) \right] n \sin n\psi \right\} \varrho d\varrho, \tag{13.29}$$

$$v_r(r, \psi, y) = \frac{1}{4} \sum_{n=-\infty}^{\infty} \sum_{m=-\infty}^{\infty} (-1)^m A_{n+m} \int_0^{\infty} e^{-\varkappa y} \varkappa d\varkappa \times$$

$$\times \int_0^R [J_{n-1}(\varkappa r) - J_{n+1}(\varkappa r)] J_m(\varkappa \varrho) \left\{ \left[F_m^{c1}(\varrho) + \frac{m}{\varkappa \varrho} F_m^{s2}(\varrho) \right] \cos n\psi - \right.$$

$$\left. - \left[F_m^{s2}(\varrho) - \frac{m}{\varkappa \varrho} F_m^{c2}(\varrho) \right] \sin n\psi \right\} \varrho d\varrho. \qquad (13.30)$$

Quantities $A_p (p = m + n)$ appearing in Eqs. (13.28)-(13.30) are constant, dependent only on parameters V_x and V'_y, characterizing the helicopter regime of flight.

Let us consider, in greater detail, Eq. (13.28) expressing v'_y perpendicular to the disc component of induced velocity, as this is of the greatest interest. In the development of that relationship, it was assumed that velocities are determined at points of the upper half of space, while the vortex wake moves into the lower half. This corresponds to the following limitations: $V'_y \geq 0$, $y > 0$. However, due to the continuity of v_y at $y \geq 0$ in Eq. (13.28); it is possible to go to the limit of $y \to 0$ and, with the so-obtained expressions, compute induced velocities directly in the rotor disc plane. In addition, it is possible in Eq. (13.28) to go to the limit for $V'_y \to 0$ independently of the y values which correspond to the case of a flat vorticity wake. However, Eq. (13.28) is of no use for the calculations of induced velocities in the half-space where, for $V'_y \neq 0$, there is a cylinder of vorticity. In particular, when $V'_y > 0$, then from Eq. (13.28), one can compute velocities only in the upper half of space, $y > 0$. If $V'_y < 0$, then by changing direction of the axes, it is possible to use Eq. (13.28) for computations of velocities in the lower half of space, $y < 0$. In order to unify all the considered cases, it is possible to modify Eq. (13.28), introducing into it, $|V'_y|$ and $|y|$ instead of V'_y and y. It should be remembered, however, that the formula is applicable only at those points in space where both y and V'_y are of the same sign.

7. NONDIMENSIONAL FORM OF VELOCITY INTEGRALS AND MODIFICATIONS OF $J_{n,m}$

Let us rewrite Eq. (13.28) in a nondimensional form. All linear dimensions will be related to the rotor radius R. Velocities V_x, V'_y and v_y will be related to the tip speed in the following way:

$$\mu=\frac{V_x}{\omega R},\qquad \lambda=\frac{V_y'}{\omega R},\qquad \bar{v}_y=\frac{v_y}{\omega R}.$$

Instead of coefficients A_p appearing in Eq. (13.28), we will introduce the corresponding nondimensional coefficients:

$$\bar{A}_p=\frac{1}{\sqrt{\mu^2+\lambda^2}}\left\{\frac{\sqrt{\mu^2+\lambda^2}-|\lambda|}{\mu}\right\}^p,\quad \bar{A}_{-p}=(-1)^p\bar{A}_p\,(p=0,1,2,3,\ldots).$$

We will also define reduced circulation g and unit thrust p (per running unit of length) of the blade by the following formulae (ρ_0 - *air density*)

$$g=\frac{2\Gamma}{a_\infty b_0\omega R^2},\qquad p=\frac{2Y}{\varrho_0 a_\infty b_0\omega^2R^2},$$

where $Y=\rho_0 W_x\Gamma$ is the unit thrust of the blade; $a_\infty=dC_y/d\alpha$ is assumed to be constant, and b_0 is the characteristic chord of the blade, say at a radius $\bar{r}=0{,}7$.

With the introduction of the above-given nondimensional quantities, the expression for induced velocity normal to the rotor disc, Eq. (13.28), assumes the following form:

$$\bar{v}_y(\bar{r},\psi,\bar{y})=-\frac{a_\infty\sigma}{8}\sum_{n=-\infty}^{\infty}\sum_{m=-\infty}^{\infty}(-1)^m\bar{A}_{n+m}\int_0^\infty e^{-z\bar{y}}z\,dz\int_0^1 J_n(\bar{r}z)\,J_m(\bar{\varrho}z)\times$$
$$\times\left\{\left[\frac{p_m^c(\bar{\varrho})}{\bar{\varrho}}+\frac{m\lambda}{z\bar{\varrho}^2}g_m^s(\bar{\varrho})\right]\cos n\psi-\left[\frac{p_m^s(\bar{\varrho})}{\bar{\varrho}}-\frac{m\lambda}{z\bar{\varrho}^2}g_m^c(\bar{\varrho})\right]\sin n\psi\right\}\bar{\varrho}\,d\bar{\varrho}. \qquad (13.31)$$

Here, p_m^c, p_m^s, g_m^c, g_m^s represent coefficients appearing in the expansion of the reduced circulation and lift per unit length into a Fourier series:

$$p(r,\psi)=\sum_{m=-\infty}^{\infty}p_m^c\cos m\psi+p_m^s\sin m\psi, \qquad (13.32)$$
$$g(r,\psi)=\sum_{m=-\infty}^{\infty}g_m^c\cos m\psi+g_m^s\sin m\psi,$$

where it is assumed, as before, that

$$p_{-m}^c=p_m^c,\quad p_{-m}^s=-p_m^s,\quad g_{-m}^c=g_m^c,\quad g_{-m}^s=-g_m^s.$$

Let us develop Eq. (13.31) by expanding coefficients of induced velocity $v_y(\bar{r},\psi,\bar{y})$ into a Fourier series

$$\bar{v}_y=\lambda_0^c+2\sum_{n=1}^{\infty}(\lambda_n^c\cos n\psi+\lambda_n^s\sin n\psi), \tag{13.33}$$

which, under the assumption of $\lambda_n^c = \lambda_{-n}^c$ $\lambda_n^s = -\lambda_{-n}^s$, can be rewritten as follows:

$$\bar{v}_y=\sum_{n=-\infty}^{\infty}(\lambda_n^c\cos n\psi+\lambda_n^s\sin n\psi). \tag{13.34}$$

Coefficients of the series of Eq. (13.34) are defined (according to Eq. (13.31)) by the following series

$$\lambda_n^c=\sum_{m=0}^{\infty}\lambda_{n,m}^c,\quad \lambda_n^s=\sum_{m=1}^{\infty}\lambda_{n,m}^s\ (n=0,1,2,3\ldots), \tag{13.35}$$

whose terms, we can present as follows:

$$\lambda_{n,m}^c=-\frac{a_\infty{}^\sigma}{8}K_{n,m}^c\tilde{\lambda}_{n,m}^c(\bar{r}),\ \lambda_{n,m}^s=-\frac{a_\infty{}^\sigma}{8}K_{n,m}^s\tilde{\lambda}_{n,m}^s(\bar{r}). \tag{13.36}$$

Here,

$$K_{n,0}^c=\bar{A}_n,\ K_{n,m}^c=\bar{A}_{n-m}+(-1)^mA_{n+m},\ K_{n,m}^s=\bar{A}_{n-m}-(-1)^m\bar{A}_{n+m}, \tag{13.37}$$

$$\tilde{\lambda}_{n,m}^c=J_{n,m}\left\{\frac{p_m^c(\bar{\varrho})}{\bar{\varrho}}\right\}+\frac{\lambda}{2}\left[J_{n,m-1}\left\{\frac{g_m^s(\bar{\varrho})}{\bar{\varrho}}\right\}+J_{n,m+1}\left\{\frac{g_m^s(\bar{\varrho})}{\bar{\varrho}}\right\}\right],$$

$$\tilde{\lambda}_{n,m}^s=J_{n,m}\left\{\frac{p_m^s(\bar{\varrho})}{\bar{\varrho}}\right\}-\frac{\lambda}{2}\left[J_{n,m-1}\left\{\frac{g_m^c(\bar{\varrho})}{\bar{\varrho}}\right\}+\right.$$

$$\left.+J_{n,m+1}\left\{\frac{g_m^c(\bar{\varrho})}{\bar{\varrho}}\right\}\right]\ (n,m=0,1,2,3\ldots), \tag{13.38}$$

where symbol $J_{n,m}\{\phi(\rho)\}$ means the following integral

$$J_{n,m}\{\varphi(\varrho)\}=\int_0^{\infty}e^{-z\bar{y}}z\ dz\int_0^1 J_n(\bar{r}z)J_m(\varrho z)\varphi(\varrho)\varrho d\varrho. \tag{13.39}$$

This integral of any arbitrary function $\phi(\rho)$ represents some new function of radius $\bar{r}$. This means that it becomes a functional operator, which we will call $J_{n,m}$ - a transform of that function.

Since, for the helicopter rotor, always $\lambda \ll 1$, hence, all terms having λ as a multiplier may be considered as small (for

a flat vorticity wake, they are equal to zero) and thus, may be neglected. In view of the above Eq. (13.38) defining functions $\tilde{\lambda}^c_{n,m}$, $\tilde{\lambda}^s_{n,m}$ will assume a simpler form

$$\tilde{\lambda}^c_{n,m}=J_{n,m}\left\{\frac{p^c_m(\bar{\varrho})}{\bar{\varrho}}\right\},\quad \tilde{\lambda}^s_{n,m}=J_{n,m}\left\{\frac{p^s_m(\bar{\varrho})}{\bar{\varrho}}\right\}. \tag{13.40}$$

For practical applications of Eq. (13.40), it is necessary to find the integral given by Eq. (13.39). In the particular case of $n=m$, this task is solved immediately, where, with the help of the Hankel integral, we obtain

$$J_{n,n}\{\varphi(\bar{\varrho})\}=\varphi(\bar{r}). \tag{13.41}$$

In the general case of $n\neq m$, the integral of Eq. (13.39) can be found analytically for a large class of functions ϕ_ν, forming a "complete system." Expanding an arbitrary function ϕ into a series with respect to functions ϕ_ν of such a system and then summing up $J_{n,m}$, transforms of those functions (with the same coefficients), we obtain $J_{n,m}$, a transform of function ϕ.

Later, as basic functions, we will take power functions of the following form

$$\varphi_m(\bar{\varrho})=\bar{\varrho}^m(1-\bar{\varrho}^2)^{q/2}, \tag{13.42}$$

as well as the associated Legendre polynomials.

We define, by $Y^q_{n,m}(\bar{r})$, the result $J_{n,m}$-transform of function $\phi_m(\bar{\rho})$. In Appendix VII, recurring formulae for $Y^q_{n,m}(\bar{r})$ are given which, starting from low values of q and m would permit one to find those functions.

8. INTERPOLATING TRIGONOMETRIC AND LEGENDRE POLYNOMIALS

For practical computations of induced velocities, we approximate function $\phi(\rho)$ appearing in Eq. (13.39). This is done with the help of the trigonometric interpolating polynomials, which assume prescribed values at a finite number of control points. In order to construct such polynomials, we will take advantage of the following identity:

$$\frac{1+z}{1-z}(1-z^{p+1})=1+2z+2z^2+\ldots+2z^p+z^{p+1},$$

assuming $z=e^{i\theta}$. Then, the left side of the identity becomes a complex function whose real part divided by $2(p+1)$, we will call $\delta(\theta)$. In this way,

$$\delta(\theta)=\frac{1}{2(p+1)}\operatorname{ctg}\frac{\theta}{2}\sin(p+1)\theta.$$

From the right side of the identity, we obtain

$$\delta(\theta)=\frac{1}{2(p+1)}[1+2\cos\theta+2\cos 2\theta+\ldots+2\cos p\theta+\cos(p+1)\theta]. \qquad (13.43)$$

It can be seen from the above that $\delta(0) = 1$ and function $\delta(\theta)$ is even, and within a range $0 < \theta < \pi$, it becomes zero at points $\theta = \theta_k$, where

$$\theta_k=\frac{\pi}{p+1}k \quad (k=1,2,3,\ldots,p).$$

Now, we are going to construct a new function

$$\delta_m^k(\theta)=\frac{\sin^m\theta}{\sin^m\theta_k}[\delta(\theta-\theta_k)+\delta(\theta+\theta_k)-\delta(\theta+\theta_k-\pi)-\delta(\theta-\theta_k+\pi)]$$
$$\left(k=1,2,3,\ldots,\frac{p-1}{2}\right), \qquad (13.44)$$

which, in consideration of Eq. (13.43), has the following form

$$\delta_m^k(\theta)=\frac{4}{p+1}\frac{\sin^m\theta}{\sin^m\theta_k}\sum_{\nu=1}^{\frac{p-1}{2}}\cos(2\nu+1)\theta\cos(2\nu+1)\theta_k \qquad (13.45)$$

(here, p is an odd number; m, an integer or zero). In considering obvious characteristics of function $\delta(\theta)$, it is easy to see that within the range $(0, \pi/2)$ at points $\theta = \theta_l$ where

$$\theta_l=\frac{\pi}{p+1}l \quad \left(l=1,2,3,\ldots,\frac{p-1}{2}\right),$$

we have $\delta_m^k(\theta_l) = 0$, if $l \neq k$, and $\delta_m^k(\theta_l) = 1$ if $l = k$. Graphs of function δ_m^k vs variable $\bar{r} = \sin\theta$ are shown in Fig. 13.4 for $p = 11$, $m = 0$, and various values of k. On radii $\bar{r}_l = \sin\theta_l$ which we will call "keys", functions $\delta_m^k(\bar{r})$ are equal to zero, if $l \neq k$ and unity, if $l = k$. It follows from the above, that a sum of the following form

$$F(\bar{r})=\sum_{k=1}^{\frac{p-1}{2}}F_k\delta_m^k(\bar{r}) \qquad (13.46)$$

represents an interpolating trigonometric polynomial, assuming, at the key radii, $\bar{r}_k$, a priori given values $F_k = F(\bar{r}_k)$. Since values of F_k do not depend on $\bar{r}$, the result $J_{n,m}$ of the transform of function $F(\bar{r})$, given under the form of Eq. (13.46), will be

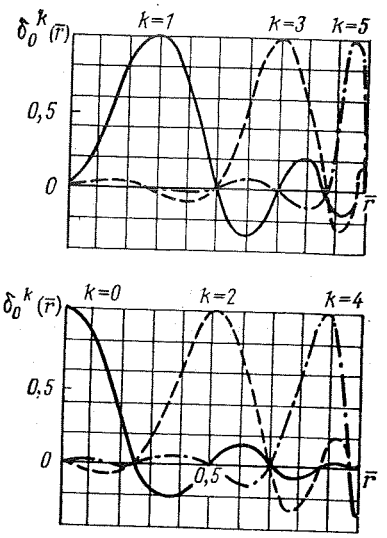

Figure 13.4

$$J_{n,m}\{F(\bar{r})\}=\sum_{k=1}^{\frac{p-1}{2}} F_k \varepsilon_{n,m}^k(\bar{r}), \qquad (13.47)$$

where

$$\varepsilon_{n,m}^k(\bar{r})=J_{n,m}\{\delta_m^k(\bar{r})\}. \qquad (13.48)$$

Functions $\varepsilon_{n,m}^k$ still remain to be calculated.

Expressing cosines of multiple arcs appearing in Eq. (13.45) through powers of cosines, we find, according to Eq. 1.331,1 of Ref. 77, that

$$\cos(2\nu+1)\theta=\sum_{\nu=1}^{\frac{p-1}{2}} d_{\nu,p}\cos^{2\nu+1}\theta,$$

where

$$d_{\nu,p}=(-1)^{p+\nu}2^{2\nu}\frac{2p+1}{p-\nu}\frac{(\nu+2)(\nu+3)\ldots(\nu+p)}{p-\nu+1} \quad \text{for } \nu<p-1,$$

$$d_{\nu,p}=0 \quad \text{for } \nu>p,$$

$$d_{p-1,p}=-2^{2(p-1)}(2p+1),\ d_{p,p}=2^p.$$

After substituting the obtained expression into Eq. (13.45), we obtain

$$\delta_m^k(\theta)=\frac{1}{\sin^m\theta_k}\sum_{\nu=1}^{\frac{p-1}{2}} c_{k,\nu}\bar{r}^m\left(1-\bar{r}^2\right)^{\frac{2\nu+1}{2}}, \qquad (13.49)$$

where

$$c_{k,\nu}=\frac{n}{p+1}\sum_{t=1}^{\frac{p-1}{2}} d_{\nu,t}\cos(2t+1)\theta_k.$$

Consequently, function δ_m^k is a superposition of functions $\phi_m(\bar{r})$ defined in Eq. (13.42). For this reason, from Eqs. (13.48)

we can obtain the sought representation of function $\varepsilon^k_{n,m}(\bar{r})$:

$$\varepsilon^k_{n,m}(\bar{r}) = \frac{1}{\sin^m \theta_k} \sum_{\nu=1}^{\frac{p-1}{2}} c_{k,\nu} Y^{2\nu+1}_{n,m}(\bar{r}). \tag{13.50}$$

As the way of calculating function $Y^q_{n,m}$ is shown in Appendix VII, hence, arrangement of tables of function $\varepsilon^k_{n,m}(\bar{r})$ according to Eq. (13.50) is not difficult. Tables of $\varepsilon^k_{n,m}(\bar{r})$, shown in Appendix IX were obtained in that way. With the help of those tables, it is easy to obtain $J_{n,m}$-transform of an arbitrary function by approxmating it by an interpolating polynomial. Suitable working formulae are developed in Ch. XIV.

Another way of computing the necessary integrals consists of the expansion of function ϕ according to the associated Legendre polynomials. Let

$$\varphi_m(\bar{r}) = P^m_{m+a}(\zeta) \quad (a=1,3,5,\ldots), \tag{13.51}$$

where

$$\zeta = \sqrt{1-\bar{r}^2} \ (0<\bar{r}<1), \ \& \ P^m_{m+a}(z)$$

is the associated Legendre polynomial. Defining

$$J_{n,m}\{P^m_{m+a}\} = S^a_{nm},$$

we obtain

$$S^a_{n,m}(\bar{r},\bar{y}) = \int_0^\infty e^{-\bar{y}z} J_n(\bar{r}z)\, z \ dz \int_0^{\pi/2} J_m(z\sin\theta') P^m_{m+a}(\cos\theta') \sin\theta' \cos\theta' d\theta'. \tag{13.52}$$

This integral is computed under the following form:

$$S^a_{n,m}(\bar{r},\bar{y}) = C P^{-n}_{m+a}(\zeta) Q^n_{m+a}(i\eta), \tag{13.53}$$

where Q^n_{m+a} is the associated Legendre function. Variables ζ and η are elliptic coordinates of point $(\bar{r},\bar{y})$ connected with variable $\bar{r},\bar{y}$ with the help of the following relationships

$$\bar{r} = \sqrt{1-\zeta^2}\sqrt{1+\eta^2}, \ \bar{y} = \eta\zeta.$$

The significance of constant C and the development of Eq. (13.53) are given in Appendix VIII.

9. THE A.V. NEKRASOV METHOD

For $\bar{y} = 0$, computation of $J_{n,m}$-transform of an arbitrary function is reduced to a single integration of the product of this function and the hypergeometric function. This way of calculation of induced velocities was developed and applied by A.V. Nekrasov to practical cases of helicopter design[64]. In determining $J_{n,m}$-transform at $\bar{y} = 0$, we have

$$J_{n,m}\{G_m(\bar{\varrho})\} = \int_0^\infty z J_n(\bar{r}z)\,dz \int_0^1 J_m(\bar{\varrho}z) G_m(\bar{\varrho})\,\bar{\varrho}\,d\bar{\varrho}. \tag{13.54}$$

Taking into consideration that function $G_m(\bar{\rho})$ is not zero only for $a \leq \rho \leq b$ and performing the integration, by parts, of Eq. (13.54), we obtain

$$J_{n,m}\{G_m(\varrho)\} = \left[G_m(\varrho) E_n^{m+1}\left(\frac{\bar{r}}{\bar{\varrho}}\right)\right]_a^b - \int_a^b \bar{\varrho}^m \left[G_m(\bar{\varrho})\,\bar{\varrho}^{-m}\right]' E_n^{m+1}\left(\frac{\bar{r}}{\bar{\varrho}}\right) d\bar{\varrho}, \tag{3.55}$$

where

$$E_n^{m+1}(x) = \int_0^\infty J_{m+1}(z) J_n(xz)\,dz, \tag{13.56}$$

while the dash means differentiation with respect to $\bar{\rho}$.

It is shown in Appendix VIII that function E_n^{m+1} is expressed through hypergeometric functions (see Eqs. (VIII.6) and VIII.7)):

$$E_n^p(x) = \frac{x^n \Gamma\left(\frac{n+p+1}{2}\right)}{\Gamma\left(\frac{p-n+1}{2}\right)\Gamma(n+1)} F\left(\frac{n+p+1}{2}, \frac{n-p+1}{2}; n+1, x^2\right) \quad (x \leqslant 1),$$

$$E_n^p(x) = \frac{\Gamma\left(\frac{p+n+1}{2}\right)}{x^{p+1}\Gamma\left(\frac{n-p+1}{2}\right)\Gamma(p+1)} F\left(\frac{p+n+1}{2}, \frac{p-n+1}{2}; n+1, \frac{1}{x^2}\right) \quad (x > 1). \tag{13.57}$$

Due to the properties of hypergeometric function F from Eq. (13.57), it follows that for $p = n + 2k - 1$ $(k=0,1,2,\ldots)$, the function E_n degenerates into polynomials when $x \leq 1$ and becomes zero for $x > 1$. For $p = n - 2k + 1$ $(k=0,1,2,\ldots)$, the function E_n^p becomes zero when $x < 1$ and for $x > 1$, it degenerates into polynomials. In those cases, computation of function $E_n^p(x)$ is not difficult. In particular, functions $E_0^0(x)$ and $E_1^1(x)$ can be expressed with the help of Eqs. (7.237), (6.113) and (6.114) from Ref. 77 as complete elliptic integrals $E(x)$ and $K(x)$.

In this way, for $|x| < 1$,

$$E_0^0(x)=\frac{2}{\pi}\mathrm{K}(x), \quad E_1^1(x)=\frac{2}{\pi x}[\mathrm{K}(x)-\mathrm{E}(x)], \tag{13.58}$$

and for $|x| > 1$,

$$E_0^0(x)=\frac{2}{\pi x}\mathrm{K}\left(\frac{1}{x}\right), \quad E_1^1(x)=\frac{2}{\pi}\left[\mathrm{K}\left(\frac{1}{x}\right)-\mathrm{E}\left(\frac{1}{x}\right)\right]. \tag{13.59}$$

At the remaining values of p and n corresponding to $p = n + 2k$ $(k=0,1,2,\ldots)$, it is possible to compute function E_n^p by taking advantage of either a direct summation of hypergeometric series or a reduction of function E_n^p (with the help of formulae known for hypergeometric functions) to functions E_0^0 and E_1^1 defined by Eqs. (13.58) and (13.59).

If functions $E_n^p(x)$ are already found, then computation of $J_{n,m}$-transform of an arbitrary function $G_m(\rho)$ is reduced to computation of an ordinary integral which, due to the condition of making $G(\rho) = 0$ at the ends of the interval $(0-1)$ has the following form:

$$J_{n,m}(G_m(\varrho))=-\int_a^b \varrho^m [G_m(\varrho)\varrho^{-m}]' E_n^{m+1}\left(\frac{r}{\varrho}\right) d\varrho \tag{13.60}$$

(dash in the subintegral function means differentiation with respect to ρ).

We obtained a formula permitting one to define, with complete accuracy, the $J_{n,m}$-transform of an arbitrary function $G_m(\rho)$ through a single integration over a finite interval. We thus avoid computation of double integrals (Eq. (13.54)) or Bessel functions. Some inconvenience in the use of Eq. (13.60) consists of that in those cases when the series in Eq. (13.57) does not reduce to polynomials, function $E_n^p(x)$ has a longarithmic peculiarity of the form

$$E_n^p(x)=\frac{\cos\frac{\pi}{2}(n-p)}{\pi}\ln|1-x|+\ldots,$$

where terms which do not become infinite as $x \to 1$ are indicated by dots. However, this peculiarity does not preclude integragration and thus, does not represent a serious obstacle in the determination of the integral in Eq. (13.60). In practical computations, it is convenient to break the interval of variation of ρ in the integral of Eq. (13.60) into parts and to replace

function $G(\rho)/\rho^m$ in those segments by a step curve. In this case, in Eq. (13.55), for every segment, an integral term becomes zero and consequently, computations are reduced to a summation of the subintegral terms corresponding to various segments.

It should be noted that when hypergeometric series of Eq. (13.57) deteriorates into polynomials, Eq. (13.60) gives (for $m = 0$)

$$\tilde{\lambda}^c_{0,0} = \frac{p^c_0(\bar{r})}{\bar{r}},$$

$$\tilde{\lambda}^c_{2,0} = -\frac{p^c_0(\bar{r})}{\bar{r}} + \frac{2}{\bar{r}^2}\int_0^{\bar{r}} p^c_0(\bar{r})\,d\bar{r},$$

$$\tilde{\lambda}^c_{4,0} = \frac{p^c_0(\bar{r})}{\bar{r}} + \frac{4}{\bar{r}^3}\int_0^{\bar{r}} p^c_0(\bar{r})\,d\bar{r} - \frac{12}{\bar{r}^4}\int_0^{\bar{r}} p^c_0(\bar{r})\,\bar{r}^2 d\bar{r}.$$

Analogous expressions, but with different coefficients, can be obtained for $m \neq 0$ as well.

CHAPTER XIV

BASIC RESULTS AND COMPUTATIONAL FORMULAE FOR TIME-AVERAGE INDUCED VELOCITIES

1. INDUCED VELOCITIES FOR LIFT PER UNIT OF BLADE SPAN INDEPENDENT OF AZIMUTH ANGLE

We will consider the induced velocities field at the rotor disc. Distribution of those velocities depends on the law of variation with the azimuth of the blade unit lift $Y(r,\psi)$ or its reduced nondimensional value $p(\bar{r},\psi)$, defined as follows:

$$p(\bar{r},\psi)=\frac{2Y(\bar{r},\psi)}{\varrho_0 a_\infty b_0 \omega^2 R^2}.$$

At the beginning, let us consider a simple case where the blade unit lift depends on the radius only (this means that we neglect the variation of that force with azimuth). In addition, in the development of the nondimensional blade unit lift into a Fourier series

$$p(\bar{r},\psi)=p_0^c(\bar{r})+2p_1^c(\bar{r})\cos\psi+2p_1^s(\bar{r})\sin\psi+2p_2^c(\bar{r})\cos 2\psi+ \\ +2p_2^s(\bar{r})\sin 2\psi+\ldots \qquad (14.1)$$

only the first term, $p_0^c(\bar{r})$ is considered. Then, the nondimensionalized vertical induced velocity, $\bar{v}_y$, at points of the rotor disc can be presented, according to Eq. (13.33), by a Fourier series containing cosines of ψ only; i.e.,

$$\bar{v}_y(\bar{r},\psi)=\lambda_{0,0}^c(\bar{r})+2\lambda_{1,0}^c(\bar{r})\cos\psi+2\lambda_{2,0}^c(\bar{r})\cos 2\psi+\ldots \qquad (14.2)$$

It follows from Eq. (14.2) that induced velocities are symmetrical with respect to the longitudinal rotor diameter.

In order to determine coefficients (harmonics) in the series in Eq. (14.2), according to Eq. (13.36), we use the following formula

$$\lambda_{n,0}(\bar{r})=-\frac{a_\infty\sigma}{8}\bar{A}_n\tilde{\lambda}_{n,0}^c(\bar{r})\ (n=0,1,2,\ldots). \qquad (14.3)$$

Dependence of the harmonics of induced velocities $\lambda_{n,0}$ on the radius is expressed only by functions $\tilde{\lambda}_{n,0}^c(\bar{r})$ which will be called the reduced (nondimensional) harmonics of velocities. Factors $\bar{A}_n$ in Eq. (14.3) determine dependence of the velocities harmonics from the helicopter regime of flight and are computed from the following formula

$$\bar{A}_n = \frac{(\sqrt{\mu^2+\lambda^2}-|\lambda|)^n}{\mu^n \sqrt{\mu^2+\lambda^2}} \quad (n=0,1,2,\ldots). \tag{14.4}$$

Some important properties of that formula should be noted. For $\lambda = 0$ when the vorticity wake becomes flat, $\bar{A}_n = 1/\mu$; i.e., all coefficients $\bar{A}_n$ become equal to each other and inversely proportional to μ. In the case of axial translation ($\mu = 0$) when the skewed vorticity cylinder becomes straight, we have $\bar{A}_0 = 1/|\lambda|$, $A_1 = A_2 = \ldots = 0$, so that the series in Eq. (14.2) stops at the zero term.

INDUCED VELOCITY AVERAGED OVER A CIRCLE

In the case of the zero harmonic ($n = 0$), the following equation exists:

$$\tilde{\lambda}^c_{0,0}(\bar{r}) = \frac{p^c_0(\bar{r})}{\bar{r}}. \tag{14.5}$$

On the basis of Eq. (14.5), the relative induced velocity averaged with respect to azimuth $\bar{v}_y = \lambda^c_{0,0}(\bar{r})$ is determined by the following very simple formula

$$\bar{v}_r = -\frac{a_\infty \sigma}{8} \frac{1}{\sqrt{\mu^2+\lambda^2}} \frac{p^c_0(\bar{r})}{\bar{r}}. \tag{14.6}$$

Since nondimensionalized unit blade lift $p(\bar{r},\psi)$ is related to relative blade circulation $\bar{\Gamma} = \Gamma/\omega R^2$ by the relationship

$$\frac{a_\infty b}{2R} p(\bar{r},\psi) = \bar{\Gamma}(\bar{r}+\mu\sin\psi),$$

hence, substituting $\mu = 0$ into Eq. (14.6), we will obtain the well-known Joukowsky formula for induced velocity of the propeller in axial flow. Just as in the case of axial translation, induced velocity given by Eq. (14.6) is proportional to the blade lift per unit length divided by the radius. However, when the flow is oblique, then that formula does not determine the whole induced velocity, but only its average with respect to the azimuth part which represents the zero harmonic term in the expansion given by Eq. (14.2).

Using Eq. (14.6), we find the averaged over the disc induced velocity, which is equal to

$$\bar{v} = \frac{1}{\pi} \int_0^{2\pi} \int_0^1 \bar{v}_y(\bar{r},\psi)\bar{r}\,d\bar{r}\,d\psi. \tag{14.7}$$

Since in the development of $\bar{v}_y(\bar{r},\psi)$ into the series of Eq. (14.2), terms having indices $n > 0$ do not influence the value of the integral in Eq. (14.7), and

$$c_T = a_\infty \sigma \int_0^1 p_0^c(\bar{r})\, d\bar{r},$$

it is easy to reduce Eq. (14.7) to the following form

$$\bar{v} = -\frac{c_T}{4\sqrt{\mu^2+\lambda^2}}. \tag{14.8}$$

Eq. (14.8) corresponds to the widely known formula for the average over-the-disc induced velocity which was postulated by Glauert without a hydrodynamic justification. As we can see, that formula is indeed correct within the framework of the linear vortex theory, but only for an airscrew with constant lift per unit of blade span with respect to the azimuth.

HARMONICS OF INDUCED VELOCITY

Let us now consider the harmonics of induced velocity given by Eq. (14.3) which are generated by the constant with azimuth thrust per unit length. Functions $\bar{\lambda}^c_{n,0}(\bar{r})$ (reduced harmonics) at fixed $\bar{r}$ are not only determined by values of p_0^c at that fixed $\bar{r}$, but also by the values of that function at other values of $\bar{r}$. To provide an example, let us consider three laws for variation of the $p_0^c(\bar{r})/\bar{r}$ ratio:

$$(p_0^c/\bar{r})^{\mathrm{I}} = \sqrt{1-\bar{r}^2},\quad (p_0^c/\bar{r})^{\mathrm{II}} = \bar{r}^2\sqrt{1-\bar{r}^2},\quad (p_0^c/\bar{r})^{\mathrm{III}} = (2\bar{r}^2-1)\sqrt{1-\bar{r}^2}. \tag{14.9}$$

The first two distributions were investigated by Mangler and Squire[109] who calculated harmonics of the induced velocities, but did not show details of the calculation method.

Let us define, by $\tilde{\lambda}^{c\,\mathrm{I}}_{n,0}$ $\tilde{\lambda}^{c\,\mathrm{II}}_{n,0}$ and $\tilde{\lambda}^{c\,\mathrm{III}}_{n,0}$, functions corresponding to $\tilde{\lambda}^c_{n,0}$ in Eq. (14.9). Those quantities, can be expressed with the functions $Y^q_{n,0}$ introduced in Ch. XIII:

$$\tilde{\lambda}^{c\mathrm{I}}_{n,0} = Y^1_{n,0},\quad \tilde{\lambda}^{c\mathrm{II}}_{n,0} = Y^1_{n,0} - Y^3_{n,0},\quad \tilde{\lambda}^{c\mathrm{III}}_{n,0} = 2Y^5_{n\,0} - 3Y^3_{n\,0} + Y^1_{n,0}.$$

In order to determine functions $Y^q_{n,0}$ for low q values, it is not difficult to establish analytical expressions, taking advantage of recurring formulae from Appendix VII. However, it is more convenient to perform numerical evaluation of functions $Y^q_{n,0}$. Graphs of reduced harmonics of induced velocities obtained in that way are shown in Figs. 14.1-14.3. It can be

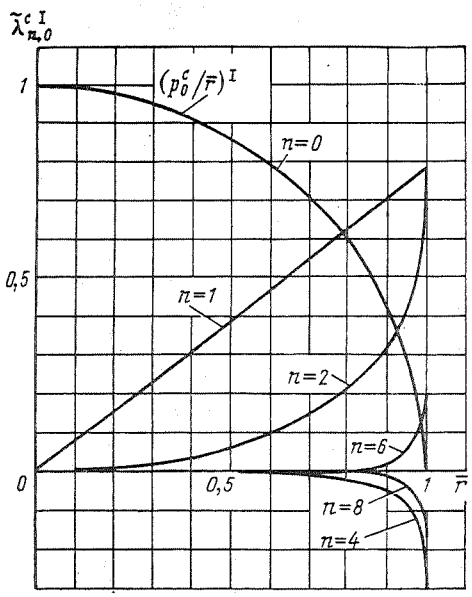

Figure 14.1

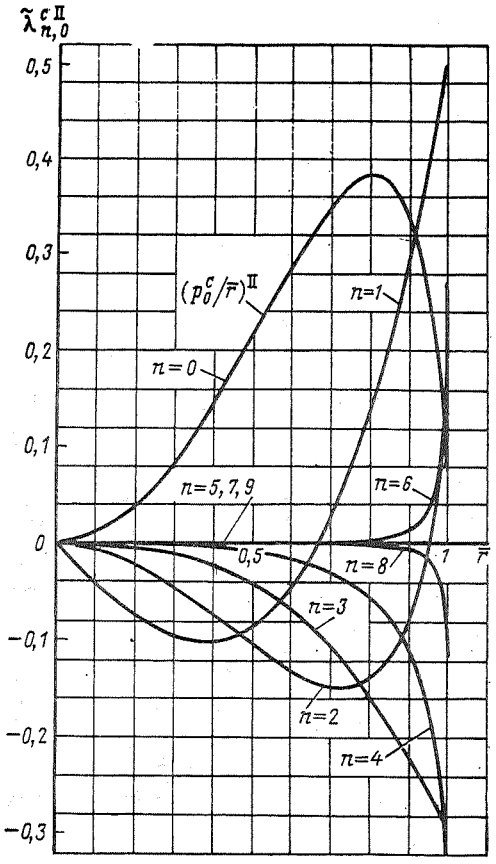

Figure 14.2

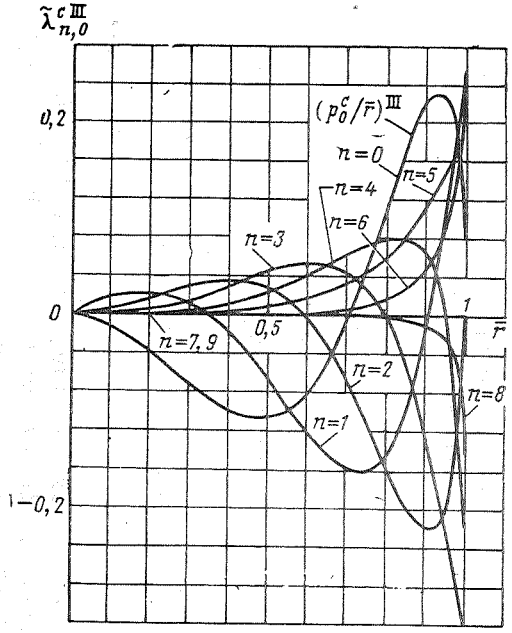

Figure 14.3

seen that the most important coefficients are those at the zero and first harmonics; the remaining ones are less significant, but decrease in values very little with the increasing harmonic number n. As the blade tip is approached, the importance of the presented harmonics quickly increases. Since, in the case of a flat vorticity wake, all $\bar{A}_n$ coefficients are equal to each other; hence, in calculating coefficients of the series given by Eq. (14.2), it is necessary to multiply each function $\bar{\lambda}^c_{n,o}(\bar{r})$ by the same quantity only. If the vorticity wake is three dimensional, then each function $\bar{\lambda}^c_{n,o}(\bar{r})$ $(n=0, 1, 2, \ldots)$ must be multiplied by a suitable coefficient, $\bar{A}_n$.

Let us investigate variation of the $\bar{A}_n$ coefficient, depending on the regime of flight. Assuming, in accordance with the Glauert formula that

$$\lambda = \frac{c_T}{4\sqrt{\mu^2+\lambda^2}} - \mu \operatorname{tg} \alpha_B,$$

we develop, from Eq. (14.4) graphs of the dependence of $\bar{A}_n$ on μ at various angles of attack α_B, of the rotor (Fig. 14.4).

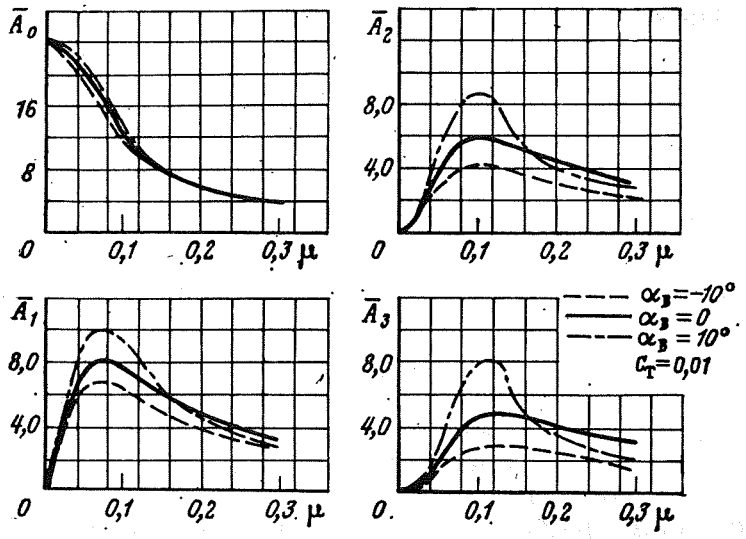

Figure 14.4

It can be seen that coefficient $\bar{A}_0$ smoothly decreases with the increasing μ. This characterizes the variation of induced velocity averaged over the azimuth or over the disc. The remaining coefficients A_n $(n=1, 2, 3, \ldots)$ are equal to zero for $\mu = 0$, while at low flying speeds $(\mu \approx 0{,}1)$, they have sharp maxima; sharper at the positive than at the negative angles of attack α_B. In this way, at low μ's and positive angles of attack α_B, all harmonics of induced velocities become maximum. This explains, in part, why at low flying speeds of helicopters, blade alternating stresses and vibrations in the cabin sharply increase. Furthermore, at the positive α_B angles, those phenomena manifest themselves more appreciably than at the negative ones.

With the help of Eq. (14.3), (14.4) and graphs in Figs. 14.1-14.3, it is easy to find harmonics of induced velocities for any of the "standard" unit load distribution shown in Eq. (14.9), or for any linear combination (with constant coefficients) of those distributions. In the latter case, it is necessary to form a suitable linear combination from functions $\tilde{\lambda}^{cI}_{n,o}$, $\tilde{\lambda}^{cII}_{n,o}$ and $\tilde{\lambda}^{cIII}_{n,o}$.

If the required accuracy of approximating function $p^c_0(\bar{r})$ by any of the given standard distributions is not sufficient, then coefficients $\lambda^c_{n,o}(\bar{r})$ should be found by interpolation based on the approximation of the unit lift distribution by a trigonometric polynomial. In such approximation, values of $\tilde{\lambda}^c_{n,o}(\bar{r})$ at the nodal points $\bar{r} = \bar{r}_l$ are defined, as was shown in Chapter XIII by the following formula*

$$\tilde{\lambda}^c_{n,0}(\bar{r}_l) = \sum_{k=0}^{5} \left(\frac{p^c_0}{\bar{r}}\right)_k \varepsilon^k_{n,0}(\bar{r}_l), \qquad (14.10)$$

where $(p^c_0/\bar{r})_k$ are the values of the $p^c_0(\bar{r})/\bar{r}$ ratio at those points. Values of $\bar{r}_k$ of the nodal points are shown in Table 14.1.

k, l	0	1	2	3	4	5
$\bar{r}_k, \bar{r}_l$	0	0,259	0,5	0,707	0,866	0,966

Table 14.1

Functions $\varepsilon^k_{n,o}$ are given in Appendix IX. In order to obtain values of $\tilde{\lambda}^c_{n,o}(\bar{r})$ at the nodal points, it is possible, according to Eq. (14.10) to compute the product of a matrix of coefficients $\varepsilon^k_{n,o}(\bar{r}_l)$ (k is the row, and l is the column number) times a column matrix of the $(p^c_0/\bar{r})_k$ values. For the distribution given in Eq. (14.9), results of calculations according to Eq. (14.10) are exact. In other cases, Eq. (14.10) gives the approximate values of the induced velocity harmonics. The accuracy of that approximation depends on the degree of exactness of expressing actual loadings through the interpolating polynomial.

*A polynomial suitable for 5 nodal points is shown.

2. INDUCED VELOCITIES WITH THRUST PER UNIT LENGTH OF BLADE SPAN VARYING WITH AZIMUTH

Let us consider a case where, in determining induced velocities, variations of the blade unit thrust along the radius, as well as with the azimuth, are considered. We will assume that reduced (nondimensionalized) unit blade thrust $p(\bar{r},\psi)$ can be represented by a sum of a finite number of harmonics

$$p(\bar{r},\psi)=p_0^c(\bar{r})+2\sum_{m=1}^{N}[p_m^c(\bar{r})\cos m\psi+p_m^s(\bar{r})\sin m\psi]. \tag{14.11}$$

Due to the linearity of the considered theory, induced velocity $\bar{v}_y(\bar{r},\psi)$ is equal to the sum of velocities generated separately by each of the harmonics of the thrust per unit length. In this way, induced velocity can be represented by a Fourier series

$$\bar{v}_y(\bar{r},\psi)=\lambda_0^c+2\sum_{n=1}^{\infty}[\lambda_n^c(\bar{r})\cos n\psi+\lambda_n^s(\bar{r})\sin n\psi],$$

where

$$\lambda_n^c=\lambda_{n,0}^c+\lambda_{n,1}^c+\lambda_{n,2}^c+\dots,$$
$$\lambda_n^s=\lambda_{n,1}^s+\lambda_{n,2}^s+\dots$$

The quantities $\lambda_{n,m}^c(\bar{r})$, $\lambda_{n,m}^s(\bar{r})$, called components of induced velocities harmonics, are determined through functions of radius $\tilde{\lambda}_{n,m}^c(\bar{r})$, $\tilde{\lambda}_{n,m}^s(\bar{r})$ and constants $K_{n,m}^c$, $K_{n,m}^s$, depending on the regime of flight.

$$\lambda_{n,m}^c(\bar{r})=-\frac{a_\infty\sigma}{8}K_{n,m}^c\tilde{\lambda}_{n,m}^c(\bar{r}),$$
$$\lambda_{n,m}^s(\bar{r})=-\frac{a_\infty\sigma}{8}K_{n,m}^s\tilde{\lambda}_{n,m}^s(\bar{r}), \tag{14.12}$$

where

$$K_{n,m}^c=\bar{A}_{n-m}+(-1)\bar{A}_{n+m},$$
$$K_{n,m}^s=\bar{A}_{n-m}-(-1)^m\bar{A}_{n+m}\quad(n,m=0,1,2,\dots). \tag{14.13}$$

Here, $\bar{A}_p(p=n+m,n-m)$ are the coefficients which for $p\geq 0$, are determined from Eq. (14.4), while for $p<0$, are obtained from the relationship $\bar{A}_{-p}=(-1)^p\bar{A}_p$.

ANALOGS TO JOUKOWSKY FORMULAE FOR VELOCITIES DUE TO THE LOADING HARMONICS

As in the case of the zero harmonics, also for $n=m$, the functionals $J_{n,m}$ degenerate and the following equalities take place

$$\tilde{\lambda}^c_{n,n}(\bar{r}) = \frac{p^c_n(\bar{r})}{\bar{r}}, \quad \tilde{\lambda}^s_{n,n}(\bar{r}) = \frac{p^s_n(r)}{\bar{r}}. \tag{14.14}$$

It follows from the above that

$$\lambda^c_{n,n}(\bar{r}) = -\frac{a_\infty \sigma}{8}\left[\overline{A}_0 + (-1)^n \overline{A}_{2n}\right]\frac{p^c_n(\bar{r})}{\bar{r}},$$

$$\lambda^s_{n,n}(\bar{r}) = -\frac{a_\infty \sigma}{8}\left[\overline{A}_0 - (-1)^n \overline{A}_{2n}\right]\frac{p^s_n(\bar{r})}{\bar{r}}. \tag{14.15}$$

It can be seen that components $\lambda^c_{n,m}$, $\lambda^s_{n,m}$ of the velocities harmonics are proportional to the reduced (nondimensional) unit thrust loads p^c_n, p^s_n divided by the blade radius $\overline{r}$. Components of the velocities harmonics with the coinciding values of n and m will be called *straight* and those not coinciding, *transverse*. Accordingly, induced velocities will also be divided into *straight* and *transverse* values. The *transverse* velocities are determined by the complete law of variation of the unit thrust load over the rotor disc . The "straight" velocities, according to Eq. (14.15), are proportional to the generating harmonics of unit thrust load, divided by $\overline{r}$. In that respect, Eq. (14.15) completely coincides with Eq. (14.5) and is analogous to the Joukowsky formula. In the particular case of axial flow ($\mu = 0$), all coefficients $K^c_{n,m}$, $K^s_{n,m}$ for $n \neq m$ become zero, while for $n = m$, we have $K^c_{n,n} = K^s_{n,n} = 1/|\lambda|$. The *transverse* induced velocities completely disappeared and the remaining "straight" ones give, in summation, an explicit expression for the relative induced velocity:

$$\bar{v}_y(\bar{r},\psi) = -\frac{a_\infty \sigma}{8|\lambda|}\frac{p(\bar{r},\psi)}{\bar{r}}. \tag{14.16}$$

If we express, through relative circulation, the nondimensional unit thrust load appearing in Eq. (14.16), then we obtain the Joukowsky formula,

$$\bar{v}_y(\bar{r},\psi) = -\frac{k_\pi \overline{\Gamma}(\bar{r},\psi)}{4\pi|\lambda|}, \tag{14.17}$$

where circulation $\overline{\Gamma}$ is a function of both $\overline{r}$ and ψ. We have to admit that Eq. (14.17) can be obtained in a completely elementary way; for instance, by considering flow generated by a system of vortex solenoids which are formed by arbitrary closed cylindrical surfaces with their infinite generatrices parallel to the rotor axis.

As an example, let us consider the following law of variation of the reduced thrust per unit length over the rotor disc

$$\frac{p}{\bar{r}} = (p_m^{\alpha}/\bar{r})^k \left\{ \begin{matrix} \cos m\psi \\ \sin m\psi \end{matrix} \right\} (k = \mathrm{I}, \mathrm{II};\ \alpha = c, s;\ m = 1, 2),$$

where

$$(p_1^{\alpha}/\bar{r})^{\mathrm{I}} = \bar{r}\sqrt{1-\bar{r}^2},\ (p_1^{\alpha}/\bar{r})^{\mathrm{II}} = \bar{r}(2\bar{r}-1)\sqrt{1-\bar{r}^2},\ (p_2^{\alpha}/\bar{r})^{\mathrm{I}} = \bar{r}^2\sqrt{1-\bar{r}^2}.$$

The corresponding functions $\tilde{\lambda}^{c\mathrm{I}}_{n,m}$, $\tilde{\lambda}^{c\mathrm{II}}_{n,m}$, etc., are expressed through functions $Y^q_{n,m}(\overline{r})$ per the following formulae

$$\begin{gathered} \tilde{\lambda}^{c\mathrm{I}}_{n,m} = \tilde{\lambda}^{s\mathrm{I}}_{n,m} = Y^1_{n,m}, \\ \tilde{\lambda}^{c\mathrm{II}}_{n,m} = \tilde{\lambda}^{s\mathrm{II}}_{n,m} = Y^1_{n,m} - 2Y^3_{n,m}\ (m = 1, 2;\ n = 0, 1, 2, 3, \ldots). \end{gathered} \tag{14.18}$$

Graphs of functions $\tilde{\lambda}^{\alpha}_{n,m}(\overline{r})$ defined by Eq. (14.18) for the rotor disc $(\overline{y} = 0)$ are shown in Figs. 14.5-14.8. They permit a ready evaluation of the influence of the nonuniformity of the unit thrust loading on the induced velocities field. For more accurate calculations, it is possible to use the interpolation method in which functions $\tilde{\lambda}^{c}_{n,m}(\overline{r})$, $\tilde{\lambda}^{s}_{n,m}(\overline{r})$ are determined by formulae analogous to those of Eq. (14.14):

$$\begin{aligned} \tilde{\lambda}^{c}_{n,m}(\bar{r}_l) &= \sum_{k=1}^{5} \left(\frac{p_m^c(\bar{r})}{\bar{r}} \right)_k \varepsilon^k_{n,m}(\bar{r}_l), \\ \tilde{\lambda}^{s}_{n,m}(\bar{r}_l) &= \sum_{k=1}^{5} \left(\frac{p_m^s(\bar{r})}{\bar{r}} \right)_k \varepsilon^k_{n,m}(\bar{r}_l). \end{aligned} \tag{14.19}$$

Tables of functions $\varepsilon^k_{n,m}(\overline{r}_l)$ at various values of n and m are given in Appendix IX.

3. AERODYNAMIC FORCES

Limiting ourselves to the case of linear dependence of blade section lift coefficients on angles of attack, we assume the following expression for the blade thrust per unit length Y

$$Y = \frac{\varrho a_\infty b}{2} \omega^2 R^2 \left[\overline{W}^2_{x\varphi} + \overline{W}_x \overline{W}_y \right]. \tag{14.20}$$

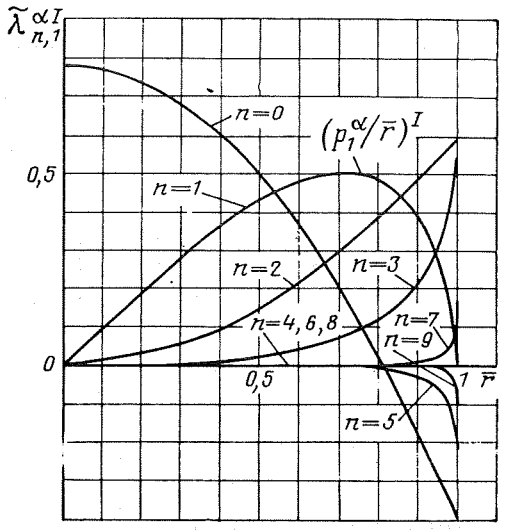

Figure 14.5

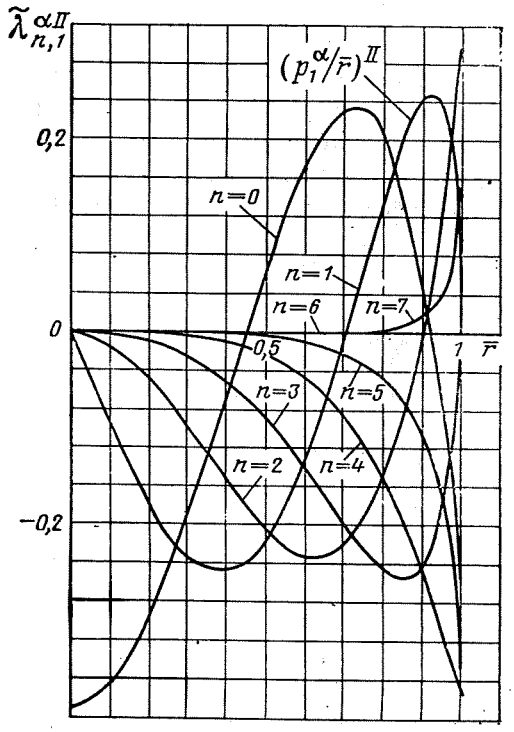

Figure 14.6

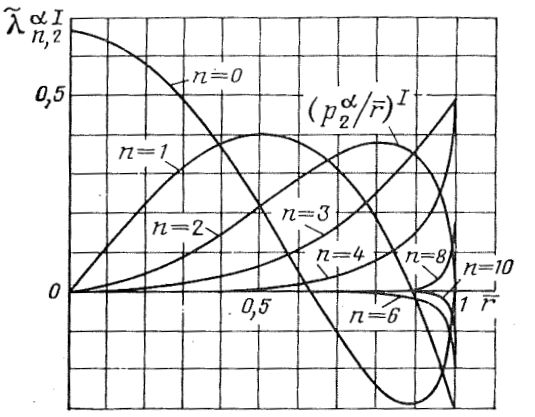

Figure 14.7

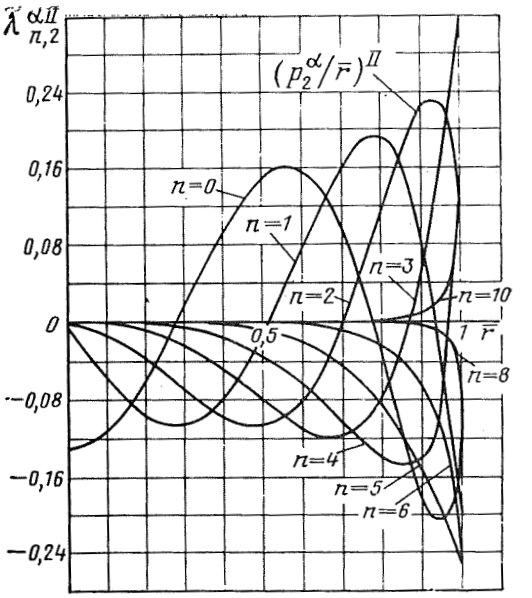

Figure 14.8

Here, $\overline{W}_x$, $\overline{W}_y$ respectively, are the horizontal & vertical components of the relative velocity of flow approaching the blade section. In the case of a rotor with a zero offset of the blade hinges,

$$\overline{W}_x=\bar{r}+\mu\sin\psi,\ \overline{W}_y=\bar{\lambda}-\beta\mu\cos\psi-\bar{r}\frac{d\beta}{d\psi},$$

where $\bar{\lambda}(\bar{r},\psi)=\bar{v}_y(\bar{r},\psi)+\mu\operatorname{tg}\alpha_в$

is the resultant velocity of flow through the rotor disc.

For β, $\bar{\lambda}$ and ϕ, let us introduce the following expansions into Fourier series

$$\begin{aligned}\beta&=\sum_{n=-\infty}^{\infty}(\bar{a}_n^c\cos n\psi+\bar{a}_n^s\sin n\psi),\\ \bar{\lambda}&=\sum_{n=-\infty}^{\infty}(\bar{\lambda}_n^c\cos n\psi+\bar{\lambda}_n^s\sin n\psi),\\ \varphi&=\sum_{n=-\infty}^{\infty}(\varphi_n^c\cos n\psi+\varphi_n^s\sin n\psi),\end{aligned}\qquad(14.21)$$

where $\bar{a}_n^c=\bar{a}_{-n}^c$; $\bar{a}_n^s=-\bar{a}_{-n}^s$, etc., for all coefficients of the series in Eq. (14.21). We should note that coefficients for β in the series of Eq. (14.21) and those in Eq. (1.16) are different.

After substituting Eq..(14.21) into Eq. (14.20), and after some simple transformations, we obtain

$$p=\sum_{-\infty}^{\infty}(p_n^c\cos n\psi+p_n^s\sin n\psi),\qquad(14.22)$$

where coefficients p_n^c, p_n^s are determined by the following formulae

$$\begin{aligned}p_n^c=\tilde{b}\Big\{&\bar{r}^2\varphi_n^c+\mu\bar{r}(\varphi_{n+1}^s-\varphi_{n-1}^s)+\frac{\mu^2}{4}(2\varphi_n^c-\varphi_{n+2}^c-\varphi_{n-2}^c)+\bar{r}\bar{\lambda}_n^c+\\&+\frac{\mu}{2}(\bar{\lambda}_{n+1}^s-\bar{\lambda}_{n-1}^s)-\bar{r}^2n\bar{a}_n^s+n\bar{r}\frac{\mu}{2}(\bar{a}_{n+1}^c-\bar{a}_{n-1}^c)-\frac{\mu^2}{4}(\bar{a}_{n+2}^s-\bar{a}_{n-2}^s)\Big\},\\ p_n^s=\tilde{b}\Big\{&\bar{r}^2\varphi_n^s+\mu\bar{r}(\varphi_{n-1}^c-\varphi_{n+1}^c)+\frac{\mu^2}{4}(2\varphi_n^s-\varphi_{n+2}^s-\varphi_{n-2}^s)+\bar{r}\bar{\lambda}_n^s+\\&+\frac{\mu}{2}(\bar{\lambda}_{n-1}^c-\bar{\lambda}_{n+1}^c)+\bar{r}^2n\bar{a}_n^c+n\bar{r}\frac{\mu}{2}(\bar{a}_{n+1}^s-\bar{a}_{n-1}^s)-\frac{\mu^2}{4}(\bar{a}_{n-2}^c-\bar{a}_{n+2}^c)\Big\}\\ &(n=0,\pm1,\pm2,\ldots),\ \tilde{b}=b/b_0.\end{aligned}\qquad(14.23)$$

It is easy to see that $p_n^c = P_{-n}^c$ and $p_n^s = -p_{-n}^s$, and consequently, the series of Eq. (14.22) can be written as

$$p(\bar{r}, \psi) = p_0^c + 2\sum_{n=1}^{\infty}(p_n^c \cos n\psi + p_n^s \sin n\psi).$$

In the absence of the horizontal hinge offset, it is possible to write the equation of the flapping motion as follows:

$$J_r\left(\frac{d^2\beta}{dt^2} + \omega^2\beta\right) = \int_0^R Yr\,dr.$$

A substitution of Eqs. (14.21) and (14.22) into the above equation leads to the following expressions

$$(1-n^2)\bar{a}_n^c = \gamma\int_0^1 p_n^c \bar{r}\,d\bar{r}, \quad (1-n^2)\bar{a}_n^s = \gamma\int_0^1 p_n^s \bar{r}\,d\bar{r}, \tag{14.24}$$

where $\gamma = \rho a_\infty b R^4/2J_\Gamma$ is the blade mass characteristic. We present the pitch angle of the blade sections in the following form

$$\varphi = \theta_0 + \Delta\varphi(\bar{r}) + \theta_1\cos\psi + \theta_2\sin\psi - \bar{k}\beta,$$

where $\bar{k}$ is the coefficient of the flapping motion control; θ_0, θ_1 and θ_2 are the coefficients of collective and cyclic pitch; $\Delta\phi(\bar{r})$ is the blade twist. Taking advantage of Eq. (14.21) we obtain

$$\varphi_0^c(\bar{r}) = \theta_0 + \Delta\varphi(\bar{r}) - \bar{k}\bar{a}_0^c, \quad \varphi_1^c = \frac{1}{2}\theta_1 - \bar{k}\bar{a}_1^c, \quad \varphi_1^s = \frac{1}{2}\theta_2 - \bar{k}\bar{a}_1^s,$$

$$\varphi_n^c = -\bar{k}\bar{a}_n^c, \quad \varphi_n^s = -\bar{k}\bar{a}_n^s \text{ for } n \geqslant 2.$$

After substituting the expressions for velocities (Eqs. (14.5) and (14.15)) into Eqs. (14.23) and (14.24), equations for coefficients $\bar{a}_n^c$, $\bar{a}_n^s$ are obtained. They are valid for the first approximation of computation of the *straight* induced velocities only (for which the Joukowsky formulae are analogical). From the values of $p_n^c(\bar{r})$, $p_n^s(\bar{r})$ obtained from Eq. (14.23), it is possible to compute the induced velocity field and obtain a more accurate determination of the corresponding coefficients $\bar{a}_n^c$, a_n^s and functions p_n^c, p_n^s. The process of consecutive approximation leads to a fast convergence.

If we limit ourselves to the determination of the zero harmonic of reduced unit thrust, then neglecting the small terms in Eq. (14.23), we readily find

$$p_0^c = \frac{\tilde{b}}{1 + \frac{a_\infty \sigma \tilde{b}}{8}\bar{A}_0}\left\{\left(\bar{r}^2 + \frac{\mu^2}{2}\right)\varphi_0^c(\bar{r}) + \mu\bar{r}\,\mathrm{tg}\,\alpha_B\right\}.$$

It is possible to accelerate calculations if, in computing the harmonics m ($m=1,2,3...$) of the unit thrust, we take into consideration in the first approximation, not only *straight* induced velocities, but also the *transverse* ones from the previously found lower harmonics of the unit thrust.

EXAMPLE OF CALCULATIONS

Let us consider a rotor with articulated, twisted, and tapered blades in a regime of flight characterized by the following parameters: $\mu = 0,2$; $\alpha_B = -10°$; $c_T = 0,008$; $\lambda = -0,045$. Curves giving reduced (nondimensional) unit thrust loads obtained from Eq. (14.23) and taking into consideration "straight" induced velocities only ($\lambda^c_{n,m}$, $\lambda^s_{n,m}$) are shown in Fig. 14.9 as dashed lines. Values of those harmonics obtained in the second approximation are also shown with the consideration of the *transverse* induced velocities ($\lambda^c_{n,m}$, $\lambda^s_{n,m}$ at $n \neq m$) taken from the first approximation. It can be seen that taking into account the *transverse* velocities has little influence on the considered coefficients p^c_n, p^s_n. Consequently, there is no need for further approximations.

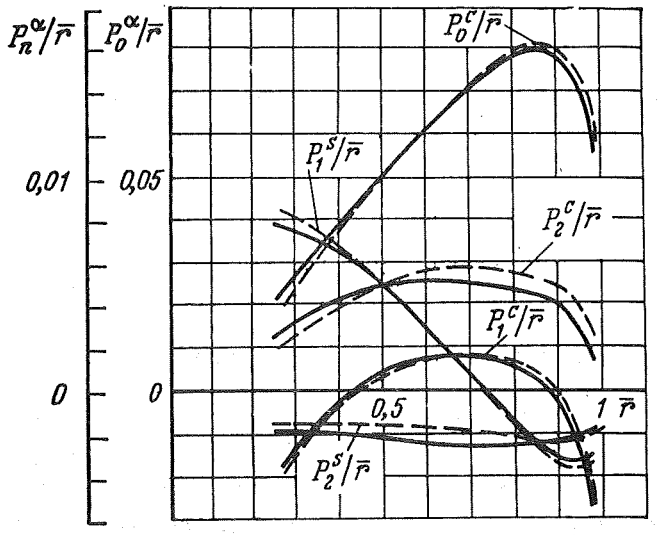

Figure 14.9

Harmonics of induced velocities, $\lambda^c_{n,m}$, $\lambda^s_{n,m}$ corresponding to the first approximation and computed from Eq. (14.19) for $0 \leq n \leq 5$ and $0 \leq m \leq 2$ are shown in Fig. 14.10. In Fig. 14.11, resultant values of velocities harmonics λ^c_n, λ^s_n obtained by summation of all considered harmonics of the unit thrust load are shown. It can be seen that consideration of the sole zero term p^c_0 in the development of the unit thrust load according to

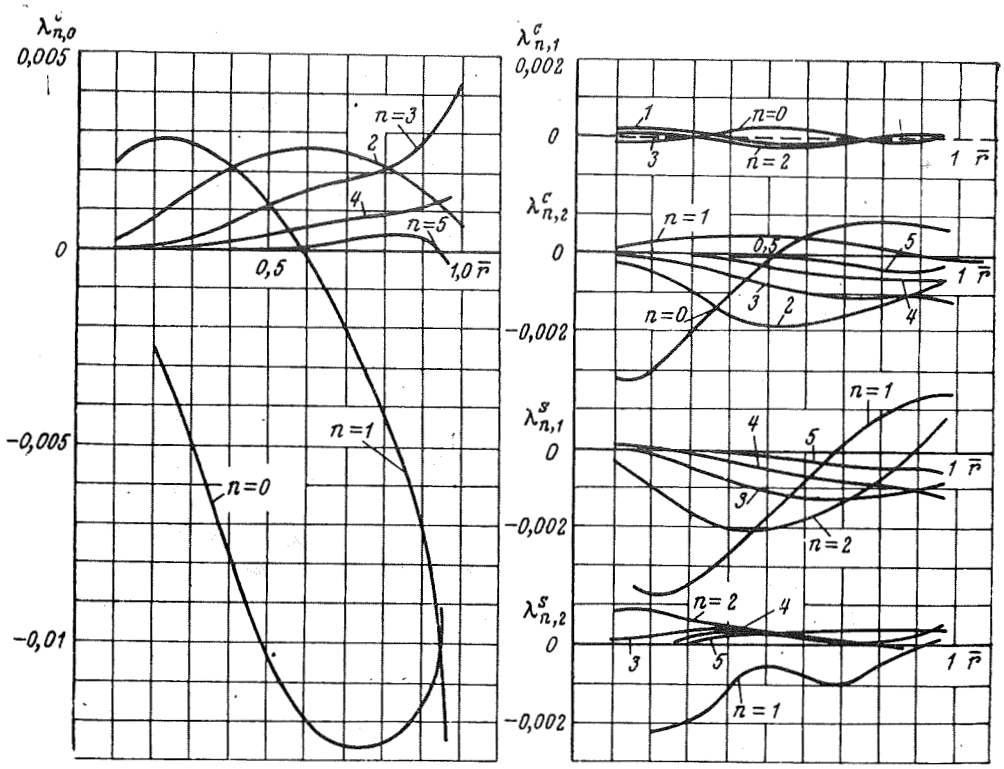

Figure 14.10

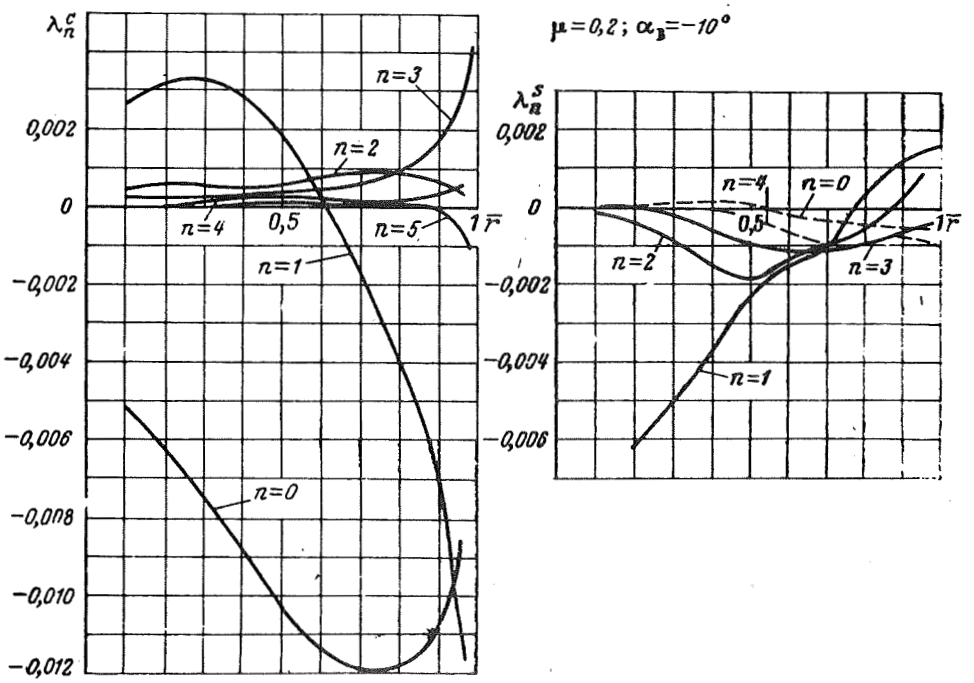

Figure 14.11

Eq. (14.1) already gives a good qualitative picture of the induced velocity distribution. Summation of the Fourier series for the considered case gives the distribution of induced velocities over the disc as shown in Fig. 14.12. It can be seen that velocities in the aft portion of the disc are much higher than in the front one, while their distribution along the lateral rotor diameter is almost symmetrical with respect to the longitudinal plane.

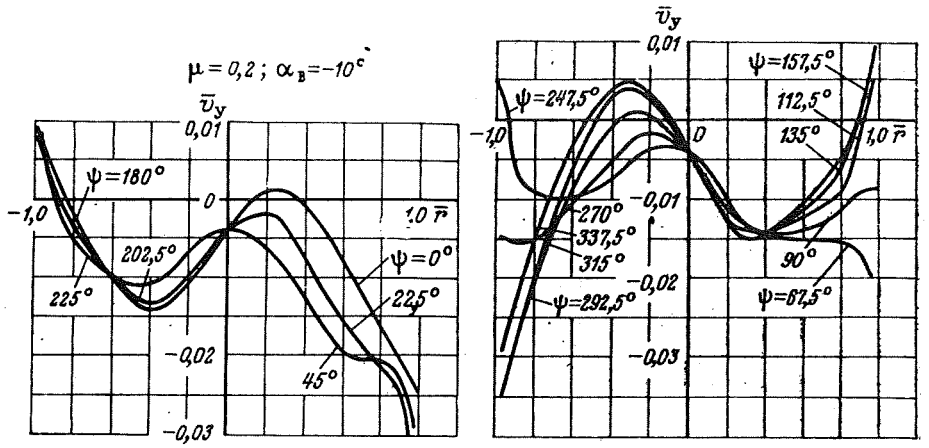

Figure 14.12

CHAPTER XV

FUNDAMENTALS OF THE LINEAR THEORY OF INSTANTANEOUS INDUCED VELOCITIES AND SOME OF ITS REFINEMENTS

In the preceding chapters, methods were presented of calculations of the fields of time-average velocities induced by helicopter rotors in horizontal flight.

However, velocities induced by the rotor vary with time. For this reason, one should talk about their true instantaneous values. In a steady-state regime of flight, dependence of instantaneous velocities on time at a fixed point in space is of a periodic character. Here, period is equal to the time required for the rotor to turn through an angle equal to that between the two consecutive blades. In the consideration of flow around aerodynamic surfaces fixed with respect to the helicopter, such as a wing, stabilizer or fuselage, instantaneous induced velocities are usually replaced by the time-average values at a given point. In addition, it is assumed (just a hypothesis) that the so-obtained aerodynamic loads also represent time-averaged values of the instantaneous loads. The smaller the pulsations are in comparison with their time-averaged values, the more correct this hypothesis would be. However, even at a high level of those pulsations, this hypothesis would still be sufficiently accurate as long as linear dependence exists between the considered aerodynamic characteristics and the flow angle. The above-mentioned time averaging would lead to serious errors only in the case of strong nonlinearities, as in the case of airfoil stall. In the case of moving aerodynamic surfaces, time averaging of instantaneous loads does not, in general, coincide with averaging of induced velocities and thus, it becomes necessary to consider actual instantaneous induced velocities.

1. APPLICATION OF THE SCHEME OF LIFTING LINE TO COMPUTATIONS OF INSTANTANEOUS INDUCED VELOCITIES

In the foundations of contemporary methods of computation of instantaneous induced velocities lies a scheme of the blade vortex theory of an airscrew in an oblique flow, as first proposed by G.I. Maykapar. A large elongation of blades should, in principle, permit one to use the lifting-line approach. However, rotor blades experience large sweep angles; hence, the application of the lifting-line scheme encounters the same difficulties as in the theory of swept-wing airplanes.

It is convenient to break the vortices springing from the blades into two classes. To the first class, we assign all those vortex elements which left the blade during the short time interval preceding the considered moment. They would form a segment of the vorticity wake directly adjacent to the blade trailing edge. To the second class, we assign all the remaining vortices which would thus appear at some distance (sometimes not too far) from the blade. In solving the task of determining induced velocities generated by vortices belonging to the first class, it is necessary to take the finite width of the blade into consideration and to use a scheme of a lifting strip or lifting surface. For vortices belonging to the second class, it is sufficient to treat the blade as an infinitely thin vortex filament.

Starting from the above-outlined principles, we will investigate the field of instantaneous induced velocities generated by a rotor in an oblique flow. The motion of the blades will be considered in a Cartesian coordinates system (see Fig. 13.2). We replace each blade with a straight-line R-long segment of bound vortex located in the $x0z$ plane, rotating about the Oy axis with an angular velocity ω. We will consider that the circulation Γ of that vortex depends on both ρ - distance of a point of the vortex from the origin of coordinates; and ψ_n - blade azimuth angle. This means that $\Gamma = \Gamma(\rho, \psi)$. Vortices leaving the blades form a skewed helical surface S_ψ defined by the following equations:

$$\begin{aligned} x &= -\varrho\cos\vartheta + \frac{V_x}{\omega}(\vartheta - \psi_n), \\ y &= \frac{V_y'}{\omega}(\vartheta - \psi_n), \\ z &= \varrho\sin\vartheta \qquad (0 < \vartheta < \psi_n;\ 0 < \varrho < R). \end{aligned} \tag{15.1}$$

In the above equations, ρ and ϑ are Gaussian coordinates of a point moving on the wake (they represent radius and azimuth of a point on the vortex at the instant of its leaving the blade), while ψ_n is the azimuth of the nth blade $(n=1,2,3,\ldots,k)$ from which the vortex wake springs (see Fig. 13.1).

Variation with time of the S_ψ surface shape consists of: (a) movement of all its points (corresponding to the fixed ρ and ϑ) with a constant velocity, and (b) appearance of new segments of that surface.

Surface S_ψ is covered by a layer of vortices whose intensity can be conveniently characterized by introducing a notion of circulation Γ at each point of the wake. This circulation is understood as circulation of a velocity vector along an

arbitrary contour C piercing the wake at that (and only at that) point. Circulation Γ does not, in principle, depend on the shape of C and blade azimuth; (ψ_n); but is a function of parameters describing the position at that point on the wake; i.e., $\Gamma = \Gamma(\rho, \vartheta)$. By assuming that $\vartheta = \psi_n$ and reducing contour C to a small circle around the bound vortex at radius ρ, it is not difficult to deduce that circulation Γ is identical with circulation of the bound vortex at $\psi_n = \vartheta$.

Eq. (15.1) and function $\Gamma(\rho, \psi)$ fully define the system of free vortices and consequently, induced velocities as well. In those cases when induced velocities have to be determined on the same blade from which the vorticity wake flows, we will cut off surface $\delta\psi$ along a straight line $\vartheta = \psi - \delta\psi$; thus, it would not touch the blade itself (here, angle $\delta\psi \sim 30^0$). Through the above approach, the influence on the flow of vortices cut off at the blade should be considered separately.

2. INSTANTANEOUS INDUCED VELOCITIES

Let us develop expressions for calculating instantaneous induced velocities. Let dS be a flat element of surface S covered with vortices, corresponding to the increment of coordinates by $d\rho$ and $d\vartheta$. That element would have the form of a parallelogram built on two infinitesimal vectors $d\mathbf{l}_1$ and $d\mathbf{l}_2$ defined as

$$d\mathbf{l}_1 = \frac{\partial \mathbf{r}}{\partial \rho} d\rho, \quad d\mathbf{l}_2 = \frac{\partial \mathbf{r}}{\partial \vartheta} d\vartheta, \tag{15.2}$$

where

$$\mathbf{r} = \mathbf{r}(\rho, \vartheta) = x\mathbf{i} + y\mathbf{j} + z\mathbf{k}$$

is the radius-vector of a point on the wake. Partial derivatives with respect to ρ and ϑ will be designated by suitable indices. According to Eq. (15.1), we have

$$\frac{\partial \mathbf{r}}{\partial \rho} = \mathbf{r}_\rho = -\cos\vartheta\,\mathbf{i} + \sin\vartheta\,\mathbf{k}, \quad \frac{\partial \mathbf{r}}{\partial \vartheta} = \mathbf{r}_\vartheta = \left(\rho\sin\vartheta + \frac{V_x}{\omega}\right)\mathbf{i} + \frac{V_y'}{\omega}\mathbf{j} + \rho\cos\vartheta\,\mathbf{k}.$$

We replace the vortices located on the little platform dS by two infinitesimal segments of vortex filaments running along vectors $d\mathbf{l}_1$ and $d\mathbf{l}_2$. The intensity of those vortex filaments will be equal to circulations $d\Gamma_1$ and $d\Gamma_2$ determined along contours C_1 and C_2 enclosing the corresponding filaments. Contour C_1 should pierce the wake surface at points with coordinates (ρ, ϑ) and $(\rho, \vartheta + d\vartheta)$, and contour C_2 at points (ρ, ϑ) and $(\rho + d\rho, \vartheta)$. Expressing circulations along the selected contours C_i $(i=1,2)$ as a difference in circulation Γ existing at points of the wake surface pierced by the contours; and coordinating

directions of the movement along the contour with the directions of vectors $d\mathbf{l}_1$ and $d\mathbf{l}_2$, we obtain

$$d\Gamma_1 = -\Gamma_\vartheta d\vartheta, \quad d\Gamma_2 = \Gamma_\varrho d\varrho. \tag{15.3}$$

Velocity $d\mathbf{v}$, induced by vortices belonging to element dS, at a space point with radius-vector $\mathbf{r}_0$ is computed from the Biot-Savart law:

$$d\mathbf{v} = \frac{1}{4\pi l^3}\,\mathbf{l} \times (d\Gamma_1 d\mathbf{l}_1 + d\Gamma_2 d\mathbf{l}_2), \tag{15.4}$$

where $\mathbf{l} = \mathbf{r} - \mathbf{r}_0$, $l = |\mathbf{l}|$. Integrating Eq. (15.4), we obtain the following formula for velocity $\mathbf{v}_1^{\text{св}}(\mathbf{r}_0, \psi_n)$, induced at an arbitrary point of space by free vortices of the wake that spring from the nth blade

$$\mathbf{v}^{\text{св}}(\mathbf{r}_0, \psi_n) = \int_0^R \int_{-\infty}^{\psi_n} \frac{\mathbf{l} \times D(\Gamma, \mathbf{r})}{4\pi l^3}\, d\varrho d\vartheta. \tag{15.5}$$

Here, $D(\Gamma, \mathbf{r})$ is the following Jacobian

$$D(\Gamma, \mathbf{r}) = \frac{\partial \Gamma}{\partial \varrho}\,\frac{\partial \mathbf{r}}{\partial \vartheta} - \frac{\partial \Gamma}{\partial \vartheta}\,\frac{\partial \mathbf{r}}{\partial \varrho}.$$

Eq. (15.5) expresses velocities induced by vortices of the skewed helical surface S_ψ shown in Fig. 13.1. Vortices on that surface extending along the helical lines of $\rho = const$ are analogous to the longitudinal vortices generated by a wing and for that reason, we will call them the longitudinal vortices, while vortices on that surface extending along the $\vartheta = const$ lines will be called the lateral ones.

Velocity induced at point $(\mathbf{r}_0)$ by bound vortices of a blade at the instant when it is at azimuth ψ_n will be

$$\mathbf{v}^{\text{пр}}(\mathbf{r}_0, \psi_n) = \int_0^R \frac{\Gamma[\mathbf{l} \times \mathbf{r}_\varrho]}{4\pi l^3}\, d\varrho, \tag{15.6}$$

where the point of integration $(\mathbf{r})$ should be located on the blade. This means that in substituting Eq. (15.1) into Eq. (15.6), it is necessary to assume that $\vartheta = \psi_n$. Velocities induced by the whole system are obtained by a summation of Eqs. (15.5) and (15.6) in which we assume that ψ_n takes values of $\psi + 2\pi(n-1)/k$, corresponding to each blade $(n=1, 2, 3, \ldots, k)$. Consequently,

$$\mathbf{v}(\mathbf{r}_0, \psi) = \sum_{n=1}^{k} \int_0^R \int_{-\infty}^{\psi_n} \frac{\mathbf{l} \times D(\Gamma, \mathbf{r})}{4\pi l^3}\, d\varrho d\vartheta + \sum_{n=1}^{k} \int_0^R \frac{\Gamma[\mathbf{l} \times \mathbf{r}_\varrho]}{4\pi l^3}\, d\varrho. \tag{15.7}$$

In the particular case of circulation Γ being constant within a region $\rho_1<\rho<\rho_2$ and zero outside of it, expressions for velocities induced by free vortices can be simplified to the following form:

$$\mathbf{v}^{\text{св}}(r_0,\psi)=\sum_{n=1}^{k}\sum_{l=1}^{2}\int_{-\infty}^{\psi_n}\frac{\Gamma_l[\mathbf{l}\times\mathbf{r}_\theta]}{4\pi l^3}\,d\vartheta. \tag{15.8}$$

Eq. (15.8) contains only single integration along the two longitudinal vortices with circulations $\Gamma_1 = \Gamma$ and $\Gamma_2 = -\Gamma$ which spring from blade stations $\rho = \rho_1$ and $\rho = \rho_2$.

3. CONSIDERATION OF THE DIFFUSION OF VORTICES

A more realistic picture of the flow phenomena associated with the blade action can be obtained if one considers the finite thickness of vortex filaments resulting from diffusion. Let us consider either an infinite or closed three-dimensional vortex filament extending along line L with circulation Γ whose vorticity field Ω at the initial instant of time $t = 0$ is included inside of the filament (tube) and then it is diffused into space according to the following equation of dissipation

$$\frac{\partial\Omega}{\partial t}=\nu_{\text{экв}}\Delta\Omega. \tag{15.9}$$

It is well known that the process of diffusion occurs in viscous fluids. Here, it takes place simultaneously with the process of transport of vortices and is described by the Helmholtz equation

$$\frac{d\Omega}{dt}=(\Omega\cdot\nabla)\,\mathbf{V}+\nu\Delta\Omega. \tag{15.10}$$

Eq. (15.9) is an approximate one, and is obtained from Eq. (15.10) by neglecting the convection terms. The influence of the microscopic mixing of fluid on the diffusion of vortices is accounted for through a substitution of the equivalent turbulent viscosity coefficient $\nu_{\text{экв}}$ for the kinematic viscosity coefficient ν. The relationships expressed by Eq. (15.9) represent an equation of heat transfer for vortex vector Ω. The solution of that equation for the above-formulated initial conditions is given by the following well-known formula

$$\Omega(\mathbf{r},t)=\int_L\frac{\Gamma}{2\,(\sqrt{\nu_{\text{экв}}\pi t})^3}\,e^{-\frac{l^2}{4\nu_{\text{экв}}t}}\,d\mathbf{L}, \tag{15.11}$$

where dL is an element of line L.

Let us find the field of velocities corresponding to the field of vortices given by Eq. (15.11). A direct inspection would show that to the field of velocities,

$$\mathbf{v}(\mathbf{r}_0)=\mathrm{rot}\int_L \frac{\Gamma}{4\pi}\frac{\varkappa(l)}{l}d\mathbf{L} \tag{15.12}$$

corresponds a field of vortices,

$$\Omega(\mathbf{r}_0)=-\int_L \frac{\Gamma}{4\pi}\frac{\varkappa''(l)}{l}d\mathbf{L}. \tag{15.13}$$

In the above formulae, $\varkappa$ is a sufficiently smooth, arbitrary function satisfying the following conditions

$$\varkappa(0)=0,\ \varkappa(l)=1 \text{ for } l>\varepsilon, \tag{15.14}$$

where ε is an arbitrary positive number. Eq. (15.12) can be rewritten as follows:

$$\mathbf{v}=\int_L \frac{\Gamma}{4\pi}\frac{\mathbf{l}\times d\mathbf{L}}{l^3}K(l), \tag{15.15}$$

where

$$K(l)=\varkappa(l)-l\varkappa'(l). \tag{15.16}$$

Eq. (15.13) represents a particular case of Eq. (15.11) and changes into Eq. (15.11) for

$$\varkappa(l)=\frac{2}{\sqrt{\pi}}\int_0^{l/\delta} e^{-x^2}dx \quad (\delta=2\sqrt{\nu_{\text{экв}}t}). \tag{15.17}$$

In addition, the second condition of Eq. (15.14) is fulfilled, with sufficient accuracy for practice, for $\varepsilon \approx 3\delta$. Consequently, velocities induced by the field of vortices from Eq. (15.11) can be determined using Eq. (15.12) or Eq. (15.15). Function $\varkappa(l)$ should be determined according to Eq. (15.17) and function $K(l)$ according to the following relationship resulting from Eqs. (15.16) and (15.17):

$$K(l)=\frac{4}{\pi}\int_0^{l/\delta} x^2e^{-x^2}dx.$$

The field of vortices of Eq. (15.13) for an arbitrary function $\varkappa(l)$ satisfying the conditions of Eq. (15.11) is contained inside of the vortex tube having line L as its axis and cross-sections with radii equal to ε. The field of vortices of Eq. (15.11) has analogous properties. In the considered tube, not all the vortices will be included, but the majority of them will be there. Eq. (15.11), determining the field of velocities due to the diffused vortex filament, differs from the Biot-Savart law through the presence of a scalar multiplier $K(l)$ which is equal to unity for $l > \varepsilon$ and which becomes zero at $l = 0$. The subsequent expression in Eq. (15.15) remains finite at $l = 0$.

Taking advantage of the above results, it is easy to obtain formulae for computation of velocities induced by rotor vortices with due consideration of the finite thickness of the vortex wake. In order to do this, it is sufficient to introduce the multiplier $K(l)$ into the subintegral functions in expressions for induced velocities. As to the time of diffusion t of every element, it may be taken as equal to the time interval $t = (\psi - \vartheta)/\omega$ during whose duration that element exists. Then Eq. (15.7) will assume the following form:

$$\mathbf{v}(\mathbf{r}_0, \psi) = \sum_{n=1}^{k} \int_0^R \int_{-\infty}^{\psi_n} \frac{\mathbf{l} \times D(\Gamma, \mathbf{r})}{4\pi l^3} K(l)\, d\varrho\, d\vartheta + \sum_{n=1}^{k} \int_0^R \frac{\Gamma[\mathbf{l} \times \mathbf{r}_\varrho]}{4\pi l^3}\, d\varrho. \qquad (15.18)$$

The field of induced velocities generated by the diffusing free vortices remains finite at all space points, both on the vortex wake as well as outside of it, as long as those points are not located on the bound vortices. The subintegral function of Eq. (15.18) is also finite everywhere with the exception of points located on the lifting vortices.

The introduction of diffusing vortices may be considered as an approximate consideration of the influence of viscosity on the phenomena of flow, while the introduction of an arbitrary time-independent function $K(l)$ may be taken as a consideration of the volumetric distribution of vortices within the framework of the ideal fluid theory.

4. SEGREGATION OF INDUCED VELOCITIES INTO PROPER AND EXTERNAL VELOCITIES

Various components of the vortex wake play different roles with respect to generation of induced velocities at the blade itself. A segment of the vortex wake leaves the blade, and when directly adjacent to the trailing edge qualitatively influences aerodynamic loads in a way similar to that of the

vortex wake which springs from a moving wing. The remaining parts of the vorticity wake generate a field of disturbances through which, or close to which, the blades have to move.

It is convenient to separately consider induced velocities corresponding to each of those cases. For this reason, as was mentioned before, in calculating velocities along any particular blade, we will divide the vorticity wake into two parts: calling one, *adjacent vortices* and the other, *separated vortices*. Those elements of vortices which spring from the blade during a short period (corresponding to rotation of the blade through a small angle, $\delta\psi$) just preceding the considered moment will be called the adjacent ones. All the remaining vortices will be called the separated ones (with respect to the considered blade). Velocities induced by adjacent vortices will be called *proper*, $v_y^{c\delta}$, and those generated by separated vortices will be called *external*, v_y^{BH}.

The magnitude of angle $\delta\psi$, enclosing the adjacent vortices, is selected in such a way that the so-enclosed vortices would be far enough from the blade to make their contribution to the generation of induced velocities at the blade relatively small. It is possible to select values of the $\delta\psi$ angle within a range from 10-20° up to 180° or even more and still meet the above-mentioned conditions. It is only important that angle $\delta\psi$ is not too small (for instance, not less than 10°) when an increase in δ_ψ would considerably influence the magnitude of the proper velocities. Also, $\delta\psi$ should not be too large (say, larger than 180°) when the blade may again come near the vortices which sprang from it during the preceding revolution.

Although resolution of vortices into adjacent and separated ones is somewhat arbitrary as directly related to the selection of the $\delta\psi$ value, nevertheless it reflects the realistic facts of different influences of the proper and external velocities on the process of generation of aerodynamic loadings. Action of the adjacent vortices is similar (as was mentioned before) to the influence of the vortex sheet which springs from an airplane wing. At the same time, the separated vortices determine the specifics of flow at the helicopter rotor blade when that blade moves in the vicinity of the vortex wake which sprang either from the other blades or from the blade itself during the preceding revolutions.

5. RESULTS OF CALCULATIONS

INFLUENCE OF TIP VORTICES

Let us consider the results of calculations of external induced velocities for a four-bladed rotor under typical

horizontal flight conditions ($\mu = 0,3$; $\alpha_B = -5°$). We will limit ourselves to the most important components of the external induced velocities; namely, to those generated by the tip vortices. A horizontal projection of the system of vortices corresponding to various azimuth positions of the blades is shown in Fig. 15.1. The proximity of those vortices to the blades is signaled by the points of intersection of the blades with the projections of those vortices on the plane of rotation. In the vicinity of those points, one may expect especially noticeable variations of induced velocities. Furthermore, it can be seen from Fig. 15.1 that the positions of those points vary on the blades as the latter change their azimuthal points.

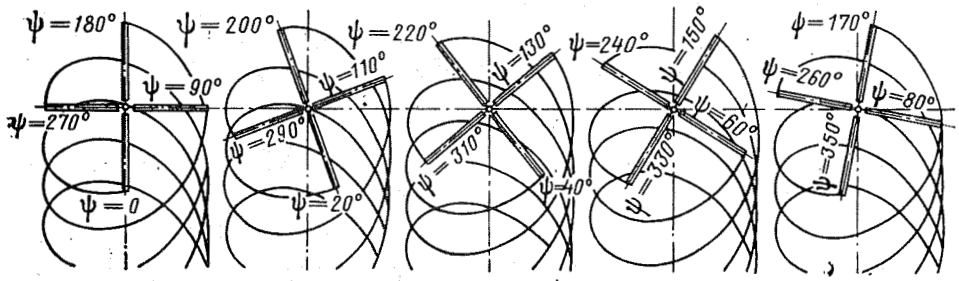

Figure 15.1

A graph of the relative induced velocity $\bar{v}_y^{BH}$ distribution along the blade at the moment when blade *I* (at which velocities are computed) assumes the $\psi = 90°$ azimuth angle, is shown in Fig. 15.2. It was assumed that tip vortices leave the blade at a radius $\bar{\rho}_2 = 1$, while their circulation $\Gamma = 0,01\omega R^2$. Curves *I*, *II*, *III* and *IV* in Fig. 15.2 represent the external induced velocities at blade *I* which are generated by vortices springing from blades *I*, *II*, *III* and *IV*. Looking at those curves, it is not difficult to detect a relationship between characteristic peculiarities in velocity distributions along the blade (at $\psi = 90°$) and the corresponding position of the tip vortices. External velocities induced at blade *I* by its own tip vortex are very low. This is due to the fact that all elements of that vortex move down with the flow and remain sufficiently far from the blade. The vortex springing from blade *II* comes close to blade *I* at radius $\bar{r} = 0,95$. Due to this fact, induced velocities increase toward the blade tip and reach very high values in the areas where the vortex approaches the blade. Close to the point of intersection of the blade axis with the vortex projection, velocities reach their maximum, then rapidly decrease and change their sign. At the very tip of the blade, velocities induced by that vortex become directed upward. A similar situation may be noticed in Fig. 15.2 with respect to the external velocities induced at blade *I* by the tip vortices of blades *III* and *IV*. Points of velocity transition through zero move to the radii $\bar{r} = 0,7$ and $\bar{r} = 0,2$, corresponding to the points of the

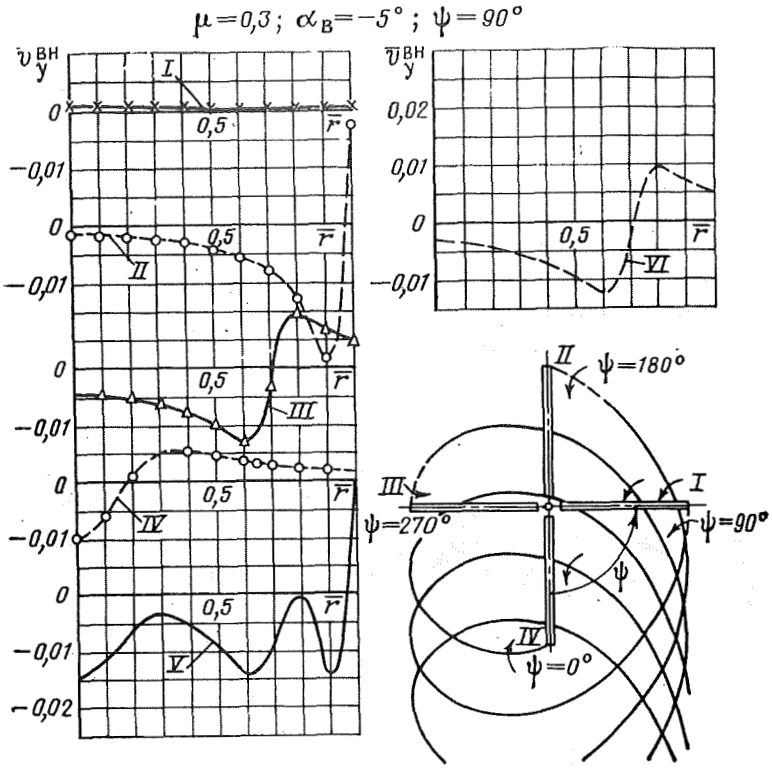

Figure 15.2

closest proximity of the elements of vortices to the blades. Induced velocities in the neighborhood of those points do not decrease as rapidly as in the case of curve *II*, since the vortices do not come as close to the blade as in the preceding case. Curve *V* in Fig. 15.2 shows variation along blade *I*, of external velocities induced by the tip vortices of all four blades. This curve shows maxima at the points where the blade (for which velocities are computed) comes close to the various tip vortices. Curve *VI* refers to the same interaction for a two-bladed rotor.

Let us now consider the variation of the external instantaneous induced velocities as a function of the azimuth angle (ψ) while the radius remains fixed. Suitable curves, corresponding to the considered case for $\overline{r} = 0,7$, are shown in Fig. 15.3. Here, velocities at blade *I*, induced by the tip vortices for the four (curve *V*) and two-bladed (curve *VI*) rotors.are also given. From a comparison of curve *II* with the remaining ones, it can be seen that the vortex which springs from the blade moving directly ahead of the considered one has the greatest influence on the external induced velocity at $\overline{r} = 0,7$. Tip vortices of other blades have a much weaker influence. Consequently, curve *V*, representing a summation of all the

influences is very similar to curve *II*. From Fig. 15.3, it can also be seen that the external instantaneous velocities induced at the blade vary with the azimuth in a very irregular fashion. When the considered blade comes close to a vortex which sprang from the preceding blade, very rapid fluctuations of induced velocity should be noticed.

Longitudinal (trailing) vortices springing from the remaining sections of the blade exert an influence analogous to that of the tip vortices. However, those vortices are much weaker and hence, velocities induced by them do not show fluctuations as strong as those resulting from the tip vortices. Furthermore, vortices springing from the root stations at all azimuth angles (with the exception of angles close to $\psi = 0$) remain relatively far from all the blade working sections.

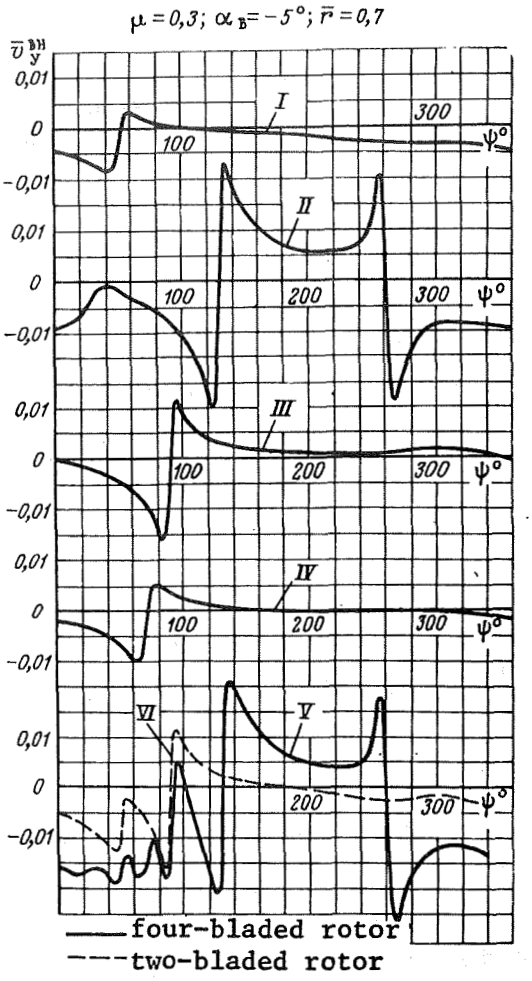

Figure 15.3

A planview of the tip and root vortices of a four-bladed rotor is shown in Fig. 15.4. The location of points from which the root and tip vortices spring from the blade were assumed as $\bar{r}_1 = 0,4$ and $\bar{r}_2 = 0,95$. It can be seen that root vortices are aggregated within a narrow strip extending from the rotor center down along the direction of flow. External induced velocities $\bar{v}_y^{вн}$ corresponding to the shown system of vortices are plotted in Fig. 15.5. Qualitatively, it can be seen that they are not much different from velocities induced by the tip vortices alone. One should notice, however, that on curves showing $\bar{v}_y^{вн}$ vs azimuth, there are considerable velocity fluctuations in the neighborhood of $\psi = 0$. These fluctuations are caused by the root vortices.

INFLUENCE OF VORTICES ADJACENT TO THE BLADE

It has already been shown that under the influence of the separated vortices, a field of nonuniform velocities is formed

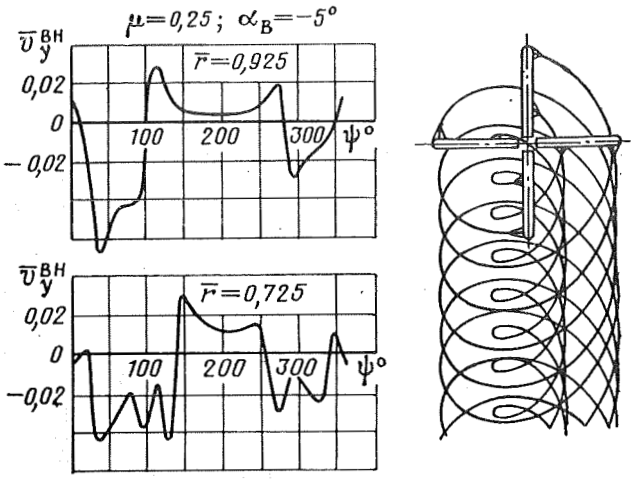

Рис. 15.4.

Figure 15.4

ahead of the blade. During blade movement in this field, supplementary adjacent vortices would spring from the blade. The character of the influence exerted on the aerodynamic loads by velocities induced by those vortices will be examined on a concrete example.

Computed values of the relative circulation Γ at $\psi = 90°$ for a blade of a two-bladed rotor are shown in Fig. 15.5. Curve *1* is computed for geometric angles of attack of blade sections with no consideration of induced velocities. Curve *2* gives values of circulation $\bar{\Gamma}^{\infty}$, computed with the consideration of the external induced velocities only $\bar{v}_y^{вн}$, as given by curve *4*. For the considered blade azimuth position, tip vortex of the preceding blade closely approaches the investigated blade at its $\bar{r} = 0,7$ station. This leads to rapid variations in the $\bar{v}_y^{вн}$ values; from the high negative at $\bar{r} < 0,65$ to the high positive at $\bar{r} > 0,75$. This variation of velocity is responsible for the step jump in the $\bar{\Gamma}^{\infty}$ graph of curve *2*. Curve *3* corresponds to circulation $\bar{\Gamma}$, computed with an approximate consideration of the proper induced velocities as obtained from a solution of the integral-differential equation of Prandtl

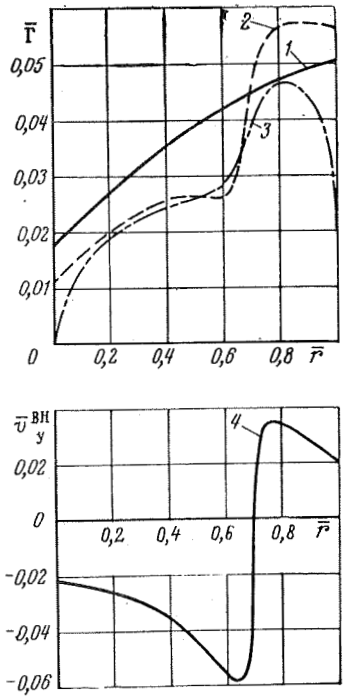

Рис. 15.5.

Figure 15.5

$$\bar{\Gamma}=\bar{\Gamma}^{\infty}+\frac{a_{\infty}b}{8\pi}\int_0^1\frac{\partial\bar{\Gamma}}{\partial\varrho'}\frac{d\varrho'}{\varrho'-\varrho}$$

(values of $\bar{\Gamma}^{\infty}$ are taken from curve *2*). From curve *3*, it can be seen that consideration of the influence of the proper induced velocities resulted in a sizeable decrease in circulation values in the blade tip region, while at both extreme blade stations, circulation becomes zero. In addition, some smoothing of the rapid variation of circulation $\bar{\Gamma}^{\infty}$ also occurred, which had been caused by the proximity of the tip vortex to the blade. It can be seen, hence, that in contrast to the perturbance-causing effects of external induced velocities $\bar{v}_y^{\text{BH}}$, the proper induced velocities have a smoothing influence.

A comparison of the external and proper induced velocities shows that it is conceivable to determine $\bar{v}_y^{\text{BH}}$ from the a priori given circulation, which will be later determined with more accuracy. However, for calculation of $\bar{v}_y^{\sigma\sigma}$, this approach is not suitable since the corresponding integral-differential equations would lead to divergent solutions by this process. It should also be noted that the order of magnitude of the proper induced velocities is determined by circulation $\bar{\Gamma}$ and depends little on the regime of flight. By contrast, the external velocities $\bar{v}_y^{\text{BH}}$ depend on the regime of flight and on the average, vary inversely-proportionally to the helicopter speed of flight. Those differences between the proper and external induced velocities justify their separate consideration, in spite of the fact that a division of vortices into the adjacent and separated ones is, to a large extent, arbitrary.

COMPARISON OF THEORETICAL AND EXPERIMENTAL RESULTS

Let us consider to what extent the theoretically predicted specific peculiarities of the blade loadings are found in practice. In order to better examine the aerodynamic loads associated with the tip vortices, we will consider those loads under special circumstances. We will consider a two-bladed rotor with flat, nontwisted blades at zero disc angle of attack. It will also be assumed that one of the blades has a pitch angle of $\phi = 7,2^{\circ}$ and carries its normal load, while the other blade is at $\phi = 0$. In this case, the second blade would experience aerodynamic loads solely due to the tip vortices of the first one. Both analytical calculations and tests were performed in accordance with the above conditions[3]. Experimental and analytical data are shown in Fig. 15.6, where quantities $c_{y1}\bar{W}_x{}^2\tilde{b}$, proportional to the blade loads per unit of span, are plotted vs the azimuth. Continuous lines represent experimental, and the broken ones, analytical, results.

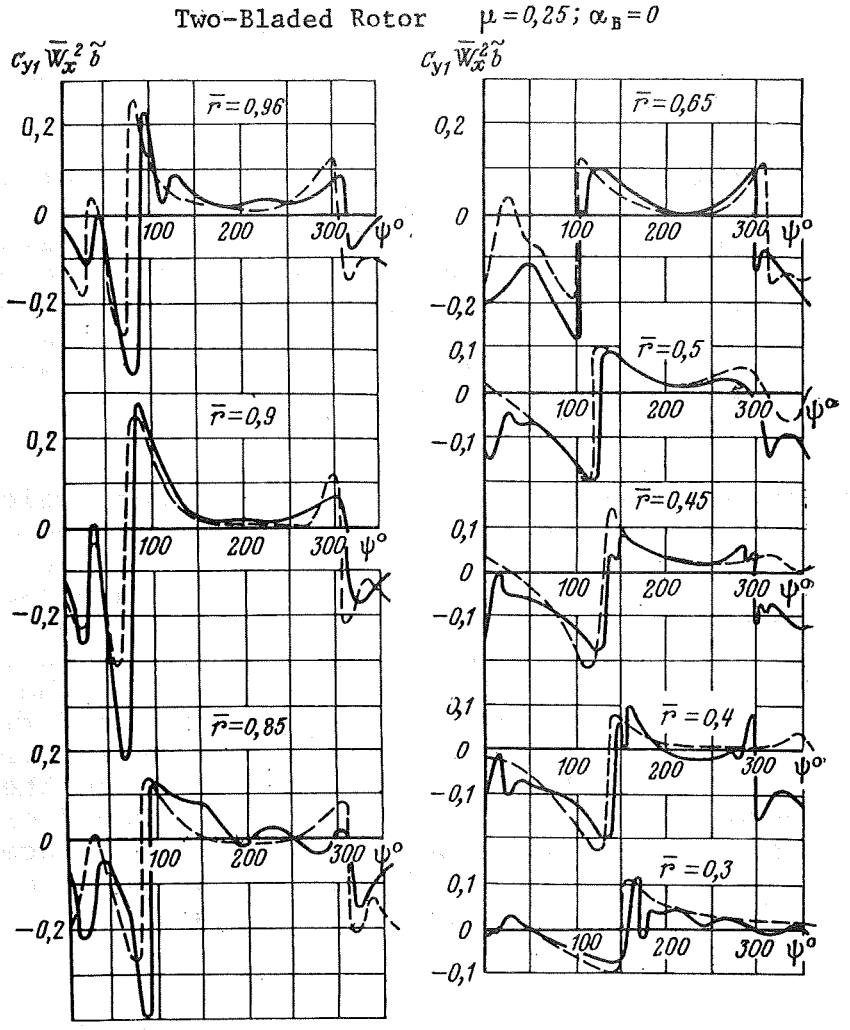

Figure 15.6

In spite of the complicated character of the curves, variation of the unit span thrust with the azimuth shows a good agreement between predicted and measured values (for this particular case). Experimental data fully confirmed the existance of almost all of the very rapid, and one might think, random, fluctuations of the curves. The only area of disagreement is in the $300° < \psi < 360°$ region where, for $\bar{r} = 0,4$, the difference between the analytical and experimental curves is significant.

The above described rapid variations of the blade unit span thrust loads (resulting from the interaction between the blade and nearby tip vortices) can also be observed in a somewhat smoother form in the more common cases of rotor operations with all blades equally loaded. As an illustration, curves giving

variations of the quantity $c_{y_1}\overline{W}_x^2\tilde{b}$ at the $\overline{r} = 0,7$ radius vs the azimuth angle are shown in Fig. 15.7. In this figure, theoretical predictions are depicted by broken lines and experimental values by the continuous ones. The above data are for a rotor with five rectangular, untwisted blades. Rapid increases in the blade unit span thrust loading for the $150° < \psi < 210°$ region can be explained by the proximity of tip vortices to the blade.

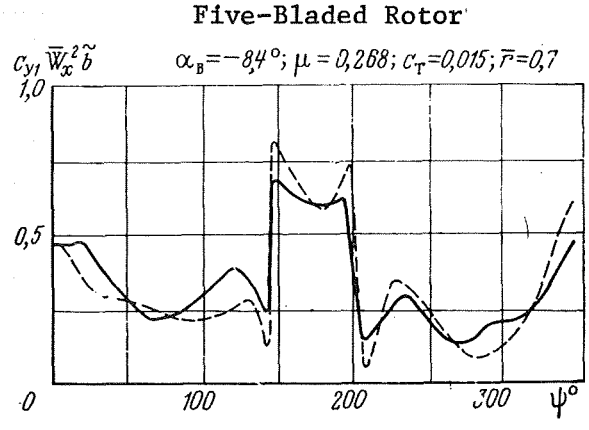

Figure 15.7

From the presented examples of calculations of instantaneous induced velocities, important conclusions can be drawn. First of all, it can be seen that the adjacent and the separated vortices play a very important role in the determination of the blade loads. Consequently, both should be considered. The separated vortices represent mutual inductive influence of the blades on their aerodynamic loads. This influence generates, in turn, a complicated field of varying external induced velocities and the whole phenomenon becomes especially characteristic for the rotor oblique flow conditions. When the blade enters into the field of rapidly varying external velocities, it experiences corresponding variations in its aerodynamic loads. The influence of the proper induced velocities is chiefly manifested as some smoothing of those rapid aerodynamic loading variations. The most significant influence on the external induced velocities is exerted by the tip vortices, and especially, by the tip vortex of the blade immediately preceding the considered one.

A model based on the tip vortices requires relatively simple analytical procedures. Thus, it offers a practical approach to the task of finding aerodynamic loads with due consideration of the instantaneous induced velocities.

Although the considered scheme of calculations (let us call it the first approximation scheme) reflects the basic laws of

the instantaneous aerodynamic loads variations, it also has drawbacks. Some of those drawbacks stem from the inaccuracy of the linear vortex scheme, while the others result from the simplified vortex system. First of all, it must be realized that the first approximation scheme exaggerates the degree of nonuniformity of the field of external induced velocities. Load peaks, associated with the braids of tip vortices coming near the blade, as indicated by calculations are higher than actually measured. This lowering of the actual load peaks can be explained through the influence of the vortex sheet. We will call this phenomenon "screening" of the braids by the vortex sheet. Let us explain in greater detail, the mechanism of that phenomenon. Screening consists of the following: If, in a particular moment, a section of the tip vortex braid comes close to the blade, then from the blade itself would spring vortices of an opposite sign to those of the braid. Those vortices would locate themselves close to the indicated section of the braid and then would move with the braid, thus considerably reducing the local induced velocities. In order to evaluate the effect of screening, it is necessary to compute external induced velocities with an accurate consideration of the variation of the vortex sheet with both the radius and the azimuth. Such calculations were performed by M.N. Tishchenko. Some of the obtained results will be quoted.

Graphs of $c_{y_2}\overline{W}_x{}^2\tilde{b}$ vs ψ are shown in Fig. 15.8 for four values of $\overline{r}$. This was done for a rotor with four tapered linearly twisted blades. Curves *1* represent quantities computed according to the first approximation scheme with vortices springing from the tip and the root of the blade; curves *2* are computed with the considerations of the vortex sheet; and curves *3* represent experimental results. It may be concluded that there is an acceptable agreement between the calculations and the experiment. The external induced velocities $\overline{v}_y^{\text{BH}}$ are shown in Fig. 15.10. Curves *1* correspond to the vortex sheet scheme and curves *2*, to the first approximation scheme. Conditions here are the same as in Fig. 15.8. In agreement with the previously made statements, it can be seen that induced velocities calculated according to the first approximation scheme are distributed less uniformly. In the curves showing induced velocities,vs the azimuth angle, one can find rapid fluctuations in their values. Those breaks in continuity considerably diminish when the vortex sheet approach is used. In Fig. 15.9 a comparison is shown of the calculations of induced velocities according to the vortex scheme, with considerations (curve *1*) and without considerations (curve *2*) of the lateral vortices. From that figure, it can be seen that the differences are small. Consequently, considerations of the lateral vortices can be omitted.

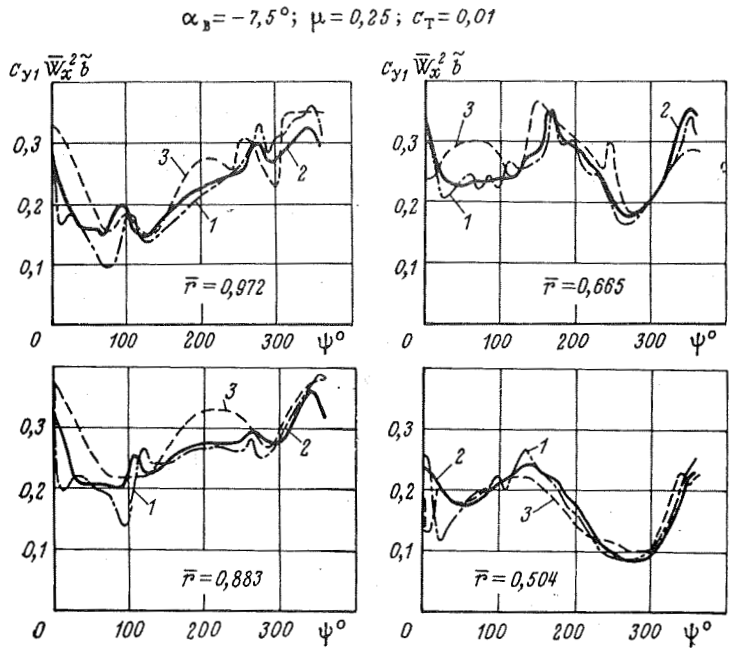

Figure 15.8

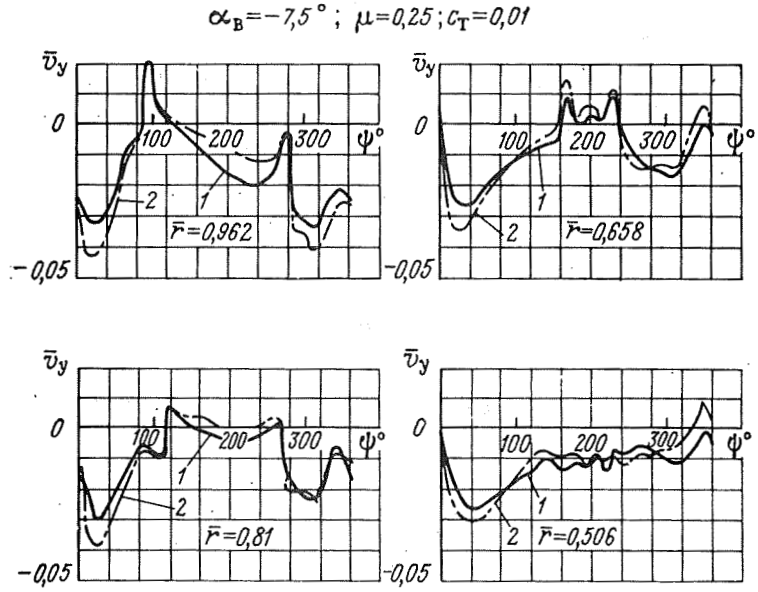

Figure 15.9

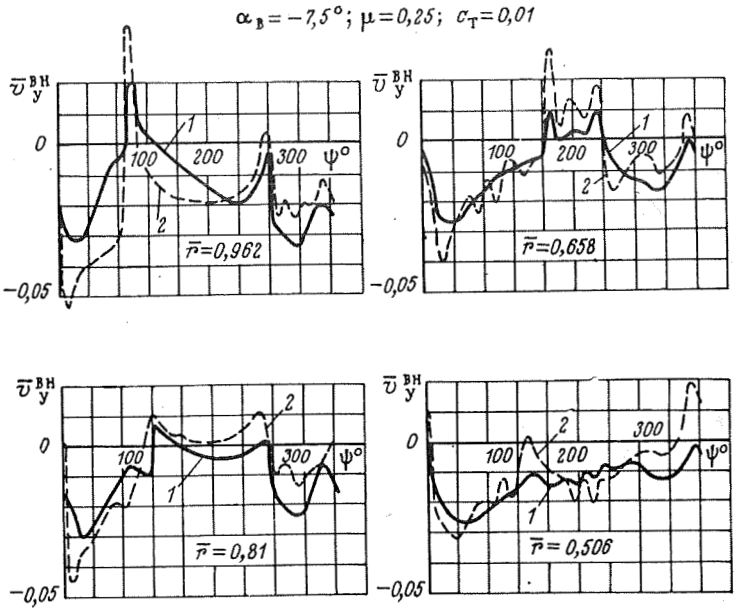

Figure 15.10

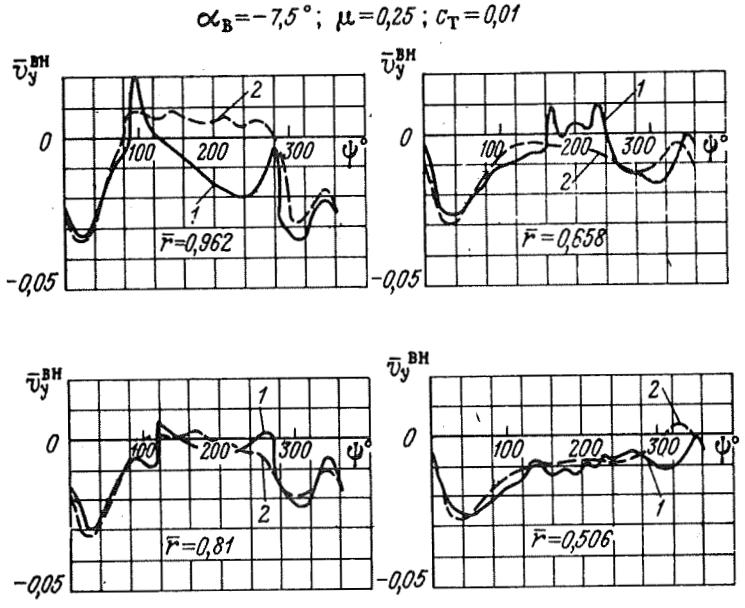

Figure 15.11

Finally, in Fig. 15.11, a comparison is shown of the relative external induced velocities for the above-considered four-bladed rotor (curves *1*) with those for a rotor with an infinite number of blades (curves *2*). In the latter case, all the peaks of induced velocities associated with the proximities of vortices to the blades disappeared. In addition, there are large differences in induced velocities in the tip region which may be related to the influence of the proper induced velocities. For this reason, it is possible to considerably improve the accuracy of blade load calculations performed according to the disc vortex theory. This can be done by considering velocities predicted by the disc theory as being external, and introducing the proper velocities as being supplementary. Values of induced velocities at the root and mid-blade stations would differ little for both cases. This provides a basis for the application of the theory of a rotor with an infinite number of blades to the calculation of the overall aerodynamic loads for conventional four- and five-bladed rotors where local load fluctuation, due to the proximity of vortices to the blades, level off with time.

6. FUNDAMENTALS OF THE NONLINEAR VORTEX THEORY OF LIFTING AIRSCREWS

The previously considered methods of induced velocity calculations were based on the fundamental assumption of the linear theory according to which the transport of the vortex elements occurs with constant velocity. This assumptions permits one to readily construct the shape of the vorticity wake, which is later used in the calculations of induced velocities. The linear theory gives good results as long as the induced velocities are small in comparison with those of the undisturbed flow approaching the rotor. In that case, the velocity of the transportation of vortices is not much different from that of the undisturbed flow. This case is typical for high-speed helicopter flight. However, at low speeds of flight, the magnitudes of the induced velocities are comparable to those of the flight itself. Furthermore, the variation of those induced velocities, in turn, causes a deformation of the real system of vortices, thus making it different from that constructed on the basis of the linear theory. In order to improve the prediction accuracy of the field of velocities generated by a rotor in those regimes of flight, it is desirable to determine the distribution of vortices together with the field of varying induced velocities generated by these vortices.

TRANSPORT SPEED OF THIN VORTEX SURFACES

With a three-dimensional distribution of free vortices, their elements are transported with the speed of movement of particles

of the fluid. If free vortices form a surface, then induced velocities experience discontinuities at that surface. Thus, the speed of motion of the points belonging to the surface becomes undetermined. However, it may be shown that this velocity is equal to one-half of the sum of the limit values of velocities at the considered point when the point is approached from different directions.

Let us consider an unsteady field of velocities $\boldsymbol{V}(\boldsymbol{r},t)$ having a discontinuity of the tangential component on some limited, moving finite surface S (Fig. 15.12). This field is continuous on the outside of the surface S and has a velocity potential $\phi(\boldsymbol{r},t)$. On the basis of the Lagrange integral, the pressure difference $\Delta p = p_B - p_A$ between two arbitrary points A and B in the flow stream is expressed by the following formula:

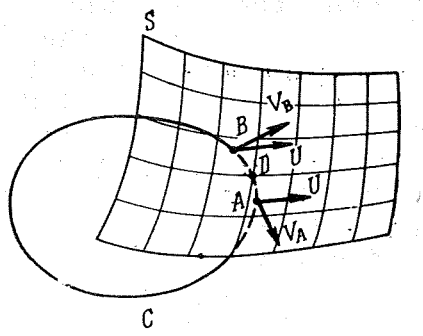

Figure 15.12

$$\Delta p=\frac{\varrho}{2}(\mathbf{V}_A^2-\mathbf{V}_B^2)+\varrho\frac{\partial\Delta\varphi}{\partial t}, \qquad (15.19)$$

where $\mathbf{V}_A$ and $\mathbf{V}_B$ are the fluid velocity vectors, and $\Delta\phi$ is the difference of potential between points A and B. Let us consider that points A and B move with the same velocity $\mathbf{V} = 0{,}5(\mathbf{V}_A + \mathbf{V}_B)$. Expressing the derivative $d\Delta\phi/dt$ at the moving point through the local derivative $\partial\Delta\phi/\partial t$ appearing in Eq. (15.19), we obtain

$$\frac{d\Delta\varphi}{dt}=\frac{\partial\Delta\varphi}{\partial t}+\frac{\mathbf{V}_A+\mathbf{V}_B}{2}\operatorname{grad}\Delta\varphi, \qquad (15.20)$$

where

$$\operatorname{grad}\Delta\varphi=\mathbf{V}_A-\mathbf{V}_B. \qquad (15.21)$$

With the consideration of Eq. (15.21), Eq. (15.20) expressing pressure difference between two arbitrary points of the flow stream is transformed to the following form

$$\Delta p=\varrho\frac{d\Delta\varphi}{dt}.$$

Let us bring points A and B, located on different sides of surface S, closer to some point D located on surface S (see Fig. 15.12). We should also note that in this case, the quantity $\Delta\phi$ will be equal to circulation Γ along an arbitrary contour piercing surface S. In considering the above, we obtain

$$\Delta p=\varrho\frac{d\Gamma}{dt}. \qquad (15.22)$$

On the surface of free vortices, $\Delta p = 0$; hence, according to Eq. (15.22), circulation along contour C is time independent. This means that free vortices of the surface, when moving, do not intersect contour C. The selection of point D was arbitrary. This means that elements of vortices forming the surface move at all its points with speeds equal to one-half of the sum of the limit velocities determined at the considered points on both sides of the surface.

7. INTEGRAL-DIFFERENTIAL EQUATION OF VORTEX SURFACE MOVEMENT

On the moving surface S formed by free vortices, let us introduce a network of curved Gaussian coordinates u,v. It will be assumed that surface points defined by such coordinates are connected with the free vortices and move together with them. In such a case, circulation Γ of the velocity vector along contour C, piercing the surface at point (u,v), will be a function of those coordinates only and not of time: $\Gamma = \Gamma(u,v)$. Defining the current vector radius of the moving points of the surface by $S(u,v,t)$, it is possible to write an expression, analogous to Eq. (15.7), which would determine the induced velocity V_S at an arbitrary space point (r_O). This expression will have a form of an integral over surface S:

$$\mathbf{v}_s(\mathbf{r}_0, t)=\iint_S \frac{1}{4\pi l^3}\mathbf{l}\times\frac{\partial(\Gamma', \mathrm{S}')}{\partial(u', v')}du'\,dv'. \tag{15.23}$$

Here, Γ' and S' define the following functions:

$$\Gamma'=\Gamma(u', v'),\ \mathrm{S}'=\mathrm{S}(u', v', t); \tag{15.24}$$

Expression $\partial(\Gamma',S')/\partial(u',v')$ which, in this case, will be a vector, is the Jacobian of functions in Eq. (15.24); i.e.,

$$\frac{\partial(\Gamma', \mathrm{S}')}{\partial(u', v')}=\frac{\partial\Gamma'}{\partial u'}\frac{\partial \mathrm{S}'}{\partial v'}-\frac{\partial\Gamma'}{\partial v'}\frac{\partial \mathrm{S}'}{\partial u'},$$

while vector $l = S' - r_O$ joins the point of integration with the point at which velocity is computed. In a particular case, the point at which velocity is computed might be on the surface itself. Then, the integral on the right side of Eq. (15.23), considered as the principal value, is equal to one-half of the sum of the limit values of velocities at a point on the surface when this point is approached from opposite directions. This half-sum is called the *straight* value of such an integral.

In addition to surface S, there can be other vortices in the stream flow. The sum of velocities induced by those vortices and the velocity of the undisturbed incoming flow will be designated as V_0, and its value will be considered to be known. Since at $V = 0$, the velocity of movement of a point with radius vector $S(u,v,t)$ is equal to the straight value of the integral of Eq. (15.23) at that point, hence, for function $S(u,v,t)$, the following nonlinear integral-differential equation can be written

$$\frac{d}{dt}\mathrm{S}(u, v, t)=\frac{1}{4\pi}\iint_S \frac{1}{l^3}\times\frac{\partial(\Gamma', \mathrm{S}')}{\partial(u', v')}\,du'\,dv'+\mathrm{V}_0, \tag{15.25}$$

where

$$1=\mathrm{S}(u', v', t)-\mathrm{S}(u, v, t).$$

Eq. (15.25) may be considered as a particular case of an infinite system of ordinary differential equations having the normal Cauchy form. Initial conditions for the corresponding Cauchy problem can be given as the form of the vorticity surface an an initial moment of time $t = t_0$. Function $\Gamma(u,v)$, appearing in Eq. (15.25) is assumed to be given.

In the application of Eq. (15.25) to the surface of free vortices springing from helicopter blades, it is convenient to take the following quantities as parameters u,v: (a) time τ of separation of the vortex elements from the blade trailing edge and (b) ρ radius of the point of separation. In that case, surface S will continuously be resupplied with new vortices whose initial position and circulation at the moment of separation from the blade are known (assuming that the movements of the blades and their loads are known).

PARTICULAR FORMS OF VORTEX SURFACE

Due to the great complexity of Eq. (15.25), it is convenient to consider some particular cases representing simple forms of surface S. Let us consider the following cases: (1) an arbitrary cylindrical surface with infinite generatrices; (2) surface of revolution; (3) surface of revolution degenerated into a line (vortex filament). In those cases, the shape of surface S is described as a function of a single variable only, and not of two variables as before.

If surface S becomes a cylinder consisting of infinite rectilinear vortices extending along its generatrices, then Eq. (15.25) can be written (after integration of velocities along the vortices) under the form of the following system of two scalar equations.

$$\frac{d}{dt}x(u,t)=-\frac{1}{2\pi}\int_{u_0}^{u_1}\frac{d\Gamma(u')}{du'}\frac{y(u,t)-y(u',t)}{l^2}du'+V_{0x},$$

$$\frac{d}{dt}y(u,t)=\frac{1}{2\pi}\int_{u_0}^{u_1}\frac{d\Gamma(u')}{du'}\frac{x(u,t)-x(u',t)}{l^2}du'+V_{0y}, \qquad (15.26)$$

where $$l^2=[x(u,t)+x(u',t)]^2+[y(u,t)-y(u',t)]^2,$$

while $x(u,t)$ and $y(u,t)$ are the Cartesian coordinates of the line representing the intersection of surface S by a plane perpendicular to its generatrices. Initial conditions for the solution of Eq. (15.26) can be given as the position of line $x = x(u,t)$, $y = (u,t)$ at $t = t_O$ and the position of new components of that line at the moment of their appearance.

If surface S represents a surface of revolution consisting of vortex rings, then after an integration of velocity along such a ring, Eq. (15.25) can be written as follows:

$$\frac{dx}{dt}=\int_{u_0}^{u_1}\frac{d\Gamma(u)}{du}K_x\left(\frac{x-x'}{r'},\frac{r}{r'}\right)\frac{du'}{r'}+V_{0x},$$

$$\frac{dr}{dt}=\int_{u_0}^{u_1}\frac{d\Gamma(u)}{du}K_r\left(\frac{x-x'}{r'},\frac{r}{r'}\right)\frac{du'}{r'}, \qquad (15.27)$$

where $x = x(u,t)$ and $r = r(u,t)$ are the equations of lines representing intersections of surface S by a radial plane, while in addition, $x' = x(u',t)$ and $y' = y(u',t)$. Axial and radial components of velocity induced at point (x,r) by a vortex ring of unit radius and unit circulation located in plane $x = 0$ are defined as $K_x(x,r)$ and $K_r(x,r)$. Those functions have the following well-known form[12].

$$K_x(x,r)=\frac{1}{4\pi}\frac{1}{\sqrt{x^2+(1+r)^2}}\left(\frac{2-k^2}{1-k^2}\mathrm{E}-2\mathrm{K}-\frac{4E}{(1-k^2)[x^2+(1+r)^2]}\right),$$

$$K_r(x,r)=\frac{1}{4\pi}\frac{-x}{r\sqrt{x^2+(1+r)^2}}\left(\frac{2-k^2}{1-k^2}\mathrm{E}-2\mathrm{K}\right), \qquad (15.28)$$

where modulus k of the complete elliptic integrals E and K is given by the following formula

$$k^2=\frac{4r}{x^2+(1+r)^2}.$$

Finally, if surface S degenerates into a line, then it becomes impossible to directly apply Eq. (15.25). This is due to the fact that the curved vortex filament would induce infinitely high velocities on itself. Consideration of the thickness of the vortex filament becomes a necessary condition in the determination of its movement. Now, we consider the vortex filament of finite cross-sections (vortex braid); in this case, we obtain the following integral-differential equation:

$$\frac{d}{dt}\mathrm{S}(u, t)=\frac{-\Gamma}{4\pi}\int_{L}\frac{\partial \mathrm{S}}{\partial u'}\times\frac{1}{l^3}K(l)\,du'+\mathbf{V}_0, \qquad (15.29)$$

which describes the motion of the vortex braid. Here, Γ is the circulation of the braid, and $S(u,t)$ is a function defining radius-vectors of points located at an instant t on the braid axis.

8. TASKS WHICH CAN BE REDUCED TO THE INVESTIGATION OF MOVEMENTS OF FLAT VORTICES AND VORTEX RINGS

The integral-differential equations of the type of Eq. (15.26) were applied by Kaden[105] to the approximate description of rolling up of the vortex sheet of a moving wing of a finite span. In the application of that method to rotors, it is possible to consider the roll-up problem of the vortex sheet leaving the blade into the tip braids. This approach can also be applied to the problem of mutual interaction between a segment of the wake of one blade with the vortex braid of another. In order to solve integral-differential Eq. (15.26), it is necessary to replace a continuous distribution of vortices by a discrete one. This reduces those equations to a system of m ordinary differential equations of the following type:

$$\frac{dx_i}{dt}=-\frac{1}{2\pi}\sum_{j=1}^{m}\frac{(\Gamma_{j+1}-\Gamma_j)(y_i-y_j)}{l_{i,j}^2},$$
$$\frac{dy_i}{dt}=\frac{1}{2\pi}\sum_{j=1}^{m}\frac{(\Gamma_{j+1}-\Gamma_j)(x_i-x_j)}{l_{i,j}^2} \qquad (i=1, 2, 3, \ldots, m) \qquad (15.30)$$

with the initial Cauchy conditions. Here,

$$l_{i,j}^2=(x_i-x_j)^2+(y_i-y_j)^2,$$

and x_i, y_i are the coordinates of discrete vortices.

Application of Eq. (15.30) to the investigation of deformation of the rotor vortex wake is based on the following approximation. It is assumed that separate sections cut out from the vortex sheet by the closely spaced $\vartheta = const$ lines may be considered as segments of a vortex sheet springing from a wing having the same distribution of circulation as the blade.

Based on the above approach, let us consider some results of calculations of the rolling-up of the vortex sheet springing out from one wing while under the influence of an external vortex braid generated by another wing (Figs. 15.13-15.15). Curves *1* in those figures give the initial span-wise distributions of circulation $\overline{\Gamma}$ for a flat constant-chord blade for various values of $\overline{h}$ determining the distance of the blade from the external braid, which is assumed to be located below the blade at relative radius $\overline{r} = 0,5$. Curves *2* and *3* give cross-sections of the rolled-up vortex sheet at various time values $t = \Delta\psi/\omega$, corresponding to blade rotation through an angle $\Delta\psi$. Calculations indicate that the rolling-up of the tip vortices appears very quickly. Root vortices roll up much slower and form braids of large cross-sections and lower circulations, since part of the vorticity remains in a sheet form. In addition to the roll-up of the tip and root vortices, one may also notice that the roll-up takes place at the middle sections of the blade where the circulation varies rapidly as a result of the proximity of the external vortex braid. For small distances $(\overline{h} = 0,025)$ of the external braid, the rolled-up middle vortex sheet is united with the external braid into a single unit. Circulation of the combined braid is lower than that of the external one. This is due to the fact that the vortices in the sheet are of the opposite sign. Here, one may find a partial explanation of the experimentally observed reduction of the induced velocity peaks, as the blade comes repeatedly close to the tip vortices.

TASKS WHICH CAN BE REDUCED TO CONSIDERATIONS OF MOVEMENTS OF VORTEX RINGS

The application of the nonlinear vortex theory to calculations of induced velocities of a helicopter rotor in an axial translation can be considerably simplified. This can be done by neglecting the lateral components of induced velocities (not too important for lifting airscrews) and replacing the three-dimensional vortices with a system of vortex rings. This type of flow is completely symmetrical with respect to the axis. Consequently, it may be investigated in one of the *Oyr* planes, which represents a much simpler task than investigation of a three-dimensional flow. If one restricts the considerations to a finite number of the vortex rings, then the task of finding movement of those rings in a field of velocities induced by them is not

chain of rings which spring from the same radius ρ_j and index "i" designates the consecutive position of the ring in the chain. The number of rings in the chain $n(t)$ increases with time. This means that the system given by Eq. (15.31) contains a variable number of equations. Integration of the systems of Eq. (15.31) is performed from the initial Cauchy conditions separately given for the coordinates of each ring at the moment of its appearance. Velocity components, corresponding to those generated by each ring on itself are omitted from the summation indicated in Eq. (15.31). However, they are accounted for through the addition of the v'_i term to the velocity V_o of the free stream. In the computation of velocity v'_i, it is necessary to consider the finite thickness of the ring using, for instance, the following approximate formula[55]:

$$v'_i = \frac{\Gamma}{4\pi r_i} \ln \varepsilon,$$

where ε is the radius of the cross-section of the ring. Velocity at the ring center is pointed in the same direction as that of the fluid flow.

In the application of Eq. (15.31) to the problem of defining the flow generated by an airscrew, it is desirable to determine, as exactly as possible, the position of the vortex filaments in the vicinity of the blades. For this reason, it is recommended to take the time interval (Δt), passing between the appearance of consecutive vortex rings, as equal to the time required to rotate the blade through the indexing angle. Furthermore, induced velocities should be computed for an instant immediately preceding the formation of a new vortex ring. Circulation γ_i of a vortex ring which springs from any part of the blade is equal to the variation of blade circulation $\Gamma(\rho)$ on that part.

As an example, let us consider the results of calculations (based on Eq. (15.31)) of the form of vortices as well as values of the corresponding external induced velocities $v_{\bar{y}}^{BH}$ in the rotor disc plane. In those calculations, circulation Γ is assumed to be constant along the blade. Consequently, only two chains of vortex rings would spring from the rotor disc. One of them would correspond to the tip and the other, to the root vortex braids. Points of the braid separation from the blades were assumed to be located at the $0,4R$ and $0,95R$ stations, while the relative circulation was assumed to be $\bar{\Gamma} = 0,02$. Axis $O\bar{y}$ coincides with the rotor axis, while the disc of the rotor is in the $\bar{y} = 0$ plane.

Fig. 15.16*a* gives the shape of the slipstream in hovering $(\bar{V}_o = 0)$. One can see outlines of the main flow as well as a cluster of dispersing vortices at its end. Contraction of the slipstream below the disc is also clearly visible. Figure 15.16*b*

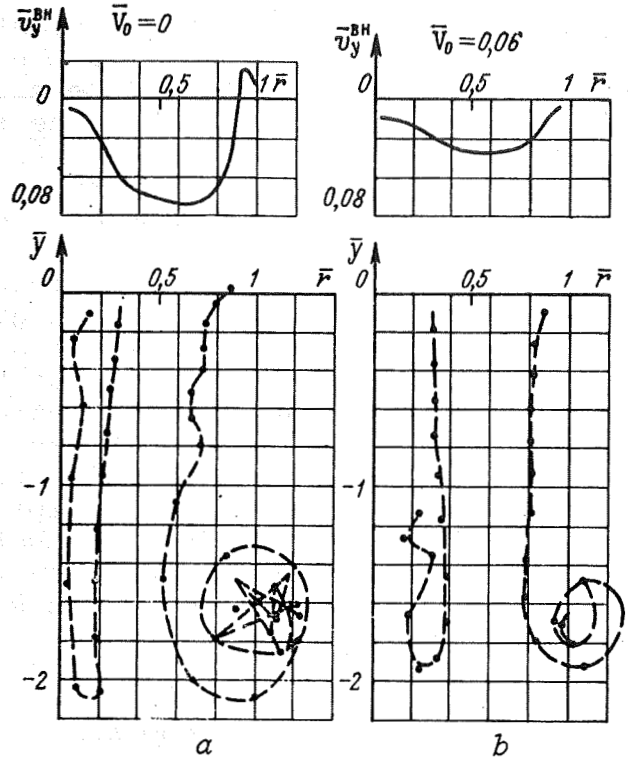

Figure 15.16

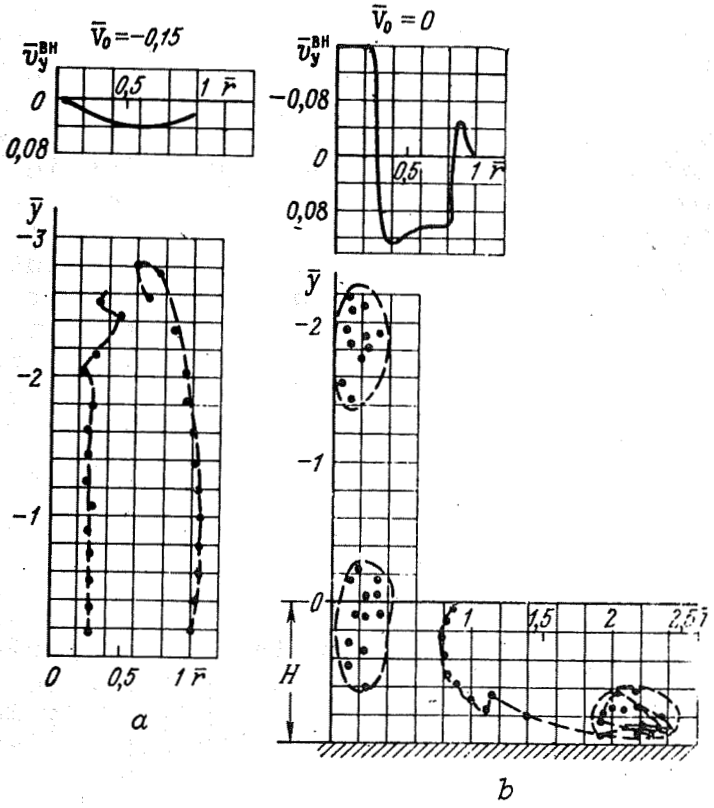

Figure 15.17

shows the same data for the case of vertical ascent ($\bar{V}_0 = 0,06$). Here, contraction of the streamtube as well as the induced velocities are considerably smaller. As in the previous case, a cluster of vortices can be seen at the end of the slipstream. The form of the slipstream in vertical descent ($\bar{V}_0 = -0,15$) is shown in Fig. 15.17*a*. Expansion of the slipstream above the disc is quite visible, while induced velocities are very low.

The form of the slipstream and values of external induced velocities for the case of hovering close to the ground are shown in Fig. 15.17*b*. Distance, H, of the rotor disc from the ground is assumed to be equal to the rotor radius. The influence of the ground was considered through the introduction of the reflection image of the vortex rings. It can be seen that the slipstream expands close to the ground and transits into a flow along the ground plane. A cluster of dissipating vortices can also be seen. It is interesting to notice that in this case, the vortex rings springing from the root section do not form a continuous chain but congregate into groups which do not move downstream, but float up over the rotor disc. The flow in this case is not steady, since groups of vortices separate themselves periodically from the disc. In that regime of flight, high induced velocities directed upward appear at the center of the disc.

9. APPLICATION OF NONLINEAR THEORY TO THE DETERMINATION OF THE ROTOR VORTEX SYSTEM IN AN OBLIQUE FLOW

Let us now consider the general case of a three-dimensional movement of vortices springing from the blades in horizontal flight. In computing the external induced velocities, it will be assumed here that the vortex sheets roll up into the tip and root vortex braids[5]. In order to find a solution for Eq. (15.29) describing the motion of such a braid, it is necessary to define its shape with the help of a finite number of parameters. Selecting coordinates of the "nodal" points located along the braid axis and connecting them by straight line segments, we obtain the following system of ordinary differential equations.

$$\frac{dS_j}{dt} = \mathbf{V}_j(S_1, S_2, \ldots, S_m) + \mathbf{V}_0 \quad [j = 1, 2, 3, \ldots, m(t)]. \qquad (15.32)$$

Here S_j is the radius vector of the nodal points and V_j is the induced velocity in the number j point. Number of the nodal points increases with time $m(t)$ as new vortex elements enter the stream. Consequently, the system defined by Eq. (15.32) has a variable number of equations. The position of each new nodal point at the moment of its appearance is known (it coincides with that point on the blade where the vortex springs off).

Since the system of Eq. (15.32) contains a very large number of unknowns; hence, it is expedient to not integrate exactly all the equations, but only a part of them, while the positions of the remaining nodal points is described in an approximate way. In the development of a suitable program of calculations, the whole vortex system was broken down into vortex "loops", defined as those sections of the braids which spring from the blade during one revolution. Integration was used to observe movement of a single loop only which is called the "reference" loop. Movement of that reference loop is described from the moment of its appearance to the time when it reaches the limit of the system of loops considered in these calculations. Approximate positions are assigned to the loops that appeared after the "birth" of the referenced one, and thus are located upstream from it. This is done by assuming that at the proper time, they would be at the same position as was the reference loop. In this way, the first computation of the reference loop movement provided the first approximation for the determination of positions of all the vortices. Next, those positions were computed more accurately in the consecutive approximations. In the first approximation, positions of the loops being downstream from the reference one were determined according to the linear theory. Actual calculations indicated that it is necessary to make from three to four iterations. After that, neither the form of the vortices nor induced velocities show practically any changes.

Let us examine some results of those calculations. The top and side views of the system of tip vortices obtained by the above method for a four-bladed rotor are shown in Fig. 15.18. These results were obtained for an advance ratio of $\mu = 0,1$ and rotor angle of attack of $\alpha_B = -11°$. The relative circulation of tip vortices was assumed as $\bar{\Gamma} = 0,02$. Due to the fact that each element of the vortex braid moves in the field of variable induced velocity, it can be seen that the shape of the whole vortex system is quite different from that predicted by the linear approach. Instead of skewed helical lines, one finds here, a system of deformed three-dimensional curves. Those curves intermingle with themselves at the edges of the vortex system where an apparent rotational motion can be identified by examining the aggregation of vortex elements springing from the disc edges.

In order to better illustrate this deformation of the vortices, a horizontal projection and a side view of a vortex loop is shown in Fig. 15.19. In Fig. 15.19*a*, the loop is shown at the moment of its formation, while in Fig. 15.19*b*, one can see it after a time length corresponding to one rotor revolution. The dash lines represent results of calculations based on linear, and continuous ones, on nonlinear theories. It can be

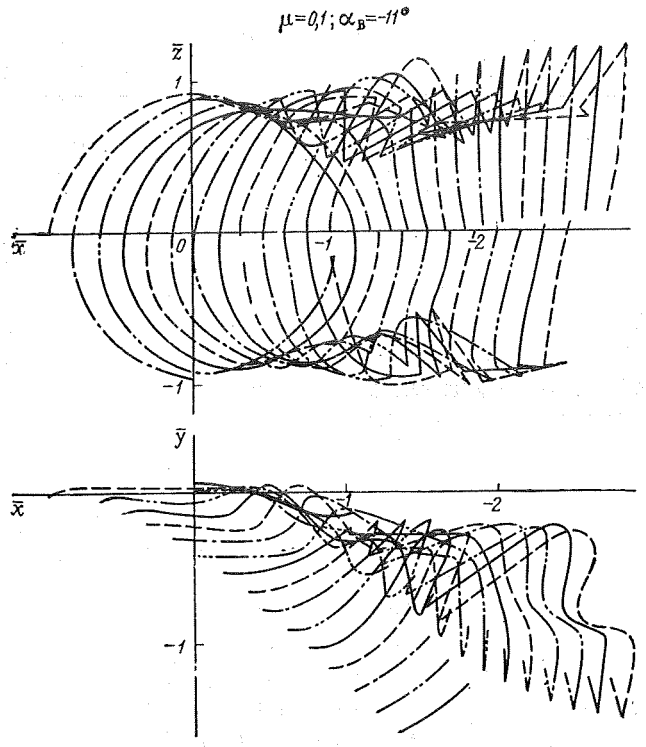

Figure 15.18

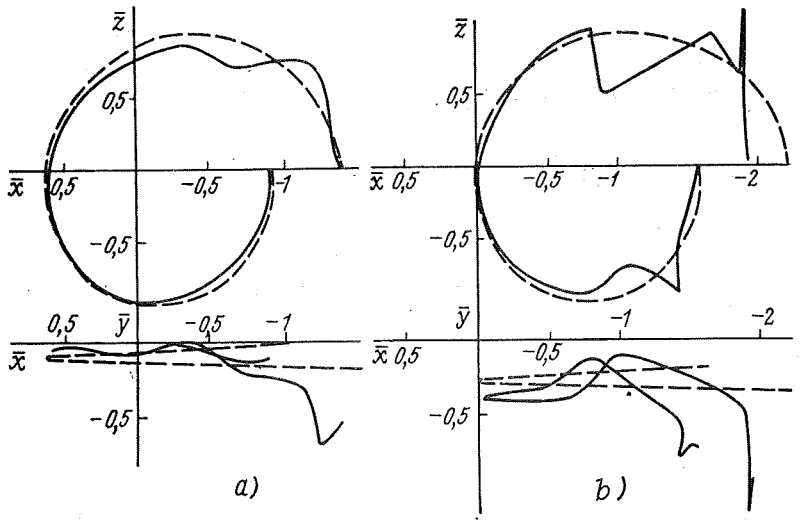

Figure 15.19

seen that even in the formulative stage of the loop, its deformation is already quite noticeable. If the horizontal projection even somewhat resembles the vortex cycloids postulated by the linear theory, then in the vertical projection, considerable differences can be spotted. It can also be seen that during one revolution, points of the loop undergo considerable displacements which markedly change its planform as well as the shape of its vertical projection.

Horizontal and vertical projections of the system of tip vortices at $\mu = 0,07$ and $\alpha_B = -11°$ are shown in Fig. 15.20. It can be seen that at the decreasing μ's, nonlinear deformations of tip vortices become more appreciable. Horizontal projections and side views of the system of vortices at $\mu = 0,2$ and $\alpha_B = -3°$ (circulation remains the same: $\bar{\Gamma} = 0,02$) are shown in Fig. 15.21.

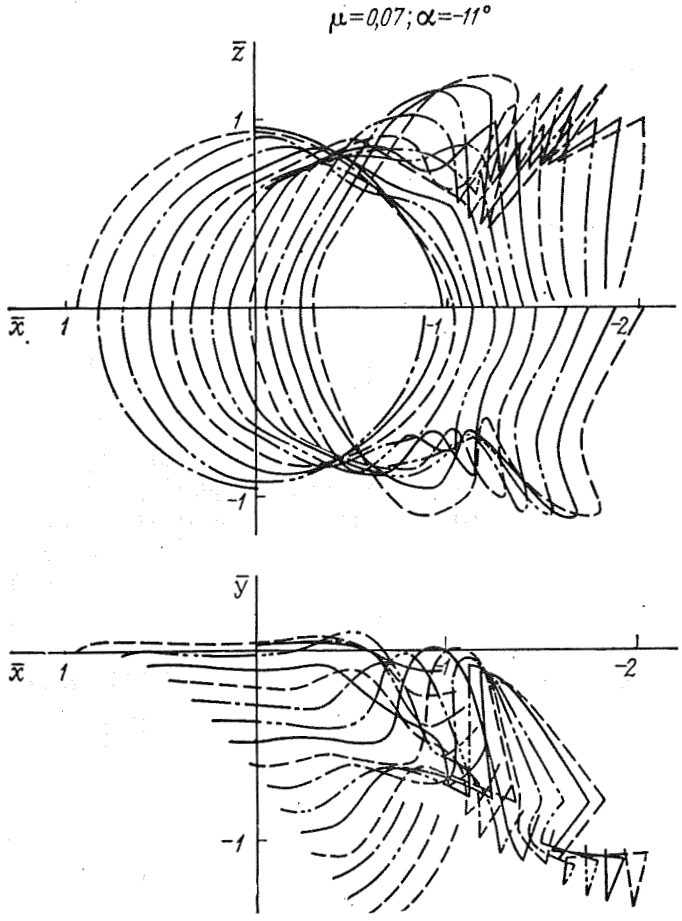

Figure 15.20

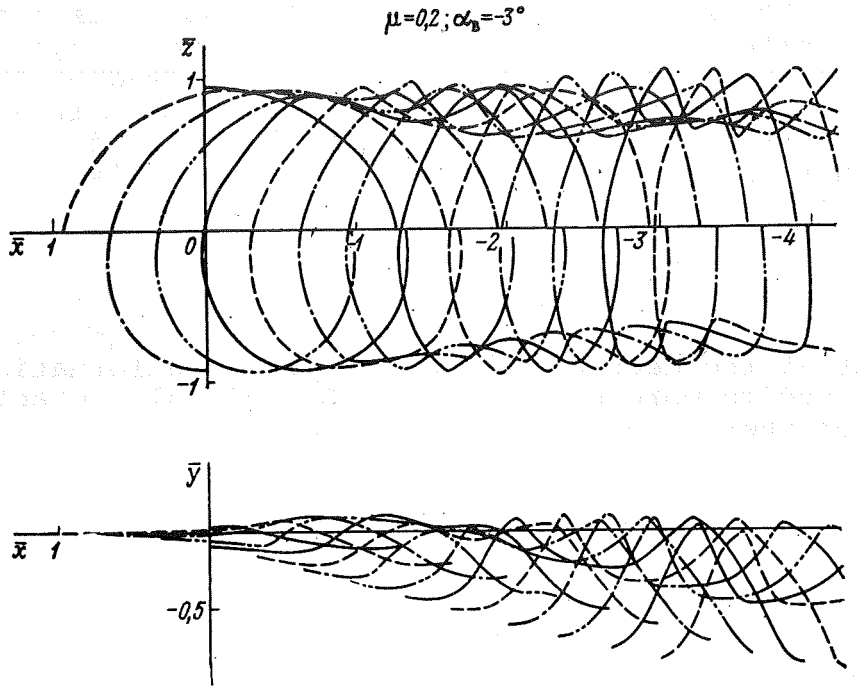

Figure 15.21

In this regime of flight, one may also observe noticeable deformations of the tip vortex braids. In the neighborhood of the rotor disc, the shape of the vortex braids is close to the cycloidal ones, but further downstream, considerable deviations from the cycloidal form can be seen. One can also see that further downstream from the rotor disc, edges of the vortex system start to turn up. In this process, the whole assembly of the tip vortex braids which moves away from the disc tends to roll up into a braid of the "second order" - similar to the roll-up of the vortex sheet springing from a circular wing. This process is quite visible in Fig. 15.22 where continuous lines show the vortex loop at the moment of its completed formation, while dash lines give its form further downstream when it reaches its assumed limit position. From the projection on the yOz plane, one can see that the initial weak upward movement of the vortex loop edge changes with time into a full $360°$ turn of that section. This represents the process of formation of the secondary vortex braid.

Let us now compare the induced velocities computed on the basis of the linear theory with those predicted by the nonlinear one. In Fig. 15.23, one can find suitable curves for the external induced velocities at the rotor disc $\bar{v}_y^{\text{вн}}$, plotted vs radius $\bar{r}$ for several azimuth angles. Those calculations

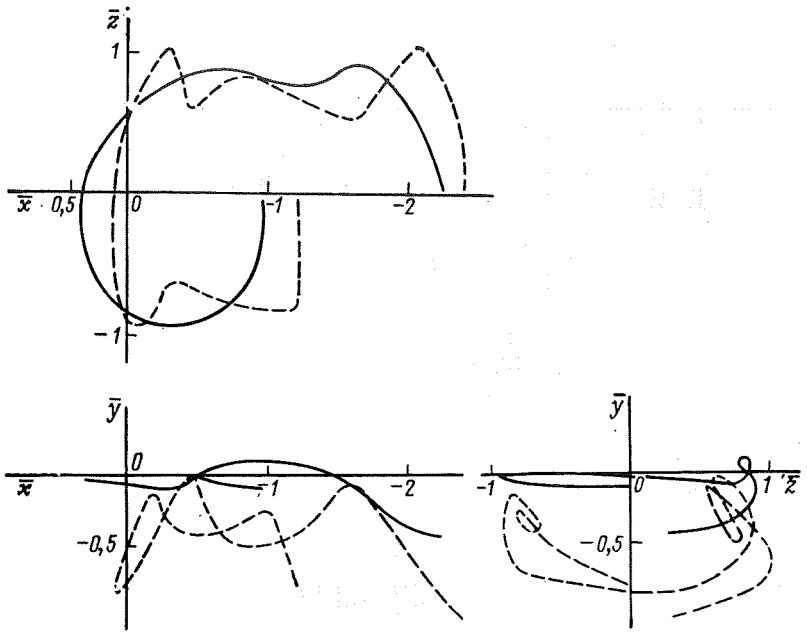

Figure 15.22

correspond to $\mu = 0,1$ and $\alpha_B = -6°$. Continuous lines depict the nonlinear and dashed lines, the linear vortex systems. It can be seen from Fig. 15.23 that in the front part of the rotor disc there is not much difference between the induced velocity values obtained from the linear and nonlinear theories. However, in the rear portion of the disc, those differences are quite noticeable, especially for azimuth angles of $\psi = 40°$ and $\psi = 20°$.

Fig. 15.24 shows the influence, on induced velocities, of the level of relative circulation $\bar{\Gamma}$ of the tip vortex braid ($\mu = 0,1$ and $\alpha_B = -11^o$). Here, the ratio of external induced velocities at the rotor disc $\bar{v}_y^{BH}$ to circulation $\bar{\Gamma}$ are plotted vs $\bar{r}$ for several values of ψ and three levels of $\bar{\Gamma}$. One may notice that the influence of $\bar{\Gamma}$ nonlinearities on induced velocities become more important as $\bar{\Gamma}$ increases from $0,01$ to $0,03$. For the most heavily loaded rotor ($\bar{\Gamma} = 0,03$), differences as high as 30% in induced velocity values predicted by the linear and nonlinear theories can be noted for $\psi = 20^o$ and $\psi = 40^o$. This indicates that for heavily-loaded rotors in low forward speeds, considerations of nonlinearities in the rotor vortex system is very important. For lightly-loaded rotors ($\bar{\Gamma} = 0,01$) and $\mu \geq 0,1$, the nonlinear theory gives corrections that are not significant for the computation of induced velocities at the rotor disc.

At medium and high speeds of flight, nonlinearity in the movements of vortices has little effect on induced velocities at the rotor disc. Exceptions will be found in those cases when vortex elements come close to the blades.

$\mu=0,1$; $\alpha_в=-6°$

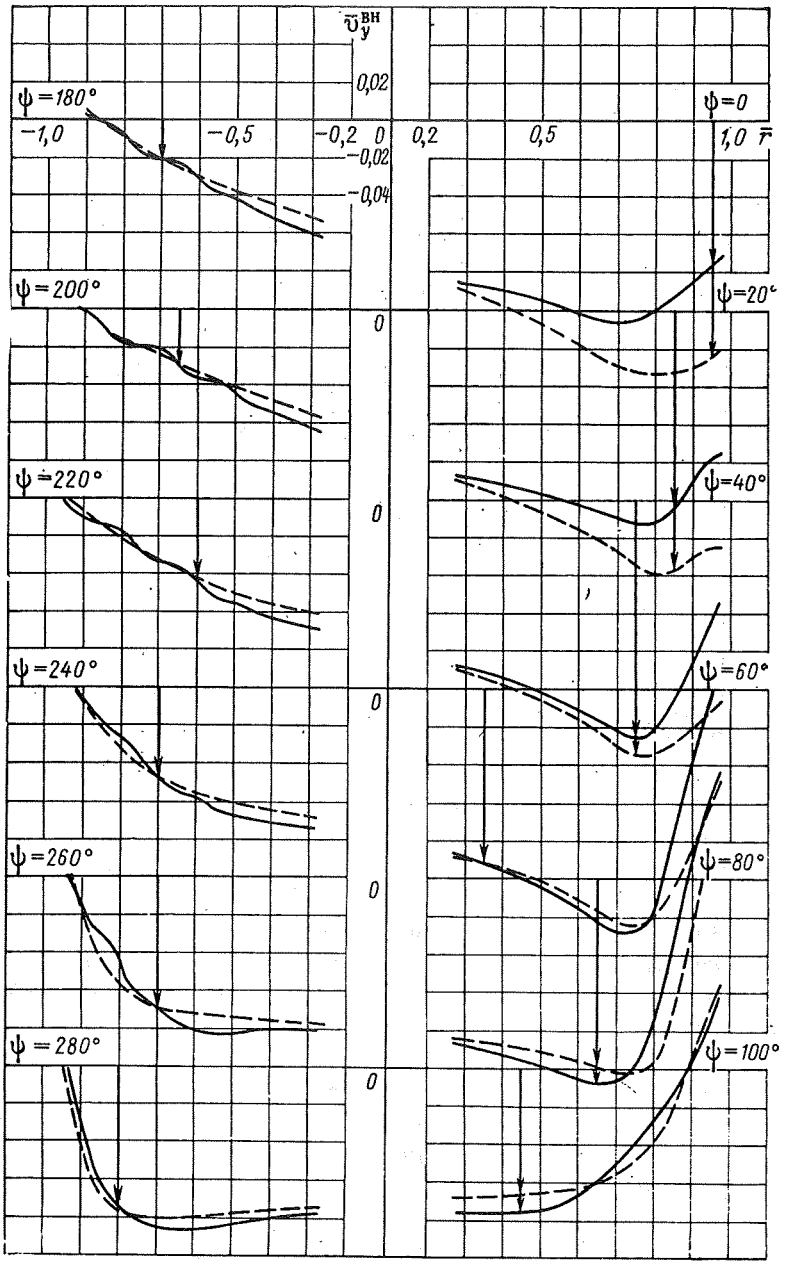

Figure 15.23

$\mu=0,1;\ \alpha_в=-11°$

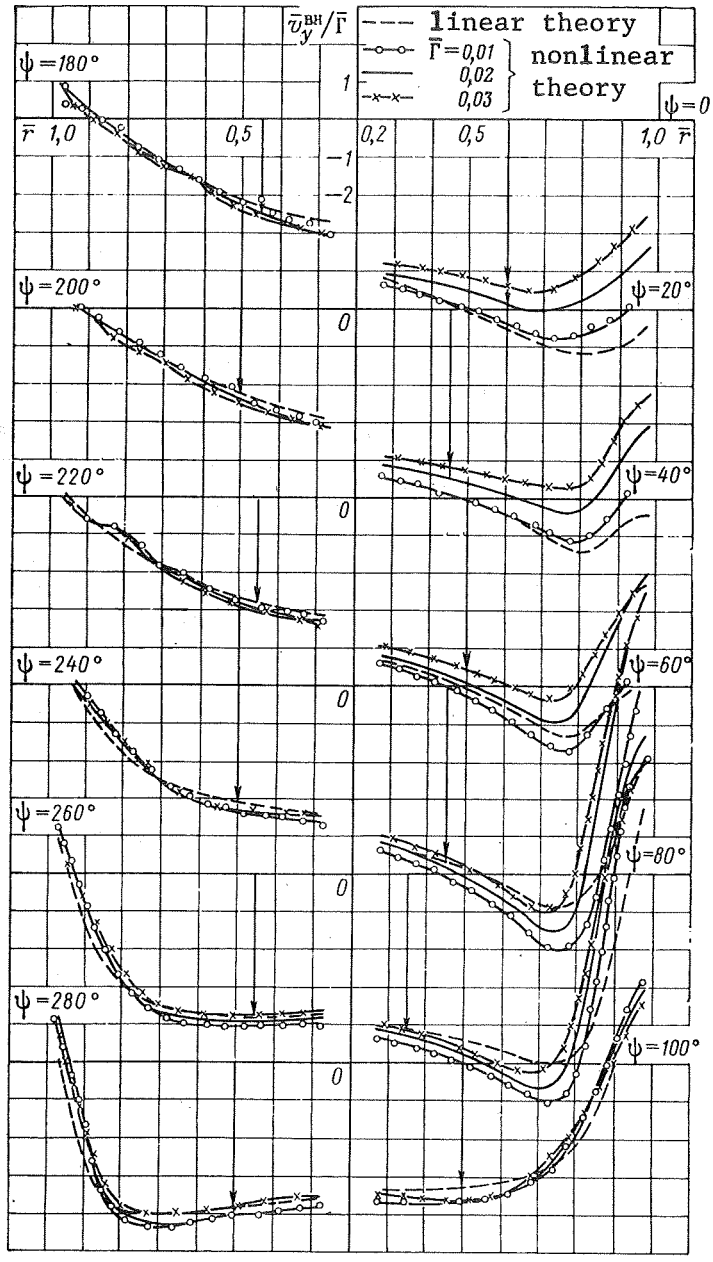

Figure 15.24

CHAPTER XVI

INDUCTION OF VORTICES IN A COMPRESSIBLE MEDIUM

It is well known that any arbitrary vector field can be uniquely defined as a field of sources and vortices. In hydrodynamic applications, it is often possible to assume the field of vortices as given a priori. As long as the fluid is incompressible, the sources are absent and velocities can be easily found from the vortices; say, by the Biot-Savart law. In a compressible fluid (gas), the field of sources is not known a priori and the Biot-Savart formula is, in general, not applicable in its usual form. However, the Biot-Savart law can be supplemented and made applicable (within linear approximations) to gases as well. The so *supplemented* Biot-Savart law permits one to obtain the field of velocities in the gas flow from a known field of vortices using equations of hydrodynamics (sources are automatically taken into consideration). This chapter is devoted to the consideration of a general theory of obtaining a field of gas flow velocities from the field of vortices formed in the gas. Attention is concentrated mainly on cases of the nonrectilinear unsteady motion in gas of lifting surfaces and lifting lines.

1. DIFFERENTIAL EQUATIONS OF GAS MOTION

Let us consider unlimited space filled with gas which, up to a moment $t = 0$, remained motionless, and then was put into motion by the action of an arbitrary three-dimensional field of external forces. Motion of the gas in fixed coordinates is determined, within the linear approximations, by the following system of differential equations (the acoustic equations):

$$\frac{\partial \mathbf{v}}{\partial t}+\frac{1}{\varrho_0}\operatorname{grad} p=\mathbf{F}(\mathbf{r}, t),\ \frac{\partial \varrho}{\partial t}+\varrho_0 \operatorname{div} \mathbf{v}=0,\ p-p_0=a^2(\varrho-\varrho_0). \tag{16.1}$$

The solution of these equations should satisfy the following initial conditions

$$p|_{t=0}=p_0,\ \varrho|_{t=0}=\varrho_0,\ \mathbf{v}|_{t=0}=0, \tag{16.2}$$

as well as the following conditions at infinity

$$p|_{r\to\infty}=p_0,\ \varrho|_{r\to\infty}=\varrho_0,\ \mathbf{v}|_{r\to\infty}=0. \tag{16.3}$$

Here, $\mathbf{v}, p, \rho$ are, respectively, velocity, pressure and density; a is the velocity of sound in the undisturbed gas, $\rho_0\mathbf{F}$ is the external force acting on a unit of gas volume, and p_0 and ρ_0 represent values of p and ρ for the gas at rest.

2. SCALAR POTENTIAL OF GAS VELOCITIES

The simplest way of integrating Eq. (16.1) consists of reducing them to a single equation of scalar velocity potential. In order to do this, let us integrate the first equation of (16.1) from the moment of the beginning of motion to the present time t. Introducing the following definitions

$$\mathbf{D}=\int_0^t \mathbf{F}(\mathbf{r}, t)\,dt, \tag{16.4}$$

$$\varphi=-\frac{1}{\varrho_0}\int_0^t (p-p_0)\,dt, \tag{16.5}$$

we obtain

$$\mathbf{v}=\mathbf{D}+\operatorname{grad}\varphi. \tag{16.6}$$

From Eq. (16.6), it can be seen that gas velocities resulting from an action of an arbitrary three-dimensional field of forces can be expressed in the form of a sum of the potential part, *grad* ϕ, and some rotational (vortex) part $\mathbf{D}$. According to Eq. (16.4). Vector $\boldsymbol{D}$ describes a field of impulses (referred to ρ_0) of external forces acting on a unit of gas volume at point $\boldsymbol{r}$ in an instant t.

Gas pressure p (Eq. (16.5)) is related to the potential by the following expression

$$p=p_0-\varrho_0\frac{\partial\varphi}{\partial t}. \tag{16.7}$$

After eliminating density ρ from the second and third equations in (16.1), we obtain

$$\frac{\partial p}{\partial t}+a^2\varrho_0\operatorname{div}\mathbf{v}=0. \tag{16.8}$$

Expressing pressure and velocity according to Eqs. (16.7 and (16.6), we arrive at the following final differential equation for the potential

$$\nabla^2\varphi-\frac{1}{a^2}\frac{\partial^2\varphi}{\partial t^2}=-\operatorname{div}\mathbf{D}. \tag{16.9}$$

This is a nonhomogeneous wave equation, the solution of which should be sought according to Eqs. (16.2) and (16.3) for the following initial conditions

$$\varphi|_{t=0}=0,\quad \left.\frac{\partial\varphi}{\partial t}\right|_{t=0}=0 \tag{16.10}$$

while the potential and its derivatives should disappear in infinity. A unique solution of Eq. (16.9) for initial conditions of Eq. (16.10) and those in infinity, is given by the Kirchoff formula

$$\varphi(\mathbf{r}_0, t_0)=\iiint_K \frac{dK}{4\pi|\mathbf{r}_0-\mathbf{r}|}\operatorname{div}\mathbf{D}\left(\vec{\mathbf{r}}, t_0-\frac{|\mathbf{r}_0-\mathbf{r}|}{a}\right). \tag{16.11}$$

Integration is performed within a region K, where the subintegral function is not zero, and an arrow over **r** indicates that the operator div is applied exclusively to the variable **r** marked by that arrow.

Eq. (16.11) defines ϕ as the retarding potential of the spatial distribution of stationary outlets with intensity Q where $Q = \operatorname{div}\mathbf{D}(\mathbf{r}, t)$. According to Eq. (16.6), gradient ϕ defines the "potential" part of velocity which, in combination with the rotational (vortex) part **D**, defines the sought velocity of the gas flow. The vortex vector $\boldsymbol{\Omega}$ is completely defined by vector **D** since determining rot **v** from the same equation (16.6), we have

$$\boldsymbol{\Omega}=\operatorname{rot}\mathbf{D}. \tag{16.12}$$

It can be seen that vector **D** completely determines the flow kinematics and, for that reason, from now on we will call it *vector of the kinematic impulse*.

In the particular case of an incompressible fluid, Eq. (16.11) expressing the potential, changes into the following expression:

$$\varphi(\mathbf{r}_0, t_0)=\iiint_K \frac{dK}{4\pi|\mathbf{r}_0-\mathbf{r}|}\operatorname{div}\mathbf{D}(\mathbf{r}, t). \tag{16.13}$$

Taking advantage of Eq. (16.13), we obtain an expression for the velocity of incompressible fluid:

$$\mathbf{v}_{\text{несж}}=\mathbf{D}+\iiint_{V}\frac{dK}{4\pi}\operatorname{grad}_0\left(\frac{1}{l}\right)\operatorname{div}\mathbf{D}(\mathbf{r},t)\quad(l=|\mathbf{r}-\mathbf{r}_0|),\tag{16.14}$$

where the operator grad_0 is taken with respect to the variable $\mathbf{r}_0$. From the Biot-Savart relationship, it is known that this velocity can also be expressed through vector Ω of the vorticity (rotation) of the velocity of flow,

$$\mathbf{v}_{\text{несж}}=\iiint_{K}\frac{\mathbf{e}\times\Omega}{4\pi l^2}\,dK\quad(\mathbf{e}=(\mathbf{r}-\mathbf{r}_0)/l).\tag{16.15}$$

It should be recalled that according to Eq. (16.12), the vortex field generated either in an incompressible fluid or gas by the action of external forces will be the same for identical forces.

3. DISCONTINUOUS FIELDS OF FORCES (VECTOR POTENTIALS OF IMPULSES AND VORTICES)

In order to be able to consider the discontinuous and degenerated fields of forces in the above obtained expressions, we will define velocity potential ϕ under the following form:

$$\varphi=\operatorname{div}\mathbf{E},\tag{16.16}$$

where $\mathbf{E}(\boldsymbol{r},t)$ is the new vector function to be defined. Vector $\mathbf{E}(\boldsymbol{r},t)$ is analogous to some extent to the known in the electrodynamics Hertz vector. After substituting Eq. (16.16) into Eq. (16.9), we obtain the following:

$$\operatorname{div}\left\{\nabla^2\mathbf{E}-\frac{1}{a^2}\frac{\partial^2\mathbf{E}}{\partial t^2}+\mathbf{D}\right\}=0.\tag{16.17}$$

From the above it can be seen that Eq. (16.16) will satisfy Eq. (16.9). It is not difficult to prove that it also would satisfy conditions of Eq. (16.10) if vector $\mathbf{E}$ is determined from the following differential equation:

$$\nabla^2\mathbf{E}-\frac{1}{a^2}\frac{\partial^2\mathbf{E}}{\partial t^2}=-\mathbf{D}\tag{16.18}$$

with the following initial conditions

$$\mathbf{E}|_{t=0}=0,\quad\left.\frac{\partial\mathbf{E}}{\partial t}\right|_{t=0}=0.\tag{16.19}$$

For the initial conditions given by Eq. (16.19), a unique solution of the nonhomogenious wave equation (16.18) is given by the following formula

$$\mathbf{E}(\mathbf{r}_0, t_0)=\iiint_K \frac{1}{4\pi l}\mathbf{D}\left(\mathbf{r}, t_0-\frac{l}{a}\right)dK. \tag{16.20}$$

It can be seen that vector $\mathbf{E}$ is represented under the form of the spatial retarding potential of effluences, the density of which is equal to the vector of kinematic impulse. For an incompressible fluid, potential of effluences is known since their vectorial intensity is equal to the vortex vector. This is called the vector potential (of vortices). By analogy, we will call $\mathbf{E}$ the vectorial potential of impulses, or the *impulse potential*, for short.

Regular scalar potential ϕ is equal to the divergence of the impulse potential. Consequently,

$$\varphi(\mathbf{r}_0, t_0)=\operatorname{div}\iiint_K \frac{1}{4\pi l}\mathbf{D}\left(\mathbf{r}, t_0-\frac{l}{a}\right)dK. \tag{16.21}$$

As yet, this formula was developed for the case of continuous vector fields of the kinematic potential. However, in using the limit concept in going from the uninterrupted fields, $\mathbf{D}$, to the fields having discontinuities of the first kind, the appearance of the relationship of Eq. (16.21) would not change. This means that it is also applicable to discontinuous fields of impulses.

On the basis of vectorial identity,

$$\operatorname{div}_0\iiint_K \frac{dK}{4\pi l}\mathbf{D}\left(\mathbf{r}, t_0-\frac{l}{a}\right)=\iiint_K \frac{dK}{4\pi l}\operatorname{div}\mathbf{D}\left(\overset{\downarrow}{\mathbf{r}}, t_0-\frac{l}{a}\right)-$$
$$-\iiint_K \operatorname{div}\left[\frac{\mathbf{D}\left(\mathbf{r}, t_0-\frac{l}{a}\right)}{4\pi l}\right]dK,$$

(verified by a direct differentiation) and the Gauss theorem, Eq. (16.21) can be rewritten under the following form:

$$\varphi(\mathbf{r}_0, t_0)=\iiint_K \frac{dK}{4\pi l}\operatorname{div}\mathbf{D}\left(\overset{\downarrow}{\mathbf{r}}, t_0-\frac{l}{a}\right)-\iint_S \frac{\mathbf{N}\cdot\mathbf{D}\left(\mathbf{r}, t_0-\frac{l}{a}\right)}{4\pi l}dS. \tag{16.22}$$

Here, S is a surface limiting region K, and $\mathbf{N}$ is the external normal to surface S. Eq. (16.22) will not change its form in the case of vector $\mathbf{D}$ fields having a discontinuity of the first kind (order) on surface S and hence, it is applicable to such fields.

In conclusion, we will obtain relationships expressing gas velocity in terms of the vectorial potential $\mathbf{A}$ which is analogous to the vectorial potential of vortices in an incompressible fluid. Substituting Eq. (16.16) into Eq. (16.6), we will obtain $\mathbf{v}$ = grad div E+D. Taking advantage of the well-known vectorial identity,

$$\text{grad div } \mathbf{E} = \text{rot rot } \mathbf{E} + \nabla^2 \mathbf{E},$$

defining $\mathbf{A}$ = rot $\mathbf{E}$ and taking into consideration Eq. (16.18), it is possible to represent the velocity of gas under the following form

$$\mathbf{v} = \text{rot } \mathbf{A} + \frac{1}{a^2} \frac{\partial^2 \mathbf{E}}{\partial t^2}. \tag{16.23}$$

Upon determining rot $\mathbf{E}$ for continuous fields $\mathbf{D}$, the vector-potential becomes

$$\mathbf{A}(\mathbf{r}_0, t_0) = \iiint_K \frac{1}{4\pi l} \Omega\left(\mathbf{r}, t_0 - \frac{l}{a}\right) dK. \tag{16.24}$$

With $a \to \infty$, Eqs. (16.23) and (16.24) give the well-known representation of velocity through the vector-potential of vortices. It can be seen from Eq. (16.23) that in order to determine velocities in the case of gas, it is not enough to have one vector $\mathbf{\Omega}$, but it is also necessary to compute the second derivative with respect to time of vector $\mathbf{E}$.

CASE OF SURFACE FORCES

Action of a body on a gas flowing around it, can be replaced by the action of a field of forces acting on the gas in points of the body surface. Let us consider a field of surface forces such as the limiting case of a volumetric field. Let region K, within which forces act on the gas, be represented by a thin layer between two immobile surfaces, W and W_1. We define an element of surface W as dS and the volume of an element constructed on dS is defined as dK; height is equal to the layer thickness. With the volumetric field of forces $\rho_0 \mathbf{F}$, the gas included within element dK will be subjected to a force $\rho_0 \mathbf{F} dK$. Referring that force to the area dS, and introducing density of the field of forces $\sigma\rho_0$, we obtain the following equation

$$\mathbf{F}dK=\sigma dS. \tag{16.25}$$

Defining the surface density of the vector of the kinematic impulse as Γ, we can write

$$\mathbf{D}\,dK=\Gamma dS, \tag{16.26}$$

while

$$\Gamma=\int_0^t \sigma dt. \tag{16.27}$$

Eqs. (16.25) and (16.26) permit one to deal with integrals containing functions F or D of surface fields instead of volumetric ones. Eqs. (16.20) and (16.26) indicate that in the case of the surface-type field of forces the impulse potential is

$$\mathbf{E}(\mathbf{r}_0, t_0)=\iint_W \frac{\Gamma\left(\mathbf{r}, t_0-\frac{l}{a}\right)}{4\pi l}\,dS, \tag{16.28}$$

and scalar velocity potential

$$\varphi(\mathbf{r}_0, t_0)=\operatorname{div}\iint_W \frac{1}{4\pi l}\Gamma\left(\mathbf{r}, t_0-\frac{l}{a}\right)dS. \tag{16.29}$$

In the presence of surface forces, the velocity of gas is equal to the gradient of ϕ, since vector $\mathbf{D}$ appearing in Eq. (16.6) vanishes outside of surface W.

4. VELOCITY OF GAS IN THE CASE OF SMOOTH FIELDS OF EXTERNAL FORCES (GENERALIZATION OF THE BIOT-SAVART LAW)

Let the field of forces $\mathbf{F}(\mathbf{r}, t)$ acting on the gas be continuous everywhere and have continuous first and second partial derivatives. Eq. (16.11) can be differentiated once under the integral sign, which leads to the following:

$$\begin{aligned}\operatorname{grad}\varphi=\iiint_K \frac{1}{4\pi}\Big[Q\left(\mathbf{r}, t_0-\frac{l}{a}\right)\operatorname{grad}_0\left(\frac{1}{l}\right)-\\ -\frac{1}{la}\dot{Q}\left(\mathbf{r}, t_0-\frac{l}{a}\right)\operatorname{grad}_0 l\Big]\,dK,\end{aligned} \tag{16.30}$$

where $$Q(\mathbf{r}, t)=\operatorname{div}\mathbf{D};\quad Q=\frac{\partial Q}{\partial t}.$$

Substituting Eq. (16.30) into (16.6) and introducing the effective intensity of effluences

$$Q_э=Q\left(\mathbf{r}, t_0-\frac{l}{a}\right)+\frac{l}{a}\dot{Q}\left(\mathbf{r}, t_0-\frac{l}{a}\right), \tag{16.31}$$

it is possible to represent gas velocity $\mathbf{v}$ under the following form

$$\mathbf{v}(\mathbf{r}_0, t_0)=\mathbf{D}(\mathbf{r}_0, t_0)+\iiint_K \frac{Q_э}{4\pi}\operatorname{grad}_0\left(\frac{1}{l}\right)dK. \tag{16.32}$$

In our consideration, let us introduce a vector field of "effective impulses" $\mathbf{D}_э(\mathbf{r}, t)$ which is related to the field of impulses $\mathbf{D}(\mathbf{r}, t)$ by an expression analogous to Eq. (16.31):

$$\mathbf{D}_э=\mathbf{D}\left(\mathbf{r}, t_0-\frac{l}{a}\right)+\frac{l}{a}\dot{\mathbf{D}}\left(\mathbf{r}, t_0-\frac{l}{a}\right). \tag{16.33}$$

It is easy to notice that

$$\operatorname{div}\mathbf{D}_э=Q_э-\frac{l}{a^2}\dot{\mathbf{F}}\left(\mathbf{r}, t_0-\frac{l}{a}\right)\operatorname{grad} l.$$

Upon finding $Q_э$ from the above expression and substituting it into Eq. (16.32), we obtain

$$\mathbf{v}=\mathbf{D}+\iiint_K \frac{dK}{4\pi}\operatorname{grad}\left(\frac{1}{l}\right)\operatorname{div}\mathbf{D}_э+\iiint_K \frac{l\,dK}{4\pi a^2}\operatorname{grad}_0\left(\frac{1}{l}\right)\dot{\mathbf{F}}\left(\mathbf{r}, t_0-\frac{l}{a}\right)\mathbf{e}. \tag{16.34}$$

For $r = r_0$, the values of vectors D and D coincide; hence, the first two terms in the right-hand side of Eq. (16.34) represent velocity $\mathbf{v}_{\text{несж}}$ at point $(\mathbf{r}_0)$ of the flow of incompressible fluid, resulting from the action of external forces with a field of impulses $\mathbf{D}_э$. Defining, by $\boldsymbol{\Omega}_э$, the vector of the flow rotation (vorticity) generated by the field of impulses $\boldsymbol{D}_э$ we find, according to Eq. (16.12), that

$$\Omega_э=\operatorname{rot}\mathbf{D}_э. \tag{16.35}$$

Upon determining, from the Biot-Savart formula, the vector of velocity $\mathbf{v}_{\text{несж}}$ induced in an incompressible fluid by a field of vortices $\Omega_э$, and substituting it for the first two terms in Eq. (16.34), we finally obtain

$$\mathbf{v}(\mathbf{r}_0, t)=\iiint_K \frac{\mathbf{e}\times\Omega_э}{4\pi l^2}\,dK+\iiint_K \frac{dK}{4\pi l a^2}\mathbf{e}\left(\mathbf{e}\cdot\dot{\mathbf{F}}\left(\mathbf{r}, t_0-\frac{l}{a}\right)\right). \tag{16.36}$$

Let us analyze the above expression. It is not difficult to find from Eq. (16.35) that

$$\Omega_э=\Omega\left(\mathbf{r}, t_0-\frac{l}{a}\right)+\frac{l}{a}\dot{\Omega}\left(\mathbf{r}, t_0-\frac{l}{a}\right)+\frac{l}{a^2}\dot{\mathbf{F}}\left(\mathbf{r}, t_0-\frac{l}{a}\right)\times\mathbf{e}. \tag{16.37}$$

After a substitution of Eq. (16.37) into Eq. (16.36) and an expansion of the triple vector product $\mathbf{e}\times[\dot{\mathbf{F}}\times\mathbf{e}]$, the sought velocity of gas can be presented in the following form

$$\mathbf{v}=\mathbf{v}^{\Omega}+\mathbf{v}^{\dot{\Omega}}+\mathbf{v}^{\dot{F}}, \tag{16.38}$$

where

$$\mathbf{v}^{\Omega}(\mathbf{r}_0, t_0)=\iiint_K \frac{dK}{4\pi l^2}\mathbf{e}\times\Omega\left(\mathbf{r}, t_0-\frac{l}{a}\right), \tag{16.39}$$

$$\mathbf{v}^{\dot{\Omega}}(r_0, t_0)=\iiint_K \frac{dK}{4\pi l a}\mathbf{e}\times\dot{\Omega}\left(\mathbf{r}, t_0-\frac{l}{a}\right), \tag{16.40}$$

$$\mathbf{v}^{\dot{F}}(\mathbf{r}_0, t_0)=\iiint_K \frac{dK}{4\pi l a^2}\dot{\mathbf{F}}\left(\mathbf{r}, t_0-\frac{l}{a}\right). \tag{16.41}$$

It can be seen that the velocity of gas is equal to the sum of three "retarded" velocities. Velocity $\mathbf{v}^{\Omega}$ is determined, according to the regular Biot-Savart formula from the actual field of vortices but a time lag appears in the development of velocity due to the time required to transmit the acoustic signal from a vortex element.

5. LIFTING SURFACE IN GAS

Let us consider infinite volume of gas which, up to the moment $t = 0$, remained at rest and then was exited by the movement in it of a lifting surface from which there are forces acting on the gas (surface *CDFE* in Fig. 16.1). We will limit our considerations to such movements of the lifting surface which can be imagined as a sliding motion along some imaginary

stationary "directing" surface W ($ABGH$ in Fig. 16.1). It will be assumed that forces acting on the gas are directed along lines N normal to the surface W. We will assume that vector σ of the surface density of those forces referred to ρ_0; the shape of the directing surface, and the law of movement on it of the lifting surface are known. Assuming the linear theory is valid under these circumstances, the task consists of the determination of velocities of the unsteady motion of the gas.

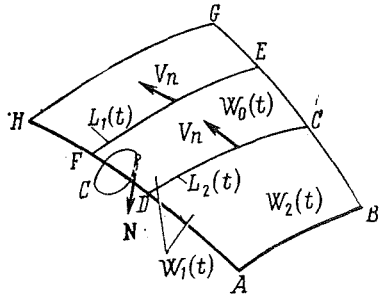

Figure 16.1

We define as $W_0(t)$ that region of the directing surface W which, at the moment t, is occupied by the lifting surface (see $CDFE$ in Fig. 16.1). With the increasing time, region $W_0(t)$ changes its position on the directing surface W. Let us assume that this region is limited on one hand, by two lines, $L_1(t)$ and $L_2(t)$ forming the "edges" of the lifting surface (lines EF and CD); while on the other, its boundaries coincide with those of the directing surface W (see Fig. 16.1). Let us also assume that lines $L_1(t)$ and $L_2(t)$ move over the directing surface W in such a way that $L_1(t+\Delta t)$ lies outside of the region $W_0(t)$; i.e., it becomes the front edge, while line $L_2(t+\Delta t)$ lies inside of the region $W_0(t)$ and becomes the rear edge ($\Delta t>0$). We assume that each of the lines $L_1(t)$ and $L_2(t)$ passes only once over the fixed point (r) on the directing surface W. We define those moments of passing as $\tau_1(\mathbf{r})$ and $\tau_2(\mathbf{r})$, respectively. In addition, we assume that at the initial time, lines $L_1(t)$ and $L_2(t)$ coincided. This does not exclude the possibility of an instantaneous formation (or disappearance) of a part of the lifting surface which will be treated as movements of lines $L_1(t)$ and $L_2(t)$ with infinite velocities. We define as $W_1(t)$ that region $ABEF$ of the directing surface W where the lifting surface was either before, or during, the considered moment t; and $W_2(t)$ defines another region where it was, but at the moment t is not there any more. It is obvious that $W_0(t)$ complements $W_2(t)$ to $W_1(t)$. Lines $L_1(t)$ and $L_2(t)$ will separate regions $W_1(t)$ and $W_2(t)$ from the remaining portions of the directing surface W.

We will assume that vector $\sigma(\mathbf{r},t)$ is given over the whole directing surface, but is equal to zero at those points where, during moment t there is no lifting surface. Such a vector, although being continuous within region W_0, will not be continuous over the whole directing surface W since, at lines $L_1(t)$ and $L_2(t)$, it may have discontinuities of the first order undergoing step variations with changing $\mathbf{r}$ or t. The previously considered relationship of Eq. (16.28) for the impulse-potential $\mathbf{E}$ retains its validity also for such variations of forces. This means that for the lifting surface we have

$$\mathbf{E}(\mathbf{r}_0, t_0) = \iint_W \frac{1}{4\pi l} \Gamma\left(\mathbf{r}, t_0 - \frac{l}{a}\right) dS, \tag{16.42}$$

where, as before, the vector of the surface kinematic impulse

$$\Gamma(\mathbf{r}, t) = \int_0^t \sigma(\mathbf{r}, t)\, dt, \tag{16.43}$$

potential of the flow velocity

$$\varphi = \operatorname{div} \mathbf{E}, \tag{16.44}$$

and velocity $\mathbf{v}$ is determined as grad ϕ.

Let us examine Eq. (16.42) in more detail. Upon determination of function $\tau_i(\mathbf{r})$ $(i=1,2)$, the question of whether point $(\mathbf{r})$ belongs to the $W_i(t)$ regions (*shorter* $(\mathbf{r}) \in W_i(t)$) is determined by the following inequality: $\tau_i(\mathbf{r}) < t$. Taking into consideration that function $\sigma(\mathbf{r}, t) = |\boldsymbol{\sigma}|$ is non-zero in the $W_0(t)$ region only, the following expression can be written for value Γ of vector $\boldsymbol{\Gamma}$

$$\Gamma(\mathbf{r}, t) = \begin{cases} 0 & \text{for } t \leqslant \tau_1(\mathbf{r}), \\ \displaystyle\int_{\tau_1(\mathbf{r})}^{t} \sigma(\mathbf{r}, t)\, dt & \text{for } \tau_2(\mathbf{r}) > t > \tau_1(\mathbf{r}),\ \mathbf{r} \in W_0, \\ \displaystyle\int_{\tau_1(\mathbf{r})}^{\tau_2(\mathbf{r})} \sigma(\mathbf{r}, t)\, dt & \text{for } t \geqslant \tau_2(\mathbf{r}),\ \mathbf{r} \in W_2. \end{cases} \tag{16.45}$$

From the above it can be seen that function $\Gamma(\mathbf{r}, t)$ is non-zero only in the $W_1(t)$ region; while in the $W_2(t)$ region, it is independent from time. After finding the retarding quantity Γ for some fixed $\mathbf{r}_0$ and t_0 from Eq. (16.45), we obtain

$$\Gamma\left(\mathbf{r}, t_0 - \frac{l}{a}\right) = \begin{cases} 0 & \text{for } t_0 - \dfrac{l}{a} \leqslant \tau_1(\mathbf{r}), \\ \displaystyle\int_{\tau_1(\mathbf{r})}^{t_0 - \frac{l}{a}} \sigma(\mathbf{r}, t)\, dt & \text{for } \tau_2(\mathbf{r}) > t_0 - \dfrac{l}{a} > \tau_1(\mathbf{r}), \\ \displaystyle\int_{\tau_1(\mathbf{r})}^{\tau_2(\mathbf{r})} \sigma(\mathbf{r}, t)\, dt & \text{for } t_0 - \dfrac{l}{a} \geqslant \tau_2(\mathbf{r}). \end{cases} \tag{16.46}$$

This function is non-zero within some region W^*_1 defined by the following inequality:

$$t_0 - \frac{l}{a} \geqslant \tau_1(\mathbf{r}), \tag{16.47}$$

while, within region W^*_2 defined by another inequality

$$t_0 - \frac{l}{a} > \tau_2(\mathbf{r}), \tag{16.48}$$

it does not depend on t_0.

The following physical interpretation can be given to regions W^*_1 and W^*_2. Let us assume that line $L_i(t)$ $(i=1,2)$, representing edges of the lifting surface, during the motion emits spherical acoustic waves. Then, region W^*_i $(i=1,2)$ will be the locus of points from which those waves would have time to reach point $(\mathbf{r}_0)$ at the moment t_0. We define the region supplementing region W^*_2 into W^*_1 as W^*_0, and we will call region W^*_i $(i=0,1,2)$ the "audible images" of the corresponding regions, $W_i(t)$.

According to Eqs. (16.47) and (16.48), the condition needed for point $(\mathbf{r})$ to be within region W^*_i $(i=1,2)$ is expressed by the following inequality:

$$|\mathbf{r}_0 - \mathbf{r}| - a[t_0 - \tau_i(\mathbf{r})] \leqslant 0. \tag{16.49}$$

The left-hand side of this inequality will be defined as $\psi_i(\mathbf{r}_0, \mathbf{r}, t_0)$. Since, outside of the W^*_1 region, function $\Gamma(\mathbf{r}, t_0 - (l/a))$ is equal to zero, Eq. (16.42) can be rewritten as follows:

$$\mathbf{E}(\mathbf{r}_0, t) = \iint\limits_{W^*_1} \frac{1}{4\pi l} \Gamma\left(\mathbf{r}, t_0 - \frac{l}{a}\right) dS. \tag{16.50}$$

Further considerations will be limited to the case when each of the equations $\psi_i(\mathbf{r}_0, \mathbf{r}, t_0) = 0$ $(i=1,2)$ at fixed $\mathbf{r}_0, t_0$ defines some line L^*_i on the surface W. In addition, line L^*_1 will separate region W^*_1 from the remaining regions of surface W. The same role will be played by L^*_2 for region W^*_2 (Fig. 16.2). From now on, we will call L^*_1 and L^*_2 the audible lines.

6. VELOCITY POTENTIAL OF LIFTING SURFACES

In order to determine the velocity potential ϕ of a lifting surface, it is necessary to find the divergence of

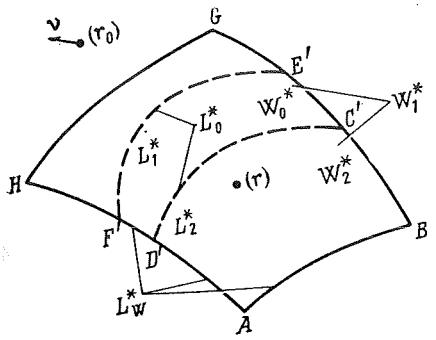

Figure 16.2

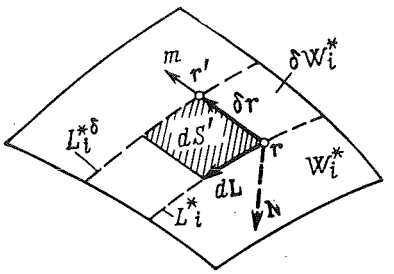

Figure 16.3

vector **E** defined by Eq. (16.50). First, we will calculate its differential $\delta\mathbf{E}$ corresponding to the condition that point $(\mathbf{r}_0)$ is displaced along an arbitrary unit vector $\boldsymbol{\nu}$ through an infinitesimal distance δh during time δt. After determination of the corresponding derivatives, we obtain

$$\delta\mathbf{E}=\delta h\iint\limits_{W_1^*}\frac{dS}{4\pi}\frac{\partial}{\partial\nu_0}\left(\frac{1}{l}\right)\boldsymbol{\Gamma}\left(\mathbf{r},t_0-\frac{l}{a}\right)+\iint\limits_{W_1^*}\frac{dS}{4\pi l}\dot{\boldsymbol{\Gamma}}\left(\mathbf{r},t_0-\frac{l}{a}\right)\times$$
$$\times\left(\delta t-\frac{\delta h}{a}\frac{\partial l}{\partial\nu_0}\right)+\iint\limits_{\delta W_1^*}\frac{dS}{4\pi l}\boldsymbol{\Gamma}\left(\mathbf{r},t_0-\frac{l}{a}\right). \qquad (16.51)$$

Let $L_i^{*\delta}$ be the position of the audible line L_i^* $(i=1,2)$ displaced during the variation. Let us take two infinitesimally close points $(\mathbf{r})$ and $(\mathbf{r}')$ on the initial and displaced audible lines, and define, by $\delta\mathbf{r}$, the connecting vector (Fig. 16.3). Upon determination of curves L_i^* and $L_i^{*\delta}$, the following equation for point **r**, located on L_i^* and vector $\delta\mathbf{r}$, can be written:

$$\boldsymbol{\nu}\delta h\cdot\operatorname{grad}_0\Psi_i+\delta\mathbf{r}\operatorname{Grad}\Psi_i+\frac{\partial\Psi_i}{\partial t_0}\delta t=0. \qquad (16.52)$$

After introducing a unit vector **e** directed from point $(\mathbf{r}_0)$, to point $(\mathbf{r})$, we obtain

$$\operatorname{grad}_0\Psi_i=-\mathbf{e},\ \operatorname{Grad}\Psi_i=\mathbf{e}-\mathbf{N}(\mathbf{eN})+a\operatorname{Grad}\tau_i,$$

and the condition expressed by Eq. (16.52) assumes the following form:

$$(\mathbf{e}+\boldsymbol{\mu}_i)\cdot\delta\mathbf{r}-(\mathbf{e}\boldsymbol{\nu})\delta h-a\delta t=0, \qquad (16.53)$$

where, for the surface gradient of function $\tau_i(\mathbf{r})$, the following symbol was introduced: $\boldsymbol{\mu}_i = a\operatorname{Grad}\tau_i(\mathbf{r})$. In the particular case of $\delta h = \delta t = 0$, lines L_i^* and $L_i^{*\delta}$ coincide and Eq. (16.53) yields the following condition of the superposition on vector $d\mathbf{L}$ of an element of curve L_i^*:

$$d\mathbf{L}(\mathbf{e}+\mu_i)=0. \tag{16.54}$$

On the directional surface W, we introduce a family of arbitrary vectors $\mathbf{m}$ which are tangent to that surface. Those vectors vary continuously along that surface, but do not touch the audible line L_i^*. Let vectors $\delta\mathbf{r}$ be directed along vectors $\mathbf{m}$. Then, $\mathbf{m}(\mathbf{e}+\mu_i)\neq 0$, and from Eq. (16.53), we find

$$\delta\mathbf{r}=\frac{\mathbf{m}\delta H}{\Delta_i}, \tag{16.55}$$

where

$$\Delta_i=\mathbf{m}(\mathbf{e}+\mu_i),\quad \delta H=\mathbf{e}\nu\delta h+a\delta t.$$

A planar element dS' is constructed on vector $\delta\mathbf{r}$ (Eq. (16.55)) and element $d\mathbf{L}$ of curve L_i^* (positive, when $\delta\mathbf{r}$ is directed away from region W_i; while $d\mathbf{L}$ when looking along N has that region to the left of its direction),

$$dS'=-\frac{[\mathbf{N}\mathbf{m}d\mathbf{L}]}{\Delta_i}\delta H. \tag{16.56}$$

Taking into consideration that $\sigma = \Gamma$ and that function $\sigma(\mathbf{r}, t_0 - (l/a))$ becomes zero in the W_2^* region, instead of Eq. (16.51), we obtain the following:

$$\delta\mathbf{E}=\delta h\iint\limits_{W_1^*}\frac{1}{4\pi}\frac{\partial}{\partial\nu_0}\left(\frac{1}{l}\right)\Gamma\left(\mathbf{r},t_0-\frac{l}{a}\right)dS+$$

$$+\iint\limits_{W_0^*}\frac{1}{4\pi l}\sigma\left(\mathbf{r},t_0-\frac{l}{a}\right)\left(\delta t-\frac{1}{a}\frac{\partial l}{\partial\nu_0}\delta h\right)dS. \tag{16.57}$$

Assuming that $\delta t = 0$ in Eq. (16.57); and dividing that equation by δh, we obtain derivative $\partial\mathbf{E}/\partial\boldsymbol{\nu}_0$ of the vector function $\mathbf{E}$ with respect to the position of point $(\mathbf{r}_0)$ in the direction of vector $\boldsymbol{\nu}$; i.e.,

$$\frac{\partial\mathbf{E}}{\partial\nu_0}=\iint\limits_{W_1^*}\frac{dS}{4\pi}\frac{\partial}{\partial\nu_0}\left(\frac{1}{l}\right)\Gamma\left(\mathbf{r},t_0-\frac{l}{a}\right)-\iint\limits_{W_0^*}\frac{dS}{4\pi la}\sigma\left(\mathbf{r},t_0-\frac{l}{a}\right)\frac{\partial l}{\partial\nu_0}. \tag{16.58}$$

Now defining the quantity div $\mathbf{E} = (\partial E_x/\partial x) + (\partial E_y/\partial y) + (\partial E_z/\partial z)$; according to Eq. (16.44), we find the following expression for the velocity potential:

$$\varphi(\mathbf{r}_0,t_0)=\iint\limits_{W_1^*}\frac{dS}{4\pi}\frac{\partial}{\partial N_0}\left(\frac{1}{l}\right)\Gamma\left(\mathbf{r},t_0-\frac{l}{a}\right)+\iint\limits_{W_0^*}\frac{l dS}{4\pi a}\frac{\partial}{\partial N_0}\left(\frac{1}{l}\right)\sigma\left(\mathbf{r},t_0-\frac{l}{a}\right). \tag{16.59}$$

Here, Γ and σ are projections of vectors $\boldsymbol{\Gamma}$ and $\boldsymbol{\sigma}$ on the normal N, and $\partial/\partial N_0$ means differentiation with respect to the position of point $(\mathbf{r}_0)$ in the direction of N.

Introducing the following definition,

$$\Gamma^*=\Gamma\left(\mathbf{r}, t_0-\frac{l}{a}\right)+\frac{l}{a}\sigma\left(\mathbf{r}, t_0-\frac{l}{a}\right), \tag{16.60}$$

Eq. (16.59) can be rewritten as follows:

$$\varphi(\mathbf{r}_0, t_0)=\iint\limits_{W_1^*}\frac{dS}{4\pi}\frac{\partial}{\partial N_0}\left(\frac{1}{l}\right)\Gamma^*. \tag{16.61}$$

In contrast to the real circulation Γ, from now on function Γ^* will be called the "audible circulation."

7. VELOCITY AND PRESSURE OF GAS ASSOCIATED WITH MOTION OF A LIFTING SURFACE

We will find derivatives of the potential (Eq. (16.54)) which are necessary in calculating velocity and pressure. First, we calculate differential

$$\delta\varphi=\delta'\varphi+\delta''\varphi+\delta'''\varphi,$$

where

$$\delta'\varphi=\delta\iint\limits_{W_1^*}\frac{dS}{4\pi}\frac{\partial}{\partial N_0}\left(\frac{1}{l}\right)\Gamma\left(\mathbf{r}, t_0-\frac{l}{a}\right)+$$
$$+\delta\iint\limits_{W_1^*}\frac{dS}{4\pi a}\frac{\partial}{\partial N_0}\left(\frac{1}{l}\right)l\sigma\left(\mathbf{r}, t_0-\frac{l}{a}\right),$$

$$\delta''\varphi=\delta\iint\limits_{W_1^*}\frac{dS}{4\pi}\frac{\partial}{\partial N_0}\left(\frac{1}{l}\right)\Gamma\left(\mathbf{r}, t_0-\frac{l}{a}\right)+\delta\iint\limits_{W_0^*}\frac{dS}{4\pi a}\frac{\partial}{\partial N_0}\left(\frac{1}{l}\right)l\sigma\left(\mathbf{r}, t_0-\frac{l}{a}\right),$$

$$\delta'''\varphi=\delta\iint\limits_{W_1^*}\frac{dS}{4\pi}\frac{\partial}{\partial N_0}\left(\frac{1}{l}\right)\Gamma\left(\mathbf{r}, t_0-\frac{l}{a}\right)+\delta\iint\limits_{W_0^*}\frac{dS}{4\pi a}\frac{\partial}{\partial N_0}\left(\frac{1}{l}\right)l\sigma\left(\mathbf{r}_0, t_0-\frac{l}{a}\right).$$

We will write differential $\delta'\phi$ under the following form:

$$\delta'\varphi=\delta h\frac{\partial}{\partial\nu_0}\iint\limits_{W_1^*}\frac{dS}{4\pi}\frac{\partial}{\partial N_0}\left(\frac{1}{l}\right)\Gamma^*, \tag{16.62}$$

where differentiation in the direction of vector ν is performed only for the variable marked with an arrow; i.e., r_0 appearing in $\partial/\partial N_0(1/l)$, while region W_i^* and function Γ^* do not vary.

After differentiation, differential $\delta''\phi$ assumes the following form:

$$\delta''\varphi=\iint\limits_{W_1^*}\frac{dS}{4\pi}\frac{\partial}{\partial N_0}\left(\frac{1}{l}\right)\sigma\left(\mathbf{r},t_0-\frac{l}{a}\right)\left(\delta t-\frac{1}{a}\frac{\partial l}{\partial \nu_0}\delta h\right)+$$
$$+\iint\limits_{W_0^*}\frac{dS}{4\pi a}\frac{\partial}{\partial N_0}\left(\frac{1}{l}\right)\left[\sigma\left(\mathbf{r},t_0-\frac{l}{a}\right)\frac{\partial l}{\partial \nu_0}\delta h+l\dot{\sigma}\left(\mathbf{r},t_0-\frac{l}{a}\right)\left(\delta t-\frac{1}{a}\frac{\partial l}{\partial \nu_0}\delta h\right)\right] \tag{16.63}$$

(derivative $\dot{\sigma}=\partial\sigma/\partial t$ is taken at the internal points of region W_0^*, where σ is continuous). Since the quantity $\sigma(\mathbf{r}, t_0-(l/a))$ is zero outside of region W_0^*, Eq. (16.63) becomes

$$\delta''\varphi=\iint\limits_{W_0^*}\frac{dS}{4\pi}\frac{\partial}{\partial N_0}\left(\frac{1}{l}\right)\left[\sigma\left(\mathbf{r},t_0-\frac{l}{a}\right)\delta t+\frac{l}{a}\dot{\sigma}\left(\mathbf{r},t_0-\frac{l}{a}\right)\left(\delta t+\frac{\delta h}{a}\mathrm{ev}\right)\right]. \tag{16.64}$$

It was considered here that since $\mathrm{grad}_0 l=-\mathbf{e}$; the derivative of the quantity l, with respect to point (r_0) in the direction of vector ν is

$$\frac{\partial l}{\partial \nu_0}=\nu\cdot\mathrm{grad}_0 l=-(\mathbf{e}\nu).$$

In addition,

$$\frac{\partial l}{\partial N_0}=-(\mathbf{eN}),\ \frac{\partial}{\partial N_0}\left(\frac{1}{l}\right)=\frac{(\mathbf{eN})}{l^2}. \tag{16.65}$$

Defining, by δW_i, an increase of region W_i^* $(i=1,2)$ associated with the displacement of point (r_0) through vector $\nu\delta h$ during time δt, we represent $\delta'''\phi$ as follows:

$$\delta'''\varphi=\iint\limits_{\delta W_0}\frac{dS}{4\pi}\frac{\partial}{\partial N_0}\left(\frac{1}{l}\right)\Gamma\left(\mathbf{r},t_0-\frac{l}{a}\right)+\iint\limits_{\delta W_1^*}\frac{dS}{4\pi a}\frac{\partial}{\partial N_0}\left(\frac{1}{l}\right)l\sigma\left(\mathbf{r},t_0-\frac{l}{a}\right)-$$
$$-\iint\limits_{\delta W_2^*}\frac{dS}{4\pi a}\frac{\partial}{\partial N_0}\left(\frac{1}{l}\right)l\sigma\left(\mathbf{r},t_0-\frac{l}{a}\right). \tag{16.66}$$

Region δW_i^* $(i=1,2)$ represents a narrow strip contained between the initial and displaced position of line L_i^* (see Fig. 16.3). Going to the limits in the integrals of Eq. (16.66), when the regions of integration δW_1^* and δW_2^* change into lines L_1^* and L_2^*, and remembering that function $\Gamma(\mathbf{r}, t_0-(l/a))$ on line L_1^* becomes zero, we obtain (in analogy with Eq. (16.51) the following:

$$\delta\varphi'''=-\int\limits_{L_0^*}\frac{1}{4\pi a\Delta_i}\frac{\partial}{\partial N_0}\left(\frac{1}{l}\right)l\sigma\left(\mathbf{r},t_0-\frac{l}{a}\right)[\mathrm{Nm}dL](\mathrm{ev}\delta h+a\delta t). \tag{16.67}$$

Here, L_0^* is the line consisting of both lines L_1^* and L_2^*, whereupon, the positive movement along line L_0 was selected in such a way that if one looks along $\mathbf{N}$, then region W_0^* is to the left. Δ_i signifies Δ_1 on line L_1^* and Δ_2 on line L_2^*.

The sought derivative $\partial\phi/\partial\nu = \nu$ grad ϕ, in the direction of vector ν, of potential ϕ with respect to the position of point $(\mathbf{r})$ can be expressed through the above found increments of the potential:

$$\frac{\partial\varphi}{\partial\nu}=\frac{1}{\delta h}(\delta'\varphi+\delta''\varphi+\delta'''\varphi)|_{\delta t=0}. \tag{16.68}$$

Substituting Eqs. (16.62), (16.64), (16.67) into the above and taking into consideration Eq. (16.65), we obtain

$$\frac{\partial\varphi}{\partial\nu}=\nu\,\mathrm{grad}_0\iint\limits_{W_1^*}\frac{dS}{4\pi}\frac{\partial}{\partial N_0}\left(\frac{1}{l}\right)\Gamma^*+\nu\iint\limits_{W_0^*}\frac{dS\,\mathrm{e\,(Ne)}}{4\pi a^2 l}\dot{\sigma}\left(\mathbf{r},t_0-\frac{l}{a}\right)-$$
$$-\nu\int\limits_{L_0^*}\frac{\mathrm{e\,(Ne)}\,[\mathrm{Nm}dL]}{4\pi a l\Delta_i}\sigma\left(\mathbf{r},t_0-\frac{l}{a}\right). \tag{16.69}$$

The multiplicand of ν in the right-hand side of Eq. (16.69) is equal to the gradient ϕ. Consequently, the sought velocity vector of the gas flow generated by the lifting surface is

$$\mathbf{v}=\mathrm{grad}_0\iint\limits_{W_1^*}\frac{dS}{4\pi}\frac{\partial}{\partial N_0}\left(\frac{1}{l}\right)\Gamma^*+\iint\limits_{W_0^*}\frac{\mathrm{e\,(Ne)}}{4\pi a^2 l}\dot{\sigma}\left(\mathbf{r},t_0-\frac{l}{a}\right)dS-$$
$$-\int\limits_{L_0^*}\frac{\mathrm{e\,(Ne)}\,[\mathrm{Nm}\,d\,\mathrm{L}]}{4\pi a l\,\mathrm{m\,(e+\mu)}}\sigma\left(\mathbf{r},t_0-\frac{l}{a}\right), \tag{16.70}$$

where μ is μ_1 on L_1^*, and μ_2 on L_2^*.

The first of the integrals appearing in Eq. (16.70) represents the gradient of the potential of the double layer (16.61), taken under the assumption that the intensity of dipoles (doublets) Γ^* and region W_0 of their distribution do not vary. Such a gradient is equal to velocity $\mathbf{v}^*$ of the flow of an incompressible fluid at point $(\mathbf{r}_0)$ generated by dipoles (doublets) with intensity equal to the audible circulation Γ^*. Replacing dipoles by the equivalent "vortices of the audible circulation" and determining velocities from such vortices by the Biot-Savart formula, we obtain the sought velocity of the flow of gas,

$$\mathbf{v}=\mathbf{v}^*+\mathbf{v}^\Delta, \tag{16.71}$$

where

$$\mathbf{v}^*=\iint\limits_{W_1^*}\frac{\mathbf{e}\times\boldsymbol{\gamma}^*}{4\pi l^2}\,dS+\int\limits_{L_0^*+L_W^*}\frac{\Delta\Gamma^*\mathbf{e}\times d\mathbf{L}}{4\pi l^2},$$

$$\mathbf{v}^\Delta=\iint\limits_{W_0^*}\frac{\mathbf{e}\,(\mathrm{Ne})}{4\pi a^2 l}\dot{\sigma}\left(\mathbf{r},t_0-\frac{l}{a}\right)dS-\int\limits_{L_0^*}\frac{\mathbf{e}\,(\mathrm{Ne})\,[\mathrm{Nm}\,d\,\mathbf{L}]}{4\pi l a\mathrm{m}\,(\mathrm{e}+\mu)}\sigma\left(\mathbf{r},t_0-\frac{l}{a}\right). \tag{16.72}$$

Vortices of audible circulation consist of a vorticity layer (vortex sheet) with vector of the surface intensity

$$\boldsymbol{\gamma}^*=-\mathbf{N}\times\mathrm{Grad}\,\Gamma \tag{16.73}$$

and discrete vortices with circulation $\Delta\Gamma^*$ extending along lines L_W^* and L_0^* (where Γ^* encounters a first order discontinuity with a jump equal to $\Delta\Gamma^*$, where

$$\Delta\Gamma^*=\begin{cases}-\dfrac{l}{a}\sigma\left(\mathbf{r},t_0-\dfrac{l}{a}\right) & \text{on line } L_0^*,\\ -\Gamma^* & \text{on line } L_W^*.\end{cases} \tag{16.74}$$

Here, L_W^* is written for the $F'ABC'$ boundary of the directing surface W which belongs to region W_1^* (see Fig. 16.2). Movement around lines L_0^* and L_W^* is positive if region W_0^* (W as well) is to the left when looking along $\mathbf{N}$.

Eq. (16.71) determines the velocity of the flow of gas at any arbitrary space point for the most general case of a non-stationary curved-line motion of a lifting surface at any speed (subsonic, supersonic, or mixed).

GAS PRESSURE

According to Eq. (16.7), gas pressure resulting from the movement of a lifting surface can be determined, within the limits of linear approximations, as a derivative of potential ϕ with respect to time. Taking advantage of the previously found potential differentials, we can write

$$\frac{\partial\varphi}{\partial t}=\frac{1}{\delta t}\{\delta'\varphi+\delta''\varphi+\delta'''\varphi\}_{\delta h=0}. \tag{16.75}$$

After substituting Eqs. (16.62), (16.64) and (16.67) into Eq. (16.75), the following expression for the pressure increment $\Delta p = p - p_0$ is obtained

$$\Delta p(\mathbf{r}_0, t_0) = \varrho_0 \int\int_{W_0^*} \frac{dS}{4\pi} \frac{\partial}{\partial N_0}\left(\frac{1}{l}\right)\dot{\Gamma}^* - \varrho_0 \int_{L_0^*} \frac{(\mathbf{eN})\,[\mathbf{N}m\,d\,\mathbf{L}]}{4\pi l\,\mathrm{m}\,(\mathrm{e}+\mu)}\,\sigma\left(\mathbf{r}, t_0 - \frac{l}{a}\right), \qquad (16.76)$$

where

$$\dot{\Gamma}^* = \frac{\partial \Gamma^*}{\partial t} = \sigma\left(\mathbf{r}, t_0 - \frac{l}{a}\right) + \frac{l}{a}\,\dot{\sigma}\left(\mathbf{r}, t_0 - \frac{l}{a}\right). \qquad (16.77)$$

8. LIFTING LINE IN GAS

In the preceding sections, means of computing gas velocities induced by vortices were considered for the case when vortices are, in turn, generated by some moving lifting surface with an arbitrary load continuously varying over the surface. We will now consider a particular case of the flow of gas when the lifting surface becomes infinitesimally narrow; or, in other words, degenerates into a lifting line.

Let it be assumed that in a gas at rest, an arbitrarily formed curved line L (filament) starts to move at some moment $t = 0$. This line acts on the gas through a known field of unitary (per unit of length) loads. Movements of that line are described with the help of directing surface W, given by the parametric equation $\mathbf{r} = \mathbf{r}(u,v)$ and by an equation of the form of the line on that surface at an arbitrary time t. This second equation we will write in the form of $\tau(u,v) = t$. Here, u,v are arbitrary (not necessarily orthogonal) Gaussian coordinates on surface W. Functions $\mathbf{r}(u,v)$ and $\tau(u,v)$ are assumed to be continuous, sufficiently smooth, and correspond to a single passage of filament L over each point $(\mathbf{r})$ of surface W.

Force per unit length, Y, representing action of the filament on the gas, is assumed to be directed along $\boldsymbol{N}$ - normal to surface W. We will treat the action of this filament on the gas as an application to the latter of a field of forces from the direction of surface W, and will find kinematic impulse $\boldsymbol{\Gamma}$ of surface density of those forces. During time dt, element $d\mathbf{L}$ of the lifting filament describes a platform, $dS = d\mathbf{L}\cdot\mathbf{V}_n dt$ on surface W. Here, $\mathbf{V}_n$ is the normal (with respect to the line) component of the filament velocity of motion on that surface. During this time element, $d\mathbf{L}$ transmits an impulse, $d\mathbf{I} = \mathbf{N}Y dL dt$, to the gas. Referring the above impulse to surface dS, we find the density vector of the relative kinematic impulse of surface forces

$$\boldsymbol{\Gamma} = \frac{1}{\varrho_0}\frac{d\mathbf{I}}{dS} = \frac{\mathbf{N}Y}{\varrho_0 V_n}. \qquad (16.78)$$

From this equation, it follows that value Γ of vector $\boldsymbol{\Gamma}$ is related to force Y by the following formula of Joukowsky

$$Y=\varrho_0 V_n \Gamma, \tag{16.79}$$

This means that it represents circulation of the bound vortex of a lifting line. At those points of surface W which at time t have not been reached as yet by the lifting line, vector $\boldsymbol{\Gamma}$ is obviously equal to zero. For this reason, at all points of surface W we have the following:

$$\Gamma(\mathbf{r}, t)=\begin{cases}\Gamma(\mathbf{r}) & \text{at} \quad t \geqslant \tau(\mathbf{r}), \\ 0 & \text{at} \quad t<\tau(\mathbf{r}),\end{cases} \tag{16.80}$$

where $\boldsymbol{\Gamma}(\mathbf{r}) = N\boldsymbol{\Gamma}$, and Γ is the circulation of the bound vortex of the lifting line. We assume that the relationship $\boldsymbol{\Gamma}(\mathbf{r})$ is known.

According to Eq. (16.29), the scalar potential ϕ of flow velocity is expressed as divergence of the vector of the impulse-potential

$$\mathbf{E}(\mathbf{r}_0, t_0)=\iint_W \frac{dS}{4\pi l} \boldsymbol{\Gamma}\left(\mathbf{r}, t_0-\frac{l}{a}\right). \tag{16.81}$$

If the condition

$$t_0-\frac{l}{a} \leqslant \tau(u, v) \tag{16.82}$$

is not fulfilled, then the potential function in Eq. (16.81) (according to Eq. (16.80)), becomes zero. After introducing notations similar to those in Eq. (16.49), we can rewrite the condition of Eq. (16.82) as follows:

$$\Psi(\mathbf{r}_0, \mathbf{r}, t_0) \leqslant 0. \tag{16.83}$$

This would define, on surface W, some "audible region" W^*. Elements of the lifting line emit acoustic signals from points of region W^* which have time to reach point $(\mathbf{r})$ at instant t_0. Form and dimensions of that region do not appear as invariant for given $\mathbf{r}(u,v)$ and $\tau(\mathbf{r})$. They also depend on the time t_0 and space point $\mathbf{r}_0$ for which vector $\mathbf{E}$ is calculated. According to the definition of audible region, Eq. (16.81) can be written as follows:

$$\mathbf{E}(\mathbf{r}_0, t_0)=\iint_{W^*} \frac{dS}{4\pi l} \boldsymbol{\Gamma}(\mathbf{r}), \tag{16.84}$$

where the region of integration W^* also depends on $\mathbf{r}_0$ and t_0.

Let us determine derivatives of vector E with respect to the coordinates of point $(\mathbf{r}_0)$ since they are necessary in obtaining potential $\phi = \operatorname{div} \mathbf{E}$. in order to do this, as before, we will find the increment $\delta\mathbf{E}$ under the condition that point $(\mathbf{r}_0)$ has shifted through vector $\boldsymbol{\nu}\delta h$ during time increment δt. By defining an enlargement of region W^* at such variations as δW^*, we obtain:

$$\delta\mathbf{E}=\delta h \iint_{W^*} \frac{\Gamma dS}{4\pi} \frac{\partial}{\partial \nu_0}\left(\frac{1}{l}\right)+\iint_{\delta W^*} \frac{\Gamma dS}{4\pi l}. \tag{16.85}$$

As before, subscript "zero" at vector $\boldsymbol{\nu}$ means that the derivative of $1/l$ in the direction $\boldsymbol{\nu}$ is taken with respect to the coordinates at point $(\mathbf{r}_0)$.

The equation $\Psi(\mathbf{r}_0, \mathbf{r}, t_0) = 0$ determines the audible line L^* on surface W. Region δW^* represents a narrow strip on surface W, contained between the initial L^* and displaced $(L^{*\delta})$ positions on the audible line. We have already considered such regions (δW_1^* and δW_2^*) in Section 7, where it was shown that an element of area dS' of such a strip corresponds to an element of line L^*, $d\mathbf{L}$ long,

$$dS'=-\frac{[\mathbf{N}\mathbf{m}\, d\mathbf{L}]}{\mathbf{m}(\mathbf{e}+\mu)}(\mathbf{e}\boldsymbol{\nu}\delta h+a\delta t). \tag{16.86}$$

Taking advantage of Eq. (16.86) to express area dS' in region δW^*, and introducing it into the second integral of Eq. (16.85), we transform the expression for $\delta\mathbf{E}$ to the following form:

$$\delta\mathbf{E}=\delta h \iint_{W^*} \frac{\Gamma dS}{4\pi} \frac{\partial}{\partial \nu_0}\left(\frac{1}{l}\right)-\int_{L^*} \frac{\Gamma(\mathbf{e}\boldsymbol{\nu}\delta h + a\delta t)[\mathbf{N}\mathbf{m}\, d\mathbf{L}]}{4\pi l\, \mathbf{m}(\mathbf{e}+\mu)}. \tag{16.87}$$

Passage around line L^* should be such that region W^* would remain on the left when looking along vector $\mathbf{N}$. In Eq. (16.87), the coefficient at δh is equal to the derivative $\partial\mathbf{E}/\partial\boldsymbol{\nu}$, so that

$$\frac{\partial\mathbf{E}}{\partial\boldsymbol{\nu}}=\iint_{W^*} \frac{\Gamma dS}{4\pi} \frac{\partial}{\partial \nu_0}\left(\frac{1}{l}\right)-\int_{L^*} \frac{\Gamma(\mathbf{e}\boldsymbol{\nu})[\mathbf{N}\mathbf{m}d\mathbf{L}]}{4\pi l\mathbf{m}(\mathbf{e}+\mu)}. \tag{16.88}$$

Assuming here that vector $\boldsymbol{\nu}$ is equal to any unit of Cartesian axes; it is not difficult fo find derivatives of the projections of vector E on those axes at coordinates x_0, y_0, z_0 of point $(\mathbf{r}_0)$. Divergence of vector E is determined with the help of

such derivatives. However, this divergence is equal to the potential ϕ of gas velocities generated by the lifting-line motion. Consequently, in analogy to Eq. (16.59)), we obtain

$$\varphi(\mathbf{r}_0, t_0)=\iint_{W^*}\frac{\Gamma dS}{4\pi}\frac{\partial}{\partial N_0}\left(\frac{1}{l}\right)-\int_{L^*}\frac{\Gamma(\mathrm{Ne})\,[\mathrm{N}\mathbf{m}d\mathbf{L}]}{4\pi l\mathbf{m}\,(\mathrm{e}+\mu)}. \tag{16.89}$$

The above formula can also be obtained in another way by considering it as a particular case of the lifting surface potential (Eq. (16.59)) when that surface degenerates into a line.

We will develop two more forms for the representation of the scalar velocity potential (Eq. (16.89)) of the lifting line.

As was previously shown in Sect. 6, a positively directed unit vector of a tangent to line L^* will be $\mathbf{t} = \mathbf{c}/|\mathbf{c}|$, where $\mathbf{c} = (\mathbf{e} + \mu) \times \mathbf{N}$. Substituting quantity $\mathbf{c}|d\mathbf{L}|\cdot|\mathbf{c}|^{-1}$ for $d\mathbf{L}$ in the second integral of Eq. (16.89), and noticing that after such substitution $[\mathbf{N}\mathbf{m}d\mathbf{L}] = -\mathbf{m}(\mathbf{e} + \mu)|d\mathbf{L}|/|\mathbf{c}|$, we will obtain velocity potential of the lifting surface under the following form:

$$\varphi(\mathbf{r}_0, t_0)=\iint_{W^*}\frac{\Gamma dS}{4\pi}\frac{\partial}{\partial N_0}\left(\frac{1}{l}\right)+\int_{L^*}\frac{\Gamma(\mathrm{Ne})\,|d\mathbf{L}|}{4\pi\,|\mathbf{r}_0-\mathbf{r}|\cdot|\mathbf{N}\times(\mathbf{e}+\mu)|}, \tag{16.90}$$

which does not contain an arbitrary vector $\mathbf{m}$.

In varying potential expressed by Eq. (16.89), it is convenient to use parametric representation of surface W and vector $\mathbf{m}$. Giving, as before, vector $\mathbf{m}$ through its coefficients m_1, m_2 on the basis of $\mathbf{r}_u, \mathbf{r}_v$, we modify Eq. (16.89) to the following form:

$$\varphi(\mathbf{r}_0, t_0)=\iint_{W^*}\frac{\Gamma\varkappa\,du\,dv}{4\pi}\frac{\partial}{\partial N_0}\left(\frac{1}{l}\right)-\int_{L^*}\frac{\Gamma\varkappa\,(\mathrm{Ne})\,(m_1dv-m_2du)}{4\pi l\,(Am_1+Bm_2)}, \tag{16.91}$$

where $A = \mathbf{r}_u\mathbf{e} + a\tau_u$; $B = \mathbf{r}_v\mathbf{e} + a\tau_v$; $\varkappa = |\mathbf{r}_u \times \mathbf{r}_v|$.

Values of m_1 and m_2 have no influence on the results of integration; consequently, they are selected as arbitrary continuous functions of the length of the arc of curve L^* under the condition that $\Delta = Am_1 + Bm_2 \neq 0$. If point $(\mathbf{r}_0)$ is not located on the Mach wave, then it is always possible to select m_1 and m_2 such that $\Delta \neq 0$, and the potential determined by Eq. (16.91) actually exists.

9. GAS VELOCITY ASSOCIATED WITH MOTION OF THE LIFTING LINE

It is possible to determine the gas velocity associated with the lifting-line motion in the gas. This can be done by calculating the gradient of the potential expressed by Eq. (16.89). As before, we will determine an increment $\delta\phi$ of the potential under the condition that during time increment δt, point $(\mathbf{r}_0)$ is displaced through vector $\nu\delta h$. Under such variation, the audible line L^* (see CD in Fig. 16.4) is displaced to some new position $L^{*\delta}$ (see EF in Fig. 16.4) and correspondingly, region W^* is increased by δW^*, which is the strip between L^* and $L^{*\delta}$. Upon determination of the differential, we obtain

$$\delta\varphi=\delta h\frac{\partial}{\partial\nu}\left[\iint\limits_{W^*=\text{const}}\frac{\Gamma dS}{4\pi}\frac{\partial}{\partial N_0}\left(\frac{1}{l}\right)\right]+\iint\limits_{\delta W^*}\frac{\Gamma dS'}{4\pi}\frac{\partial}{\partial N_0}\left(\frac{1}{l}\right)-$$
$$-\int\limits_{L^{*\delta}}\left[\frac{(\Gamma e)\,[\mathrm{N}md\mathrm{L}]}{4\pi l\Delta}\right]_{\mathbf{r}_0,\,t_0}^{\delta}+\int\limits_{L^*}\frac{(\Gamma e)\,[\mathrm{N}md\mathrm{L}]}{4\pi l\Delta}, \qquad (16.92)$$

where the superscript "δ" and subscripts "$\mathbf{r}_0, t_0$" to the term contained in square brackets indicate that it was taken at the increased values of $\mathbf{r}_0 + \nu\delta h$ and $t_0 + \delta t$ of the variables $\mathbf{r}_0$ and t_0.

Appearing in Eq. (16.92, integral

$$\Phi=\iint\limits_{W^*}\frac{\Gamma}{4\pi}\frac{\partial}{\partial N_0}\left(\frac{1}{l}\right)dS$$

represents the potential of the flow of incompressible fluid put into motion by a double layer of sources with intensity Γ which covers area W^* on the directing surface W. Derivative of Φ in the direction of vector ν, at invariant region W^* represents a projection on that direction of velocity $\mathbf{v}_{\text{несж}}$ of the indicated flow of incompressible fluid. System of vortices being equivalent to the dipoles (doublets) would consist of: (1) a layer of vortices covering region W^*, the intensity of which would be $\gamma = -\mathbf{N} \times \mathrm{Grad}\ \Gamma$, and (2) a discrete vortex with circulation $-\Gamma$. which would go around that region. Velocity induced by all those vortices can be expressed by the Biot-Savart formula

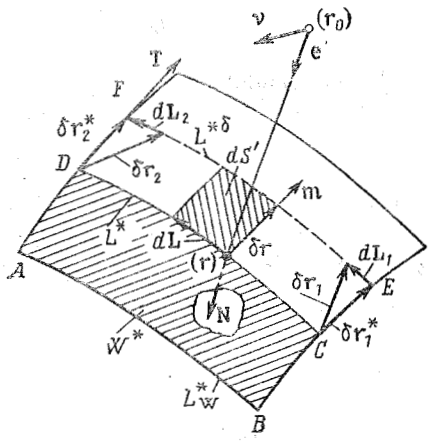

Figure 16.4

$$\mathbf{v}_{\text{несж}}=\mathbf{v}_0-\int\limits_{L^*}\frac{\Gamma e\times d\mathrm{L}}{4\pi l^2}, \qquad (16.93)$$

where

$$\mathbf{v}_0=\iint\limits_{W^*}\frac{\mathbf{e}\times\boldsymbol{\nu}}{4\pi l^2}\,dS-\int\limits_{L_W^*}\frac{\Gamma\mathbf{e}\times d\mathbf{L}}{4\pi l^2}\,, \tag{16.94}$$

while L_W^* is the part *(CBAD)* of the boundary of surface W which is in the audible zone (Fig. 16.4). As was indicated before,

$$\frac{\partial}{\partial\nu}[\Phi|_{W^*=\text{const}}]=\nu\cdot\mathbf{v}_{\text{несж}}.$$

In order to further transform Eq. (16.92), we will fix some family of vectors $\mathbf{m}$ on surface W and will use those which originate at points of curve L^*. We will also construct vectors $\delta\mathbf{r}=(\delta H\mathbf{m})/\Delta$ connecting curves $L^{*\delta}$ and L^*. When point $(\mathbf{r})$ moves from the beginning to the end of curve L^*, point $(\mathbf{r}+\delta\mathbf{r})$ would move along curve $L^{*\delta}$ and will describe on it some segment L^{*0} which perhaps, would differ from $L^{*\delta}$ because of infinitesimal vectors $d\mathbf{L}_1$ and $d\mathbf{L}_2$ at the beginning and end of that curve (Fig. 16.4). We define, by $\delta\mathbf{r}_i$, vectors $\delta\mathbf{r}$ in the initial $(i=1)$ and final $(i=2)$ points of curve L^*; by $\delta\mathbf{r}_1^*$, the vector connecting the initial points of curves L^* and $L^{*\delta}$ (see Fig. 16.4); and the final points, by $\delta\mathbf{r}_2^*$. Then, $d\mathbf{L}_i=(-1)^i(\delta\mathbf{r}_i^*-\delta\mathbf{r}_i)$. After introducing vector $\mathbf{T}$ of the tangent to line L_W bordering region W, it is possible, according to Eq. (16.55), to write $\delta\mathbf{r}_i^*=(\delta H\cdot\mathbf{T})/\mathbf{T}(\mathbf{e}+\boldsymbol{\mu})$. In the third integral in Eq. (16.92), upon switching from the variable of integration $\mathbf{r}'$ to a new variable $\mathbf{r}$ related to $\mathbf{r}'$ by the expression $\mathbf{r}'=\mathbf{r}+\delta\mathbf{r}$, we obtain

$$\int\limits_{L^{*\delta}}\left[\frac{(\Gamma\mathbf{e})\,[\mathbf{N}\mathbf{m}d\mathbf{L}]}{4\pi l\Delta}\right]_{\mathbf{r}_0,t_0}^{\delta}=\int\limits_{L^*}\left[\frac{(\Gamma\mathbf{e})\,[\mathbf{N}\mathbf{m}d\mathbf{L}]}{4\pi l\Delta}\right]_{\mathbf{r}_0,t_0,\mathbf{r}}^{\delta}+\sum_{i=1}^{2}\left[\frac{(\Gamma\mathbf{e})\,[\mathbf{N}\mathbf{m}d\mathbf{L}]}{4\pi l\Delta}\right]_{\mathbf{r}_0,t_0,\mathbf{r}}^{\delta} \tag{16.95}$$

Superscripts δ and subscripts $\mathbf{r}_0$, t_0, $\mathbf{r}$ indicate that the quantities included within those brackets are taken at the increased values $\mathbf{r}_0$, t_0 and $\mathbf{r}$ equal to $\mathbf{r}_0+\delta\mathbf{r}$, $t_0+\delta t$, $\mathbf{r}+\delta\mathbf{r}$ $(\delta\mathbf{r}=\delta H\mathbf{m}/\Delta)$. According to Eq. (16.56), the second integral of Eq. (16.92) transfers into a curved-line integral along the audible line L^*.

$$\iint\limits_{\delta W^*}\frac{\Gamma dS'}{4\pi}\,\frac{\partial}{\partial N_0}\left(\frac{1}{l}\right)=-\int\limits_{L^*}\frac{\Gamma\,[\mathbf{N}\mathbf{m}d\mathbf{L}]\,\delta H}{4\pi\Delta}\,\frac{\partial}{\partial N_0}\left(\frac{1}{l}\right). \tag{16.96}$$

Since

$$[\mathbf{N}\mathbf{m}d\mathbf{L}_i]=[\mathbf{N}\mathbf{T}]\,\frac{\delta H(-1)^i}{\mathbf{T}(\mathbf{e}+\boldsymbol{\mu})}\,,\quad\frac{\partial}{\partial N_0}\left(\frac{1}{l}\right)=\frac{\mathbf{N}\mathbf{e}}{l^2}\,,$$

therefore, in consideration of Eqs. (16.94)-(16.96), Eq. (16.97) can be written as follows:

$$\delta\varphi = \nu\delta h\left(\nu^0 - \int\limits_{L^*}\frac{\Gamma e\times dL}{4\pi l^2}\right) - \int\limits_{L^*}\frac{(\Gamma e)\,[Nm\,d\,L]\,\delta H}{4\pi l^2\Delta} -$$

$$-\int\limits_{L^*}\delta'\left[\frac{(\Gamma l)\,[Nm\,d\,L]}{4\pi l^2\Delta}\right] - \prod_{i=1}^{i=2}\frac{(\Gamma e)\,[NmT]\,\delta H}{4\pi l T\,(e+\mu)\Delta}. \qquad (16.97)$$

Symbol δ' signifies that differentiation is performed under the condition that points (r_0) and (r) are displaced through vectors $\nu\delta H$ and δr, while time increases through δt. As always, the sign of substitution in the last terms means that summation is performed with the change of sign when the lower limit is substituted. Applying the operator of differentiation to the fractions following it, we obtain

$$\delta\varphi = \nu\delta h\left(\nu^0 - \int\limits_{L^*}\frac{\Gamma e\times dL}{4\pi l^2}\right) - \int\limits_{L^*}\frac{[Nm\,d\,L]}{4\pi l^2\Delta}\{(\Gamma e)\,\delta H + \delta'\Gamma\cdot l + \Gamma\delta' l\} -$$

$$-\int\limits_{L^*}\frac{(\Gamma l)\,\delta'\,[Nm\,d\,L]}{4\pi l^2\Delta} + \int\limits_{L^*}\frac{(\Gamma e)\,[Nm\,d\,L]}{4\pi l\Delta}\left\{\frac{\delta' l^2}{l^2} + \frac{\delta'\Delta}{\Delta}\right\} - \prod_{i=1}^{i=2}\frac{(\Gamma e)\,[NmT]\,\delta H}{4\pi l T\,(e+\mu)\,\Delta}. \qquad (16.98)$$

According to the condition of variation, increments of vectors $\nu r_0 \nu$ and $\nu r \nu$ will be $\nu\delta h$ and $\delta r = m\delta H/\Delta$. Consequently,

$$\begin{aligned}
&\delta' l = \delta'(r - r_0) = \frac{\delta H}{\Delta}\,m - \nu\delta h,\\
&\delta' l^2 = \delta'(l\cdot l) = 2l\left[\frac{em}{\Delta}\,\delta H - e\nu\delta h\right],\\
&\delta' e = \delta'\left(\frac{l}{l}\right) = \frac{\delta H}{l\Delta}[m - e(me)] - \frac{\delta h}{l}[\nu - e(\nu e)].
\end{aligned} \qquad (16.99)$$

Since Γ, m and μ do not depend on r_0 and t_0, then

$$\delta'\Gamma = (\delta r\cdot\nabla)\Gamma,\ \delta' m = (\delta r\cdot\nabla)m,\ \delta'\mu = (\delta r\cdot\nabla)\mu.$$

Hamilton's operator ∇ is determined on the surface under the form $([r_v\times N]\frac{\partial}{\partial u} + [N\times r_u]\frac{\partial}{\partial v})/\varkappa$, and vector $\delta r = (m_1 r_u + m_2 r_v)\ \delta H\Delta^{-1}$. From this,

$$\begin{aligned}
&\delta'\Gamma = \frac{\delta H}{\Delta}[m_1\Gamma_u + m_2\Gamma_v],\ \delta' m = \frac{\delta H}{\Delta}[m_1 m_u + m_2 m_v],\\
&\delta'\mu = \frac{\delta H}{\Delta}[m_1\mu_u + m_2\mu_v].
\end{aligned} \qquad (16.100)$$

Subscripts "u, v" always signify partial differentiation. Since $\delta'\Delta = \delta m(e+\mu) + m(\delta' e + \delta'\mu)$, hence taking advantage of Eqs. (16.99) and (16.100) and taking into account that $\delta H = (e\nu)\delta h + a\delta t$, after small transformations, we obtain the following:

$$\delta'\Delta=\frac{\delta H}{\Delta}\Lambda+\frac{E(\mathrm{ev})\,\delta h+E'a\delta t}{l\Delta}-\frac{(\mathrm{mv})\,\delta h}{l}. \tag{16-101}$$

Here,

$$\Lambda=m_1[(\mu\mathrm{m})_u+\mathrm{e}\cdot\mathrm{m}_u]+m_2[(\mu\mathrm{m})_v+\mathrm{em}_v],$$
$$E=\mathrm{m}^2+(\mathrm{me})(\mathrm{m}\mu),\quad E'=\mathrm{m}^2-(\mathrm{me})^2. \tag{16.102}$$

Finally, we compute the differential

$$\delta'[\mathrm{Nm}d\mathrm{L}]=[\delta'\mathrm{Nm}d\mathrm{L}]+[\mathrm{N}\delta'\mathrm{m}d\mathrm{L}]+[\mathrm{Nm}\delta'd\mathrm{L}]. \tag{16.103}$$

Since vector $\delta'\mathrm{N}$ is perpendicular to N, and lies in the plane of vectors m and $d\mathrm{L}$; hence, $[\delta'\mathrm{N}\mathrm{m}d\mathrm{L}] = 0$. Vector $d\mathrm{L}$ in its displaced position is obtained by a transfer of the points of its beginning and end from their initial positions through vectors $\delta\mathrm{r}$ and $\delta\mathrm{r} + (d\mathrm{L}\nabla)\delta\mathrm{r}$. From this, $\delta' d\mathrm{L} = (d\mathrm{L}\cdot\nabla)\delta\mathrm{r}$; or assuming here that $\delta\mathrm{r} = \delta H\mathrm{m}/\Delta$ and differentiating, we obtain

$$\delta' d\mathrm{L}=\frac{\delta H}{\Delta}(d\mathrm{L}\cdot\nabla)\,\mathrm{m}+\mathrm{m}(d\mathrm{L}\cdot\nabla)\frac{\delta H}{\Delta}.$$

Substituting the above expression into the first part of Eq. (16.103), as well as $\delta'\mathrm{m}$ from Eq. (16.100), and taking into consideration that $d\mathrm{L} = \mathrm{r}_u du + \mathrm{r}_v dv$, we obtain

$$\delta'[\mathrm{Nm}\,d\,\mathrm{L}]=\frac{\delta H}{\Delta}\{[\mathrm{Nm}_u\mathrm{r}_v]-[\mathrm{Nm}_v\mathrm{r}_u]\}(m_1dv-m_2du). \tag{16.104}$$

If the derivatives of vector m appearing in the above equation are written in an expanded form of

$$\mathrm{m}_u=(m_1)_u\mathrm{r}_u+(m_2)_u\mathrm{r}_v+m_1\mathrm{r}_{uu}+m_2\mathrm{r}_{uv},$$
$$\mathrm{m}_v=(m_1)_v\mathrm{r}_v+(m_2)_v\mathrm{r}_v+m_1\mathrm{r}_{uv}+m_2\mathrm{r}_{vv},$$

then Eq. (16.104) will assume the following form:

$$\delta'[\mathrm{Nm}\,d\,\mathrm{L}]=\frac{\delta H dP}{\Delta}[(m_1\varkappa)_u+(m_2\varkappa)_v], \tag{16.105}$$

where $dP = m_1 dv - m_2 du$, while $[\mathrm{Nm}d\mathrm{L}] = \varkappa dP$.

In this way, all differentials appearing in Eq. (16.98) have been found. After substituting the found values into Eq. (16.98) and after some regrouping, we obtain

$$\delta\varphi = \nu\delta h\left(\nu^0 - \int\limits_{L^*}\frac{\Gamma e\times dL}{4\pi l^2} + \int\limits_{L^*}\frac{\Gamma[N-e(Ne)]\varkappa dP}{4\pi l^2\Delta}\right) - \int\limits_{L^*}\frac{dP\delta H(Gl)}{4\pi l^2\Delta^2} +$$

$$+\int\limits_{L^*}\frac{(\Gamma^z e)\,dP}{4\pi l^2\Delta^2}\left\{\left[2(em)+\frac{\Delta l+E}{\Delta}\right]\delta H - [2(ev)\Delta + mv]\,\delta h - \right.$$

$$\left. - [2(em)+m\mu]\,a\delta t\right\} - \sum_{l=1}^{l=2}\frac{(\Gamma e)[NmT]\,\delta H}{4\pi l\Gamma(e+\mu)\Delta}. \qquad (16.106)$$

Here,

$$G = (m_1\Gamma^z)_u + (m_2\Gamma^z)_v;\quad \Gamma^z = \Gamma\nu.$$

Assuming, in Eq. (16.106) that $\delta t = 0$ (while $\delta H = (ev)\delta h/\Delta$) and dividing the so-obtained expression by δh, we find the derivative

$$\frac{\partial\varphi}{\partial\nu} = \frac{1}{\delta h}(\delta\varphi)|_{\delta t=0}.$$

In the above found expression for $\partial\phi/\partial\nu$, the arbitrary unit vector ν appears linearly under the form of its scalar product with respect to the remaining part of that expression which, consequently, will be equal to gradient of ϕ. In this way,

$$\operatorname{grad}\varphi = \nu_0 - \int\limits_{L^*}\frac{\Gamma e\times dL}{4\pi l^2} + \int\limits_{L^*}\frac{\Gamma[N-e(Ne)]\varkappa dP}{4\pi l^2\Delta} - \int\limits_{L^*}\frac{dP(Gl)\,e}{4\pi l^2\Delta^2} +$$

$$+\int\limits_{L^*}\frac{(\Gamma^z e)\,dP}{4\pi l^2\Delta^2}\left\{\left[2(em)+\frac{\Delta l+E}{\Delta}-2\Delta\right]e - m\right\} - \sum_{l=1}^{l=2}\frac{(\Gamma e)[NmT]\,e}{4\pi l\Gamma(e+\mu)\Delta}. \qquad (16.107)$$

Let us modify the first integral in Eq. (16.107) into a slightly different form. As we have already seen in Sect. 8,

$$dL = |dL|\frac{c}{|c|},\quad [Nmd L] = -\frac{\Delta|dL|}{|c|},$$

where $c = (e+\mu)\times N$. In addition to dL, let us introduce two other elementary vectors dL^* and dL^{**} at an arbitrary point of curve L^*. They are defined by the following equations

$$dL^* = [e\times N]\frac{|dL|}{|c|},\quad dL^{**} = -[\mu\times N]\frac{|dL|}{|c|}, \qquad (16.108)$$

in such a way that $dL = dL^* - dL^{**}$. Both vectors lie in a plane tangent to surface W, with vector dL^* perpendicular to vector e, and vector dL^{**} is perpendicular to vector μ (Fig. 16.5). Since vector μ is normal with respect to the lifting line, hence, dL^{**} is directed along a tangent to the lifting line. Taking advantage of Eq. (16.108), it is not difficult to establish the following identity:

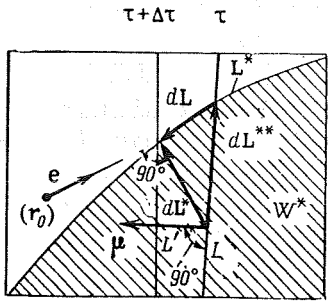

Figure 16.5

$$\int_{L^*} \frac{\Gamma \mathbf{e} \times d\mathbf{L}^*}{4\pi l^2} = -\int_{L^*} \frac{\Gamma [\mathbf{N} - \mathbf{e}(\mathbf{Ne})][\mathbf{N} m d\mathbf{L}]}{4\pi l^2 \Delta}.$$

Taking into consideration the above identity, it is possible to represent velocity of the gas flow, $\mathbf{v} = \operatorname{grad} \phi$, resulting from a movement in that gas of the lifting line, under the following final form:

$$\mathbf{v} = \mathbf{v}_0 + \mathbf{v}_1 + \mathbf{v}_2, \tag{16.109}$$

where

$$\mathbf{v}_0 = \iint_{W^*} \frac{\mathbf{e} \times \boldsymbol{\gamma}}{4\pi l^2} dS - \int_{L_W^*} \frac{\Gamma \mathbf{e} \times d\mathbf{L}}{4\pi l^2}, \tag{16.110}$$

$$\mathbf{v}_1 = \int_{L^*} \frac{\Gamma \mathbf{e} \times d\mathbf{L}^{**}}{4\pi l^2}, \tag{16.111}$$

$$\mathbf{v}_2 = \int_{L^*} \frac{m_1 dv - m_2 du}{4\pi l^2 \Delta^2} \left\{ \frac{\mathbf{e}(\Gamma^{\times}\mathbf{e})}{\Delta} (E + \Delta l) - \mathbf{e}(\mathbf{Gl}) - \right.$$

$$\left. - (\Gamma^{\times}\mathbf{e})[\mathbf{m} + 2\mathbf{e}(\mathbf{m}\mu)] \right\} - \Big|_{i=1}^{i=2} \frac{(\Gamma \mathbf{e})\, \mathbf{e}[m_1\beta - m_2\alpha]}{4\pi l (A\alpha + B\beta)\Delta}. \tag{16.112}$$

Here, $A = (\mathbf{r}_u \mathbf{e}) + a\tau_u$; $B = (\mathbf{r}_v \mathbf{e}) + a\tau_v$; α and β are the coefficients of vector $\mathbf{T}$ on the basis of $\mathbf{r}_u, \mathbf{r}_v$; i.e., $\mathbf{T} = \alpha \mathbf{r}_u + \beta \mathbf{r}_v$. If the equation of the limit L_W of the region W is given as $f(u,v) = const$, then the value of the ratio α/β appearing in Eq. (16.112) is determined from the following equation: $\alpha f_u + \beta f_v = 0$. Vector $d\mathbf{L}^{**}$ appearing in Eq. (16.111) can be presented (in spite of Eq. (16.108)) in the following form:

$$d\mathbf{L}^{**} = -a \frac{\partial(\tau, \mathbf{r})}{\partial(u, v)} \frac{m_1 dv - m_2 du}{A m_1 + B m_2}. \tag{16.113}$$

The symbol of substitution in Eq. (16.112) means summation (with change of sign for $i=1$) of the expression following it at the beginning $(i=1)$ and the end $(i=2)$ of curve $\mathbf{L}^*$ while moving on that curve in the positive direction (if we look along $\mathbf{N}$, then region W^* should remain on the left).

Functions $m_1(u,v)$ and $m_2(u,v)$, appearing in the expression for velocities, show no influence on the results. It is possible to select them arbitrarily; however, with a restriction that everywhere on the audible line L^*, the following condition is fulfilled: $\Delta = Am_1 + Bm_2 \neq 0$. If the network of coordinates u,v is selected in such a way that vector $\mathbf{r}_u$ does not touch the audible line L^*, then condition $\Delta \neq 0$ will be fulfilled for $\mathbf{m} = \mathbf{r}_u$ (i.e., $m_1 = 1$, $m_2 = 0$). Under this condition, Eq. (16.112) is considerably simplified and takes the following form:

$$\mathbf{v}_2 = \int_{L^*} \frac{dv}{4\pi l^2 A^2} \left\{ \frac{\mathbf{e}(\Gamma^x \mathbf{e})}{A} \left[\mathbf{r}_u^2 + a\tau_u (\mathbf{r}_u \mathbf{e}) + l(\mathbf{r}_{uu}\mathbf{e} + a\tau_{uu}) \right] - \right.$$

$$\left. - (\mathbf{r}_u + 2\mathbf{e}a\tau_u)(\Gamma^x \mathbf{e}) - \mathbf{e}(\Gamma_u^x \mathbf{e})\, l \right\} - \sum_{i=1}^{i=2} \frac{(\Gamma^x \mathbf{e})\, \mathbf{e}\beta}{4\pi l A (A\alpha + B\beta)}. \qquad (16.114)$$

Eqs. (16.109) and (16.112) represent the general law determining the field of velocities induced by the system of vortices of a lifting line moving in an arbitrary fashion in the gas. Velocity at an arbitrary point of space consists of three components. Two of them ($\mathbf{v}_0$ and $\mathbf{v}_1$) are determined from the Biot-Savart formula suitably applied to the audible elements of the free and bound vortices. The third component, $\mathbf{v}_2$, is of a wave character. In the case most interesting from a practical point of view; namely, that of a motion of the lifting line along a plane and determination of induced velocity in that plane, the wave components become zero.

The above obtained formula can be applied, in particular, to the case of instantaneous forces acting on the gas. Here, function $\tau(r)$ degenerates into a constant and velocities $\mathbf{v}_1$ disappear.

Gas pressure caused by the motion of a lifting line is

$$p = p_0 - \varrho_0 \frac{\partial \varphi}{\partial t}. \qquad (16.115)$$

The derivative $\partial\phi/\partial t$ appearing here is equal to the coefficient at δt in Eq. (16.106). Upon calculating that coefficient, we obtain

$$\frac{\partial \varphi}{\partial t} = \int_{L^*} \frac{adP}{4\pi l^2 \Delta^2} \left\{ (\Gamma^x \mathbf{e}) \left[\frac{E + \Delta l}{\Delta} - \mathbf{m} \cdot \boldsymbol{\mu} \right] - \mathrm{Gl} \right\} - a \sum_{i=1}^{i=2} \frac{\Gamma \mathbf{e}\,[\mathrm{NmT}]}{4\pi l \mathrm{T}\,(\mathrm{e} + \mu)\,\Delta}. \qquad (16.116)$$

Eqs. (16.115) and (16.116) permit one to calculate acoustic gas pressure generated by an arbitrary motion of the lifting line in the gas.

10. FORMULATION OF PRINCIPLE RESULTS FOR THE CASE OF PLANAR MOTION

RULE OF "AUDIBLE CIRCULATION"

Let it be assumed that in an infinite volume of gas at rest, at some moment of time $t=0$, a lifting surface appears and starts to move in an arbitrary way; however, remaining within some plane W. Velocities of the resulting gas flow can be determined in the W plane (for the known loads on the surface) through the use of the following rules of *audible circulation*.

1) Selection is made of a point $(\mathbf{r}_0)$ in the W plane for which gas velocity $\mathbf{v}(\mathbf{r}_0, t_0)$ at a moment t_0 has to be determined. For those $(\mathbf{r}_0)$ and t_0 functions, Γ^* for point $(\mathbf{r})$ on plane W is formulated according to the following relationship:

$$\Gamma^*(\mathbf{r})=\Gamma\left(\mathbf{r},\ t_0-\frac{l}{a}\right)+\frac{l}{a}\sigma\left(\mathbf{r},\ t_0-\frac{l}{a}\right)\quad(l=|\mathbf{r}-\mathbf{r}_0|). \tag{16.117}$$

Here, a is the velocity of sound; $\sigma(\mathbf{r}, t)$ is the force divided by the air density expressing action of the lifting plane elements on a stationary unit of area at an arbitrary point $(\mathbf{r})$ of plane W; $\Gamma(\mathbf{r}, t)$ is the lifting surface circulation taken along contour C, piercing surface W at point $(\mathbf{r})$ and some other point which, as yet, has not been approached by the lifting surface. Circulation, in terms of the surface density (σ) of the forces, is expressed by the following formula:

$$\Gamma(\mathbf{r},\ t)=\int_0^t \sigma(\mathbf{r},\ t)\,dt. \tag{16.118}$$

2) Circulation Γ^* (the so-called "audible circulation") is taken as circulation of some "transformed" system of vortices covering surface W, and distribution of those vortices is determined. The system of vortices generated by "audible circulation" may consist of a vorticity layer on surface W and discrete vortices passing through those places where function (16.117) encounters discontinuities of the first order.

3) Using the Biot-Savart formula (or by some other means) velocity induced at point $(\mathbf{r}_0)$ by vortices of the *audible circulation* is computed. This velocity is equal to the sought gas velocity at point $(\mathbf{r}_0)$ at time t_0. (If point $\mathbf{r}_0$ happens to be on the vortex layer of *audible circulation*, then the velocity integral, taken in the sense of principle value, gives a half-sum of the limit value of velocity on different sides of surface W).

RULE FOR THE "AUDIBLE ELEMENTS OF VORTICES"

In gas being initially in a state of rest, let us imagine that at some instant of time, a lifting line (bound vortex) appears which performs an arbitrary movement (possibly with some deformations of its original shape), but still always remaining on a stationary plane W. It is assumed that circulation Γ of the bound vortex varies with the position of the vortex as well as time. Consequently, in its wake, a system of free vortices is generated with circulation $\Gamma(\mathbf{r})$. Gas velocities induced by those vortices at points of plane W can be determined with the help of the following rules of the "audible elements of vortices."

1) Select and fix point $(\mathbf{r}_0)$ on plane W as well as the time instant t_0 for which gas velocity $\mathbf{v}(\mathbf{r}_0, t)$ is to be computed. For $(\mathbf{r}_0)$ and t_0, on surface W find the "audible region" W^*. Region W^* is constituted of such points of surface W from which, at instant t_0, acoustical signals have time to reach point $(\mathbf{r}_0)$. The question of whether point $(\mathbf{r})$belongs to the zone of audibility is answered by the following condition:

$$\Psi \equiv |\mathbf{r}-\mathbf{r}_0| - a[t_0 - \tau(\mathbf{r})] \leqslant 0, \tag{16.119}$$

where $\tau(\mathbf{r})$ is the time of passing of the lifting line over point $(\mathbf{r})$ of surface W.

2) Construct a system of free vortices springing from the bound vortex (filament) with circulation Γ. (Free vortices will be the same for both imcompressible fluid and gas). Elements of free vortices belonging to the region W^* will be called "audible".

3) Locate "audible elements" $d\mathbf{L}^{**}$ of the bound vortex on line L^* determined by the equation $\Psi = 0$. (Means of determining $d\mathbf{L}^{**}$ will be discussed below).

4) Using the Biot-Savart formula, at point $(\mathbf{r}_0)$ compute the velocity generated by the "audible elements" of free and bound vortices. That velocity is equal to the sought gas velocity at the point at instant t_0 (integrals needed for velocities on vortex layers should be taken as their principal values).

DETERMINATION OF THE "AUDIBLE ELEMENTS" OF THE BOUND VORTEX

If, on surface W, an arbitrary network of Gauss coordinates u, v is given, then the distribution along line L^* of the "audible elements" $d\mathbf{L}^{**}$ of the bound vortex is determined from the following formula

$$d\mathrm{L}^{**}=\frac{m_2du-m_1dv}{Am_1+Bm_2}\frac{\partial(\tau,\mathrm{r})}{\partial(u,v)}a.$$

Here, $\tau(u,v)$ is the time of passing of the filament over point (u,v) of surface W, and m_1,m_2 are the arbitrarily chosen continuous functions of u and v for which the following condition is fulfilled: $Am_1 + Bm_2 \neq 0$, where

$$A=(\mathrm{r}_u\mathrm{e})+a\tau_u,\quad B=(\mathrm{r}_v\mathrm{e})+a\tau_v,\quad \mathrm{e}=[\mathrm{r}-\mathrm{r}_0]/|\mathrm{r}-\mathrm{r}_0|.$$

The value of element $d\mathrm{L}^{**}$ does not change with the various selections of m_1 and m_2.

Element $d\mathrm{L}^{**}$ can also be determined by the following geometric considerations. Let L and L' be two consecutive positions of the lifting line at two infinitesimally close moments of time τ and $\tau + \Delta\tau$ $(\Delta\tau>0)$, with $d\mathrm{L}$ being a segment of the boundary of audibility region included between L and L' (see Fig. 16.5). Then, element $d\mathrm{L}^{**}$ will be represented by a segment of the bound vortex (filam nt) at position L, which is included between the beginning of vector $d\mathrm{L}$ and the point of intersection of L with a line perpendicular to vector e passing through the end of $d\mathrm{L}$.

11. EXAMPLES

NONSTATIONARY MOVEMENT WITH CONSTANT VELOCITY OF A STRAIGHT LIFTING LINE

A straight infinite lifting line with constant circulation Γ appears in an infinite volume of gas being at rest at time $t=0$. Afterwards, that line moves in the gas with a constant velocity.

Without limiting the generality of our considerations, it is possible to assume that the filament moves in the xOy plane in a direction opposite to the Ox axis with a speed V, which is perpendicular to the filament. At an instant t_0, the position of the filament coincides with the Oy axis. Let the velocity of gas be calculated at point $Q(x_0,0)$ of the Ox axis. Let us consider point P at the intersection of the audible line L^* and the lifting filament at some arbitrary instant of time τ (Fig. 16.6). From point P to axis Oy, distance x is equal to $V(t_0 - \tau)$; and distance l, between points P and Q, is equal to $a(t_0 - \tau)$. The ratio of the above distances is constant. Consequently, the audible line L^* will represent a conic section with axis Oy as its directrix, the focus at point Q, and excentricity equal to a/V - inverse of the Mach number. (For movements of the lifting filament with supersonic velocities, L^* becomes an ellipse; for subsonic, a hyperbola; and sonic, a parabola).

By introducing angle θ between vector e and axis Ox (see Fig. 16.6), it is possible to write the following equation for line L^* in polar coordinates

$$l=\frac{x_0}{M-\cos\theta}. \qquad (16.120)$$

For $M \geq 1$ (supersonic, or sonic flows), it is necessary to take $x_0 > 0$; otherwise, the audible zone would disappear. In order to find the "audible elements" $d\mathbf{L}^{**}$ of the bound vortex, we will take advantage of the geometric interpretation developed in Sect. 10. Let L and L_1 be the positions of the lifting filaments during infinitesimally close moments of time t and $t+dt$, while P and P' are points of intersection of those lines and the boundary of audibility (see Fig. 16.6). Distances from points P and P' to point Q are equal to $a(t_0-t)$ $a(t_0-t-\Delta t)$, respectively. Consequently, segment PD is equal to $a\Delta t$ and is related to segment PE by the following: $PD = PE \sin\theta$. Since, according to definition, element $d\mathbf{L}^{**}$, by itself, represents vector EP (assuming that elements of the bound vortex are directed along axis Oy), then

$$d\mathbf{L}^{**}=\frac{adt}{\sin\theta}\mathbf{j}=\frac{dx}{M\sin\theta}\mathbf{j}. \qquad (16.121)$$

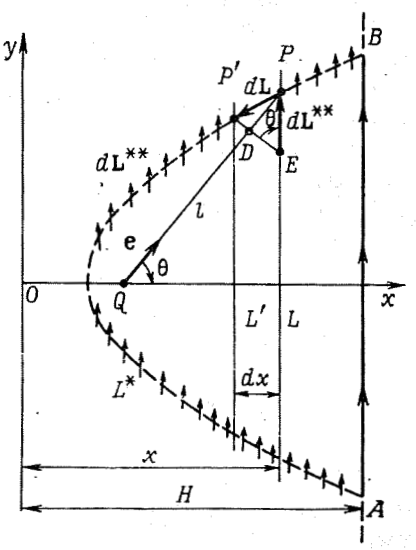

Figure 16.6

The lifting filament, appearing at instant $t=0$, leaves (at a distance $H = Vt_0$ from the Oy axis) a straight vortex whose circulation is opposite to that of the lifting filament. Segment AB of the vortex falls into the audible zone. In this way, the system of audible elements of vortices consists of the straight segment AB and elements $d\mathbf{L}^{**}$, with circulation Γ, distributed along line L^* (shown by arrows in Fig. 16.6). At point Q, vortex AB with circulation $-\Gamma$ induces the following velocity:

$$v_z'=-\frac{\Gamma}{2\pi(H-x_0)}\sin\theta_B, \qquad (16.122)$$

where θ_B signifies θ at point B. Elements of vortices $d\mathbf{L}^{**}$ located on the segment of line L^* and contained between points with the polar angles θ_1 and θ_2 $(\theta_2>\theta_1)$ will generate, at point Q, the following velocity directed downward along axis Oz:

$$v_z''=\int_{\theta_2}^{\theta_1}\frac{\Gamma\,|d\mathbf{L}^{**}|}{4\pi l^2}\cos\theta,$$

where dependence of l on θ is determined by Eq. (16.120). After integrating, we find

$$v_z''=\frac{\Gamma}{4\pi x_0}(\sin\theta_2-\sin\theta_1). \tag{16.123}$$

Noticing that in the case of an infinitely long filament $\theta_1 = \theta_B$ and $\theta_2 = 2\pi - \theta_B$, and summing up velocities given by Eqs. (16.122) and (16.123), we finally obtain the velocity of gas, v_z^∞, induced by an infinite filament

$$v_z^\infty=-\frac{\Gamma}{2\pi}\left\{\frac{1}{H-x_0}+\frac{1}{x_0}\right\}\sin\theta_B, \tag{16.124}$$

where

$$\sin\theta_B=\sqrt{1-\frac{(H-x_0)^2}{H^2}M^2}\,. \tag{16.125}$$

If $sin\ \theta_B$ happens to be imaginary, then it is necessary to take $v_z^\infty = 0$.

INDUCED VELOCITIES OF THE LIFTING AIRSCREW IN A COMPRESSIBLE MEDIUM

We will adapt the above obtained law of induction associated with an arbitrary motion of the lifting filament in gas to the case of an airscrew in an oblique translation. As in the case of an incompressible fluid, the airscrew blade will be represented by a straight, R-long, segment of a lifting filament which rotates with a constant velocity ω around an axis perpendicular to that filament, while the axis itself moves in a rectilinear motion with speed V. It will be assumed that circulation Γ of the bound vortex filament is zero at both ends, while it varies in an arbitrary fashion with both spanwise position and time. We will limit ourselves to the single-bladed airscrew as, in a more general case, it would suffice to superimpose fields of velocities induced by each blade.

Let $Oxyz$ represent the stationary Cartesian coordinate axes with respect to which undisturbed gas remains at rest. Orientation of the axes is selected in such a way that at time t_0, the axis of rotation coincides with axis Oy, and the plane of rotation with plane xOy. Let $(\mathbf{r})$ be an arbitrary point on the filament located at a distance ρ from the axis of rotation. Radius-vector $\mathbf{r}$, determining the position of that point,

extends from the origin of system $Oxyz$; at an arbitrary time τ it will be $\mathbf{r} = -\mathbf{V}(t_0 - \tau) + \rho\mathbf{e}_\rho$ where $\mathbf{e}_\rho = -\mathbf{i}\cos\vartheta + \mathbf{k}\sin\vartheta$ is the unit vector directed along the filament segment. Angle ϑ is the angle between the filament and the half-plane $(z=0, x<0)$. For an arbitrary instant of time τ and for the blade azimuth angle ψ at the moment t_0, that angle may be assumed as $\omega\tau$ and ωt_0, respectively. Consequently,

$$\mathbf{r} = -\frac{\mathbf{V}}{\omega}(\psi - \vartheta) + \rho\mathbf{e}_\rho. \qquad (16.125)$$

For the variation of parameters ϑ and ρ within the limits $-\infty < \vartheta \leq \psi$, $0 \leq \rho \leq R$, the above equation represents a skewed helical surface S_ψ (see Fig. 13.1) which appears as the directing surface W. Circulation of the lifting filament $\Gamma(\vartheta, \rho)$ and function $\tau = \vartheta/\omega$ (showing the time of the passage of the filament over an arbitrary point of surface W) completely define the system of free vortices springing from the filament as well as velocities induced by those vortices. In order to calculate those velocities, we will use Eq. (16.109), where we assume $u=\vartheta$, $v=\rho$; and for functions $\mathbf{r}(u,v)$ and $\tau(u,v)$, we will take the relationships shown above.

In this case, the region of audibility is determined by the following inequality:

$$l - \frac{a}{\omega}(\psi - \vartheta) \leqslant 0. \qquad (16.126)$$

By making Eq. (16.126) an equality, we obtain an equation for the boundary of audible zone. Let us enlarge the surface given by Eq. (16.125) by assuming that parameter ρ varies from $-\infty$ to ∞, and we determine those values of ρ which correspond to the audible boundary. Let $\mathbf{H}$ be perpendicular, extending from point $(\mathbf{r}_0)$ to the line $\vartheta = const$ where, in addition, the end of vector $\mathbf{H}$ coincides with the point having coordinates ϑ, ρ_0. Then,

$$\mathbf{H} = -\frac{\mathbf{V}}{\omega}(\psi - \vartheta) + \rho_0\mathbf{e}_\rho - \mathbf{r}_0. \qquad (16.127)$$

As a result of the condition $\mathbf{H}\mathbf{e}_\rho = 0$, we find $\rho_0 = (\mathbf{r}_0 + \mathbf{V}(\psi - \vartheta)/\omega)\mathbf{e}_\rho$ which, when substituted into Eq. (16.127), yields

$$\mathbf{H} = (\mathbf{r}_0\mathbf{e}_\rho)\mathbf{e}_\rho - \mathbf{r}_0 + [(\mathbf{V}\mathbf{e}_\rho)\mathbf{e}_\rho - \mathbf{V}]\frac{\psi - \vartheta}{\omega}. \qquad (16.128)$$

Values of parameter ρ at points of the audible boundary are defined as ρ_1 and ρ_2. Considering that these points are at distance $l = (\psi - \vartheta)a/\omega$ from point $(\mathbf{r}_0)$, we find that

$$\varrho_{1,2}=\varrho_0 \pm \sqrt{\frac{a^2}{\omega^2}(\psi-\vartheta)^2-H^2}. \tag{16.129}$$

In our considerations, let us introduce function $E^*(\vartheta,\rho)$ which is equal to unity in the audible regions and zero outside; i.e.,

$$E^*=\begin{cases} 1 \text{ for } l \leqslant \frac{a}{\omega}(\psi-\vartheta), \\ 0 \text{ for } l > \frac{a}{\omega}(\psi-\vartheta). \end{cases} \tag{16.130}$$

Then, velocity $\mathbf{v}_0$ induced by the audible elements of free vortices can be expressed as follows:

$$\mathbf{v}_0=\int_{\vartheta=-\infty}^{\vartheta=\psi} d\vartheta \int_0^R \frac{E^*}{4\pi l^2}\mathbf{e}\times\frac{\partial(\mathbf{r},\Gamma)}{\partial(\vartheta,\varrho)}d\varrho, \tag{16.131}$$

where $\mathbf{r}(\vartheta,\rho)$ is given by Eq. (16.125). Velocity $\mathbf{v}_1$, induced by the audible elements of the bound vortices, is given by the following integral

$$\mathbf{v}_1=\int_{L^*}\frac{\Gamma\mathbf{e}\times d\mathbf{L}^{**}}{4\pi l^2}, \tag{16.132}$$

where $$d\mathbf{L}^{**}=\frac{a}{\omega}\frac{\mathbf{r}_\varrho d\vartheta}{(\mathbf{e}\mathbf{r}_\varrho)}. \tag{16.133}$$

A positive direction of movement along curve L^* corresponds to an increase of ϑ on the $\rho = \rho_2(\vartheta)$ branch of that curve and a decrease of ϑ on the $\rho = \rho_1(\vartheta)$ branch. Substituting Eq. (16.133) into Eq. (16.132) and unifying the integrals taken along the two branches into one expression; it is possible to present the results in the following final form:

$$\mathbf{v}_1=\int_{\vartheta=-\infty}^{\vartheta=\psi} d\vartheta \int_{\varrho=\varrho_1(\vartheta)}^{\varrho=\varrho_2(\vartheta)} \frac{E^*\Gamma\mathbf{e}\times\mathbf{e}_\varrho}{4\pi l^2(\mathbf{e}\cdot\mathbf{e}_\varrho)}. \tag{16.134}$$

The wave component $\mathbf{v}_2$ of the gas velocity can be found in an analogical way. It should be noted that for the more important case of the flat wake, velocities at the airscrew disc are simply $\mathbf{v}_2 = 0$.

CHAPTER XVII

RESULTS OF WORK ON THE THEORY OF AIRSCREWS

1. EXPERIMENTAL CONFIRMATION OF BASIC ASSUMPTIONS AND REPRESENTATIONS OF THE VORTEX THEORY

The most convincing confirmation of the validity of the vortex-type interaction between airscrew blades on the surrounding medium is obtained through visualization of the flow in the wake. The original investigations should be credited to Flamm[83] who photographed free vortices springing from the blade tips where they are especially strong (Fig. 17.1). These Very interesting photographs show smoke streams passing through the airscrew: filaments passing close to the trailing tip vortices form curls indicating the positions of the cores of the helical vortex (Fig. 17.2)[97]. The region of separated flow behind the propeller forms a helical cavity having a few coils (Fig. 17.3)[96].

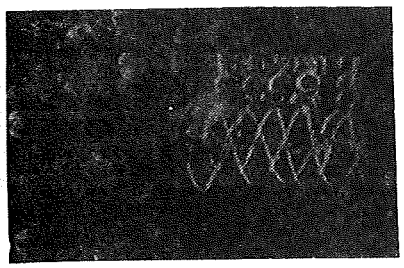

Figure 17.1

Figure 17.2

In the case of coaxial airscrews, no clear picture of vortices has been obtained. This is due to the fact that the vortices generated by the leading airscrew, once chopped up by the blades of the following one do not become reestablished. Instead, vortex rings are formed and the flow becomes unsteady (Fig. 17.4)[100]. If the propeller is located in front of a wing, the slipstream generated by the propeller changes its shape downstream of the wing. Parts of this slipstream, once separated by the wing, remain separated (Fig. 17.5)[101].

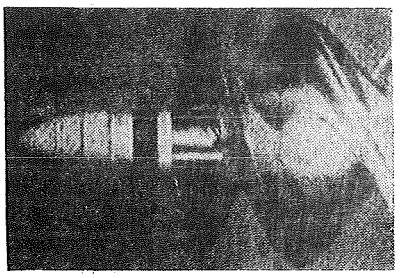

Figure 17.3

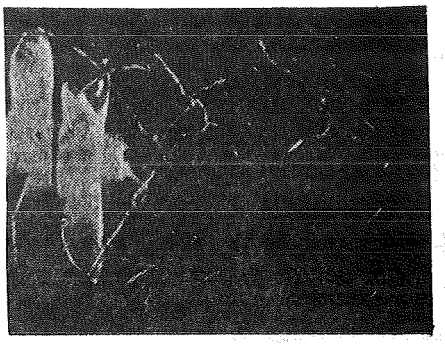

Figure 17.4

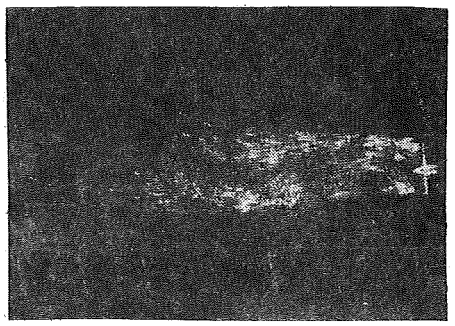

Figure 17.5

It can be seen, hence, that an approach based on systems of free (trailing) helical vortices is fully justified; not only for isolated airscrews, but also for those cases where a body of revolution is located on the propeller axis. However, if free vortices are chopped up by a wing or blades of another propeller, then this approach is justified only for those cases when the influence of distant vortices is insignificant. A direct verification of the validity of the application of two-dimensional airfoil characteristics in the case of unstalled flow is obtained by comparing pressure distributions at various blade stations for rotating and stationary airscrews when values of the c_{y_1} coefficients are the same (Fig. 17.6). A comparison of pressure distributions predicted on the basis of the flow of ideal fluid with those obtained experimentally is quite satisfactory (Fig. 17.7). Also, an agreement can be shown between pressure distributions computed for flat airfoil cascades and those experimentally obtained for axial compressors (Fig. 17.8)[35]. An agreement can also be shown for the same airfoil sections at various blade stations. Similar results were obtained on models

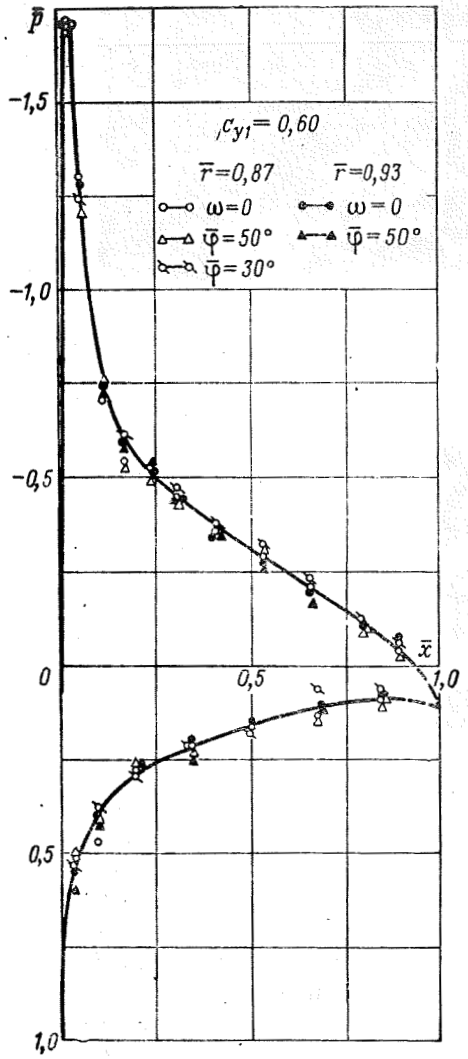

Figure 17.6

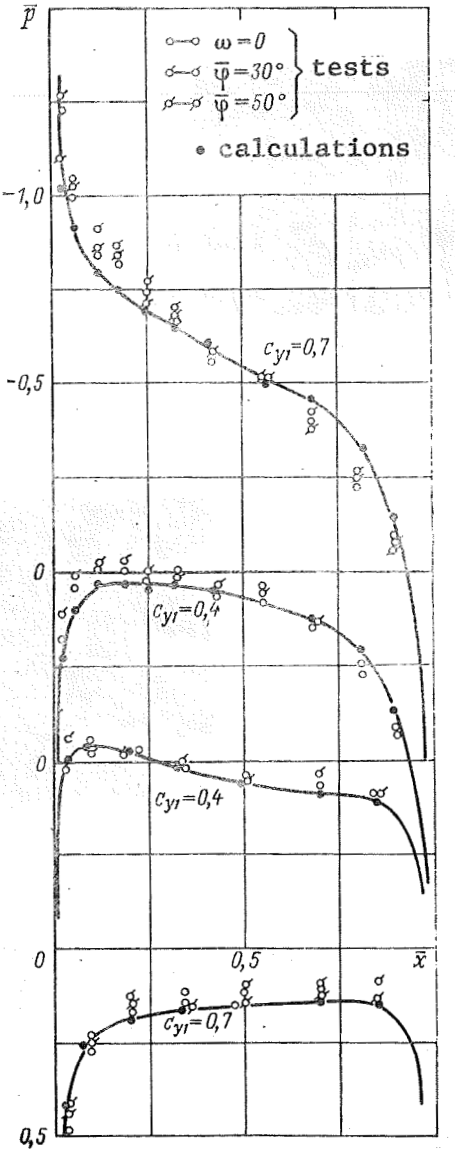

Figure 17.7

of lifting rotors in the horizontal regime of flight[3]. Experimental data covering wide ranges of Mach numbers *(up to M = 1,1)*, blade pitch angles, and advance ratio values for full-scale propellers, propeller models, and axial compressors, verified the applicability of the two-dimensional approach. The appearance of local supersonic flow in the thicker regions of airscrew blade airfoils was no different than the same phenomenon encountered on fixed wings having identical airfoil sections (Fig. 17.9). The permissibility of neglecting the influence of yaw angle was confirmed by investigations of pressure

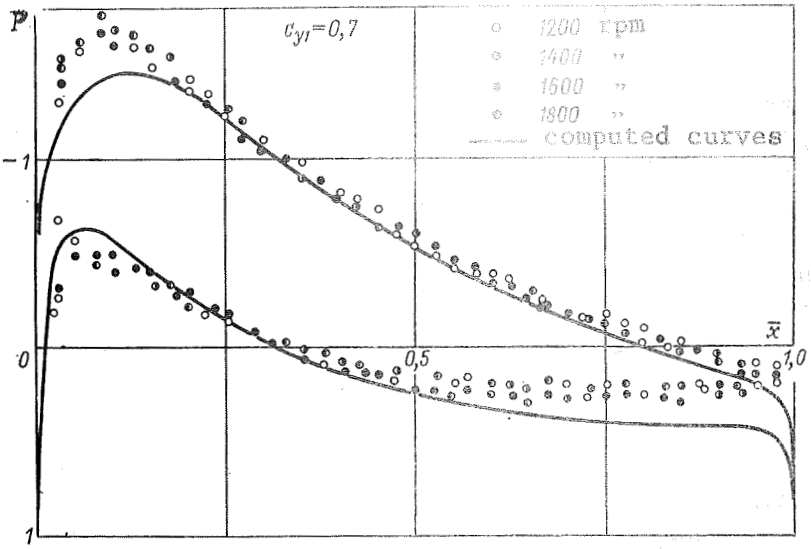

Figure 17.8

distribution on a straight wing up to a yaw angle of $\sim 45°$. However, the angle of yaw has an influence on the incipience of stall. The two-dimensional approach is not applicable to blade sections close to the tip and the spinner. Rotation of the propeller has no significant influence on the stall of sections located close to the blade tips (Fig. 17.10). Observation also showed no significant influence of rotation on the inception of stall for other blade stations.

The stall picture of a rotating blade is completely different from that of a wing. In the region of separation, the velocity of flow is low, and conditions are similar to the static ones. Consequently, pressure is determined from the condition of equilibrium of force generated by the pressure gradient and the centrifugal force acting on the air stream entrained due to rotation. This means that

$$\frac{dp}{dr} = \varrho\omega^2 r.$$

Assuming that the flow is adiabatic in the stall (separation) region, this condition leads to[47]

$$\frac{p(r)}{p(R)} = \left[1 - \frac{\varkappa - 1}{2}\left(\frac{\omega}{a}\right)^2 (R^2 - r^2)\right]^{\frac{\varkappa}{\varkappa-1}} \quad \left(\varkappa = \frac{c_p}{c_v}\right).$$

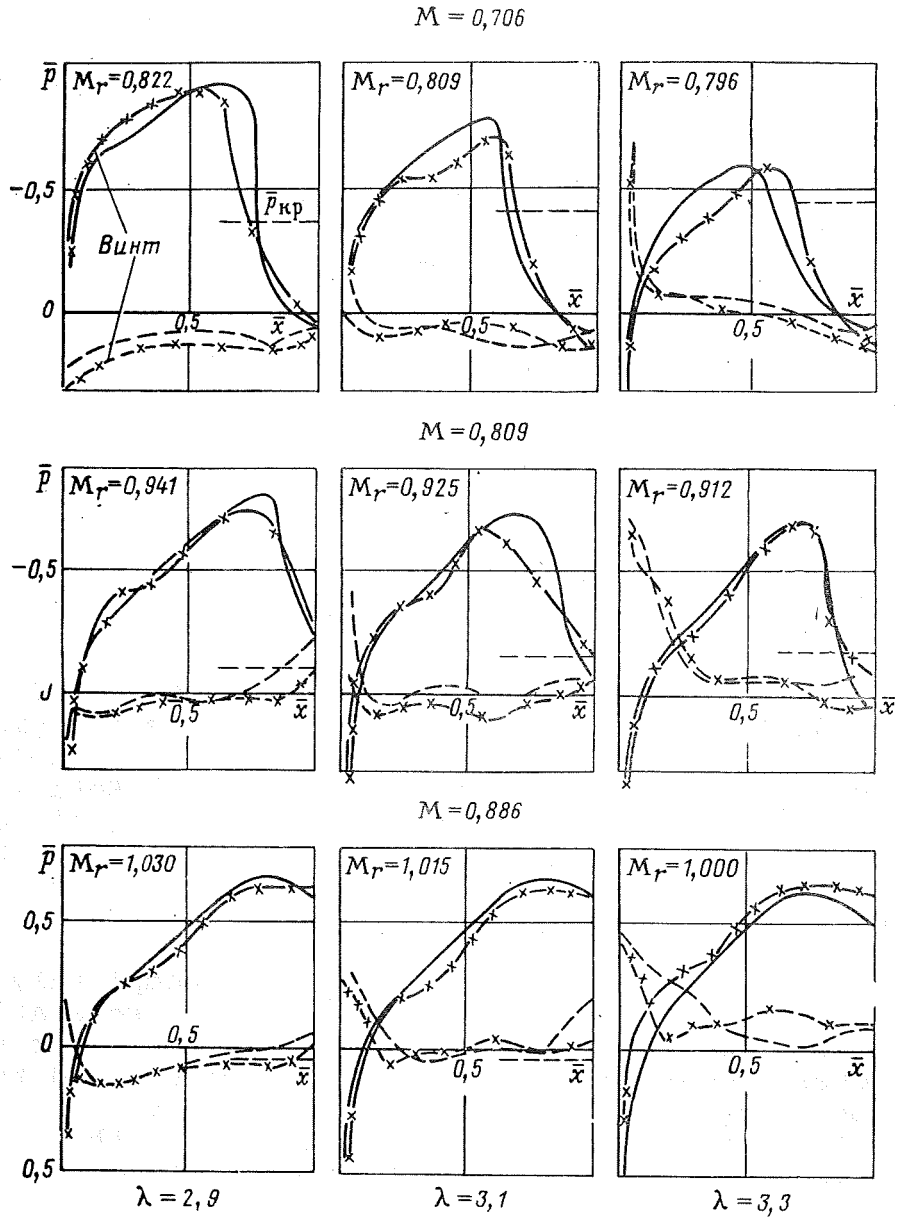
M = 0,706
$\bar{p}$
M_r=0,822
M_r=0,809
M_r=0,796
−0,5
0
$\bar{p}_{кр}$
Винт
0,5
$\bar{x}$
M = 0,809
M_r=0,941
M_r=0,925
M_r=0,912
M = 0,886
M_r=1,030
M_r=1,015
M_r=1,000
λ = 2,9
λ = 3,1
λ = 3,3

Figure 17.9

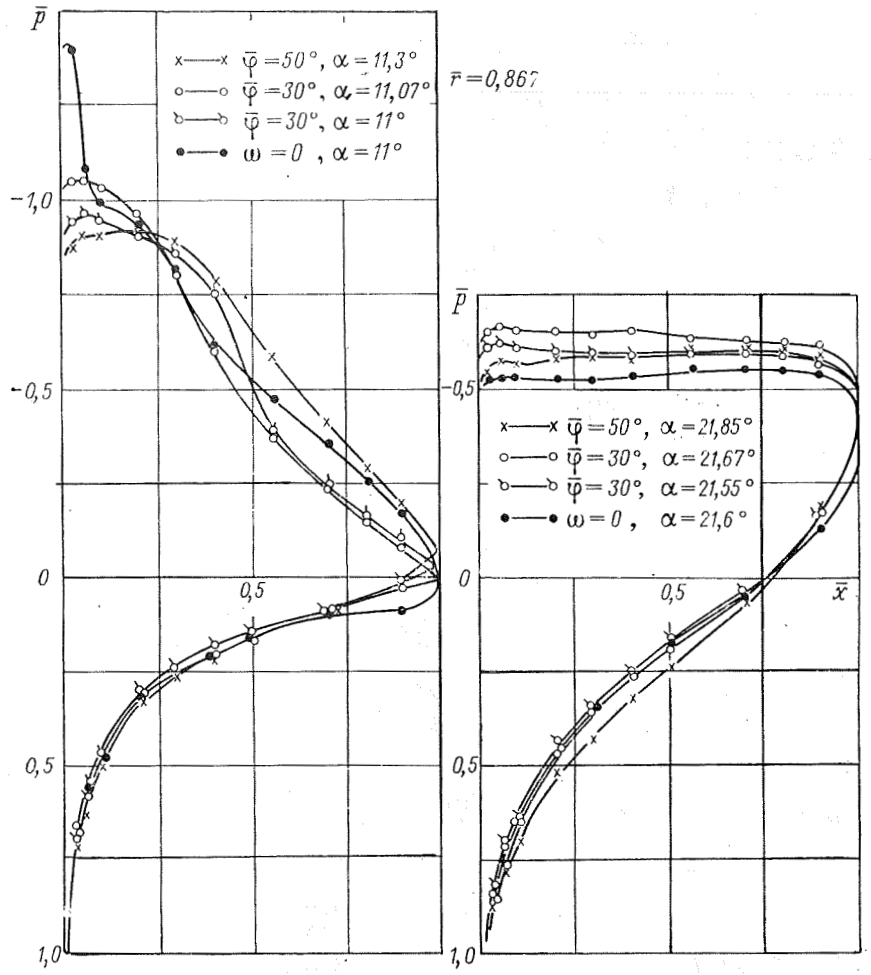

Figure 17.10

Flow in the stalled region is similar to the flow in a rotating tube, the outer end of which is open and the internal one is on the axis of rotation. Reduction of pressure on the upper surface of the rotating blade (inboard sections) considerably exceeds that on a stationary blade. With increasing angle of attack, the reduced pressure region gradually spreads over the whole chord (Figs. 17.11-17.13) and becomes close to that calculated by the above formula. For the inner sections of the rotating blade, the linear character of the $c_{y1}(\alpha)$ dependence is maintained up to higher values of the angles of attack than for a wing, and the c_{y1} values stop increasing only when the reduced pressure area is extended over the whole chord. For stalled flow, it is obvious that the hypothesis of the

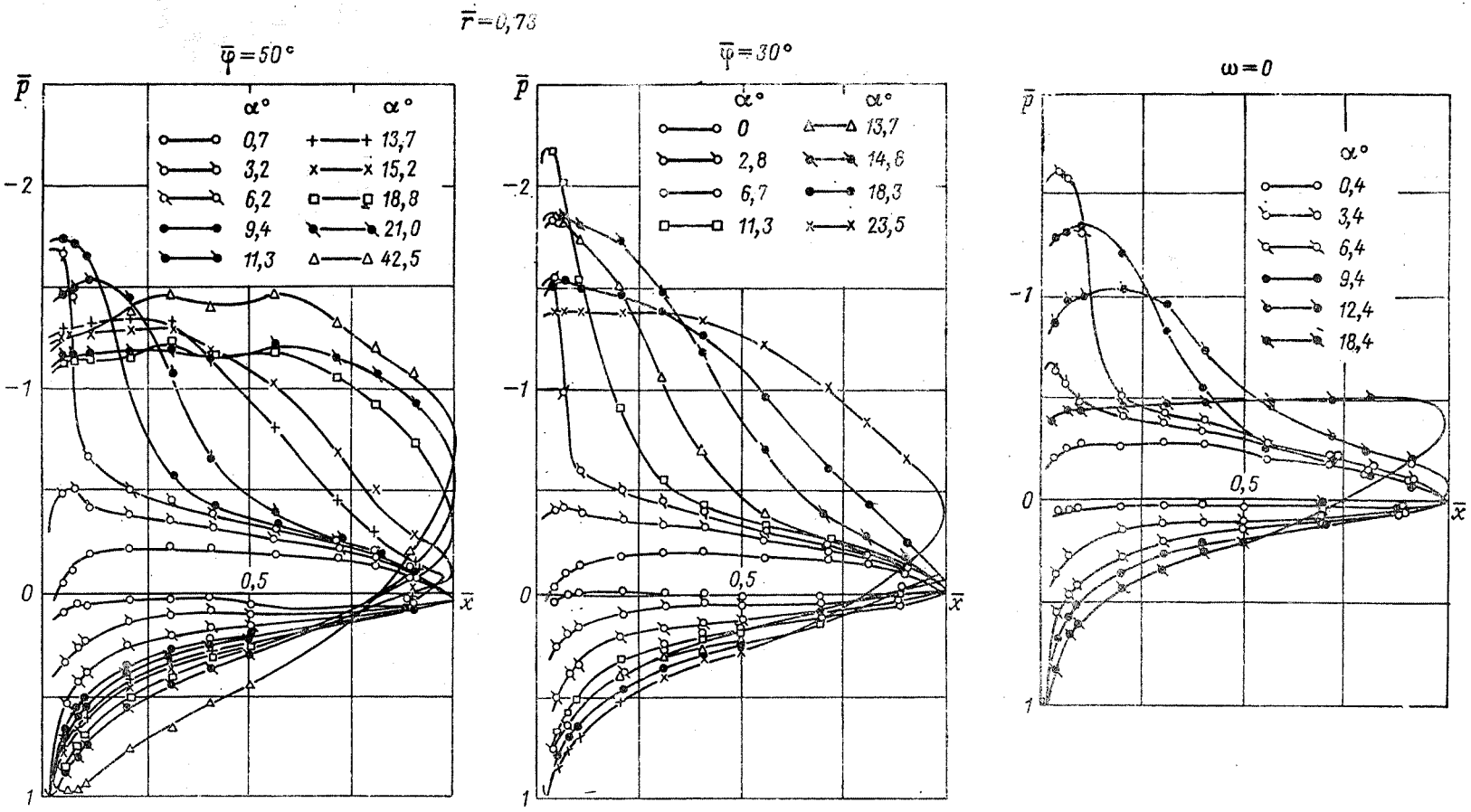
$\bar{r}=0,73$
$\bar{\varphi}=50°$
$\bar{p}$
α°
α°
0,7
3,2
6,2
9,4
11,3
13,7
15,2
18,8
21,0
42,5
-2
-1
0
1
0,5
$\bar{x}$
$\bar{\varphi}=30°$
$\bar{p}$
α°
α°
0
2,8
6,7
11,3
13,7
14,6
18,3
23,5
-2
-1
0
1
0,5
$\bar{x}$
ω=0
$\bar{p}$
α°
0,4
3,4
6,4
9,4
12,4
18,4
-1
0
1
0,5
$\bar{x}$

Figure 17.11

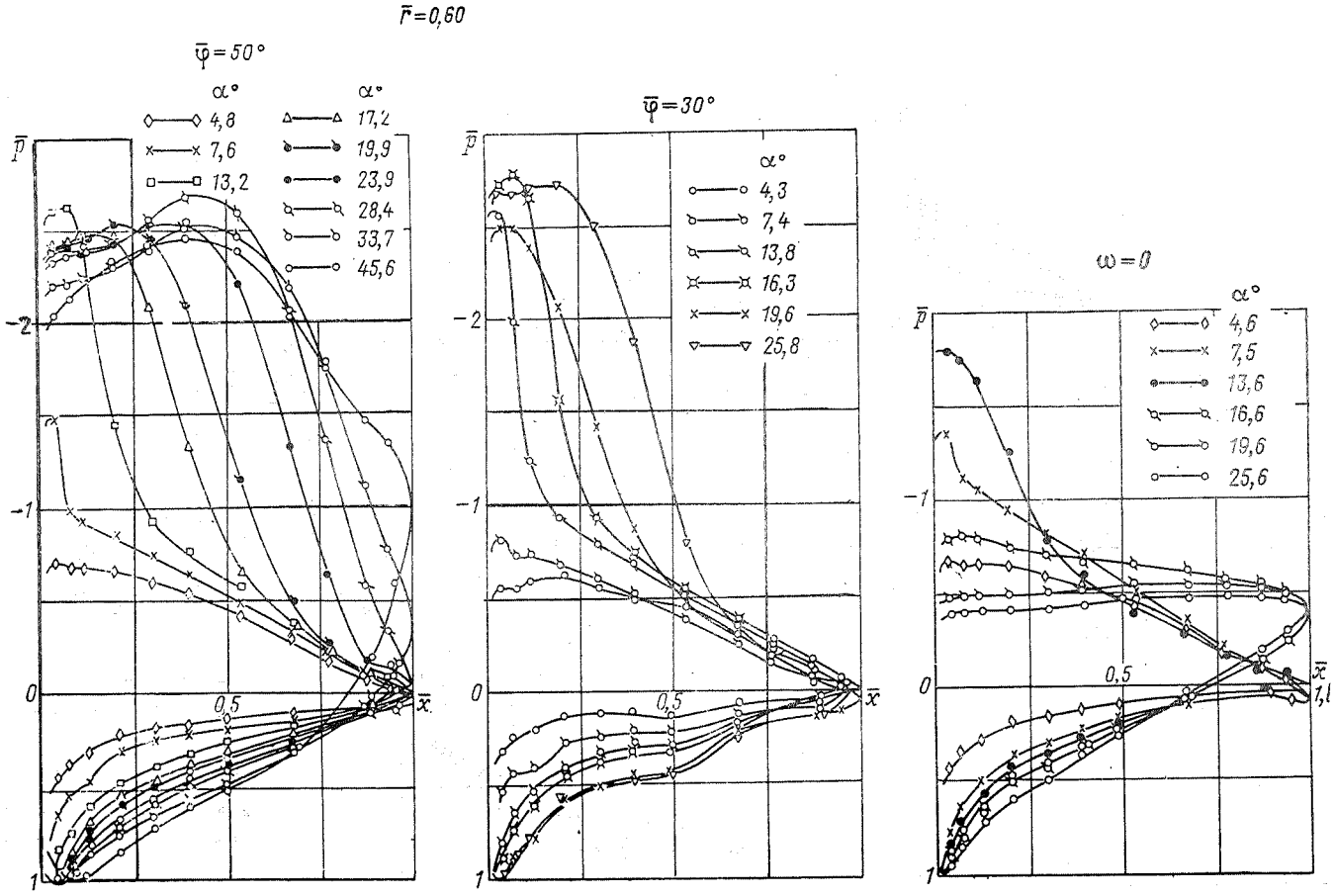
$\bar{r}=0,60$
$\bar{\varphi}=50°$
α°
4,8
7,6
13,2
17,2
19,9
23,9
28,4
33,7
45,6
$\bar{p}$
$\bar{x}$
$\bar{\varphi}=30°$
α°
4,3
7,4
13,8
16,3
19,6
25,8
$\omega=0$
α°
4,6
7,5
13,6
16,6
19,6
25,6
0,5
7,1

Figure 17.12

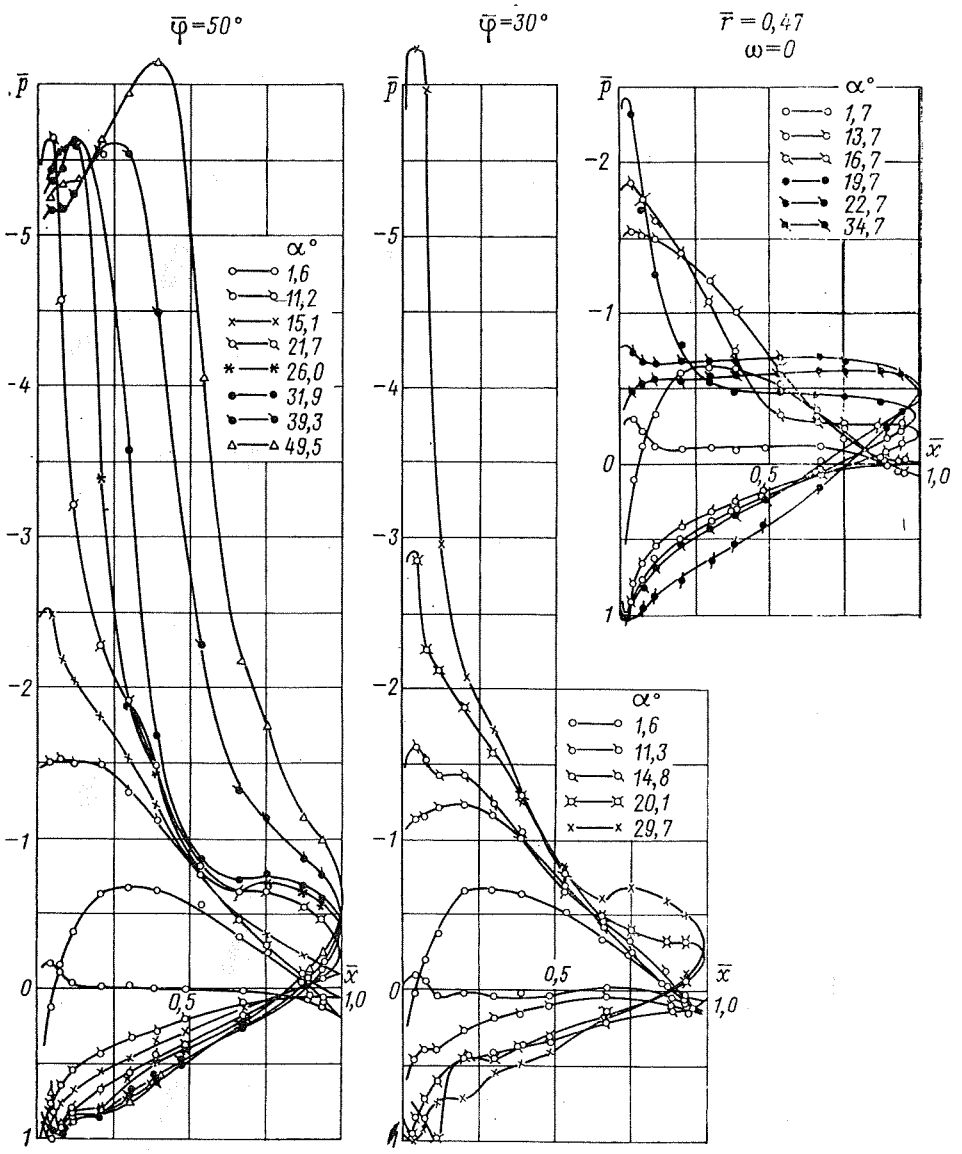
$\bar{\varphi}=50°$
$\bar{\varphi}=30°$
$\bar{r}=0,47$
$\omega=0$
$\bar{p}$
$\bar{x}$
$\alpha°$
1,6
11,2
15,1
21,7
26,0
31,9
39,3
49,5
11,3
14,8
20,1
29,7
1,7
13,7
16,7
19,7
22,7
34,7
0,5
1,0

Figure 17.13

two-dimensional flow is not applicable. A completely satisfactory agreement between performance (thrust, power, etc.) predicted by the vortex theory with those experimentally measured further confirms the reliability of the theory for the regimes of unstalled flow[63]. However, for cases of stalled flow, only approximate evaluations are possible at the present time.

2. COMPUTATION OF INDUCED VELOCITY

Computation of velocities induced by a vortex surface, especially at points located on the surface itself, represents the most difficult task in the airscrew analysis. The necessary solutions can be obtained in an elementary way only for the most simple cases of straight-line vortices. In the case of helical vortices, it is necessary to take advantage of special functions either directly, or with the help of expansion into series[63]. Time-average induced velocity can be calculated more easily, as in the case of $\alpha_B = \pi/2$ for which N.E. Joukowsky obtained simple formulae[41].

Let us consider a vortex surface, given either in a vectorial form $\mathbf{r} = \mathbf{r}(u,v)$, or described by coordinates: $\xi = \xi(u,v)$, $\eta = \eta(u,v)$, $\zeta = \zeta(u,v)$. Velocity circulation Γ, determined along a closed contour, penetrating the vortex surface at one point only, will also be a functions of parameters u and v, which means that $\Gamma = \Gamma(u,v)$. In the computation of induced velocity $\mathbf{v}$ at point (x, y, z), one may take advantage of the potential of a twin layer with the help of which we obtain

$$v_x = -\frac{1}{4\pi}\iint\left\{\eta_u\zeta_v-\zeta_u\eta_v-\frac{3(x-\xi)}{l^2}[(\eta_u\zeta_v-\zeta_u\eta_v)(x-\xi)+\right.$$
$$\left.+(\zeta_u\xi_v-\xi_u\zeta_v)(y-\eta)+(\xi_u\eta_v-\eta_u\xi_v)(z-\zeta)]\right\}\frac{\Gamma du\,dv}{l^3}, \tag{17.1}$$

$$v_y = -\frac{1}{4\pi}\iint\left\{\zeta_u\xi_v-\xi_u\zeta_v-\frac{3(y-\eta)}{l^2}[(\eta_u\zeta_v-\zeta_u\eta_v)(x-\xi)+\right.$$
$$\left.+(\zeta_u\xi_v-\xi_u\zeta_v)(y-\eta)+(\xi_u\eta_v-\eta_u\xi_v)(z-\zeta)]\right\}\frac{\Gamma du\,dv}{l^3}, \tag{17.2}$$

$$v_z = -\frac{1}{4\pi}\iint\left\{\xi_u\eta_v-\eta_u\xi_v-\frac{3(z-\zeta)}{l^2}[(\eta_u\zeta_v-\zeta_u\eta_v)(x-\xi)+\right.$$
$$\left.+(\zeta_u\xi_v-\xi_u\zeta_v)(y-\eta)+(\xi_u\eta_v-\eta_u\xi_v)(z-\zeta)]\right\}\frac{\Gamma du\,dv}{l^3}. \tag{17.3}$$

It is also possible to start from the Biot-Savart formula.

A vortex filament represents a line of $\Gamma(u, v) = const$; consequently, along this line, $\Gamma_u\, du + \Gamma_v\, dv = 0$. As a result of this, elements of the vortex filament can be described in the following form:

$$d\mathbf{l} = \mathbf{r}_u du + \mathbf{r}_v dv = \frac{du}{\Gamma_v}(\mathbf{r}_u\Gamma_v - \mathbf{r}_v\Gamma_u).$$

Integration with respect to parameter u represents an integration along the vortex filament. With an increment of parameter v, circulation Γ also increases by $\Gamma_v dv$. Integration with respect to all values of u, v corresponding to the vortex surface gives induced velocity

$$d\mathbf{v} = \frac{du\, dv}{4\pi l^3}[\mathbf{r}_u\Gamma_v - \mathbf{r}_v\Gamma_u, \mathbf{l}] \tag{17.4}$$

or, in component form,

$$v_x = \frac{1}{4\pi}\iint \{\Gamma_v[\eta_u(z-\zeta) - \zeta_u(y-\eta)] - \Gamma_u[\eta_v(z-\zeta) - \zeta_v(y-\eta)]\}\frac{du\, dv}{l^3}, \tag{17.5}$$

$$v_y = \frac{1}{4\pi}\iint \{\Gamma_v[\zeta_u(x-\xi) - \xi_u(z-\zeta)] - \Gamma_u[\zeta_v(x-\xi) - \xi_v(z-\zeta)]\}\frac{du\, dv}{l^3}, \tag{17.6}$$

$$v_z = \frac{1}{4\pi}\iint \{\Gamma_v[\xi_u(y-\eta) - \eta_u(x-\xi)] - \Gamma_u[\xi_v(y-\eta) - \eta_v(x-\xi)]\}\frac{du\, dv}{l^3}. \tag{17.7}$$

In agreement with general assumptions of the theory of small perturbations, we will assume that the bound as well as the free (trailing) vortices are located on a surface generated by a straight-line segment of length R. This segment rotates around axis x with an angular velocity ω and translates at a speed V (Fig. 17.14). This surface can be presented in a parametric form as follows:

$$\xi = \lambda(\psi - \vartheta)\sin\alpha_в,\quad \eta = \lambda(\psi - \vartheta)\cos\alpha_в + \varrho\cos\vartheta,\quad \zeta = \varrho\sin\vartheta. \tag{17.8}$$

Here, $\lambda = V/\omega R$, $r_0 \leq \rho \leq 1$, while ρ and ϑ are the parameters. It will be assumed that the positive direction of the normals is toward axis x. Substituting into Eqs. (17.1)-(17.3), expressions for coordinates of a point on the vortex surface,

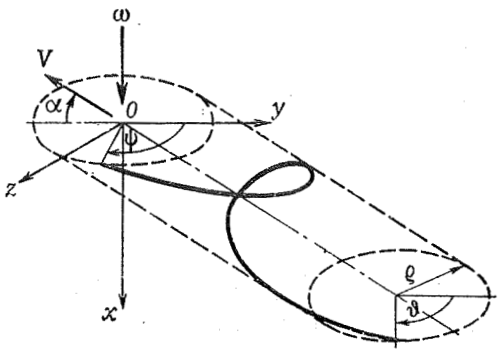

Figure 17.14

we obtain

$$v_x = -\iint \left\{\varrho + \lambda \cos\alpha_в \sin\vartheta - \frac{3[x - \lambda(\psi - \vartheta)\sin\alpha_в]}{l^2}[\varrho x + \lambda x \cos\alpha_в \sin\vartheta - \right.$$
$$\left. - \lambda y \sin\alpha_в \sin\vartheta + \lambda z \sin\alpha_в \cos\vartheta - \varrho\lambda(\psi - \vartheta)\sin\alpha_в]\right\} \frac{\Gamma d\varrho d\vartheta}{l^3}, \tag{17.9}$$

$$v_y = \iint \left\{\lambda \sin\alpha_в \sin\vartheta + \frac{3[y - \lambda(\psi - \vartheta)\cos\alpha_в - \varrho\cos\vartheta]}{l^2}[\varrho x + \right.$$
$$\left. + \lambda x \cos\alpha_в \sin\vartheta - \lambda y \sin\alpha_в \sin\vartheta + \lambda z \sin\alpha_в \cos\vartheta - \lambda\varrho(\psi - \vartheta)\sin\alpha_в]\right\} \frac{\Gamma d\varrho d\vartheta}{l^3}, \tag{17.10}$$

$$v_z = -\iint \left\{\lambda \sin\alpha_в \cos\vartheta - \frac{3(z - \varrho\sin\vartheta)}{l^2}[\varrho x + \lambda x \cos\alpha_в \sin\vartheta - \right.$$
$$\left. - \lambda y \sin\alpha_в \sin\vartheta + \lambda z \sin\alpha_в \cos\vartheta - \lambda\varrho(\psi - \vartheta)\sin\alpha_в]\right\} \frac{\Gamma d\varrho d\vartheta}{l^3}. \tag{17.11}$$

According to Eqs. (17.5)-(17.7), we have

$$v_x = \iint \{\Gamma_\vartheta [z\cos\vartheta - y\sin\vartheta + \lambda(\psi - \vartheta)\cos\alpha_в \sin\vartheta] - \Gamma_\varrho [\varrho^2 - \varrho(z\sin\vartheta + $$
$$+ y\cos\vartheta) + \lambda\varrho\cos\alpha_в((\psi - \vartheta)\cos\vartheta + \sin\vartheta) - \lambda z\cos\alpha_в]\} \frac{d\varrho d\vartheta}{l^3}. \tag{17.12}$$

$$v_y = \iint \{\Gamma_\vartheta \sin\vartheta [x - \lambda(\psi - \vartheta)\sin\alpha_в] - \Gamma_\varrho [\varrho x\cos\vartheta + \lambda z\sin\alpha_в - $$
$$- \varrho\lambda\sin\alpha_в(\sin\vartheta + (\psi - \vartheta)\cos\vartheta)]\} \frac{d\varrho d\vartheta}{l^3}, \tag{17.13}$$

$$v_z = -\iint \{\Gamma_\vartheta \cos\vartheta [x - \lambda(\psi - \vartheta)\sin\alpha_в] + \Gamma_\varrho [\lambda(x\cos\alpha_в - y\sin\alpha_в) + \\ + \lambda\varrho\sin\alpha_в(\cos\vartheta - (\psi - \vartheta)\sin\vartheta) + \varrho x\sin\vartheta]\} \frac{d\varrho d\vartheta}{l^3}, \qquad (17.14)$$

where $$l^2 = x^2 + y^2 + z^2 + \varrho^2 + \lambda^2(\psi - \vartheta)^2 + 2\lambda(\psi - \vartheta)(\varrho\cos\alpha_в\cos\vartheta - \\ - x\sin\alpha_в - y\cos\alpha_в) - 2\varrho(y\cos\vartheta + z\sin\vartheta).$$

Velocities induced by various blades can be obtained by substituting $\psi = \psi_1 + (2\pi/n)(n-1)$, $n = 1, 2, \ldots, k$. The tangent component of velocity shows a discontinuity on the vortex surface itself (in the computation of velocity on a vortex surface, it is generally necessary to use the limit approach)[61].

In those particular cases when there is no need to compute derivatives of Γ_ϱ, Γ, Eqs. (17.9)-(17.11) may have an advantage over Eqs. (17.12)-(17.14). For computation of velocities on the vortex surface, Eqs. (17.12)-(17.14) are more suitable, especially when circulation is presented as a sum of analytic functions. The basic difficulty associated with the computation of integrals in those formulae consists of the fact that the denominator is related in a complicated form to the variable of integration. It is somewhat easier to compute the time-average induced velocity generated by the free (trailing) vortices (which begin in the yz plane). In order to compute components of the average velocity, it is necessary to integrate Eqs. (17.12)-(17.14) with respect to ψ from 0 to 2π. Since circulation of free (trailing) vortices depends only on coordinates ρ and ϑ and not on ψ, it is permissible to integrate; first, with respect to ψ from ϑ to ∞ and then, to integrate with respect to ϑ from 0 to 2π. Upon performing the above operation, we obtain

$$\overline{v}_x = \frac{1}{2\pi\lambda}\int_{\varrho_0}^{1}\int_{0}^{2\pi}\left\{\Gamma_\vartheta\left[(z\cos\vartheta - y\sin\vartheta)\int_\vartheta^\infty \frac{d\lambda(\psi-\vartheta)}{l^3} + \right.\right. \\ + \cos\alpha_в\sin\vartheta\int_\vartheta^\infty \frac{\lambda(\psi-\vartheta)\,d\lambda(\psi-\vartheta)}{l^3}\Big] - \Gamma_\varrho\Big[(\varrho^2 - \varrho(z\sin\vartheta + y\cos\vartheta) + \\ + \varrho\lambda\cos\alpha_в\sin\vartheta - \lambda z\cos\alpha_в)\int_\vartheta^\infty \frac{d\lambda(\psi-\vartheta)}{l^3} + \qquad (17.15) \\ \left.\left. + \varrho\cos\alpha_в\cos\vartheta\int_\vartheta^\infty \frac{\lambda(\psi-\vartheta)\,d\lambda(\psi-\vartheta)}{l^3}\Big]\right\} d\varrho d\vartheta,$$

$$\overline{v}_y = \frac{1}{2\pi\lambda}\int_{\varrho_0}^{1}\int_{0}^{2\pi}\left\{\Gamma_\vartheta \sin\vartheta\left[x\int_{\vartheta}^{\infty}\frac{d\lambda(\psi-\vartheta)}{l^3} - \sin\alpha_в\int_{\vartheta}^{\infty}\frac{\lambda(\psi-\vartheta)\,d\lambda(\psi-\vartheta)}{l^3}\right] - \right.$$

$$- \Gamma_\varrho\left[(\varrho x\cos\vartheta + \lambda z\sin\alpha_в - \varrho\lambda\sin\alpha_в\sin\vartheta)\int_{\vartheta}^{\infty}\frac{d\lambda(\psi-\vartheta)}{l^3} - \right. \qquad (17.16)$$

$$\left.\left. - \varrho\sin\alpha_в\cos\vartheta\int_{\vartheta}^{\infty}\frac{\lambda(\psi-\vartheta)\,d\lambda(\psi-\vartheta)}{l^3}\right]\right\} d\varrho d\vartheta,$$

$$\overline{v}_z = -\frac{1}{2\pi\lambda}\int_{\varrho_0}^{1}\int_{0}^{2\pi}\left\{\Gamma_\vartheta\cos\vartheta\left[x\int_{\vartheta}^{\infty}\frac{d\lambda(\psi-\vartheta)}{l^3} - \sin\alpha_в\int_{\vartheta}^{\infty}\frac{\lambda(\psi-\vartheta)\,d\lambda(\psi-\vartheta)}{l^3}\right] + \right.$$

$$+ \Gamma_\varrho\left[(\lambda(x\cos\alpha_в - y\sin\alpha_в) + \lambda\varrho\sin\alpha_в\cos\vartheta + \varrho x\sin\vartheta)\int_{\vartheta}^{\infty}\frac{d\lambda(\psi-\vartheta)}{l^3} - \right. \qquad (17.17)$$

$$\left.\left. - \varrho\sin\alpha_в\sin\vartheta\int_{\vartheta}^{\infty}\frac{\lambda(\psi-\vartheta)\,d\lambda(\psi-\vartheta)}{l^3}\right]\right\} d\varrho d\vartheta.$$

where

$$\int_{0}^{\infty}\frac{d\lambda(\psi-\vartheta)}{l^3} = \frac{1}{l_0}(\varrho\cos\alpha_в\cos\vartheta - x\sin\alpha_в - y\cos\alpha_в + l_0)^{-1},$$

$$\int_{\vartheta}^{\infty}\frac{\lambda(\psi-\vartheta)\,d\lambda(\psi-\vartheta)}{l^3} = \frac{1}{l_0},$$

$$l_0^2 = x^2 + y^2 + z^2 + \varrho^2 - 2\varrho(y\cos\vartheta + z\sin\vartheta).$$

Parameter λ appears in Eqs. (17.15)-(17.17) as an explicit factor only. This corresponds to the resolution of vortices into circular and straight components[61]. Velocity induced by free vortices was examined in more detail for some particular cases which we are now going to consider.

AIRSCREWS EXPOSED TO AXIAL FLOW

In the case of $\alpha_в = \pi/2$, it is convenient to take advantage of expressions for the axial, peripheral, and radial velocity components. Defining these projections as v_a, v_t, v_r respectively, and the coordinates of the point at which

these velocities are computed as x, r, θ, we obtain

$$v_a=\iint \{\Gamma_\vartheta r\sin(\theta-\vartheta)-\varrho\Gamma_\varrho[\varrho-r\cos(\theta-\vartheta)]\}\frac{d\varrho d\vartheta}{l^3}, \tag{17.18}$$

$$v_t=\iint \{-\Gamma_\vartheta\cos(\theta-\vartheta)[x-\lambda(\psi-\vartheta)]+\Gamma_\varrho[\varrho\sin(\theta-\vartheta)(x-\lambda(\psi-\vartheta))+ +\lambda(r-\varrho\cos(\theta-\vartheta))]\}\frac{d\varrho d\vartheta}{l^3}, \tag{17.19}$$

$$v_r=-\iint \{\Gamma_\vartheta\sin(\theta-\vartheta)[x-\lambda(\psi-\vartheta)]+\Gamma_\varrho[\varrho\cos(\theta-\vartheta)(x- -\lambda(\psi-\vartheta))+\lambda\varrho\sin(\theta-\vartheta)]\}\frac{d\varrho d\vartheta}{l^3}, \tag{17.20}$$

$$l^2=[x-\lambda(\psi-\vartheta)]^2+r^2+\varrho^2-2\varrho r\cos(\theta-\vartheta).$$

As long as blade pitch angle remains constant, $\Gamma_\vartheta = 0$, and it is necessary to calculate velocity induced by the free vortices only. In this case, Eqs. (17.18)-(17.20) become substantially simplified:

$$v_a=-\int_{\varrho_0}^{1}\varrho\Gamma_\varrho d\varrho\int_{-\frac{x}{\lambda}}^{\infty}\frac{\varrho-r\cos(\tau-t)}{l^3}d\tau, \tag{17.21}$$

$$v_t=\lambda\int_{\varrho_0}^{1}\Gamma_\varrho' d\varrho\int_{-\frac{x}{\lambda}}^{\infty}\{r-\varrho[\cos(\tau-t)+\tau\sin(\tau-t)]\}\frac{d\tau}{l^3}, \tag{17.22}$$

$$v_r=-\lambda\int_{\varrho_0}^{1}\varrho\Gamma_\varrho d\varrho\int_{-\frac{x}{\lambda}}^{\infty}\frac{\sin(\tau-t)-\tau\cos(\tau-t)}{l^3}d\tau, \tag{17.23}$$

$$l^2=(\lambda\tau)^2+r^2+\varrho^2-2\varrho r\cos(\tau-t);\quad \tau=\psi-\vartheta-\frac{x}{\lambda};\quad t=\psi-\theta-\frac{x}{\lambda}.$$

The internal integrals can be presented in the following form:

$$\int_{-\frac{x}{\lambda}}^{\infty}f(\tau-t)d\tau=\int_{0}^{\infty}f(\tau-t)d\tau\pm\int_{0}^{\frac{|x|}{\lambda}}f(\tau+t)d\tau$$

and their values can then be tabulated.

Let us compute the induced velocity projection v_s on a tangent to the helical line passing through point (x, r, θ):

$$v_s = v_a \sin\beta - v_t \cos\beta =$$

$$= -\frac{\lambda}{\sqrt{\lambda^2 + r^2}} \int_{\varrho_0}^{1} \Gamma_\varrho d\varrho \int_{-\frac{x}{\lambda}}^{\infty} \frac{\varrho^2 + r^2 - 2\varrho r \cos(\tau - t) - \varrho r \tau \sin(\tau - t)}{l^3} d\tau =$$

$$= \frac{-\lambda}{\sqrt{\lambda^2 + r^2}} \int_{\varrho_0}^{1} \Gamma_\varrho d\varrho \int_{-\frac{x}{\lambda}}^{\infty} \left(l^2 - \frac{\tau}{2} \frac{dl^2}{d\tau} \right) \frac{d\tau}{l^3} = \qquad (17.24)$$

$$= -\frac{1}{\sqrt{\lambda^2 + r^2}} \int_{-\varrho_0}^{1} \Gamma_\varrho d\varrho \left(1 + \frac{x}{\sqrt{x^2 + \varrho^2 + r^2 - 2\varrho r \cos\left(t + \frac{x}{\lambda}\right)}} \right).$$

It can be seen from the above that there is no necessity to compute both internal integrals in Eqs. (17.21) and (17.22). It is sufficient to compute only one of them; for instance, the simpler one from Eq. (17.21) and then take advantage of Eq. (17.24) in determining v_t. If $x = 0$, or $x \to \infty$, and $\Gamma(1) = \Gamma(\rho_0) = 0$, then $v_s = 0$. Consequently, induced velocity $\sqrt{v_a^2 + v_t^2}$ must be perpendicular to the vortex surface passing through the considered point[63].

In the determination of integral

$$\int_0^{\tau} \frac{\varrho[\varrho - r\cos(\tau - t)]\, d\tau}{[(\lambda\tau)^2 + \varrho^2 + r^2 - 2\varrho r \cos(\tau - t)]^{3/2}}$$

the following parameters were introduced in order to reduce the volume of computations $\tilde{\rho} = \rho/r$ and $\mathrm{tg}\beta = \lambda/r$. It was shown that the accuracy of the earlier computations of T. Moriya and B.L. Minukhin[65, 67, 68] for parameters ρ, r, λ was not sufficient, as the scatter of points was too large[57]. Tables were developed[61] for function

$$i_t(\tilde{\varrho}, \mathrm{tg}\beta, t; \tau) = -\mathrm{tg}\beta \int_0^{\tau} \frac{\tilde{\varrho}[\tilde{\varrho} - \cos(\tau - t)]\, d\tau}{[(\tau\,\mathrm{tg}\beta)^2 + 1 + \tilde{\varrho}^2 - 2\tilde{\varrho}\cos(\tau - t)]^{3/2}}$$

and, as an illustration, Fig. 17.15 is shown.

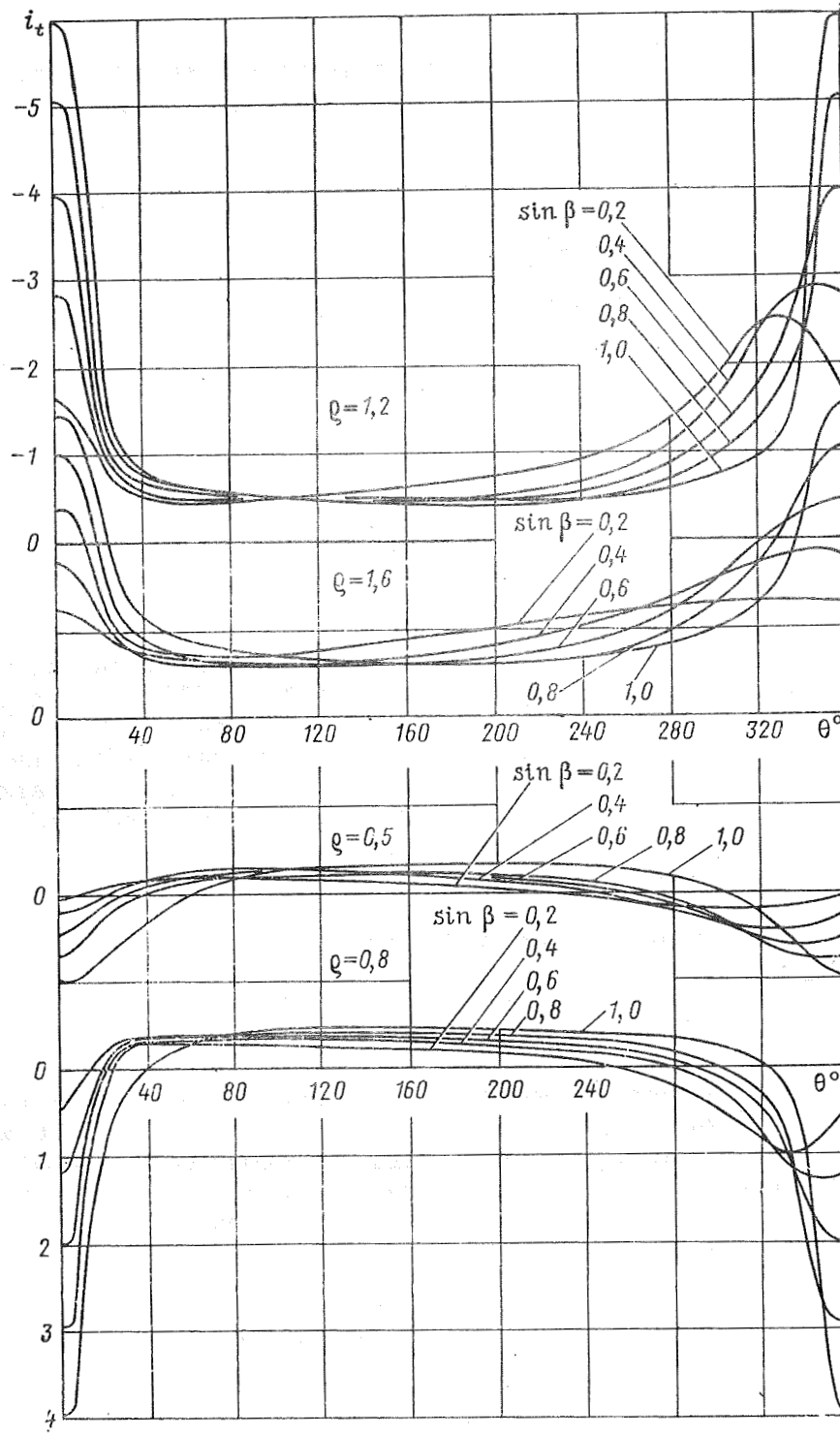
i_t
-5
-4
-3
-2
-1
0
sin β=0,2
0,4
0,6
0,8
1,0
ϱ=1,2
sin β=0,2
0,4
0,6
ϱ=1,6
0,8
1,0
40
80
120
160
200
240
280
320
θ°
sin β=0,2
0,4
ϱ=0,5
0,6
0,8
1,0
0
sin β=0,2
0,4
ϱ=0,8
0,6
0,8
1,0
40
80
120
160
200
240
θ°
1
2
3
4

Figure 17.15

When $\lambda \to 0$, then we have

$$i_t = -\lambda \sum_{n=0}^{\infty} \int_0^{2\pi} \frac{\varrho\,[\varrho - r\cos(\tau - t)]\,d\tau}{[\lambda^2(\tau + 2\pi n)^2 + r^2 + \varrho^2 - 2r\varrho\cos(\tau - t)]^{3/2}} =$$

$$= -\frac{1}{2\pi} \lim_{\lambda \to 0} \int_0^{\infty} \int_0^{2\pi} \frac{\varrho\,[\varrho - r\cos(\tau - t)]\,d\tau d\xi}{[(\lambda\tau + \xi)^2 + r^2 + \varrho^2 - 2\varrho r\cos(\tau - t)]^{3/2}} =$$

$$= -\frac{1}{2\pi} \int_0^{2\pi} \frac{\varrho\,[\varrho - r\cos(\tau - t)]\,d\tau}{r^2 + \varrho^2 - 2\varrho r\cos(\tau - t)} = \begin{cases} -1 & \text{for } \varrho > r, \\ -1/2 & \text{for } \varrho = r, \\ 0 & \text{for } \varrho < r. \end{cases}$$

Those limit values of function i_t coincide with the ones averaged over the circle. It can be seen from Fig. 17.15 that the higher the value of β, the more the discrepancy appears between the actual velocity and its average value.

Average velocity at an arbitrary point (x, r, θ) is computed by reducing i_t to the elliptic integrals[44]. If the translation of an airscrew differs only through a small angle, $(\pi/2) - \alpha_B$, from the axial direction, then for the sake of simplicity, it is possible to expand some subintegral function of Eqs. (17.12)-(17.17) into a power series with respect to $[(\pi/2) - \alpha_B]$ and to retain the first terms only. For example, for v_x at $x = 0$, from Eq. (17.12) we obtain

$$\frac{z\cos\vartheta - y\sin\vartheta + \lambda(\psi - \vartheta)\sin\vartheta\cos\alpha_B}{l^3} = \frac{r\sin(\theta - \vartheta)}{l_0^3} + \frac{\lambda(\psi - \vartheta)}{l_0^3}\left[\sin\vartheta - \right.$$

$$\left. - \frac{3r\sin(\theta - \vartheta)(\varrho\cos\vartheta - r\cos\theta)}{l_0^2}\right]\left(\frac{\pi}{2} - \alpha_B\right) + \ldots,$$

$$\frac{\varrho^2 - \varrho(z\sin\vartheta + y\cos\vartheta) + \lambda\cos\alpha_B[\varrho((\psi - \vartheta)\cos\vartheta + \sin\vartheta) - z]}{l^3} =$$

$$= \frac{\varrho[\varrho - r\cos(\theta - \vartheta)]}{l_0^3} + \frac{\lambda}{l_0^3}\left\{\varrho[(\psi - \vartheta)\cos\vartheta + \sin\vartheta] - r\sin\theta - \right.$$

$$\left. - \frac{3(\psi - \vartheta)(\varrho\cos\vartheta - r\cos\theta)\varrho[\varrho - r\cos(\theta - \vartheta)]}{l_0^2}\right\}(\pi/2 - \alpha_B) + \ldots,$$

$$l_0^2 = \lambda^2(\psi - \vartheta)^2 + r^2 + \varrho^2 - 2\varrho r\cos(\theta - \vartheta).$$

If the motion were unsteady, then circulation of the free (trailing) vortices would depend on ϑ and the preliminary integration with respect to ϑ needed for the development of tables would be possible only through the representation of the circulation as a series. In the case of circulation being independent of ϑ, computation of the average velocity is reduced to the evaluation of the elliptic integrals.

AIRSCREW EXPOSED TO OBLIQUE FLOW

This case is of great interest for helicopters and VTOL aircraft. As in the case of $\alpha_B = \pi/2$, early in the investigations, time-average induced velocity was computed for circulation constant with time.[61] It was found that average velocity varies considerably with the azimuth (Fig. 17.16), while the actual induced velocity fluctuates even more radically with the azimuth (Figure 17.17). With the increasing number of blades, actual velocity approaches the average. Nevertheless, it is obvious that in the determination of actual blade loads, it is not permissible to use average velocity. However, it is convenient to take advantage of the average velocity values when determining the mutual interference between airscrews and other components of aircraft. It may also be of interest for the particular case of horizontal flight of helicopters when $\alpha_B = 0$. L.S. Vil'dgrube indicated that under those conditions, averaging with respect to time leads to the presence of straight-line vortices only behind the airscrew (see Ch. II of this book). It was shown in Ref. 76 that for $\alpha_B = 0$, the average velocity can be expressed through the elliptic integrals.

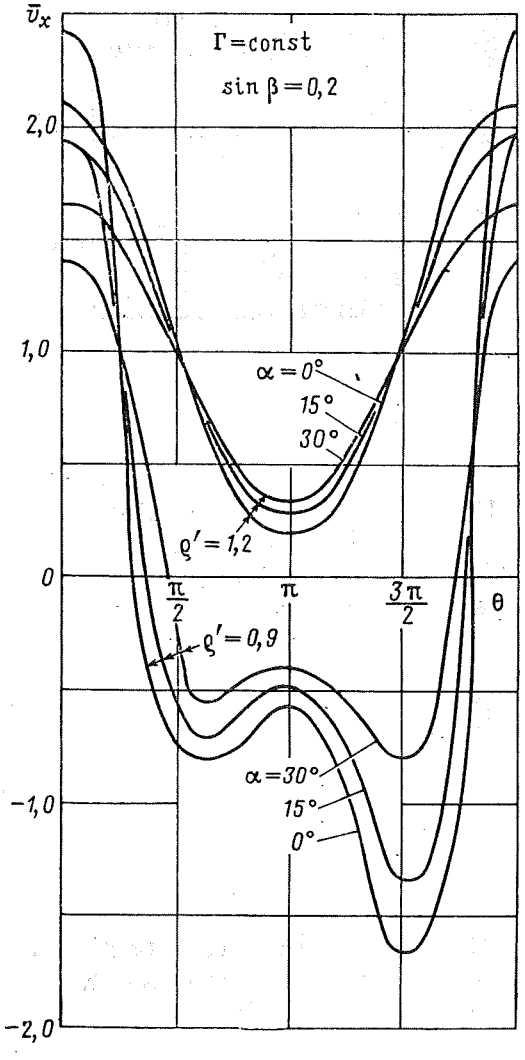

Figure 17.16

Determination of average induced velocity for an arbitrary angle α_B was worked out in Ref. 56 with the help of elliptic integrals. This approach also permitted computation of the induced velocity harmonics.

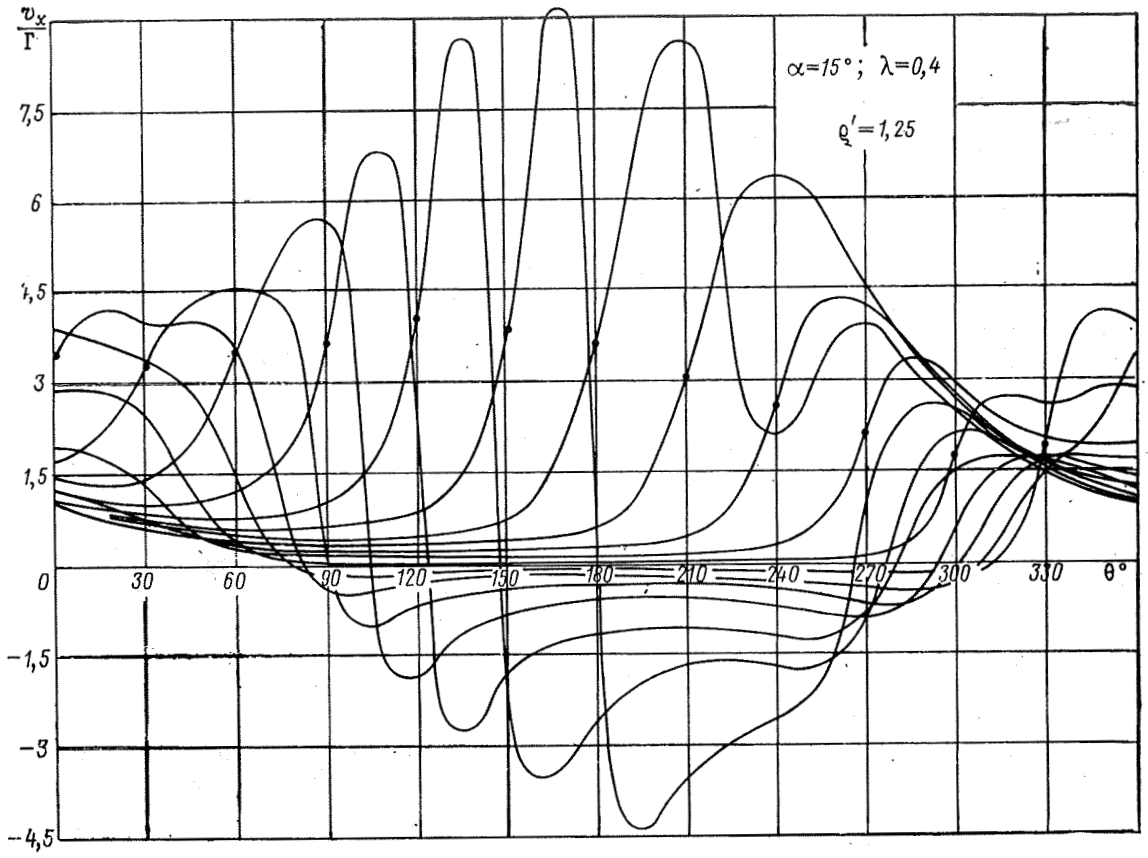

Figure 17.17

Integration with respect to ρ and ψ, required for the evaluation of the harmonic components, becomes possible through reduction to elliptic integrals. This is done by presenting circulation in the form of a double sum

$$\Gamma=\sum_m\sum_n(\Gamma_{mn}\sin m\psi+\Gamma'_{mn}\cos m\psi)\sin n\varphi,$$

where

$$\varphi=\arccos\frac{1+\varrho_0-2\varrho}{1-\varrho_0}.$$

In the case of small angles of attack, it is also possible to take advantage of the expansion into a power series with respect to α_B. For example, from Eq. (17.12) we obtain

$$\frac{z\cos\vartheta - y\sin\vartheta + \lambda(\psi-\vartheta)\sin\vartheta\cos\alpha_в}{l^3} = \frac{z\cos\vartheta - y\sin\vartheta + \lambda(\psi-\vartheta)\sin\vartheta}{l_0^3} +$$

$$+\frac{3\lambda(\psi-\vartheta)[z\cos\vartheta - y\sin\vartheta + \lambda(\psi-\vartheta)\sin\vartheta]\,x}{l_0^5}\alpha_в + \ldots,$$

$$\frac{\varrho[\varrho - z\sin\vartheta - y\cos\vartheta] + \lambda\cos\alpha_в[\varrho(\psi-\vartheta)\cos\vartheta + \sin\vartheta) - z]}{l^3} =$$

$$= \frac{\varrho(\varrho - z\sin\vartheta - y\cos\vartheta) + \lambda[\varrho((\psi-\vartheta)\cos\vartheta + \sin\vartheta) - z]}{l_0^3} +$$

$$+\frac{3\lambda(\psi-\vartheta)\,x}{l_0^5}\{\varrho(\varrho - z\sin\vartheta - y\cos\vartheta) + \lambda[\varrho((\psi-\vartheta)\cos\vartheta + \sin\vartheta) - z]\}\alpha_в + \ldots,$$

$$l_0^2 = x^2 + y^2 + \varrho^2 + \lambda^2(\psi-\vartheta)^2 + 2\lambda(\psi-\vartheta)(\varrho\cos\vartheta - y) - 2\varrho(y\cos\vartheta + z\sin\vartheta).$$

For a point located in the airscrew plane ($x = 0$), only terms starting with $\alpha_в^2$ appear in the expansion.

INDUCED VELOCITY ON THE VORTEX SURFACE

In order to calculate blade loads, it becomes necessary to determine velocity components perpendicular to the vortex surface.

$$v_n = \frac{1}{\sqrt{G(r,\theta) - F^2(\theta)}}\int\int\{\Gamma_\vartheta[(r\sin\tau + \lambda\cos\alpha\tau\sin(\theta-\tau))H(\varrho,\vartheta) +$$

$$+\lambda^2\sin^2\alpha_в\tau\cos\tau] - \Gamma_\varrho[(\varrho(\cos\tau + \tau\sin\tau) - r)\lambda^2\sin^2\alpha_в +$$

$$+H(\varrho,\vartheta)(\varrho(\varrho - r\cos\tau) + \lambda\cos\alpha_в(\varrho\sin(\theta-\tau) - r\sin\theta + \varrho\tau\cos(\theta-\tau)))]\}\times$$

$$\times\frac{d\varrho d\vartheta}{l^3}, \qquad (17.25)$$

$$l^2 = (\lambda\tau)^2 + \varrho^2 + r^2 - 2r\varrho\cos\tau + 2\lambda\tau\cos\alpha_в[\varrho\cos(\theta-\tau) - r\cos\theta],$$

$$G(r,\theta) = \lambda^2 + r^2 + 2\lambda r\cos\alpha_в\sin\vartheta,$$

$$H(r,\theta) = r + \lambda\cos\alpha_в\sin\theta,$$

$$F(\theta) = -\lambda\cos\alpha_в\cos\theta.$$

Assuming that $\varepsilon = \rho - r$ and $\tau = \theta - \vartheta$ may be considered as small quantities, Eq. (17.25) will be integrated in order to isolate the singularities. It will be assumed that circulation and its derivatives are represented by continuous functions, while the circulation itself can be expressed in the following form:

$$\Gamma_\vartheta = \Gamma_\theta + \Gamma_{\theta\theta}\tau + \Gamma_{\theta r}\varepsilon + \ldots,\quad \Gamma_\varrho = \Gamma_r + \Gamma_{r\theta}\tau + \Gamma_{rr}\varepsilon + \ldots,$$

where coefficients Γ_{ij} are functions of r and θ. Subintegral functions are now expanded into series, where only those terms are maintained which become infinite either for a point located inside of the region of integration $-\Delta \leq \tau \leq \Delta$ (Δ being a small but non-zero quantity), or for a point located near the limit of the region of integration; i.e., for $-\delta \leq \tau \leq \Delta$, where the small quantity δ may become zero (the computed point approaches the limit of the region of integration). In the first case, we obtain

$$v_n = -2\int\left\{\frac{F(\theta)\Gamma_\theta/\sqrt{G(r,\theta)}-\sqrt{G(r,\theta)}\,\Gamma_r}{\varepsilon\sqrt{G(r,\theta)-F^2(\theta)}}-\right.$$
$$-\left[F(\theta)\Gamma_\theta\left(\frac{H(r,\theta)}{\sqrt{G(r,\theta)-F^2(\theta)}}-\frac{3r\sqrt{G(r,\theta)-F^2(\theta)}}{2G(r,\theta)}\right)-\right. \qquad (17.26)$$
$$\left.\left.-(\Gamma_{\theta\theta}+r\Gamma_r/2)\sqrt{G(r,\theta)-F^2(\theta)}\right]\frac{\ln|\varepsilon|}{G^{3/2}(r,\theta)}\right\}d\varepsilon,$$

In particular, if $\alpha = \pi/2$, then $\Gamma_\theta = \Gamma_{\theta\theta} = 0$, and

$$v_n = 2\int\Gamma_r\left[\frac{1}{\varepsilon}-\frac{r\ln|\varepsilon|}{2(\lambda^2+r^2)}\right]d\varepsilon. \qquad (17.27)$$

Singularities $1/\varepsilon$, $\ln|\varepsilon|$ can be integrated.

In the second case,

$$v_n = -\int\left\{\frac{1}{\sqrt{G(r,\theta)-F^2(\theta)}}\left[\frac{\Gamma_\theta F_\theta(\theta)/\sqrt{G(r,\theta)}-\Gamma_r\sqrt{G(r,\theta)}}{\varepsilon}+\right.\right.$$
$$+\frac{(\Gamma_\theta F(\theta)-\Gamma_r G(r,\theta))\delta}{\varepsilon\sqrt{G(r,\theta)\delta^2+2F(\theta)\delta\varepsilon+\varepsilon^2}}+\frac{\Gamma_\theta-F(\theta)\Gamma_r}{\sqrt{G(r,\theta)\delta^2+2F(\theta)\delta\varepsilon+\varepsilon^2}}\left.\right]-$$
$$-\left[F(\theta)\Gamma_\theta\left(\frac{H(r,\theta)}{\sqrt{G(r,\theta)-F^2(\theta)}}-\frac{3r\sqrt{G(r,\theta)-F^2(\theta)}}{2G(r,\theta)}-\right.\right. \qquad (17.28)$$
$$\left.\left.-(\Gamma_{\theta\theta}+r\Gamma_r/2)\sqrt{G(r,\theta)-F^2(\theta)}\right]\frac{\ln|\varepsilon|}{G^{3/2}(r,\theta)}\right\}d\varepsilon.$$

The remaining part of the subintegral function has a finite value for both $\varepsilon \to 0$ and $\delta \to 0$. In Eq. (17.28), the term $[G(r,\theta)\delta^2 + 2F(\theta)\varepsilon\delta + \varepsilon^2]^{-1/2}$ produces a singularity $2\ln|\delta|$, regardless of whether the point of interest approaches the vortex surface, either from within or from without. This logarithmic singularity is due to the fact that the vortex component $\Gamma_\theta - F(\theta)\Gamma_r$ is non-zero, and is directed along the

tangent to the boundary. If this boundary is represented by the trailing edge of the blade, then the logarithmic singularities due to free vortices and vortices distributed over the blade cancel each other as being of equal magnitude, but with opposite signs.

The remaining singularities in Eq. (17.28) can be evaluated through integration. In particular,

$$\lim_{\delta\to 0}\int_{Q_0-r}^{1-r}\frac{\delta d\varepsilon}{\varepsilon\sqrt{G(r,\theta)\delta^2+2F(\theta)\delta\varepsilon+\varepsilon^2}}=\frac{1}{\sqrt{G(r,\theta)}}\ln\frac{\sqrt{G(r,\theta)}-F(\theta)}{\sqrt{G(r,\theta)}+F(\theta)}.$$

On the basis of the above-outlined analysis of singularities, the following method of determining velocities can be obtained. From the subintegral functions, particular terms are selected which can be analytically integrated:

$$\int_{Q_0-r}^{1-r}\varepsilon^{-1}d\varepsilon=\ln\frac{1-r}{r-Q_0},\quad\int_{Q_0-r}^{1-r}\ln|\varepsilon|d\varepsilon=(1-r)[\ln(1-r)-1]+$$
$$+(r-Q_0)\ln[(r-Q_0)-1],$$

while integration of the remainder, which does not contain singularities, is performed numerically. At the transition to the system of lifting vortices, it is finally possible to assume $\delta = 0$. This approach was taken in Refs. 57 and 63 for $\alpha = \pi/2$ and, in Ref. 61, a table of the following limited function is given

$$i_{t0}=i_t(\tilde{Q},\lambda,0;\infty)+\sin\beta\left(\frac{1}{\tilde{Q}-1}-\frac{\cos^2\beta}{2}\ln|\tilde{Q}-1|\right).$$

3. COMPUTATION OF BLADE LOADS AND AIRSCREW PERFORMANCE, SELECTION OF BLADE FORM

SCHEME OF THE LIFTING VORTICES

Considering absolute unsteady motion, and neglecting squares of velocities induced by the airscrew, we find, from the Cauchy integral, the following relationship expressed in nondimensional quantities:

$$\frac{1}{\omega}\frac{\partial\varphi}{\partial t}+p=\text{const.}$$

Consequently, the load on the blade is (see footnote*)

$$p_{\text{нижн}} - p_{\text{верх}} = -\frac{1}{\omega}\frac{\partial}{\partial t}(\varphi_{\text{нижн}} - \varphi_{\text{верх}}) = \frac{1}{\omega}\frac{\partial \Gamma}{\partial t}.$$

The position of the blade trailing edge is defined by angle ψ; the position of a point on the blade is given by angle θ, computed from the trailing edge. The increment of circulation at a fixed point through which the blade passes is composed of two increments; $-\partial\Gamma/\partial\theta$ due to displacement of the blade with unchanged circulation, and increment $\partial\Gamma/\partial\psi$ resulting from the azimuth variation. In this way,

$$p_{\text{нижн}} - p_{\text{верх}} = \frac{\partial \Gamma}{\partial \psi} - \frac{\partial \Gamma}{\partial \theta}.$$

The Joukowsky-Chaplygin requirement for the blade trailing edge is fulfilled under the condition of continuity of circulation derivatives

$$(p_{\text{нижн}} - p_{\text{верх}})_0 = \frac{\partial \Gamma_0}{\partial \psi} - \left(\frac{\partial \Gamma}{\partial \theta}\right)_0 = 0,$$

where Γ_0 is the circulation at the blade trailing edge $(\partial\Gamma/\partial\theta)_0$ is the derivative of this circulation.

Loading on the blade section is equal to

$$dq = \int_0^{\theta_\pi} \left(\frac{\partial \Gamma}{\partial \psi} - \frac{\partial \Gamma}{\partial \theta}\right) \sqrt{G(r, \theta) - F^2(\theta)}\, d\theta dr$$

and, if the blade is narrow,

$$dq = \sqrt{G(r, \theta) - F^2(\theta)} \left(\Gamma_0 + \frac{\partial}{\partial \psi}\int_0^{\theta_\pi} \Gamma d\theta\right) dr,$$

where θ_π is the coordinate of the leading edge.

---

*NOTE: Subscript нижн = lower, and
верх = upper

In order to determine loading, it is necessary to find circulation. This can be done by using the above presented method of induced velocity calculation applied to the condition that no flow can go through the blade. For narrow blades, numerous simplifications of this task are possible; in particular, transition to the lifting-line concept. In this scheme, blade vortices at every section normal to the blade axis are replaced by a system of straight infinite vortices. Velocities induced by those vortices, when combined with velocities induced by the free (trailing) vortices, should satisfy the no-flow through the blade condition. From this latter condition, an integral-differential equation is obtained which determines circulation on the blade. This equation differs from that for an airfoil or a wing of finite span in a steady flow by the presence of the term $(\Gamma_\theta - \Gamma_\gamma F(\theta))_0 \ln\theta$ in the expression for velocities induced by free vortices. Due to this, the intensity of vortices at the trailing edge does not go to zero. For the case of $\alpha = \pi/2$; the computations, according to the lifting-line scheme, are no different than those for a wing of finite span. In this case, it is most expedient to represent circulation in the form of an interpolating polynomial

$$\Gamma(r)=\sum_{n=1}^{m}\Gamma_n\frac{(-1)^{n+1}\sin\theta_n\sin(m+1)\theta}{(m+1)(\cos\theta-\cos\theta_n)},$$

where

$$\cos\theta=\frac{1+r_0-2r}{1-r_0},\quad \theta_n=\frac{n\pi}{m+1}. \tag{17.29}$$

Coefficients of the polynomial are equal to the circulation at points

$$r_n=\frac{1+r_0}{2}-\frac{1-r_0}{2}\cos\theta_n.$$

Induced velocity is also given as a polynomial

$$v_\nu=v(r_\nu)=\sum_{n=1}^{m}\Gamma_n v_{n\nu}. \tag{17.30}$$

Among the various methods which can be applied to the solution of the integral-differential equation, one may use the method of minimization of the mean-squared error[59,63].

It is necessary to develop more precise computational methods for blades which do not taper to zero at the tip and do not transition into a cylinder at the root. Flow at the blade tip is three-dimensional and application of the hypothesis

of two-dimensional sections is no longer applicable. However, in order to achieve zero load at the blade tip (even within the accuracy of the two-dimensional flow hypothesis) it is required that the induced inflow angle be equal to the geometric angle of attack. If the blade root section is also considered as free, then the same condition should be applied to it. In order to fulfill those conditions, a new term (for instance, $y_0 sin(m+1)\theta$) must be introduced into the polynomial approximating circulation. Thus, derivatives of the circulation at the blade ends may be more precisely defined. If the blade roots adjoin a rigid wall, then circulation in that region may not drop down to zero and in order to define its value, a new term of the $\Gamma_0 [sin(m+1)\theta/(m+1) sin\,\theta]$ type must be introduced into Eq. (17.29). In the latter case, it should be noted that it is necessary to consider the influence of a rigid boundary.

For coaxial propellers, computations are performed, assuming that the system of free (trailing) vortices in the wake of each propeller is the same as for the isolated ones. Mutual interference is accounted for through mean velocities induced by one propeller in the plane of another.

It was shown that the total force and moment acting on a propeller with $k > 3$ is time-independent when the following conditions are fulfilled: (1) dependence of induced velocity on circulation is the same as for $\alpha_B = \pi/2$, and (2) the hypothesis of steady state is acceptable to the regime of a propeller in a skewed flow at small values of $(\pi/2) - \alpha_B$. The projection of total aerodynamic force on the plane of rotation is

$$Y = \frac{1}{4}(\pi - 2\alpha_B)\frac{\varrho V^2}{2}\pi R^2 \int_{r_0}^{1} \left(\frac{dc_y}{d\alpha}\right)_\infty \bar{b} \sin\varphi dr \qquad (17.31)$$

and does not depend on rotational velocity.

THEORY OF IMPULSES AND ENERGY

At some distance downstream from an airscrew, free (trailing) vortices roll-up and then dissipate under the influence of viscosity. For this reason, extension of vortices to very long distances should be considered only as a scheme permitting computational evaluation of the action of an airscrew on the medium in the neighborhood of the airscrew itself.

Under the assumption of small perturbations, the force acting on an arbitrary system of bodies and the power required to agitate the medium are, respectively, equal to the vector of momentum and the kinetic energy of the medium contained in a volume separated by two parallel planes, infinitely distant from the bodies, and separated from each other by a distance

corresponding to velocity V. If the free vortices of an airscrew working in the presence of other rigid bodies remain helical in infinity, then any arbitrary system composed of an airscrew and rigid bodies satisfying this condition would require the same power and have the same effective thrust as a corresponding isolated airscrew with the same distribution of circulation in infinity[60]. Flow around an airscrew remains axisymmetric only in the presence of a body(s) of revolution coaxial with that of the airscrew itself. If, in the case of a body of revolution, the airscrew is lightly loaded, then free vortices become distributed on the stream surfaces and transition from the airscrew plane of rotation (r) to the plane of an equivalent isolated airscrew (r_∞) is performed with the help of the continuity equation.

$$\left(1+\frac{v_x}{V}\right)r\,dr=r_\infty dr_\infty.$$

Let us consider two coaxial, contrarotating propellers having angular velocities ω_1 and ω_2 and moving along their axes $(\alpha_B = \pi/2)$ with constant velocity V. In contrast to the isolated airscrew, the field of velocities of each of the propellers is nonstationary with respect to the other propeller. The period of variation of the velocity field infinitely far downstream from the propellers will be $\tau = 2\pi/(\omega_1 + \omega_2)$. In order to determine the time average thrust and power expenditure, it is sufficient to find the quantity of momentum and energy of the air contained between two planes infinitely distant (downstream) from the propellers and separated from each other by a distance $\Delta x = \tau V$. Increments of the axial component of momentum and kinetic energy of the air, respectively are equal to:

$$\Delta R=\varrho\iiint_Q v_x dQ,\qquad \Delta E=\frac{\varrho}{2}\iiint_Q v^2 dQ,$$

where Q is the volume contained between the planes. The flow has the potential ϕ, equal to the sum of potentials of the free vortices of both propellers, $\phi_1 = \phi_1 + \phi_2$. In infinity, ϕ no longer depends on time. Let us apply the formulae of Gauss and Green to the expressions for ΔR and ΔE. Then

$$\Delta R=\varrho\iint\varphi dS_x,\quad \Delta E=\frac{\varrho}{2}\iint\varphi\frac{\partial\varphi}{\partial n}dS.$$

Here, dS_x is the projection on axis x of an element of the surface containing volume Q. Integrals along the planes mutually cancel each other, and vortex surfaces represent surfaces of discontinuity of the potential. For this reason, it is necessary to integrate along both sides of the surface, keeping in mind that the normals have opposite directions. On surface S_1, the discontinuity has potential ϕ_1, and on surface S_2, has potential ϕ_2. Consequently,

$$\Delta R=\varrho k_1\int\limits_{r_{01}}^{R_1}\int\limits_{0}^{\theta_1}[\varphi_1]\,r\,d\,r\,d\theta+\varrho k_2\int\limits_{r_{02}}^{R_2}\int\limits_{0}^{\theta_2}[\varphi_2]\,r\,d\,r\,d\theta,$$

while $\theta_1=\tau\omega_1$, $\theta_2=\tau\omega_2$. Since

$$\frac{1}{\theta_1}\int\limits_0^{\theta_1}[\varphi_1]\,d\theta=\Gamma_{10},\ \frac{1}{\theta_2}\int\limits_0^{\theta_2}[\varphi_2]\,d\theta=\Gamma_{20},$$

where Γ_{10}, Γ_{20} are average values for the period, then thrust

$$T=T_1+T_2=\varrho k_1\omega_1\int\limits_{r_{01}}^{R_1}\Gamma_{10}r\,dr+\varrho k_2\omega_2\int\limits_{r_{02}}^{R_2}\Gamma_{20}r\,dr,$$

which means that thrust of the coaxial propellers is equal to the sum of the thrust of the isolated propellers.

When computing ΔE, remember that velocity is continuous and its component $v_s = 0$ (this is strictly correct only for the case of $\Gamma^\theta = 0$) and in considering Green's formula

$$\iint\left(\varphi_1\frac{\partial\varphi_2}{\partial n}-\varphi_2\frac{\partial\varphi_1}{\partial n}\right)dS=0.$$

Consequently,

$$\Delta E=\frac{\varrho}{2}\left(\iint\varphi_1\frac{\partial\varphi_1}{\partial n_1}\,dS_1+\iint\varphi_2\frac{\partial\varphi_2}{\partial n_2}\,dS_2+2\iint\varphi_1\frac{\partial\varphi_2}{\partial n_1}\,dS_1\right).$$

Since $\frac{\partial\varphi_2}{\partial n_1}=v_{n2}\cos(\beta_1+\beta_2)$, then

$$\Delta E=\frac{\varrho}{2}\left\{k_1\int\limits_{r_{01}}^{R_1}\int\limits_{0}^{\theta_1}[\varphi_1]\,v_{n1}\sqrt{r^2+\left(\frac{V}{\omega_1}\right)^2}\,r\,d\,r\,d\theta+\right.$$

$$+k_2\int\limits_{r_{02}}^{R_2}\int\limits_{0}^{\theta_2}[\varphi_2]\,v_{n2}\sqrt{r^2+\left(\frac{V}{\omega_2}\right)^2}\,r\,d\,r\,d\theta+$$

$$\left.+2k_1\int\limits_{r_{01}}^{R_1}\int\limits_{0}^{\theta_1}[\varphi_1]\,v_{n2}\cos(\beta_1+\beta_2)\sqrt{r^2+\left(\frac{V}{\omega_1}\right)^2}\,r\,d\,r\,d\theta\right\}.$$

In general, an average with respect to θ can be computed by neglecting time variation of circulation and velocity:

$$\frac{1}{\theta_1}\int_0^{\theta_1}[\varphi_1]\,v_{n1}d\theta=\Gamma_{10}v_{n1}^0,\quad \frac{1}{\theta_2}\int_0^{\theta_2}[\varphi_2]\,v_{n2}d\theta=\Gamma_{20}v_{n2}^0,\ \frac{1}{\theta_1}\int_0^{\theta_1}[\varphi_1]\,v_{n2}d\theta=\frac{k_2\Gamma_{10}\Gamma_{20}}{2\pi r\sin\beta_2}.$$

Finally, power losses can be expressed as follows:

$$E=\frac{\varrho}{2}\left\{k_1\omega_1\int_{r_{01}}^{R_1}\Gamma_{10}v_{n1}^0\sqrt{r^2+\left(\frac{V}{\omega_1}\right)^2}\,r\,dr+\right.$$
$$\left.+k_2\omega_2\int_{r_{02}}^{R_2}\Gamma_{20}v_{n2}^0\sqrt{r^2+\left(\frac{V}{\omega_2}\right)^2}\,r\,dr+\frac{k_1k_2}{\pi}\int\Gamma_{10}\Gamma_{20}\left(\frac{\omega_1\omega_2}{V}r^2-V\right)dr.\right. \tag{17.32}$$

Depending on the sign of the last integral in Eq. (17.32), power losses of the coaxial propellers can be either larger, or smaller, than the sum of losses of isolated propellers.

Let us now apply the theory of impulses and energy to the isolated propeller at an angle of attack α_B (see Fig. 17.14), and calculate momentum and energy of the air enclosed between two planes parallel to the propeller disc, and separated by $2\pi V\ sin\ \alpha_B$. Finally, for the components of the time-average total force and power losses, we obtain the following:

$$X=\frac{\varrho\omega}{2\pi}\iint\varphi n_x dS=\frac{\varrho k\omega}{2\pi}\int_{r_0}^{R}\int_0^{2\pi}\Gamma\left(r+\frac{V}{\omega}\cos\alpha_B\sin\theta\right)dr\,d\theta,$$

$$Y=\frac{\varrho\omega}{2\pi}\iint\varphi n_y dS=-\frac{\varrho kV\sin\alpha_B}{2\pi}\int_{r_0}^{R}\int_0^{2\pi}\Gamma\sin\theta d\theta\,dr,$$

$$Z=\frac{\varrho\omega}{2\pi}\iint\varphi n_z dS=\frac{\varrho kV\sin\alpha_B}{2\pi}\int_{r_0}^{R}\int_0^{2\pi}\Gamma\cos\theta d\theta\,dr,$$

$$E=\frac{\varrho\omega}{4\pi}\iint\varphi\frac{\partial\varphi}{\partial n}dS=$$

$$=\frac{k\varrho\omega}{4\pi}\iint_{r_0}\Gamma v_n\sqrt{\left(\frac{V}{\omega}\sin\alpha_B\right)^2+r^2+\left(\frac{V}{\omega}\cos\alpha_B\sin\theta\right)^2}\,dr\,d\theta, \tag{17.33}$$

where n_x, n_y, n_z are projections of the unit vector, normal to the vortex surface.

OPTIMAL DISTRIBUTION OF CIRCULATION

The solution of variational problems should be considered as a rational basis for the design of propeller blades. The variational problem of the optimum distribution of circulation can be formulated as follows: With a given projection on direction l of force

$$L=\frac{\varrho\omega}{2\pi}\iint \varphi n_l dS,$$

acting on the propeller, or for a given power, find circulation $\Gamma(\theta,r)$ which assures the lowest power losses

$$E=\frac{\varrho\omega}{4\pi}\iint \varphi\,\frac{\partial\varphi}{\partial n}\,dS.$$

We write a functional, $E - \lambda L$, where λ is an undefined multiplier. Its first variation may be equal to zero; i.e,

$$\delta\iint \varphi\left(\frac{1}{2}\,\frac{\partial\varphi}{\partial n}-\lambda n_l\right)dS=0.$$

But, according to the Green formula,

$$\iint\left(\delta\varphi\frac{\partial\varphi}{\partial n}-\varphi\frac{\partial\delta\varphi}{\partial n}\right)dS=0.$$

Consequently,

$$\iint\delta\varphi\left(\frac{\partial\varphi}{\partial n}-\lambda n_l\right)dS=0$$

and, since the variation of $\delta\phi$ is arbitrary, then

$$v_n=\frac{\partial\varphi}{\partial n}=\lambda n_l. \tag{17.34}$$

Eq. (17.34) represents a generalization of the well-known Betz formula: A propeller with optimum distribution of circulation should generate the same velocities far downstream as those generated by a rigid vortex surface moving with velocity λ in direction l. At a given thrust (or power) level, the coaxial propellers ($\alpha_B = \pi/2$) will experience minimum power losses under the following condition: Circulation with respect to r and θ varies in such a way that the free vortex surfaces generate the same velocities far away in the propeller slipstream as those that would have been generated by rigid helical surfaces moving in direction x with velocity λ:

$$\frac{\partial(\varphi_1+\varphi_2)}{\partial n_1}=v_{n1}+\bar{v}_{n2}\cos(\beta_1+\beta_2)=\lambda\cos\beta_1,$$
$$\frac{\partial(\varphi_1+\varphi_2)}{\partial n_2}=\bar{v}_{n1}\cos(\beta_1+\beta_2)+v_{n2}=\lambda\cos\beta_2. \qquad (17.35)$$

At high subsonic velocities of flight, the largest part of the power loss is due to the wave drag of airfoil sections. For this reason, in the formulation of variational tasks, it is necessary to consider the *profile* power losses. Power required by the propeller and the power losses are as follows:

$$N=k\varrho\omega V\int_{r_0}^{R}\Gamma r\,dr,\quad E=k\varrho\int_{r_0}^{R}\left(\Gamma v_n+\frac{c_x}{2}bW^2\right)W\,dr,$$

where $W=\sqrt{V^2+(\omega r)^2}$. According to Green's formula,

$$\int_{r_0}^{R}(\delta\Gamma v_n-\Gamma\delta v_n)W\,dr=0$$

and the condition of equality to zero of the first variation of functional $E-\lambda N$ can be written in the following form:

$$\delta(E-\lambda N)=\int_{r_0}^{R}\left[\delta\Gamma(2v_nW-\lambda\omega Vr)+\frac{1}{2}\delta(c_xb)W^3\right]dr=0.$$

The profile drag coefficient $c_x=c_x(c_y,\ c/b,\ M,\ Re)$. For this reason, the preceding equation can also be expressed as

$$\int_{r_0}^{R}\left[b\left(2v_n-\lambda V\cos\beta+W\frac{\partial c_x}{\partial c_y}\right)\delta c_y+c_y\left(2v_n-\lambda V\cos\beta+\right.\right.$$
$$\left.\left.+W\frac{c_x}{c_y}-\frac{W}{c_y}\frac{c}{b}\frac{\partial c_x}{\partial\left(\frac{c}{b}\right)}\right)\delta b+W\frac{\partial c_x}{\partial\left(\frac{c}{b}\right)}\delta c\right]W^2dr=0.$$

If all variations are independent and arbitrary, then for the determination of c_y, b, c, we obtain the following three equations:

$$2v_n-\lambda V\cos\beta+W\frac{\partial c_x}{\partial c_y}=0,$$
$$2v_n-\lambda V\cos\beta+W\left(\frac{c_x}{c_y}-\frac{c}{bc_y}\frac{\partial c_x}{\partial\left(\frac{c}{b}\right)}\right)=0, \qquad (17.36)$$
$$\frac{\partial c_x}{\partial\left(\frac{c}{b}\right)}=0.$$

Usually, thickness and chord of a blade are tied up with some additional condition; i.e., stress requirements, and consequently, variations of δb and δc are mutually dependent. Hence, it is possible to assume that c_x depends on c_y and b. Then, for the determination of c_y and b, we will have only two equations instead of three:

$$2v_n-\lambda V\cos\beta+W\frac{\partial c_x}{\partial c_y}=0,$$
$$2v_n-\lambda V\cos\beta+W\left(\frac{c_x}{c_y}+\frac{b}{c_y}\frac{\partial c_x}{\partial b}\right)=0. \qquad (17.37)$$

From the last equation, we can determine

$$b=\left(\frac{\partial c_x}{\partial b}\right)^{-1}\left(c_y\frac{\partial c_x}{\partial c_y}-c_x\right)^{*}.$$

If the blade chord is given, then the first equation from Eqs. (17.37) remains for the determination of c_y. When c_y is given, the second equation remains. Values of b, c_y can be given for some segments of the blade, and Eqs. (17.37) will be correct for these particular blade segments[81]. As long as the relative thickness of the blade sections is given and there are no restrictions with respect to the blade chord, minimum power losses will be achieved at $c_x/c_y = min$. This means that the quantity c_y can also be considered as having been given. In this case, from the second equation in Eqs. (17.37), we obtain

$$2v_n-\lambda V\cos\beta+W\left(\frac{c_x}{c_y}\right)_{\min}=0.$$

In the presented formulation, selection of the airfoil section appears as a part of the variational problem. Solutions can be extended to the considerations of a system composed of a propeller and a body of revolution. This can be done with the help of the theory of equivalence of such a system to an isolated propeller. Appplication of the Betz theory to a propeller with a finite cylindrical spinner gives circulation that does not become zero at the spinner (Fig. 17.18). However, at the wall of a body of finite length, as indicated by the theory of equivalence, circulation should go to zero if maximum effective thrust is to be realized.

---

*Analogous results were obtained by L.S. Vil'dgrube.

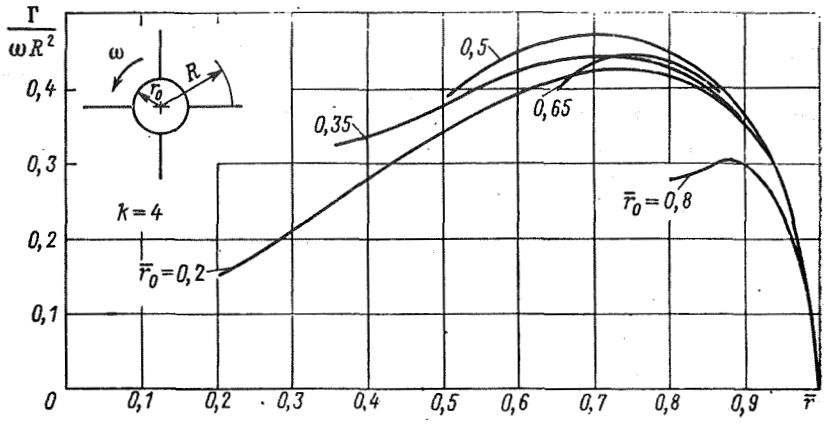

Figure 17.18

4. PROPELLERS IN A COMPRESSIBLE MEDIUM

At subsonic speeds of flight with blade tip speeds only slightly exceeding the speed of sound, compressibility effects are chiefly demonstrated through changes of the airfoil characteristics. These changes are related to the presence of supersonic flow regions, appearance of shock waves, and stall generated by the shock waves. Nevertheless, even at subsonic flight speeds, mutual blade interference becomes substantial for sections close to the nacelle. With a sufficiently large number of blades, at supersonic flight speeds the *cascade* effect may be considerable, while mutual interaction between the propeller and fuselage becomes quite distinct. In investigations of a propeller in a stream of gas, it is possible to solve the wave equation for the velocity potential under the small perturbation assumption. Let us briefly present the results of such investigations.

We will restrict ourselves to angle $\alpha_B = \pi/2$; at which the flow is steady with respect to the propeller. Using cylindrical coordinates attached to the propeller*, we have

$$\frac{\partial\varphi}{\partial t}=V\frac{\partial\varphi}{\partial x}+\omega\frac{\partial\varphi}{\partial\theta},\quad \frac{\partial^2\varphi}{\partial t^2}=V^2\frac{\partial^2\varphi}{\partial x^2}+2V\omega\frac{\partial^2\varphi}{\partial x\partial\theta}+\omega^2\frac{\partial^2\varphi}{\partial\theta^2}.$$

Consequently, the wave equation can be written in the following form:

---

*The propeller rotates in a direction opposite to the positive θ, and moves in the opposite direction to the x axis.

$$\frac{1}{r}\frac{\partial}{\partial r}\left(r\frac{\partial\varphi}{\partial r}\right)+\frac{\partial^2\varphi}{\partial x^2}\left(1-\frac{V^2}{a^2}\right)+\left(\frac{1}{r^2}-\frac{\omega^2}{a^2}\right)\frac{\partial^2\varphi}{\partial\theta^2}-\frac{2\omega V}{a^2}\frac{\partial^2\varphi}{\partial x\,\partial\theta}=0. \tag{17.38}$$

With the help of nondimensional coordinates, Eq. (17.38) can be transferred to a canonical form and V/a and ω can be explicitly eliminated. Let us assume that

$$\bar{x}=\frac{a\omega x}{a^2-V^2},\quad \bar{r}=\frac{\omega r}{\sqrt{a^2-V^2}},\quad \vartheta=\theta+\frac{\omega V x}{a^2-V^2}\ \text{for}\ V<a,$$

$$\bar{x}=\frac{a\omega x}{V^2-a^2},\quad \bar{r}=\frac{\omega r}{\sqrt{V^2-a^2}},\quad \vartheta=\theta-\frac{\omega V x}{V^2-a^2}\ \text{for}\ V>a.$$

Then

$$\frac{1}{\bar{r}}\frac{\partial}{\partial\bar{r}}\left(\bar{r}\frac{\partial\varphi}{\partial\bar{r}}\right)+\frac{\partial^2\varphi}{\partial\bar{x}^2}+\left(\frac{1}{\bar{r}^2}-1\right)\frac{\partial^2\varphi}{\partial\vartheta^2}=0\ \text{for}\ V<a, \tag{17.39}$$

$$\frac{1}{\bar{r}}\frac{\partial}{\partial\bar{r}}\left(\bar{r}\frac{\partial\varphi}{\partial\bar{r}}\right)-\frac{\partial^2\varphi}{\partial\bar{x}^2}+\left(1+\frac{1}{\bar{r}^2}\right)\frac{\partial^2\varphi}{\partial\vartheta^2}=0\ \text{for}\ V>a. \tag{17.40}$$

Particular integrals of Eq. (17.39) are mixed - elliptical for $\bar{r} < 1$ and hyperbolic for $\bar{r} > 1$ - with functions[98]

$$J_n\left(\bar{r}\sqrt{n^2+\lambda^2}\right)e^{\lambda\bar{x}}\sin n\vartheta\ \text{and}\ J_n\left(\bar{r}\sqrt{n^2+\lambda^2}\right)e^{\lambda\bar{x}}\cos n\vartheta,$$

while for Eq. (17.40), they are of the hyperbolic kind - with functions

$$I_n\left(\bar{r}\sqrt{n^2+\lambda^2}\right)e^{\lambda\bar{x}}\sin n\vartheta\ \text{and}\ I_n\left(\bar{r}\sqrt{n^2+\lambda^2}\right)e^{\lambda\bar{x}}\cos n\vartheta,$$

where J_n and I_n are Bessel functions.

Far downstream from the propeller, the field of flow in the fixed system of coordinates is steady and depends on two parameters only; $\bar{r} = \omega r/V$, $\tau = \theta - \omega x/V$. Consequently,

$$\frac{1}{\bar{r}}\frac{\partial}{\partial\bar{r}}\left(\bar{r}\frac{\partial\varphi}{\partial\bar{r}}\right)+\left(1+\frac{1}{\bar{r}^2}\right)\frac{\partial^2\varphi}{\partial\tau^2}=0 \tag{17.41}$$

does not differ from the equation for an incompressible medium, and particular integrals of that equation (as well as Eq. 17.38)) become products of Bessel functions $I_n(n\bar{r})$, $K_n(n\bar{r})$ times $\sin n\tau$ and $\cos n\tau$[63]. On the basis of Eq. (17.41) it is impossible to prove that compressibility of the air has no influence on the induced velocity value in the propeller plane. This is due to the fact that the velocity field in a compressible medium is not symmetrical with respect to the propeller plane, and velocity in that plane is not equal to one-half its value in infinity[86]. In the particular case of $\omega = 0$ and $k = \infty$, a suitable substitution of variables permits one to transform Eq. (17.38) into an

equation for incompressible fluids; thus making it possible to obtain that proof[79,85]. Since, in the case of small perturbations, velocity potential and enthalpy i are related by the equation $i + \partial\phi/\partial t = 0$, while the derivative $\partial\phi/\partial t$ satisfies Eq. (17.38), then particular integrals of Eq. (17.38) can also be used for the determination of i. Computation of a propeller in a compressible medium represents a difficult task. For this reason, in most investigations, only simplified schemes were considered; for example, actuator disc (infinite number of blades), no interference between blades, flat airfoil cascades.

5. IDEAL PROPELLER

Let us consider an actuator disc of radius R which supplies energy to the flow. If we assume that all of the energy supplied is transferred into kinetic energy of the medium and, in addition, assume that the flow does not rotate, then such a scheme may be considered as that of the *ideal* propeller. There are discontinuities in pressure, density and axial component of velocity at the disc. Pressure $i = (p - p_\infty)/p$ satisfies the wave equation and since acceleration potential is equal to $-i$, the component velocities are

$$v_x = -\frac{i}{V}, \quad v_y = -\frac{1}{V}\int \frac{\partial i}{\partial y}\,dx, \quad v_z = -\frac{1}{V}\int \frac{\partial i}{\partial z}\,dx.$$

If we assume that the density, γ, of doublets covering the disc is constant along the radius, then in the case of $M = V/a < 1$ it will be related to the propeller thrust through the following equation*

$$\gamma = -\frac{\beta^2 [i]}{4\pi} = -\frac{T}{4\pi\rho F}.$$

At $M < 1$, the pressure is higher and the axial component of velocity is lower behind the disc than in front of it. Perturbation velocity on axis x (Fig. 17.19) is

$$\frac{v_x}{v_{x\infty}} = \begin{cases} \dfrac{1}{2\beta^2}\left(1 + \dfrac{\bar{x}}{\sqrt{1+\bar{x}^2}}\right) & \text{for } \bar{x} < 0, \\ \dfrac{1}{2\beta^2}\left(1 - 2M^2 + \dfrac{\bar{x}}{\sqrt{1+\bar{x}^2}}\right) & \text{for } \bar{x} > 0, \end{cases}$$

where

$$v_{x\infty} = \frac{T}{\rho F V^2}, \quad \bar{x} = \frac{x}{\beta R}, \quad \beta = \sqrt{1 - M^2}.$$

*Square brackets are used to designate a jump in value at the surface of discontinuity.

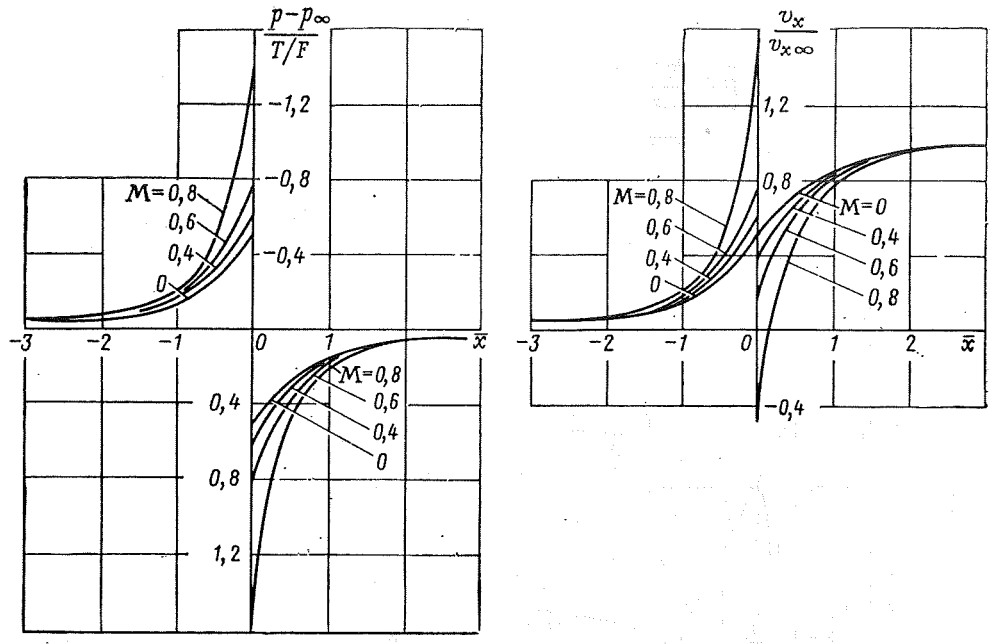

Figure 17.19

The average velocity of perturbation in the disc plane ($\bar{x} = 0$) does not depend on Mach number, M.

For $M > 1$, the intensity of the doublets is

$$\gamma = \frac{\mu^2 [i]}{2\pi} = -\frac{T}{2\pi\varrho F}, \quad \mu = \sqrt{M^2 - 1},$$

and the region of disturbance is limited by a cone $(\bar{r} - 1)^2 \leq \bar{x}^2$ (Fig. 17.20). The pressure behind the disc is lower than in the undisturbed stream; while inside of the $(1 - \bar{x})^2 = \bar{r}^2$ cone, the pressure is constant, and the axial component of the velocity of perturbation is

$$\frac{v_x}{v_{x\infty}} = \frac{M^2}{\mu^2}.$$

Within the region limited by the $(\bar{x} - 1)^2 = \bar{r}^2$ cone with its vertex at point $\bar{x} = 1$, $\bar{y} = \bar{z} = 0$, on axis x we have

$$\frac{v_x}{v_{x\infty}} = \frac{M^2}{\mu^2}\left(1 - \frac{\bar{x}}{M^2\sqrt{\bar{x}^2 - 1}}\right).$$

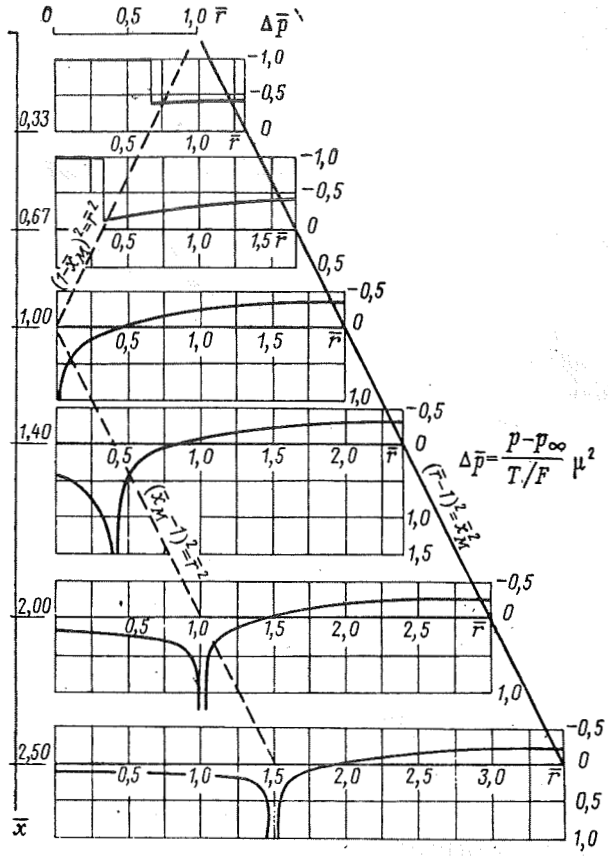

Figure 17.20

On the surface of this cone, the pressure goes to infinity. Consequently, the assumption of small perturbations is not valid and the whole theory is not applicable. Surfaces of cones $(1 - \bar{x})^2 = \bar{r}^2$ and $(\bar{r} - 1)^2 = \bar{x}^2$ become surfaces of discontinuity; whereupon,

$$\frac{[p]}{p_\infty} = \frac{T}{p_\infty F} \cdot \frac{1}{2\mu^2 \sqrt{1 \mp \bar{x}}}.$$

The average velocity of perturbation in the disc plane is not equal to the one-half of velocity at an infinite distance behind the disc. Pressure and velocity distributions behind the disc along the x axis is shown in Fig. 17.21. Computation of function i at an arbitrary space point is reduced to the use of elliptic integrals. Differences in the mutual interference of propeller and body of revolution at subsonic and supersonic

speeds is explained by the corresponding differences in the pressure fields behind the propeller. At a supersonic velocity, it is possible to reduce the wave drag of a body due to the rarefication of the air behind the propeller.

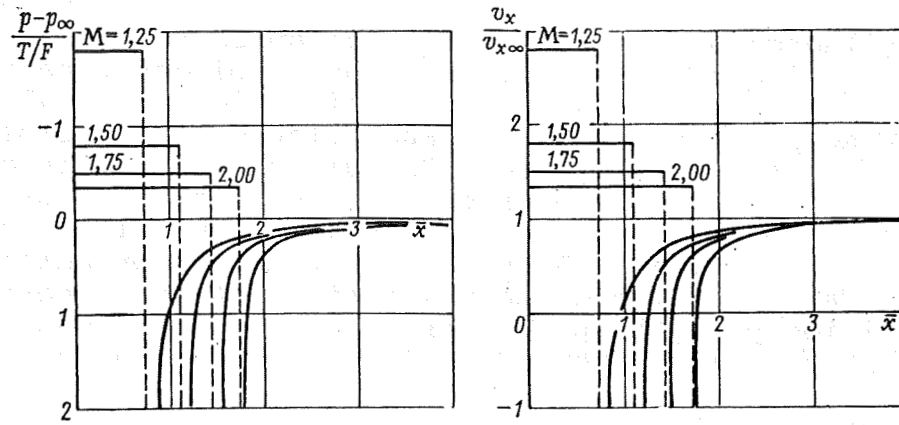

Figure 17.21

6. PROPELLER WITH FINITE NUMBER OF BLADES IN A CYLINDRICAL TUBE

We are going to consider a propeller of radius R working at Mach number $M < 1$ in an infinitely long cylindrical tube of radius R_T. The blades of the propeller have a helical form, limited by the planes $x = \pm H$, while the load along the chord is constant: $[i] = (p_{\text{нижн}} - p_{\text{верх}})/p = q(r)$. Enthalpy i will be presented in the form of a sum of function i_0, satisfying Eq. (17.38) in the case of infinite helical surfaces of discontinuities of function i and functions i_1, i_2 and i_3 respectively, defined for $x \leq -H$, $-H \leq x \leq H$ and $x \geq H$, and guaranteeing continuity of function i and its derivatives everywhere except for the blade surfaces. Function i_0 is presented in the form of a series of the products of Bessel functions I_η and K_η times the trigonometric functions, and functions i_1, i_2 and i_3 are represented as a series from particular integrals of Eq. (17.39). Calculations indicated that for the scheme of lifting surfaces, induced velocities at the blades are finite, including the critical radius, $\bar{r} = 1$.

7. PROPELLERS WITH WIDE BLADES

Let us assume that the propeller blades, while thin, are so wide that in the equation for velocity potential

$$\frac{1}{\bar{r}}\frac{\partial}{\partial \bar{r}}\left(\bar{r}\frac{\partial \varphi}{\partial \bar{r}}\right)+\left(1+\frac{1}{\bar{r}^2}\right)\frac{\partial^2 \varphi}{\partial \tau^2}+\beta^2\frac{\partial^2 \varphi}{\partial \bar{x}^2}-2\frac{\partial^2 \varphi}{\partial \bar{x}\partial \tau}=0$$

derivatives with respect to $\bar{x}$ can be considered as quantities of a lower order than derivatives with respect to $\bar{r}$ and τ. Then the above equation becomes the same as Eq. (17.41), which means that the influence of compressibility disappears. It is possible to assume that for every section $\bar{x} = const$, blades generate the same flow as that generated by an infinite rigid helical surface moving along the x axis. Such flow would be close to the optimum one for ideal fluid. Propulsive efficiency of a propeller with thin, wide blades should differ from that of a propeller with an optimum circulation distribution. This is mostly due to the friction drag. Actual model tests of propellers with thin, wide blades confirmed the predictions of the theory: propulsive efficiency of the propeller was quite high and with an increase of Mach number from $0,6$ to $0,95$, it decreased by only 5 percent.

8. PROPELLERS WITH NONINTERACTING BLADES AND A LARGE NUMBER OF BLADES

At supersonic speeds of flight, as long as the propeller has a small number of blades, it is possible to neglect blade interference and use two-dimensional characteristics for load calculations. The influence of the front propeller on the aft propeller is considered through the introduction of average induced velocity. The propulsive efficiency of coaxial propellers is higher than that of an isolated one. The influence of the relative blade thickness on propulsive efficiency was investigated, and variational problems of an optimum planform of the coaxial propeller blades were solved. For calculations of blades with radial leading edges, we assume a retarding potential of sources moving along helical lines. For another particular case - that of an infinitely large number of blades having axisymmetrical flow in the slipstream behind the propeller corresponding to the minimum wave drag of a flat cascade - the variational problem of optimum circulation was solved for the case of isolated, as well as coaxial propellers.

9. FLAT CASCADES OF AIRFOILS IN SUPERSONIC FLOW

The cylindrical cross-section of a multibladed propeller can be considered as a flat, infinite, cascade of airfoils. An ideal cascade in a slightly inclined flow is considered in Ref. 85. For computations of a cascade of thin, lightly loaded, airfoils at a low angle of attack with respect to the flow whose velocity only slightly exceeds the speed of sound, it is possible to use the theory of small perturbations with the corresponding linear equation for velocity potential. Depending on the ratio of the pitch

of the cascade t to the airfoil chord b, angle of the elevation of the grid β, angle of attack of the airfoil θ, and the angle of inclination of characteristic $\alpha = \sin^{-1}M^{-1}$; three regimes of flow are possible:

(1) At $t/b \geq [\sin(\alpha + \theta)]/[\sin(\beta - \alpha - \theta)]$, $\beta - \theta > \alpha$, there is no mutual interference between the airfoils and the field behind the cascade is doubly periodic, and nonuniform.

(2) At $t/b < [\sin(\alpha + \theta)]/[\sin(\beta - \alpha - \theta)]$, $\beta - \theta \geq \alpha$, the flow ahead of the cascade is not disturbed, and the flow at the front part of the airfoil is the same as for isolated airfoils at the upper (верх) and lower (нижн) sides

$$\bar{x}_{\text{верх}} = \frac{t}{b}\,\frac{\sin(\alpha+\beta)}{\sin\alpha}, \quad \bar{x}_{\text{нижн}} = \frac{t}{b}\,\frac{\sin(\beta-\alpha)}{\sin\alpha}$$

therefore, there is no noticeable influence on the neighboring airfoils and a uniform flow is possible behind the cascade.

(3) At $\beta - \theta < \alpha$, the velocity component normal to the cascade axis is subsonic and the flow in front of the cascade is disturbed.

In the two latter cases, characteristics of airfoils in the cascade are considerably different from those of isolated airfoils. In case (2), an important role is played by the quantity $\Delta = 1 - n\bar{x}_T$ ($\bar{x}_T = \bar{x}_{\text{верх}} + \bar{x}_{\text{нижн}}$, and n is an integer) connected with the reflection of waves inside of the cascade coming from the airfoil edges. In the case of $\Delta = 0$, all waves moving inside the channel between the airfoils are reflected the same number of times and the coefficients c_x and c_y depend only on the airfoil shape and not on the angle of attack. In this case, for a cascade composed of flat plates, $c_x = c_y = 0$. For $\Delta \neq 0$, the airfoil characteristics depend on angle of attack. For instance, for a cascade composed of flat plates,

$$c_y = \frac{4(\bar{x}_T - \Delta)\theta}{\mu}, \quad c_x = c_y\theta \text{ for } \bar{x}_{\text{верх}} \leqslant \Delta \leqslant \bar{x}_T,$$

$$c_y = \frac{4\bar{x}_{\text{нижн}}\theta}{\mu}, \quad \bar{c}_x = \frac{c_y^2\mu}{4\bar{x}_{\text{нижн}}} \text{ for } \bar{x}_{\text{нижн}} \leqslant \Delta \leqslant \bar{x}_{\text{верх}},$$

$$c_y = \frac{4\Delta\theta}{\mu}, \quad c_x = \frac{c_y^2\mu}{4\Delta} \text{ for } 0 \leqslant \Delta \leqslant \bar{x}_{\text{нижн}},$$

and for the airfoil section, the dependence of $dc_y/d\theta$ on Δ is periodic. Minimum wave drag does not correspond to a flat plate, but to airfoils with finite thickness. In addition, for given c_y, M, b/t and β, there is no unique solution. This means

that identical characteristics can be obtained for airfoils of different shapes. The coefficient of the lowest drag is

$$c_{x\,\min}=\frac{c_y^2\mu^2\,\frac{b}{t}}{4\left[M^2\sin^2(\beta-\theta)-1\right]}.$$

Under defined conditions, flow behind the cascade is uniform.

10. BLADE ROOT SECTIONS AND SPINNER SHAPE

When designing a propeller for a turboshaft powerplant with the air intake behind the propeller, it is necessary to devote special attention to the shape of the blade root sections and the spinner (nacelle). This is necessary, since an increase in the profile drag of those sections and the corresponding pressure losses can considerably reduce the engine power. The flow between the root sections of the blade is considerably different from that of two-dimensional flow. Angles of incidence of the root sections are close to 90°. In order to evaluate the influence of the three-dimensionality, it is permissible to assume that the angles of incidence are equal to 90°. Let us introduce the velocity of flow between the blades averaged over a circle, then equations of gas motion are

$$\frac{\partial\rho us}{\partial r}+\frac{\partial\rho ws}{\partial z}=0,\quad \frac{\partial\rho w^2 s}{\partial z}+\frac{\partial\rho uws}{\partial r}=-s\frac{\partial p}{\partial z},$$

$$\frac{\partial\rho uws}{\partial z}+\frac{\partial\rho u^2 s}{\partial r}=-s\frac{\partial p}{\partial r},\quad \frac{\partial u}{\partial z}-\frac{\partial w}{\partial r}=0,$$

where

$$s=\left(1-\frac{kc}{2\pi r}\right)r,$$

Under the assumption of small velocity perturbations, u' and w', the above equations can be reduced to the following equation

$$\frac{1}{r}\frac{\partial u' r}{\partial r}+\beta^2\frac{\partial w'}{\partial z}=\frac{kV}{2\pi r}\frac{\partial c}{\partial z}.$$

Through a substitution of variables $\bar{z}=z/\beta$, $\bar{r}=r$ and $\bar{c}=c/\beta$, this last equation can be transformed into the Poisson equation for the potential of perturbation velocities

$$\frac{1}{\bar{r}}\frac{\partial}{\partial\bar{r}}\left(\bar{r}\frac{\partial\varphi}{\partial\bar{r}}\right)+\frac{\partial^2\varphi}{\partial\bar{z}^2}=\frac{kV}{2\pi\bar{r}}\frac{\partial\bar{c}}{\partial\bar{z}}.$$

Distributed sources are substituted for the blades.

Calculations show that due to the three-dimensional character of flow, *blockage* of the flow in the channels between the blades occurs at Mach numbers 0,1- 0,15 higher than for two-dimensional airfoils. Losses of the total pressure can be reduced by decreasing the speed of flow between the blades by *compressing* the spinner at the area of attachment of the blades. Reduction of the spinner cross-section area in those places where the channel between the blades is the most narrow can be such that perturbation velocities will be reduced to zero. Test results fully confirmed the effectiveness of the local narrowing of the spinner, which permits avoidance of the total head losses with the increasing number of blades. The influence of three-dimensionality for radial blades was also investigated for the case of supersonic speed. Here, the character of the section loading changes considerably. On parts of the blades, it is possible to obtain thrust instead of resistance.

Results of investigations by A.Ya. Bokareva, V.I. Ganabov, V. V. Keldysh, I. M. Nosarev, D.V. Khalezov, etc., are reflected in this chapter.

DETERMINATION OF INDUCED VELOCITY AVERAGED OVER A CIRCLE

Let us find induced velocity averaged over a circle corresponding to the blade station at radius r. This induced velocity will be

$$\bar{v}_r = \frac{1}{\pi}\int_{\pi/2}^{\frac{3}{2}\pi} \bar{v}_{y0}(\bar{z})\, d\psi. \tag{I.1}$$

In analogy with Eq. (2.18)

$$\bar{v}_r = -\frac{k}{4\pi\bar{V}}\int_{\bar{\varrho}=\bar{r}_0}^{\bar{\varrho}=1} \Delta\hat{v}_r^0 d\bar{\Gamma}_\varrho. \tag{I.2}$$

According to Eq. (I.1),

$$\Delta\hat{v}_r^0 = \frac{1}{\pi}\int_{\pi/2}^{\frac{3}{2}\pi} \Delta\hat{v}_{y_0}^0(\bar{z})\, d\psi, \tag{I.3}$$

where $\bar{z} = \bar{r}\ sin\ \psi$; $\bar{\rho}$ is the relative radius of the circle from which springs a layer of free vortices; $\bar{r}$ is the relative radius of circle along which the induced velocity is computed. If $|\bar{r}| \leq |\bar{\rho}|$, then according to Eq. (2.17), $\Delta\hat{v}_{y0}(\bar{z}) = -1$. If, however, $|\bar{r}| > |\bar{\rho}|$, then as indicated in Ch. 4, distribution of $\Delta\hat{v}_{y0}(\bar{z})$ would contain the following three sections:* (1) $\bar{\rho} \leq \bar{z} \leq \bar{r}$, (2) $-\bar{\rho} \leq \bar{z} \leq \rho$, (3) $-\bar{r} \leq \bar{z} \leq -\bar{\rho}$. Switching now to the variable ψ, limits of integration for those three sections will be as follows (Fig. I.1):

$$\frac{\pi}{2} - \psi_1,\ \psi_1 - \psi_2,\ \psi_2 - \frac{3}{2}\pi^*.$$ Hence,

$$\Delta\hat{v}_r^0 = \frac{1}{\pi}\left[\int_{\pi/2}^{\psi_1} \Delta\hat{v}_{y_0}^0(\bar{z})\, d\psi + \int_{\psi_1}^{\psi_2} \ldots d\psi + \int_{\psi_2}^{\frac{3}{2}\pi} \ldots d\psi\right], \tag{I.4}$$

*Horizontal plane $x0z$ in which is located circle of radius $\bar{r}$, is shown in Fig. I.1, together with vertical plane $y\theta z$ in which the $\Delta\hat{v}_{y0}$ distribution is given.

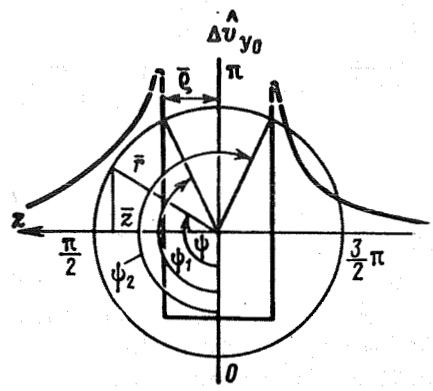

Figure I.1

where $\psi_1=\arcsin\frac{\bar{\rho}}{\bar{r}}<\pi$, $\psi_2=2\pi-\psi_1>\pi$.

We assume

$$\text{for region } \frac{\pi}{2}-\psi_1 \quad \Delta\hat{v}_{y0}(\bar{z})=-1+\frac{\bar{V}+\bar{z}}{\sqrt{\bar{z}^2-\bar{\rho}^2}},$$

$$\text{for region } \psi_1-\psi_2 \quad \Delta\hat{v}^0_{y_0}(\bar{z})=-1,$$

$$\text{for region } \psi_2-\frac{3}{2}\pi \quad \Delta\hat{v}^0_{y_0}(\bar{z})=-1-\frac{\bar{V}+\bar{z}}{\sqrt{\bar{z}^2-\bar{\rho}^2}}.$$

Substituting the above expressions into Eq. (I.4), we obtain

$$\Delta\hat{v}^0_r=\frac{1}{\pi}\left[-\int_{\pi/2}^{\frac{3}{2}\pi}d\psi+\int_{\pi/2}^{\psi_2}\frac{\bar{V}+\bar{z}}{\sqrt{\bar{z}^2-\bar{\rho}^2}}\,d\psi-\int_{\psi_2}^{\frac{3}{2}\pi}\frac{\bar{V}+\bar{z}}{\sqrt{\bar{z}^2-\bar{\rho}^2}}\,d\psi\right].$$

And after a substitution of $\bar{z}=\bar{r}\sin\psi_1$, $\bar{\rho}=\bar{r}\sin\psi_1$ in the region $\pi/2<\psi<\psi_1$; and $\bar{\rho}=\bar{r}\sin\psi_2$ in the region $\psi_2<\psi<(3/2)\pi$, as well as some transformations, we find

$$\Delta\hat{v}^0_r=-1+\frac{1}{\pi}\left(\frac{\bar{V}}{\bar{r}}E+F\right), \tag{I.5}$$

where

$$E=\int_{\pi/2}^{\psi_1}\frac{d\psi}{\sqrt{\sin^2\psi-\sin^2\psi_1}}-\int_{\psi_2}^{\frac{3}{2}\pi}\frac{d\psi}{\sqrt{\sin^2\psi-\sin^2\psi_2}},$$

$$F=\int_{\pi/2}^{\psi_1}\frac{\sin\psi d\psi}{\sqrt{\sin^2\psi-\sin^2\psi_1}}-\int_{\psi_2}^{\frac{3}{2}\pi}\frac{\sin\psi d\psi}{\sqrt{\sin^2\psi-\sin^2\psi_2}}.$$

For $\psi = \psi_1$ and $\psi = \psi_2$, the subintegral functions become discontinuous and integrals E and F become improper. Let us consider the integrals determining F:

$$\int_{\pi/2}^{\psi_1}\frac{\sin\psi d\psi}{\sqrt{\sin^2\psi-\sin^2\psi_1}}=\lim_{\varepsilon\to 0}\int_{\pi/2}^{\psi_1-\varepsilon}\frac{\sin\psi d\psi}{\sqrt{\sin^2\psi-\sin^2\psi_1}}=$$

$$=\lim_{\varepsilon\to 0}\int_{\pi/2}^{\psi_1-\varepsilon}\frac{\sin\psi d\psi}{\sqrt{\cos^2\psi_1-\cos^2\psi}}=-\lim_{\varepsilon\to 0}\arcsin\left(\frac{\cos\psi}{|\cos\psi_1|}\right)\Bigg|_{\pi/2}^{\psi_1-\varepsilon}=\frac{\pi}{2}.$$

The second integral is equal to $-\pi/2$. Consequently, $F = \pi$.

Taking advantage of the Cauchy criterion, we ascertain that limit values of integrals expressing E are finite. Integrals determining E are equal to each other. Consequently, $E = 0$. Then, from Eq. (I.5), we find

$$\begin{aligned}\Delta\hat{v}_r^{\varrho}&=-1 \quad \text{for } |\bar{r}|\leqslant|\bar{\varrho}|,\\ \Delta\hat{v}_r^{\varrho}&=0 \quad \text{for } |\bar{r}|>|\bar{\varrho}|,\end{aligned} \tag{I.6}$$

This means that free vortices springing from a circle of relative radius $\bar{\rho}$, having a constant circulation along it, generate the same average induced velocity at all circles having radii smaller than $\bar{\rho}$. At circles with radii larger than $\bar{\rho}$, the average induced velocities are zero.

Now we can determine $\bar{v}_r$. From Eq. (I.2) we have

$$\bar{v}_r=-\frac{k}{4\pi\bar{V}}\int_{\bar{\varrho}-\bar{r}_0}^{\bar{\varrho}-1}\Delta\hat{v}_r^{\varrho}\,d\bar{\Gamma}_{\varrho}=-\frac{k}{4\pi\bar{V}}\left[\int_{\bar{\varrho}-\bar{r}_0}^{\bar{\varrho}-\bar{r}}\Delta\hat{v}_r^{\varrho}\,d\bar{\Gamma}_{\varrho}+\int_{\bar{\varrho}-\bar{r}}^{\bar{\varrho}-1}\Delta\hat{v}_r^{\varrho}\,d\bar{\Gamma}_{\varrho}\right].$$

In the first integral, $\Delta\hat{v}_r{}^{\rho} = 0$; and in the second, $\Delta\hat{v}_r{}^{\rho} = -1$. Consequently,

$$\bar{v}_r=\frac{k}{4\pi\bar{V}}\int_{\bar{\varrho}-\bar{r}}^{\bar{\varrho}-1}d\bar{\Gamma}_{\varrho}=\frac{k}{4\pi\bar{V}}\left[\bar{\Gamma}_{\varrho}(1)-\bar{\Gamma}_{\varrho}(\bar{r})\right].$$

Circulation at the blade tip, averaged over the circle, is zero; i.e., $\Gamma_\rho(1) = 0$. From this

$$\bar{v}_r = -\frac{k\bar{\Gamma}_Q(\bar{r})}{4\pi\bar{V}}. \tag{I.7}$$

Eq. (I.7) is also correct for those cases when $\bar{\Gamma}_\rho(1) \neq 0$. As a matter of fact, in that case in Eq. (I.2) determining $\bar{v}_r$ due to the free vortex layer, a new term will be added. It would consider velocity induced at radius $\bar{r}$ by a discrete tip vortex with circulation $k\bar{\Gamma}_\rho(1)$. This induced velocity is determined according to Eq. (2.11) at $\Delta\hat{v}_{y_0} = -1$. As the final result, we obtain Eq. (I.7).

APPENDIX II

DETERMINATION OF COEFFICIENT $\bar{v}_{s1}(\bar{r})$ FOR THE $\sin\psi$ EXPANSION OF INDUCED VELOCITY INTO FOURIER SERIES

We define

$$\bar{v}_\mu(\bar{r}) = -\frac{k}{4\pi\bar{V}}\int_{\bar{Q}=1}^{\bar{Q}=\bar{r}_0}\Delta\hat{v}^{\rho}_{\mu}(\bar{r})\,d\bar{\Gamma}_Q. \tag{II.1}$$

Coefficient of that average induced velocity is

$$\Delta\hat{v}^{\rho}_{\mu}(\bar{r}) = \frac{\mu}{\pi\bar{r}}\int_{\pi/2}^{\frac{3}{2}\pi}\Delta\hat{v}^{\rho}_{y_0}(\bar{z})\sin\psi\,d\psi. \tag{II.2}$$

Determination of the above integral is performed similarly to the determination of the Integral in Eq. (I.3). Following the logic discussed in Appendix I, we substitute the three segments, $(\pi/2) - \psi$, $\psi_1 - \psi_2$ and $\psi_2 - (3/2)\pi$ instead of the integration limits, $(\pi/2) - (3/2)\pi$. In this way, we will take advantage of the previously obtained results. Then, for $\bar{r} \leq \bar{\rho}$ (i.e., when the radius at which the average induced velocity is calculated is smaller than that from which the vortices spring), $\Delta\hat{v}_{y_0}{}^{\rho}(z) = -1$, and

$$\Delta\hat{v}^{\rho}_{\mu}(\bar{r}) = -\frac{\mu}{\pi\bar{r}}\int_{\pi/2}^{\frac{3}{2}\pi}\sin\psi\,d\psi = 0. \tag{II.3}$$

For $\bar{r} \geq \bar{\rho}$, we represent integral (II.2) in the following form:

$$\Delta\hat{v}_{\mu}^{\rho}(\bar{r})=\frac{\mu}{\pi\bar{r}}\left[\int_{\pi/2}^{\psi_1}\Delta\hat{v}_{y_0}^{\rho}(\bar{z})\sin\psi\,d\psi+\int_{\psi_1}^{\psi_2}\ldots d\psi+\int_{\psi_2}^{\frac{3}{2}\pi}\ldots d\psi\right]$$

Introducing values of $\Delta\hat{v}_{y\,0}^{\rho}(\bar{z})$ for the singled out regions of integration; as in the determination of integrals in Eq. (I.4), we obtain

$$\Delta\hat{v}_{\mu}^{\rho}(\bar{r})=\frac{\mu}{\pi\bar{r}}\left[-\int_{\pi/2}^{\frac{3}{2}\pi}\sin\psi\,d\psi+\int_{\pi/2}^{\psi_1}\frac{(\bar{V}+\bar{z})}{\sqrt{\bar{z}^2+\bar{\rho}^2}}\sin\psi\,d\psi-\right.$$
$$\left.-\int_{\psi_2}^{\frac{3}{2}\pi}\frac{(\bar{V}+\bar{z})}{\sqrt{\bar{z}^2+\bar{\rho}^2}}\sin\psi\,d\psi\right]. \qquad \text{(II.4)}$$

We perform the same substitutions as for Eq. (I.5). Then, taking into consideration that the first integral is zero, we will have

$$\Delta\hat{v}_{\mu}^{\rho}(\bar{r})=\frac{\mu}{\pi\bar{r}}\left(\frac{\bar{V}}{\bar{r}}F+S\right). \qquad \text{(II.5)}$$

Here, as in Eq. (I.5), $F = \pi$, while

$$S=\int_{\pi/2}^{\psi_1}\frac{\sin^2\psi\,d\psi}{\sqrt{\sin^2\psi-\sin^2\psi_1}}-\int_{\psi_2}^{\frac{3}{2}\pi}\frac{\sin^2\psi\,d\psi}{\sqrt{\sin^2\psi-\sin^2\psi_2}} \qquad \text{(II.6)}$$

consists of the two improper integrals having finite values. Since $\psi_2 = 2\pi - \psi$; hence, both integrals are equal. Consequently, $S = 0$. Now we have

$$\Delta\hat{v}_{\mu}^{\rho}(\bar{r})=0 \quad \text{for} \quad \bar{r}<\bar{\rho},$$
$$\Delta\hat{v}_{\mu}^{\rho}(\bar{r})=\frac{\mu\bar{V}}{\bar{r}^2} \quad \text{for} \quad \bar{r}\geqslant\bar{\rho}. \qquad \text{(II.7)}$$

According to Eq. (II.1)

$$\bar{v}_{\mu}(\bar{r})=-\frac{k}{4\pi\bar{V}}\left[\int_{\bar{\rho}-\bar{r}_0}^{\bar{\rho}-\bar{r}}\Delta\hat{v}_{\mu}^{\rho}(\bar{r})\,d\bar{\Gamma}_{\rho}+\int_{\bar{\rho}-\bar{r}}^{\bar{\rho}-1}\ldots d\bar{\Gamma}_{\rho}\right]. \qquad \text{(II.8)}$$

On the basis of Eq. (II.7), the second integral here is zero and

$$\bar{v}_\mu(\bar{r}) = -\frac{k}{4\pi}\frac{\mu}{\bar{r}^2}\left[\bar{\Gamma}_\rho(\bar{r}) - \bar{\Gamma}_\rho(\bar{r}_0)\right]. \tag{II.9}$$

At the blade root, $\bar{\Gamma}_\rho(\bar{r}_0) = 0$. Then*

$$\bar{v}_\mu(\bar{r}) = -\frac{\mu}{\bar{r}^2}\frac{k\bar{\Gamma}_\rho(\bar{r})}{4\pi}. \tag{II.10}$$

In light of Eq. (2.92), we obtain

$$\bar{v}_{s1}(\bar{r}) = -\frac{k\bar{\Gamma}_\rho(\bar{r})}{2\pi\bar{r}}. \tag{II.11}$$

Taking into consideration Eq. (I.7), we can, in addition, write the following expression

$$\bar{v}_{s1}(\bar{r}) = 2\frac{\bar{V}}{\bar{r}}\bar{v}_r. \tag{II.12}$$

APPENDIX III

DETERMINATION OF COEFFICIENTS $\bar{v}_{s(2n+1)}(\bar{r})$ AND $\bar{v}_{c2n}(\bar{r})$ FOR THE $\sin(2n+1)\psi$ AND $\cos 2n\psi$ EXPANSION OF INDUCED VELOCITY INTO FOURIER SERIES

Let us represent relative induced velocity at any point of the rotor disc under the following form

$$\bar{v}_y(\bar{r}, \psi) = \bar{v}_r + \sum_{n=1}^{n=\infty}\left[\bar{v}_{cn}(\bar{r})\cos n\psi + \bar{v}_{sn}(\bar{r})\sin n\psi\right], \tag{III.1}$$

where

$$\bar{v}_r = \frac{1}{2\pi}\int_0^{2\pi}\bar{v}_y(\bar{r}, \psi)\,d\psi, \tag{III.2}$$

---

*It is possible to show that this formula is also correct when at the blade root, $\bar{\Gamma}_\rho \neq 0$.

$$\bar{v}_{cn}(\bar{r})=\frac{1}{\pi}\int_0^{2\pi}\bar{v}_y(\bar{r},\ \psi)\cos n\psi\, d\psi, \tag{III.3}$$

$$\bar{v}_{sn}(\bar{r})=\frac{1}{\pi}\int_0^{2\pi}\bar{v}_y(\bar{r},\ \psi)\sin n\psi\, d\psi. \tag{III.4}$$

Expressions for $\bar{v}_r$ and $v_{s1}(\bar{r})$ have already been obtained in Eqs. (I.7), (II.11) and (II.12). It was shown that*

$$\bar{v}_{c2}(\bar{r})=\frac{k\bar{\Gamma}_r}{2\pi\bar{V}}\,\frac{\bar{\varrho}_c^2}{\bar{r}^2}=2\bar{v}_r\tilde{\varrho}_c^2, \tag{III.5}$$

where

$$\bar{\varrho}_c^2=\frac{\int_{\bar{\varrho}=\bar{r}}^{\bar{\varrho}=\bar{r}_0}\bar{\varrho}^2 d\bar{\Gamma}_\varrho}{\int_{\bar{\varrho}=\bar{r}}^{\bar{\varrho}=\bar{r}_0}d\bar{\Gamma}_\varrho}, \qquad \tilde{\varrho}_c^2=\frac{\bar{\varrho}_c^2}{\bar{r}^2}. \tag{III.6}$$

At $\bar{\Gamma}_\rho = a\bar{\rho}$, we will have $\bar{\rho}_c^2 = (1/3)\bar{r}^2$. In this case,

$$\bar{v}_{c2}(\bar{r})=\frac{k\bar{\Gamma}_r}{6\pi\bar{V}}=-\frac{2}{3}\bar{v}_r. \tag{III.7}$$

Now, we determine $\bar{v}_{s(2m+1)}(\bar{r})$ and $\bar{v}_{c2(m+1)}(\bar{r})$ where $m=1,2,3\ldots$ Omitting intermediate calculations (analogous to those discussed in Appendix II), we present the final results:

$$\bar{v}_{s3}(\bar{r})=\bar{v}_{s1}(\bar{r})(1-2\tilde{\varrho}_c^2), \tag{III.8}$$

$$\bar{v}_{s5}(\bar{r})=\bar{v}_{s1}(\bar{r})(1-6\tilde{\varrho}_c^2+6\tilde{\varrho}_c^4), \tag{III.9}$$

$$\bar{v}_{s7}(\bar{r})=\bar{v}_{s1}(\bar{r})(1-12\tilde{\varrho}_c^2+30\tilde{\varrho}_c^4-20\tilde{\varrho}_c^6), \tag{III.10}$$

$$\bar{v}_{s9}(\bar{r})=\bar{v}_{s1}(\bar{r})(1-20\tilde{\varrho}_c^2+90\tilde{\varrho}_c^4-140\tilde{\varrho}_c^6+70\tilde{\varrho}_c^8), \tag{III.11}$$

$$\bar{v}_{s11}(\bar{r})=\bar{v}_{s1}(\bar{r})(1-30\tilde{\varrho}_c^2+210\tilde{\varrho}_c^4-560\tilde{\varrho}_c^6+630\tilde{\varrho}_c^8-252\tilde{\varrho}_c^{10}), \tag{III.12}$$

*Eqs. (III.5)-(III.7) were obtained by G.R. Kvasha

where

$$\tilde{\varrho}_c^{2m}=\frac{\int_{\bar{\varrho}=\bar{r}}^{\bar{\varrho}=\bar{r}_0}\bar{\varrho}^{2m}d\tilde{\Gamma}_{\varrho}}{\bar{r}^{2m}\int_{\bar{\varrho}=\bar{r}}^{\bar{\varrho}=\bar{r}_0}d\tilde{\Gamma}_{\varrho}}. \tag{III.13}$$

For $m = 1$, Eq. (III.13) changes into relationships given by Eq. (III.6). Similar to Eqs. (III.8)-(III.12), we also find that

$$\bar{v}_{c4}(\bar{r})=-2\bar{v}_r(2\tilde{\varrho}_c^2-3\tilde{\varrho}_c^4), \tag{III.14}$$

$$\bar{v}_{c6}(\bar{r})=-2\bar{v}_r(3\tilde{\varrho}_c^2-12\tilde{\varrho}_c^4+10\tilde{\varrho}_c^6), \tag{III.15}$$

$$\bar{v}_{c8}(\bar{r})=-2\bar{v}_r(4\tilde{\varrho}_c^2-30\tilde{\varrho}_c^4+60\tilde{\varrho}_c^6-35\tilde{\varrho}_c^8), \tag{III.16}$$

$$\bar{v}_{c10}(\bar{r})=-2\bar{v}_r(5\tilde{\varrho}_c^2-60\tilde{\varrho}_c^4+210\tilde{\varrho}_c^6-280\tilde{\varrho}_c^8+128\tilde{\varrho}_c^{10}). \tag{III.17}$$

During the development of the relationships given by Eqs. (III.14)-(III.17), the following recurring formula was established

$$\bar{v}_{s(2m+1)}(\bar{r})-\bar{v}_{s2(m-1)}(\bar{r})=\bar{v}_{c2m}(\bar{r})\frac{\bar{v}_{s1}(\bar{r})}{\bar{v}_r}. \tag{III.18}$$

In order to facilitate quantitative estimates, we are going to develop a simple formula for $\tilde{\rho}_c^{2m}$ which corresponds to the $\tilde{\Gamma}$ distribution given by the following relationship

$$\tilde{\Gamma}=a\bar{\varrho}^s(1-\bar{\varrho}^t). \tag{III.19}$$

According to the condition of Eq. (3.12), at $\bar{r}_0 = 0$,

$$a=\frac{(s+2)(s+t+2)}{2t}. \tag{III.20}$$

For $t \to \infty$ and $s = 1$, quantity $\tilde{\Gamma} \to (3/2)\bar{\rho}$, while for $t \to \infty$ and $s = 0$, circulation $\tilde{\Gamma} \to 1$. In this way, properly selecting values of s and t, one can always get a practical approximation of the circulation $\tilde{\Gamma}$ close to the real one as given by Eqs.

(2.98) and (3.35). Substituting Eq. (III.19) into Eq. (III.13) and assuming, for simplicity, that $\bar{r}_0 = 0$, we obtain

$$\tilde{\varrho}_c^{2m} = \frac{s(1-p\bar{r}^t)}{(2m+s)(1-\bar{r}^t)}, \tag{III.21}$$

where

$$p = \frac{(s+t)(2m+s)}{s(2m+s+t)}. \tag{III.22}$$

It should be realized that the higher value of the t power, the less is the dependence of $\tilde{\rho}_c^{2m}$ on $\bar{r}$. For $t \to \infty$, quantity $\tilde{\rho}_c^{2m} \to s/(2m+s)$. In other words, it becomes constant along the blade. In addition if $s \to 0$ also, then $\tilde{\rho}_c^{2m} \to 0$.

In the particular case of $\tilde{\Gamma} = 1,5\tilde{\rho}$ $(s = 1,\ t \to \infty)$, the quantity $\tilde{\rho}_c^{2m} = 1/(2m+1)$ and the relationships expressed by Eqs. (III.8)-(III.12), and (III.14)-(III.17) can be expressed by the following recurring formulae

$$\bar{v}_{s(2m+1)}(\bar{r}) = \frac{1}{2m+1}\bar{v}_{s1}(\bar{r}), \tag{III.23}$$

$$\bar{v}_{c2(m+1)}(\bar{r}) = -\frac{2}{4(m+1)^2-1}\bar{v}_r. \tag{III.24}$$

APPENDIX IV

DETERMINATION OF COEFFICIENTS $\bar{v}_{s2n}(\bar{r})$ AND $\bar{v}_{c(2n-1)}(\bar{r})$ FOR THE $\sin 2n\psi$ AND $\cos(2n-1)\psi$ EXPANSION OF INDUCED VELOCITY INTO FOURIER SERIES

Let us begin with the determination of $\bar{v}_{c1}(\bar{r})$. According to Eq. (III.3)

$$\bar{v}_{c1}(\bar{r}) = \frac{1}{\pi}\int_0^{2\pi} \bar{v}_y(\bar{r},\ \psi)\cos\psi\, d\psi. \tag{IV.1}$$

We take the same approach as that in the development of the formula for $\bar{v}_r$ by summing up induced velocities at points summetrical with respect to the Oz axis (see Fig. 2.30). Then,

$$\bar{v}_y(\bar{r},\ \psi)\cos\psi + \bar{v}_y(\bar{r},\ \pi-\psi)\cos(\pi-\psi) = 2\left[\bar{v}_{y1}(\bar{x},\ \bar{z}) + \bar{v}_{y2}(\bar{x},\ \bar{z})\right]\cos\psi. \tag{IV.2}$$

Next, we have

$$\bar{v}_{c1}(\bar{r})=\frac{2}{\pi}\int_{-\pi/2}^{\pi/2}[\bar{v}_{y1}(\bar{x},\ \bar{z})+\bar{v}_{y2}(\bar{x},\ \bar{z})]\cos\psi\,d\psi.$$

We replace the variable of integration ψ by the variable z. Then,

$$\bar{v}_{c1}(\bar{r})=\frac{2}{\pi\bar{r}}\int_{-\bar{r}}^{\bar{r}}[\bar{v}_{y1}(\bar{x},\ \bar{z})+\bar{v}_{y2}(\bar{x},\ \bar{z})]\,d\bar{z}. \tag{IV.3}$$

In analogy with Eqs. (2.68) and (2.71), we obtain

$$\bar{v}_{c1}(\bar{r})=\frac{k\tilde{\Gamma}_c}{4\pi\bar{V}}\hat{v}_{c1}(\bar{r}), \tag{IV.4}$$

where

$$\hat{v}_{c1}(\bar{r})=\sum_{\bar{Q}=\bar{Q}_0}^{\bar{Q}=1,0}\Delta\hat{v}^{\rho}_{c1}(\bar{r})\,\Delta\tilde{\Gamma}_Q. \tag{IV.5}$$

Here,

$$\Delta\hat{v}^{\rho}_{c1}(\bar{r})=\frac{2}{\pi\bar{r}}\int_{-\bar{r}}^{\bar{r}}[\Delta\hat{v}^{\rho}_{y1}(\bar{x},\ \bar{z})+\Delta\hat{v}^{\rho}_{y2}(\bar{x},\ \bar{z})]d\bar{z},$$

$$\bar{z}=\bar{r}\sin\psi,\qquad \bar{x}=\bar{r}\cos\psi. \tag{IV.6}$$

Using formulae and graphs from Sects. 3 and 5 of Ch. II, we find $\bar{z}$ and $\bar{x}$ for given $\bar{r}$ at various angles ψ. Next, for every $\bar{\rho}$ (radius of the station from which spring the free vortices), we compute $\tilde{x}=\bar{x}/\bar{\rho}$, $\tilde{z}=\bar{z}/\bar{\rho}$ and from suitable graphs we find $\Delta\hat{v}^{\rho}_{y1}(\tilde{x},\tilde{z})$. Then, we find M and N from the graphs, and upon defining $\bar{V}_*=\bar{V}/\bar{\rho}$, we compute $\Delta\hat{v}^{\rho}_{y2}(\tilde{x},\tilde{z})$ from Eq. (2.36). After the completion of those calculations, explicit formulae for $\hat{v}_{c1}(\bar{r})$ at $\bar{V}=0{,}15;\ 0{,}25$, and $0{,}35$ were obtained.

According to Eq. (III.4), we have

$$\bar{v}_{s2}(\bar{r})=\frac{1}{\pi}\int_0^{2\pi}\bar{v}_y(\bar{r},\ \psi)\sin 2\psi\,d\psi, \tag{IV.7}$$

$$\bar{v}_{s4}(\bar{r})=\frac{1}{\pi}\int_0^{2\pi}\bar{v}_y(\bar{r},\ \psi)\sin 4\psi\,d\psi. \tag{IV.8}$$

From Eq. (III.3), we find

$$\bar{v}_{c3}(\bar{r})=\frac{1}{\pi}\int_0^{2\pi}\bar{v}_y(\bar{r},\ \psi)\cos 3\psi\, d\psi, \tag{IV.9}$$

$$\bar{v}_{c5}(\bar{r})=\frac{1}{\pi}\int_0^{2\pi}\bar{v}_y(\bar{r},\ \psi)\cos 5\psi\, d\psi. \tag{IV.10}$$

These coefficients are analogous to $\bar{v}_{c1}(\bar{r})$ in the sense that the sum of subintegral expressions in the symmetrical points here is also determined as a doubled sum of $\bar{v}_{y_1}(\bar{x},\bar{z})+\bar{v}_{y_2}(\bar{x},\bar{z})$ multiplied by either sine or cosine, whichever is appropriate. In this way, in analogy with Eq. (IV.4), one can write

$$\bar{v}_{s2}(\bar{r})=\frac{k\bar{\Gamma}_{cp}}{4\pi\bar{V}}\hat{v}_{s2}(\bar{r}), \tag{IV.11}$$

$$\bar{v}_{s4}(\bar{r})=\frac{k\bar{\Gamma}_{cp}}{4\pi\bar{V}}\hat{v}_{s4}(\bar{r}), \tag{IV.12}$$

$$\bar{v}_{c3}(\bar{r})=\frac{k\bar{\Gamma}_{cp}}{4\pi\bar{V}}\hat{v}_{c3}(\bar{r}), \tag{IV.13}$$

$$\bar{v}_{c5}(\bar{r})=\frac{k\bar{\Gamma}_{cp}}{4\pi\bar{V}}\hat{v}_{c5}(\bar{r}). \tag{IV.14}$$

Without concentrating on details connected with the computation of the proper coefficients, we will present the results of calculations of $\hat{v}_{c1}(\bar{r})$, $\hat{v}_{s2}(\bar{r})$* for $\bar{V}=0{,}15;\ 0{,}25;\ 0{,}35$ and calculations of $\hat{v}_{c3}(\bar{r})$, $\hat{v}_{s4}(\bar{r})$, $\hat{v}_{c5}(\bar{r})$ for $\bar{V}=0{,}25$.

Coefficients $\hat{v}_{sn}$ and $\hat{v}_{cm}$ are found from the following formulae

$$\hat{v}_{sn}(\bar{r})=\sum_{k=1}^{10}\Delta\hat{v}_{sn}^{k}(\bar{r})\,\Delta\bar{\Gamma}_k,\quad \hat{v}_{cm}(\bar{r})=\sum_{k=1}^{10}\Delta v_{cm}(\bar{r})\,\Delta\bar{\Gamma}_k,$$

where $k=10\bar{\rho}$. Functions $\Delta\hat{v}_{sn}(\bar{r})$ $(n=2,4)$ and $\Delta\hat{v}_{cm}(\bar{r})$ $(m=1,3,5)$ are given in the tables.

---

*Quantity $\hat{v}_{s2}(\bar{r})$ as determined by G.R. Kvasha

$\Delta \widehat{v}^{0}_{s2}(\bar{r})$

$\bar{r}$ \ k	1	2	3	4	5	6	7	8	9	10	$\bar{V}$
0,15	1,030	—0,220	—0,034	—0,025	—0,004	0,001	0,003	0,001	0,002	0,001	
0,35	0,820	0,620	0,145	—0,220	—0,095	—0,060	—0,041	—0,025	—0,009	—0,012	
0,55	0,730	0,590	0,405	0,190	—0,018	—0,210	—0,073	—0,062	—0,036	—0,020	0,15
0,75	0,480	0,470	0,428	0,330	0,230	0,100	—0,033	—0,200	—0,100	—0,032	
0,95	0,350	0,380	0,380	0,307	0,250	0,150	0,032	—0,093	—0,160	—0,088	
0,15	1,733	—0,320	—0,063	—0,025	—0,017	—0,012	—0,006	—0,005	—0,004	0,005	
0,35	1,250	0,900	0,152	—0,250	—0,110	—0,057	—0,036	—0,020	—0,010	—0,009	
0,55	0,960	0,810	0,570	0,300	—0,120	—0,250	—0,120	—0,054	—0,047	—0,031	0,25
0,75	0,718	0,620	0,540	0,450	0,300	0,120	—0,107	—0,314	—0,164	—0,110	
0,95	0,550	0,540	0,500	0,440	0,370	0,260	0,120	—0,020	—0,150	—0,160	
0,15	2,560	—0,470	—0,056	—0,023	—0,009	—0,008	—0,008	—0,013	—0,011	—0,013	
0,35	1,770	1,240	0,162	—0,285	—0,125	—0,054	—0,031	—0,015	—0,011	—0,008	
0,55	1,460	1,140	0,910	0,495	—0,190	—0,430	—0,194	—0,072	—0,030	—0,030	0,35
0,75	1,130	0,990	0,820	0,645	0,480	0,113	—0,290	—0,485	—0,210	—0,140	
0,95	0,931	0,874	0,820	0,730	0,640	0,432	0,200	—0,100	—0,380	—0,375	

$\Delta \widehat{v}^{0}_{s4}(\bar{r})$

0,15	0,187	—0,035	—0,005	0,009	0,015	0,010	0,005	0,015	0,004	0,004	
0,35	—0,049	—0,105	0,052	—0,044	—0,022	—0,002	—0,007	—0,003	—0,011	—0,028	
0,55	—0,042	0,007	0,055	0,156	0,067	—0,010	—0,015	—0,007	0,002	—0,010	0,25
0,75	—0,071	—0,027	0,010	0,022	—0,190	0,137	0,397	0,021	—0,020	—0,022	
0,95	—0,044	—0,040	—0,035	—0,045	—0,005	0,050	0,183	0,183	0,282	0,010	

$\Delta \widehat{v}^{0}_{s1}(\bar{r})$

0,15	—0,640	—1,109	—0,569	—0,396	—0,291	—0,241	—0,204	—0,174	—0,151	—0,123	
0,35	—0,042	—0,344	—1,286	—1,560	—0,898	—0,661	—0,555	—0,467	—0,394	—0,333	
0,55	0,143	—0,050	—0,372	—0,774	—1,740	—1,820	—1,230	—0,885	—0,722	—0,620	0,15
0,75	0,005	0	—0,119	—0,308	—0,602	—1,070	—1,910	—2,040	—1,390	—1,080	
0,95	0,096	0,104	0,040	—0,120	—0,356	—0,600	—0,920	—1,280	—2,040	—2,020	

$\Delta\hat{v}^{0}_{c1}(\bar{r})$

$\bar{r}$ \ k	1	2	3	4	5	6	7	8	9	10	$\bar{V}$
0,15	−0,160	−1,065	−0,562	−0,384	−0,308	−0,256	−0,215	−0,181	−0,149	−0,132	0,25
0,35	−0,048	−0,450	−1,277	−1,530	−0,923	−0,672	−0,545	−0,448	−0,383	−0,320	
0,55	0,080	−0,107	−0,407	−0,801	−1,750	−1,710	−1,307	−0,878	−0,748	−0,620	
0,75	−0,086	−0,084	−0,179	−0,340	−0,650	−1,046	−1,920	−2,010	−1,410	−1,080	
0,95	0,041	−0,010	−0,099	−0,240	−0,420	−0,570	−0,835	−1,240	−1,960	−1,980	
0,15	−0,910	−1,110	−0,540	−0,375	−0,294	−0,235	−0,210	−0,176	−0,155	−0,141	0,35
0,35	−0,054	−0,430	−1,320	−1,450	−0,920	−0,676	−0,560	−0,480	−0,415	−0,360	
0,55	0,080	−0,080	−0,350	−0,780	−1,650	−1,810	−1,185	−0,910	−0,730	−0,640	
0,75	−0,100	−0,094	−0,190	−0,340	−0,600	−1,035	−1,930	−2,050	−1,390	−1,060	
0,95	0,078	0,091	−0,013	−0,140	−0,330	−0,531	−0,830	−1,220	−1,990	−1,840	

$\Delta\hat{v}^{0}_{c3}(\bar{r})$

0,15	−0,061	0,010	−0,008	−0,278	−0,011	−0,008	−0,010	0,002	0,002	0,002	0,25
0,35	−0,309	−0,679	0,124	0,124	0,035	0,008	−0,015	−0,010	−0,014	−0,026	
0,55	−0,391	−0,328	−0,565	−0,230	0,220	0,162	0,092	0,017	−0,038	−0,014	
0,75	−0,366	−0,376	−0,382	−0,454	−0,965	0,080	0,310	0,141	0,064	0,040	
0,95	−0,338	−0,370	−0,388	−0,426	−0,521	−0,746	−0,190	0,155	0,430	0,552	

$\Delta\hat{v}^{0}_{c5}(\bar{r})$

0,15	−0,047	0,020	−0,001	0,038	0,012	0,006	0,010	0,015	0,019	0,026	0,25
0,35	−0,039	0,243	0,022	0,038	−0,026	0,011	0,019	0,010	0,001	−0,004	
0,55	−0,155	−0,187	−0,323	0,008	0,273	0,007	−0,009	0,002	−0,010	0,016	
0,75	−0,160	−0,161	−0,176	−0,260	−0,594	0,106	0,243	0,040	0,015	0,008	
0,95	−0,301	−0,321	−0,341	−0,407	−0,522	−1,057	0,216	0,261	−0,007	−0,191	

APPENDIX V

FORMULAE FOR CALCULATIONS OF THE $\hat{v}_y$ COEFFICIENTS

The $\hat{v}_y$ coefficients for $\bar{y} = 0$ are found from the following formula

$$\hat{v}_y(\bar{r}, \psi) = \sum_{k=1}^{10} \Delta\hat{v}_y^k(\bar{r}, \psi)\,\Delta\bar{\Gamma}_k,$$

where $k = 10\bar{\rho}$. Functions $\Delta\hat{v}_y^k(\bar{r}, \psi)$ are given in the tables. For $\psi = 0$ and $\psi = 180°$, the coefficients $\Delta\hat{v}_y^k(r, \psi)$ are independent of $\bar{V}$.

$\psi=0$

$\bar{r}$ \ k	1	2	3	4	5	6	7	8	9	10	$\bar{V}$
0,15	—2,54	—1,85	—1,51	—1,35	—1,28	—1,23	—1,21	—1,16	—1,14	—1,14	
0,35	—2,00	—2,10	—2,45	—2,54	—1,90	—1,70	—1,60	—1,50	—1,43	—1,39	
0,55	—2,00	—2,04	—2,09	—2,20	—2,56	—2,57	—2,09	—1,88	—1,74	—1,65	
0,75	—2,00	—2,03	—2,06	—2,09	—2,16	—2,29	—2,60	—2,66	—2,24	—2,00	
0,95	—2,00	—2,02	—2,04	—2,06	—2,07	—2,12	—2,23	—2,40	—2,63	—2,65	
$\psi=45°$											
0,15	—1,45	—1,65	—1,30	—1,22	—1,15	—1,14	—1,13	—1,12	—1,10	—1,06	
0,35	1,38	3,20	—2,75	—2,27	—1,75	—1,50	—1,40	—1,33	—1,28	—1,24	
0,55	0,76	1,05	2,20	—1,35	—2,95	—2,47	—1,94	—1,70	—1,54	—1,45	0,15
0,75	0,58	0,67	1,00	1,82	5,40	—2,40	—3,00	—3,02	—2,07	—1,82	
0,95	0,47	0,51	0,65	0,90	1,36	3,35	—1,94	—2,50	—3,12	—3,00	
0,15	—2,50	—1,75	—1,40	—1,20	—1,14	—1,10	—1,10	—1,08	—1,07	—1,05	
0,35	2,00	4,80	—3,08	—2,55	—1,75	—1,54	—1,40	—1,35	—1,28	—1,23	
0,55	1,35	1,60	2,78	—1,50	—3,25	—2,65	—1,97	—1,71	—1,54	—1,47	0,25
0,75	0,96	1,05	1,35	2,15	6,10	—2,55	—3,17	—3,00	—2,14	—1,85	
0,95	0,64	0,72	0,87	1,20	1,90	3,55	—1,80	—2,50	—3,10	—3,15	
0,15	—2,50	—1,77	—1,38	—1,24	—1,17	—1,14	—1,13	—1,10	—1,08	—1,07	
0,35	2,93	5,75	—3,20	—2,57	—1,82	—1,54	—1,43	—1,35	—1,30	—1,25	
0,55	1,72	2,07	3,50	—1,75	—3,25	—2,80	—2,02	—1,72	—1,60	—1,48	0,35
0,75	1,22	1,34	1,76	2,72	6,20	—2,66	—3,30	—3,07	—2,16	—1,84	
0,95	0,97	1,03	1,24	1,57	2,21	4,15	—2,00	—2,70	—3,27	—3,70	
$\psi=90°$											
0,15	1,7	—1,00	—1,00	—1,00	—1,00	—1,00	—1,00	—1,00	—1,00	—1,00	
0,35	0,50	0,75	1,90	—1,00	—1,00	—1,00	—1,00	—1,00	—1,00	—1,00	
0,55	0,30	0,36	0,55	0,90	2,13	—1,00	1,00	—1,00	—1,00	—1,00	
0,75	0,20	0,26	0,30	0,43	0,60	1,01	2,60	—1,00	—1,00	—1,00	0,15
0,95	0,12	0,20	0,24	0,29	0,36	0,50	0,72	1,20	2,95	—1,00	
1,00	0,10	0,18	0,23	0,27	0,33	0,44	0,61	0,92	1,80	—1,00	
1,05	0,10	0,16	0,21	0,24	0,30	0,40	0,53	0,75	1,30	2,75	
1,15	0,08	0,15	0,18	0,24	0,26	0,32	0,47	0,60	0,84	1,37	

$\psi=90°$

$\bar{r}$ \ k	1	2	3	4	5	6	7	8	9	10	$\bar{V}$
0,15	2,57	—1,00	—1,00	—1,00	—1,00	—1,00	—1,00	—1,00	—1,00	—1,00	
0,35	0,80	1,10	2,50	—1,00	—1,00	—1,00	—1,00	—1,00	—1,00	—1,00	
0,55	0,50	0,57	0,75	1,12	2,70	—1,00	—1,00	—1,00	—1,00	—1,00	
0,75	0,33	0,38	0,45	0,60	0,80	1,25	2,85	—1,00	—1,00	—1,00	0,25
0,95	0,21	0,25	0,33	0,38	0,49	0,65	0,91	1,38	3,22	—1,00	
1,00	0,19	0,23	0,31	0,36	0,46	0,58	0,79	1,14	1,90	—1,00	
1,05	0,18	0,22	0,30	0,35	0,42	0,52	0,66	0,92	1,50	3,07	
1,15	0,17	0,21	0,27	0,30	0,35	0,43	0,57	0,67	0,97	1,57	
0,15	3,47	—1,00	—1,00	—1,00	—1,00	—1,00	—1,00	—1,00	—1,00	—1,00	
0,35	1,25	1,45	3,15	—1,00	—1,00	—1,00	—1,00	—1,00	—1,00	—1,00	
0,55	0,67	0,75	0,94	1,46	3,25	—1,00	—1,00	—1,00	—1,00	—1,00	
0,75	0,47	0,54	0,61	0,77	0,97	1,50	3,40	—1,00	—1,00	—1,00	0,35
0,95	0,30	0,38	0,45	0,55	0,64	0,85	1,05	1,57	3,42	—1,00	
1,00	0,26	0,34	0,40	0,50	0,57	0,77	0,94	1,25	2,25	—1,00	
1,05	0,25	0,34	0,40	0,46	0,54	0,64	0,80	1,07	1,70	3,40	
1,15	0,22	0,30	0,36	0,40	0,45	0,52	0,64	0,82	1,10	1,77	

$\psi=135°$

0,15	0,10	—0,32	—0,65	—0,75	—0,83	—0,86	—0,89	—0,90	—0,91	—0,92	
0,35	0,20	0,54	0,75	0,35	—0,22	—0,50	—0,58	—0,67	—0,73	—0,75	
0,55	0,11	0,15	0,34	—0,35	0,90	0,70	—0,10	—0,32	—0,45	—0,53	0,15
0,75	0,05	0,06	0,18	0,30	0,70	0,41	1,20	0,65	0,02	—0,17	
0,95	0	0,02	0,06	0,07	0,13	0,50	—0,17	0,50	1,02	0,93	
0,15	0	—0,25	—0,68	—0,80	—0,84	—0,87	—0,92	—0,96	—0,96	—0,95	
0,35	0,22	0,61	1,15	0,60	—0,22	—0,45	—0,56	—0,67	—0,72	—0,75	
0,55	0,20	0,25	0,43	—0,65	1,27	0,67	—0,02	—0,30	—0,42	—0,51	0,25
0,75	0,05	0,17	0,22	0,31	1,50	0,52	1,20	0,50	0,10	—0,17	
0,95	0	0,10	0,15	0,20	0,24	0,43	—0,17	0,60	1,25	0,80	
0,15	1,00	—0,22	—0,64	—0,80	—0,82	—0,87	—0,90	—0,93	—0,94	—0,93	
0,35	0,25	0,75	1,15	0,70	—0,17	—0,44	—0,56	—0,65	—0,71	—0,75	
0,55	0,12	0,37	0,57	—0,50	1,30	0,80	—0	—0,26	—0,40	—0,50	0,35
0,75	0,07	0,22	0,21	0,42	0,90	0,57	1,25	0,87	0,15	—0,10	
0,95	0,05	0,15	0,10	0,30	0,44	0,60	—0,12	0,70	1,35	1,45	

$\psi=180°$

$\bar{r}$ \ k	1	2	3	4	5	6	7	8	9	10	$\bar{V}$
0,15	0,40	—0,22	—0,50	—0,64	—0,72	—0,77	—0,79	—0,84	—0,87	—0,88	
0,35	0,03	0,09	0,50	0,53	—0,11	—0,32	—0,41	—0,51	—0,57	—0,61	
0,55	0,01	0,04	0,08	0,20	0,56	0,57	0,09	—0,12	—0,26	—0,35	
0,75	0	0,02	0,05	0,08	0,15	0,30	0,60	0,62	0,24	0	
0,95	0	0,02	0,04	0,06	0,08	0,12	0,22	0,42	0,62	0,63	
$\psi=225°$											
0,15	—0,78	—0,32	—0,63	—0,72	—0,79	—0,83	—0,87	—0,88	—0,92	—0,92	
0,35	—0,15	—0,11	0,09	—0,06	—0,31	—0,45	—0,60	—0,67	—0,74	—0,77	
0,55	—0,09	—0,10	—0,16	0,30	0,38	0,08	—0,17	—0,32	—0,43	—0,52	0,15
0,75	0	—0,09	—0,03	0	0,26	0,18	0,38	0,19	—0,04	—0,19	
0,95	0,07	—0,06	0,04	0	0,03	0,10	—0,32	0,30	0,45	0,39	
0,15	—0,84	—0,50	—0,66	—0,76	—0,80	—0,86	—0,88	—0,91	—0,94	—0,93	
0,35	—0,24	—0,27	—0,17	—0,14	—0,36	—0,49	—0,61	—0,68	—0,73	—0,76	
0,55	—0,10	—0,05	—0,16	—0,27	0,10	0	—0,20	—0,34	—0,45	—0,54	0,25
0,75	—0,04	—0,14	—0,06	—0,08	0,21	0,06	0,25	0,14	—0,08	—0,24	
0,95	0	—0,12	—0,09	—0,05	—0,04	0,10	—0,29	0,23	0,29	0,46	
0,15	—0,92	—0,60	—0,68	—0,74	—0,80	—0,85	—0,89	—0,91	—0,93	—0,91	
0,35	—0,42	—0,40	—0,43	—0,27	—0,42	—0,52	—0,60	—0,67	—0,73	—0,76	
0,55	—0,21	—0,17	—0,24	0,35	—0,08	—0,06	—0,22	—0,37	—0,46	—0,55	0,35
0,75	—0,04	—0,16	—0,09	—0,18	0,04	—0,02	0,31	0,25	—0,11	—0,38	
0,95	0,04	—0,16	—0,03	—0,08	—0,24	—0,38	—0,24	0,14	0,34	0,35	
$\psi=270°$											
0,15	—1,00	—1,00	—1,00	—1,00	—1,00	—1,00	—1,00	—1,00	—1,00	—1,00	
0,35	—0,40	—0,30	0,02	—1,00	—1,00	—1,00	—1,00	—1,00	—1,00	—1,00	
0,55	—0,26	—0,22	—0,12	0,04	0,80	—1,00	—1,00	—1,00	—1,00	—1,00	
0,75	—0,19	—0,18	—0,12	—0,06	0,07	0,32	1,25	—1,00	—1,00	—1,00	
0,95	—0,16	—0,15	—0,12	—0,07	0	0,12	0,25	0,53	1,75	—1,00	0,15
1,00	—0,16	—0,15	—0,12	—0,07	0	0,09	0,20	0,40	0,90	—1,00	
1,05	—0,15	—0,13	—0,10	—0,08	—0,02	0,07	0,16	0,34	0,67	1,84	
1,15	—0,17	—0,12	—0,10	—0,07	—0,02	0,04	0,12	0,20	0,38	0,77	

$\psi=270°$

$\bar{r}$ \ k	1	2	3	4	5	6	7	8	9	10	$\bar{V}$
0,15	—1,88	—1,00	—1,00	—1,00	—1,00	—1,00	—1,00	—1,00	—1,00	—1,00	
0,35	—0,71	—0,65	—0,42	—1,00	—1,00	—1,00	—1,00	—1,00	—1,00	—1,00	
0,55	—0,45	—0,41	—0,34	—0,19	0,35	—1,00	—1,00	—1,00	—1,00	—1,00	
0,75	—0,33	—0,31	—0,27	—0,18	—0,11	0,12	0,94	—1,00	—1,00	—1,00	0,25
0,95	—0,26	—0,25	—0,22	—0,18	—0,12	—0,05	0,12	0,38	1,35	—1,00	
1,00	—0,25	—0,25	—0,21	—0,17	—0,11	—0,08	0,07	0,29	0,66	—1,00	
1,05	—0,24	0,24	—0,20	—0,17	—0,12	—0,08	0,03	0,16	0,50	1,50	
1,15	—0,22	—0,22	—0,19	—0,15	—0,13	—0,08	—0,02	0,08	0,22	0,62	
0,15	—2,8	—1,00	—1,00	—1,00	—1,00	—1,00	—1,00	—1,00	—1,00	—1,00	
0,35	—1,00	—1,00	—1,00	—1,00	—1,00	—1,00	—1,00	—1,00	—1,00	—1,00	
0,55	—0,64	—0,60	—0,57	—0,53	—0,19	—1,00	—1,00	—1,00	—1,00	—1,00	
0,75	—0,48	—0,44	—0,42	—0,40	—0,28	—0,13	0,55	—1,00	—1,00	—1,00	0,35
0,95	—0,43	—0,38	—0,34	—0,32	—0,25	—0,20	—0,07	0,18	1,05	—1,00	
1,00	—0,42	—0,38	—0,33	—0,30	—0,25	—0,20	—0,09	0,08	0,55	—1,00	
1,05	—0,39	—0,33	—0,30	—0,28	—0,24	—0,17	—0,10	0,01	0,32	1,27	
1,15	—0,37	—0,30	—0,28	—0,27	—0,22	—0,18	—0,10	—0,03	0,11	0,45	
					$\psi=315°$						
0,15	—2,65	—1,67	—1,37	—1,26	—1,20	—1,17	—1,14	—1,12	—1,08	—1,07	
0,35	—1,00	—0,50	—2,05	—1,94	—1,62	—1,47	—1,37	—1,30	—1,25	—1,20	
0,55	—0,64	—0,52	—0,05	—1,50	—2,25	—2,10	—1,80	—1,62	—1,52	—1,42	0,15
0,75	—0,50	—0,44	—0,22	+0,27	+2,00	—2,15	—2,42	—2,20	—1,92	—1,75	
0,95	—0,45	—0,27	—0,20	0	0,32	1,42	—1,70	—2,32	—2,44	—2,75	
0,15	—1,50	—1,40	—1,27	—1,20	—1,16	—1,13	—1,10	—1,05	—1,05	—1,05	
0,35	—1,80	—1,75	—1,82	—1,82	—1,60	—1,45	—1,37	—1,30	—1,27	—1,22	
0,55	—1,10	—1,05	—0,71	—1,45	—2,10	—2,10	—1,80	—1,60	—1,50	—1,45	0,25
0,75	—0,82	—0,74	—0,63	—0,30	1,02	—2,05	—2,24	—2,15	—1,90	—1,75	
0,95	—0,67	—0,60	—0,52	—0,37	0	0,70	—1,75	—2,25	—2,35	—2,55	
0,15	—1,75	—1,35	—1,25	—1,20	—1,15	—1,12	—1,10	—1,07	—1,06	—1,05	
0,35	—1,05	—3,15	—1,90	—1,80	—1,55	—1,45	—1,38	—1,30	—1,24	—1,29	
0,55	—1,10	—1,65	—1,37	—1,45	—2,10	—2,05	—1,77	—1,60	—1,50	—1,42	0,35
0,75	—1,40	—1,25	—1,05	—0,87	—0,35	—1,97	—2,25	—2,25	—1,85	—1,70	
0,95	—1,50	—1,10	—0,88	—0,75	—0,55	+0,22	—1,57	—2,15	—2,30	—2,80	

APPENDIX VI

TABLES OF THE INFLUENCE FUNCTIONS

Table VI.1

$k=3$

$\bar{\varrho}_j$	$\sin\beta_R$	$\bar{v}_{ij/k}$									
		$i=1$	$i=2$	$i=3$	$i=4$	$i=5$	$i=6$	$i=7$	$i=8$	$i=9$	$i=10$
0,24	0,03	—2,7470	0,0530			0,0001	—0,0001				
($j=1$)	0,04	—2,1869	0,1107	0,0003							
	0,05	—1,8889	0,1665	0,0013							
	0,06	—1,7099	0,2137	0,0036	0,0001						
	0,07	—1,5913	0,2513	0,0070	0,0002						
	0,08	—1,5063	0,2800	0,0114	0,0006						
	0,09	—1,4410	0,3013	0,0161	0,0011	0,0001					
0,32	0,03	0,0447	—2,7485	0,0524							
($j=2$)	0,04	0,0928	—2,1911	0,1099	0,0003						
	0,05	0,1391	—1,8970	0,1661	0,0013						
	0,06	0,1785	—1,7226	0,2143	0,0036	0,0001					
	0,07	0,2104	—1,6094	0,2534	0,0071	0,0002					
	0,08	0,2354	—1,5303	0,2842	0,0116	0,0006					
	0,09	0,2550	—1,4714	0,3079	0,0166	0,0012	0,0001				
0,40	0,03		0,0458	—2,7492	0,0520						
($j=3$)	0,04	0,0002	0,0955	—2,1931	0,1092	0,0003					
	0,05	0,0009	0,1437	—1,9008	0,1653	0,0013					
	0,06	0,0024	0,1849	—1,7287	0,2137	0,0036	0,0001				
	0,07	0,0048	0,2185	—1,6183	0,2534	0,0071	0,0002				
	0,08	0,0078	0,2453	—1,5422	0,2850	0,0116	0,0006				
	0,09	0,0111	0,2663	—1,4866	0,3099	0,0167	0,0012	0,0001			
0,48	0,03			0,0465	—2,7496	0,0517					
($j=4$)	0,04		0,0002	0,0972	—2,1942	0,1086	0,0003				
	0,05		0,0010	0,1465	—1,9029	0,1646	0,0013			0,0005	—0,0005
	0,06		0,0026	0,1889	—1,7321	0,2131	0,0036	0,0001			
	0,07	0,0001	0,0052	0,2236	—1,6232	0,2529	0,0071	0,0002			
	0,08	0,0003	0,0084	0,2514	—1,5489	0,2849	0,0116	0,0006			
	0,09	0,0007	0,0121	0,2734	—1,4952	0,3103	0,0167	0,0012	0,0001		
0,56	0,03				0,0470	—2,7499	0,0514				
($j=5$)	0,04			0,0002	0,0983	—2,1948	0,1081	0,0003			
	0,05			0,0010	0,1484	—1,9042	0,1639	0,0013			

Table VI.1 (cont'd)

	0,06			0,0027	0,1916	—1,7342	0,2123	0,0035	0,0001		
	0,07		0,0001	0,0054	0,2270	—1,6262	0,2523	0,0071	0,0002		
	0,08		0,0004	0,0088	0,2555	—1,5530	0,2845	0,0116	0,0006		
	0,09		0,0007	0,0127	0,2782	—1,5005	0,3102	0,0167	0,0012	0,0001	
0,64	0,03					0,0473	—2,7500	0,0512			
(j=6)	0,04				0,0002	0,0992	—2,1953	0,1077	0,0002		
	0,05				0,0010	0,1497	—1,9050	0,1633	0,0013		
	0,06				0,0028	0,1935	—1,7356	0,2117	0,0035	0,0001	
	0,07			0,0002	0,0056	0,2295	—1,6228	0,2517	0,0070	0,0002	
	0,08			0,0004	0,0091	0,2585	—1,5557	0,2839	0,0115	0,0006	
	0,09			0,0008	0,0131	0,2817	—1,5040	0,3098	0,0166	0,0012	0,0001
0,72	0,03						0,0476	—2,7501	0,0510		
(j=7)	0,04					0,0002	0,0998	—2,1956	0,1074	0,0002	
	0,05					0,0010	0,1508	—1,9056	0,1629	0,0013	
	0,06					0,0029	0,1949	—1,7365	0,2111	0,0035	
	0,07				0,0002	0,0057	0,2313	—1,6296	0,2511	0,0070	0,0002
	0,08				0,0004	0,0093	0,2607	—1,5575	0,2834	0,0115	0,0006
	0,09				0,0008	0,0135	0,2842	—1,5064	0,3093	0,0166	0,0012
0,80	0,03							0,0478	—2,7502	0,0509	
(j=8)	0,04						0,0002	0,1002	—2,1958	0,1071	0,0002
	0,05						0,0010	0,1516	—1,9060	0,1625	0,0012
	0,06						0,0029	0,1961	—1,7372	0,2107	0,0035
	0,07					0,0002	0,0058	0,2327	—1,6306	0,2505	0,0069
	0,08					0,0004	0,0095	0,2624	—1,5589	0,2829	0,0114
	0,09					0,0009	0,0137	0,2862	—1,5082	0,3089	0,0165
0,88	0,03								0,0479	—2,7503	0,0507
(j=9)	0,04							0,0002	0,1006	—2,1960	0,1069
	0,05							0,0010	0,1522	—1,9064	0,1621
	0,06							0,0029	0,1969	—1,7377	0,2102
	0,07						0,0002	0,0059	0,2339	—1,6313	0,2501
	0,08						0,0004	0,0096	0,2638	—1,5599	0,2824
	0,09						0,0009	0,0139	0,2878	—1,5095	0,3084
0,96	0,03					—0,0001	—0,0001	—0,0001	—0,0001	0,0481	—2,7504
(j=10)	0,04								0,0002	0,1009	—2,1961
	0,05								0,0010	0,1527	—1,9066
	0,06								0,0029	0,1977	—1,7381
	0,07							0,0002	0,0059	0,2348	—1,6319
	0,08							0,0004	0,0097	0,2649	—1,5607
	0,09						0,0009	0,0009	0,0141	0,2890	—1,5105

Table VI.2

$k=4$

$\bar{q}_j$	$\sin\beta_R$	$\bar{v}_{ij/k}$									
		$i=1$	$i=2$	$i=3$	$i=4$	$i=5$	$i=6$	$i=7$	$i=8$	$i=9$	$i=10$
0,24	0,03	—2,6760	0,0136			0,0001	—0,0001				
($j=1$)	0,04	—2,0579	0,0389								
	0,05	—1,7153	0,0701	0,0001							
	0,06	—1,4288	0,1156	0,0008							
	0,07	—1,3656	0,1290	0,0012							
	0,08	—1,2666	0,1528	0,0025							
	0,09	—1,1923	0,1722	0,0041	0,0001						
0,32	0,03	0,0116	—2,6765	0,0135							
($j=2$)	0,04	0,0330	—2,0597	0,0389							
	0,05	0,0594	—1,7196	0,0704	0,0001						
	0,06	0,0980	—1,4380	0,1171	0,0008						
	0,07	0,1095	—1,3767	0,1312	0,0013						
	0,08	0,1301	—1,2821	0,1564	0,0026						
	0,09	0,1474	—1,2124	0,1776	0,0043	0,0001					
0,40	0,03		0,0119	—2,6768	0,0134						
($j=3$)	0,04		0,0341	—2,0607	0,0387						
	0,05	0,0001	0,0615	—1,7215	0,0703	0,0001					
	0,06	0,0005	0,1020	—1,4425	0,1175	0,0008					
	0,07	0,0009	0,1142	—1,3822	0,1318	0,0013					
	0,08	0,0017	0,1362	—1,2897	0,1576	0,0026					
	0,09	0,0029	0,1549	—1,2226	0,1796	0,0044	0,0001				
0,48	0,03			0,0121	—2,6769	0,0134					
($j=4$)	0,04			0,0347	—2,0611	0,0386					
	0,05		0,0001	0,0628	—1,7226	0,0701	0,0001				
	0,06		0,0006	0,1045	—1,4450	0,1174	0,0008				
	0,07		0,0009	0,1171	—1,3853	0,1318	0,0013				
	0,08		0,0019	0,1399	—1,2940	0,1580	0,0025	0,0001			
	0,09	0,0001	0,0032	0,1595	—1,2283	0,1803	0,0045	0,0001			
0,56	0,03				0,0122	—2,6770	0,0133				
($j=5$)	0,04				0,0351	—2,0614	0,0384				
	0,05			0,0001	0,0636	—1,7233	0,0699	0,0001			

Table VI.2 (Cont'd)

	0,06			0,0006	0,1061	—1,4465	0,1172	0,0008			
	0,07			0,0010	0,1191	—1,3871	0,1317	0,0013			
	0,08			0,0020	0,1425	—1,2967	0,1580	0,0026			
	0,09		0,0001	0,0034	0,1625	—1,2318	0,1806	0,0045	0,0001		
0,64	0,03					0,0123	—2,6770	0,0133			
(j=6)	0,04					0,0354	—2,0616	0,0383			
	0,05				0,0001	0,0642	—1,7238	0,0697	0,0001		
	0,06				0,0006	0,1073	—1,4476	0,1170	0,0008		
	0,07				0,0010	0,1204	—1,3884	0,1315	0,0013		
	0,08				0,0021	0,1442	—1,2984	0,1579	0,0026		
	0,09			0,0001	0,0035	0,1647	—1,2342	0,1806	0,0045	0,0001	
0,72	0,03						0,0124	—2,6771	0,0132		
(j=7)	0,04						0,0356	—2,0618	0,0382		
	0,05					0,0001	0,0647	—1,7241	0,0696	0,0001	
	0,06					0,0007	0,1082	—1,4482	0,1168	0,0008	
	0,07					0,0010	0,1215	—1,3892	0,1313	0,0013	
	0,08					0,0021	0,1456	—1,2996	0,1577	0,0026	
	0,09				0,0001	0,0036	0,1663	—1,2358	0,1805	0,0045	0,0001
0,80	0,03							0,0124	—2,6771	0,0132	
(j=8)	0,04							0,0358	—2,0619	0,0381	
	0,05						0,0001	0,0650	—1,7243	0,0694	0,0001
	0,06						0,0007	0,1088	—1,4487	0,1166	0,0008
	0,07						0,0010	0,1222	—1,3898	0,1311	0,0012
	0,08						0,0022	0,1466	—1,3005	0,1575	0,0026
	0,09					0,0001	0,0037	0,1676	—1,2369	0,1803	0,0044
0,88	0,03								0,0124	—2,6772	0,0131
(j=9)	0,04								0,0359	—2,0620	0,0380
	0,05							0,0001	0,0653	—1,7245	0,0693
	0,06							0,0007	0,1094	—1,4491	0,1165
	0,07							0,0011	0,1229	—1,3903	0,1309
	0,08							0,0022	0,1474	—1,3012	0,1573
	0,09						0,0001	0,0038	0,1685	—1,2378	0,1801
0,96	0,03							—0,0001	—0,0001	0,0125	—2,6772
(j=10)	0,04						0,0001	—0,0002		0,0360	—2,0620
	0,05								0,0001	0,0655	—1,7246
	0,06								0,0007	0,1098	—1,4494
	0,07								0,0011	0,1233	—1,3906
	0,08								0,0022	0,1480	—1,3017
	0,09							0,0001	0,0038	0,1693	—1,2385

Table VI.2 (Cont'd)

$\bar{Q}_j$	$\sin\beta_R$	$\bar{v}_{ij/k}$									
		$i=1$	$i=2$	$i=3$	$i=4$	$i=5$	$i=6$	$i=7$	$i=8$	$i=9$	$i=10$
0,24	0,1	—1,1337	0,1876	0,0061	0,0002						
($j=1$)	0,2	—0,8237	0,2192	0,0232	0,0040	0,0007	0,0001				
	0,3	—0,639	0,1844	0,0254	0,0064	0,0019	0,0006	0,0002	0,0001		
	0,4	—0,5025	0,1481	0,0222	0,0065	0,0023	0,0009	0,0004	0,0002	0,0001	
	0,5	—0,3982	0,1182	0,0184	0,0057	0,0022	0,0010	0,0004	0,0002	0,0001	
	0,6	—0,3152	0,0938	0,0148	0,0048	0,0019	0,0009	0,0004	0,0002	0,0001	0,0001
	0,7	—0,2455	0,0732	0,0116	0,0038	0,0016	0,0007	0,0004	0,0002	0,0001	0,0001
0,32	0,1	0,1616	—1,1588	0,1950	0,0065	0,0003					
($j=2$)	0,2	0,2100	—0,8981	0,2478	0,0276	0,0050	0,0010	0,0002			
	0,3	0,1962	—0,7398	0,2232	0,0328	0,0088	0,0027	0,0009	0,0003	0,0001	
	0,4	0,1701	—0,6074	0,1877	0,0303	0,0094	0,0036	0,0015	0,0006	0,0003	0,0001
	0,5	0,1409	—0,4956	0,1543	0,0259	0,0086	0,0036	0,0016	0,0008	0,0004	0,0002
	0,6	0,1176	—0,4000	0,1248	0,0213	0,0074	0,0032	0,0015	0,0008	0,0004	0,0002
	0,7	0,0939	—0,3157	0,0986	0,0169	0,0060	0,0027	0,0013	0,0007	0,0004	0,0002
0,40	0,1	0,0043	0,1704	—1,1716	0,1979	0,0067	0,0003				
($j=3$)	0,2	0,0198	0,2293	—0,9422	0,2636	0,0302	0,0056	0,0011	0,0002		
	0,3	0,0262	0,2225	—0,8093	0,2493	0,0379	0,0105	0,0033	0,0011	0,0004	0,0001
	0,4	0,0267	0,1995	—0,6890	0,2180	0,0366	0,0119	0,0046	0,0019	0,0008	0,0004
	0,5	0,0245	0,1724	—0,5780	0,1844	0,0322	0,0112	0,0048	0,0023	0,0011	0,0006
	0,6	0,0214	0,1447	—0,4763	0,1522	0,0271	0,0098	0,0044	0,0022	0,0012	0,0007
	0,7	0,0178	0,1175	—0,3817	0,1220	0,0219	0,0081	0,0038	0,0020	0,0011	0,0006
0,48	0,1	0,0001	0,0048	0,1759	—1,1788	0,1992	0,0067	0,0003			
($j=4$)	0,2	0,0031	0,0230	0,2419	—0,9697	0,2728	0,0316	0,0059	0,0012	0,0002	
	0,3	0,0063	0,0306	0,2408	—0,8576	0,2668	0,0413	0,0117	0,0038	0,0013	0,0004
	0,4	0,0078	0,0320	0,2217	—0,7513	0,2407	0,0413	0,0137	0,0055	0,0023	0,0010
	0,5	0,0080	0,0303	0,1961	—0,6463	0,2090	0,0375	0,0134	0,0059	0,0028	0,0014
	0,6	0,0075	0,0269	0,1679	—0,5435	0,1762	0,0322	0,0120	0,0056	0,0029	0,0016
	0,7	0,0066	0,0228	0,1386	—0,4426	0,1435	0,0265	0,0101	0,0048	0,0026	0,0015
0,56	0,1		0,0002	0,0051	0,1795	—1,1834	0,1997	0,0068	0,0002		
($j=5$)	0,2	0,0005	0,0036	0,0245	0,2505	—0,9878	0,2783	0,0325	0,0061	0,0012	0,0002
	0,3	0,0017	0,0076	0,0338	0,2539	—0,8917	0,2787	0,0436	0,0125	0,0041	0,0014
	0,4	0,0027	0,0097	0,0360	0,2385	—0,7989	0,2578	0,0449	0,0151	0,0061	0,0026

Table VI.2 (Cont'd)

	0,5	0,0032	0,0103	0,0347	0,2152	—0,7020	0,2290	0,0417	0,0152	0,0068	0,0033
	0,6	0,0032	0,0098	0,0315	0,1878	—0,6017	0,1969	0,0366	0,0139	0,0066	0,0035
	0,7	0,0030	0,0090	0,0271	0,1575	—0,4981	0,1629	0,0306	0,0119	0,0058	0,0032
0,64	0,1			0,0002	0,0053	0,1821	—1,1864	0,1999	0,0068	0,0003	
(j=6)	0,2	0,0001	0,0006	0,0041	0,0260	0,2566	—1,0002	0,2819	0,0331	0,0063	0,0013
	0,3	0,0005	0,0022	0,0087	0,0362	0,2636	—0,9164	0,2870	0,0453	0,0130	0,0043
	0,4	0,0010	0,0035	0,0112	0,0390	0,2515	—0,8354	0,2707	0,0475	0,0162	0,0066
	0,5	0,0014	0,0042	0,0120	0,0382	0,2308	—0,7474	0,2451	0,0451	0,0167	0,0075
	0,6	0,0015	0,0044	0,0117	0,0352	0,2047	—0,6518	0,2145	0,0404	0,0155	0,0075
	0,7	0,0015	0,0042	0,0106	0,0308	0,1743	—0,5481	0,1804	0,0343	0,0135	0,0067
0,72	0,1				0,0002	0,0055	0,1840	—1,1884	0,1999	0,0068	0,0003
(j=7)	0,2		0,0001	0,0007	0,0044	0,0270	0,2612	—1,0090	0,2842	0,0334	0,0064
	0,3	0,0002	0,0007	0,0026	0,0094	0,0380	0,2709	—0,9347	0,2930	0,0464	0,0135
	0,4	0,0004	0,0014	0,0041	0,0123	0,0414	0,2617	—0,8636	0,2804	0,0495	0,0170
	0,5	0,0006	0,0019	0,0051	0,0134	0,0410	0,2435	—0,7844	0,2580	0,0478	0,0178
	0,6	0,0008	0,0022	0,0054	0,0133	0,384	0,2191	—0,6946	0,2295	0,0435	0,0169
	0,7	0,0008	0,0022	0,0051	0,0122	0,0340	0,1893	—0,5928	0,1960	0,0376	0,0150
0,80	0,1					0,0002	0,0056	0,1854	—1,1899	0,1998	0,0067
(j=8)	0,2			0,0001	0,0008	0,0046	0,0278	0,2647	—1,0155	0,2857	0,0337
	0,3		0,0002	0,0008	0,0028	0,0101	0,0394	0,2766	—0,9485	0,2973	0,0472
	0,4	0,0002	0,0006	0,0017	0,0046	0,0132	0,0433	0,2699	—0,8858	0,2879	0,0510
	0,5	0,0003	0,0009	0,0023	0,0057	0,0145	0,0433	0,2540	—0,8145	0,2685	0,0500
	0,6	0,0004	0,0011	0,0028	0,0062	0,0145	0,0410	0,2314	—0,7311	0,2422	0,0462
	0,7	0,0005	0,0012	0,0028	0,0060	0,0135	0,0368	0,2026	—0,6327	0,2098	0,0405
0,88	0,1						0,0002	0,0057	0,1866	—1,1911	0,1996
(j=9)	0,2				0,0001	0,0009	0,0048	0,0284	0,2674	—1,0204	0,2868
	0,3		0,0001	0,0002	0,0009	0,0031	0,0105	0,0405	0,2811	—0,9592	0,3005
	0,4	0,0001	0,0002	0,0007	0,0019	0,0050	0,0139	0,0448	0,2764	—0,9035	0,2938
	0,5	0,0001	0,0004	0,0011	0,0027	0,0063	0,0154	0,0452	0,2626	—0,8394	0,2770
	0,6	0,0002	0,0006	0,0014	0,0031	0,0068	0,0156	0,0432	0,2420	—0,7622	0,2530
	0,7	0,0003	0,0007	0,0016	0,0033	0,0067	0,0147	0,0393	0,2144	—0,6680	0,2220
0,96	0,1							0,0002	0,0058	0,1845	—1,1919
(j=10)	0,2					0,0002	0,0009	0,0050	0,0289	0,2696	—1,0243
	0,3			0,0001	0,0003	0,0010	0,0033	0,0109	0,0414	0,2847	—0,9676
	0,4		0,0001	0,0003	0,0008	0,0021	0,0054	0,0145	0,0461	0,2817	—0,9176
	0,5	0,0001	0,0002	0,0006	0,0013	0,0030	0,0067	0,0162	0,0468	0,2698	—0,8598
	0,6	0,0001	0,0003	0,0008	0,0017	0,0035	0,0074	0,0165	0,0452	0,2510	—0,7888
	0,7	0,0002	0,0004	0,0009	0,0019	0,0037	0,0073	0,0157	0,0415	0,2249	—0,6993

TABLE VI.3

$k=5$

$\bar{\varrho}_j$	$\sin\beta_R$	$\bar{v}_{ij/k}$									
		$i=1$	$i=2$	$i=3$	$i=4$	$i=5$	$i=6$	$i=7$	$i=8$	$i=9$	$i=10$
0,24	0,03	—2,6578	0,0035								
($j=1$)	0,04	—2,0130	0,0139								
	0,05	—1,6439	0,0303								
	0,06	—1,4121	0,0493								
	0,07	—1,2563	0,0684	0,0002			—0,0003	0,0003			
	0,08	—1,1454	0,0861	0,0005							
	0,09	—1,0626	0,1018	0,0010							
0,32	0,03	0,0030	—2,6580	0,0035							
($j=2$)	0,04	0,0120	—2,0138	0,0140							
	0,05	0,0260	—1,6462	0,0306							
	0,06	0,0422	—1,4165	0,0502							
	0,07	0,0588	—1,2633	0,0701	0,0002						
	0,08	0,0742	—1,1556	0,0890	0,0006						
	0,09	0,0881	—1,0765	0,1060	0,0011				—0,0003	0,0003	
0,40	0,03		0,0032	—2,6580	0,0035						
($j=3$)	0,04		0,0124	—2,0142	0,0140	0,0041	—0,0041				
	0,05		0,0270	—1,6472	0,0307						
	0,06		0,0441	—1,4186	0,0504						
	0,07	0,0001	0,0616	—1,2668	0,0708	0,0002					
	0,08	0,0004	0,0782	—1,1607	0,0901	—0,0001	0,0007				
	0,09	0,0007	0,0932	—1,0834	0,1077	0,0011	0,0001				
0,48	0,03			0,0032	—2,6581	0,0035					
($j=4$)	0,04			0,0126	—2,0144	0,0140					
	0,05			0,0276	—1,6478	0,0307					
	0,06			0,0452	—1,4197	0,0505					
	0,07		0,0002	0,0633	—1,2687	0,0710	0,0002				
	0,08		0,0004	0,0805	—1,1636	0,0905	0,0006				
	0,09		0,0008	0,0963	—1,0874	0,1085	0,0012				
0,56	0,03				0,0032	—2,6581	0,0035				
($j=5$)	0,04				0,0128	—2,0146	0,0139				
	0,05				0,0280	—1,6482	0,0306				

Table VI-3 (Cont'd)

	0,06				0,0460	—1,4205	0,0505				
	0,07			0,0002	0,0644	—1,2700	0,0710	0,0002			
	0,08			0,0004	0,0821	—1,1654	0,0907	0,0006			
	0,09			0,0009	0,0983	—1,0898	0,1088	0,0012			
0,64	0,03					0,0032	—2,6581	0,0035			
(j=6)	0,04					0,0129	—2,0147	0,0139			
	0,05					0,0282	—1,6484	0,0306			
	0,06					0,0465	—1,4209	0,0504			
	0,07				0,0002	0,0652	—1,2707	0,0710	0,0002		
	0,08				0,0005	0,0832	—1,1666	0,0907	0,0006		
	0,09				0,0009	0,0977	—1,0915	0,1090	0,0012		
0,72	0,03						1,0032	—2,6582	0,0034		
(j=7)	0,04						0,0130	—2,0147	0,0138		
	0,05						0,0284	—1,6486	0,0305		
	0,06						0,0468	—1,4213	0,0504		
	0,07					0,0002	0,0658	—1,2712	0,0710	0,0002	
	0,08					0,0005	0,0840	—1,1674	0,0907	0,0006	
	0,09					0,0010	0,1007	—1,0926	0,1090	0,0012	
0,80	0,03							0,0032	—2,6582	0,0034	
(j=8)	0,04							0,0130	—2,0148	0,0138	
	0,05							0,0286	—1,6487	0,0304	
	0,06							0,0471	—1,4215	0,0503	
	0,07						0,0002	0,0662	—1,2716	0,0709	0,0002
	0,08						0,0005	0,0846	—1,1679	0,0907	0,0006
	0,09						0,0010	0,1015	—1,0934	0,1090	0,0012
0,88	0,03								0,0032	—2,6582	0,0034
(j=9)	0,04								0,0130	—2,0148	0,0138
	0,05								0,0287	—1,6488	0,0304
	0,06								0,0473	—1,4217	0,0502
	0,07							0,0002	0,0666	—1,2719	0,0708
	0,08							0,0005	0,0851	—1,1684	0,0906
	0,09							0,0010	0,1022	—1,0940	0,1089
0,96	0,03									0,0032	—2,6582
(j=10)	0,04									0,0131	—2,0149
	0,05									0,0288	—1,6489
	0,06									0,0475	—1,4218
	0,07								0,0002	0,0669	—1,2721
	0,08								0,0005	0,0855	—1,1687
	0,09								0,0010	0,1026	—1,0944

CALCULATIONS OF $J_{m,n}$-TRANSFORMS OF POWER FUNCTIONS

Let us calculate integrals

$$J_{n,m}(\varphi_m)=\int_0^\infty e^{-z\bar{y}}z\,dz\int_0^1 J_n(\bar{r},z)J_m(\bar{\varrho}z)\varphi_m(\bar{\varrho})\bar{\varrho}d\bar{\varrho},$$

to which the problem of determining harmonics of induced velocities is reduced in that case when

$$\varphi_m=\bar{\varrho}^m(1-\bar{\varrho}^2)^{q/2}\ (q=1,3,5\ldots).$$

The $J_{n,m}$ result of a transform of such a function will be designated as $Y^q_{n,m}$. This means that

$$Y^q_{n,m}(\bar{r})=\int_0^\infty e^{-z\bar{y}}z\,dz\int_0^1 J_n(\bar{r}z)J_m(\bar{\varrho}z)\bar{\varrho}^m(1-\bar{\varrho}^2)^{q/2}\bar{\varrho}d\bar{\varrho}. \qquad \text{(VII.1)}$$

The internal integral in Eq. (VII.1) is directly computed from Eq. 4.4536 in Ref. 77. We have

$$\int_0^{\pi/2} J_p(z\sin x)\sin^{p+1}(x)\cos^{q+1}x\,dx=\frac{2^{q/2}\Gamma\left(\frac{q}{2}+1\right)}{z^{q/2+1}}J_{p+q/2+1}(z)$$

$$(q>-1,\ p>-1).$$

Substituting the above expression into Eq. (VII.1), we obtain

$$Y^q_{n,m}=2^{q/2}\Gamma\left(\frac{q}{2}+1\right)\int_0^\infty e^{-z\bar{y}}J_n(\bar{r}z)J_{q/2+m+1}(z)z^{-q/2}dz. \qquad \text{(VII.2)}$$

For the half-integer values of the indexes, Bessel functions are expressed through the elementary ones. In particular,

$$J_{1/2}(z)=\sqrt{\frac{2}{\pi z}}\sin z.$$

Taking into consideration the above relationship, it is not difficult to prove that at $\bar{y}=0$, $m=-1$ and $q=1$, the integral in Eq. (VII.2) can readily be computed on the basis of the known for Bessel functions formula 4.4621 (see Ref. 77).

$$\int_0^\infty J_p(\alpha x)\sin\beta x\,\frac{dx}{x}=\begin{cases}\dfrac{1}{p}\sin\left(p\arcsin\dfrac{\beta}{\alpha}\right) & \text{for } \beta\leqslant\alpha,\\ \dfrac{\alpha^p\sin\dfrac{p\pi}{2}}{p\{\beta+\sqrt{\beta^2-\alpha^2}\}^p} & \text{for } \beta\geqslant\alpha.\end{cases}$$

In this way,

$$Y^1_{n,-1}=\begin{cases}\dfrac{\bar r^n}{n(1+\sqrt{1-\bar r^2})^n}\sin\dfrac{\pi n}{2} & \text{for } \bar r\leqslant 1,\\ \dfrac{1}{n}\sin\left(n\arcsin\dfrac{1}{\bar r}\right) & \text{for } \bar r\geqslant 1.\end{cases}\qquad\text{(VII.3)}$$

For the value of $n = 0$ in the right-hand part of Eq. (VII.3), it is necessary to go to the limit with $n \to 0$. If $\bar y \neq 0$, then the quantity $y^1_{n,-1}$ is computed from Eq. 4.432 in Ref. 77.

$$\int_0^\infty e^{-\alpha x}J_p(\beta x)\,\frac{dx}{x}=\frac{\{\sqrt{\alpha^2+\beta^2}-\alpha\}^p}{p\beta^p}\ (p>0,\ \mathrm{Re}\,\alpha>\mathrm{Im}\,\beta),$$

in which it is necessary to assume $\alpha = \bar y + i$, $\beta = \bar r$ and to separate real and imaginary parts. In that case,

$$Y^1_{n,-1}=-\frac{D^n}{n\bar r^n}\sin n\Phi,\qquad\text{(VII.4)}$$

where

$$D=\sqrt{(A-\bar y)^2+(B-1)^2};\quad A=\sqrt{\frac{a+\sqrt{a^2+b^2}}{2}};$$

$$B=\sqrt{\frac{-a+\sqrt{a^2+b^2}}{2}};\quad a=\bar y^2+\bar r^2-1;\quad b=2\bar y,$$

and parameter Φ is given by the following equalities

$$\sin\Phi=\frac{B-1}{D},\quad \cos\Phi=\frac{A-\bar y}{D}.$$

In order to determine the integrals in Eq. (VII.2) for the remaining values of m and q, we are going to develop the recurring formulae. Replacing, in Eq. (VII.2), one of the Bessel functions according to the following formula

$$\frac{2p}{z}J_p(z)=J_{p-1}(z)+J_{p+1}(z),$$

after a few simple transformations, we obtain the following two recurring formulae

$$nY^q_{n,m}=\frac{q}{2}\bar{r}\left(Y^q_{n-1,m+1}+Y^q_{n+1,m+1}\right), \tag{VII.5}$$

$$Y^q_{n,m}=\frac{q}{q+2m+2}\left(Y^{q-2}_{n,m}+Y^{q-2}_{n,m+2}\right). \tag{VII.6}$$

Next, after taking advantage of a formula for the derivative of Bessel function

$$J_{q/2+m+1}(z)z^{-q/2-m}=-\frac{d}{dz}z^{-q/2-m}J_{\frac{q}{2}+m}(z),$$

integrating Eq. (VII.2) by parts and taking into consideration that $2J_p'(z) = J_{p-1}(z) - J_{p+1}(z)$, we obtain

$$Y^q_{n,m}=\frac{q}{m+q}\left[Y^{q-2}_{n,m}-\bar{y}Y^{q-2}_{n,m+1}+\frac{\bar{r}}{2}\left(Y^{q-2}_{n-1,m+1}-Y^{q-2}_{n+1,m+1}\right)\right]. \tag{VII.7}$$

where $A = 1$ when $n = m = 0$, while in the remaining cases, $A = 1$. As the result of Eqs. (VII.6) and (VII.7), we obtain the following formula

$$Y^q_{n,m}=A-\bar{y}Y^q_{n,m-1}+\frac{m}{q+2}Y^{q+2}_{n,m-2}+\frac{\bar{r}}{2}\left[Y^q_{n-1,m-1}-Y^q_{n+1,m-1}\right], \tag{VII.8}$$

Combining Eqs. (VII.7) and (VII.5), one can obtain one more recurring formula

$$Y^q_{n,m}=\frac{n-q-m-2}{n+q+m}Y^q_{n-2,m}-\frac{2(n-1)\bar{y}}{n+m+q\bar{r}}Y^q_{n-1,m}+$$
$$+\frac{q}{n+m+q}\left(Y^{q-2}_{n-2,m}+Y^{q-2}_{n,m}\right). \tag{VII.9}$$

Assuming in Eqs. (VII.7) and (VII.8) respectively, $m = 0$ and $m = -1$, we will obtain two recurring formulae which would permit us to find values of $Y^{q+2}_{n,-1}$ and $Y^{q+2}_{n,0}$ for $n=0,1,2,\ldots,s-2$ for known values of $Y^q_{n,-1}$ $(n=0,1,2,3,\ldots,s)$. If, in addition, advantage is taken of Eq. (VII.9), then the above quantities can now be found for $n = 0 \div s$.

Since for $q = -1$ and all values of n, quantities Y^q_{n-1} are known, hence Eqs. (VII.5)-(VII.9) permit one through the full induction method to find functions $Y^q_{n,-1}$, $Y^q_{n,0}$ for the

odd q values. After that, it is possible from Eq. (VII.6) to determine $Y^q_{n,m}$ of other values of m.

Calculations can be checked with the help of the already known Eq. (13.41) relationship $Y^q_{n,m}=\bar{r}^n(1-\bar{r}^2)^{q/2}$.

Calculations performed according to the above discussed recurring formulae indicated that the accuracy of the obtained results does not decrease in proportion to the calculations.

APPENDIX VIII

CALCULATIONS OF $J_{n,m}$-TRANSFORMS OF THE ASSOCIATED LEGENDRE POLYNOMIAL

In order to calculate the internal integral in Eq. (13.25), we will take advantage of the well-known in theory of cylindrical functions formula of Gegenbauer (see Eq. 4.623, Ref. 77).

$$\int_0^{\pi} J_m(z\sin x\sin\varphi)\sin(z\cos x\cos\varphi)C_a^{m+\frac{1}{2}}(\cos x)\sin^{m+1}x\,dx=$$

$$=(-1)^{\frac{a-1}{2}}\left(\frac{2\pi}{z}\right)^{\frac{1}{2}}\sin^m\varphi C_a^{m+\frac{1}{2}}(\cos\varphi)\,J_{m+a+\frac{1}{2}}(z), \qquad \text{(VIII.1)}$$

where a is an odd number. In that formula, $C_a^p(\cos\phi)$ stands for the Gegenbauer polynomial, linked to the associated Legendre polynomial through the relationship in Eq. 6.921 of Ref. 77.

$$C_a^{m+\frac{1}{2}}(\cos\theta)\sin^m\theta=\frac{(-1)^m m!\,2^m}{(2m)!}P^m_{m+a}(\cos\theta). \qquad \text{(VIII.2)}$$

We divide both sides of Eq. (VIII.1) by $z\cos\phi$ and will find the limit of the so-obtained expression for $\phi\to\pi/2$. Taking into consideration that according to Eq. 6.921 of Ref. 77, for the odd values of a,

$$\lim\frac{C_a^{m+\frac{1}{2}}(t)}{t}=\frac{(-1)^{\frac{a-1}{2}}2\Gamma\left(m+\frac{a}{2}+1\right)}{\Gamma\left(\frac{a+1}{2}\right)\Gamma\left(m+\frac{1}{2}\right)},$$

and taking advantage of Eq. (VIII.2), we obtain

$$\int_0^{\pi} J_m(z\sin x)\,P^m_{m+a}(\cos x)\sin x\cos x\,dx=$$

$$=\frac{(-1)^m(2\pi)^{1/2}2\Gamma\left(m+\frac{a}{2}+1\right)\Gamma(2m+1)}{\Gamma\left(\frac{a+1}{2}\right)\Gamma\left(m+\frac{1}{2}\right)\Gamma(m+1)2^m}\,\frac{J_{m+a+\frac{1}{2}}(z)}{z^{3/2}}. \qquad \text{(VIII.3)}$$

Here, $\Gamma(x)$ represents Euler Γ function. It is known that if $x = m$ where m is a natural number, then

$$\Gamma(m+1)=m!$$

Taking advantage of the formula for duplication of the argument of Γ functions, we have

$$\Gamma(2x)=\frac{2^{2x-1}}{\sqrt{\pi}}\Gamma(x)\Gamma\left(x+\frac{1}{2}\right)$$

and noticing that for $a = 1, 3, \ldots,$ the subintegral function in Eq. (VIII.3) is even with respect to the $x - \pi/2$ variable; instead of Eq. (VIII.3), the following formula can be written:

$$\int_0^{\infty} J_p(\alpha t)J_q(\beta t)t^{-s}dt=\frac{\alpha^p\Gamma\left(\frac{p+q-s+1}{2}\right)}{2^s\beta^{p-s+1}\Gamma\left(\frac{-p+q+s-1}{2}\right)\Gamma(p+1)}\times$$

$$\times F\left(\frac{p+q-s+1}{2},\ \frac{p-q-s+1}{2},\ p+1,\ \frac{\alpha^2}{\beta^2}\right) \qquad \text{(VIII.4)}$$

$$(0<\alpha<\beta).$$

The left side of the above equation represents the internal integral in Eq. (13.52). Substituting the right side of Eq. (VIII.4) for that integral, we obtain

$$S^a_{n\,m}(\bar r,\bar y)=\frac{(-1)^m 2^{m+\frac{1}{2}}\Gamma\left(m+\frac{a}{2}+1\right)}{\Gamma\left(\frac{a+1}{2}\right)}\int_0^{\infty} e^{-\bar y z}J_n(\bar r z)J_{m+a+\frac{1}{2}}(z)\frac{dz}{\sqrt{z}}. \qquad \text{(VIII.5)}$$

Now, we can turn our attention to the determination of the last integral of Eq. (VIII.5) with respect to the variable z. First of all, let us consider the particular case of $\bar y = 0$. In other words, we will determine the value of that integral in the plane of the rotor disc. We take advantage of the integral formula, 4.415 of Ref. 77, developed by Shafheitlin within the theory of cylindrical functions

$$\int_0^{\pi/2} J_m(z\sin x)\,P^m_{m+a}(\cos x)\sin x\cos x\,dx=$$

$$=\frac{(-1)^m 2^{m+\frac{1}{2}}\Gamma\left(m+\frac{a}{2}+1\right)}{\Gamma\left(\frac{a+1}{2}\right)}\,\frac{J_{m+a+\frac{1}{2}}(z)}{z^{3/2}}. \qquad \text{(VIII.6)}$$

Here, the symbol $F(\alpha,\beta,\gamma,x)$ stands for a hypergeometric function determined for $|x| < 1$ by the following series:

$$F(\alpha,\beta,\gamma,x)=1+\frac{\alpha,\beta}{\gamma}x+\frac{\alpha(\alpha+1)\beta(\beta+1)}{\gamma(\gamma+1)2!}x^2+\ldots$$

In order to calculate the integral of Eq. (VIII.6) for $\alpha > \beta$, it is sufficient to substitute β instead of α in the left and right-hand sides of that formula. This gives

$$\int_0^\infty J_p(\alpha t)J_q(\beta t)t^{-s}dt=\frac{\beta^q\Gamma\left(\frac{p+q-s+1}{2}\right)}{2^s\alpha^{q-s+1}\Gamma\left(\frac{p-q+s+1}{2}\right)\Gamma(q+1)}\times$$

$$\times F\left(\frac{p+q-s+1}{2},\ \frac{-p+q-s+1}{2},\ q+1,\ \frac{\beta^2}{\alpha^2}\right)\ldots \qquad \text{(VIII.7)}$$

In the case of $\bar{r} < 1$, $\bar{y} = 0$ appearing in Eq. (VIII.5), the integral is computed according to Eq. (VIII.6) by assuming that $\alpha = \bar{r}$, $\beta = 1$, $s = 1/2$, $p = n$, $q = m + a + 1/2$. In this way, we will have

$$S^a_{n,m}(\bar{r},0)=\frac{(-1)^m 2^m\Gamma\left(m+\frac{a}{2}+1\right)\Gamma\left(\frac{m+n+a+1}{2}\right)}{\Gamma\left(\frac{a+1}{2}\right)\Gamma\left(\frac{-n+m+a}{2}+1\right)\Gamma(n+1)}\times \qquad \text{(III.8)}$$

$$\times\bar{r}^n F\left(\frac{m+n+a+1}{2},\ \frac{n-m-a}{2},\ n+1,\ \bar{r}^2\right).$$

The hypergeometric function appearing here can be rewritten under a slightly different form. Taking advantage of formula 7.235 of Ref. 77 showing transformations of hypergoemetric functions, we have

$$F\left(\alpha, \beta; \alpha+\beta+\frac{1}{2}; \bar{r}^2\right)=F\left(2\alpha, 2\beta, \alpha+\beta+\frac{1}{2}; \frac{1-\zeta}{2}\right), \qquad \text{(VIII.9)}$$

where $$\zeta=\sqrt{1-\bar{r}^2}.$$

According to the determination of the associated Legendre function of the first kind with a negative superscript "n"

$$P^{-n}_{m+a}(\zeta)=\frac{1}{n!}\left(\frac{1+\zeta}{1-\zeta}\right)^{-n/2} F\left(-m-a,\ m+a+1;\ n+1;\ \frac{1-\zeta}{2}\right). \qquad \text{(VIII.10)}$$

Taking into consideration one more formula for transformation of hypergeometric functions

$$F(\alpha, \beta, \gamma, z)=(1-z)^{\gamma-\alpha-\beta}F(\gamma-\alpha,\ \gamma-\beta;\ \gamma;\ z)$$

Eq. (VIII.10) can be rewritten in the following form

$$P^{-n}_{m+a}(\zeta)=\frac{1}{n!\,2^n}(1-\zeta)^{n/2}F\left(m+n+1;\ n-m-a;\ n+1;\ \frac{1-\zeta}{2}\right)\ldots \qquad \text{(VIII.11)}$$

It can be seen from Eq. (VIII.9) that the same hypergeometric function appears in the right-hand sides of Eqs. (VIII.11) and (VIII.8). By excluding it from those equations, we find the following expression for the sought integral of Eq. (13.52) for $\bar{r} < 1$ and $\bar{y} = 0$:

$$S^a_{n,m}(\bar{r}, 0)=\frac{(-1)^m 2^{m+n}\Gamma\left(m+\frac{a}{2}+1\right)\Gamma\left(\frac{m+n+a+1}{2}\right)}{\Gamma\left(\frac{a+1}{2}\right)\Gamma\left(\frac{-n+m+a}{2}+1\right)} P^{-n}_{m+a}(\zeta). \qquad \text{(VIII.12)}$$

In this way, we computed the integrals encountered at the $J_{n,m}$ transform of the associated Legendre functions P^m_{m+a} at $\bar{y} = 0$. The result is expressed through the Legendre function P^{-n}_{m+a} (with a negative superscript) multiplied by a constant coefficient $K^a_{n,m}$.

$$J_{n,m}\{P^m_{m+a}(\zeta)\}=K^a_{n,m}P^{-n}_{m+a}(\zeta), \qquad \text{(VIII.13)}$$

where $$K^a_{n,m}=\frac{(-1)^m 2^{m+n}\Gamma\left(m+\frac{a}{2}+1\right)\Gamma\left(\frac{m+n+a+1}{2}\right)}{\Gamma\left(\frac{a+1}{2}\right)\Gamma\left(\frac{n+m+a}{2}+1\right)}.$$

There are tables for the associated Legendre functions which can be used in calculations indicated by Eq. (VIII.12). An analytic expression for the associated Legendre polynomials with negative superscripts, for example, can be found by taking advantage of the following formula:

$$P_k^{-m}(x)=(-1)^m\frac{(k-m)!}{(k+m)!}P_k^m(x)\quad(k\geqslant m),$$

where $P_k(x)$ is the general Legendre polynomial. Constant coefficient $K_{n,m}^a$ appearing in Eq. (VIII.13) is computed using Γ-functions for the integer and half-integer argument values expressed by the following elementary relationships:

$$\Gamma(n+1)=n!,\ \Gamma\left(n+\frac{1}{2}\right)=\frac{\sqrt{\pi}}{2^n}(2n-1)!!$$

The integral in Eq. (VIII.5) for points in the plane of rotation, but being outside of the rotor disc; i.e., for $\bar{r}>1$, $\bar{y}=0$, can be computed in an analogous way.

$$S_{n,m}^a(\bar{r},0)=\frac{(-1)^m2^m\Gamma\left(m+\frac{a}{2}+1\right)\Gamma\left(\frac{n+m+a+1}{2}\right)}{\Gamma\left(\frac{a+1}{2}\right)\Gamma\left(\frac{n-m-a+1}{2}\right)\Gamma\left(m+a+\frac{3}{2}\right)}\times$$
$$\times\frac{1}{\bar{r}^{m+a+1}}F\left(\frac{n+m+a+1}{2},\ \frac{m+a-n+1}{2},\ m+a+\frac{3}{2};\ \frac{1}{\bar{r}^2}\right).\qquad\text{(VIII.14)}$$

According to the definition of the associated Legendre function of the second kind $Q_p^q(z)$ in the case of an imaginary argument $z=i\eta$ is

$$Q_{m+a}^n(i\eta)=\frac{(-1)^n\Gamma(m+n+a+1)\sqrt{\pi}}{2^{m+a+1}\Gamma\left(m+a+\frac{3}{2}\right)}(\eta^2+1)^{n/2}(i)^{-m-a-1}\eta^{-n-m-a-1}\times$$
$$\times F\left(\frac{m+n+a+2}{2},\ \frac{m+a+n+1}{2};\ m+a+\frac{3}{2},\ -\frac{1}{\eta^2}\right).\qquad\text{(VIII.15)}$$

Hypergeometric functions appearing in the right-hand sides of Eqs. (VIII.14) and (VIII.15) change, one into the other, with the help of Eq. 7.231, Ref. 77:

$$F(\alpha,\beta,\gamma,z)=(1-z)^\alpha F\left(\alpha,\gamma-\beta,\gamma,\frac{z}{z-1}\right),$$

Making use of the above as well as the formula for doubling of the Γ-function, it is possible to represent Eq. (VIII.14) under the following form

$$S^a_{n,m}(\bar{r},0)=$$

$$=\frac{(-1)^{m-n}2^{m-n+1}\Gamma\left(m+\frac{a}{2}+1\right)}{\Gamma\left(\frac{a+1}{2}\right)\Gamma\left(\frac{n-m-a+1}{2}\right)\Gamma\left(\frac{m+a+n}{2}+1\right)}\frac{Q^n_{m+a}(i\eta)}{i^{-m-a-1}}, \qquad \text{(VIII.16)}$$

where

$$\eta=\sqrt{\bar{r}^2-1}\,.$$

In this way, by taking advantage of the integrating formulae known in the theory of cylindrical functions, we succeeded in evaluating the integral for $\bar{y}=0$; i.e., when velocities are calculated at the rotor disc plane. In order to find values of that integral in the upper half-space ($\bar{y}\geq 0$), we will take advantage of the fact that the following expression $f=exp(-\bar{y}z)J_\eta(\bar{r}z)\,sin\,n\psi$ represents a solution of the Laplace equation in cylindrical coordinates $\bar{y},\bar{r},\psi$. As a result of this function, $S^a_{n,m}(\bar{r},\bar{y})\,sin\,n\psi$ which, according to Eq. (13.52), can be represented as an infinite superposition of such expressions, will also represent a solution of the Laplace equation. Supported by the uniqueness of the Dirichlet solution to the Laplace equation, we will not start from Eq. (VIII.5), but will seek function $S^a_{n,m}(\bar{r},\bar{y})$ which at $y\neq 0$ would satisfy the boundary conditions corresponding to the solution of the Laplace equation.

Taking into consideration the character of Eqs. (VIII.12) and (VIII.16), we will try to construct the indicated expression by assuming

$$S^a_{n\,m}(\bar{r},\bar{y})=CP^{-n}_{m+a}(\zeta)Q^n_{m+a}(i\eta). \qquad \text{(VIII.17)}$$

Here, P^{-n}_{m+a} and Q^n_{m+q} are the associated Legendre functions of the first and second kind; C is a constant; parameters ζ and η are elliptic coordinates related to the cylindrical ones $(\bar{r},\bar{y})$ through the following relationships:

$$\bar{r}=\sqrt{1-\zeta^2}\sqrt{1+\eta^2},\ y=\eta\zeta.$$

Eq. (VIII.17) multiplied by $sin\,m\psi$ $(or\ cos\,m\psi)$ represents a solution of the Laplace equation in elliptic coordinates h,z,ψ.

When a point with coordinates $\bar{r},\bar{y}$ moves in the upper hemispace, then parameters η and ζ vary within the following limits $0<\eta<\infty$, $0<\zeta<1$. Points on the rotor disc correspond to the $\eta=0$ values, while $\bar{r}$ and η are related by the following

relationship $\bar{r} = \sqrt{1 - \zeta^2}$. Points of the plane of rotation located outside of the rotor disc correspond to the $\zeta = 0$ values. In addition, $r = \sqrt{1 + \eta^2}$, which corresponds to the earlier established definitions of η and ζ.

Let us find limit values of Eq. (VIII.17) for $\bar{y} \to 0$.

Substituting $\eta = 0$ into Eq. (VIII.17), we obtain the following for points located on the rotor disc

$$S^a_{n,m}(\bar{r},0)=CP^{-n}_{m+n}(\zeta)Q^n_{m+a}(i0) \quad (\bar{r}<1).$$

The above equation becomes the same as Eq. (VIII.12) if

$$C=\frac{(-1)^m 2^{n+m}\Gamma\left(m+\frac{a}{2}+1\right)\Gamma\left(\frac{m+n+a+1}{2}\right)}{\Gamma\left(\frac{a+1}{2}\right)\Gamma\left(\frac{-n+m+a}{2}+1\right)Q^n_{m+a}(i0)}. \qquad \text{(VIII.18)}$$

Substituting $\zeta = 0$ in Eq. (VIII.17), we will obtain the following for points located outside of the rotor disc

$$S^a_{n,m}(\bar{r},0)=CP^{-n}_{m+a}(0)Q^n_{m+a}(i\eta),$$

which becomes identical with Eq. (VIII.16) for

$$C=\frac{(-1)^{m-n}2^{m-n+1}\Gamma\left(m+\frac{a}{2}+1\right)i^{m+a+1}}{\Gamma\left(\frac{a+1}{2}\right)\Gamma\left(\frac{n-m-a+1}{2}\right)\Gamma\left(\frac{m+a+n}{2}+1\right)P^{-n}_{m+a}(0)}. \qquad \text{(VIII.19)}$$

Eq. (VIII.16) actually gives values of the integral in Eq. (13.52) if the right-hand sides of Eq. (VIII.18) and (VIII.19) are equal. Taking advantage of the formulae for the needed values of the associated Legendre functions of zero argument:

$$P^q_p(0)=\frac{2^q\sqrt{\pi}}{\Gamma\left(\frac{p-q}{2}+1\right)\Gamma\left(\frac{-p-q+1}{2}\right)},$$

$$Q^q_p(i0)=(-1)^q i^{-p-1}2^{q-1}\sqrt{\pi}\,\frac{\Gamma\left(\frac{p+q+1}{2}\right)}{\Gamma\left(\frac{p+q}{2}+1\right)} \qquad \text{(VIII.20)}$$

it is not difficult to verify that it is indeed so where, in addition, constant C may be expressed under the following form

$$C=\frac{(-1)^{m-n}2^{m+1}\Gamma\left(m+\frac{a}{2}+1\right)}{\Gamma\left(\frac{a+1}{2}\right)\sqrt{\pi}}\,i^{m+a+1}.$$

In this way, we obtained the results of the $J_{n,m}$ transform of the associated Legendre function on the rotor disc, as well as in the space above the disc.

APPENDIX IX

TABLES OF FUNCTION $\mathcal{E}^{k}_{nm}(\bar{r})$

$n=0,\ m=0$

$\bar{r}$	$\varepsilon^{(0)}_{0,0}$	$\varepsilon^{(1)}_{0,0}$	$\varepsilon^{(2)}_{0,0}$	$\varepsilon^{(3)}_{0,0}$	$\varepsilon^{(4)}_{0,0}$	$\varepsilon^{(5)}_{0,0}$
0,259	0	1,00	0	0	0	0
0,5	0	0	1,00	0	0	0
0,707	0	0	0	1,00	0	0
0,866	0	0	0	0	1,00	0
0,966	0	0	0	0	0	1,00
1,00	0	0	0	0	0	0

$n=1,\ m=0$

$\bar{r}$	$\varepsilon^{(0)}_{1,0}$	$\varepsilon^{(1)}_{1,0}$	$\varepsilon^{(2)}_{1,0}$	$\varepsilon^{(3)}_{1,0}$	$\varepsilon^{(4)}_{1,0}$	$\varepsilon^{(5)}_{1,0}$
0,259	0,415	0,129	—0,374	0,028	—0,069	0,012
0,5	—0,142	0,772	0,114	—0,431	0,014	—0,057
0,707	0,133	—0,123	0,804	0,086	—0,439	0,009
0,866	—0,086	0,296	—0,043	0,830	0,065	—0,389
0,966	0,094	—0,108	0,360	—0,008	0,906	0,038
1,00	—0,077	0,241	—0,052	0,461	0,015	1,315

$n=2,\ m=0$

$\bar{r}$	$\varepsilon^{(0)}_{2,0}$	$\varepsilon^{(1)}_{2,0}$	$\varepsilon^{(2)}_{2,0}$	$\varepsilon^{(3)}_{2,0}$	$\varepsilon^{(4)}_{2,0}$	$\varepsilon^{(5)}_{2,0}$
0,259	0,412	—0,361	—0,066	0,026	—0,012	0,005
0,5	0,008	0,632	—0,598	—0,057	0,023	—0,009
0,707	0,047	0,212	0,518	—0,753	—0,034	0,011
0,866	0,009	0,190	0,280	0,384	—0,849	—0,018
0,966	0,019	0,128	0,254	0,268	0,259	—0,925
1,00	0,014	0,127	0,228	0,261	0,227	0,130

$n=3,\ m=0$

$\bar{r}$	$\varepsilon_{3,0}^{(0)}$	$\varepsilon_{3,0}^{(1)}$	$\varepsilon_{3,0}^{(2)}$	$\varepsilon_{3,0}^{(3)}$	$\varepsilon_{3,0}^{(4)}$	$\varepsilon_{3,0}^{(5)}$
0,259	0,221	—0,289	0,074	—0,013	0,008	—0,002
0,5	0,226	0,063	—0,493	0,233	—0,067	0,037
0,707	—0,066	0,560	—0,307	—0,481	0,290	—0,051
0,866	0,127	0,016	0,487	—0,630	—0,385	0,287
0,966	—0,066	0,370	0,016	0,292	—0,893	—0,254
1,00	0,108	—0,005	0,421	—0,188	0,071	—1,433

$n=4,\ m=0$

$\bar{r}$	$\varepsilon_{4,0}^{(0)}$	$\varepsilon_{4,0}^{(1)}$	$\varepsilon_{4,0}^{(2)}$	$\varepsilon_{4,0}^{(3)}$	$\varepsilon_{4,0}^{(4)}$	$\varepsilon_{4,0}^{(5)}$
0,259	0,084	—0,128	0,058	—0,022	0,009	—0,004
0,5	0,321	—0,351	—0,069	0,131	—0,052	0,021
0,707	—0,022	0,48	—0,722	0,180	0,115	—0,039
0,866	0,079	0,160	0,105	—0,853	0,456	0,064
0,966	0,015	0,245	0,060	—0,295	—0,757	0,711
1,00	0,029	0,201	0,116	—0,264	—0,566	—0,471

$n=5,\ m=0$

$\bar{r}$	$\varepsilon_{5,0}^{(0)}$	$\varepsilon_{5,0}^{(1)}$	$\varepsilon_{5,0}^{(2)}$	$\varepsilon_{5,0}^{(3)}$	$\varepsilon_{5,0}^{(4)}$	$\varepsilon_{5,0}^{(5)}$
0,259	0,024	—0,041	0,024	—0,011	0,005	—0,002
0,5	0,268	—0,399	0,153	—0,022	0,004	—0,004
0,707	0,149	0,044	—0,486	0,401	—0,119	0,023
0,866	—0,037	0,417	—0,521	—0,174	0,518	—0,193
0,966	0,132	0,022	0,116	—0,808	0,408	0,441
1,00	—0,054	0,396	—0,271	—0,213	—0,606	1,390

$n=6,\ m=0$

$\bar{r}$	$\varepsilon_{6,0}^{(0)}$	$\varepsilon_{6,0}^{(1)}$	$\varepsilon_{6,0}^{(2)}$	$\varepsilon_{6,0}^{(3)}$	$\varepsilon_{6,0}^{(4)}$	$\varepsilon_{6,0}^{(5)}$
0,259	0,006	—0,010	0,007	—0,004	0,002	—0,001
0,5	0,146	—0,241	0,137	—0,054	0,019	—0,007
0,707	0,271	—0,330	—0,049	0,210	—0,138	0,046
0,866	—0,024	0,361	—0,731	0,487	0,008	—0,122
0,966	0,096	0,093	—0,225	—0,476	0,936	—0,402
1,00	0,050	0,180	—0,245	—0,399	0,429	0,878

$n=7,\ m=0$

$\bar{r}$	$\varepsilon_{7,0}^{(0)}$	$\varepsilon_{7,0}^{(1)}$	$\varepsilon_{7,0}^{(2)}$	$\varepsilon_{7,0}^{(3)}$	$\varepsilon_{7,0}^{(4)}$	$\varepsilon_{7,0}^{(5)}$
0,259	0,001	—0,001	0	0	0	0
0,5	0,058	—0,102	0,068	—0,034	0,014	—0,005
0,707	0,261	—0,416	0,191	—0,015	—0,038	0,022
0,866	0,122	—0,011	—0,406	0,54	—0,319	0,073
0,966	—0,025	0,315	—0,648	0,388	0,276	—0,498
1,00	0,161	—0,073	—0,155	—0,329	1,128	—1,111

$n=8,\ m=0$

$\bar{r}$	$\varepsilon_{8,0}^{(0)}$	$\varepsilon_{8,0}^{(1)}$	$\varepsilon_{8,0}^{(2)}$	$\varepsilon_{8,0}^{(3)}$	$\varepsilon_{8,0}^{(4)}$	$\varepsilon_{8,0}^{(5)}$
0,259	0	0	0	0	0	0
0,5	0,021	—0,038	0,029	—0,018	0,010	—0,004
0,707	0,172	—0,303	0,203	—0,099	0,033	—0,007
0,866	0,251	—0,365	0,061	0,185	—0,230	0,121
0,966	—0,005	0,221	—0,631	0,797	—0,518	0,068
1,00	0,073	0,068	—0,427	0,387	0,273	—1,179

$n=9,\ m=0$

$\bar{r}$	$\varepsilon_{9,0}^{(0)}$	$\varepsilon_{9,0}^{(1)}$	$\varepsilon_{9,0}^{(2)}$	$\varepsilon_{9,0}^{(3)}$	$\varepsilon_{9,0}^{(4)}$	$\varepsilon_{9,0}^{(5)}$
0,259	0	0	0	0	0	0
0,5	0,06	—0,012	0,010	—0,007	0,004	—0,002
0,707	0,084	—0,156	0,122	—0,079	0,042	—0,016
0,866	0,258	—0,453	0,294	—0,115	—0,007	0,037
0,966	0,168	—0,202	—0,118	0,424	—0,540	0,369
1,00	—0,032	0,230	—0,614	0,957	—0,999	0,639

$n=10,\ m=0$

$\bar{r}$	$\varepsilon_{10,0}^{(0)}$	$\varepsilon_{10,0}^{(1)}$	$\varepsilon_{10,0}^{(2)}$	$\varepsilon_{10,0}^{(3)}$	$\varepsilon_{10,0}^{(4)}$	$\varepsilon_{10,0}^{(5)}$
0,259	0	0	0	0	0	0
0,5	0,001	—0,002	0,002	—0,001	0,001	0
0,707	0,031	—0,058	0,050	—0,037	0,023	—0,009
0,866	0,170	—0,318	0,259	—0,178	0,096	—0,033
0,966	0,292	—0,523	0,360	—0,143	—0,053	0,144
1,00	0,119	—0,145	—0,112	0,469	—0,847	1,200

$n=0,\ m=1$

$\bar{r}$	$\varepsilon_{0,1}^{(1)}$	$\varepsilon_{0,1}^{(2)}$	$\varepsilon_{0,1}^{(3)}$	$\varepsilon_{0,1}^{(4)}$	$\varepsilon_{0,1}^{(5)}$	
0,259	0,453	0,971	0,099	0,267	0,024	
0,5	—0,324	0,273	0,769	0,080	0,138	
0,707	0,068	—0,458	0,173	0,673	0,032	
0,866	—0,076	0,076	—0,571	0,114	0,496	
0,966	0,038	—0,151	0,072	—0,714	0,609	
1,00	—0,053	0,056	—0,265	0,063	—1,194	

$n=1,\ m=1$

$\bar{r}$	$\varepsilon_{1,1}^{(1)}$	$\varepsilon_{1,1}^{(2)}$	$\varepsilon_{1,1}^{(3)}$	$\varepsilon_{1,1}^{(4)}$	$\varepsilon_{1,1}^{(5)}$
0,259	1,00	0	0	0	0
0,5	0	1,00	0	0	0
0,707	0	0	1,00	0	0
0,866	0	0	0	1,00	0
0,966	0	0	0	0	1,00
1,00	0	0	0	0	0

$n=2,\ m=1$

$\bar{r}$	$\varepsilon_{2,1}^{(1)}$	$\varepsilon_{2,1}^{(2)}$	$2_{2,1}^{(3)}$	$\varepsilon_{2,1}^{(4)}$	$\varepsilon_{2,1}^{(5)}$
0,259	0,664	—0,384	0,143	—0,094	0,038
0,5	0,48	0,498	—0,447	0,114	—0,074
0,707	—0,022	0,678	0,348	—0,423	0,057
0,866	0,103	0,023	0,788	0,241	—0,372
0,966	—0,020	0,224	0,059	0,910	0,137
1,00	0,071	0,006	0,386	0,090	0,135

$n=3,\ m=1$

$\bar{r}$	$\varepsilon_{3,1}^{(1)}$	$\varepsilon_{3,1}^{(2)}$	$\varepsilon_{3,1}^{(3)}$	$\varepsilon_{3,1}^{(4)}$	$\varepsilon_{3,1}^{(5)}$
0,259	0,276	—0,253	0,135	—0,076	0,035
0,5	0,655	—0,198	—0,162	0,078	—0,034
0,707	0,155	0,731	—0,508	—0,081	0,028
0,866	0,114	0,323	0,626	—0,699	—0,04
0,966	0,069	0,262	0,393	0,466	—0,850
1,00	0,067	0,227	0,371	0,391	0,252

$n=4,\ m=1$

$\bar{r}$	$\varepsilon^{(1)}_{4,1}$	$\varepsilon^{(2)}_{4,1}$	$\varepsilon^{(3)}_{4,1}$	$\varepsilon^{(4)}_{4,1}$	$\varepsilon^{(5)}_{4,1}$
0,259	0,084	—0,097	0,065	—0,038	0,021
0,5	0,521	—0,442	0,156	—0,055	0,027
0,707	0,400	0,223	—0,588	0,262	—0,066
0,866	0,112	0,586	—0,241	—0,528	0,269
0,966	0,179	0,239	0,487	—0,692	—0,372
1,00	0,069	0,426	0,121	0,210	—1,42

$n=5,\ m=1$

$\bar{r}$	$\varepsilon^{(1)}_{5,1}$	$\varepsilon^{(2)}_{5,1}$	$\varepsilon^{(3)}_{5,1}$	$\varepsilon^{(4)}_{5,1}$	$\varepsilon^{(5)}_{5,1}$
0,259	0,020	—0,027	0,021	—0,013	0,006
0,5	0,290	—0,333	0,208	—0,101	0,044
0,707	0,506	—0,287	—0,149	0,201	—0,077
0,866	0,210	0,445	—0,767	0,213	0,104
0,966	0,201	0,323	—0,036	—0,892	0,572
1,00	0,170	0,345	—0,004	—0,587	—0,659

$n=6,\ m=1$

$\bar{r}$	$\varepsilon^{(1)}_{6,1}$	$\varepsilon^{(2)}_{6,1}$	$\varepsilon^{(3)}_{6,1}$	$\varepsilon^{(4)}_{6,1}$	$\varepsilon^{(5)}_{6,1}$
0,259	0,004	—0,006	0,004	—0,004	0,002
0,5	0,125	—0,168	0,133	—0,078	0,036
0,707	0,429	—0,46	0,209	—0,026	—0,005
0,866	0,361	—0,016	—0,526	0,508	—0,153
0,966	0,190	0,359	—0,695	0,039	0,510
1,00	0,274	0,155	—0,180	—0,837	1,265

$n=0,\ m=2$

	$\varepsilon^{(1)}_{0,2}$	$\varepsilon^{(2)}_{0,2}$	$\varepsilon^{(3)}_{0,2}$	$\varepsilon^{(4)}_{0,2}$	$\varepsilon^{(5)}_{0,2}$
0,259	—0,124	1,024	0,489	0,322	0,131
0,5	—0,105	—0,573	0,586	0,280	0,149
0,707	0,04	—0,057	—0,756	0,338	0,129
0,866	—0,019	0,022	—0,036	—0,858	0,158
0,966	0,007	—0,008	0,010	—0,016	—0,937
1,00	0	0	0	0	0

$n=1,\ m=2$

$\bar{r}$	$\varepsilon_{1,2}^{(1)}$	$\varepsilon_{1,2}^{(2)}$	$\varepsilon_{1,2}^{(3)}$	$\varepsilon_{1,2}^{(4)}$	$\varepsilon_{1,2}^{(5)}$
0,259	1,010	0,655	0,08	0,105	0,015
0,5	—0,451	0,635	0,681	0,085	0,098
0,707	0,248	—0,494	0,435	0,629	0,056
0,866	—0,214	0,214	—0,563	0,290	0,501
0,966	0,175	—0,22	0,188	—0,688	0,160
1,00	—0,173	0,176	—0,291	0,163	—1,158

$n=2,\ m=2$

$\bar{r}$	$\varepsilon_{2,2}^{(1)}$	$\varepsilon_{2,2}^{(2)}$	$\varepsilon_{2,2}^{(3)}$	$\varepsilon_{2,2}^{(4)}$	$\varepsilon_{2,2}^{(5)}$
0,259	1,00	0	0	0	0
0,5	0	1,00	0	0	0
0,707	0	0	1,00	0	0
0,866	0	0	0	1,00	0
0,966	0	0	0	0	1,00
1,00	0	0	0	0	0

$n=3,\ m=2$

$\bar{r}$	$\varepsilon_{3,2}^{(1)}$	$\varepsilon_{3,2}^{(2)}$	$\varepsilon_{3,2}^{(3)}$	$\varepsilon_{3,2}^{(4)}$	$\varepsilon_{3,2}^{(5)}$
0,259	0,537	—0,156	0,038	—0,010	—0,001
0,5	0,569	0,522	—0,310	0,086	—0,049
0,707	—0,214	0,730	0,403	—0,335	0,049
0,866	0,229	—0,134	0,852	0,290	—0,318
0,966	—0,173	0,282	—0,043	0,974	0,176
1,00	0,185	—0,133	0,427	0,0[illegible]	1,406

$n=4,\ m=2$

$\bar{r}$	$\varepsilon_{4,2}^{(1)}$	$\varepsilon_{4,2}^{(2)}$	$\varepsilon_{4,2}^{(3)}$	$\varepsilon_{4,2}^{(4)}$	$\varepsilon_{4,2}^{(5)}$
0,259	0,202	—0,094	0,035	—0,016	0,006
0,5	0,807	—0,064	—0,123	0,049	—0,020
0,707	—0,029	0,880	—0,345	—0,09	0,030
0,866	0,110	0,227	0,810	—0,577	—0,050
0,966	0,006	0,223	0,415	0,739	—0,781
1,00	0,027	0,170	0,392	0,510	0,366

$n=5,\ m=2$

$\bar{r}$	$\varepsilon_{5,2}^{(1)}$	$\varepsilon_{5,2}^{(2)}$	$\varepsilon_{5,2}^{(3)}$	$\varepsilon_{5,2}^{(4)}$	$\varepsilon_{5,2}^{(5)}$
0,259	0,058	—0,034	0,017	—0,008	0,003
0,5	0,649	—0,276	0,064	—0,020	0,011
0,707	0,408	0,419	—0,477	0,158	—0,034
0,866	—0,102	0,720	—0,015	—0,521	0,212
0,966	0,254	0,115	0,751	—0,553	—0,413
1,00	—0,131	0,503	0,196	0,462	—1,422

$n=6,\ m=2$

$\bar{r}$	$\varepsilon_{6,2}^{(1)}$	$\varepsilon_{6,2}^{(2)}$	$\varepsilon_{6,2}^{(3)}$	$\varepsilon_{6,2}^{(4)}$	$\varepsilon_{6,2}^{(5)}$
0,259	0,014	—0,006	0,006	—0,003	0,001
0,5	0,348	—0,203	0,086	—0,033	0,013
0,707	0,683	—0,104	—0,188	0,146	—0,049
0,866	—0,007	0,745	—0,639	0,069	0,105
0,966	0,191	0,341	0,302	—0,957	0,460
1,00	0,102	0,390	0,266	—0,513	—0,812

SOME PROBLEMS ASSOCIATED WITH COMPUTATIONS OF PROPELLERS

We are going to show solutions to some problems which were encountered in the computation of propellers.

INDUCED VELOCITY DUE TO k HELICAL VORTICES IN THE PRESENCE OF A CYLINDRICAL HUB

With the help of particular integrals of Eq. (17.41) satisfying boundary conditions at an infinite rigid cylinder of radius r_0, we obtain the following expression for the potential of velocity induced by k vortices with circulation Γ:

$$\varphi = -\frac{k\Gamma}{\pi}\left\{\frac{\tau}{2}+\frac{1}{\lambda}\sum_{n=1}^{\infty}(-1)^n\left[\frac{K'_{kn}\left(\frac{kn}{\lambda}\right)I'_{kn}(kn\bar{r}_0)}{K'_{kn}(kn\bar{r}_0)}K_{kn}(kn\bar{r})-\right.\right.$$

$$\left.\left.-K'_{kn}\left(\frac{kn}{\lambda}\right)I_{kn}(kn\bar{r})\right]\sin kn\tau\right\} \text{ for } \bar{r}_0 \leqslant \bar{r} \leqslant \frac{1}{\lambda},$$

$$\varphi = -\frac{k\Gamma}{\pi\lambda}\sum_{n=1}^{\infty}(-1)^n\left[\frac{K'_{kn}\left(\frac{kn}{\lambda}\right)I'_{kn}(kn\bar{r}_0)}{K'_{kn}(kn\bar{r}_0)}-I_{kn}\left(\frac{kn}{\lambda}\right)\right]K_{kn}(kn\bar{r})\sin kn\tau$$

$$\text{for } \bar{r} \geqslant \frac{1}{\lambda}.$$

COMPUTATION OF THE VELOCITY OF FLOW AROUND A BODY OF REVOLUTION AT ZERO ANGLE OF ATTACK

If a body of revolution is replaced by sources distributed along axis x on segment $(0\text{-}a)$[62], then computation is reduced to the solution of the following integral equation

$$\int_0^1 \frac{Q(\bar{\xi})\,d\bar{\xi}}{[(\bar{x}-\bar{\xi})^2+\bar{r}^2(\bar{x})]^{3/2}} = 1,$$

where $\bar{x} = x/a$; $\bar{r} = r/a$ and $\bar{r} = \bar{r}(\bar{x})$ is the equation of the body contour. The above integral equation can be transformed to the following form:

$$Q(\bar{x})=\left\{1-\int_0^1 \frac{Q(\bar{\xi})-Q(\bar{x})}{[(\bar{x}-\bar{\xi})^2+\bar{r}^2(\bar{x})]^{3/2}}\,d\bar{\xi}\right\}\left\{\int_0^1 \frac{d\bar{\xi}}{[(\bar{x}-\bar{\xi})^2+\bar{r}^2(\bar{x})]^{3/2}}\right\}^{-1}$$

and solved through a method of consecutive approximations. Velocity components are expressed through function Q:

$$\bar{v}_x=\frac{v_x}{V}=1+\frac{1}{2}\int_0^1 \frac{(\bar{x}-\bar{\xi})\,dQ(\bar{\xi})}{[(\bar{x}-\bar{\xi})^2+\bar{r}^2]^{3/2}},$$

$$\bar{v}_r=\frac{v_r}{V}=-\frac{\bar{r}}{2}\int_0^1 \frac{dQ(\bar{\xi})}{[(\bar{x}-\bar{\xi})^2+\bar{r}^2]^{3/2}}.$$

COMPUTATION OF FLOW AROUND A SYMMETRICAL AIRFOIL

The airfoil section is replaced by sources distributed along segment $-l \leq x \leq l$ of the x axis, and integration required for the determination of the outflow from the sources

$$\int_{-1}^1 \frac{Q(\bar{\xi})\,d\bar{\xi}}{(\bar{x}-\bar{\xi})^2+\bar{y}^2(\bar{x})}=1 \quad \left(\bar{x}=\frac{x}{l},\ \bar{y}=\frac{y}{l}\right)$$

is transformed to the following

$$Q(\bar{x})=\left\{1-\int_{-1}^1 \frac{Q(\bar{\xi})-Q(\bar{x})}{(\bar{x}-\bar{\xi})^2+\bar{y}^2(\bar{x})}\,d\bar{\xi}\right\}\left\{\int_{-1}^1 \frac{d\bar{\xi}}{(\bar{x}-\bar{\xi})^2+\bar{y}^2(\bar{x})}\right\}^{-1}$$

and then solved by the method of consecutive approximations. Velocity components are defined with the help of function Q:

$$\bar{v}_x=\frac{v_x}{V}=1+\int_{-1}^1 \frac{(\bar{x}-\bar{\xi})\,dQ(\bar{\xi})}{(\bar{x}-\bar{\xi})^2+\bar{y}^2},$$

$$\bar{v}_y=\frac{v_y}{V}=\bar{y}\int_{-1}^1 \frac{dQ(\bar{\xi})}{(\bar{x}-\bar{\xi})^2+\bar{y}^2}.$$

The magnitude of velocity on the surface of a symmetrical airfoil at an arbitrary angle of attack is related to the velocity existing at zero angle of attack through the following

$$\frac{v(0)}{V}=\bar{v}(0)=\begin{cases}\dfrac{\bar{v}_{\text{верх}}(\alpha)+\bar{v}_{\text{нижн}}(\alpha)}{2\cos\alpha} & \text{for } -1\leqslant\bar{x}\leqslant\bar{x}_0,\\ \dfrac{\bar{v}_{\text{верх}}(\alpha)-\bar{v}_{\text{нижн}}(\alpha)}{2\cos\alpha} & \text{for } \bar{x}_0\leqslant\bar{x}\leqslant 1,\end{cases}$$

where $\bar{x}_0$ is the coordinate of the critical point. The above relationship permits calculation of velocity at any angle of attack once its distribution for $\alpha = 0$ is known.

DETERMINATION OF THE SHAPE OF A THIN AIRFOIL FOR GIVEN PRESSURE DISTRIBUTION

Presentations of the compressibility effects and considerations of boundary layer separation at subsonic velocities are related to pressure distribution corresponding to the incompressible flow. For this reason, the pressure distribution becomes a starting point for the determination of the airfoil shape. For thin airfoil sections, the airfoil is replaced by sources and vortices distributed on segment $-1 \leq \bar{x} \leq 1$ of the x axis. This permits one to obtain the following equations with the help of which it is possible to find the angle of attack, camber $\bar{y}_0 = 1/2(\bar{y}_{\text{верх}} + \bar{y}_{\text{нижн}})$ and airfoil thickness $\bar{c} = \bar{y}_{\text{верх}} - \bar{y}_{\text{нижн}}$:

$$\alpha-\frac{d\bar{y}_0(\bar{x})}{d\bar{x}}=\frac{1}{2\pi}\int_{-1}^{1}\frac{g_2(\bar{\xi})\,d\bar{\xi}}{\bar{x}-\bar{\xi}},$$

$$\frac{d\bar{c}(\bar{x})}{d\bar{x}}=\frac{2}{\pi\sqrt{1-\bar{x}^2}}\int_{-1}^{1}\frac{g_1(\bar{\xi})\sqrt{1-\bar{\xi}^2}}{\bar{x}-\bar{\xi}}\,d\bar{\xi},$$

where

$$g_1=\frac{1}{2}\left(\frac{\bar{p}_{\text{верх}}}{1+\sqrt{1-\bar{p}_{\text{верх}}}}+\frac{\bar{p}_{\text{нижн}}}{1+\sqrt{1-\bar{p}_{\text{нижн}}}}\right),$$

$$g_2=\frac{\bar{p}_{\text{нижн}}-\bar{p}_{\text{верх}}}{\sqrt{1-\bar{p}_{\text{нижн}}}+\sqrt{1-\bar{p}_{\text{верх}}}},\quad \bar{p}=\frac{p-p_\infty}{q_\infty}.$$

According to the *a priori* given pressure distribution, an airfoil was developed using the above outlined method. With the help of conformal transformations to a circle, pressure distributions were obtained for this airfoil. A comparison of the so-obtained pressure distributions with those originally given as a starting point indicated a satisfactory agreement.

BIBLIOGRAPHY

NOTE: Names and titles are transliterated according to the U.S. Board on Geographic Names (B.G.N. System).

1. Durand, W.F. Aerodinamika *(Aerodynamic Theory)* translated from English. Vols. II and IV, Oborongiz, 1939.

2. Aleksandrov, V.L. Vozdushnyye vinty *(Airscrews)*. Oborongiz, 1951.

3. Baskin, V. E., D'yachenko, A.C., Maykapar, G.I., Martynov, A.I. Issledovanniye techeniya vozdukha i nagruzok na lopasti vinta vetroleta v gorizontalnom polete *(Investigations of the Air Flow and Blade Loads of a Helicopter Rotor in Horizontal Flight)*. "Inzhenernyy Zhurnal" *("Engineering Journal")*. 1963, Vol. III, No. 2.

4. Baskin, V. E. O dvizhenii prostranstvennoy diffundiruyushchey vikhrevoy trubki v nyeszhimaemoy vyaskoy zhidkosti *(Movement of a Three-Dimensional Vortex Filament in an Incompressible Viscous Fluid)*. DAN SSSR*, 1965, Vol. 165, No. 6.

5. Baskin, V. E., Koroleva, K.K. K nyelineynoy vikhrevoy teorii vinta vertoleta v gorizonyalnom polete *(Nonlinear Vortex Theory of the Helicopter Rotor in Horizontal Flight)*. Trudy TsAGI *(Publications of TsAgi)*. 1966, No. 1013.

6. Baskin, V. E. K teorii nyestatsionarnogo krivolineynogo dvizheniya nyesushchey poverkhnosti v gaze *(Theory of Nonstationary Curvilinear Motion of a Lifting Surface in Gas)*. "Uchebnyye zapiski TsAGI" *("Scientific Notes of TsAGI")*. 1970, Vol. I, No. 2.

7. Baskin, V. E. K lineynoy teorii nyestatsionarnogo dvizheniya gaza pod deystviem nyepotentsialnykh vnyeshnikh sil *(Linear Theory of Unstationary Motion of Gas under the Influence of Nonpotential External Forces)*. Izv. AN SSSR *(News of the Academy of Sciences of USSR)*. "Mekhanika zhidkostey i gazov" *(Mechanics of Liquids and Gases)*. 1969, No. 4.

8. Baskin, V. E. Induktirovnyye skorosti u vozdushnogo vinta, obduvayemogo pod uglom k yego osi *(Induced Velocities of an Airscrew in a Nonaxial Flow)*. "Vsesoyuznyy s"yezd po teoreticheskoy i prikladnoy mekhanike. Annotatsii dokladov" *("All-*

*Doklady Akademii Nauk SSSR *(Proceedings of the Academy of Sciences of USSR)*.

Union Meeting on Theoretical and Applied Mechanics. Proceedings of Lectures). Izd. AN SSSR*, 1960.

9. Baskin, V. E. Nyelineynaya teoriya i raschety skorostey vikhrevogo techeniya vinta vertoleta *(Nonlinear Theory and Computations of Velocities of Vortex Flow of a Helicopter Rotor.* "Tretiy vsesoyuzhyy s"yezd po teoreticheskoy i prikladnoy mekhanike. Annotatsii dokladov" *("Third All-Union Meeting on Theoretical and Applied Mechanics. Proceedings of Lectures").* Izd. AN SSSR, 1968.

10. Belkin, S.A., Druzhinin A.S. Prakticheskiy metod podscheta kharateristik vintov *(Practical Methods of Computation of Characteristics of Propellers).* Trudy TSAGI *(Publications of TsAGI).* 1939, No. 429.

11. Belotserkovskiy, S.M. Kol'tsevoy vikhr pri nyeustanovivshemsya dvizhenii *(Ring Vortex in Unsteady Motion).* PMM, 1956, Vol. XX, No. 2.

12. Belotserkovskiy, S.M. Tonkaya nesushchaya poverkhnost' v dozvukovom potoke *(Thin Lifting Surface in Subsonic Flow).* M. Nauka *(Science).* 1965.

13. Betts, A. O propellere s naymen'shey poterey moshnosti *Betz, A. About Propellers with the Lowest Power Loss).* TVF**, 1927, No. 5/6.

14. Bratukhin, I.P. Aerodinamicheskiy raschet avtozhira *(Aerodynamic Computations of Autogiros).* TSF, 1934, No. 3.

15. Bratukhin, I.P. Avtozhiry (teoriya i raschet). [*Autogiros (Theory and Computations)*]. M. Gosmashmetizdat, 1934.

16. Van Shi-Tsun'. Obobshchennaya vikhrevaya teoriya nesushchego vinta vertoleta *(Generalized Vortex Theory of Helicopter Rotor).* Trudy *(Publications)* MAI, No. 142, M. Oborongiz, 1961.

17. Vedrov, V.S. Otnositel'nyy koeffitsient poleznogo deystviya grebnogo vinta *(Relative Coefficient of Propulsive Efficiency of a Propeller).* TVF**, 1927, No. 4.

18. Vetchinkin, V.P. Raschet grebnogo vozdushnogo vinta *(Calculations of a Propulsive Airscrew).* Byulletin politekhnicheskogo obshchestva (Bulletin of the Polytechnical Society), No. 5, 1913.

---

*Publications of the Academy of Sciences of USSR.

**Tekhnika Vozdushnogo Flota *(Technology of the Air Fleet).*

19. Vetchinkin, V.P. Raschet grebnogo vinta *(Calculations of a Propeller)*. "Trudy Aviatsionnogo raschetnoispytatel'nogo byuro" *("Publications of the Analytical and Experimental Aviation Bureau")*. Izd. upr. voenno-vozdushnogo flota *(Publications of the Air-Force Command)*. Moscow, 1918.

20. Vetchinkin, V.P. Ob invariantakh grebnogo vinta *(About the Invariants of a Propeller)*. "Trudy otdeleniya fizicheskikh nauk Obshchestva lyubitieley estestvoznania *(Publications of the Physical-Sciences Branch of the Society of Natural Sciences)*. 1914, Vol. XVII, No. 1.

21. Vetchinkin, V.P. Polyakhov, N.N. Teoriya i raschet vozdushnogo grebnogo vinta *Theory and Calculation of a Propeller)*. M., Oborongiz, NKAP, 1940.

22. Vil'dgrube, L.S. Nekotoryye graficheskiye priyemy aerodinamicheskikh raschetov *(Some Graphical Methods of Aerodynamic Calculations)*. TVF, 1945, No. 4.

23. Vil'dgrube, L.S. Optimal'nyye parametry gelikoptera na rezhimakh vertikal'nogo poleta *(Optimal Parameters of Helicopters in Vertical Regimes of Flight)*. TVF, 1946, Nos. 3 and 5.

24. Vil'dgrube, L.S. Opredeleniye letno-tekhnicheskikh kharacteristik gelikoptera na vsekh rezhimakh poleta i vybor yego parametrov pri proyektirovanii *(Determination of Helicopter Performance in all Regimes of Flight and Selection of its Parameters during Design)*. TVF. 1947, No. 6.

25. Vil'dgrube, L.S. Teoriya nesushchikh vintov s ploskoy vikhervoy sistemoy *(Theory of Lifting Airscrews with a Flat Vortex System)*. "Vsesoynznyy s"yezd po teoreticheskoy i prikladnoy mekhanike. Annotatsii dokladov" *(All-Union Meeting on Theoretical and Applied Mechanics. Proceedings of Lectures)*. Publication of AN SSSR, 1960.

26. Vil'dgrube, L.S. Variatsionnyye zadachi v teorii dvukhvitovykh nesushchikh sistyem *(Variational Problems in the Theory of the Two-Airscrew Lifting Systems)*. "Tretiy vsesoyuznyy s"yezd po teoreticheskoy i prikladnoy mekhanike. Annotatsii dokladov" *("Third All-Union Meeting on Theoretical and Applied Mechanics. Proceedings of Lectures")*. Publications of AN SSSR, 1968.

27. Vozhdayev, Ye.S. Ob odnom prilozhenii obobshchennogo zakona Bio-Savara *(About One Application of the Generalized Biot-Savart Law)*. Inzhenernyy zhurnal *(Engineering Journal)*. Vol. V, No. 2, 1965.

28. Vozhdayev, Ye. S. Lopastnaya teoriya nyesushchego vinta vertikalno vzletayuschego apparata v osevom potoke *(Blade Theory of Lifting Airscrew of Vertically Rising Aircraft in Axial Flow)*. Publications of TsAGI, 1970, Report 1234.

29. Vozhdayev, Ye. S. Teoriya nyesushchego vinta na rezhimakh vkhrevogo kol'tsa *(Theory of Lifting Airscrew in Vortex-Ring Regimes)*. Publications of TsAGI, 1970, Report 1184.

30. Vozhdayev, Ye. S. O nyekotorykh funktsyakh gipergeometricheskogo tipa vstrechayushchikhsya v mekhanike *(About Some Hypergeometric-Type Functions Encountered in Mechanics)*. "Uchenyye zapiski *(Scientific Notes of)* TsAGI", 1970, Vol. I, No. 6.

31. Vozhdayev, Ye. S. Metod nyesushchey poverkhnosti v teorii vinta vertoleta *(Method of Lifting Surface in Theory of Helicopter Rotor)*. Tretiy vsesoyuznyy s"yezd po teoreticheskoy i prikladnoy mekhanike. Annotatsii dokladov." AN SSSR, 1968.

32. Gessou G., Meyers, G. Aerodinamika vertoleta (per. c angl.) [*(Gessow, G., Myers, G. Helicopter Aerodynamics (translated from English)*]. M. Oborongiz, 1954.

33. Glauert, G. Osnovy teorii kryl'yev i vinta (per. s angl.). [*Glauert, H. Fundamentals of Wing and Propeller Theory (translated from English)*]. GNTI, 1931.

34. Dzhevetskiy, S.K. Teoria vozdushnykh vintov i spocob ikh vychisleniya *(Drzewiecki, S.K. Theory of Airscrews and Method of Their Calculations)*. Kiyev, 1910.

35. Dovzhik, S.A. Profilirovaniye lopatok osevogo dozvukovogo kompressora *(Selection of Airfoils of Axial Subsonic Compressor)*. Promyshlennaya aerodynamika *(Industrial Aerodynamics)*. Vol. II, M. Oborongiz, 1958.

36. Dorodnitsyn, A.A. Obobshcheniye teorii nyesushchey linii na sluchay kryla s izognutoy os'yu i os'yu nye perpendikulyarnoy potoku *(Generalization of the Lifting-Line Theory for the Case of Curved Wing Axis and Axis Nonperpendicular to the Flow)*. PMM, 1944, Vol. VIII, Report 1.

37. Zhukovskiy, N.Ye. O prisoyedinennykh vikhrakh *(About Bound Vortices)*. Collected Works, GITTL. Vol. IV, 1949.

38. Zhukovskiy, N.Ye. Opyt teoreticheskogo opredeleniya effekta vetra, duyushchego v ploskosti gelikopternogo vinta *(Attempt at Theoretical Determination of the Effect of Wind Blowing in the Plane of a Helicopter Rotor)*. Collected Works of GITTL, Vol. 1, 1949.

39. Zhukovskiy, N.Ye. Teoriya vinta gelikopternogo i grebnogo *(Theory of Helicopter and Propulsive Airscrews).* Collected Works of GITTL, Vol. VI, 1950.

40. Zhukovskiy, N.Ye. Raschet vinta dla aeroplana i dirizhabla *(Calculation of Propeller for Airplane and Dirigible).* Collected Works of GITTL, Vol. VI, 1950.

41. Zhukovskiy, N.Ye. Vikhrevaya teoriya grebnogo vinta *(Vortex Theory of Propelling Airscrew)* stat'ya pervaya *(First Article).* Collected Works of GITTL, Vol. IV, 1949.

42. Zhukovskiy, N.Ye. Vikhrevaya teoriya grabnogo vinta *(Vortex Theory of Propelling Airscrew)* stat'ya vtoraya *(Second Article).* Collected Works of GITTL, Vol. IV, 1949.

43. Zhukovskiy, N.Ye. Vikhrevaya teoriya grebnogo vinta *(Vortex Theory of Propelling Airscrew)* stat'ya tret'ya *(Third Article).* Collected Works of GITTL, Vol. IV, 1949.

44. Zhukovskiy, N.Ye. Vikhrevaya teoriya grobnogo vinta *(Vortex Theory of Propelling Airscrew)* stat'ya chetvertaya *(Fourth Article).* Collected Works of GITTL, Vol. IV, 1949.

45. Zhukovskiy, N.Ye. Teoreticheskiye osnovy vozdukhoplavaniya, izd 2, vyp 2 *(Theoretical Foundations of Aeronautics, Second Edition, Second Printing).* GONTI, 1925.

46. Keldysh, M.V., Frankl', F.I. Strogoye obosnovaniye teorii vinta N.Ye. Zhukovskogo *(Rigorous Foundation of the Zhukovskiy Airscrew Theory)* Matematicheskiy sbornik *(Mathematical Archives).* 1935, Vol. 42, No. 2.

47. Keldysh, V.V. Obtekaniye vinta s otryvom potoka *(Flow around an Airscrew with Stall).* "Inzhenernyy Zhurnal" *("Engineering Journal")*, Vol. III, Issue 1.

48. Keldysh, V.V. Reshetki profiley v sverkhsvukavom potoke *(Airfoil Cascade in Supersonic Flow).* Sbornik teoreticheskikh rabot po aerodinamike *(Collection of Theoretical Works on Aerodynamics).* M. Oborongiz, 1947.

49. Kolesnikov, G.A. Metod rascheta raspredeleniya tsirkulyatsii kryl'yev malogo udlinyeniya *(Method of Calculating Circulation Distribution of Low-Aspect-Ratio Wings).* Sbornik teoreticheskikh rabot po aerodinamike *(Collection of Theoretical Works on Aerodynamics).* M. Oborongiz, 1957.

50. Kozhevnikov, V.A. Vliyaniye blizosti zemli na aerodinamicheskiye kharakteristiki nesushchego vinta gelikoptera *(Influence of the Ground Proximity on Aerodynamic Characteristics of the Lifting Rotor of a Helicopter).* TVF, 1947, No. 4.

51. Kochin, N.Ye. Ob ustanovivshikhsya kolebaniyakh kryla krugovoy formy v plane *(About Steady-State Oscillations of a Wing of Circular Planform)*. PMM, 1942, Vol. VI, Report 4.

52. Kochin, N.Ye. Kibel', I.A., Roze, N.V. Teoreticheskaya Gidromekhanika *(Theoretical Hydromechanics)*. OGIZ-GITTL, 1947.

53. Kuz'min, G.I. Issledovaniye raboty vozdushnykh vintov *(Investigation of the Working of Airscrews)*. Publications of TsAGI, 1930, Report 45.

54. Kuz'min, G.I. Raschet vinta po vikhrevoy teorii *(Calculations of Propeller According to Vortex Theory)*. Publications of TsAGI, 1932, Report 132.

55. Lamb, G. Gidrodinamika *(Hydrodynamics)* translated from English, OGIZ-GTI, 1947.

56. Lepilkin, A.M. Vikhrevaya teoriya nesushchego vinta i vzaimnogo vliyaniya vintov *(Vortex Theory of a Lifting Airscrew, and Mutual Interaction of Airscrews)*. "Izv. AN SSSR; Mekhanika i matematika" *(The USSR Academy of Sciences News; Mechanics and Mathematics)*.

57. Lepilkin, A.M. K vikhrevoy teorii izolirovannogo vinta *(About the Vortex Theory of an Isolated Airscrew)*. Publications of TsAGI, 1940, Report 529.

58. Maykapar, G.I. Opredeleniye induktivnykh skorostey vinta s pomoshch'yu besselevykh funktsiy *(Determination of Induced Velocities with the Help of Bessel Functions)*. Publications of TsAGI, 1940, Report 529.

59. Maykapar, G.I. Aerodinamicheskiy raschet izolirovannogo propellera *(Aerodynamic Calculations of an Isolated Propeller)*. TVF, 1939, No. 7/8.

60. Maykapar, G.I. Issledovaniye po vichrevoy teorii propellera *(Investigation of the Vortex Theory of Propellers)*. Publications of LII GVF, 1940, Report 21.

61. Maykapar, G.I. Prilozheniya vikhrevoy teorii vinta *(Applications of the Vortex Theory of Airscrews)*. Publications of TsAGI, 1947, Report 21.

62. Maykapar, G.I. Raschet skorosti potoka, obtekayushchego tela vrashcheniya *(Calculations of Velocities of Flow Around Bodies of Revolution)*. Publications of TsAGI, 1944, Report 547.

63. Maykapar, G.I., Lepilkin, A.M., Khalezov, D.V. Aerodynamicheskiy raschet vintov po lopastnoy teorii *(Aerodynamic Calculations of Airscrews According to Blade Theory)*. Publications of TsAGI, 1940, Report 529.

64. Mil', M.L., Nekrasov, A.V., Braverman, A.S., Grodko, L.N., Leykand, M.A. Vertolety *(Helicopters)*. Vol. I, M. "Mashinostroyeniye", 1966.

65. Milyukhin, B.L. Raschet vinta po otnositel'noy teorii *(Airscrew Calculations According to Relative Theory)*. Publications of TsAGI, 1939, Report 401.

66. Mikhaylov, A.N. Teoriya rotora avtozhira s peremennym uglom ustanovki *(Theory of the Autogiro Rotor with Variable Pitch Angle)*. TVF, 1940, No. 3.

67. Moriya, T. Induktivnaya skorost' i kharakteristika propellera *(Induced Velocity and Characteristics of Propellers)*. TsAGI Bulletin, 1933, No. 20.

68. Moriya, T. Diagrammy induktivnoy skorosti i metod rascheta aerodinamicheskikh kharakteristik vinta *(Diagrams of Induced Velocity and Method of Aerodynamic Calculations of an Airscrew)*. Publications of TsAGI, 1936, No. 119.

69. **Paine,** P. R. Dinamika i aerodinamika vertoleta *(Dynamics and Aerodynamics of Helicopters)* translated from English. M. Oborongiz, 1969.

70. Polyakhov, N.N. Teoriya vinta s konechnym chislom lopastey *(Theory of Propellers with Finite Number of Blades)*. cations of TsAGI, 1937, Report 324.

71. Polyakhov, N.N. K teorii grebnogo vinta *(About the Theory of Propellers)*. Publications of TsAGI, 1935, Report 184.

72. Polyakhov, N.N. O nayvygodneyshem vinte *(About the Most Suitable Proepller)*. Publications of TsAGI, 1939, Report 455.

73. Polyakhov, N.N. Teoriya nesushchey vintovoy poverkhnosti *(Theory of Lifting Helical Surface)* "Vestnik LGU". 1963, No. 13.

74. Proskuryakov, A.P. Vliyaniye nyestatsionarnosti potoka na aerodinamiku lopasti avtozhira *(Influence of the Unsteadyness of Flow on Aerodynamics of an Autogiro Blade)*. Publications of TsAGI, 1939, Report 460.

75. Proskuryakov, A.P. Aerodinamicheskiy raschet nesushchego vinta s peremennym po azimutu uglom lopasti *(Aerodynamic Calculations of Lifting Airscrew with the Azimuth-Varying Blade Pitch Angle).* Publications of LII, 1946, No. 16.

76. Proskuryakov, A.P. Teoriya nesushchego vinta pri nulevom ugle ataki *(Theory of Lifting Airscrew at Zero Angle of Attack).* PMM, 1956, Vol. XX, No. 4.

77. Ryzhik, I.M. Gradshteyn, M.C. Tablitsy integralov, summ, ryadov i proizvedeniy.*(Tables of Integrals, Sums, Series and Products).* M. GITTL, 1951.

78. Sabinin, G.Kh. Teoriya ideal'nogo vetryaka *(Theory of the Ideal Windmill).* Publications of TsAGI, 1927, Report 32.

79. Simonov, L.A., Khristianovich, S.A. Vliyaniye szhimayemosti na induktivnyye skorosti kryla i vinta *(Influence of Compressibility on Induced Velocities of Wing and Airscrew).* PMM, 1944, Vol. VIII, No. 2.

80. Simonov, L.A. Raschet obtekaniya krylovykh profiley i postroyeniye profilya po raspredeleniyu skorostey na yego poverkhnosti *(Calculations of Flow Around Wing Airfoils and Design of Airfoil According to the Velocity Distribution on Its Surface).* PMM, 1947, Vol. XI, No. 1.

81. Slutskiy, A.I. Optimal'naya tsirkulatsiya s uchetom kachestva profilya dla vinta s konechnym chislom lopastey *(Optimum Circulation with Considerations of Airfoil Suitability for an Airscrew with a Finite Number of Blades).* Publications of TsAGI, 1940, Report 529.

82. Struminskiy, V.V., Lebed', N.K., Metod rascheta tsirkulyatsii po razmakhu strelovidnogo kryla *(Method of Circulation Calculation Along the Span of an Arrow-Shaped Wing).* Sbornik teoreticheskikh rabot po aerodinamike *(Collection of Works on Aerodynamics).* M. Oborongiz, 1957.

83. Flamm, O. Sudovoy grebnoy vint i yego deystviye v vode *(Ship Propeller and its Operation in Water)* translated from German. Moscow, 1910.

84. Frankl', F.I. Rabota vinta pri bol'shikh skorostyakh *(Operation of Propeller at High Speeds).* TVF, 1933, No. 9.

85. Frankl', F.I. K teorii vinta s beskonechuym chislom lopastey pri bolshikh skorostyakh *(Theory of High-Speed Propellers with Infinite Number of Blades).* Publications of TsAGI, 1937, Report 301.

86. Frankl', F.I. Teriya vinta s konechnym chislom lopastey pri bol'shikh postupatel'nykh i okruzhnykh skorostyakh *(Theory of Propeller with Finite Number of Blades at High Translatory and Tip Speeds)*. Publications of TsAGI, 1942, Report 540.

87. Chushkin, P.I. Raschet raspredeleniya tsirkulatsii po pryamougol'nym kryl'yam malogo udlineniya *(Calculation of Circulation Distribution for Straight Wings of Low Aspect Ratio)*. Sbornik teoreticheskikh rabot po aerodinamike *(Collection of Works on Aerodynamics)*. M. Oborongiz, 1957.

88. Shaydakov, V.I. Issledovaniniye rezhimov vertikal'nogo snizheniya vertoleta *(Investigation of Descending Regimes of Helicopters)*. Publications of MAI, Report 142, M. Oborongiz, 1961.

89. Yur'yev, B.N. O sovremennom polozhenii teorii grebnogo vinta *(About the Current Status of Theory of Propulsive Airscrew)*. "Vestnik Vozdushnogo flota" *(Air Fleet News")* 1923, No. 5.

90. Yur'yev, B.N. Vozdushnyye vinty *(Airscrews)*. M. ONTI, 1934.

91. Yur'yev, B.N. Izbrannyye trudy, t.I. Vozdushnyye vinty, vertolety *(Collected Works, Vol. I, Airscrews, Helicopters)*. M. AN SSSR, 1961.

92. Yur'yev, B.N. Aerodinamicheskiy raschet vertoletov *(Aerodynamic Calculations of Helicopters)*. M. Oborongiz, 1956.

93. Yur'yev, B.N. Izbrannyye trudy t. II. Aerodinamika, istoriya aviatsionnoy tekhniki *(Collected Works, Vol. II. Aerodynamics, History of Aeronautical Technology)*. M. AN SSSR, 1961.

94. Yang, R.A. Teoriya i raschet gelikoptera *(Theory and Calculations of Helicopters)* translated from English. M. Oborongiz, 1951.

95. Brotherhood, P. *Flow through a Helicopter Rotor in Vertical Descent*. ARC R&M No. 2735, 1952.

96. Brown, C.E. *Challenge in Marine Systems*. Astronautics and Aeronautics, Vol. II, No. 2, 1965, pp. 64-66.

97. Brown, F.N. *An American Method of Photographing Flow Pictures*. Aircr. Ing., Vol. XXIV, No. 280, 1952.

98. Buseman, A. *Theory of the Propeller in Compressible Flow*. Proc. Third Mid-West Conf., Fluid Mechanics, 1953.

99. Castles, W., deLeeuw, J.H. *Induced Velocity in the Vicinity of a Lifting Rotor and Some Examples of Its Applications.* NACA TR No. 1184, 1954.

100. Eisenhuth, I.I., McCormick, B.W. *An Observation on the Vortex System of a Dual-Rotation Propeller.* JAS, Vol. 20, No. 6, 1953.

101. Flügge-Lotz, I., Solf, K. *Strömungsaufnahen eines durch einen Tragflügel gestörten Schraubenstrahles,* Luftfahrtforschung, Bd. 17, Lfg. 6, 1940.

102. Gersten, K.A. *Nonlinear Lifting-Surface Theory Especially for Low-Aspect Ratio Wings.* AIAA Journal IV, Vol. 1, No. 4, 1963.

103. Goldstein, S. *On the Vortex Theory of Screw Propellers.* Proc. of the Royal Soc. (A) 123, 440, 1929.

104. Keyson, H.H., Katzoff, S. *Induced Velocity Near a Lifting Rotor with Nonuniform Disc Loading.* NACA TR No. 1319, 1957.

105. Kaden, K. *Auf Wicklung einer unstabilen Unstetigkeitsfläche.* Ing.-Arch. Bd. 11, H.2, 1931.

106. Kawada, S. *Induced Velocity by Helical Vortices.* JAS, Vol. 3, No. 3, 1936.

107. Kinner, W. *Die kreisförmige Tragfläche auf potential theoretischer Grundlage.* Ing-Arch. Bd. 8, H.1, 1937.

108. Lock, C.N.H. *Further Development of Autogiro Theory.* ARC R&M, No. 1127, 1927.

109. Mangler, K.W., Squire, H.B. *The Induced Velocity Field of a Rotor.* ARC R&M, No. 2642, 1953.

110. Miller, R.H. *Rotor Blade Harmonic Air Loading.* IAS Paper 62-82, 1962.

111. Nishiyma, T. *Lifting-Surface Theory of Wide-Bladed Propellers.* Pt. I - Tech. Rep Tokoku Univ., Vol. 29, No. 2, 1964.

112. Piziali, R., Daughaday, H., DuWaldt, F. *Rotor Airloads.* Proc. CAL/TRECOM Symposium, Vol. 1, 1964.

113. Reissner, M. *On the Vortex Theory of the Screw Propeller.* JAS, Vol. 5, No. 1, 1937.

114. Schade, Th. *Theorie der Schwingen kreisformigen Tragflache auf potential theoretischer Grundlage.* Luftfahrtforschung, Bd. 17, Lfg. 11/12, 1940.

115. Sissingh, G. *Beitrag zur Aerodynamic der Drehflugeflugzeuge.* Luftfahrtforschung, Nr. 6, 1938; Nr. 7, 1940.

116. Stewart, W. *Helicopter Behaviour in the Vortex Ring Condition.* ARC Current Paper No. 99, 1952.

117. Wheatley, J., Hood, M.J. *Full-Scale Wind Tunnel Tests of a PCA-2 Autogiro Rotor.* NACA Rep. No. 515, 1935; also see TVF No. 10, 1937.

*U.S. GOVERNMENT PRINTING OFFICE: 1976 - 635-275/69

1. Report No. NASA TT F-823	2. Government Accession No.	3. Recipient's Catalog No.
4. Title and Subtitle Theory of the Lifting Airscrew		5. Report Date February 1976 6. Performing Organization Code
7. Author(s) V. E. Baskin, L. S. Vil'dgrube, Ye. S. Vozhdayev, G. I. Maykapar		8. Performing Organization Report No. 10. Work Unit No.
9. Performing Organization Name and Address Boeing Vertol Company, P.O. Box 16858 Philadelphia, Pa. 19142		11. Contract or Grant No. NAS-2-8081 13. Type of Report and Period Covered Translation
12. Sponsoring Agency Name and Address National Aeronautics and Space Administration U.S. Army Air Mobility R&D Laboratory		14. Sponsoring Agency Code

15. Supplementary Notes

Translation of "Teoriya Nesushchego Vinta", edited by A. K. Martynov, Moscow, Mashinostroyeniye Press, 1973, pp. 1-364.
Translated by W. Z. Stepniewski
Transcribed by W. L. Metz

16. Abstract

The text is chiefly based on the vortex theory. However, some aspects of velocity potential are also discussed. Oblique and axial translations of a lifting airscrew in an ideal fluid are considered first, within the limits of linear and nonlinear theories. Then, viscosity and compressibility effects are introduced. Exposition of some aspects of propeller operation in a compressible medium concludes this presentation.

17. Key Words (Selected by Author(s))	18. Distribution Statement
Rotor Aerodynamics Vortex Theory	Unlimited - Unclassified Subject Category 02

19. Security Classif. (of this report)	20. Security Classif. (of this page)	21. No. of Pages	22. Price *
Unclassified	Unclassified	481	$12.00

For sale by the National Technical Information Service, Springfield, Virginia 22161

NATIONAL AERONAUTICS AND SPACE ADMINISTRATION
WASHINGTON, D.C. 20546

OFFICIAL BUSINESS
PENALTY FOR PRIVATE USE $300

SPECIAL FOURTH-CLASS RATE
BOOK

POSTAGE AND FEES PAID
NATIONAL AERONAUTICS AND
SPACE ADMINISTRATION
451

U.S.MAIL

POSTMASTER: If Undeliverable (Section 158 Postal Manual) Do Not Return

"The aeronautical and space activities of the United States shall be conducted so as to contribute . . . to the expansion of human knowledge of phenomena in the atmosphere and space. The Administration shall provide for the widest practicable and appropriate dissemination of information concerning its activities and the results thereof."

—NATIONAL AERONAUTICS AND SPACE ACT OF 1958

NASA SCIENTIFIC AND TECHNICAL PUBLICATIONS

TECHNICAL REPORTS: Scientific and technical information considered important, complete, and a lasting contribution to existing knowledge.

TECHNICAL NOTES: Information less broad in scope but nevertheless of importance as a contribution to existing knowledge.

TECHNICAL MEMORANDUMS: Information receiving limited distribution because of preliminary data, security classification, or other reasons. Also includes conference proceedings with either limited or unlimited distribution.

CONTRACTOR REPORTS: Scientific and technical information generated under a NASA contract or grant and considered an important contribution to existing knowledge.

TECHNICAL TRANSLATIONS: Information published in a foreign language considered to merit NASA distribution in English.

SPECIAL PUBLICATIONS: Information derived from or of value to NASA activities. Publications include final reports of major projects, monographs, data compilations, handbooks, sourcebooks, and special bibliographies.

TECHNOLOGY UTILIZATION PUBLICATIONS: Information on technology used by NASA that may be of particular interest in commercial and other non-aerospace applications. Publications include Tech Briefs, Technology Utilization Reports and Technology Surveys.

Details on the availability of these publications may be obtained from:

SCIENTIFIC AND TECHNICAL INFORMATION OFFICE

NATIONAL AERONAUTICS AND SPACE ADMINISTRATION

Washington, D.C. 20546